# EFFECTS OF URBANIZATION ON LAND SURFACE TEMPERATURE IN PARTS OF SUDAN SAVANNA AND RAINFOREST ZONES OF NIGERIA

**BY**

**SULE, Isaiah Majin**
**PhD/SPS/2018/7763**

**DEPARTMENT OF GEOGRAPHY**
**FEDERAL UNIVERSITY OF TECHNOLOGY MINNA**

**AUGUST, 2023**

# EFFECTS OF URBANIZATION ON LAND SURFACE TEMPERATURE IN PARTS OF SUDAN SAVANNA AND RAINFOREST ZONES OF NIGERIA

**BY**

**SULE, Isaiah Majin**
**PhD/SPS/2018/7763**

**THESIS SUBMITTED TO THE POSTGRADUATE SCHOOL, FEDERAL UNIVERSITY OF TECHNOLOGY, MINNA, NIGERIA IN PARTIAL FULLFILMENT OF THE REQUIREMENTS FOR THE AWARD OF THE DEGREE OF DOCTOR OF PHILOSOPHY (PhD) IN GEOGRAPHY**

**AUGUST, 2023**

## ABSTRACT

The study aimed at assessing the effects of urbanization on Land Surface Temperature (LST) in four selected cities in Sudan Savanna and Rainforest Ecological Zones of Nigeria. The cities are Ibadan and Owerri in the Rainforest zone, and Kano and Birnin Kebbi in the Sudan Savanna zone, Kano, Owerri and Birnin Kebbi. The study utilized Landsat TM, ETM+ OLI data from the United States Geological Service from the global visualization repository for the years 1990 to 2019, and ERA-Interim (European Reanalysis) grid-based 2 meter above ground daily temperature data from ECMWF repository for the four surveyed cities from 1990 to 2019. To achieve this, the study analyzed LULC change, NDVI, NDBI and LST for the four cities using Idrisi Terrset version 18.21 software and ArcGIS ArcMap 10.8 software. For the ERA-Interim data, R Statistical package software version 3.6.1 was employed to detect the trend and seasonality in the maximum noon-time temperature of the four cities using non-parametric Mann-Kendall trend and seasonal trend tests. The statistical properties of the data were first analyzed by graphical examination of the data, using time plots, and boxplots. Also, the normality test of Shapiro-Wilk (S-W test) was applied. Pettitt test was then employed to test for single change-point detection in the temperature series. The thesis established that built-up areas increased from 312.90 $km^2$ (9.19%), 70.32 $km^2$ (12.94%), 58.48 $km^2$ (11.85 %) and 14.06 $km^2$ (1.13%) in Ibadan, Owerri, Kano and Birnin Kebbi respectively in 1990 to 1,039.54 $km^2$ (30.55%), 209.16 $km^2$ (38.50%), 216.03 $km^2$ (43.77%) and 123.03 $km^2$ (9.85%) in 2019 respectively. This implied a high rate of urbanization process in all the cities, and a concomitant decrease in other land cover types; with a resultant imbalance in the ecosystem of the urban environment. The study also established differences in values of the mean noon-time air temperature; indicating higher temperature values in Birnin Kebbi (27.49°C) and Kano (25.56°C) both in the Sudan, in contrast with lower temperature values of 24.08°C and 23.17°C for Ibadan and Owerri respectively located in the Rainforest. Furthermore, the thesis established a Tau statistics of 0.070, 0.098 and 0.091, and corresponding p-values are 0.045, 0.005 and 0.0098 which are less than 0.05 confidence level for Kano, Ibadan and Owerri respectively; indicating significant rising trends of noon-time temperature in the three cities. Aside the mean LST-NDBI correlation of 0.94, 0.98, 0.96, 0.98 in Ibadan, Owerri, Kano and Birnin Kebbi respectively, the study established an increase in coverage areas of high LST areas from 18.12%, 18.07% and 14.71% respectively in Ibadan, Owerri and Birnin Kebbi respectively in 1990 to 27.00%, 52.12% and 64% in 2019. This implied that as the urban sizes increase in the cities, the coverage area of higher LST increases. The study recommended adequate urban land use planning and initiation of urban greening processes and carbon sequestration as mitigating measures for high LSTs in the cities.


## TABLE OF CONTENTS

## LIST OF TABLES

**Table** **Page**

## LIST OF FIGURES

**Figure** **Page**

## LIST OF PLATES

(CLAMPS-2)

## ABBREVIATIONS AND ACRONYMS

| | |
|---|---|
| DEM | Digital Elevation Models |
| ECMWF | European Centre for Medium-Range Weather Forecasts |
| ERA-Interim | European Reanalysis Interim |

| | |
|---|---|
| ETM+ | Enhanced Thematic Mapper Plus |
| GIS | Geographic Information System |
| GLCF | Global Land Cover Facility |
| GLOVIS | Global Visualizations |
| GPS | Global Positioning System |
| LST | Land Surface Temperature |
| LULC | Landuse/Landcover |
| LULCC | Landuse/Landcover Change |
| NDBI | Normalized Difference Built-up Index |
| NDVI | Normalized Difference Vegetation Index |
| NIR | Near Infrared |
| OLI | Operational Land Imager |
| SWIR | Short-Wave Infrared |
| TIRS | Thermal Infrared Sensor |
| TM | Thematic Mapper |
| UHI | Urban Heat Island |
| USGS | United States Geological Survey |
| UTM | Universal Transverse Mercator |

# CHAPTER ONE

## 1.0 INTRODUCTION

### 1.1 Background to the Study

The past three or four decades have undergone unprecedented urbanization, especially in the developing countries (Kumi-Boateng *et al*., 2015). Particularly, Sub-Saharan Africa is urbanizing fast, with cities and towns growing at an annual rate of about four percent over the past 2 decades (Henderson *et al.,* 2017). Due to unprecedented urbanization, more than half of the world's population now resides in urban location and this number may continue to rise (United Nations, 2014; UN DESA, 2012). The United Nations (UN, 2010) estimated a global rise in the population of city inhabitants from 790 million in 1950 to approximately 3.5 billion in 2010, and projected that given the present pace of increase, the population will rise to 5.9 billion in 2045.

Approximately three-quarters of the urban population of the world as well as its largest cities are at present concentrated in low and middle income countries (Revi *et al*., 2014), particularly in informal settlements and slums (McMichael *et al*., 2008). In these countries rapid urban sprawl is closely related to rapid economic growth (World Bank, 2008; Satterthwaite *et al*., 2010). This is occasioned by the fact that in the developing nations, cities, particularly capital cities, are locations where majority of modern productive activities are concentrated, where the vast majority of paid employment opportunities abound (Cohen, 2006), and where there is availability of basic and better services such as better transportation, sewer, water, educational and health care services among others (Bhatta, 2010). Urbanization is therefore largely attributed to rapid population increase caused by a mass immigration of people (Josh and Bhatta, 2012) into urban areas in search of economic opportunities; with rural-urban migration being the principle component of rapid and unplanned growth of towns and cities in the developing countries (Jahan, 2012).

About ninety per cent of the projected rise in global urban population is expected to occur in Africa and Asia (United Nations, 2014). For instance, Nigeria, India, and China

combined are predicted to account for thirty-seven percent of the projected growth of the world urban population between 2014 and 2050 (Aliyu and Amadu, 2017). Predictions have suggested that by 2030 Africa will attain the urban age when half of Africans will live in urban areas (Opoko and Oluwatayo, 2014). Specifically, Nigeria's urban population has expanded rapidly over the past 50 years and may continue to grow relatively fast in the coming decades (Bloch *et al.,* 2015). At the current growth rate of about 2.8 percent to three percent annually, it is estimated that Nigeria's urban population will double in the next two decades (Aliyu and Amadu, 2017). Consequently, the number of people living in Nigeria's urban centres will likely hit 100 million by 2020 (Oyeleye, 2013).

Several drivers of urbanization have been identified. The main drivers include natural population increase, growth of urban areas through merger processes, transformation of countrysides into small urban settlements, and rural-urban migration (Aliyu and Amadu, 2017). Specifically, in Nigeria, urbanization has been largely attributed to rapid population increase caused by a high entrance of people into cities from the countrysides (Ohwo and Abotutu, 2015). Other important factors influencing urbanization in Nigeria as highlighted by Ohwo and Abotutu (2015) include creation of new states and new Local Government Areas (LGAs) with consequent establishment of state capitals and LGA headquarters, as well as the establishment of new universities and colleges in virtually every state (Aliyu and Amadu, 2017). The major pull factor of population to urban areas in the country is the perceived opportunities offered by these urban centres (Ohwo and Abotutu, 2015). It has been predicted that by year 2030, agglomeration of cities and population migration from rural areas to urban centres will raise world-wide proportion of urban coverage by seventy percent of the world's present urban population (Kumar *et al.,* 2015). Similarly, the amount of global urban land is expanding at twice the population

growth rate and is predicted to triple by 2030 if present trends in population density continue (Angel *et al.,* 2011; Seto *et al*., 2012). A major implication of urbanization in Nigeria is that most urban centres in the country lack adequate planning and effective management strategies to accommodate the influx of people (Ohwo and Abotutu, 2015). This results in serious pressure on the socioeconomy supporting structures and the environment (Ohwo and Abotutu, 2015).

Urbanization is known to be the prime anthropogenic activity with enormous irreparable consequences on adjoining ecosystems (Mahmoud *et al.*, 2016). Some of its impacts have been highlighted by Cui and Shi (2012). The impacts include increased air and water contamination, decreased water supply, inadequate housing and poor sanitation facilities. Others are drastic reduction in natural vegetal cover and carbon sequestration, and traffic jams. Another important impact of urbanization process is its effects on land surface temperarue (LST) which refers to the radiative skin temperature of the land surface which plays a significant role in the science of the land surface through the processes of energy and water exchange with the air (Zhang *et al.*, 2009). LST is a very important biophysical parameter which modulates the the lowest layers of the atmosphere and plays vital roles in the energy balance of the surface (Zoran, 2011). Urbanization process results in the conversion of natural vegetal cover, exposed soil, and surface water to modern non-evaporating impervious land use/land cover (LULC) classes (Polydoros *et al*., 2018; Paranunzio *et al.*, 2019). The modern urban surfaces which have replaced natural landscapes include buildings, rooftops, asphalt, concrete, bricks, tiles, metals, roads, parking lots, pavements and other impervious surfaces (Goswami *et al*., 2013; Kaiser, 2014; Jiang *et al*., 2015; Liu *et al*., 2015). The high proportions of impervious surfaces of the urban landscapes are largely created for transportation, commercial usage, industrial uses, and housing units (Jin and Dickinson, 2010). These materials inhibit the penetration

of water into the soil; resulting in the absorption of most of the incident shortwave radiation which is transformed into sensible heat (Gusso *et al*., 2017).

These impervious surfaces alter the thermodynamic properties of soil, surface energy budget of the Earth, change the nature of the circulation of ambient atmosphere, and create large amount of waste heat from human activities (Van and Bao, 2015). Moreover, the rooftops and walls of high-rise structures with darker surfaces, parking lots, roads and pavements constructed with asphalt and concrete tend to have low albedos. These dark low-albedo surfaces absorb higher amount of solar radiation and convert it to thermal energy, resulting in excess amounts of heat energy accumulation in the immediate vicinity to above average levels (Effat *et al*., 2014). The subsequent energy release from these processes causes cities to possess higher temperatures than the adjacent unurbanized areas, resulting in Urban Heat Island (UHI) (Gusso *et al*., 2017). UHI is an environmental phenomenon which results when cities possess higher air temperatures than their adjacent countryside surroundings due to the anthropogenic modifications of land surfaces (Abutaleb *et al*., 2015).

Furthermore, urban areas are responsible for the production of more than seventy percent of the Green House Gas (GHG) emissions with implications on the changing climate (Sabel *et al.*, 2016). It is therefore, unequivocally evidenced from many scientific studies that urbanization negatively alters the natural environment and leads to modifications in microclimates of urban areas (Ashraf, 2015). Consequently, it is a key contributor to innumerable modifications in the earth's surface temperatures (Singh *et al*., 2014). Therefore, LULC changes, municipal heating, as well as alterations in urban climatic variables have been identified as some of the profound signatures of urbanization (Morris *et al*., 2016).

Existing studies have established relationships between long term trends in air temperature of large urban centres and intensities of urban sprawls (Chen *et al.*, 2011; Babalola and Akinsanola, 2016; Liu *et al.*, 2016; Ukaegbu *et al*., 2017; Aremu *et al*., 2017; Chaithanya *et al.*, 2017; Kotharkar and Bagade, 2018; Dissanayake *et al*., 2019). Studies have also shown that increasing urbanization has brought about changes in the energy balance in densely built city centres such as Shanghai (China), Guangzhou (China) and Cairo in Egypt (Jin *et al*., 2011; Xiong *et al*., 2012; Frey and Parlow, 2012); resulting in higher mean air and LST than those of their neighbouring countrysides.

Concerns have been expressed on these local climate modifications within cities across the globe. The implication of this urbanization trend in cities is that increasing number of people are influenced by the microclimate of cities and vice versa. Furthermore, apart from new economic, managerial and social challenges associated with growing cities, there is a deformed energy budget which pulls them toward a warmer climatic condition (Mirzaei, 2015).

With an increase in local ambient temperature, human exposure to heat increases, particularly during hot seasons in hot regions of the world in the low and middle income countries, where urban dwellers who cannot afford the cost of air conditioning and other cooling methods are subjected to very severe heat stress and health risks (Ojeh *et al*., 2016). Consequently, the socio-economic development, health leisure activities, and productivity of the workers are negatively affected (Ojeh *et al*., 2016). The increasing thermal load in warm and hot tropical cities, raises the feelings of discomfort and places higher demands on cooling and a concomitant increase in energy utilization (Elsayed, 2012). Also, there are indications that the elevated night-time temperatures often associated with the UHI will make it more difficult for many city-dwellers to recover from

any heat stress they may have experienced during the day (Loughnan *et al.*, 2009; Martiello and Giacchi, 2010).

There is a consensus that rising daytime and nocturnal temperatures will put vulnerable populations and groups across all social strata and geographical locations at higher risk of heat-related diseases and death, particularly infants; frail older people; and those with existing physical or mental illnesses (McMichael *et al.*, 2008). Diseases associated with temperature, especially those transmitted by arthropod vectors are influenced by temperature increase (Araujo *et al.*, 2015). Increased urban temperatures also exacerbate pollution levels due to increased energy consumption for cooling purposes (Campbell-Lendrum and Corvalan, 2007; Blake *et al.*, 2011; Liu and Zhang, 2011; Xie and Zhou, 2015). This is because increased use of electricity generating sets raises the level of carbon-monoxide in the atmosphere.

Since heat is a peculiar problem urban dwellers experience in their everyday lives, it becomes absolutely necessary to develop effective strategies capable of reducing impacts of urban heat. There is an urgent need to implement heat watch-warning technologies that will mitigate the impacts of heat waves and related phenomenon and protect the vulnerable populations of the ever-growing urban centres. As such, it is very important that these cities incorporate climatological considerations in their design to provide for sustainable living and working environments (Roth and Chow, 2012).

## 1.2 Statement of the Research Problem

In well-planned cities, there are potentials for the inhabitants to have better access to employment opportunities, health care, education and public services compared to their rural counterparts (UNDP, 2016). Also, well-managed city centres possess lower per capita energy, climate and ecosystem footprints as well as lower costs per person for infrastructure and basic services. Furthermore, the concentration of resources, ideas and energy in cities is a fertile ground for the creativity and technological innovation needed to solve the many developmental challenges facing the world today (UNDP, 2016).

Unfortunately, in developing countries like Nigeria, the inherent opportunities of urbanization are lost due to lack of adequate resources, basic infrastructure, services and well-conceived planning (Opoko and Oluwatayo, 2014). This is because urban Centres in developing countries, particularly, the urban fringes are associated with unplanned and uncontrolled development, and occupation of unsuitable sites (Ukoje, 2016). Poorly maintained, inadequate, or non-existent infrastructure; poor land use planning and enforcement have been identified as non- climatic stressors that aggravate urban climate problem (Barata *et al.,* 2011).

Unplanned, hasty, rapid urbanization in modern cities affects the ecosystems of cities and often results in adverse ecological impacts; which include eradication and breaking-up of natural biomes, production of man-made pollutants, increased LST, and reduced moistness (Efe and Eyefia, 2014). The incessant increase in urban air temperature occurs mainly as a result of heat release from higher energy consumption, increase in built-up surfaces which possess high heat capacities and conductions, as well reduced vegetal cover (Coutts *et al.,* 2008; Chaithanya *et al., 2017*).

Owing to high rates of environmental deterioration being witnessed in Nigerian cities, they are rated among urban areas with the lowest liveability index in the world. As a

result, it is estimated that only between 20 and 30 percent of the urban population enjoy decent urban life in Nigeria (Daramola and Ibem, 2010). Furthermore, Opoko and Oluwatayo (2014) have posited that virtually every city in Nigeria is susceptible to the changing climate, as well as other natural or anthropogenic disasters. Urban centres like Birnin Kebbi, Ibadan, Owerri and Kano which are the focal cities of this study are all state administrative headquarters that are rapidly growing and experiencing similar conditions with other cities in Nigeria. Ukoje (2016) has pointed out that the administrative functions of towns as state capitals and their strategic location have encouraged immigration and accelerated the urbanisation process and the geographical expansion of the towns. These capital cities have therefore witnessed unprecedented physical haphazard expansion (Oriye, 2013).

Globally, studies have shown that there are negative associations between cities and urban health, especially, high surrounding temperatures which are known to be responsible for higher mortality or morbidity rates (Heaviside *et al*., 2016); with steady increase in such fatalities in the last few decades (Stone and Norman, 2006). These problems associated with rising urban temperatures place ever increasing demands on planners and public officials to devise effective strategies for managing climate in these urban centres. Consequently, globally, urban planning and management strategies are increasingly employed in addressing the challenges associated with local climate effects (Sailor *et al.*, 2016). In Nigeria, master plans may exist for most of the urban centres particularly for new developing areas within and around the cities, however, such plans more often than not are either not implemented at all, or are poorly implemented and enforced. As such, areas designated as green areas and meant to make such centres liveable are often converted into other uses as in the case of Festac Town, Lagos (Fasona and Omojola (2004) and Abuja (Jibril, 2010; Fanan *et al*., 2011).

To provide information that will guide policy formulation in physical development planning and mitigate the effects of anticipated increase in the heat islands of these cities for improved environments, there is a need for regular up to date assessment of changes in the thermal environments of these urban centres. A good understanding of the spatial and periodic differences in local climates of these city centres is very expedient for effective and coherent development of adaptation strategies (van Hove *et al.,* 2015). In the light of problems associated with rising urban LSTs and the need for city planning and management, several attempts have been made to characterize LST in different urban centres in Nigeria. For example, Babalola and Akinsanola (2016) and Dissanayake *et al*. (2019) assessed land temperature characteristics of the coastal City of Lagos located in Fresh and Swamp water rainforest belt of Nigeria.

Ukaegbu *et al*. (2017) assessed land temperature characteristics in Owerri, while Aremu *et al*. (2017) assessed urban growth and intensity of UHI in Akure, both located within the Rainforest Belt of the country. Similarly, Ifatimehin *et al*. (2010) and Alabi (2012) documented LULC change and LST characteristics in Lokoja, while Ifatimehin *et al*. (2015) studied LST in Anyigba both located within Southern-Guinea Savanna, Nigeria. In addition, Ogunjobi *et al*. (2018) examined LULC change and its implication on Sokoto Metropolis, Sahelian belt of Nigeria.

However, there is more to be done with respect to making comparison between and within different ecological zones. This work intended to fill this gap. The work attempted characterizing LST dynamics of four (4) cities located in two different ecological zones utilizing the same time frame to map trend variability between the different ecological zones. It considered one large metropolitan city each for Sudan Savanna and Rainforest zones of Nigeria and one moderately populated city each for the two ecological zones.

Hence, the study attempted to provide a wider outlook of the temperature characteristics of urban centres in Nigeria. Moreover, most documented studies utilized single data sources such as meteorological data (Alabi, 2012) or remotely sensed data (Babalola and Akinsanola, 2016; Ukaegbu *et al*., 2017; Ogunjobi *et al*., 2018; Dissanayake *et al*., 2019). In contrast, this work combined both data sources for more explicit characterization of temperature in the cities and analysed other related biophysical indices of land surface temperature as done by Dissanayake *et al*. (2019).

The study examined cities in two critical ecological zones of Nigeria; namely the Rainforest and the Sudan Savanna. The Rainforest zone is undergoing unprecedented deforestation or loss of vegetal cover due to anthropogenic activities which may consequently lead to several deleterious effects and may worsen the challenge of global climate change, particularly higher temperatures. Similarly, the Sudan Savanna region which is located on already dry marginal lands may be exposed to greater challenges associated with vegetal cover removal, urbanization and climate change.

Specifically, Ibadan and Kano Metropolis were chosen as case studies of urban agglomerates for the Rainforest and Sudan Savanna respectively, while Owerri and Birnin Kebbi were selected to represent relatively small urban centres in the Rainforest and Sudan Savanna belts respectively. Kano and Ibadan Metropolitan cities are highly populated agglomerates with population of 3,820,000 and 3,383,000 respectively according to United Nations (UN, 2018). Kano Municipal has a population density of about 1,000 persons per $km^2$ within Kano closed-settled zone (Nabegu, 2010). Owerrii and Birnin Kebbi are cities with relatively small populations with estimated figures of 873,000 (United Nations, 2020 estimate) and 375, 550 estimated from the 2006 population census respectively (Nigeria Bureau of Statistics, 2012). Apart from their

locations in different ecological zones and demographic size, the surveyed urban centres also differ considerably in economic and administrative functions.

## 1.3 Research Questions

Consequent upon the preceding section, the research addressed the following questions:

i. What is the nature of the LULC trends in the study areas (Birnin Kebbi, Ibadan Metropolis, Kano Metropolis and Owerri Metropolis) from 1990 to 2019?

ii. What are the trends in air temperature in the study areas from 1990 to 2019?

iii. What are the trends in the LST in the study areas from 1990 to 2019?

iv. Is there a variation in LST trend across the two ecological zones (Rainforest and Sudan Savanna) from 1990 -2019?

v. What are relationships between LSTs and NDVI and NDBI in the selected settlements from 1990 to 2019.

vi. How has urbanization affected LST in the study area from 1990 to 2019?

## 1.4 Aim and Objectives

The aim of this work was to examine the effects of urbanization on LST in parts of Sudan Savanna and Rainforest Ecological Zones of Nigeria.

The specific objectives of this study were to:

i. Examine LULC trends in the study areas (Birnin Kebbi, Ibadan Metropolis Kano Metropolis, and Owerri) from 1990 to 2019.

ii. Analyse the trends in air temperature in the study areas from 1990 to 2019.

iii. Examine the trends in LST in the study areas from 1990 to 2019.

iv. Compare the variation in LST trend across the two ecological zones (Tropical Rainforest and Sudan Savanna) from 1990 -2019.

v. Examine relationships between LSTs and NDVI and NDBI in the selected settlements from 1990 to 2019.

vi. Analyse the effect of urbanization on LST in the study area from 1990 to 2019?

## 1.5 Justification for the Study

Rising urban temperatures have far reaching implications. High surrounding temperatures have adverse implications on urban dwellers' health in terms of increased mortality or morbidity (Heaviside *et al*., 2016). Higher urban heat not only negatively influences human health through increased mortality rates brought about by heat stress (Nastos and Matzarakis, 2012) and more frequent sleeplessness events during hot nights (Vineis, 2010), there are also implications on labour productivity (Zander *et al*., 2015).

Furthermore, it has been opined that there are thresholds for human to cope with temperature changes (Kenney *et al*., 2004; Lin *et al*., 2015). As urban areas expand, there may be a corresponding increase in the number of people who are potentially vulnerable to risks of rising temperatures (Smith *et al.,* 2011). Consequently, public health costs may become higher as the magnitude of urban heat increases because adapting urban centres to the new optimum climatic scenario will require large capital (Jeong, 2012). In addition, there is an expected rise in the cost required for cooling urban buildings (Santamouris *et al.*, 2001).

Aside implications on human well-being, higher urban air temperatures result in an increase in the emissions of biogenic hydrocarbons and higher evaporation rates of synthetic volatile organic compounds (Elsayed, 2012). Urban thermal fluxes also have implications on tourism as warmer temperatures may result in extra cooling costs,

changes in plant, wildlife and insect population and distribution, and an altered seasonality which may negatively impact the agreeable temperatures that draw tourists to tourism destinations (Gonzales, 2016). Furthermore, higher urban temperatures have implications on the local meteorological conditions by changing local wind patterns; stimulating clouds and fog formation; increasing frequency of lightning episodes; and altering the formation of precipitation (Liu and Zhang, 2011).

With rapid urbanization in a changing climate, the consequences and the magnitude of rising urban temperatures will increase. Therefore, assessing urban temperatures and the consequences of increased temperature in the selected cities of Ibadan, Kano, Owerri and Birnin Kebbi is very expedient; as it will provide precise information to urban planners in those cities to reduce heat risk in the cities. Identifying causes and implications of intra-urban variability of the thermal environment has been pointed out as the necessary action in improving urban planning and development (Lehoczky *et al*., 2017).

This study is timely as it provides insight into the present temperature characteristics in the cities of Ibadan, Kano, Owerri and Birnin Kebbi, and will serve as a framework for policy formulation by urban planners towards the mitigation of the current trends. Moreover, micoclimatic studies is key in climate science. This study will therefore offer a good appreciation of the spatio-temporal variability in local climate/surface temperature regimes of Ibadan, Kano, Owerri and Birnin Kebbi to allow for the identification of places with thermal and/or thermodynamically-related local climatic effects.

The outcome of this study will also ameliorate information gap arising from the relatively few long-term observational data on the spatial variability of local climate within cities in Nigeria, particularly, within the selected cities in the different climatic zones. Since data on the thermal behaviour and characteristics of urban surface is important for urban

planning, environmental management, and improving the quality of urban centres, the time series information that this study yielded would serve as basis for decision making and necessary action by urban planners, environmental managers/protection agencies, and development partners working in the selected cities and states in their bid to make the urban environment worth living. Furthermore, the outcome of the study on LST characteristics, as well as LULC dynamics in the two climatic zones will stimulate interests in further researches on related subject matters and at the same time provide the basis for such researches. Finally, the original contribution of this work will add to existing body of knowledge on urbanization and its attendant issues.

## 1.6 Scope and Limitations of the Study

This work focused on the LST and LULC dynamics in selected Nigerian cities. The choice of the focus area is necessitated by the fact that the urban microclimate is a vulnerable system that is highly sensitive to temperature changes often escalated by unprecedented urbanization (Benali *et al*., 2012). This work centred on four selected cities in the Rainforest and Sudan Savanna zones of Nigeria namely, Ibadan, Kano, Owerri and Birnin Kebbi (Figure 1.1). The selection consists of one metropolitan city and one small city in each of the two ecological zones. Kano and Ibadan Metropolitan Centres were selected to represent large-sized cities in the Sudan Savanna and the Tropical Rainfall respectively. For the small-sized cities, Birnin Kebbi and Owerri were selected to represent the Sudan and Rainforest respectively.

The essence for this selection criterion is to enable comparisons of LST dynamics between small and large cities in the two ecological zones. Remotely sensed Landsat images and ERA Interim (European Reanalysis) gridded satellite temperature data (maximum) were the data used for the study. Remotely sensed Landsat images were

chosen for this study because of their relatively high spatial resolution, and their ability to depict temperature variations in the heterogeneous urban/suburban environments (Morabito *et al*., 2016).

The temporal scope for the study was 1990 to 2019. The study adopted decadal intervals (1990, 2000, 2010, and 2019) due to the unprecedented urbanization witnessed in urban centres in the developing countries over the last four decades (Kumi-Boateng *et al*., 2015). However, due to the non-availability of useful imageries for Ibadan in 2000 and 2010, and Kano in 1990, 2000 and 2010, satellite imageries of the succeeding years (1991, 2001 and 2011) were used. In addition, satellite datasets corresponding to the same month and date were not available for virtually all the years and locations.

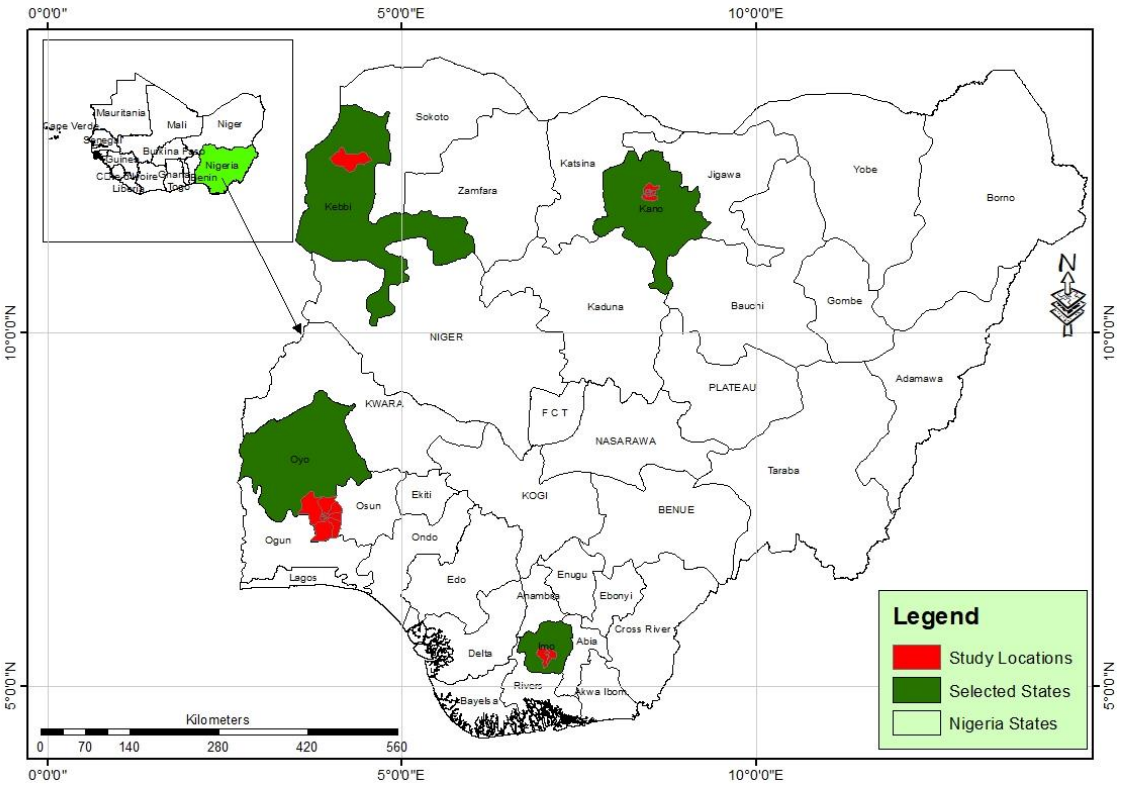


**Figure 1.1** Nigeria Showing the study cities
**Source:** Department of Geography, Federal University of Technology, Minna (2019)

## 1.7 Study Areas

### 1.7.1 General overview of Rainforest and Sudan Savanna ecological zones of Nigeria

#### *1.7.1.1 Rainforest ecological zone of Nigeria*

The Rainforest Ecological Zone coincides with Koppen's tropical humid climate (Af) climate (Figure 1.2). The zone occupies only about 9.7 percent of Nigeria's total land mass, and is the most densely populated and the source of Nigeria's bulk timber and a home to an enormous number of plants and animals (Adaohuru *et al*., 2012). The zone covers Ogun, Ondo, Osun, Ekiti, Abia, Ebonyi, Imo, Edo, Anambra, Enugu and parts of Oyo states. Some major towns and cities within the zone are Benin City, Abeokuta, Akure, Ijegu Ode, Ibadan, Ogoja, Owerri, Ado Ekiti, Asaba, Awka, Enugu, Uyo, Umuahia, and Abakaliki, among others.

The mean annual rainfall of the ecological zone ranges from 2,500mm at the southern fringes to 1,220mm at the northern fringes of the zone, and a mean yearly relative humidity of about 76.05 percent (Adepoju and Salami, 2017; Gbiri *et al*., 2019). The zone is characterized by a long period of rainfall; lasting between March/April and November; and a dry period lasting between December and March (Adepoju and Salami, 2017). The zone experiences a monthly mean minimum temperature of about 22.49°C; a monthly mean maximum temperature of about 31.24°C; and mean yearly temperature of about 26.6°C (Adepoju and Salami, 2017).

The Rainforest ecological zone is the richest in terms of tree species composition, abundance and diversity (Akpan-Ebe, 2017). Structure-wise, the vegetation is well stratified into distinguishable layers with some trees exceeding a height of more than 50 metres (Adekunle *et al*., 2013; Akpan-Ebe, 2017; Ambe and Onnoghen, 2019). The zone houses the largest number of economic trees such as *Khaya spp., Entandrophragma spp,*

*Lovoa trichiliodes, Milicia excelsa Triplochiton scleroxylon, Diospyros spp, Celtis milbraedii, Ceiba pentandra, Lophira alata, Terminalia spp., Gossweilerodendron balsamiferum, Afzelia bipindensis, Antiaris africana, and Brachystegia nigerica* and etc (Orimoogunje *et al*., 2009; Akpan-Ebe, 2017).

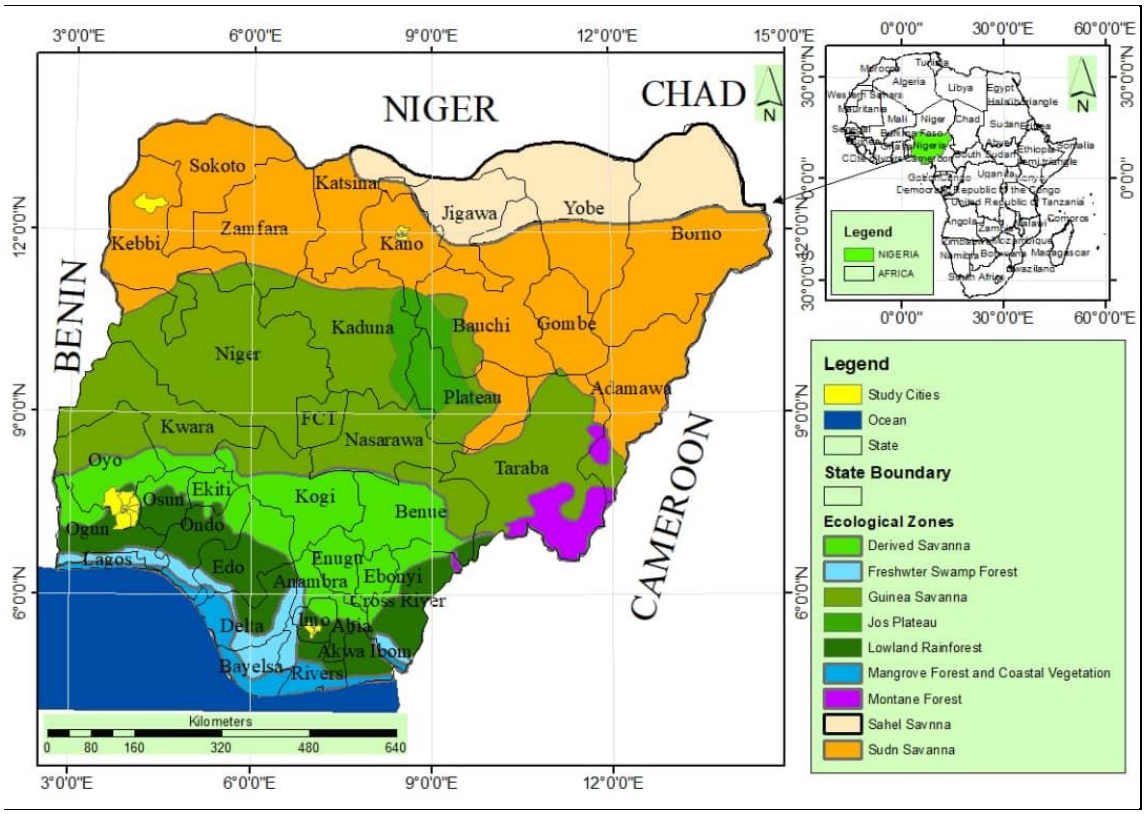


**Figure 1.2** Nigeria showing Ecological Zones

**Source:** Department of Geography, Federal University of Technology, Minna (2019)

The trees are ever-green throughout the year because the temperature and precipitation are sufficiently high for continuous growth (Adekunle *et al*., 2013).

### *1.7.1.2 Sudan Savanna ecological zone of Nigeria*

The Sudan Savanna zone of Nigeria lies between latitudes 9°30' and 12°31' N and longitudes 4° and 14°30' E (Figure 1.2) . It covers approximately 22.8 million hectares (Damisa *et al*., 2010). The region runs east-west of the Northern part of Nigeria and occupies an area over 250 km band width and covering almost the entire northern states

bordering the Niger Republic. The zone covers over one quarter of Nigeria's total area. According to the Federal Department of Forestry (FDF, 2019), it stretches from the Sokoto Plains through the Northern section of the High Plains of Nigeria, to the Chad Basin. It comprises areas around Sokoto, Kano, Birnin Kebbi, Zamfara, Katsina and Borno States of Nigeria (Haruna and Murtala, 2019). Some of the major towns and cities within the Sudan Savanna include Kano, Sokoto, Katsina, Birnin Kebbi, Gusau, Kaura Namoda, Potiskum, Dutse, Damaturu, Nguru and Hadejia, among others.

The climate of Sudan Savanna is of the tropical wet and dry type, symbolized as Aw by Koppen. The region has a single annual rainfall regime with total amount ranging from 600 mm in the northern fringe to 1,140 mm at the southern fringe (Damisa *et al*., 2010; Butu and Emeribe, 2019). The rainy season lasts for a period of 100-150 days, falling from May/June to September, while the dry period lasts from September to April. The relative humidity of the zone is generally less than 40 percent, except during the few rainy months when it rises to 60 percent and above (FDF, 2019).

Vegetation of this zone is made up of short grasses (about 1- 2 m high), and trees which vary in density from place to place. Most of these have umbrella-shaped canopies which become smaller as one move northwards. Examples of trees include stunted species, such as Acacia species, *Ceiba pentandra* (silk cotton) and the *Adansonia digitata* (baobab). The length of growing period provides opportunities for the cultivation of rainfed cereals, groundnuts, cowpea, cotton, pigeonpea, irrigated rice and wheat, and vegetables. Cropping systems are based on cereal-legume. The zone is considered very suitable for the cultivation of grain crops like as millet, sorghum, acha and rice, and grain legumes such as beans, cowpea etc (Butu and Emeribe, 2019). The zone has the highest population density in Northern Nigeria. It is also worthy to note that the main concentration of cattle production in the country occurs in the zone, primarily because it is relatively free from

tsetse fly infestation (Butu and Emeribe, 2019). Intense cultivation in this region, coupled with heavy grazing, bush burning and trees-cutting for fuel and building construction have promoted desertification in the zone (Butu and Emeribe, 2019).

### 1.7.2 Birnin Kebbi

#### *1.7.2.1 Location and size of Birnin Kebbi*

Birnin Kebbi is the capital of Kebbi State and the headquarters of Gwandu Emirate. Located in the north-western part of Nigeria, it it is positioned between latitudes 12º 15' N and 12º 35' N; and longitudes 4º 01'E and 4º 38'E (Figures 1.3). The mean elevation of the metropolis is about 250 metres above sea level. The metropolis covers about 1,385 $km^2$. It is bounded to the north-east by Argungu LGA; to the south by Kalgo LGA; to the east by Gwandu LGA; and to the west by Arewa Dandi LGA (Abubakar and Sawa, 2016).

#### *1.7.2.2 Weather and climate of Birnin Kebbi*

Kebbi State enjoys a Tropical Continental (cT) type of climate which is characterized by distinct wet and dry seasons. In Birnin Kebbi and environs, the highest mean daily temperature is recorded at the peak of the dry season, just before the onset of the rains in April, while the lowest is recorded during the peak of the Harmattan period. The mean temperature during the hot season is 37ºC but this falls to as low as 8ºC during the peak of Harmattan (December-February). Higher relative humidity is is recorded in the southern areas where Birnin Kebbi is located than in the north. The season notwithstanding, relative humidity is generally lower in the afternoon compared to the morning. This is because water holding capacity of the air increases during the day with rising air temperature (Abubakar, 2015).

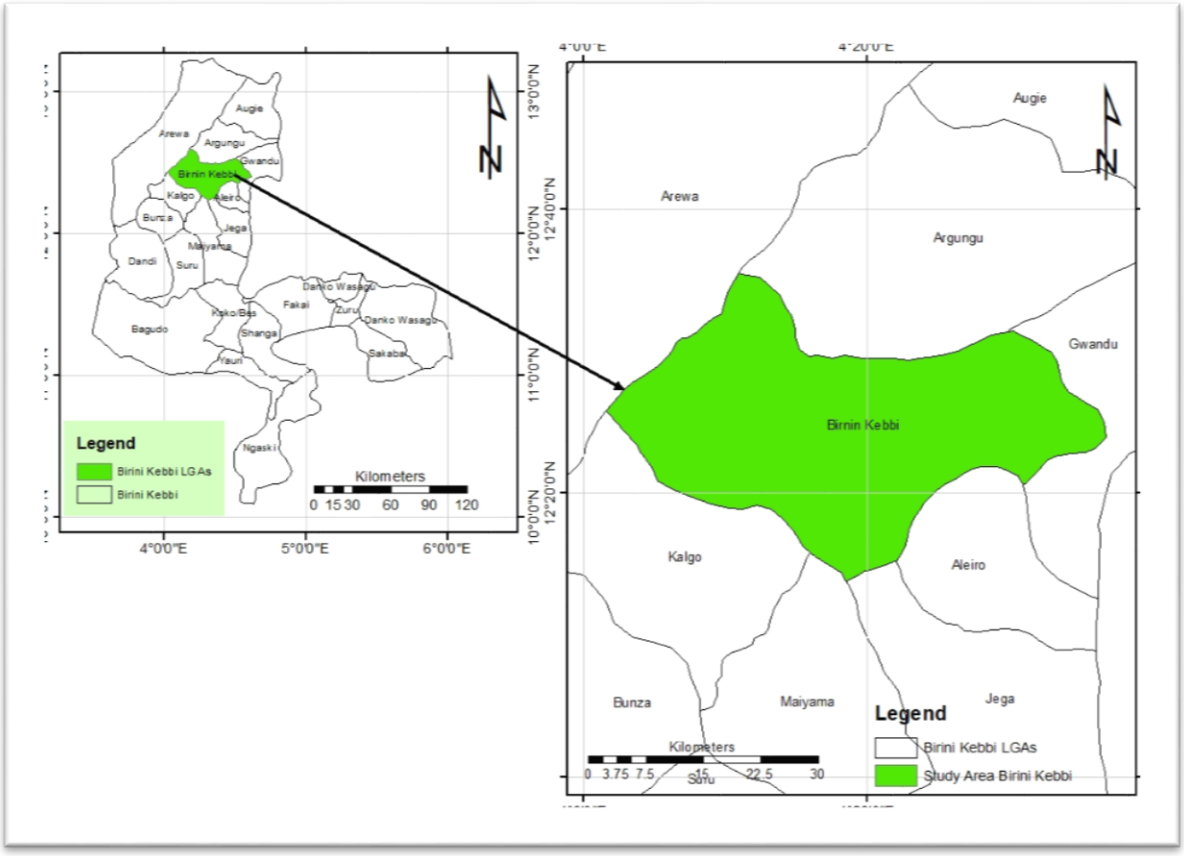


**Figure 1.3** Birnin-Kebbi
**Source:** Department of Geography, Federal University of Technology, Minna (2019)

### *1.7.2.3 Geology of Birnin Kebbi*

The geology of Birnin Kebbi comprises thick vast sequences of sedimentary deposits of the Sokoto basin, underlaying about fifty percent of the area. The Sokoto basin is part of an elongated sedimentary basin underlying most of north-western Nigeria and part of eastern Niger republic. The remaining part of the area is underlain by the precambrian basement complex rocks (Abubakar and Sawa, 2016).

### *1.7.2.4 Relief of Birnin Kebbi*

The relief of Kebbi State is generally gently rolling to undulating. There are outcrops and steep cliffs of limestone, which sometimes reach 15 metres in height within the town and up to 30 metres outside. The elevation of the state is largely less than 300 metres (Abubakar, 2015).

### *1.7.2.5 Soils of Birnin Kebbi*

The principal soils that make up the Birnin Kebbi region are the vertisols, which are heavy, cracking clay soils with more than 35 percent clay, and have shrinking and swelling properties. The soils are high in minerals but have problems associated with spillage, poor drainage, flood and erosion (Abubakar, 2015).

### *1.7.2.6 Vegetation of Birnin Kebbi*

The vegetation of the area is heterogeneous in nature and heavily disturbed by intense anthropogenic influences such as long periods of intensive cultivation, grazing, fuelwood extraction and bush burning. These influences have transformed the vegetation into a form of parkland dominated by trees like, *Piliostigma, Ziziphus, Mangifera Indica and Tamarindus* (Abubakar, 2015; Mohammed and Jeb, 2014). Acacia and neem trees, shrubs and grasses dominate the vegetative cover of Birnin Kebbi (Abubakar, 2015). The grasses and herbs of the savanna serve as sources of food for herbivorous wild life.

### *1.7.2.7 Drainage of Birnin Kebbi*

Birnin Kebbi is sandwiched between two fertile extensive flood plains (Ogunbajo *et al*., 2015). It is drained by the Rima and the Shella rivers covering broad flood plains, located in the north and south-east of the town respectively. Shella river flood plain is situated about 3 km south-east of the town and is about 1.5 km wide. The Rima river flood plain occupies north-west of the town, and runs southerly before finally emptying into the River Niger (Ogunbajo *et al*., 2015). The major tributaries of the Rima river include Gawon, Zamfara and Gubinka which take their sources from the basement complex region of Sokoto State (Abubakar, 2015).

#### *1.7.2.8 Population of Birnin Kebbi*

Birnin Kebbi has an estimated population of about 375, 550 from the 2006 population census (NBS, 2012). The population of the city is a mix of multiple ethnic groups, major among who are Kabawas, Fulanis, Zabarmawas Dakarkaris, Kambaris, Gungawas, Dandawas, and more recently Yorubas, Igbos, Urhobos, etc. However, the diversity of the ethnic composition within the metropolis has greatly multiplied, especially with the present status as a state capital and a host to several higher institutions of learning.

#### *1.7.2.9 Socio-economy of Birnin Kebbi*

Birnin Kebbi functions as the state capital, local government headquarters, and the seat of Gwandu Emirate. These functions have made the city a centre of trade and commerce for the entire northwest sub-region and neighbouring Niger and Benin Republics. Opportunities facing the people of Birnin Kebbi have been determined principally by its economic base (Danboyi, 2006). The local economy has continued to attract migrants, from within and outside the country; resulting in rapid population increase, physical growth, and development of the town (Abubakar, 2015).

### 1.7.3 Ibadan metropolis

#### *1.7.3.1 Location and size of Ibadan metropolis*

The city of Ibadan is located in the south-western part of Nigeria, approximately on longitude $3^{o}5'$ to $4^{o}36'$ East of the Greenwich Meridian, and latitude $7^{o}23'$ to $7^{o}55'$ north of the Equator (Figure 1.4), and has a mean elevation of 230 metres. It covers about 3,400 $km^2$ and is made up of eleven (11) Local Government Councils, of which six comprise the outer areas namely: Akinyele, Lagelu, Egbeda, Ona-Ara, Oluyole and Iddo. The remaining five LGAs occupy the inner city or the core area where the metropolis is

situated and comprise Ibadan North East, Ibadan North, Ibadan North West, Ibadan South West, and Ibadan South East.

### *1.7.3.2 Weather and climate of Ibadan*

Ibadan lies within the tropical rain forest region. The temperature of this area is almost uniform throughout the year, with little deviation from the mean annual temperature of 27°C. February and March are the hottest with 28$^{o}$C and 29$^{o}$C respectively, while August with temperature of 25 $^{\circ}$C is the coolest (Awopetu and Baruwa, 2017). The range between month of highest temperature and the month of lowest temperature is 3.7$^{o}$C (Owolabi and Adebayo, 2016). The mean annual rainfall is 1,400 mm with a low co-efficient of variation of about 10 percent. Rainfall is highly seasonal with well-marked rainy and dry seasons. The wet season commences in March and lasts till October, with double maxima rainfall occurring in July and September and a break in August (Owolabi and Adebayo, 2016; Awopetu and Baruwa, 2017).

### *1.7.3.3 Geology of Ibadan*

Ibadan and environs falls within the Pre-Cambrian rocks of Southwestern Nigeria. The major rock types are schist-quartzites, granite-gneiss, banded gneiss, augen-gneiss, and migmatites, while minor rock types such as pegmatite, aplites, quartz veins, and dolerite dykes intruded the main rocks in places.

### *1.7.3.4 Relief of Ibadan*

Ibadan lies mostly on lowlands influenced by rocky outcrops and series of hills which contain mainly granite. The average elevation of the city is 230 m above mean sea level (Onyebuchi *et al*., 2016).

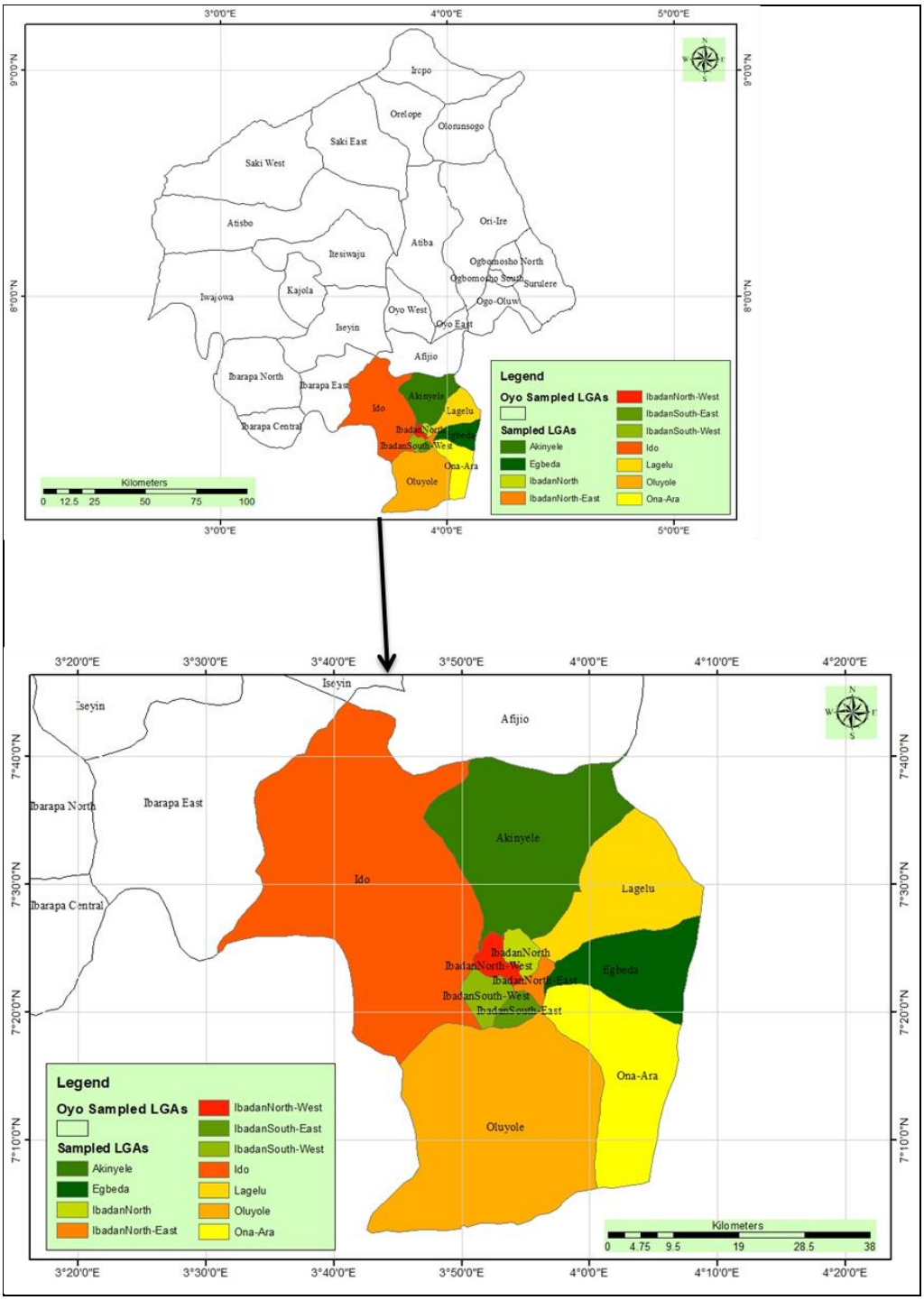


**Figure 1.4** Ibadan Metropolis in Oyo State Setting

**Source:** Department of Geography, Federal University of Technology, Minna (2019)

### *1.7.3.5 Vegetation of Ibadan*

The vegetation of Ibadan area consists of evergreen tree compositions which range from shrubs to dense vegetation, made up of a number of recognizable strata (Olatoye *et al*.,

2021). The tallest stratum consists of intermittent foliage canopies which comprise emergent trees with rounded tops, followed by trees with an unbroken layer of spreading crowns with heights ranging from 15 - 30 metres. The third layer consists of an irregular stratum comprising varying sizes of trees with thick undergrowth. Below this stratum are shrubs which are quite distinct from small trees comprising significant foliage and possessing heights around two metres (Olatoye *et al*., 2021). Aside trees, the vegetation also comprises herbs, climbers as well as epiphytic, saprophytic, and parasitic plants. Examples of tree species include *Celtis zenkeri, Sterculia rhinopetala, Strombosia spp., Trilepsium madagascariensis, Triplochiton scleroxylon, Terminalia superba, Antiaris africana, Milicia excelsa, Terminalia ivorensis, Tectona grandis, Gmelina arborea*, and *Pinus caribaea* (Olatoye *et al*., 2021).

#### *1.7.3.6 Soils of Ibadan*

Soils in Ibadan are closely related to the geological formations and the rock type. The Soils are predominantly ferruginous, typical of basement complex rock areas of South Western Nigeria (Arohunsoro and Omotoba, 2017). The soils are highly erodible due to the availability of thick depth of weathered overburden averagely varying in thickness between 0 and 14 metres (Arohunsoro *et al*., 2017). The charnockite rock forms the predominant rock type in the basin and the parent material from which the soils are formed basically (Arohunsoro *et al*., 2017).

#### *1.7.3.7 Drainage of Ibadan metropolis*

Ibadan metropolis is drained by three major rivers, Rivers Ogunpa, Ona and Ogbere and their several tributaries include Omi, Kudeti, Alaro and Alapata. The combinations of hills and river valleys provide a good drainage for the city (Onyebuchi *et al*., 2016).

#### *1.7.3.8 Population of Ibadan metropolis*

Ibadan Metropolitan is a highly populated agglomerate with population of 3,383,000 respectively according to United Nations (UN, 2018).

#### *1.7.3.9 Socio-economy of Ibadan*

Ibadan is an important commercial centre. Virtually every street and corner in the traditional core and the inner suburbs of the city is a market square or stall. The largest daily market stretches in a belt from the railway station in the west to the centre of the city and is Ibadan's commercial core. Other economic activities include agriculture (carried out by many urban part-time farmers who augment their earnings with other work), manufacturing, service industries and handicrafts (such as weaving, spinning and dyeing, pottery making, and blacksmithing.

### 1.7.4 Kano metropolis

#### *1.7.4.1 Location and size of Kano metropolis*

Kano Metropolis is situated between latitude 12°25′ and 12°40′N, and longitude 8°35′E and 8°45′E with a mean elevation of 482 metres (Figure 1.5). The city covers about 500 $km^2$ and is the largest city in the Sudan Region of Nigeria and the third largest town in Nigeria after Lagos and Ibadan (Nabegu, 2010; Ayila *et al*., 2014).

The Metropolis is made up of eight (8) LGAs. They are Dala, Fagge, Gwale, Kano Municipal, Nassarawa, Tarauni and parts of Ungogo and Kumbotso local governments. It is bordered by Madobi and Tofa Local Government Areas (LGAs) at the south-west, Gezawa LGA at the east, Dawakin Kudu LGA at the south-east, and Minjibir LGA at the north-east (Figure 1.5).

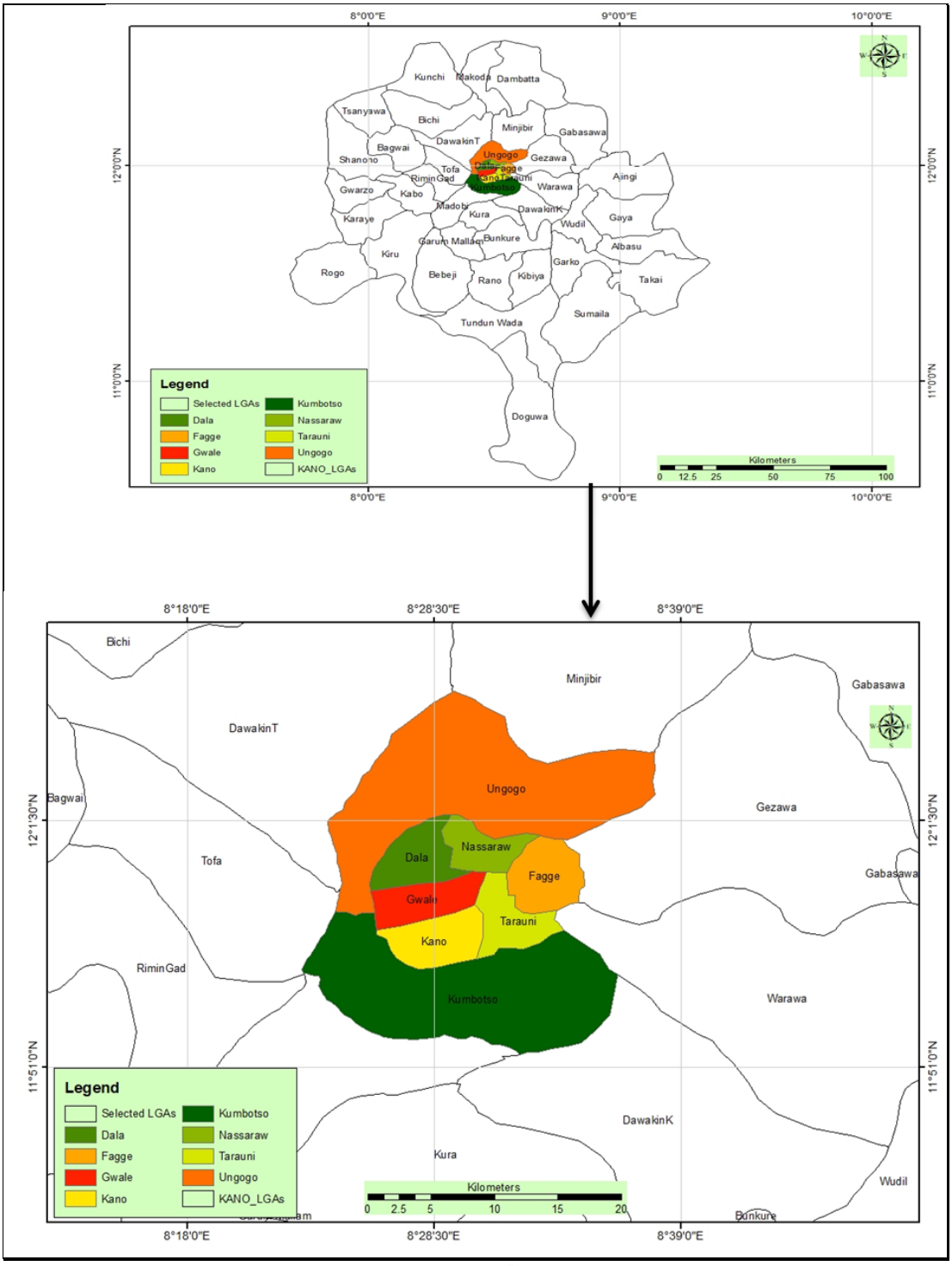


**Figure 1.5** Kano Metropolis in Kano State Setting

**Source:** Department of Geography, Federal University of Technology, Minna (2019)

### *1.7.4.2 Weather and climate of Kano metropolis*

Kano Metropolis is located in the Sudan Savanna. The climate of the area is influenced by the movement of two air masses namely; the maritime air masses originating over

Atlantic Ocean and the dry air masses coming from the Sahara desert. Consequently, the area is characterized by wet season (May to September) which is characterized by south western maritime winds that carry warm and humid air, and the dry season (October to April) characterized by the tropical dry continental wind (Harmattan) from the north. The annual average rainfall of about 690 mm majorly falls from June through September. The temperature is generally very hot throughout the year, though from December through February, the city is noticeably cool. The average nighttime temperatures during the cold months range from 11° to 14 °C. During the hot season (mid – March to mid-May), the maximum temperature reading may be as high as 40$^{o}$C. The average temperature for these hot months may range between 30$^{o}$C and 32$^{o}$C.

#### *1.7.4.3 Geology of Kano metropolis*

Geologically, more than four fifth of Kano is underlain by quartzite, undifferentiated Meta-sediments and basement complex rocks of the Precambrian origin (Mallam *et al*., 2016; Kankara, 2019). Prolonged weathering of the rock produced deep clayish regoliths which have been subjected to lateralization (Kankara, 2019).

#### *1.7.4.4 Relief of Kano metropolis*

Kano Municipal area lies within the Hausa plains and its highest elevation is in a village called Husure at eastern part of the area, about 564 m above sea level and minimum elevation of 488 m down south of the area (Kankara, 2019).

#### *1.7.4.5 Vegetation of Kano metropolis*

The vegetation of Kano metropolitan area has been largely affected by human interference through cultivation, grazing, construction and annual bush burning, which has now reduced it to parkland (Mallam *et al*., 2016). Small short trees and shrubs are

more common on fallow lands where regeneration takes place (Mallam *et al*., 2016). Dominant vegetation in the study area include *Acacia albida, Acacia nilotica , Adanosia digitata, Angogeissus leiocarpus, Aoedirachata indica, Balanties aegyptica*), *Diospyros mespiliformis, Khaya senegalensis*, *Selecarya birrea*, and *Ziziphus spina-christi* (Kankara, 2019) which are very resistant to drought.

The dominant soils in Kano Metropolitan area are the less rich, slightly acid soils derived from wind rip soils which are generally shallow and coarse (Mallam *et al*., 2016). Some parts of the study area are covered hydromorphic soils which are used for wetland cultivation and block construction for building purposes (Mallam *et al*., 2016).

#### *1.7.4.6 Drainage of Kano metropolis*

The drainage of Kano Metropolitan area is largely influenced by the relief. River Challawa is the only big river with tributaries, Magaga, Takwami, Guzu-guzu, Kutumbulu, Iyaka and some lakes. Other major rivers that drain the town are the Jakara and the Kano Rivers. The rivers are largely demanded, particularly the Challawa where the popular Challawa Gorge dam was constructed in the year 1972 (Kankara, 2019). The area has a drainage density of 1.46 $km^2$ (Kankara, 2019). The general pattern of drainage in the area is dendritic, mostly running in the north-south direction. The gentle slopes and undulating relief give the river a moderate to flowing character (Kankara, 2019).

#### *1.7.4. 7 Population of Kano metropolis*

Kano metropolis is among the fastest growing cities in Nigeria, with a current estimated of population of 3,820,000 according to United Nations (UN, 2018). Compared to the national average of 267 inhabitants per $km^2$, it is one of the most crowded cities in Nigeria with a population density of about 1,000 inhabitants per $km^2$ within the Kano closed-

settled zone (Nabegu, 2010). Immigration and natural growth rate of 3 percent is expected to continue to increase the population and waste stream in the years to come.

#### *1.7.4.8 Socio-economy of Kano*

Kano Metropolis has been the largest and most influential commercial town in the Sudan zone (Dankani and Abubakar, 2011) and for centuries, the most important commercial and industrial nerve centre of northern Nigeria attracting; millions from all parts of the country and beyond (Nabegu, 2010). It is called Nigeria's centre of commerce due to its long flourishing marketing activities (Ayila *et al*., 2014). So, marketing and trading has been the dominant economic activity of the populace of the metropolitan Kano, although the land is mostly exploited by urban agriculture through waste water utilization to sustain daily needs (Ayila *et al*., 2014). It has about 43 existing market places and over 400 privately owned manufacturing industries (Maigari, 2016).

### 1.7.5 Owerri metropolis

#### *1.7.5.1 Location and size of Owerri metropolis*

Owerri is located in the south eastern part of Nigeria within latitudes 5°20′ and 5°32′N, and longitudes 6°51′ and 7°08′ E (Figure 1.6). It is located on mean elevation of 159 metres and covers about 540 $km^2$. It comprises Owerri Municipal, Owerri-west and Owerri-north local government areas, and parts of Mbaitoli and Ikeduru local government areas (Nwanya *et al*., 2019). It is the administrative, commercial, and entertainment capital of Imo state (Okere *et al.*, 2018), being the landlord to most government ministries, departments and agencies and the epicentre of all socio-economic and religious activities in the State (Okeke, 2015).

### *1.7.5.2 Weather and climate of Owerri metropolis*

Owerri experiences a tropical climate with two main regimes; a dry season (November to March, and a wet season (April to November). The Rainfall values for Owerri ranges from 2,000 mm to 2,900mm annually. The driest months record less than 23 mm rainfall per month. The mean daily temperature hovers around 25°C - 27°C throughout the year (Ogbomida *et al.*, 2013; Okeke *et al.*, 2015). Average humidity of 80 to 85 percent occurs during the rainy season, but the dry season records very low relative humidity with the absence of clouds.

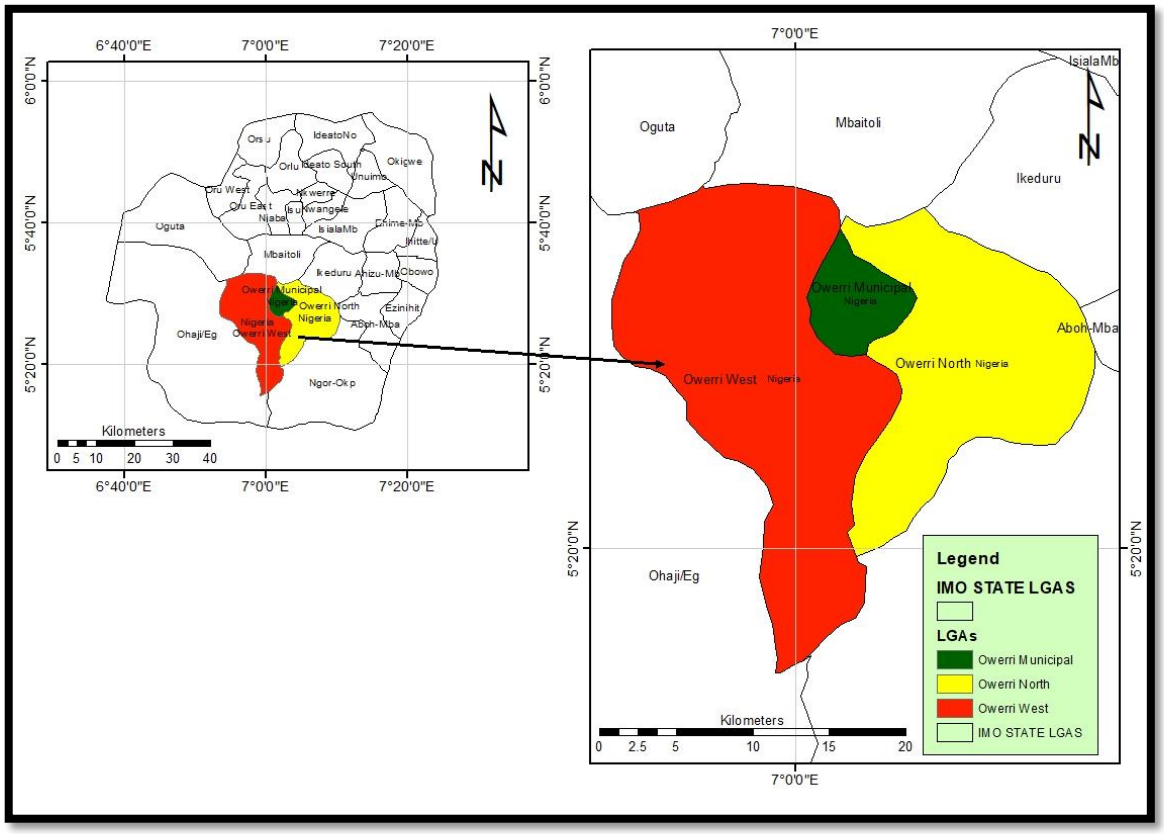


**Figure 1.6 Owerri Metropolis in Imo State Setting**

**Source:** Department of Geography, Federal University of Technology, Minna (2019)

### *1.7.5.3 Geology of Owerri metropolis*

Owerri Metropolitan area is underlain by the Benin Formation and consists largely of friable sands, conglomerates, coarse sandstone and isolated gravel units and intercalation of shale/clay lenses of Pliocene to Miocene age (Nwanya *et al*., 2019).

### *1.7.5.4 Relief of Owerri metropolis*

It lies at the northern section of the eastern coastal lowland, which is characterized by southward dipping slope. To the southwest of the town, the terrain is flat with rolling hills running in a north-south direction to the east at about an elevation of 30m (Ogbomida and Emeribe, 2013).

### *1.7.5.5 Soils of Owerri metropolis*

The Benin Formation upon which Owerri is situated has lithologies consisting of sands, silt, gravel and clayey intercalations. In many places within the area, the formation of the study area is overlain by a considerable thickness of lateric soil, composed of iron-stained regolith formed by the weathering and subsequent ferruginization of the weathered materials (Nwanya *et al*., 2019).

### *1.7.5.6 Vegetation of Owerri metropolis*

The most important vegetation of the Owerri is the tropical rainforest which has long been disturbed and almost dominated by anthropogenic interference (Okeke, 2015), given rise to a mix of different types of plants; reflecting the extent of anthropogenic interference on the original vegetal cover (Ogbomida and Emeribe, 2013). In some parts of the city, vegetal cover is marked by frequent occurrence of umbrella trees (*Musanga decropoides*). According to Ogbomida and Emeribe (2013), the southern part of Owerri is relatively undisturbed with a dense forest consisting of 3 tree layers; high dominant trees, low

dominant trees, shrubs and herbs which are interwoven by lianas and climbers. Trees here attain the heights of between 25 and 30 metres.

#### *1.7.5.7 Drainage of Owerri metropolis*

Owerri Metropolis is drained by two major rivers namely: Nworie River which flows from the west and covering an area of about 5 kilometres along its course, before emptying into the second river, which is Otamiri River flowing from the east. From the confluence of the two rivers around Emmanuel College Owerri, the Otamiri River flows southwards towards Nekede, Ihiagwa and Umuagwo, before emptying into the River Niger, around Imo and Rivers States border (Ogbomida and Emeribe 2013; Nnaji *et al*., 2014; Echebima *et al*., 2019).

#### *1.7.5.8 Population of Owerri metropolis*

National Population Commission (NPC, 2007) puts the 2006 estimated population of Owerri Metropolis at 401,873 (211,298 male and 190,575 female) with a population density of 729 per square kilometre, a figure nearly 400 percent higher than more than present national population density (given the 2006 national estimate of 175,000,000 population and land area of 923,768 $km^2$). The high density was attributed to the spiralling rural-urban migration (Okere *et al*., 2018). Due to the high rate of urbanization, the United Nations (UN, 2020) put the population of the Owerri metropolitan area in 2020 at 873,000, a 4.05 percent increase from 2019.

#### *1.7.5.9 Socio-economy of Owerri metropolis*

Civil services and trading are the dominant socio-economic activities of the residents of Owerri Metropolitan area. However, learned professionals, entrepreneurs, seasoned

artists and farmers who are predominantly natives also occupy the study area (Chukwuocha *et al*., 2016).

# CHAPTER TWO

## 2.0 LITERATURE REVIEW

### 2.1 Urbanization and Urbanization Theories

#### 2.1.1 Urbanization explained

Urbanization is often used to refer to a broad-based rural to urban transition relating to population; land utilization; economic activity; culture; or any one of these (McGranahan and Satterthwaite, 2014). Thus, it is frequently used to refer to changes in land-use for specific areas (McGranahan and Satterthwaite, 2014). Blaschke *et al*. (2011) do not only see urban areas as geographical entities comprising dense accumulation of people or buildings, but also a multi-layered construct comprising manifold dimensions of social, technological and physical interconnections and services. Urban places are usually defined by demographers on the basis of population size and density (Weeks, 2003). For a place to be classified as urban, there has to be a sufficient quantum of people living in very close proximity to one another; life being obviously different from that in rural areas often expressed in terms of economic activities (Weeks, 2003). The urban thermal environment is affected by the physical characteristics of the land surface, and by human socioeconomic activities (Yue *et al*., 2007).

Urbanization has been explained as the development of metropolises and sub-urban areas occasioned by population increase; resulting in key modifications in LULC in accordance with anthropogenic activities (Kaya *et al*., 2012). It is the process through which the population of urban areas increases, and is usually expressed relative to the total population (Kok *et al.*, 2003)**.** It has been recognized as a key anthropogenic process that does not only influence climate but also adversely affects the functioning of terrestrial

ecosystems (Zhang *et al*., 2014). Therefore, it has been identified as the key influential and noticeable anthropogenic force on earth (Dawson *et al*., 2009). Accelerating urbanization has been identified as one of the most salient social phenomena (features) which characterize human civilization in the last millennium, particularly following the era of industrial revolution (Gu *et al*., 2012; Wu *et al*., 2014). It occurs with great vitality and energy and pervades the entire globe (Gu *et al*., 2012), and the process may continue in the coming decades (van Hove *et al*., 2015).

The global increase in urbanization is creating both opportunities and challenges for fostering people's quality of life and managing the transition towards sustainability (Luederitz *et al*., 2015). It has thus been argued that urban living has the potential to fulfil basic human needs at the least cost due to economies of scale (Bettencourt *et al*., 2007). Some of the positive implications of urban growth as highlighted by Bhatta (2010) are increased economic production; opportunities for the underemployed and unemployed; and accessibility to basic and better services such as better transportation, sewer, water, as well as educational and health care facilities. Furthermore, urban development plays a significant role in the transition to lower birth rates and lower childhood infections while increasing life spans (Luederitz *et al*., 2015), and in fostering economic development and facilitating innovation (UN-Habitat, 2012).

Therefore, urbanization has been described as a gift to humanity if it is controlled, coordinated and planned, but a curse if otherwise (Mohan *et al*., 2011). It has been recognized as both a driver for, and a consequence of governance, socioeconomic development**,** production, trade, knowledge, cultural transformation, and technological inventions (Wu *et al*., 2014**;** Ali *et al*., 2017**).** As such, higher levels of urbanization often correspond to higher levels of economic and social development (Wu *et al*., 2014).

Urbanization, therefore does not only accommodate the core of the economy but in addition, the rising rate of population increase **(**Ali *et al*., 2017)). The rapid and unprecedented growth in urban centres has resulted in serious challenges (Zupancic *et al*.**,** 2015). United Nations Development Project (UNDP, 2016) has expressed that development trends in cities have largely impacted on various fabrics of the urban areas such as, environmental pollution emanating from traffic gridlocks; the concentration of industries; and insufficient refuse disposal systems. Others are environmental degradation, loss of natural habitat and species diversity, and increased human health risks associated with heat, noise, and crowding (Zupancic *et al*.**,** 2015). Bhatta (2010) has opined that in many large urban centres in developing countries, unplanned urban expansion is a common situation; resulting in high population of urban inhabitants in shantytowns within the cities or in urban fringes in poverty and degraded environments, due to the lack of vital urban services.

Owing to the functions performed by them, urban dwellers have substantially greater and more diverse demands for resource consumption than agrarians, thereby adversely affecting ecosystems and landscapes at the local and regional scales (Wu *et al*., 2014). Consequently, urbanization puts increasing demand on additional infrastructures for housing, business and transport networks, generally achieved at the expense of natural landscapes such as agricultural lands, open spaces, and water (Byomkesh *et al*., 2012); with resultant consequences such as drastic and irreversible LULC conversion in and around city centres (Zhang, 2015), as well as significant reduction in such natural areas of the urban centres (Kong and Nakagoshi 2006; Swanwick *et al.,* 2003**).** Urban centres in developing countries, where rates of urbanization are high because of mass exodus of migrants from rural to urban or from smaller to bigger cities (Mohan *et al*., 2011) are particularly subjected to more severe environmental and socioeconomic problems,

especially as their small- and medium-sized cities are predicted to be future homes to many (Redman and Jones, 2005; Wu, 2008).

### 2.1.2 Theories of urbanization

Bodo (2019), Kasarda and Crenshaw (1991) identified several theories from existing literature on drivers of urbanization and emergence of cities. Some of the theories have intersecting ideas with others while others emerged as a built up from other theories. Some of the theories include: the theory of self generated urbanization; modernization-theory; dependency/world-system theory; and theory of urban bias.

#### *2.1.2.1 Theory of self-generated urbanization*

The theory of self-generated urbanization express that, urbanization process requires two distinct conditions. The first condition is the generation of excess products which sustain people who are engaged in non-agricultural activities. The second condition is the accomplishment of a level of social advancement which enables big societies to work alone successfully (Bodo, 2015). These theorists are of the view that, these changes resulted in urbanization simultaneously in the Neolithic period when the first cities emerged in the Middle East (Wheatley, 1971). This theory expresses that rural to urban migration was the foundation of this form of urbanization; as migrants started trooping into cities for work at factories (Childe, 1950). This theory theory therefore identifies industrialization as the key factor responsible for the exodus of people from the rural areas to urban centres. This theory has however been criticized for over emphasizing rural to urban drift as the reason for urbanization, considering the fact that other cities have urbanized due to other reasons aside rural-urban migration (Bodo, 2015).

#### *2.1.2.2 Modernization/ecological theory*

The modernization theory, which was prevalent between the 1950s and the 1970s affirms that urban growth occurs as a result of new inventions and novelties in cities brought about by industrialization, use/application of technology, information dissemination and cultural diffusion. These theorists consider urbanization from the perspective of modernization. There are three fundamental concepts to modernization/ecological set of theories. The first concept is that, the present levels of urban development in particular societies is not separable from their initial states at the begining of the modernization process, which normally begins with a differential set of institutional and infrastructural patterns derived from past technological-economic capacities (Kasarda and Crenshaw, 1991).

Secondly, these theories assume that, technology is essentially more imperative than the social organization of the society. They agree that social organization creates innovation and technology, but that the untilization of automation is the key driver of social transformation which boosts or increases economies. They therefore view industrialism rather than capitalism as having a unique impact on Third World societies. Thirdly, the model asserts that cultural diffusion, despite breeding inevitable social disequilibria eventually forces a rough convergence of First World and Third World development patterns.

The theorists express that this kind of urbanization may be triggered by the concentration of social amenities and developmental projects in certain parts of the society occasioned by ethnic, racial or religious divisions and corrupt politics which create economic dichotomy and uneven developments in the world today. According to these theorists, the concentration of investments and opportunities in few places, particularly cities

necessitates unprecedented rural-urban migration stemming from rural-push and urban-pull factors (Bodo, 2019).

#### *2.1.2.3 Dependency/world-system theory*

Dependency/world-system urbanization theory arose as a result of the inability of modernization theory to justify the conditions and implications of urbanisation in less developed nations (Bodo, 2015). Proponents of this theory are of the view that, this system is introduced either intentionally through coercion or by the intrinsic reasoning of capitalism in certain areas; and the attendant underdevelopment among the populace. The dependency/world-system theory rests on some assumptions. The first assumption is that there is the existence of a distinct system of industrialist development ideal in civilizations; attributed to a system of communal organisation. The Second assumption is that for capitalism to thrive, certain social structures will have to be apparent in the form of disparate deals, unequal advancement, individual social disparity, core-periphery echelons, and sovereign architectures (Kasarda and Crenshaw, 1991). The views of these theorists are that the social changes in the third world were as a result of structures and processes of the capitalist world system.

#### *2.1.2.4 Theory of urban bias*

The urban biase theory is premised on studies that revealed a growing disparity in urban-rural centres in the poor countries. This is occasioned by the fact that administrations of poor countries lean towards intervening in markets in ways that impose levies on agribusinesses; while leaders of the richer countries are inclined towards the reverse by mediating in strategies that grant subsidies to agriculturists. By implication, the proponents of this theory describe how the countryside populace as being parasitized by urban dwellers, who benefit tremendously by consuming low-priced produce from the

countrysides and inhabiting attractive urban edifices from the levies imposed on the contrysides. Hence, proponents of this theory are of the perspective that this bias in favour of the urban settlements creates disparity between the rural and urban areas; as regards consumption, wage and productivity levels. This necessitates mass exodus of the rural dwellers to cities for greener pastures and an improved standard of living. The sufferings and abject poverty among the rural populace may be attributed to city bias which results from the uneven distribution of available resources among the populace. The urban bias theorists believed that there are groups that hinder the economical development of the rural areas by pressuring the government to protect their interest by their location in urban areas at the expense of the rural areas.

Summarily, the urbanization processes in developing and poor income countries may be explained by these theories collectively, This may be the reason such countries are currently experiencing unprecedented population explosion and urbanization in such countries.

## 2.2 Urban Thermal Characteristics

The subsequent transformation of vegetal and associated lands in urban areas leads to the modification of physical characteristics of land cover such as soil water, material thermal capacity, conductivity, reflectivity, and emmitance; with a consequent decrease in evapotranspiration (Hamilton and Erickson, 2012). The alterations are due to the substitution of the native surfaces with heat-trapping impermeable ones, which directly change the local climate in urban areas; leading to higher near surface air temperature than those of countrysides, especially at night (Kok *et al*, 2003). Urban areas, therefore, typically are characterized by impervious land cover surfaces. Impervious surfaces, often described as land cover types which inhibit water penetration are mostly associated with

transport facilities (streets, boulevard, parking-lots and walk-paths) and structures roof-tops (Zhang *et al*., 2009). These surfaces modify the thermodynamic characteristics of soil, the earth's surface energy budget, nature of circulation of ambient atmosphere, and create a large amount of waste heat from human activities (Van and Bao, 2015) such as heat released from urban houses, transportation and industries (Weng and Yang, 2004).

The high proportions of impervious surfaces of the urban landscapes are largely created for transportation, commercial, industrial, and residential purposes (Jin and Dickinson, 2010). In remotely sensed data, classified impermeable surface areas (ISA) have been extensively utilized in quantifying and mapping the extent of urban growth/development and urban landuse in urban areas (Yuan and Bauer, 2007).

Cities are known to have significant impact on climate both at local and regional scales (Sarrat *et al.*, 2006) since the morphological characteristics and the thermal and radiative properties of the built-up surfaces have direct effects on the surface energy exchanges, much different from those observed above natural soils and vegetation (Oke, 1987**).** They alter atmospheric conditions at local to regional climate on daily, seasonal, and annual scales (Seto, 2009), through the modification of surface albedo and run-off, and the surface energy budget by the release of heat from anthropogenic heating, and the increasing atmospheric aerosols (Krehbiel and Henebry, 2016). As a consequence, increasing urbanization has resulted in diminished natural surfaces like vegetation, open ground or water (van Hove *et al.*, 2015); leading to modifications in the energy budget in densely built city centres (Jin *et al.*, 2011; Xiong *et al*., 2012; Frey and Parlow, 2012). This is because the decrease and fragmentation of large vegetated areas inhibit atmospheric cooling due to advection resulting from the temperature gradient between vegetated and urbanized areas (Kumar *et al*., 2015).

Building density contributes to higher temperature in urban areas due to the fact that most buildings are not located near open spaces but rather face other warm buildings; resulting in trapping of more heat (Hamilton and Erickson, 2012). Thus, the urban microclimate is a vulnerable system that is highly sensitive to temperature changes often escalated by unprecedented urbanization (Benali *et al*., 2012). Cities are, therefore, known to possess higher warming rates, with some already established to have warmed twice the rate of the globe during the past 50 years (Stone, 2006). There is no doubt that a changing climate, coupled with a growing urban population raises both the frequency and rates of intensity of heat, and raises the UHI effects, thereby posing increasing risks to the urban populace (Schatz and Kucharik, 2015).

## 2.3 Land use/ Land Cover (LULC)

### 2.3.1 Definition of LULC

Land cover may be defined as the natural and cover of the earth surface, which may include water, vegetation, bare soils, and artificial surfaces (Obeidat *et al*., 2019). Land use, on the other hand, refers to the socioeconomic purposes and contexts for which lands are managed (Roy and Roy, 2010). Land use comprises more complicated aspects, because it incorporates social sciences and management principles. The terminogies "land use and land cover" are mostly used together.

However, there is a glaring distinction between the two terminologies. On one hand, land cover implies the spatial dispersal of the different land cover classes on the surface of the earth, and may be directly estimated qualitatively or quantitatively with the use of remotely sensed data. On the other hand, land use and its modification requires the incorporation of natural and socio-scientific techniques in determining which

anthropogenic activities are taking place in different locations of the land-scape (Roy and Roy, 2010).

### 2.3.2 Land use and land cover change (LULCC)

LULCCs are probably the most important forms of environmental modifications globally, because they occur at spatial and time-based scales and have direct relevance in the daily survival of humans (Roy and Roy, 2010). Land cover change may be defined as the transformation of the physical or biotic cover of the earth's surface, while land use change simply means modifications in utilization of lands by humans (Obeidat *et al*., 2019). According to Patel *et al.* (2019), land cover change implies modifications in certain unceasing properties of the land like vegetal type and soil property, among others, while land-use change denotes alteration in how certain areas of land are being utilized/managed by human beings.

Technically, LULCC refers to the measurable modifications in spatial extent of a given type of land use and land cover (Roy and Roy, 2010). LULCC in a generalized term may therefore be described as the anthropogenic modifications of the earth's superficial coverage (Iwuji *et al*., 2017). They are manifestations of both human and natural/climate driven forces (Liu *et al*., 2009). Alterations in land use in several spatial and time-based spheres are the material evidences, and are pointers to ecological and anthropogenic dynamics as well as their relationships intermediated by availability of land (Roy and Roy, 2010). Singh *et al*. (2016) noted that LULCC varies across regions. For rural areas, changes may be attributable to agricultural expansion, forest fires and illegal tree felling, whereas in urban areas it may be attributable to urbanization and commercialization.

LULCC, aside from altering the physical dimension of the spatial coverage of the various land cover classes, also stimulate many of the secondary courses that results in the

subsequent depletion of the earth's ecosystems (Roy and Roy, 2010). This is because LULCCs result in the decrease in vegetal cover. The loss of a vegetal cover consequently results in many other harmful effects on the environment, vis-a viz: biodiversity loss; climate change; alterations in radiative forcing; pollution of other natural ecosystems and a decrease in their values; and alterations in hydrological regimes, among others (Niyogi *et al*., 2009).

### 2.3. 3 Causes of LULCC

Humans have modified land for food and other essential purposes from time immemorial (Iwuji *et al*., 2017; Obeidat *et al*., 2019). LULC modification also occurs substantially through natural processes such as volcanic eruption, earthquake, landslide and climatological events (Bekele *et al*., 2019). It is also believed that climate change indirectly affects LULC change by increasing the demand for more farmlands, especially in development countries whose economies are largely dependent on agriculture and by forcing climate change vulnerable communities to adjust their land use choices in order to handle such changes/alterations (Bekele *et al*., 2019).

Some socio-economic factors of land cover change such as poverty, tenure insecurity, and availability of market and credit facilities have further been suggested as major contributing factors to land cover changes (Wubie *et al*., 2016). Technological advances, political and socio-economic decisions or constraints have also been recognized as prominent drivers of LULC change (Cousins *et al*., 2015). Population explosion has been a dominant cause of LULC change in may emerging nations (Tewabe and Fentahun, 2020). Consequently, in recent times, the intensity, degree, and rate of changes in LULC are far bigger than ever in history; with attendant unprecedented effects on ecosystems and environment processes at all scales (Iwuji *et al*., 2017; Obeidat *et al*., 2019). At

present, the magnitude of LULC changes induced by anthropogenic activities is greater in developing countries than in advanced nations (Obeidat *et al*., 2019); attributable to the higher rate of urbanization and urban sprawl (Mohan *et al*., 2011).

### 2.3.4 Consequences of urban LULCC

LULC changes, particularly the conversion of farmlands and forest covers into urban uses, are very important environmental changes which impact on ecology and human beings (Liu and Yang, 2015). Apart from depletion of biological diversity; water and land pollution and the emission of greenhouse gases (Iwuji *et al*., 2017; Namugize *et al*., 2018), LULCC has also been identified as the most important anthropogenic factor influencing the climate (Arsiso *et al*., 2018). Alemayehu *et al*. (2019) highlighted some consequences of LULCC to include changes in biological diversity; bio-geochemical cycles; soil nutrient richness, hydrological cycles, energy balance, land productivity, as well as the sustainability of ecological services. These changes also have associated consequences on human health (Patel *et al*., 2019). The LULCC brought about by the urbanization processes, eliminates and fragments natural habitats, leads to haphazard growth in urban areas, deterioration in the living conditions of cities, and worsening of urban environment scenery (Hassan *et al*., 2016). Consequently, there is a need to continuously monitor the changes and prediction (Alemayehu *et al*. (2019).

### 2.3.5 The role of space technology in LUCC studies

Understanding the spatial distribution and expansion of urban centres is key in urban spatial planning in relation to the advancement of environmental quality and sustainable land resource management (Bhatti and Tripathi 2014; Tewabe and Fentahun, 2020; Zaitunah and Sahara, 2021). Spatial information on LULC in an area is a requirement in the determination of changes in the quality and quantity of LULC (Roy and Roy, 2010)

and a basic requirement for this purpose is mapping the built-up areas (Bhatti and Tripathi 2014). Conventional techniques such as ground surveys and aerial photography which are quite tasking and expensive are often employed in the mapping process (Bhatti and Tripathi 2014). With the quick expansion of city centres, the task of timely and precise mapping of urban built-up surfaces are somewhat challenging (Bhatti and Tripathi, 2014).

Remote sensing alongside geographic information systems have been identified as viable scientific tools in studying and monitoring LULC, and mapping built-up areas (Bhatti and Tripathi 2014; Zaitunah and Sahara, 2021). The numerous capabilities of remotely sensed data make them valuable for measuring, examining and studying environmental changes (Zaitunah and Sahara, 2021). Progress made in remote sensing in recent decades has enabled repetitive surveillance of the earth's environment (Roy and Roy, 2010).

In addition, the advancement in sensor capabilities in terms of spatial resolution, spectral variability and revisit frequency, makes it highly practicable to estimate the even slightest changes on the surface of the earth precisely (Roy and Roy, 2010). Provision of synoptic and comprehensive views which are quite important for large urban areas and the availability of historical archives help in mapping and understanding urban sprawl over time (Bhatti and Tripathi 2014). According to He *et al*. (2010), the techniques employed in automatic mapping of land cover of city centres using remote sensing techniques may be classified into two categories. The categories are those based on the classification of the input data, including pixel- and object-based classifications, and those based on the process of direct segmentation using the indices,like the normalized difference vegetation index (NDVI) and leaf area index.

### 2.3.6 Assessing LULCC

Conventionally, LULC change detection has been carried out using the vegetation indices (Obeidat *et al*., 2019). Two common biophysical indices used in mapping urban areas are the NDVI and the normalized difference built-up index (NDBI). These indices help in depicting the effect of green and built-up surfaces on UHIs (Nádudvari, 2021). Built-up areas are effectively mapped through the arithmetic manipulation of recorded NDVI and NDBI images derived from satellite imagery (He *et al*., 2010). The NDVI index is used in detecting and quantifying vegetation coverage of a given area for different periods, particularly changes occasioned by anthropogenic activities using remote sensing procedures (Aburasa *et al*., 2015; Nwaerema and Moses 2019). It is used to measure the difference between near infrared (NIR) channel where vegetation is highly reflective due to the presence of chlorophyll in leaves, and the red channel which absorbs light (Nwaerema and Moses 2019).

The NDVI is therefore computed by combining the Red and NIR bands of a sensor system (Aburasa *et al*., 2015). NDVI values range between -1 and +1. When NDVI value is negative, it signifies likely presence of water, if it is close to +1 it implies dense/ green vegetation and values close to zero indicate a likely absence of green (Nwaerema and Moses 2019). NDVI is therefore crucial in managing urban greening and the thermal environment (Nwaerema and Moses 2019). NDVI is controlled by factors like dry or wet vegetatal cover, greenness of vegetatal cover, atmospheric contamination, moisture content of the atmosphere, mix of anthropogenic materials, dry or moist soils, among others (Guha and Govil, 2021).

Zha *et al*. (2005) suggested the use of NDBI to map built environments in city centres due to the advantage of the unique spectral responses of built-up areas and other land

covers. Built-up index is a subset of the spectral indices classes, which is one of the most commonly used approaches for analyzing data in the optical domain (Azmi *et al*., 2016). The NDBI index supports an efficient method for mapping built surfaces due to its utilization of the reflectivity of built surfaces higher in the short-wave infrared region but less reflectivity in the near-infrared region (Nádudvari, 2021). The NDBI value ranges between -1 and +1, with greater NDBI numbers for built-up areas, and negative numbers for the non-built-up areas (Jothiman *et al*., 2021). Generally, the key interest in NDBI is in the fact that urban mapping is based on the extraction of constructed surfaces or impervious areas (Azmi *et al*., 2016).

### 2.3.7 Empirical studies on LULCC

Iwuji *et al*. (2017) in their study examined LULCC in Orlu LGA, Imo State, Nigeria between 1986 and 2013 using GIS, remotely sensed data. The result of this analysis provided four major classifications of LULC namely; bare soil, built up, water body and vegetal cover. Results of the study indicated that built surfaces increased rapidly between 2000 and 2013 by 46.21 percent while bare soil and water bodies recorded drastic decrease occasioned by developmental trends in the area over the period. Consequently, vegetal cover decreased from 58.03 percent in 1986 to about 52.09 percent in 2013; an indication that Orlu is developing rapidly with regards to changes brought about by rapid increase in socioeconomic activities of the population.

Bekele *et al*. (2019) examined LULC cover drivers in more fragile and dynamic landscapes of the East African Rift Valley region for the period 1986 to 2016. They utilized a combination of remotely sensed data, GIS, logistic regression, as well as descriptive statistics to quantify and analyze the data. Results of the image analysis revealed that during the overall study period grasslands/grazing areas, agricultural land,

and bare surfaces increased by 124, 42, and 34 percent respectively. On the other hand scattered acacia woodland, bush/shrubland, and swampy/marshy land have declined by 52, 50, and 31 percent respectively. Further analysis of the data revealed that the most influential drivers of LULC change in the region include population growth (95 percent), firewood extraction (93 percent), agricultural land expansion (92 percent), charcoal making (92 percent), climate change/recurrent drought (79 percent), and overgrazing (71 percent) in descending order of percentage of respondents.

Meera *et al*. (2015) carried out vegetation change detection of Vellore District. They used remotely sensed Landsat TM image and SRTM DEM data layers to characterize the NDVI of the district in 2001 and 2006. The result shows different NDVI threshold values such as 0.1, 0.15, 0.2, 0.25, 0.3, 0.35, 0.4 and 0.5. The results show that forest/shrub land and barren lands decreased in coverage by about 6 percent and 23 percent from 2001 to 2006 respectively, while agricultural land, built-up and water areas increased by about 19 percent, 4 percent and 7 percent respectively. The Simulation results indicated that NDVI is beneficial for decision-making by policymakers.

Nwaerema and Moses (2019) examined the NDVI of Port Harcourt metropolis and environs from 1986 to 2018 using algorithm of the Google Earth Engine (GEE) from Geographic Information Systems (GIS). The results indicate that in 1986, NDVI recorded lowest value of -0.08 and highest value of 0.43 with a range of 0.5. In 2003, NDVI was ranged between 0.53 and -0.10 with a range of 0.63. Lastly, in 2018, NDVI values ranged between 0.043 and -0.06 with a range of 0.49. The study therefore established that there is a rapid and intense decline of vegetal cover on the city's green surface areas.

## 2.4 Urban Air Temperature

Air temperature has been identified as an essential variable in various investigation fields, such as impact of global warming and climatic change, ecosystem, hydrological, agricultural, and human health studies (He *et al*., 2022). As an important consideration in urban microclimate, it is largely affected by the radiative and thermal properties of built surfaces, as well as heat release occasioned by human activities (Potgieter *et al*., 2021). Depending on the method of retrieval, meteorological data (air temperature data) may be classified as ground observations via meteorological station networks, simulated numerical model outputs, and remotely sensed data, with varying characteristics and utilization (Cheval *et al*., 2020; He *et al*., 2022).

The in-situ or ground-based observations are the oldest methods for acquiring information on the urban atmosphere, but currently, such observations in urban areas are carried out through World Meteorological Organizations (WMO) stations and urban meteorological networks (Cheval *et al*., 2020). Effective application of climate data in urban study/management requires a combined utilization of meteorological and ancillary data for comparable quality, continuity and fine temporal and spatial resolution (Cheval *et al*., 2020).

### 2.4.1 Data acquired from in situ measurements

In-situ measurements of the various surface fluxes have traditionally been performed in a bid to have a better understanding of energy balance of urban centres (Xu *et al*., 2008). These conventional observation techniques, particularly weather observatories utilize point atmospheric temperature information acquired from ground observatory networks to interpolate and depict atmospheric temperature differences at comparatively smaller

scales (Chen *et al.*, 2016). An example of ground-based *in-situ* weather measuring system is depicted in Plate I.

Apart from the traditional meteorological observatories, many *in-situ* techniques have been employed in acquiring urban thermal data. For instance, Zipper *et al.* (2016) acquired urban thermal data by installing 151 HOBO U23 Pro v2 temperature/RH sensors equipped with radiation shields on utility and streetlight poles on urban, rural, park, lake, or wetland LULC types in/and around Madison WI (USA). The sensors were mounted at an elevation of 3.5m, and logged instantaneous temperature data every 15 minutes.

Plate I Campbell ground-based weather station with different meteorological instruments (**Source:** Naipal *et al*., 2013)

*In-situ* thermal data especially that from permanent meteorological observatories provide high temporal resolution and long period coverage but has a low spatial resolution (Srivanit and Hokao, 2012). Also, these traditional in-situ approaches of urban thermal data acquisition are somewhat limited in developing cities where meteorological stations are either unavailable or infrequent (Yow, 2007). In addition, there are also other factors inhibiting their use for measuring urban fluxes. Ground-based observations which are

reflections of only thermal condition around the weather observatories can hardly be used to estimate LST with desired precision (James and Charles, 2014). Also, conventional techniques of in-situ surface temperature estimation are often not feasible for all types of terrain conditions and are time consuming (Suresh *et al*., 2014). Moreover, weather observatories are often situated in park-like grounds where temperatures are consistently lower than those of nearby densely built areas where people live and work.

Another limitation is that, because of the complexity of urban surfaces, the relative degree of the energy balance typically vary widely across a city and this may depart significantly from those of the restricted area covered by the *in-situ* measurement (Xu *et al.*, 2008). Due to the uneven distribution and limited conditions of isolated meteorological observation stations, the observed LST data may not be a full representation of the distribution of LST across the region (Liu and Zhang, 2011). Lastly, as an independent technique constrained by physical and economic factors, ground observation have been employed only over small local-scale areas (Liu *et a*l., 2016).

### 2.4.2 Mobile ground-based temperature measurements

Stationary *in-situ* measurements are often insufficient in describing and depicting fully, the spatial variability of air temperature in city centres (Hart and Sailor, 2009; Dobrovolný and Krahula, 2015). To overcome some of the limitations of stationary measurements, some systematic mobile measurements are made by thermometers attached to vehicles. Plate II is an example of ground-based mobile van used in meteorological data acquisition.

Szymanowski and Kryza (2009) collected mobile air measurements (car traverses) and automatic weather stations located in various land use types with the automatic meteorological units mounted on cars using radiation-shielded, aspirated resistance

sensors (Pt-100) connected to the data logger. Dobrovolný and Krahula (2015) employed a special resistance thermometer, featuring a NiCr-Ni sensor with a rapid response time of 0.8 second for up to 90 percent of temperature change mounted on the left roof of an automobile approximately 1.8 m above ground level.

**Plate II** Picture of Collaborative Lower Atmosphere Profiling System (CLAMPS-2)
**Source:** Wagner *et al*. (2019)

Similarly, Makido *et al*. (2016) utilized a Type-T fine (30 gauge) thermocouple on vehicle traverses to examine spatial variations in summer-time air temperatures in Doha. Tsin *et al*. (2016) collected Mobile temperature data in greater Vancouver, Canada on foot using a Met One 064-2 temperature sensor inside a radiation shield with an accuracy of ± 0.1 °C and a response time of 10s in still air. Moving observations overcome the limitation of insufficient spatial details to an extent, but unable to provide synchronized views over cities (Srivanit and Hokao, 2012).

### 2.4.3 Ground-based crowd sourcing

Benjamin *et al*. (2021) has identified crowdsourcing as a relatively new form of atmospheric data collection technique which provides a high spatial density of data and a continuous, long time series. Crowdsourcing is the acquisition of data by enlisting the services of a large number of people and/or from a range of public sensors, typically

connected via the internet. A typical example of crowdsourcing is the use of Citizen Weather Stations (CWS) which are affordable and user-friendly weather stations established by members of the public for personal interest or education (Benjamin *et al*., 2021). Figure 2.1 is an illustration of ground-based crowdsourcing network

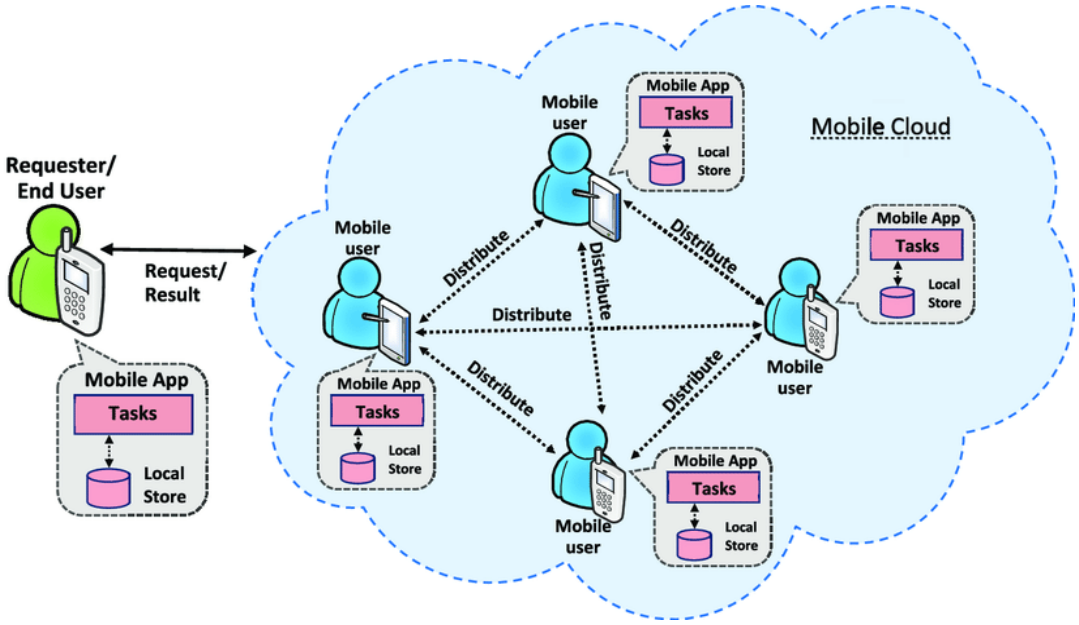


**Figure 2.1** An illustration of ground-based crowdsourcing network
**Source:** Jurairat and Seng (2018)

Due to the proximity of crowdsourced weather points to anthropogenic heat emissions, urban materials with high thermal inertia, and areas of reduced sky view factor, they record higher night-time temperatures, higher maximum temperatures on warm days, and cooler maximum temperatures on cool days (Potgieter *et al*., 2021). Crowdsourced weather stations provide very relevant data for health monitoring and urban planning (Potgieter *et al*., 2021). Furthermore, the large number of crowdsourced weather stations provide a high-resolution understanding of the variability of urban heat which is lacking traditional networks (Potgieter *et al*., 2021). The limitations of this climate data source, however, is the absence of metadata and the uneven distribution of stations with a possible socio-economic biases (Potgieter *et al*., 2021).

### 2.4.4 Climate simulation models

Sophisticated mathematical and physical models have been developed and employed in studying land surface temperatures (Xiao *et al*., 2008). Notable among these replicas are energy equilibrium models (Oke *et al.*, 1999), laboratory replicas (Cendese and Monti, 2003), three-dimensional simulations (Saitoh *et al*., 1996), Gaussian models (Streutker, 2003), as well as many other mathematical simulations. Energy simulation models normally employ statistical analysis to establish relationship between causative factors and are more widely employed than other models (Xiao *et al*., 2008).

Climate simulation models have proved to be useful data sources for urban thermal mapping (Nichol and Hang, 2012). They are, however, limited by the complexity of the roughness of the municipal canopy layer structure, difficulty of carrying out a detailed mapping of surface materials across cities (Herold *et al*., 2006), and non-inclusion of heat contributions from human activities (Nichol and Hang, 2012). Also, these models are either representations of local scale or neighborhood scale (Arnfield, 2000; Grimmond *et al.*, 2010), which are not easily scaled up to the entire urban centres and are therefore not readily useful in predicting temperature patterns at city scale, or permit studies of urban heat islands (Nichol and Hang, 2012). Of late, models are capable of simulating energy balance and air temperatures across entire urban centres but they utilize very huge and highly sophisticated databases (Ashie and Kono, 2011).

### 2.4.5 Gridded temperature datasets

Gridded climate datasets are alternative datasets to instrumental measurements, particularly for areas with spatially scarce distribution of meteorological stations or poor quality measurements (Cheval *et al*., 2020). Therefore, the scientific research community uses high-resolution gridded temperature datasets due to their spatial completeness and

their inclusion of variations resulting from topographic effects (Walton and Hall, 2018). They are reliable *in-situ* observations from various meteorological stations located at different locations globally, which are interpolated to grids using different interpolation methods (Kanda *et al*., 2020). One method is to interpolate or smooth data from irregularly spaced stations to a regular grid (Walton and Hall, 2018). Such datasets are referred to as station based. Other datasets utilize interpolation algorithms which match observations exactly at the station locations. Gridded data sets exist globally for different meteorological parameters such as temperature (maximum, minimum and Mean), precipitation and atmospheric pressure.

Examples of interpolated temperature datasets include Asian Precipitation Highly-resolved Observational Data Integration towards Evaluation of Water Resources (APHRODITE), Climate Research Unit Time-Series(CRU-TS), University of Delaware (UDEL), Hadley Centre/Climatic Research Unit Temperature (HadCRUT) series such as HadCRUT3 HadCRUT5, Climatic Research Unit Temperature (CRUTEM) series, and Ensembles gridded observational (E-OBS) dataset for precipitation, temperature and sea level pressure (Yasutomi *et al*., 201;Walton and Hall, 2018; Kanda *et al*., 2020).

There is another category of gridded datasets whereby datasets are reconstructed to run atmospheric models which assimilate historical observations (Walton and Hall, 2018). These gridded datasets are called reanalysis datasets. In reanalysis datasets, irregular ground-based observations are fused with modelled outputs to synthesize state of the system which is uniform and homogenous across a grid with complete temporal coverage (Kanda *et al*., 2020). There is another category of gridded datasets whereby datasets are reconstructed to run atmospheric models which assimilate historical observations (Walton and Hall, 2018). These gridded datasets are called reanalysis datasets.

In reanalysis datasets, irregular ground-based observations are fused with modelled outputs to synthesize state of the system which is uniform and homogenous across a grid with complete temporal coverage (Kanda *et al*., 2020). Both gridded data and reanalysis originate from terrestrial and airborne observations, however, the reanalyzed data provide a multivariate, spatially complete, and coherent record of the global atmospheric circulation (Skoulikaris *et al*., 2020). Several studies compared reanalysis products with meteorological station data and revealed a strong correlation between the two datasets. (Skoulikaris *et al*., 2020). Examples of reanalysis datasets include European Centre for Medium-Range Weather Forecasts Reanalysis-Interim and Era 5, National Centre for Atmospheric Prediction (NCEP) and the National Centre for Atmospheric Research (NCAR) NCEP-NCAR-Reanalysis and North American Regional Reanalysis (NARR) among others (Walton and Hall, 2018; Kanda *et al*., 2020).

Generally, gridded datasets are widely utilized in computing historical trends, evaluation of regional climate models and for training statistical models for downscaling low-resolution climate data to higher resolution (Walton and Hall, 2018). Meteorological reanalysis datasets are among the most widely utilized gridded datasets (Skoulikaris *et al*., 2020). They are particularly very s useful in areas whether in areas with excess data or where weather stations are inadequate or even non-existent (Bosilovich, 2013). However, the reliability of reanalysis datasets depends on the efficiency of data assimilation procedures, spatial resolution, and realism of land surface processes being represented (Kanda *et al*., 2020).

ERA-Interim which is one of the latest global reanalysis products developed by the European Centre for Medium-Range Weather Forecasts (ECMWF) was utilized for the study. ERA-Interim has been widely utilized, particularly for regions with scarce observations (Skoulikaris *et al*., 2020). The quality, accuracy and reliability of this data

has been attested by several studies. Donat *et al*. (2014) compared ECMWF's ERA-Interim, National Centre for Environmental Prediction (NCEP) reanalyses, and Japanese 25-year Reanalysis Project (JRA25) and the result revealed that ERA-Interim demonstrated a greater agreement with the gridded in situ–based datasets than the rest two. Cornes and Jones (2013) revealed that the ERA-Interim reanalysis data are generally quite good at replicating both the seasonally and spatially varying trends in the indices and also able to depict the observed trends remarkably well at the station level. Zhao *et al*. (2020) compared ERA-Interim data with 2 meter air temperature data from 24 meteorological stations in the Qilian Mountains (QLM), China and the results generally depicts that the monthly, seasonal, and annual variation show very high daily correlations with the observed records ranging from 0.956 to 0.996.

Meteorological reanalyses utilise a wide variety of observation databases assimilated in a complex fashion into a numerical weather prediction model to produce a spatially and temporally coherent synthesis of various meteorological variables over the recent historical. The reanalysis forecast model remains unchanged for consistency of simulated weather data (Essou *et al*., 2016). Data assimilated by reanalysis come from measurements derived from different sources recorded for decades throughout the world.

The dominant sources are terrestrial measurements networks, radiosondes, aircrafts, satellites, and floats (Wang *et al*., 2011). Terrestrial measurement networks comprise weather stations, buoys, and ships which provide surface data for variables such as temperature, relative humidity, atmospheric pressure, wind direction, as well as wind speed. Radiosondes, aircrafts, and satellites provide various atmospheric data, like radiance, wind, humidity, and pressure at different atmospheric heights (Essou *et al*., 2016).

An advantage of reanalyses data is that though they are not direct observations, they provide variables throughout the world, including in areas where weather stations are nonexistent or scattered (Bosilovich, 2013). Many studies have compared data from reanalyses to weather station data in several regions of the world and generally conclude that in many cases, reanalyses are comparable to observations. (Bosilovich, 2013; Lorenz and Kunstmann 2012; Manzanas *et al*., 2014; Rusticucci *et al*., 2014; Vose *et al*., 2012; Zhang *et al*., 2013).

## 2.5 Land Surface Temperature

Land Surface Temperature refers to the emmisive skin temperature of the earth surface; playing key roles in the physics of the land surface through the mechanism of energy and water exchanges with the encompassing air (Zhang *et al.*, 2009). It has been recognised as a key biophysical parameter which modulates the atmospheric heat in the lowest atmospheric layers and plays vital roles in the radiation balance of the surface (Zoran, 2011). It controls the physical and biochemical mechanisms occuring at the interface between the earth and its surrounding air (Zhang *et al.*, 2009). It also determines the interior climate of structures and influences energy transfers that affect the well-being of urban inhabitants (Zoran, 2011). Studies have proven LST to be very effective in partitioning hidden heat fluxes, and consequently surface radiative response as a function of changing surface soil water content and vegetal cover (Zhang *et al.*, 2009).

LST as a key factor in the physics of land surface processes combines surface-atmosphere relations and the energy fluxes between the atmosphere and land (Gorgani e*t al*., 2013). The relationship between LST and surface energy/and water balance occurs from local to global scales (Rozenstein *et al.*, 2014). Apart from the passive microwave, most LST measurements utilize the thermal infrared (TIR) channel in the electromagnetic spectrum

covering 8 to 15 µm (Tomlinson *et al*., 2011**).** TIR remote sensing offers exclusive technique for extracting LST information because most of the energy recorded by the sensing device in this chanel is directly produced by land surfaces (Yu *et al*., 2014). With the exception of solar irradiation components, it is with the use of LST that most fluxes at the surface/atmosphere interface are parameterized (Sobrino *et al*., 2008). LST values are dependent on LULC; with waterbodies and vegetated areas possessing the lowest surface temperatures, while urban built- surfaces likeas airports, residential locations, industrial layouts exhibit very high surface temperatures values (Feizizadeh and Blaschke, 2013; Mallick *et al*., 2013). LST is applied in a large number of fields such as city climate chang, water cycle , and vegetal cover evalution. Other applications according to them include estimation of other geophysical parameter like evapotranspiration, vegetal water stress, soil water, and global circulation (Rozenstein *et al.*, 2014; Sobrino *et al.*, 2009). Owing to the increasing recognition of the roles of LST and applications in estimating several geophysical variables, keen interests have been stimulated in the development of techniques for its measurement from space (Yu *et al*., 2014).

LST has been largely employed in studying urban climate. Wang *et al*. (2016) identified three categories of LST studies. The groups include investigating LST pattern and its potential relation to urban factors; studying the thermal equilibrium of city surfaces; as well as exploring relationships between LST and air temperature. The physical characteristics of the numerous urban land surface coverages, their colour, the ratio of received radiation by planar surfaces, arranement/orientation of streets, vehicular traffic congestion, and other human actions are key determinants of LSTs in city centres (Chudnovsky *et al*., 2004). LST has been widely utilized in several fields, notably in environmental studies, hydrology, urban climate studies, ecological, biophysical and

biochemical studies and very recently, the changing climate (Mildrexler *et al*., 2011; Rehman *et al.*, 2015). For example, LST derived from remotely sensed imageries are utilized in validating and improving global meteorological model prediction, analyzing LULCC, monitoring drought, soil water estimation, as well as frost estimation (Wan *et al*., 2004). LST and information on emmision are largely utilized in the study of built up environments' climate for establishing LST patterns and their interrelationships with surface features; and evaluating UHI relationship with surface thermal fluctuations so as to categorise landscape characteristics, patterns, and courses (Weng, 2009).

It is, therefore, an important variable in studying temperature dynamics in cities (Falahatkar *et al.*, 2011). It has been expressed that LST corresponds closely to the atmospheric temperature of the layer lying directly over it, as a result of heat energy transfer from the former to the latter (Voogt, 2002; Weng and Quattrochi, 2006). The LST of urban surfaces are also largely known to be closely related to the distribution of LULC properties (Weng, 2003; Weng *et al*., 2004), with each component surface of the urban landscapes (such as lawn, parking lot, road, building, cemetery, and garden) exhibiting distinct emmisivity, heat, moistness, and aerodynamic characteristics (Xiao *et al*., 2008).

LST, therefore, regulates the atmosphericheat of the lower atmosphere, contributes to the earth'surface radiation equilibrium, and determines the interior heat of urban structures (Voogt and Oke, 2003; Srivanit *et al*., 2012). Advanced applications and techniques in remote sensing have revealed that LST exercises strong influence on the physical, and biochemical processes which occur at the boundary between the earth and its surrounding air (Zhang *et al*., 2009). Particularly, TIR remotely sensed imageries have been employed

in studying the thermal characteristics of urban environments, largely for analysis of LST and its interrelationship with surface features (Weng, 2009).

### 2.5.1 Urban Heat Islan (UHI) phenomenon

UHI is a climatic situation whereby cities have elevated air temperature above the rural surroundings due to the anthropogenic modifications of land surfaces (Abutaleb *et al*., 2015). UHI is an instance of an unintentional alteration of the microclimate primarily due to changes in the energy equilibrium brought about by changes in land use, surface characteristics, and configuration of the of the city (Tomlinson *et al*., 2011). The modifications are largely as a result of conversion of pervious surfaces into impervious land covers arising from unprecedented urbanization (Benali *et al*., 2012). These water-resistant surfaces possess lower heat absorption capacities and energy conduction capabilities, leading to a faster increase in atmospheric heat when compared to pervious materials (Shen *et al*., 2015).

In their submission, Li *et al*. (2016) considered general reduction of surface albedo in urban areas as a key contributor to the UHI. Heisler and Brazel (2010) attributed lower surface albedo to the dark surfaces that make up the urban montage as well as the absorption of short-wave radiation through the upward walls and the urban forms.

UHI is also influenced by the relative absence of vegetation, the anthropogenic heat (AH) emission from human activities (Yow, 2007; Li *et al*., 2016) seasonal climatic conditions, daily synoptic conditions, and the diurnal cycle (Li and Norford, 2016). Anthropogenic heat refers to the energy released through man-made sources like vehicles, commercial and residential structures, industry, power plants and human metabolism (Quah and Roth, 2012). It significantly influences the urban environment directly by changing the surface

air temperature, and indirectly by the modification of urban boundary layer structure, precipitation, and other conditions (Lin *et al.*, 2008; Bohnenstengel *et al*., 2014).

UHI is measured by surface temperature, which can vary between cities and countrysides by up to five degrees (United Nations, 2010b). The effects and magnitude of UHI vary according to LULC patterns, urban morhorlogy, urban size, seasonal disparities, ecology, urban form, landscape and setting of the study area (Aslan and Koc-San, 2016). The UHI is most noticeable during conditions of light winds and cloudless skies particularly at night (Li and Norford, 2016; Cardoso *et al*., 2017) especially in large urban centres where its values may be as high as 10 °C in large cornubations (Heaviside *et al*., 2016). The reason being that the urban infrastructure radiates the shortwave solar energy absorbed during the day as longwave thermal infrared (TIR) radiation more slowly (Nguyen and Henebry, 2016).

The degree of UHI is normally determined by computing the difference between the maximun mean temperature of city centres and neighbouring country sides (De Joanna and Francese, 2012). Its effects are keenly associated with many important issues, such as urban climatology, environmental change, and human–ecological interactions, which impact on the well-being of human life (Lu and Weng, 2006).

### 2.5.2 Urban heat island types

The scientific community has identified a number of UHI kinds observeable in city centres **(**Voogt and Oke, 2003; Oke, 2009) namely: Subsurface UHI, Surface UHI, Urban canopy layer UHI and Urban boundary layer UHI. Subsurface UHI refers to the subsurface heat in cities resulting from transmission of heat surface soils and materials. The variability in the Subsurface UHI is attributed to the interface between radiant energy and the ground as well as the abilities of surfaces to reflect, engross or release energy**.**

Solar radiation has been identified as one of the vital factors that determine human thermal comfort under hot conditions (Norton *et al*., 2015). Surface is the temperature over full three dimensional urban surface interface of cities (Norton *et al*., 2015)**.** It is important to differentiate between energy exchanges at the roof top surfaces, walls, and ground surfaces because their processes are quite diverse. The Surface UHI is normally strongest at day times (Yuan and Bauer, 2007), particularly in open areas exposed to direct sunlight (Norton *et al*., 2015).

Urban canopy layer air UHI (UCL air UHI) refers to the air temperatures of the urban canopy layer such as as air around streets and under roof-tops levels; utilizing the height of the buildings as boundaries **(**Mills, 2007**).** In UHI studies, UCL temperatures are usually determined using approximately the height of people or the lower stories of buildings, between 1.5 and 3 m above ground (Heisler and Brazel, 2010). The UCL air UHI expresses the surface energy equilibrium affecting the air volume of the urban canopy (Oke, 2009)**.** Processes within the UCL are determined by the urban structure and geometry. For instance, densely built urban areas tend to reveal a stronger urban-rural temperature difference (Hughes, 2006). The canopy-layer UHI is primarily a nocturnal phenomenon resulting from reduced cooling rates over the city in the late afternoon and evening compared to the non- built-up areas resulting in higher urban minimum temperatures (Roth, 2013). Given its accessibility and relevance to human activities, the canopy layer UHI which is a local scale phenomenon is the most studied of all heat island types (Roth, 2013).

Urban boundary layer air UHI (UBL air UHI) is caused by a mixture of many local scale effects on city-wide scales and may extend hundred of metres above the surface. It varies greatly in thickness and turbulence over the course of a clear day **(**Heisler and Brazel,

2010). The development of this UHI layer is as a resultof a mixture of frictional drag of the atmosphere over the earth surface and the rising air over warmth surfaces. This UBL air UHI more obvious durin night time**.** Due to experimental difficulties in probing the air at higher heights, less attention is given to the UHI of this layer when compared to the canopy-layer, but a few airplane, helicopter, remote sensing, balloon, and tower studies have been conducted since the 1960s in a wide range of cities (Roth, 2013).

### 2.5.3 Relationship between LSTs and other biophysical parameters

There exists relationships between LSTs and other biophysical parameters such as vegetation and non-vegetation indices; as such several Vegetation and non-vegetation indices have been employed in land surface temperature studies. This is due to the fact that intensity of UHI is interrelated with the area coverage and what makes up the vegetal cover and built areas as well as their modifications over time (Zhang *et al*., 2009). Vegetation indices are ratios of bands that are designed to numerically separate or stretch the pixel values of different features on remotely sensed images (Mwakapuja *et al*., 2013). They are determined by using the distinctive feature of leaf chlorophyll absorption in the visible channel and lack of absorption in the adjacent near infrared region to isolate different features (Mwakapuja *et al*., 2013). The contrasts are utilized by combining multispectral red band and near-infrared reflectance.

There are several vegetation indices employed in LST studies notably the Normalized Differential Vegetation Index (NDVI). These indices provide for simple and fast interpretation of remotely sensed data in terms of vegetation health (Mwakapuja *et al*., 2013). NDVI is a characterization of vegetative density based on the amount and wavelength of the radiation reflected by the leaves of a plant (Ra *et al*., 2012). When vegetation is photosynthetically active, it is highly reflective in the near infrared channel

of the spectrum but reflects low in the red channel (Ra *et al*., 2012). Extensive documented evidence in the scientific community have established a strong interrelationship between LST and NDVI and other vegetation indices (Weng, 2009).

Several of these works have revealed a strong negative correlation between LST and the NDVI (Liu *et al.*, 2014). There exists a non-linear relationship between NDVI and LST due to the predominance of bare ground surfaces which display greater differences in surface temperature than the more luxuriant vegetated land covers (Zhang *et al*., 2009). NDVI measurements are dependent on seasonal changes which affect outcomes of surface urban heat island investigations (Li and Liu, 2008). The variability and nonlinearity of NDVI point to the fact that quantitative investigations of urban heat islands may not be sufficiently determined by it alone (Zhang *et al*., 2009). Thus, there is a possibility that combining NDVI and NDBI as substitutes to LULC may reveal relationships between them and LST in UHI studies (Zhang *et al*., 2009).

NDBI was designed for identifying built surfaces and areas in cities (Zha *et al.*, 2005). It is utilized in exploring the implications of green areas and built environments on UHI by estimating the ecological assessment indices of sub-urban locations (Liu and Zhang, 2011). NDBI is not only utilized as pointer of city expansion and extent of growth, but also as indicator of urban imperviousness that favours more exchange of sensible heat (Li and Liu, 2008).

LST has direct control on the UHI effect (Feizizadeh and Blaschke, 2013). The difference between LST of the urban areas and the surrounding non-urbanized surbubs is generally higher during the night time as a result of the transformation of urban areas into urban sceneries which are largely categorized by high albedo (Joshi *et al*., 2015). The UHI effect varies from place to place and is a function of spatial factors such as the

magnitude of urbanization and the amount of urban green space, and temporal factors such as season and the time of the day (Al-Gretawee *et al*., 2016). It is also affected by urban thermal, physical and geometric properties, and man-made water and heat causes existing in the area (Manik and Syaukat, 2015). The urban areas tend to have an above average temperature all year around. The difference in temperature between urban-built environment and rural centres ranges between 3˚C and 5˚C during the daytime but nocturnal differences may be up to 12 degrees celcius due to slow radiation of heat from urban surfaces due to canyon effects (Effat *et al.*, 2014; Joshi *et al*., 2015). They are direct consequences of differences between urban structure and materials in cities and those of rural areas, and indirect consequences by urban influences on hydro-climate and atmospheric pollutants (Heisler and Brazel, 2010).

They possess sparse vegetal cover but largely dominated by anthropogenic surfaces which absorb radiant energy from the sun and emit greater heat but retain limited moisture when compared with na, tural surfaces (Araujo *et al.*, 2015). Reduced water retention by artificial surfaces is attributable to rapid draining of rainfall through storm water pipes; with a consequent reduction of evapotranspiration and increased perceiveable warming of the local urban environment (Coutts *et al.,* 2007).

The magnitude of surface UHI varies with seasonal changes, because of seasonal variations in solar intensity, groundcover and weather (Effat *et al.,* 2014). Due to these variations, UHIs are typically higher in summertime. Apart from seasonal variations, the severity of the intensity of urban heat also depends on a city's location and characteristics (Parham and Haghighat, 2010) such as size and density of population, level of industrialization, as well as traffic pattern and density **(**Odindi *et al.*, 2015**).** The UHI has a thoroughly investigated feature of inadvertent anthropogenic climate modification

(Roth and Chow, 2012). Rapid urbanization and increased temperature in urban centres (UHI) exist all around the world; both contributing to global climate change and, in turn, are exacerbated by global climate change (Mills, 2007; Heisler and Brazel, 2010). Several approaches have been employed in studying thermal conditions in urban settlements (Singh *et al*., 2014).

### 2.5.4 The implications of urban land surface temperature (LST)

#### *2.5.4.1 The effects of urban LST on human health*

There are heightened awareness among bio-meteorologists, epidemiologists, climatologists and environmental health workers on health risk posed by rising rsing LST in urban areas (Tomlinson *et al*., 2011b) because there are intricate relationships between built environments, local temperatures, human health and well-being. Increased frequency, intensity, and long-lasting extremes of urban heat events; air pollution risks and ecosystem changes have been identified among the numerous major weather and climate drivers which affect human health (Luber *et al*., 2014).

Excessive rainfall and increasing temperatures are believed to aggravate problems associated with interior air quality, which include the evolution of fungi and moulds; known for increasing breathing and asthma-related situations (Fisk *et al*., 2007). In addition, warmth, concentration of harbinger substances, and methane releases have been identified as some factors which contribute to worsened ground-level ozone and particle pollution levels (Luber *et al*., 2014) responsible for premature deaths. Also, temperature increase across the globe may result in related rise in untimely deaths associated with worsening ozone and particle contamination. Urban Centres impact on the health of their residents both negatively and positively (Nieuwenhuijsen, 2016).

Apart from genetic and lifestyle causes, disease and mortality rates are affected by numerous social and environmental factors that form a complex system of causality (Fecht *et al.*, 2016), especially urban heat. In recent times, several studies have established positive relationship between cities and urban health; focusing on how specific urban characteristics potentially promote the health of urban dwellers. For instance, a study by Villeneuve *et al*. (2012) established associations between access to green spaces and lower rates of mortality while the study of Ward *et al.* (2012) established associations between green spaces and reduced stress levels. The health paybacks may result from mitigation measures like carbon sequestration strategies targeted at reducing greenhouse gas emissions through improving energy efficiency in buildings (Vardoulakis *et al*., 2014).

On the other hand, studies have also been done to establish undesirable interrelationships between cities and urban wellbeing, especially, high surrounding temperatures which negatively impacts on human health by way of increased death or illness; as they can increase markedly during episodes of persistent very hot weather (heat waves) especially among the aged (Heaviside *et al*., 2016). Sherwood and Huber (2010) have opined that heat stress imposes a robust upper limit to climate change adaptation, because at air temperature of 35.8°C and above, humans (and other mammals) lose the ability to dissipate metabolic heat.

Observations and climate change projections have been utilized by several studies in attempts to measure heat-associated health impacts currently and in future (Kinney *et al*., 2008; Huang *et al*., 2011; Vardoulakis and Heaviside, 2012; Hajat *et al*., 2014; Vardoulakis *et al*., 2014). Such epidemiological studies in various urban centres, particularly in high-income countries of Europe and North America and Japan's

conurbations have revealed that temperature extremes are associated with marked increases in mortality (McMichael *et al*., 2008). For instance, Fujibe (2009) revealed that incidences of heat related mortalities in Japan now outweighs those of other natural factors like typhoon and cyclones. During summer, over one hundred thousand persons suffering from heat-stroke related ailments were hospitalized in Tokyo metropolitan area of Japan (Fire and Disaster Management Agency of Japan, 2011). This is supported by Rey *et al.* (2007), Knowlton *et al.* (2009), Lin *et al.* (2009) who expressed that heat-waves are related with rising hospital admissions for cardiac, kidney, and breathing disorders.

The severe heat waves recorded across European cities in 2003 were reported to have had far reaching effects on public health, the economy, infrastructure, and general environmental health (Garcia-Herrera *et al*., 2010). The consequences were particularly more obvious and severe in cities across northern and central Europe where an estimated 70,000 deaths were related to the high temperatures recorded in August that year (Robine *et al.*, 2008). France alone recorded 14,802 excess deaths with the city of Paris accounting for 2,085 of the heat related deaths (Le Tertre *et al.*, 2006).

Researches have shown strong relationships between urban hotness and mental health. Dodgen *et al.* (2016) observed that persons suffering mental illness are very susceptible to excessive heat or heatwaves and noted aggressive behaviour, violence, and suicide as some implications of extreme heat on mental health and incidence of morbidity and mortality. Bouchama *et al.* (2007) who carried out six case-controlled studies that involved one thousand and sixty five heatwave related mortalities revealed that pre-existing mental-illness tripled the danger of death; as a result of exposure to heatwave. An empirical study showed that the danger of mortality rises for patients with psychosis,

dementia, and substance abuse when the weather is hot (Hsiang *et al.*, 2013). It has been established that the number of people admitted in hospitals for mental-illhealths associated with excessive heat, rising surrounding temperatures, and dampness have increased, especially for those with mental illness (Vida *et al.*, 2012; Wang *et al.*, 2014).

Urban heat strain is also related with physiological and behavioural changes ranging from vasodilatation and sweating, heat syncope or fainting, nausea and headache, to heat strokes, and heart attacks, particularly during extreme conditions (Moonen *et al.*, 2012). Other benign disorders include heat edema, heat tetanilla, heat pawns, heat exhaustion vomits, and frailty (Bhatta, 2010**).** Given these risks and health implications of a warming urban environment, Sherwood & Huber (2010) have suggested that continued global temperature rises could eventually lead to human abandonment of large regions of the presently inhabited world.

#### *2.5.4.2 Effects of urban LST on urban energy consumption*

Moonen *et al.* (2012) has posited that heat islands in warm-climate urban centres can have grave implications on the overall energy consumption of the cities, particularly demand for air conditioning. Ohashi *et al*. (2007) noted that urban cooling also raises urban temperature; as their study revealed that heat emanated from air-conditioners used for cooling within buildings increased external air temperatures in the Tokyo central business area by as much as 1-2 °C. Cities contribute about 60 to 85 percent of the world's energy consumption not only to meet the demand for heating/cooling but also because they are the main centres of fuel intensive industries (O'Malley *et al*., 2014). Santamouris *et al.* (2001) carried out studies in 30 urban and suburban stations and ten urban canyons in Athens (Greece). The study established a doubling of the air-

conditioning burden for urban houses and a tripling of peak electricity load for cooling in the study area.

#### *2.5.4.3 Effects of urban LST on urban environment*

UHI affects the local meteorological conditions by changing local-wind pattern; stimulating the formation of clouds; raising the incidences of lightning occurrence; and inducing the occurence of precipitation (Liu and Zhang, 2011). Decreased wind speed in the urban centres due to their morphology results in significant reduction in their potential natural ventilation (Santamouris *et al.*, 2001)**.** The need for increased air conditioning due to higher ambient temperatures directly raises pollution levels (particularly the formation of smog) resulting from the burning of fossil fuels by power plants (Elsayed, 2012) and transfers the indoor heat burden to the external local environment (Roth and Chow, 2012).

It has also resulted in the rise of greenhouse gas concentrations in the atmosphere (Roth and Chow, 2012). Some of the emissions and pollutants generated by majority of power plants include carbon dioxide, grainy substances, sulphur oxides, nitrous oxides, and noxious air (Bhatta, 2010). There are also indications already that higher urban temperatures increase the formation and concentration of smog (Elsayed, 2012). In addition, atmospheric chemical processes which lead to increase in ground-level ozone concentration may be accelerated with rise in urban temperature (Streutker, 2003). It has been posited that higher air temperatures may result in an increase in the emissions of biogenic hydrocarbons and higher evaporation rates of synthetic volatile organic compounds which are related to ground-level ozone (Elsayed, 2012). There is also a probability that additional warming of urban centres may stimulate urban ecological

activities due to alterations in the local distribution of plants and animals (Roth and Chow, 2012).

#### *2.5.4.4 Effects of higher temperature on water quality and quantity*

Warmer urban climates are believed to substantially reduce the quality of water through thermal pollution (Hamilton and Erickson, 2012). This occurs when urban structures such as roofs, pavements, buildings or landscapes which have temperatures 27°C to 50°C higher than that of the atmosphere transfer the heat to water and aggravates storm water runoff (Hamilton and Erickson, 2012). Urban runoff which may be 11-17°C warmer than those from country sides, discharge into streams, rivers, and lakes; posing threats to the aquatic fauna and flora in and around the water bodies (Hamilton and Erickson, 2012). The aquatic lives, which are particularly sensitive to immediate changes in temperature, may die as a result of shock and their carcasses create bastions of bacteria; posing health hazards to neighbourhoods of streams (Hamilton and Erickson, 2012). In addition, increased run-off may carry contaminants such as oil, chemicals and microbes into drinking water sources, with implications for public health (Manik and Syaukat, 2015). Also, higher water temperatures decrease the dissolved oxygen level thereby increasing the risk of contamination (Manik and Syaukat, 2015).

On the quantity of urban water supply, Barata *et al*. (2011) have noted that rising urban temperatures threaten water systems that capture, store, and transfer water to cities. They added that increased evaporation rates reduce surface water levels and fresh water availability. Furthermore, higher urban temperatures increase demand for water (Barata *et al*., 2011), thereby exacerbating the extraction of greater quantities of water from superficial and subterranean springs (Ashley and Cashman, 2006). A consequence of reduced surface water levels is an alteration in the exchange rate between groundwater

and surface water; further reducing the accessibility to fresh water supplies (Bates *et al*., 2008).

#### *2.5.4.5 Economic implications of higher urban climates*

Higher urban temperatures are also known to have some economic implications. One of such is the higher cost related to higher consumption of electricity for the purpose of indoor air conditioning systems, refrigerators, and water use (Izquierdo *et al.* 2011). Public health costs may become higher as the magnitude of urban heat increases (Jeong, 2012). Also, adapting urban centres to the new optimum climatic scenario will require capital that may be too complicated and large to be estimated (Jeong, 2012). Furthermore, economic projections have it that rising temperatures may result in loss of labour capacity during the peak months of heat stress and may double by 2050 (Dunne *et al*., 2013), leading to a decrease in the normal income globally by twenty-three percent by 2100 (Burke *et al*., 2015).

## 2.6 Data Sources for Assessing Land Surface Temperature

### 2.6.1 Airborne thermal data

This section summarizes roles of airborne thermal remote as highlighted by Harris and Coutts (2011). Airborne thermal remote sensing has been identified as is an striking opportunity for recognizing locations of exposure to high surface-heat in urban areas. It offers outstanding spatial image of the municipal scenery in time; giving room for a relative investigation of places of high surface temperature. A benefit of air-borne thermal remote sensing is its capability of observing high resolution (1-5 m) surface temperatures; permitting the recognition and investigation of discrete scenes elements. Also, in comparison with satellite remote sensing, air-borne heat-mapping permits for adjustibility in flying times. There are however, some limitations in air-borne thermal mapping. One

of such limitations is that it offers data on the surface UHI, instead of the urban canopy layer UHI which is of most concern, and the most pertinent to human thermal well-being. Secondly, it views the earth surface from a steep viewing angle; thereby leading to sampling biases, as some three-dimensional surfaces (like walls) are overlooked. In addition, for most air-borne thermal remote sensing information, other auxiliary data (such as aerial photographs, vegetation indices, and ground-based air temperature data) needed in processing, examining and interpreting the imagery.

### 2.6.2 Remotely sensed thermal data

A veritable tool and data source which has become indispensable and very reliable in environmental studies is remote sensing. Lillesand *et al*. (2004) defined remote sensing as the science and technique of gathering data about objects, areas, or phenomena by analyzing the information acquired, using devices that are not in contact with the objects, areas or phenomena under investigation. Remote sensing has also been defined as the science and technology through which features of objects of can be recognized, measured or analyzed without direct interaction with the object (Yadav *et al*., 2013), rather sensor devices such as cameras and scanners borne by aircrafts or satellite platforms are used in recording electro-magnetic radiation (Yadav *et al*., 2013).

Joshi *et al*. (2016) expressed that remote sensing devices record the electromagnetic properties of land surfaces such as reflected energy (optical sensors), emitted energy (thermal infrared or passive microwave sensors) or scattered energy (active radar sensors). Technically, remote sensing systems/sensors have three resolutions namely: spatial resolution, spectral resolution and temporal resolution (Yadav *et al*., 2013). Spatial resolution implies the smallest detectable pixel size of features on the ground in the direction of and across the flight. Spectra resolution is the number, location in the

electromagnetic spectrum and bandwidth of the specific wavelength bands or spectral bands. Temporal resolution refers to the time lapse between two successive images of the same area.

In terms of orbit, satellite remote sensing platforms are of two types; polar orbiting satellites and geostationary orbiting satellites. Polar Orbiting satellites are low-flying satellites platforms which orbit the earth in a nearly north-south path at an altitude of approximately 700 km - 1,700 km**.** They are positioned in a sun-synchronous orbit, which means that they cross a given latitude at the same solar time each day so that a particular area is seen under the same lighting conditions every time it is visited. This makes it easier to detect changes that have occurred between visits. The swath of each polar orbiting satellite is approximately 2600 km wide and they complete 14 orbits per day. They can provide global coverage twice in 24 hours. Because they operate at a distance closer to the earth, the images produced are of high spatial resolution. The advantage of higher spatial resolution (i.e. the smaller the pixel size) is that it yields more accuracy in image classification (Weeks, 2003). They provide comprehensive monitoring of the entire globe including the Polar Regions. They are however, capable of taking images of a limited area of the earth each time and have poor temporal resolution.

Examples of polar orbiting satellites are National Oceanic and Atmospheric Administration (NOAA) Advanced Very High Resolution Radiometer (AVHRR); Polar Operational Environmental Satellites (POES)**;** NASA's Earth Observation Systems such as Landsat and Terra/Aqua Moderate Resolution Imaging Spectroradiometer (MODIS); Indian Remote Sensing Satellite **(**IRS), European Resource Satellite (ERS-1 and ERS-2); Tropical Rainfall Measuring Mission (TRMM) and Defense Meteorological Satellites

Program (DMSP). MODIS and AVHRR have higher temporal resolution and are capable of producing 1–2 images per day for the same area, but have low spatial resolution ranging from 250–1000 m. As such, they may not be able to detect the high level of detailed information and seriously impede their potential applications (Bai *et al.,* 2015). Therefore to generate synthetic LST data with high spatial and temporal resolution, it may be necessary to develop new image fusions methods that can integrate complementary characteristics from multi-sensors (Bai *et al.,* 2015).

Geostationary orbiting satellites hover over the earth around the equator at an altitude of about 36,000 km. They complete one orbit in 24 hours synchronised with earth's rotation about its own axis. This implies that geostationary satellites orbit the earth in the same time it takes the earth to rotate once. Therefore, the satellite appears to stay still, always above the same area of the earth. This orbit allows the satellite to monitor the same region all the time. The main advantages of geostationary satellites lie in their synoptic coverage and the high time-scale resolution of their data; since new scenes are captured every 15-30 minutes. They are however characterized by a much coarser spatial resolution of 4 km (Jiang *et al.,* 2015b**).** Therefore, a common solution for characterizing surface temperatures from these sensors is to downscale the images from 4 to 1 km while keeping its temporal resolution (Jiang *et al.,* 2015b). Thermal downscaling is the technique to derive LSTs at high spatial and/or high temporal resolution. The classical way for this purpose is to utilize the inverse association between the NDVI and LST as evident in previous studies (Jiang *et al.,* 2015b).

Geostationary orbiting satellites are however limited by their coarse spatial resolution as compared to the polar orbiting satellites in view of their distance from the earth. In addition, due to the satellite's viewing angle, useful information is restricted to the belt

between 70 degrees north and south of the latitudes. A disadvantage of coarse or lower spatial resolution images is reduced accuracy in image classification, because there is more likelihood that a the pixel may represent a mixture of different land covers (Weeks, 2003). E xamples of sensors on geostationary platforms include NOAA's Geostationary Operational Environmental Satellite series (GOES) and METEOSAT's Second Generation (MSG) geostationary meteorological satellites.

Remote sensing systems are either passive or active Passive remote-sensing systems operate by measuring the energy which is reradiated or reflected from the object of interest back to the remote sensor (Weeks, 2003). The sensors are most often optical (measuring light reflectance), but they may also be thermal (measuring heat reflection), depending on the wavelength of the energy that the sensor is designed to measure (Weeks, 2003). Optical remote sensing has offered data for over four decades (Joshi *et al*., 2016). Optical products are commonly available as multispectral images (ranging from visible to infrared wavelengths) consisting of several bands of data (Joshi *et al*., 2016). They provide a varied array of information on land-cover depending on its spectral reflectance (Joshi *et al*., 2016). Landsat, SPOT and MODIS satellites are examples of optical sensors that dominate land use /land cover analyses owing to their length of consistent datasets and the ease of availability (Joshi *et al*., 2016).

Passive microwave sensors are remote sensing devises that do not possess their own radiation or illumination but instead are only sensitive to radiations from natural origins such as the Sun or artificial light (Kerle *et al*., 2004; Yadav *et al*., 2013). Passive sensor systems based on reflection of the Sun's energy are only operational during daylight (Kerle *et al*., 2004). On the other hand, passive sensors which measure the longer wavelengths related to the Earth's temperature do not depend on the sun as a

source of illumination and can be operated at any time (Kerle *et al*., 2004). Passive microwave measurement tends to be limited since they characteristically provide a very coarse spatial resolution (Tomlinson *et al*., 2011).

Active sensors such as RADAR (Radio Detection and Ranging), LIDAR (Light Detection and Ranging) and SONAR (Sound Navigation and Ranging) are systems which generate their own source of illumination (Kerle *et al*., 2004). They emit a controlled beam of energy to the surface and measure the amount of energy reflected back to the sensor (Kerle *et al*., 2004). The main advantages of active sensor systems is that they have a controlled illuminating signal, are typically not affected by the atmosphere and possess the ability to be operated day and night (Kerle *et al*., 2004).

Although not as widespread as the optical sensors, active microwave technology, particularly Radar has also been employed in land surface and atmospheric mapping over the last two decades and is gaining more ground (Joshi *et al*., 2016). Spaceborne Imaging Radar-C/X-Band Synthetic Aperture Radar (SIR-C/X-SAR), European Remote Sensing (ERS-1 and -2), Advanced Synthetic Aperture Radar (ASAR), Japanese Earth Resources Satellite (JERS-1), RADARSAT-1 and -2, Advanced Land Observation Satellite (ALOS-1) are some examples of active microwave systems that have been largely used in studies at regional scales.

A limitation of Radar remote sensing is the inherent presence of speckle which results in measurement uncertainty and poor classification accuracies (Maghsoudi *et al*., 2012). Another major constraint in the utilization of Radar remote sensors, particularly over hilly regions is topographic effects such as radar shadow caused by foreshortening and layover on ground-range images (Quegan and Yu, 2001) Moreover Observations using Synthetic Aperture Radar (SAR) require a relatively high

energy provision on satellite platforms; thereby reducing the availability of dense time series of SAR data over several areas across the world (Joshi *et al*., 2016). In addition, until recently, satellite-based SAR data for large-scale multi-temporal assessments were constrained by low spatial and temporal coverage of medium resolution data (Rosenqvist *et al*., 2007).

For panchromatic images which are mainly shades of gray, information is recorded for only one band of reflectance, using the brightness of the pixel in the visible range of wavelengths between 0.4 and 0.7 micrometres (Weeks, 2013). The panchromatic images are not utilized in image classification but are employed in deriving information about brightness and about the texture at the earth's surface (Weeks, 2003).

In recent times, important advancements have been achieved in satellite remote sensing technology (Walawender *et al*., 2014). There has been a continuous improvement in accessibility to satellite data (Walawender *et al*., 2014). Accessibility to remote sensing information stems in the fact there are different sensors on-board several satellites, covering a broad spectrum of spatial, temporal, radiometric and spectral-channel resolutions (Melesse *et al*., 2007) as well as their global coverage and diverse verification methods **(**Tomlinson *et al*., 2011). In addition, there are tremendous advancements in object-based image processing soft wares and methodologies (Blaschke *et al*., 2011). These advantages have resulted in the widening of its application in the monitoring of different processes occurring on the surface of the earth and its atmosphere (Walawender *et al*., 2014**)** and its wide utilization in natural resource mapping and as source of input data for environmental processes modeling (Melesse *et al*., 2007).

Satellite remote sensing has provided major advances in understanding the climate system and its changes, by quantifying processes and spatio-temporal states of the

atmosphere, land and oceans (Yang *et al*., 2013). It contributes to the description of urban climate and provides a better understanding of the underlying climatic processes (Bechtel *et al*., 2012). It has proven to be highly valuable in estimating spatially continuous near surface air temperature **(**Chen *et al*., 2016c).

Remote sensing plays crucial roles in detecting general environmental changes, including man-made transformations of the natural environment (Walawender *et al*., 2014**).** Some of the applications include modelling water resources, drainage basin delineation, radiation and water changes estimation, fractional vegetal coverage mapping, impermeable surface area delineation, urban designing and drought predictions based on soil water index using remotely-sensed data (Melesse *et al*., 2007). Using remote sensing technique in unison with GIS is increasing in the areas of meteorology and climatology (Tomlinson *et al*., 2011), particularly in urban centres**.** Driven by increasing societal needs, urban remote sensing is particularly attracting growing interests especially with advances in fine resolution imaging and more efficient methods (Melesse *et al*., 2007).

One aspect of urban study that largely employs remote sensing techniques is the exploration of LST/UHIs (Tomlinson *et al*., 2011)**.** Land surface temperature changes take advantage of thermal remotely sensed data which supply a practicable approach for the investigation of LST on extensive scales (Abutaleb *et al*., 2015). Thermal remote sensing is the branch of remote sensing which is concerned with acquiring, processing and interpreting information gathered principally in TIR channel of the light spectrum (Prakash, 2000). It measures the radiations 'emitted' from the surface of the target, as opposed to optical remote sensing where the radiations 'reflected' by the target under consideration are measured (Prakash, 2000). Its realm may be broadened to encompass not only the TIR but also the SWIR, NIR and in extreme cases even the visible channel of the light spectrum (Prakash, 2000). Thermal sensing devices measure data using

microwave wave-length range of 8 µm to 14 µm which are directly related to an object's temperature (Kerle *et al*., 2004).

Remotely sensed thermal infrared images provide a unique method for obtaining LST information at large scales (Jime´nez-Munoz *et al*., 2008). They are widely utilized in assessing the thermal urban environment, in identifying UHI in highly urbanized areas and in investigating LST patterns and its interrelationship with surface features (Weng, 2009; Kaya *et al*., 2012). Sobrino *et al*. (2009) pointed out two reasons for TIR data contribution to a better knowledge of land surface processes. The first reason being the measurement of surface temperatures as co-related with specific scenes and biophysical elements, while the second is by relating surface temperatures with energy variations for specific scenes phenomena.

In contrast with *in situ* measurement, remote sensing possesses the advantages of large spatial and temporal coverage and a relatively high spatial resolution. It provides good quality realtime information over wide areas; revealing the spatio-temporal variations in urban thermal environments at both local, regional and global levels (Chen *et al*., 2016c). Remote sensed data also provide outstanding cost-effective and timesaving technique for analyzing spatio-temporally dispersed LST (Senanayake *et al.*, 2014). An advantage in using satellite data with respect to ground-based observations is the provision of spatially representative measurements of surface temperature over large areas of cities through quasi-continuous monitoring of the urban surfaces (Fabrizi *et al.*, 2010). Sensors on satellite platforms can provide a great deal of variable information for various global applications such as environmental monitoring and natural resource management on account of their repetitive measurement capability. Other related parameters which are inputs for estimating surface heat fluxes that remotely sensed data can provide

information on include surface albedo, vegetation index, surface emissivity **(**Chakraborty *et al*.**,** 2013). It is difficult obtaining the spatial information from traditional ground based in situ measurements.

Owing to these advantages, remote sensing techniques have been widely utilized in analysing surface temperature dynamics in urban areas (Mitraka *et al.,* 2015). Particularly, TIR remote sensing techniques are employed in urban climate investigations, chiefly for analysing LST patterns and its interrelationship with surface features (Weng, 2009). Extracting LST values from remotely sensed thermal imagery requires several methodologies like sensor radiometric corrections, atmospheric and surface emissivity corrections, and classification of spatial variability in land cover, among others.

Satellite data at spatial resolutions of 100–1000 m are capable of providing dependable information on the extent of urban coverage and spatial distribution at a large scale, because of their synoptic view and wide coverage (Zhang *et al.,* 2015). Moreover, improvements in sensor technologies and broadening knowledge of atmospheric physics have remarkably enhanced both the quality and the quantity of satellite data acquisition; making a multi-scale investigation of urban climate possible (Tomlinson *et al*., 2011). In addition, thermal digital sensing of the urban location does not only measure the magnitude of surface temperature of the entire metropolis, but also the spatial distribution of the surface UHI effects **(**Srivanit *et al*., 2012**).** These attributes make remote sensing a veritable tool in studying the changes of the earth's surface and air. It has proven to be the most appropriate tool in assessing the spatio- temporal patterns and changes in city thermal landscapes, as well as urban surface energy budget (Weng, 2009).

In contemporary times, different categories of satellite images have been employed by scientists to extract information on LST. The first category of sensors are those on board

polar orbiting satellites, such as the Advanced Spaceborne Thermal Emission and Reflectance Radiometer (ASTER) Landsat Thematic Mapper (TM), Enhanced TM Plus (ETM+), Operational Land Imager (OLI), Synthetic Aperture Radar Imager (SAR), and Satellite Pour l'Observation de la Terre (SPOT) which obtain TIR data between 60 m and 120 m spatial resolution (Anderson *et al.*, 2012; Almeida *et al*., 2006; Şahin *et al.,* 2011; Zhou *et al.,* 2013; Ding and Shi, 2013; Sameen and Kubaisy, 2014) can provide thermal infrared (TIR) and are capable of providing details for LST and have proven to be appropriate in examining the spatial structures of urban heat islands (Zhou *et al.,* 2013).

Satellite sensors in this category have been frequently and extensively utilized in analyzing surface temperature changes and regional and global LST studies (Bai *et al.,* 2015). However, their low temporal resolutions render them insufficient for LST monitoring. International research programmes extensively utilize satellite observations; especially as they possess potentials to derive quantitative measurements of the dynamics of many atmospheric, oceanographic and terrestrial surface characteristics (Donoghue, 2002**).** Its utilization has resulted in key advances in understanding the climate system and its changes, through quantifying processes and spatio-temporal states of the atmosphere, land and oceans (Yang *et al*., 2013).

The availability of several satellite remote sensing platforms has provided volumes of very valuable datasets for measuring LST (Tomlinson *et al*., 2011)**.** The thermal infrared sensors on board satellite platforms thermal measure top of the atmosphere (TOA) radiances, from which brightness temperatures are extracted (Dash *et al.,*2002). The TOA radiance is the outcome of the interaction between three fractions of energy vis-a-viz earth's surface emitted radiance, atmosphere upwelling radiance, and sky down welling radiance scales (Abutaleb *et al*., 2015). TOA radiances are transformed to LST by

correcting for mospheric attenuation, angular effects and spectral emissivity values at the surface (Tomlinson *et al*., 2011)**.** Remote sensing has also been employed in studying other aspects of the urban environment such as calculation of cooling degree-days, monitoring hot spells, assessing the effects of city development on runoff and measuring soil surface moisture (Tomlinson *et al*., 2011). In addition, biophysical attributes from remotely sensed optical data possess great potentials for parameterizing urban construction materials and composition, and for linking pixel-based LST measurements for a better understanding and modeling of the surface energy budget and the UHI phenomenon (Blaschke *et al*., 2011; Bechtel *et al*., 2012).

In spite of the aforementioned benefits of TIR remote sensing, it is not without limitations. One limitation is that they are incapable of fully capturing radiant energy from vertical surfaces like walls of buildings, since the sensors largely record emissions from horizontal tops such as streets, roof tops and tree tops (Goldreich, 2006). Also, remotely acquired data represent radiation which travelled through the atmosphere, first as wavelength from the sun to the earth surface and, secondly, as wavelength from the earth to the atmosphere (Mirzaei and Haghighat, 2010). Hence, the need for the correction of the data for accurate estimations of surface properties including solar reflectance and temperature **(**Abutaleb et *al*., 2015).

Cloud coverage is another constraint of these satellites because, Clouds cause serious problems in optical wavelength remote sensing because they do not only hide the ground but also cast their shadows on the ground thereby impeding many applications. They reduce the usage of the image data and thus increases the time between two image acquisitions. In spite of the limitations, sensors in this category have been employed for

characterization of intra-annual variations of UHIs (Huang *et al*., 2006; Pongracz *et al.*, 2006; Wang *et al*., 2007; Zhou *et al*., 2008, 2011).

Satellite data and GIS have also become the commonest methods for quantifying, mapping and detecting patterns of land use owing to their accurate geo-referencing procedures, digital format suitable for computer processing and repetitive data acquisition (Hassan *et al*., 2016). Du *et al*. (2014) pointed out that remotely sensed imagery is an effective source of information suitable for providing information on urban land surface features and their variations over time at various spatial and temporal scales. They added that the data sources are widely employed in various urban applications like urban structure extraction, urbanization monitoring, and change detection among others. They also identified image classification and change detection as the most popular techniques for assessing LULCC in urban areas.

Lu and Weng (2006) pointed out change detection is a complex process that involve key steps. The steps highlighted by them include the choice of suitable data, selection of a suitable classification or detection system, carrying out necessary image pre-processing, feature selection/extraction, choice of suitable classification techniques as well as carrying out post-classification processing and accuracy assessment. The choice of classification algorithms and remotely sensed data for urban LUCC analysis are functions of the characteristics of the satellite data, land use/cover categories, atmospheric condition, the objectives of the study, the capacity of hard and softwares, and the expertise of the user (Du *et al*., 2014).

Automated urban land cover extraction methods have been developed and utilized for good resolution satellite images, like QuickBird, Ikonos, and WorldView, to map mixed ranges of urban land surface/cover (Bach *et al*., 2013). One of such extraction methods is

Object-Based-Image Analysis (Benz *et al*., 2004; Blaschke, 2010) which are preferred to pixel-based methods (Myint *et al*., 2011) which consider only spectral properties. In addition to spectral properties, Object Based Image Analysis (OBIA) consider other characteristics like shape, texture or adjacency criteria (Bach *et al*., 2013).

## 2.7 Some Common Airborne/Space borne Sensors Employed in LST Studies

### 2.7.1 Airborne imagery

Airborne sensors possess higher spectral resolution than satellite sensors, and due to low altitude in which the flights are performed, they offer higher spatial resolution images, with pixel sizes of only a few metres (Sobrino *et al*., 2008). Some examples of available airborne sensors are the digital-airborne imaging spectro-meter (DAIS), the airborne hyperspectral scanner (AHS), the airborne reflective/emissive spectrometer (ARES), the airborne hyperspectral Operative Modular Imaging Spectrometer (OMIS) among others (Sobrino *et al*., 2006; Xu *et al*., 2008).

### 2.7.2 Advanced along-track scanning radiometer (AATSR)

AATSR is one of the sensors onboard the Envisat satellite designed to obtain the high levels of sea surface temperature (SST) and LST for global climate change studies (Ouyang *et al*., 2017). AATSR measures seven channels of reflected and emitted radiation at 0.55 μm, 0.66 μm, 0.87 μm, 1.6 μm, 3.7 μm, 11 μm and 12 μm with both a nadir view resolution of $1 \times 1$ km$^2$ and a forward view resolution of $1.5 \times 2$ km$^2$. The AATSR swath width is 512 km and able to provide a global LST coverage about every three days (Sòria and Sobrino, 2007; Ghent, 2012). AATSR-derived LST products have been widely used in climate change, land–atmosphere feedbacks, modeling studies, land cover changes and many other applications (Ouyang *et al*., 2017). Currently, there are two methods of LST derivation and validation in AATSR and other satellite sensors (Li

*et al*., 2013; Coll *et al*., 2011). One method is the temperature based method (T-based) which directly compares the satellite-derived LST with *in-situ* observation data. The second method is radiance based method (R-based) which utilizes the atmospheric transfer equation to compute the at-sensor LST based on the land surface emissivity (LSE) spectra of the *in-situ* location and the atmospheric profiles.

### 2.7.3 Moderate resolution imaging spectroradiometer (MODIS)

The MODIS sensor is one of the sensors on board NASA's Aqua and Terra satellites. Each of the two satellites have near polar orbits, given them a high temporal coverage. The Aqua has two acquisitions at nighttime and during daytime and vice-versa for Terra. They however have coarse spatial resolution of 1 km compared to Advanced Thermal Emission and Reflection Radiometer (ASTER), the Landsat series such as Enhanced Thematic Mapper Plus (ETM+) and the TIRS, all of which have spatial resolutions less than 100 m. LSTs are derived from MODIS bands 31 and 32 which are its TIR bands of (Srivastava *et al*., 2010). Despite the low resolution of MODIS data, their high temporal resolution have made them useful for LST and UHI studies (Tomlinson *et al*., 2012; Sobrino *et al*., 2013; Lehoczky *et al*., 2017). MODIS TIR data are also employed for water resource management and assessing agricultural drought and environmental biogeochemistry processes (Wang *et al*., 2015).

However, the coarse spatial resolution of retrieved LST images from MODIS thermal infrared data has limited their applications in studies that require high spatial resolution in identifying detailed variation of thermal heat flux over places being investigated (Zhan *et al*., 2013) such as urban heat island monitoring and agro-drought monitoring (Wang *et al*., 2015). The need to increase its spatial resolution is therefore expedient if it is to be useful for more studies (Clinton *et al*., 2014; Nichol and Wong, 2009). Hence, several efforts

have been made to down-scale the coarse pixel of MODIS thermal infrared band data into better spatial resolution using several indices (Zhu *et al*., 2013: Wang *et al*., 2015).

Kustas *et al*. (2003) developed and utilized an approach called DisTrad in establishing a simple linear regression equation between LST and NDVI to decompose MODIS LST image into a better spatial resolution while Essa *et al*. (2012) improved the evaluation of DisTrad by developing the E_DisTrad method for urban areas. To further improve the resolution of down-scaled MODIS thermal images, Wang *et al*. (2015) designed a more efficient technique called Double-step Pixel Decomposition (DSPD), which yields a higher spatial resolution with the thermal radiance of sub-pixels in the resulting decomposed LST image similar to those of the parent pixel from which the sub-pixels are generated.

### 2.7.4 Advanced very high resolution radiometer (AVHRR) sensor

The AVHRR sensor is one of the sensors commonly onboard several National Oceanic and Atmospheric Administration (NOAA) satellite platforms (Tomlinson *et al*., 2011). AVHRR has a spatial resolution of 1.1 kilometre and offers daily daytime global coverages. The data are frequently utilized in national or global scale studies (Lu and Weng, 2006). The thermal infrared (TIR) channels of the sensor namely: channels 4 (10.3 – 11.3 μ) and 5 (11.5 – 12.5μ), are increasingly utilized for LST assessments.

### 2.7.5 Advanced space-borne thermal emission and reflection radiometer (ASTER)

LST is extracted using ASTER's thermal bands (bands 10–14). The ASTER data, with spatial resolutions ranging from 15 m to 90 m ASTER, is capable of providing much more comprehensive information than some sensors and is therefore very suitable for the urban-related studies at local and regional scales (Lu and Weng, 2006).

### 2.7.6 Advanced microwave scanning radiometers (AMSRs)

AMSRs were successfully deployed on two satellite systems; AMSR-E onboard the National Aeronautics and Space Administration's (NASA's) Aqua, and AMSR2 on-board the Japan Aerospace Exploration Agency's Global Change Observation Mission-Water1 (JAXA's GCOM-W1) satellites (Nguyen and Henebry, 2016). The AMSR-E sensor is a passive microwave radiometer operating at 6 frequencies ranging from 6.925 to 89.0 GHz. Both horizontally and vertically polarized radiation are measured at each frequency with an incidence angle of 55°. The ground spatial resolution at nadir is 75 × 45km for the 6.925GHz channel (C-band). The AMSR-E is one of six sensors onboard Aqua, which was launched in 2002. They were designed to retrieve global data on precipitation, sea surface temperature, oceanic surface winds and integrated cloud water and water vapor, vegetation, sea ice, and snow cover (Lobl *et al*., 2003). AMSR-E data has however been employed in measuring LSTS in Urban centres (Nguyen and Henebry, 2016). AMSR2 is a single-mission instrument satellite that was launched in May 2012 and its data made are available beginning in August 2012 (Wu *et al*., 2016).

### 2.7.7 Landsat sensors

Landsat Thematic Mapper (TM) and Landsat Enhanced Thematic Mapper Plus (ETM+) provide thermal information using just one long-wave infrared (LWIR) band at a higher spatial resolution of 60 metres and has re-vist period of 16 days. Landsat-8 which was successfully deployed into space on 11 February 2013 has two principal sensors on-board. One sensor is the Operational Land Imager (OLI) which has nine spectral bands in the visible (VIS), near infrared (NIR), and the shortwave infrared (SWIR) regions. The second is the Thermal Infrared Sensor (TIRS) which has two spectral bands in the Long Wave Infrared (LWIR) region.

The thermal bands have spatial resolution of 100 metres with a revisit period of 16 days. The high spatial resolution of Landsat thermal bands places it at an advantage of studying meso and small scale phenomena but it is limited by its low temporal resolution (Oguro *et al*., 2011). As such, its applications are different from those of other sensors with coarser spatial resolutions and shorter revisit times (Rozenstein *et al.*, 2014). Landsat TIR imagery are widely utilized at the regional or local scale (Lu and Weng, 2006) because the sequence of Landsat sensors offers the lengthiest incessant archives of satellite based observations (Chander *et al*., 2009). Landsat has therefore become priceless and vital in observing worldwide change and a significant basis for moderate spatial resolution earth observations **(**Chander *et al*., 2009).

## 2.8 The Role of Geographic Information System in Studying Urban Thermal Fluxes

Walsund (2013) defined Geographic Information System (GIS) as a computerized information system with functions for collecting, storing, processing, analysing and visualizing geographical data vis-a viz maps, statistics and satellite images. GIS has also been defined as a computer-based system that allows for the combination of maps with other data pertaining to particular places in order to analyse those data and present the results as thematic maps or in graphic formats (Weeks, 2003). According to Saleh (2010), GIS technologies provide flexible avenues for recording, investigating and presenting digital information from several sources for urban elements identification, modification and database development. GIS presents a set of concepts, methods, and tools for exploring spatial patterns in data and is an invaluable tool for integration, analysis, and visualization of spatial information (Wilhelmi *et al.*, 2004). It is often widely utilized with other ancillary data to convert remotely sensed urban data into tangible useful information (Blaschke *et al*., 2011).

Walsund (2013) has highlighted some common applications of GIS in urban centres namely: visualization, selection and search, graphical analysis, spatial correlation and localization. It provides a means to display and analyze comprehensive remotely sensed large-scale datasets (Chapman and Thornes, 2003). Remote sensing and GIS technologies have been extensively integrated and proven to be very effective in analysing and modelling cities (Saleh, 2010; Blaschke *et al*., 2011). Variables generated from processed remotely sensed information, GIS thematic overlays, and enumeration information have been identified as three essential data sources for urban analyses; thus their integration is a central theme in urban analysis (Blaschke *et al*. 2011). GIS offers practical and relevant working environments for integrating, analyzing and visualizing climatological/meteorological information together with other spatial data sources (Dobesch *et al*., 2007).

Lately, Global Positioning Systems (GPS) have played vital roles in GIS and remote sensing analyses. Merchant and Narumalani (2009) have pointed out some of its applications in various steps in GIS and remote sensing analysis. Some of the steps employed in GPS as highlighted by them include: image rectification, georeferencing thematic data in a GIS, collection of field data to support image analysis (such as ground truthing, calibration, or accuracy assessment), and development, or updating, of GIS databases portraying features such as roads and utilities.

## 2.9 Algorithms for Extracting Land Surface Temperatures (LST)

Several procedures have been advanced for retrieving LSTs from remotely sensed information. Commonly utilized algorithms are the Universal Single-Channel (USC) algorithm (Jime´nez-Munoz and Sobrino, 2003) and the split window procedure (Stathopoulou *et al*., 2004). For single-channel algorithms, the best wavelength for

retrieving LST depends on the atmospheric water vapor and varies from 11 mm to 10.5 mm (Roy *et al.,* 2010). The USC procedure is more frequently utilized in estimating from Landsat TIR remotely sensed infomation due to its comparatively straightforward data demands and precision. It only requires one TIR channel, makes use of same equation and constants for diverse sensing platforms, and requires only the atmospheric moistness contents and land surface emmitances as input (Chen *et al*., 2016c). In addition**,** Single-channel methods provide similar or better results than split-window methods for low atmospheric water vapor content (Roy *et al.,* 2010). Owing to these advantages the USC algorithm has been extensively utilized in studying UHI in urban centres globally (Dash *et al.,* 2002; Sobrino *et al.,* 2004).

In contrast, split-window algorithms otherwise called two channels algorithms require concurrent information from no less than two frequencies (Chen *et al*., 2016). This algorithm has been largely employed by the scientific community in LST studies (Sobrino *et al*., 2009). With regard to the split-window technique, the best simulated results were obtained for wavelength combinations near to 11 mm and 12 mm (Roy *et al.,* 2010). The algorithm provide better results for atmospheres with high humidity (Roy *et al.,* 2010).

Liu and Zhang (2011) in a study employed the mono-window algorithm to the Landsat TM, and the split-window algorithm to ASTER's five thermal bands for the analysis of LST in Hong Kong. The split window algorithm allows for correction of atmospheric effects by using differential absorption in adjacent TIR bands instead of depending on absolute atmospheric transmission in one band and is therefore less sensitive to the optical properties of the atmosphere (Srivastava *et al*., 2010).

In addition to these algorithms Sobrino *et al.* (2006) identified two other algorithms namely: temperature and emissivity separation algorithm (TES) which utilizes at least

four thermal bands; and two-angle algorithm, which utilizes just one thermal band but two view angles. Abutaleb *et al*. (2015) also identified radiative transfer equation as another algorithm for extracting LST. Among these three LST retrieval methods: radiative transfer equation, mono-window procedure and single-channel procedure can be applied to Landsat data with good results (Abutaleb *et al*., 2015).

## 2.10 Scales Employed in Urban Climate Studies

Climates of cities are categorized by varying processes occuring at different scales, occasioned by the biological/physical composition of urban centres, and the structural arrangement of urban atmospheres **(**Roth, 2013). Roth (2013) also pointed out that scale determines the size of the area from where the thermal influence emanates and how it changes over time. Oke (2004; 2009) identifies three scales which are often utilized for urban climate studies. The first according is the micro-scale climates which are consequences of the surface radiation equilibrium and entails the heat condition of individual structures, trees, streets and their intervening spaces. Typical micro-scales extend from one to hundreds of metres (Roth, 2013).

The second is the local-scale which encompasses the temperature of localities which integrates microclimate consequences with similar combinations of city features. It is the resultant effect of the surface and urban canopy layer energy balances**.** Typical local scales extend from one to several kilometres (Roth, 2013). The third and largest scale is the meso-scale which entails the influence of urban centres on large scale weather spanning more than tens of kilometre. Plumes from discrete local-scale systems spread upwards and fuse, resulting in urban boundary layer (UBL) across entire cities.

## 2.11 The Role of Vegetation in Ameliorating Temperatures in Urban Centres

Urban vegetation is known to play crucial functions in mitigating climate change both locally and globally through several mechanisms of simultaneous cooling and a reduction in summertime energy demand for indoor cooling (Alavipanah *et al.*, 2015). Its modifying roles in the urban thermal Environment makes it an indispensable component of urban sustainability (Shen *et al*., 2015). Emmanuel (2005) identified three complementary roles played by tree shades in combating urban heat islands. First, they limit solar penetration thereby restricting energy storage and the heating of the local environment. Secondly, tree shades reduce the direct gain of energy through windows and the resultant internal greenhouse effect. Thirdly, shades provide shelter from direct exposure to the sun. The magnitude of cooling provided by tree shades is a function of tree crown shape, density, tree growth rate and longevity, and the relative position of trees to buildings they shade (Doick and Hutchings, 2013).

It is now unequivocal that urban green spaces are beneficial for mitigating UHI, evapotranspiration and provision of shades which cool the urban environment (Voogt and Oke, 2003; Chen *et al*,. 2011). Urban green areas are known to provide numerous ecological services like food, materials as well as biodiversity supplies; air-pollutants removal; climate regulation; and soil erosion prevention (Qing *et al*., 2013). Other socio-economic benefits of vegetation/green areas include provision of accessible green spaces in the vicinities of those inhabiting densely populated areas (Alexandri and Jones, 2008); improving human health and well-being (Tzoulas *et al*., 2007); capturing and retaining stormwater (Buccola and Spolek, 2011; Rowe, 2011); and the creation of habitats for other species (Solecki and Rosenzweig, 2004; Lundholm and Richardson, 2010). They play crucial roles in adjusting the microclimate, eliminating noise, beautifying the

environment among other roles (Davis *et al*., 2008), thereby supporting the creation and construction of high-quality human settlements (Jim and Chen, 2006).

Studies have already documented significant negative correlations between land-surface temperatures and city-scale vegetation density (Zupancic *et al*., 2015). Apart from the impact of higher temperature, McCarthy and Pataki (2010) and Peters *et al*. (2010) have observed that in spite of the roles played by trees, they are subjected to a lot of hostilities by the urban centres. Some of such hostilities include high impervious surfaces, low soil moisture, soil compaction, deficiencies in nutrient and trace elements, toxicities, lack of rooting volume, frequent soil disturbance and air/water pollutants as well as high wind speeds in inner-city canyons.

Consequent upon the functions of vegetal cover, urban green spaces have become indispensable for proper functioning of the urban ecosystem (Byomkesh *et al.*, 2012) and in ameliorating the urban thermal environment. Greening of the urban environment has therefore been suggested as a stragegy for mitigating the human health implications of increasing urban temperatures (Alavipanah *et al*., 2015). This could be achieved through the provision of Green Infrastructure (GI). Norton *et al.* (2015) defined GI as "the network of designed and natural vegetation in cities and towns, such as public parks, recreation areas, residual vegetation, residential gardens, street trees, community gardens, and other innovative and emerging new urban greening technologies such as rain gardens, green roofs and green walls".

## 2.12 Review of Empirical Studies

### 2.12.1 Review of historic trends in LST/UHI studies

Initiatives in the scientific study of urban thermal environments could be attributed to the early observations by Luke Howard some two hundred years ago (Hebbert and Mackillop,

2013). In his classic work, Howard (1833) revealed that the climate of London was warmer than surrounding areas. His conclusion was drawn on the analysis of his daily recordings of the pressure, temperature, humidity, precipitation and evaporation at locations outside London from 1806 to 1830, a maintained diary of his observations and collated newspaper articles on any event of meteorological interest, as well as recorded meteorological data from the Royal Society in central London. Howard was not actually particular about the climate of the city of London, rather with climate generally as viewed from the vantage point of London. His interest in UHI was stimulated by the observed deviation between his recordings and those gathered at London's Royal Society.

Howard therefore identified UHI as the variation between the atmospheric temperature of the city and that of the rural environments ($\Delta$Tu-r) and hypothesized that this difference surges from the fringes of the city toward its centre, and particularly greatest during night-time of winter months. In Howard's analysis, four basic factors of UHI were pointed out namely: anthropogenic sources of heat, the geometry of the urban landscape, effects of urban roughness, and limited evaporation in the rural areas.

Howard's publications were followed by increased attention in urban climate studies from the 1930s to 1960s (Heisler and Brazel, 2010**).** However, after the second world war, particularly during environmental era of the 60s and 70s, there was an unprecedented rise in urban climate surveys (Heisler and Brazel, 2010**)**. The investigations simultaneously became less descriptive, rather they were more inclined towards numerical and hypothetical modeling, and became more consolidative and interdisciplinary (Brazel and Quatrocchi, 2005).

### 2.12.2 Empirical studies on land surface temperature in the US, Canada and Europe

Roth and Chow (2012) reviewed the work of Nieuwolt (1966) who documented a study of ambient temperature in Singapore by a team of university student scholars in 1984. The team combined measured dry ambient and wet bulb temperature records acquired from nine urban locations across southern Singapore over several days and compared the data simultaneous readings taken at Paya Lebar Airport, which was then located in a predominantly rural area 10 km northeast of the city centre. The study revealed that maximum daytime temperature was as high as 3.5°C, with the peak magnitudes recorded at the city's centre now the city's Central Business District (CBD) on days when 'the weather was fine, with occasional cloudiness but no precipitation. The study suggested that the temperature differences were attributed to increased radiation absorption and lower surface moisture in urban areas.

Oke (1973) demonstrated the relationship between the sizes of villages, towns or cities as determined by their number of inhabitants, and the degree of the UHIs they produce. He achieved this by analyzing information collected using automobile traverses in ten locations on the St. Lawrence Lowland with population sizes ranging between a thousand and two million residents. The outcome of the study showed an inverse relationship between the UHI under cloudless skies with the regional wind speed, and the logarithm of the population.

Block (1978) demonstrated the scientific validity of making use of air-borne and satellite TIR sensing as a technique for measuring the UHIs of selected towns/cities in eastern Nebraska (USA). The study revealed the superiority of these techniques over traditional temperature measurement techniques as it revealed many interlaced pockets of warm and cool areas that were previously undetected by conventional sensors.

Quattrochi and Luvall (1997) utilized 15- channel 5 metre resolution Advanced Thermal and Land Applications Sensor (ATLAS) airborne thermal infrared record of Alabama, Huntsville (USA) to investigate modifications in the temperature values of LULC during daytime and nighttime. At the same time, the work investigated the interrelationship between land-cover radiance and vegetation quantity, by assessing NDVI. The study revealed a strong inverse relationship between NDVI and radiance of inhabited lands , farmlands, and unused land-cover types, revealing that the radiance of land-cover types are significantly determined by the quantity of flora present. The predominance of forestlands, farmlands, and built-up surfaces associated with different levels of vegetal cover demonstrated noticeable differences with commercial facilities land-cover types in the city core, and supports the occurence of UHIs.

Benali *et al.* (2012) utilized a statistical approach to estimate maximum, minimum and average temperatures of Portugal over a 10 year period using remotely sensed LST data from MODIS and auxiliary data. The study employed an expanded technique with a mixed reboot and pocketknife re-sampling. The statistical models estimated average temperature with Model Efficiency (MEF) Index of 0.941 and a root mean square error (RMSE) of 1.33 °C. For the maximum and minimum temperatures, the best MEF achieved was 0.919 and 0.871, respectively, with a 1.83 and RMSE of 1.74 °C. The developed datasets provided weekly 1 km estimations and accurately described both the intra and inter annual temporal and spatial patterns of air temperature.

Shen *et al.* (2015) spatiotemporally explored the characteristics of urban temperatures of Saskatoon (SK), Canada using multitemporal remotely sensed information and historic *insitu* observations. The study involved several processes such as surface brightness retrieval, Pearson correlation, linear regression modelling, and buffer analysis applied on

different remotely sensed data. Result showed that both Landsat and MODIS datasets are capable of yielding obvious estimates of diurnal air temperature with a significant adjusted $R^2$ of 0.803 and 0.518 respectively at the spatial resolution of 120 metres and 1000 metres, respectively.

Findings of the study also revealed that the Saskatchewan River and urban green area demonstrated statistically significant cooling effects on the ambient urban surface temperatures within 500 m and 200m. In addition, a multiple linear regression model with four influential factors as independent variables can be developed to estimate urban surface temperatures with a highest adjusted $R^2$ of 0.649 and a lowest standard error of 0.076.

Simiarly, Landsat TM imagery has been largely employed in several other studies of heat island effects (Ifatimehin *et al*., 2009; Ifatimehin *et al*., 2010; Rehman *et al.*, 2015; Xie and Zhou, 2015; Kumar *et al.*, 2015; Chen *et al.*, 2016**,** Alhawiti and Mitsova, 2016) because it provides sufficient spatial resolution at 120 m for analyzing the sub-urban heat island at both local and micro levels. Alhawiti and Mitsova (2016) utilized Operational Land Imager (OLI) data over four time frames to analyze the relationship between urban thermal environments and urban land use in the City of Fort Lauderdale, located in Broward County, Florida's southeast coast. The study also computed Normalized Difference Vegetation Index and Normalized Difference Built-up Index and examined their correlations with LST for each land use. The results indicate that the highest maximum land surface temperature was observed in high density residential and commercial areas near the city's downtown while coastal areas and areas near water bodies were found to have lower land surface temperatures.

Morabito *et al*. (2018) used a replicable framework tagged "Building Thermal Functional Area" (BTFA) to carry out summer building-proxy thermal analyses of Parma, Northern Italy using remote sensing data. The study integrated daytime and nighttime ASTER images, the local urban cartography and the Italian imperviousness databases. For each residential building ($n$ = 8898), the BTFA was assessed and the correspondent ASTER-LST value and the imperviousness density were calculated.

Results of the study revealed that both daytime and nighttime surface temperature (ST) and BTFA significantly increased ($p < 0.001$) when high levels of imperviousness density surrounded the residential buildings, particularly during daytime and in densely urbanized areas. It also indicated that ST_BTFA differences between urban and park/rural areas were higher during nighttime (above 1 °C) than daytime (about 0.5 °C). The study therefore demonstrated its usefulness in identifying urban thermal hot-spots that would benefit most from mitigation responses.

Goddard and Tett (2019) estimated the effect of Urbanization on daily maximum and mini- mum temperatures in the United Kingdom. Urban fractions were calculated for 10 km × 10 km areas surrounding meteorological weather stations. The study utilized a robust linear regression to estimate relationship between urban fraction and temperature difference between station measurements and ERA-Interim reanalysis temperatures. The study shows that for an urban fraction of 1.0, the daily minimum 2-m temperature increased by 1.90 ± 0.88 K while the daily maximum temperature was not significantly affected by urbanization.

### 2.12.3 Empirical studies in land surface temperature in Asia and Middle East

Saaroni *et al*. (2000) studied the Surface UHI of Tel-Aviv, Israel using night-time radiant surface temperatures acquired by a thermal sensor installed on a helicopter, in combination with a number of on the ground and in-situ measurements including air temperatures acquired by automobile transects through the city and fixed location sensors on roof tops. The study revealed that while the inner city area had a higher air temperature than the city margins at night, it was cooler than that of a station that was based along the seashore (reversed during the day) due to the moderating effect of the ocean.

Chang *et al.* (2010) utilized Moderate Resolution Imaging Spectroradiometer (MODIS) satellite, images acquired by a high resolution airborne campaign and meteorological data to estimate the surface heat fluxes over a large portion of Chiayi urban area of Taiwan. The results indicated that surface heat fluxes determined from both airborne and satellite images were feasible for estimating surface heat flux. The correlation coefficient of surface heat fluxes with *in-situ* corresponding observations exceeded 0.80. The satellite-observed surface skin temperature and land surface energy fluxes were analyzed for different land cover types. For the urban surface which was rather dry, half of net radiation was converted to sensible heat flux for heating the surface, whereas over 90 percent net radiation was converted to latent heat flux for wet surfaces such as evergreen broadleaf or water. Surface heat flux was also proven to be an indicator of the magnitude of urban heat island effect.

Srivanit *et al.* (2012) assessed the urban area thermal characteristics of Bangkok metropolitan area (BMA) by investigating the relationships between the land surface temperature (LST) and the Normalized Difference Vegetation Index (NDVI), using Landsat imageries of 1994, 2000 and 2009**.** The study revealed that average surface

temperature (Mean±S.D.) in the BMA was about 26.01±5.89°C in 1994 increased to 37.76±2.84°C in 2000 and further to 39.79±2.91°C in 2009; leading to an intensified urban thermal effect in the urban area.

Joshi *et al*. (2015**)** carried out isotherm mapping of Ahmedabad City, Gujarat State, India using Geo-informatics technology. He combined data collected using in situ Infrared Gun for different time periods of the day at different administrative zones of the city from January to April, 2014 and Landsat TM data covering the city was acquired during the winter of January 2013 and the summer of April 2013.

Xiong *et al*. (2012) assessed the impacts of rapid urbanization on the thermal environment of Guangzhou, South China. The study utilized quantitative thermal remote sensing and spatial statistics techniques to establish relationships between UHI, LST, NDBI, and NDVI. It analyzed 1990, 2000, 2005 and 2009 Landsat TM/ETM+ images of the city in a bid to investigate the spatiotemporal variations in the land surface temperature (LST) over five land use/land cover types and over different urban/rural zones. It revealed an obvious existence of the UHI effect between 1990 and 2009, and showed that high temperature anomalies were closely related with built-up land and densely populated and heavily industrialized districts. It also shows that the mean LST difference between the urban downtown area and the suburban area were on average 0.88, 0.49, 0.90 and 1.16 K for 1990, 2000, 2005 and 2009 respectively at the 99.99percent confidence level. In addition, it showed a positive relationship between LST and NDBI, and a negative relationship between LST and NDVI.

Omran (2012) assessed the impact of land-use/land-cover change (LULCC) on surface temperature in the Ismailia Governorate, using Landsat images to quantify the changes from 1984 to 2011. The study identified six land-use/land-cover classes in the area

namely: urban, vegetation, waterlogged 1 and 2, bare land, and water with the highest overall accuracy and Kappa coefficient of 93.04 percent and 80.65 percent, respectively. The results revealed a notable land-use change in the study area. The study revealed a marked increase in built-up area during the 27 year period. It revealed that built-up area with temperature of 37.65˚C in 1984 and 43.876˚C in 2011; and Barren land with temperature of 37.34˚C in 1984 and 42.801˚C in 2011 exhibited the highest surface radiant temperature, while vegetated surfaces (28.73˚C in 1984 and 32.96˚C in 2011), water (25.94˚C in 1984 and 27.32˚C in 2011), waterlogged (34.54˚C in 1984 and 35.60˚C in 2011) recorded low radiant temperatures respectively.

Xie and Zhou (2015) assessed the impact of urbanization on urban heat island effect in Wuhan, China using Landsat Thermal imageries of 1987 and 2007. The study shows that Wuhan experienced rapid urban expansion from 1987 to 2007. While the areal extent with higher temperatures did not always correspond to the urbanized area, the percent impervious surface area (ISA) was found to efficiently explain the LST variation in urban areas, especially in high-density ones. The normalized difference vegetation index (NDVI) generated by the study was a sufficient indicator to express surface temperature variation only in natural context.

Ashraf (2015) investigated the temporal changes in surface temperature of Patna Municipal Corporation (PMC), India over a period of 25 years (1989 – 2014) using Remote Sensing and GIS Techniques. He employed spatiotemporal model and statistical techniques to determine the variations in Urban Heat Island (UHI) effect in the study area. The results show that the dense built up and commercial/residential areas had higher surface temperature in comparison with adjoining areas while the urban greens

(vegetation) were cooler. The study showed a strong correlation ($R^2$=0.742 between LST and Urban Heat Island with time.

Rehman *et al*. (2015) utilized a geospatial approach to analyze land surface temperature (LST) and Normalized Difference Vegetation Index (NDVI) in Keti Bunder, Sindh, Pakistan. Multi-date Landsat-5 TM Landsat-7 ETM+, and Landsat-8 OLI / TIRS satellite images of 2000, 2010 and 2014 respectively were utilized for the study. The study revealed a gradual increase in the maximum LST from 39°C in 2000, to 42°C in 2010 and 45°C in 2014. On the contrary, there was an increase in the mean NDVI value from (-0.165 in 2010 to - 0.009 in 2014, attributed to the growth of government-established mangroves plantations.

Kumar *et al.* (2015) studied urban surface temperature changes of Vijayawada City (India) by comparing remotely sensed Landsat satellite images of the study area in 2001 and 2014. The result indicates that the urban LST not only increased but the area with high temperature also increased significantly with a corresponding decrease in areas with low temperatures. It shows an increase in the areas of high temperature (30 to 39°C) from 31104.8 hectares in 2001 to 47502.2 hectares in 2014. In contrast the areas with low temperature range (24 to 30°C) decreased from 54410.9 hectares in 2001 to 38013.6 hectares in 2014.

Zhou *et al.* (2016) studied the spatiotemporal trends of urban heat island effect along the urban development intensity gradient (UDI) in 32 major Chinese cities from 2003 to 2012, utilizing Aqua MODIS data and Landsat TM/ETM+ images. The study revealed that daytime and night-time temperature increased significantly ($p < 0.05$, mostly in linear form) along a rising UDI for 27 and 30 out of 32 cities, respectively, with the south eastern and north western parts of the country experiencing more rapid increases. The study also

showed that trends in temperature change differed greatly by season and during daytime in particular; with the temperature increasing more rapidly in summer than in winter during the day and the reverse occurring at night for most cities. Inter-annually, temperature increased significantly in about one-third of the cities during both the day and night times from 2003 to 2012, especially in suburban areas ($0.25 < UDI \leq 0.5$).

Insignificant trends were however observed for most of the remaining cities. The study also established that temperature patterns along the UDI gradient were largely a function of local climate-vegetation conditions, while that across years were dominated by human activities. The study therefore showed that strong and highly diverse urbanization has effects on local climate cross China.

Chen *et al.* (2016) examined the effects of continuously expanding concretized anthropogenic urban surfaces on its thermal environment. They studied the spatiotemporal variation of the daily surface urban heat island (SUHI) in Shanghai from 1989 to 2013, which was a period of massive developmental changes in the metropolitan area. They utilized a set of remotely sensed Landsat data (TM and OLI) to derive the spatial patterns of Shanghai's LST). The derived LST pattern was further classified into five LST classes to examine the relative SUHI intensity level across the entire metropolis.

They also conducted spatial association and centroid movement analysis to establish the trends of LST changes at both local and holistic scales. The study further investigated the potential drivers for the present spatiotemporal variation of SUHI by analyzing different indicators such as land use change, population density, nocturnal light data, and vegetation and compared such with LST changes. Using the quantitative analysis and the socioeconomic context of the metropolis, the study identified the areas of rising LST,

proffered possible reasons for such variations, and districts that are most susceptible to extreme heat conditions were projected.

Chen *et al*. (2016b) simulated UHI in Guangzhou, China, utilizing the Weather Research and Forecasting (WRF) model coupled with an Urban Canopy Model (UCM) with new land-use data extracted from Remotely Sensed data. The simulations revealed that experiments with the extracted data have the potentials to reasonably reproduce majority of the observed temporal characteristics of the 2-m temperature, and can capture the characteristics of Urban Heat Island (UHI).

Makido *et al*. (2016) established the relationship between urban form and temperature moderation, by examining the spatial and temporal variation of air temperature throughout Doha (Qatar) by conducting vehicle traverses using highly resolved temperature and GPS data logs. They utilized Ordinary Least Squares (OLS), Regression Tree Analysis (RTA), and Random Forest (RF) statistical approaches to explain near-surface air temperatures using land cover variables. The predictions of the statistical models were validated by computing the Root Mean Square Error (RMSE). The study suggests that temporal variations in urban heat are mediated by different factors throughout the day. The average RMSE for OLS, RTA and RF is 1.25, 0.96, and 0.65 (in Celsius), respectively, suggesting that the RF is the best model for predicting near-surface air temperatures in Doha.

Liu *et al.* (2016) assessed the contribution of LCTs, vegetation fractional coverage (VFC) and percentage of impervious surface area (ISApercent) to urban surface energy fluxes using remote sensing. They utilized an advanced urban surface energy flux algorithm in combination with satellite images and meteorological data to investigate the thermal environments in the city of Suzhou, China. Multiple Endmember Spectral-

unmixing Analysis (MESMA) were used to retrieve the per-pixel sensible heat flux (H) and latent heat flux (LE) and the resultant heat fluxes were assessed using evaporation pan data collected from meteorological stations and ratios of the heat fluxes to the net radiation (Rn). They also investigated, spatial patterns of urban heat energy using an integrated analysis among LST, heat fluxes, LCTs, VFC and ISA percent.

The study revealed high values of sensible heat flux and LST over the urbanized areas, but low values for latent heat flux. Conversely, the vegetated area was characterized with high LEs but low LSTs and sensible heat flux. The study also revealed a statistically-significant correlation ($p < 0.05$; $R^2 = 0.88$) between LE and VFC at the zonal level, and a statistically-significant correlation ($p < 0.05$; $R^2 = 0.90$) between H and ISApercent.

Yang *et al.* (2017) mapped the influence of land use/land cover changes on the urban Heat Island Effect of Changchun. They examined Landsat data acquired in 1984, 1992, 2000, 2007, and 2014 to establish their spatio-temporal patterns. The results revealed dramatic changes in both land use / land cover and UHI patterns of the city over the 30 year period. It shows that the urban area grew more than four times from 143.15 km2 in 1984 to 577.45 km2 in 2014 while the percentage of UHI regions rose from 15.27percent in 1984 to 29.62percent in 2014. The study established that average LST of the city rose continuously consistent with the transformation in different land uses and land cover type into urban areas. It established a very strong positive relationship between LST with impervious surface area (ISA).

Ali *et al*. (2017) studied the spatial variation in the land surface temperature across specific zones in Bhopal city (India) in a bid to understand how the surface temperature varies with the spatial characteristics of the landscape. Mono Window Algorithm was used to extract LST from Landsat 8 TIRS imagery data. The study revealed that green

spaces had the lowest surface temperature of about 30.5°C in parks with dense tree cover and possessed highest mean normalized difference vegetation index value of about 0.5. The built up/barren areas on the other hand had surface temperature as high as 36.1 °C. The study reveals the correlation that exists between surface vegetation and surface temperature across the landscape of the city; as dense tree cover and land surface temperature exhibited a strong negative correlation, while decreased vegetation cover and successive increase in urban built up area were found to be related with high surface temperatures.

Chaithanya *et al.* (2017) estimated land surface temperature of Calicut City and Suburbs, India using Mono Window Algorithm from Landsat images of 2003, 2008 and 2015. The study classified the satellite data into land use categories such as vegetation, built up and water bodies; calculated land surface temperature; and derived NDVI of the study locations over the study period. The study revealed a gradual rise in LST from 2003 to 2015 owing to the decrease in urban vegetation as observed in the land use. They also found negative correlation between NDVI and LST.

Miles and Nansen (2017) assessed the UHI in 28 cities in northern West Siberia (NWS) utilizing MODIS MOD 11A2 land surface temperature (LST) 8-day composite product. The study demonstrated that all 28 cities exhibited a persistent UHI in both summer and winter. It also revealed differences in summer and winter regarding the UHI effect. Correlation analysis employed by the study revealed the strongest relationships between the UHI and population (log P)while regression models using log P alone explained 65–67 percent of the variability of UHIs in the region.

Kotharkar and Bagade (2018) utilized data collected from fixed station points and mobile traverse survey conducted during the month of December 2015 and February 2016 of

winter season to measure canopy layer heat island (CLHI) in a compact city of Nagpur, India using Local Climate Zone (LCZ) classification. The study also assessed the inter-LCZ temperature difference within the city and identified areas that require intervention in curbing heat island. The methodologies employed by the study include temperature buffer analysis, sensor lag determination, forecasting, outlier analysis and Pearson – correlation technique. The result reveals that during winter period the UHI intensity within built LCZ in the city ranges from 1.76 to 4.09 °C, with the compact low-rise LCZs at the urban core having warmer temperatures than other major LCZ in the inner areas of the city. It further reveals thermal variation between traditional LCZs and the LCZs with subclasses.

### 2.12.4 Empirical studies on land surface temperature in Africa

Odindi *et al.* (2015) quantified multi-seasonal heat contribution of major Land-Use-Land-Cover (LULC) within the Ethekwini Municipal Area (EMA), South Africa using Landsat 8 and MODIS Land Surface and Temperature (LST) data-sets. In order to assess the contribution of urban greenery as possible remedy to Urban Heat Island (UHI), major LULCs were grouped into four functional zones. Contribution Index (CI) was used to determine multi-seasonal heat contribution to the area. Results revealed that impervious surfaces were the major heat source while the green spaces were the major heat sinks. It also showed that the built-up/green spaces transition zones accounted for significantly lower heat contribution to the entire landscape; revealing the value of developing greenery mosaics within the often densely built-up urban areas. The study further demonstrates the value of remotely sensed data-sets in understanding the implication of LULC types on the urban micro-climate.

Aremu *et al*. (2017) utilized a time series of Landsat data from 1986 to 2014 to determine the urban growth and the intensity of urban heat island in Akure town (Nigeria). From the remotely sensed data, the study evaluated the spatial distribution of urban surface temperature and NDVI in the urban area. The study indicated that the greatest urban growth occurred in Akure South with 54.22 percent and 58.96 percent for 1986-1999 and 1999-2014 periods respectively. The study further revealed that greater growth occurred in the second period with a total of 60.20 km² compared to the total of 49.96 km² in the first period.

The study also demonstrated that urban growth over the entire study area had a yearly increase of 47.79 km². It showed that changes in LULC were accompanied by changes in NDVI and LST. In 1986, average NDVI (mean ± S.D.) in the non-built up area was 0.30 ± 0.07 and for the built-up area, it was 0.16 ± 0.09. However, this statistics reduced to 0.28 ± 0.06 and 0.13 ± 0.06 the non-built up area and the built-up area respectively in 1999. In 2014 the statistics was 0.24 ± 0.05 for non-built up and 0.06 ± 0.04 for built-up. It revealed that temperature in the non-built up area in 1986 was 24.01 ± 2.21 and 27.28 ± 1.12 for the built-up area but this difference increased to 26.52 ± 2.02 and 29.86 ± 1.66 for non-built up and the built-up respectively in 1999. Year 2014 saw a further increase to 31.48 ± 2.03 and 33.82 ± 1.07 respectively. Lastly, difference between the urban/built-up and non-built up significantly widened; leading to a higher intensity of UHI in the town.

Nse *et al*. (2020) examined land cover changes and the relationship with LST and NDVI in Uyo, Nigeria using multispectral Landsat imageries of the study area for the years 1986, 2000 and 2018. Maximum Likelihood Classification (MLC) algorithm to extract land cover classes. LST was derived using a single channel algorithm applied on the

imagery thermal bands, while the NDVI equation was employed in computing the NDVI of the imageries. Lastly, the relationship between land cover, LST and NDVI was evaluated using the Contribution Index (CI) and Pearson's Correlation analysis. The result shows that vegetation decreased from 278 $km^2$ in 1986 to 219 $km^2$ in 2018, wetlands declined from 20 $km^2$ to 17 $km^2$ during the period. Barren lands also declined from 33$km^2$ to 25$km^2$ while built-up areas increased from 69 $km^2$ to 139 $km^2$. Furthermore, the results shows that the mean LSTs in the city were 21.67 °C (1986), 25.40 °C (2000) and 26.04 °C (2018) with built up areas making the highest contribution to LST and the lowest was by vegetation. The study also revealed a high negative correlation between LST and NDVI at the three periods of study.

## 2.13 Review of Statistical Studies on Urban LST

Eliasson and Svensson (2003) statistically surveyed spatial air temperature variations in Göteborg, Sweden in relation to urban land use. The study utilized temperature data collected during an 18-month period at 30 sites in the city; a continuously updated land use/land cover data base of the town, the Master Plan of the city, and a separate site description analysis. The essence of the study was to investigate whether or not the temperature variations which revealed intra-urban air temperature differences of up to 9 °C in the urban district are statistically significant. The study applied two statistical methods; one stepwise multiple regression analysis and an analysis of variance test. Temperature anomalies, calculated as the temperature deviation at every station from the mean of all stations during each hour, were used in the statistical analysis. The multiple regression analysis was performed on monthly, seasonal and single day data sets to determine the relative effect of surface cover on the temperature pattern.

The results of the multiple regression analysis revealed that surface cover played an important role in governing air temperature differences in the area. The analysis of variance was carried out to test if the 12 land use classes contained in the Master Plan could be differentiated on the basis of temperature data. The results showed that only the air temperature deviations in land use classes, urban dense, multi-family and single houses, could be differentiated on a statistical basis.

The study also employed a site description analysis which includes a test of three methods using aerial or fish-eye photos for characterization of surface cover in the urban district. The results show statistically significant temperature variations between different land use/land cover categories on a diurnal basis and for all weather conditions.

Makido *et al*. (2016) examined the spatial and temporal variation of air temperature throughout Doha (Qatar). They acquired summer time near surface air temperature data across the city by means of vehicle traverses using highly resolved temperature and GPS data logs to determine spatial differences in summertime air temperatures. The study used three statistical approaches vis a viz  Ordinary Least Squares (OLS), Regression Tree Analysis (RTA), and Random Forest (RF). The study revealed that temporal variations in urban heat are mediated by different factors throughout the day. The average RMSE for OLS, RTA and RF is 1.25, 0.96, and 0.65 (in Celsius), respectively, suggesting that the RF is the best model for predicting near-surface air temperatures.

Silva *et al.* (2017) utilized statistical techniques to study the spatial and temporal variability patterns of the urban heat island (UHI) in the Metropolitan Area of Sao Paulo (MASP) using hourly temperature observations for a 10-year period (January 2002 to December 2011). The study used principal component analysis (PCA) and cluster analysis (CA) multivariate analysis techniques to determine the dominant modes of UHI

variability and to identify the homogeneity between the temperature observations in the area. The PCA method was employed in obtaining the spatial patterns and to define temporal variability. For the spatial patterns three major modes of variability were recognized; explained by 66.7 percent, 24.0 percent and 7.8 percent of the total variance in the air temperature.

The results revealed that the first and third PCAs were associated with wind movement in the area while the second which was related to the level of urbanization, the release of heat stored in the urban canopy and the release of heat by human sources was considered the most important mode. For the temporal variability, the PCA revealed two modes of variability explained by 49.4percent and 30.9percent of the total variance in the area. The result of the CA identified six homogeneous groups corresponding to the PCA patterns observed. The study further revealed that the standard UHI based on the scale and annual seasons for the period shows maximum values between 14:00 and 16:00 local time while minimum values were obtained between the hours of 07:00 and 09:00 local time.

# CHAPTER THREE

## 3.0 MATERIALS AND METHODS

### 3.1.1 Field surveys

A preliminary reconnaissance field visit was paid to the selected cities to garner firsthand information about the urban/suburban environments of the cities. Interactions with residents of the cities during the pre-field visit already indicated a rapid expansion of the cities and a somewhat higher temperature in recent times. A thorough field survey was then performed in all the cities under focus. The field surveys utilized a Global Positioning System (GPS) receiver to acquire needed geographic coordinates. Information acquired during the field survey was used for several purposes

The field survey was used to get acquainted with different LULC patterns in the study locations and was utilized in LULC classification procedure. Secondly, it was used to associate the ground-truth information of specific land use types with their imaging characteristics to enable image classification and production of land use maps. The recce provided information on anthropogenic activities within the cities and to obtain ancillary data like knowledge-based, existing land-use, and topographic maps. Office reconnaissance was also carried out on the selected city centres. This involved review of documented literatures, journals, information guides, and cadastral maps etc. related to each of the selected cities to develop a very sound knowledge base of the study centres.

### 3.1.2 Climatic data

Temperature data used for this study is daily ERA Interim (European Reanalysis) grid-based 2 metre above ground daily noontime maximum temperature ($^{o}$C) data products of the European Centre for Medium-Range Weather Forecasts (ECMWF) from 1990 to 2019. ERA-Interim is a global frequently used atmospheric reanalysis data. The spatial

resolution of the data set is approximately 80 km on a default grid size of 0.75° x 0.75° latitude/longitude but was projected on 0.125° x 0.125° (14km by 14km) latitude/longitude grid. Maximum temperature was used because; being an hourly data there was no significant variation between the minimum and maximum values of the same hour. The ERA-Interim data were downloaded at ECMWF website. The data points for each of the four cities are presented on Table 3.1

**Table 3.1** Temperature data coordinates for the surveyed cities

| City | Latitude | Longitude | Ecological Zone |
|---|---|---|---|
| Birnin Kebbi | 12° 22' 30" | 4° 22' 30" | Sudan |
| Kano | 12° 0' 00" | 8° 30' 00" | Sudan |
| Ibadan | 7° 22' 30" | 3° 52' 30" | Tropical Rainforest |
| Owerri | 5° 22' 30" | 6° 52' 30" | Tropical Rainforest |

**Source:** Author's work (2023)

The data utilized are those of 12:00hrs time-interval at 2m above the ground and step 12. ERA-Interim is a spatially and temporally complete data set of multiple variables at high spatial and temporal resolution, improved low-frequency variability and improved stratospheric circulation. The fair spatial distribution of the observation point justifies it adoption for interpolation between the non-observed points.

### 3.1.3 Satellite imageries

Remotely sensed Landsat satellite imageries were used for this study because of their relatively high spatial resolution and their ability to depict temperature variations in the heterogeneous urban/suburban environments. The datasets were also chosen on the basis of their quality, consistency, resolution, duration of program, time of observation, frequency of observation and availability. The datasets are freely available at the Global Visualization (Glovis), Earth Explorer and Global Land Cover Facility (GLCF) web

interfaces of the United States Geological Survey (USGS), which enable users to preview data for quality issues like presence of clouds, data loss or sensor introduced errors. Quality control by USGS includes resampling of the data, projection using the Universal Transverse Mercator (UTM) Projection System and WGS-84 datum, systematic radiometric correction along with geographic referencing, and topographic correction using Digital Elevation Models (DEM) from several official sources.

Cloud-free multi-temporal remotely sensed Landsat data sets were acquired for the work. Cloud-free imageries were utilized because clouds cause serious problems in optical wavelength remote sensing, since they do not only hide the ground but also cast their shadows on it thereby impeding many applications. The utilized data sets include Thematic Mapper (TM) imageries, Enhanced Thematic Mapper Plus (ETM+) imageries, and Operational Land Imager (OLI) imageries for the urban centres surveyed.

The spectral characteristics and the band resolution of Landsat data images are presented in Table 3.2. Landsat TM sensor which was onboard Landsat 4 and Landsat 5 satellite series has seven spectral bands with a spatial resolution of 30 metres for Bands 1 to 5 and 7. ETM+ sensor onboard Landsat 7 has eight spectral bands with a spatial resolution of 30 metres for Bands 1 to 7, and 15 metres resolution for Band 8 (panchromatic). The OLI and Thermal Infrared Sensor (TIRS**)** have nine spectral bands with a spatial resolution of 30 metres for Bands 1 to 7 and band 9. The spatial resolution for Band 8 (panchromatic) is 15 metres. Thermal bands (band 6 for Landsat TM and ETM+, and bands 10 and 11 for Landsat OLI) are useful in providing more accurate surface temperatures. The approximate scene dimension of all Landsat series is 170 km north-south by 183 km east-west. The approximate area coverage of each Landsat scene is 31,110 kilometres square.

**Table 3.2 The Band Characteristics of the Landsat Satellite Data**

| | Bands | Wavelength (micrometres) | Resolution (metres) |
|---|---|---|---|
| **Landsat 4 and 5 Thematic Mapper(TM)** | Band 1 – Blue | 0.45-0.52 | 30 |
| | Band 2 – Green | 0.52-0.60 | 30 |
| | Band 3 – Red | 0.63-0.69 | 30 |
| | Band 4 - Near Infrared (NIR) | 0.76-0.90 | 30 |
| | Band 5 - Shortwave Infrared (SWIR) 1 | 1.55-1.75 | 30 |
| | Band 6 – Thermal | 10.40-12.50 | 120* (30) |
| | Band 7 - Shortwave Infrared (SWIR) 2 | 2.08-2.35 | 30 |
| | * TM Band 6 was acquired at 120-metres resolution, but products are resampled to 30-metres pixels. | | |
| **Landsat 7 Enhanced Thematic Mapper Plus (ETM+)** | Band 1 – Blue | 0.45-0.52 | 30 |
| | Band 2 – Green | 0.52-0.60 | 30 |
| | Band 3 – Red | 0.63-0.69 | 30 |
| | Band 4 - Near Infrared (NIR) | 0.77-0.90 | 30 |
| | Band 5 - Shortwave Infrared (SWIR) 1 | 1.55-1.75 | 30 |
| | Band 6 – Thermal | 10.40-12.50 | 60 * (30) |
| | Band 7 - Shortwave Infrared (SWIR) 2 | 2.09-2.35 | 30 |
| | Band 8 – Panchromatic | .52-.90 | 15 |
| | * ETM+ Band 6 is acquired at 60-meter resolution, but products are resampled to 30-metres pixels. | | |
| **Landsat 8 Operational Land Imager (OLI) and Thermal Infrared Sensor(TIRS)** | Band 1 - Ultra Blue (coastal/aerosol) | 0.43 - 0.45 | 30 |
| | Band 2 – Blue | 0.45 - 0.51 | 30 |
| | Band 3 – Green | 0.53 - 0.59 | 30 |
| | Band 4 – Red | 0.64 - 0.67 | 30 |
| | Band 5 - Near Infrared (NIR) | 0.85 - 0.88 | 30 |
| | Band 6 - Shortwave Infrared (SWIR) 1 | 1.57 - 1.65 | 30 |
| | Band 7 - Shortwave Infrared (SWIR) 2 | 2.11 - 2.29 | 30 |
| | Band 8 – Panchromatic | 0.50 - 0.68 | 15 |
| | Band 9 – Cirrus | 1.36 - 1.38 | 30 |
| | Band 10 - Thermal Infrared (TIRS) 1 | 10.60 - 11.19 | 100 * (30) |
| | Band 11 - Thermal Infrared (TIRS) 2 | 11.50 - 12.51 | 100 * (30) |
| | *TIRS bands are acquired at 100 meter resolution, but are resampled to 30 meter in delivered data product. | | |

**Source:** USGS (2016)

The Landsat satellite images were ortho-rectified/georeferenced L2T (terrain corrected) products from source. However, the geometric accuracy was verified by overlaying and comparing with existing maps. Coordinate system verification and projection to Universal UTM Zone 32, WGS 1984, Minna Datum was ascertained. The data were used to map the LULC of the surveyed cities during the period under review. The thermal bands (band

6 for TM, and ETM+ or Bands 10 and 11 for OLI) were used to assess the thermal properties of land surfaces (i.e. LST) in the surveyed urban centres. The thermal bands were also used to elucidate multi-temporal and multi-spatial variations of thermal properties of land in the surveyed urban centres. The study adopted decadal intervals (1990, 2000, 2010, and 2019) due to the unprecedented urbanization witnessed in urban centres in the developing countries over the last four decades. However, due to the non-availability of useful imageries for Ibadan in 2000 and 2010, and Kano in 1990, 2000 and 2010, satellite imageries of the succeeding years (1991, 2001 and 2011) were used.

In addition, no satellite image was obtained during the wet season between April and October due to the presence of clouds which limit the radiometric resolution and consequently, their usability. Available Landsat data sets which were available, sourced and used for the study are presented in Table 3.3.

**Table 3.3 Landsat Image Datasets**

| S/N | Location | Data Source | Path | Row | Acquisition Data |
|---|---|---|---|---|---|
| 1. | Birnin Kebbi | Landsat TM | 191 | 051 | 16th October, 1990 |
| | | Landsat ETM+ | | | 3rd October, 2000 |
| | | Landsat ETM+ | | | 15th October, 2010 |
| | | Landsat OLI | | | 16th October, 2019 |
| 2. | Owerri | Landsat TM | 188 | 056 | 12th December, 1990 |
| | | Landsat ETM+ | | | 17th December, 2000 |
| | | Landsat ETM+ | | | 16th December, 2010 |
| | | Landsat OLI | | | 3rd February, 2019 |
| 3. | Ibadan | Landsat TM | 191 | 055 | 27th December, 1991 |
| | | Landsat ETM+ | | | 7th March, 2000 |
| | | Landsat ETM+ | | | 3rd January, 2011 |
| | | Landsat OLI | | | 1st January, 2019 |
| 4. | Kano | Landsat TM | 188 | 052 | 11th November, 1991 |
| | | Landsat ETM+ | | | 13th October, 2001 |
| | | Landsat ETM+ | | | 29th October, 2011 |
| | | Landsat OLI | | | 25th October, 2019 |

**Source:** Author (2023)

### 3.2.4 Software components

Basically three (3) main softwares were used for this study namely:

**(a) Idrisi Terrset version 18.21**

This is an integrated software system used for the analysis and display of spatial data. It includes tools for GIS analysis, image processing, surface analysis, vertical applications for land change analysis, earth trend modeler, climate change and adaptation modeler, ecosystem services and more. The software also includes a comprehensive suite of image processing tools; making it an excellent choice for land cover mapping application with remotely –sensed data which is an important aspect of this study. Tools are also provided for image restoration, enhancement, classification and transformation. The software also provides a host of machine learning tools, among which include artificial neural network classifiers, maximum likelihood classier, and land change and time series analysis most of which were utilized for this study.

**(b) ArcMap 10.8**

ArcMap 10.8 was used in producing National, State and Local government boundary maps of the study area and to extract the study area from each satellite scene and thereafter exported to Idrisi for further image analysis. ArcGIS is both vector and raster based software designed by ESRI. It provides a scalable framework for implementing GIS (Geographic Information System) for users. ArcGIS is an integrated family of GIS software products for building a complete GIS. More specifically, modules such as Arc-Map, Arc-Catalogue and spatial analysis were used in digitl image processing. The software was also used for LST mapping, as well as computation of NDVI and NDBI. The software was also used for the embellishment of images that were processed in the Idrisi environment due to its greater flexibility and choice of tools.

**(c) Microsoft Excel**

This is a flexible statistical and data management tool. It was used to generate tabulated report, charts, trends and descriptive display and analysis.

## 3.2 Methodology for Data Analysis

### 3.2.1 Methodology for achieving objective 1

#### *3.2.1.1 Importing the image into processing softwares*

All the required satellite images (TM, ETM+ and Landsat OLI) were imported into the ArcGIS software to create sub-scenes covering the urban areas and fringes of the surveyed urban centres, using the shape files of each urban centre. The subset images were then imported into the Idrisi Terrset for further processing such as LULC trend mapping/classification, LST mapping, as well as computation of NDVI and NDBI. The final outputs from these softwares were re-imported into ArcGIS for final editing. Details of the methodology are shown in Figure 3.1

#### *3.2.1.2 Image enhancement*

Image enhancement processes are employed to improve the appearance of images or convert them to formats better suited for analysis by a human or a machine. Image enhancement techniques are used to improve the appearance of certain features by modifying the colours or intensities. Two image enhancement techniques were employed to improve the quality of the satellite images that were processed and analyzed. The techniques are contrast stretching and Histogram equalization.

Contrast refers to the difference between the intensity of two adjacent pixels in an image. Low- contrast images emerged from non-uniform lighting conditions, non-linearity or small dynamic range of the imaging sensor. Contrast stretching focuses on improving the

contrast in an image by `stretching' its range of intensity values to span a desired or permissible range.

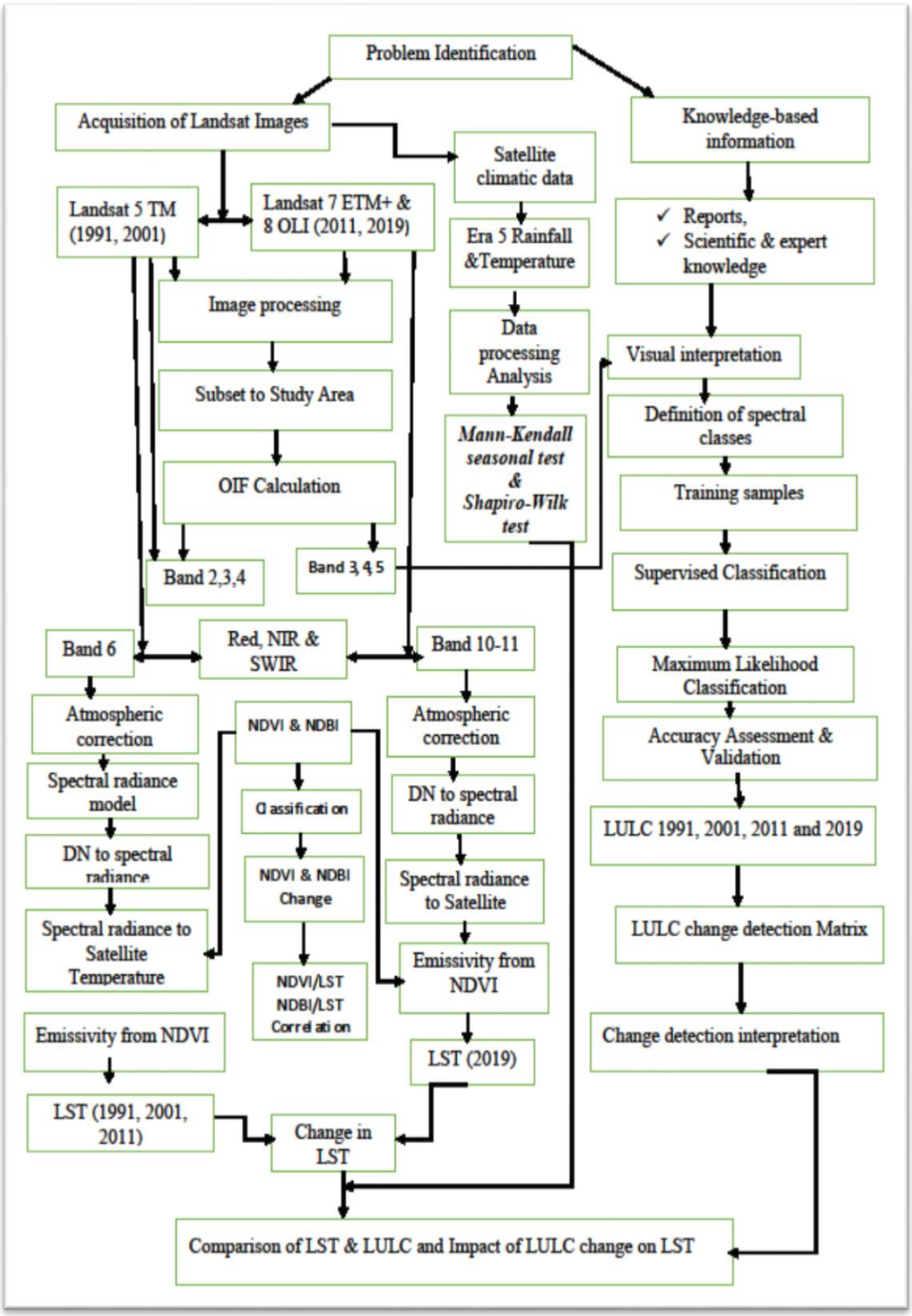


**Figure 3.1** Work Flow Chart
**Source:** Author (2023)

It equalizes the contrast throughout the image via simultaneous adjustment of each grey value at the darkest and lightest portions, thereby promoting the visualization of the details and structure of the very light or dark regions. It differs from the other algorithms in that it only applies a linear scaling function to the image pixel values resulting in a less harsh result. Prior to stretching, the upper and lower pixel value limits over which the image is to be normalized will be specified.

Histogram equalization is a very common technique for enhancing the images. Histogram equalization stretches the histogram across the entire spectrum of pixels (0 – 255). It increases the contrast of images for the finality of human inspection and can be applied to normalize illumination variations in image understanding problems (Shukla *et al*., 2017). It is one of the operations that are applied in obtaining new images based on histogram specification or modification (Shukla *et al*., 2017). Generally, histogram equalization preserves the image details such that both global and local contrasts are enhanced with minimum distortion in the image appearance (Iwasokun and Akinyokun, 2014).

#### *3.2.1.3 Layer stacking or image compositing*

To further enhance the images for easy identification of land surface features, the TM and ETM+ satellite images were displayed in False Color Composite (FCC) that is a combination of band (4,3,2) while those of OLI were displayed in 5,3,2 combination because it produces superior results due to the sensitivity of band 4 and 3 to vegetal cover and sensitivity of band 4 to water contents. The FCC provides better visualization and identification of built up areas, bare lands, vegetation, and farm land. The 2019 images were rescaled from sixteen (16) to eight such that it could correlate with the 1990, 2000 and 2010 images.

### *3.2.1.4 Creation of training sites for image classification*

The first operation was the sub-setting of the imageries by using boundary file of Area of interest (AOI) to extract the study area from the entire satellite image scene, this is because a single scene of Landsat image covers 170km by 185km and 16km radius. Thus, the major reasons for this operation was to define the study area more precisely, reduce file size, reduce processing time, and reduced storage space. Creation of training sites or Areas Of Interest (AOI) were carried out as pre-classification exercise on the layer stacked images. The next step towards achieving this is by developing spectral signatures from specified locations in the image.

The ground-truthing experience, geographical coordinates taken during the field visit, and high resolution google earth images were used in developing the spectral signatures. These specified locations were given the generic name 'training sites' and were defined by the user. Generally, vector layers were digitized over the raster scenes. The vector layers consisted of various polygons overlaying different land use types.

The LULC categories of interest in this study include forest cover; light vegetation; bare surfaces; built up areas; agricultural lands; and water bodies. Details of the classification scheme in the study are presented in Table 3.4. Multiple polygons were created for each land use category to help ensure that the software has sufficient information to create the spectral signatures. The training sites helped the Idrisi software develop spectral signatures for the outlined areas.

### *3.2.1.5 Image classification*

The multi-temporal images were classified into the desired six classes. The essence of classification was to categorize all pixels in a digital image into one of several land cover classes or themes. These categorized data were then used to produce thematic maps of

the land cover present in an image. Layer stacked multispectral data were used to perform the classification and the spectral pattern present within the data for each pixel was used as the numerical basis for categorization. The objective of image classification is to identify and portray as unique colours, the features occurring in an image in terms of the object or type of land cover these features actually represent on the ground. The training sites or ROIs already generated were used for the image classification exercise.

**Table 3.4 Classification Scheme Used for this Study**

| S/N | Class | Description |
|---|---|---|
| 1 | River/ water bodies | Open water features such as rivers, streams, lakes and reservoirs, permanent open water, ponds, canals, permanent/seasonal wetlands, low-lying areas, marshy land, and swamps. |
| 2 | Built-up | Areas under urban and rural built-up including homestead areas. All infrastructure—residential, commercial, mixed use industrial areas, villages, settlements, road network, pavements, and man-made structures. |
| 3 | Forest cover | Area cover with thick vegetation |
| 4 | Bare surfaces | Open land devoid of vegetation |
| 5 | Farmland/Agricultural lands | Fallow land, earth and sand land in-fillings, construction sites, developed land, excavation sites, open space, bare soils, and the remaining land cover types. |
| 6 | Light Vegetation | Trees, natural vegetation, mixed forest, gardens, parks and playgrounds, grassland, vegetated lands, agricultural lands, and crop fields. |

**Source: Author's Analysis (2023)**

Supervised classification was done on the images. Unlike unsupervised classification where the groupings of pixels with common characteristics are based on the software analysis of an image without the user providing sample classes, in supervised classification, a user selects sample pixels in an image that are representatives of specific classes and then directs the image processing software to use these training sites as references for the classification of all other pixels in the image. In this study, the created areas of interest were used by the image processing software to develop a statistical characterization of the reflectance (signature analysis) for each information class.

Maximum likelihood supervised classifier algorithm of the Idrisi Terrset was used for classifying the images into classes using the training sites already established on the images. The algorithm served as a statistical decision criterion to assist in the classification of overlapping signatures by assigning pixels to the class of highest probability. The maximum likelihood classifier was chosen because it is considered to give more accurate results than other hard classifiers since its procedure assumes that each training class in each band is normally distributed (Gaussian). Idrisi carries out maximum likelihood classification by calculating the following discriminant functions for each pixel in the image (Richards, 1999):

$$g_i(x) = 1n\, p(\omega_i) - {}^1/_2\, 1n\, |\sum_i| - {}^1/_2 (x - m_i)^T \sum_i^{-1} (x - m_i) \qquad (3.1)$$

Where:

$i$ = class

$x$ = $n$-dimensional data (where $n$ is the number of bands)

$p(\omega_i)$ = probability that class $\omega_i$ occurs in the image and is assumed the same for all classes

$|\Sigma_i|$ = determinant of the covariance matrix of the data in class $\omega_i$

$\Sigma_i^{-1}$ = its inverse matrix

$m_i$ = mean vector

The Idrisi software was chosen because the processes involved in the classification are less complicated. It has been effectively and widely employed in Digital Image Processing (DIP). Its algorithm for carrying out accuracy assessment of the classified images is also quite simple and straight forward. Field observations and site visits were done to aid in correlating the LST against the land cover categories. Also, high resolution google earth images were employed in enhancing the accuracy of the classification

exercise. The statistical coverage of the classes were extracted from the software and used to derive percentage changes calculated after Bissadu (2015) as follows:

$$\text{Percentage change} = \frac{\text{observe change}}{\text{sum of chnge}} \times 100 \quad (3.2)$$

The classification results were utilized in correlating the land surface temperatures with the existing land cover to accurately classify and map the land cover categories. Field observations and site visits were done to aid in correlating the LST against the land cover categories.

#### *3.2.1.6 Accuracy assessment*

Accuracy assessment otherwise known as thematic accuracy was performed on each of the classified images. This was achieved using the function of accuracy in the processing software. An accuracy assessment is carried out by determining a confusion matrix, which establishes relationships between the mapped class label and that observed on the ground or reference data for a sample of cases at specific locations. The overall accuracy is determined by dividing the number of correctly classified pixels by the total number of reference pixels. It is the most suitable technique for calculating accuracy assessment.

The Kappa coefficient of agreement is utilized in improving the overall accuracy. It it is used in expressing the proportional reduction in error generated by a classifier compared to the error in an entire random classification (Al-Ahmadi and Hames, 2009). In an error matrix, the producer's accuracy is the ratio calculated by the number of correctly classified pixels in one class divided by the total number of referenced pixels of this class. On the other hand, the user's accuracy refers to the ratio which is calculated by the number of correct classified pixels in one class divided by the total number of classified pixels in this class. The overall classification accuracy is calculated by the number of correct

classified pixels divided by the total number of classified pixels. The kappa coefficient is often used for estimating the accuracy of the classification (Bakr *et al.*, 2010). The Kappa values such as: 0.80 (i.e., 80 percent) represents strong agreement; 0.40 and 0.80 (i.e., 40–80 percent) represent moderate agreement; and a value below 0.40 (i.e., 40 percent) represent poor agreement (Congalton and Ross, 1999).

#### *3.2.1.7 Post classification LULC change detection*

After classification of imageries for the individual years and carrying out accuracy assessment of each classified image in Idrisi environment, change detection was carried out in ArcGIS environment. The change detection was carried out in two phases namely; change detection by area calculation and change detection by nature.

Three steps were utilized for determining change detection. The first step was to calculate the magnitude of change, by subtracting observed change of each period of years from the previous years. The second step was to calculate the trends through subtracting the percentage of the previous land use from the recent land use and dividing by the previous land use and multiplying by 100 (B-A/Ax100). The last step was to calculate the annual rate of change by dividing the percentage change by 100 and multiplying by the number of the study years, that is 30 years (199-2019).

The nature of change was derived through map overlay. The four classified imageries for each study location were exported to ArcGIS in TIF (Geo Tiff) format TIFF, overlayed and analyzed in ArcMap. The areas of the classified LULC in each image were then calculated using the area module of the ArcMap in generating the magnitude, trends and percentage change of each of the classes in each image.

### *3.2.1.8 Computation of normalized difference vegetation index (NDVI)*

The NDVI, which is the most commonly used satellite-based measure of vegetated regions is used for determining the vigour or health of vegetation/vegetation abundance. It was calculated to estimate the relationship between LST and vegetation for all the cities being investigated. NDVI makes it possible to compare images over time to assess ecologically significant changes. The formula for computing NDVI after Qin *et al*. (2004) is given below:

$$\text{NDVI} = \frac{\text{NIR} - \text{RED}}{\text{NIR} + \text{RED}} \tag{3.3}$$

Where $NIR$ and $RED$ are reflectances in the near-infrared band (0.76-0.90$\mu m$) and the red band (0.63-0.69 μm) respectively for Landsat TM, ETM+ and OLI.

NDVI values range between -1 and 1 with vegetated areas generally yielding high values due to their relatively higher near-infrared reflectances and low reflectances in the visible. In contrast, water, clouds, and snow possess higher reflectance potentials in the visible range than near-infrared reflectance and thereby yield negative index values. The equation was adopted because of its wide usage arising from its advantages, such as lower influence of atmospheric variations, its high sensitivity to chlorophyll, reduced noise through normalization between −1 and +1, as well as the possibility to assess and monitor ecologically significant seasonal changes (Ogashawara and Bastos, 2012).

The Multi-temporal NDVI layers for all the cities were re-classified using the mean-standard deviation method after Bozorgi and Nejadkoorki (2019). Accordingly, the NDVI layers were grouped into five interval classes namely: the low NDVI, secondary low-NDVI, medium NDVI, secondary high-NDVI, and high NDVI areas (Table 3.5).

**Table 3.5 Threshold values for NDVI Classes**

| NDVI classification | Category interval |
|---|---|
| High NDVI area | Ts>μ+std |
| Secondary high NDVI area | μ+0.5std<Ts ≤ μ+std |
| Medium NDVI area | μ-0.5std ≤ Ts ≤ μ+0.5std |
| Secondary low NDVI area | μ-std ≤ Ts<μ-0.5std |
| Low NDVI area | Ts<μ-std |

**Source: Author's Analysis, 2023**

Where:

Ts = Normalized NDVI Value
μ = Mean
std Standard Deviation

### *3.2.1.9 Computation of normalized difference built-up index (NDBI)*

The NDBI is a useful measure of the intensity of imperviousness using satellite data (Bhatti and Tripathi, 2014) It was computed for all the selected cities. This index was initially developed for use in bands 4-5 of Landsat TM imagery but has worked accurately with with successive Landsat series or other multi-temporal sensors. NDBI is useful in highlighting the distribution of urban surfaces due to their typically higher reflectances in the short-wave infrared band in comparison with the near-infrared band. It was calculated using the following Equation by Limin and George (2003).

$$\text{NDBI} = \frac{\text{SWIR} - \text{NIR}}{\text{SWIR} + \text{NIR}} \quad (3.4)$$

Where

$SWIR$ is the short-wave infrared band ranging from 1.57 - 1.65$\mu m$, while $NIR$ is the near-infrared band ranging from 0.85 to 0.88$\mu m$.

The Multi-temporal NDBI layers for all the cities were re-classified using the mean-standard deviation method after Bozorgi and Nejadkoorki (2019). Accordingly, the NDBI

layers were characterized into five interval classes namely: the low NDBI, secondary low-NDBI, medium NDBI, secondary high-NDBI, and high NDBI areas (Table 3.6).

**Table 3.6 Threshold values for** NDBI Classes

| NDBI classification | Category interval |
|---|---|
| High NDBI area | $Ts>\mu+std$ |
| Secondary high NDBI area | $\mu+0.5std<Ts\leq\mu+std$ |
| Medium NDBI area | $\mu-0.5std\leq Ts\leq\mu+0.5std$ |
| Secondary low NDBI area | $\mu-std\leq Ts<\mu-0.5std$ |
| Low NDBI area | $Ts<\mu-std$ |

**Source: Author's Analysis, 2023**

Where:

Ts = Normalized NDBI Value
$\mu$ = Mean
std Standard Deviation

### 3.2.2 Methodology for achieving objective 2

Temperature data was downloaded in Network Common Data Form (NetCDF) format but were extracted for the four study cities using the Grid Analysis and Display System (*GrADS*) software into Comma Separated Values (CSVs). To detect the trend and seasonality in the maximum noon-time temperature for the four selected cities in the two ecological zones of Nigeria, non-parametric Mann-Kendall trend and seasonal trend tests were done. To achieve these, statistical properties of the data were first determined through graphical examination of the data; using time plots, boxplots, density plots and Q-Q plots. In addition, the normality test of Shapiro-Wilk (S-W test) was applied. Pettitt test was employed in testing for single change-point detection in the temperature series. The brief discussions of the statistics are as follows:

#### *3.2.2.1 Shapiro-Wilk test for normality*

The Shapiro-Wilk test is a powerful test for verifying if climatic data series are normally distributed (Shapiro, 1980; Gilbert, 1987). In recent times, Shapiro-Wilk test has become

highly preferred because of its good power properties as compared to a wide range of alternatives (Mendes and Pala, 2003). The S-W test is similar to computing correlations between the quantiles of the standard normal distribution and ordered data points of the climatic series. The null hypothesis assumes that the population follows a normal distribution while the alternative assumes that the population does not follow normal distribution. The test statistic equation by Shapiro and Wilk (1965) is given as follows:

$$SW = \frac{\left(\sum_{i=1}^{n} a_i y_{(i)}\right)^2}{\sum_{i=1}^{n}\left(y_i - \bar{y}\right)^2} \tag{3.5}$$

where, $y_{(i)}$ is the ordered sample values and $a_i$ is the constance generated from the means, variances and covariances of the order statistics of a sample of size (n) from a normally distributed population (Pearson and Hartley, 1972).

#### *3.2.2.2 Mann-Kendall trend test*

Mann-Kendall test is a non-parametric method which is widely employed to check the null hypothesis of no trend versus the alternative that there exists a monotonic increase or decrease in trend of a climatic time series data. The test statistic S is computed as follows:

$$S = \sum_{k=1}^{n-1}\sum_{j=k+1}^{n} \operatorname{sgn}\left(X_j - X_k\right) \tag{3.6}$$

$$\text{with } \operatorname{sgn}(x) = \begin{cases} 1 & if \quad x > 0 \\ 0 & if \quad x = 0 \\ -1 & if \quad x < 0 \end{cases}$$

The mean of S is E[S] =0 and the variance $\sigma^2$ is:

$$\sigma^2 = \frac{1}{18}\left( n(n-1)(2n+5) - \sum_{j=1}^{p} t_j (t_j - 1)(2t_j + 5) \right) \tag{3.7}$$

where $p$ is the number of the tied groups in the data set and $t_j$ is the number of data points in the $jth$ tied group. The statistic S is approximately normally distributed for data values greater than or equal to 10 and provided that the following Z-transformation is employed:

$$Z = \begin{cases} \dfrac{S-1}{\sigma} & if \quad x > 0 \\ 0 & if \quad x = 0 \\ \dfrac{S+1}{\sigma} & if \quad x < 0 \end{cases}$$

The significance of trend is usually measured using Z critical values. A positive Z value indicates rising or increasing trends while the negative Z value reveals downward or decreasing trends.

The statistic S is closely related to Kendall's $\tau$ as given as follows:

$$\tau = \frac{S}{D} \tag{3.8}$$

where

$$D = \left[ \frac{1}{2} n(n-1) - \frac{1}{2} \sum_{j=1}^{p} t_j (t_j - 1) \right]^{1/2} \left[ \frac{1}{2} n(n-1) \right]^{1/2}$$

#### *3.2.2.3 Sen's slope estimator*

A simple non-parametric technique to estimate the true slope, and an intercept, if a linear trend is present in a time series was developed by (Sen, 1968). The slope is calculated thus:

$$q_i = \frac{X_i - X_j}{i - j} \qquad i = 1,2,3,.\cdots, N \;\; j > k \tag{3.9}$$

for ( $(1 \le i < j \le n)$, where q is the slope, X denotes the variable, n is the number of data, and i, j are indices.

Sen's slope is then computed as the median from all slopes: b = median $q_i$ . The intercepts are calculated for each time (t) as given by:

$$a_t = X_t - bt \tag{3.10}$$

Also, the corresponding intercept, as well as the median of all intercepts.

The Sen's estimator of slope is the median of these N values of $q_i$ . The N values of $q_i$ are ranked from the smallest to the largest. The Sen's estimator is:

$$q = \begin{cases} q_{N+1/2} & if \quad N \; is \; odd \\ \frac{1}{2}\left( q_{N/2} + q_{N+1/2} \right) \end{cases}$$

A hundred $(1-\alpha)$ percent two-sided confidence interval about the slope estimate was obtained by the non-parametric technique based on the normal distribution.

#### *3.2.2.4 Pettitt's test for change-point detection*

The Pettitt test non-parametric test after Pettitt (1979), is used to detect a single change-point in climatic or hydrological series with continuous data. The null hypothesis assumed

that the observations followed one or more distributions that have the same location parameter (no change) while the alternative hypothesis assumed that there existed a change point. The ranks $r_1, r_2, \ldots\ldots\ldots\ldots, r_n$ of $x_1, x_2, \ldots\ldots\ldots\ldots, x_n$ were used to calculate the statistics:

$$U_{(k)} = 2\sum_{i=1}^{k} r_i - k(n+1), \qquad k = 1,2,\ldots\ldots\ldots\ldots, n$$

The test statistic is the maximum of the absolute value given as:

$$K_T = \max\left|U_{t,T}\right|, \tag{3.11}$$

where

$$U_{t,T} = \sum_{i=1}^{t}\sum_{j=t+1}^{T} \operatorname{sgn}(X_i - X_j)$$

The change-point of the series is located at $K_T$, provided that the statistic is significant. The significant probability of $K_T$ is approximated for $p \le 0.05$ with:

$$p \approx 2\exp\left(\frac{-6K_T^2}{T^3 + T^2}\right),$$

### *3.2.2.5 Mann-Kendall seasonal test*

The Mann-Kendall statistic for the gth season is given as follows:

$$S_g = \sum_{i=1}^{n-1}\sum_{j=i+1}^{n} \operatorname{sgn}\left(X_{jg} - X_{ig}\right) \qquad g = 1,2,\ldots., m$$

The mean of $S_g$ is $\mu_g = 0$ and the variance including the correction term for ties is:

$$\sigma_g^2 = \frac{1}{18}\left( n(n-1)(2n+5) - \sum_{j=1}^{p} t_{jg}(t_{jg}-1)(2t_{jg}+5) \right), \quad (1 \le g \le m)$$

According to Hirsch *et al.* (1982), seasonal Mann-Kendall statistic for the entire series is calculated as:

$$\hat{S} = \sum_{g=1}^{m} S_g \quad and \quad \hat{\sigma}_g^2 = \sum_{g=1}^{m} \sigma_g^2$$

The statistic $S_g$ is approximately normally distributed, with:

$$z_g = S_g / \sigma_g$$

If continuity=TRUE then a continuity correction will be employed:

$$z = \text{sgn}(S_g)(|S_g| - 1) / \sigma_g$$

### 3.2.3 Methodology for achieving objective 3

This objective was achieved by extracting LST from processed Landsat imageries. The universal single-channel (USC) algorithm was used for retrieving/investigating LST values from the thermal-infrared bands of Landsat Images, with the aid of ArcGIS application software. The LSTs were extracted from Landsat TM and ETM+ band 6, and Landsat 8 (OLI) band 10. Band 11 data of Landsat 8 TIR was not used because it is significantly more contaminated by stray light than Band 10 and is therefore not recommended for any quantitative analysis (USGS, 2016).

The Digital Numbers (DN) values for each image were converted to radiance, and radiance was further converted to reflectance. Emissivity was estimated from reflectance, and subsequently the emissivity corrected surface temperature; which served as part of atmospheric correction was derived. The formula for approximating the LST was then

inputted and the final output was the LST map for each of the stipulated years. The various steps and processes adopted have been detailed as follows:

### *3.2.3.1 Radiometric calibrations*

In order to minimise radiometric differences between images, the digital numbers of the Landsat images were converted to normalised atmospheric reflectance, using the equation by Trotter *et al*. (2017) as follows:

$$L_\lambda = \text{Gain} \times DN + \text{bias} \quad (3.12)$$

Where:

$L_\lambda$ = the normalised atmospheric reflectance (in Watts * m−2 * sr−1 * μm−1)
DN = Digital numbers of the Landsat images
Gain and Bias = conversion coefficients

### *3.2.3.2. Conversion to at-sensor spectral radiance ($Q_{cal} – L_\lambda$)*

Calculating At-Sensor spectral radiance is crucial in converting image data from multiple sensors and platforms into physically meaningful common radiometric scales (Chander and Markham, 2003). Radiometric calibration of the Landsat images encompasses rescaling of the digital numbers (Q) transmitted from the satellite to calibrated digital number ($Q_{cal}$), with same radiometric scaling for all scenes processed on the ground for a specific period. The Landsat image calibration formula was adapted from Chander and Markham (2003) and Chander *et al*. (2009) as folllows:

$$L_\lambda = \frac{LMAX\lambda - \text{LMIN}\lambda}{(QCalmax - Qcalmin)} (\text{Qcal} - \text{Qcalmin}) + \text{LMIN}\lambda \quad (3.13)$$

Or

$$L\lambda = Grescale \times Qcal + Brescale \quad (3.14)$$

Where:

$$Grescale = \left(\frac{LMAX\lambda - LMIN\lambda}{(QCalmax - Qcalmin)}\right)$$

$$Brescale = LMIN\lambda - \frac{LMAX\lambda - LMIN\lambda}{(QCalmax - Qcalmin)} Qcalmin$$

$L_\lambda$ = Spectral radiance at the sensor's aperture [W/ ($m^2$srμm)]
$Q_{cal}$ = Quantised calibrated pixel value (DN)
$Q_{calmin}$ = Minimum quantised calibrated pixel value corresponding to LMIN ($DN_\lambda$)
$Q_{calmax}$ = Maximum quantised calibrated pixel corresponding to LMAX ($DN_\lambda$)
$LMIN_\lambda$ = Spectral At-sensor radiance that is scaled to Qcalmin [W/ ($m^2$srμm)]
$LMAX_\lambda$ = Spectral At-sensor radiance that is scaled to Qcalmax [W/ ($m^2$srμm)]
$G_{rescale}$ = Band-specific rescaling gain factor [W/ ($m^2$srμm))/DN]
$B_{rescale}$ = Band-specific rescaling bias factor [W/ ($m^2$srμm)]

### *3.2.3.3 Conversion of radiance top of atmosphere (TOA) reflectance ($L_\lambda - \rho_\lambda$)*

This was done to achieve a reduction in scene-to-scene variability and this was achieved by converting the At-sensor spectral radiance to exo-atmospheric TOA reflectance, also known as in-band planetary albedo (Gallo *et al., 1993).* The TOA reflectance of the earth was computed using the equation by Chander and Markham (2003) and Chander *et al*. (2009).

$$\rho\lambda = \frac{\pi \bullet L\lambda \bullet d2}{ESUN\lambda \bullet \cos\Theta s} \quad (3.15)$$

Where;

$\rho\lambda$ = Planetary TOA reflectance (unitless)
$\pi$ = Mathematical constant approximately equal to 3.14159 (unitless)
$L_\lambda$ = Spectral radiance at the sensor's aperture [W/ ($m^2$srμm)]
d = Earth-sun distance (astronomical units)
$ESUN_\lambda$ = Mean exo-atmospheric solar irradiance [W/ $m^2$lam)]
$\Theta s$ = Solar zenith angle (degrees)

### *3.2.3.4 Conversion from at-sensor spectral radiance to land surface temperature ($L_\lambda$ - LST) or brightness temperatures*

The thermal bands data of Landsat 5, 7 and 8 were converted from At-sensor spectral radiance to effective Land Surface Temperature. The LST assumes that the earth surface

is a black body and includes atmospheric effects (absorption and emission along path). The LST uses the pre-launched calibration constants given by Plank's equation (Gallo *et al., 1993).* The conversion formula from the At-sensor spectral radiance to LST utilized is the one given by Chander and Markham (2003) and Chander *et al*. (2009) as follows:

$$LST = \frac{K2}{In\left(\frac{K1+E}{L\lambda}+1\right)} \quad (3.16)$$

Where:

| | | |
|---|---|---|
| LST | = | Land Surface Temperature (Kelvin) |
| $K_2$ | = | Calibration constant 2 (Kelvin) |
| $K_1$ | = | Calibration constant 1 [W/ ($m^2$srμm)] |
| $L\lambda$ | = | Spectral radiance at the sensor's aperture [W/ ($m^2$srμm)] |
| E | = | Emissivity corrected reflectance |
| In | = | Natural Logaritm |

Temperature values was converted from degree kelvin (K) to degree Celsius (°C) by subtracting 272.15 from the kelvin value, which is the conversion rate from kelvin to Celsius.

### *3.2.3.5 Re-classification of LST ranges*

To garner a better understanding of the SUHI intensity, which is the LST difference between the city centre and the surbubs, the multi-temporal LST layers for all the cities were re-classified using the mean-standard deviation method after Bozorgi and Nejadkoorki (2019). Accordingly, the LST layers were grouped into five interval classes namely: the low temperature, secondary low-temperature, medium temperature, secondary high-temperature, and high temperature (Table 3.7)

**3.7 Threshold values for classification of LST**

| Temperature classification | Category interval |
|---|---|
| High temperature area | Ts>μ+std |
| Secondary high temperature area | μ+0.5std<Ts ≤ μ+std |
| Medium temperature area | μ-0.5std ≤ Ts ≤ μ+0.5std |
| Secondary low temperature area | μ-std ≤ Ts<μ-0.5std |
| Low temperature area | Ts<μ-std |

**Source: Author's Analysis, 2023**

Where:

Ts = Normalized LST Value
μ = Mean
std Standard Deviation

The threshold values for the classification are indicated in Table 3.7. For instance**,** if a pixel's LST is lower than the mean LST, $\mu$, minus the standard deviation (std), then the heat intensity of this pixel will be classified as "low". The other threshold values will be $\mu$-std/3, $\mu$+std/3, and $\mu$+1std and $\geq$ $\mu$+1std for low, medium, high, and very high respectively.

The benefit of using mean value and standard deviation is that spatial differences of LST can be revealed regardless of the actual LST values which vary between different years.

### 3.2.4 Methodology for achieving objective 4

To achieve objective 4, statistics of the results of the analysed data in objective three for each city in the two ecological zones were extracted and compared using analytical charts.

### 3.2.5 Methodology for achieving objective 5

This was achieved by relating the results of the derived NDBI and NDVI in objective one with LST results of objective three. The Pearson Product Moment Correlation coefficient was performed for a relationship between the two variables. Pearson Product Moment Correlation coefficient as used by Mukaka (2012) is given as:

$$r = \frac{N\sum xy - \sum x \sum y}{\sqrt{[N\sum x^2 - (\sum x)^2][N\sum y^2 - (\sum y^2 - (\sum y)^2]}} \quad (3.17)$$

Where:

N = Number of pairs of scores
$\sum xy$ = Sum of pairs of scores
$\sum x$ = Sum of x Scores

$\sum y$ = Sum of y Scores

$\sum x^2$ = Sum of squared x scores

$\sum y^2$ = Sum of squared y scores

### 3.2.6 Methodology for achieving objective 6

To achieve objective 6, temperature values (in ℃) for each city were extracted randomly from the LST maps generated in objective three for each year and overlaid on the classified land use/land cover maps generated in objective one for each year.

# CHAPTER FOUR

# 4.0 RESULTS AND DISCUSSIONS

## 4.1 Landuse /Landcover trends of Ibadan, Owerri, Kano and Birnin Kebbi from 1990 to 2019

This section presents the results of the analysis of landuse/land cover changes, Normalized Difference Vegetation Index (NDVI) and Normalized Difference Built-up Index for the four cities from 1990 to 2019. The results are presented in sections 4.1.1 to 4.1.5.

### 4. 1.1 Landuse/ landcover (LULC) changes in Ibadan

#### *4.1.1.1 LULC trends in Ibadan from 1990 to 2019*

Results of the landuse/landcover classification of Ibadan in 1990 and 2019 are presented in Figures 4.1 - 4.3. Figures 4.1 and 4.2 are the classified images of 1990 and 2019 repectively while Figure 4.3 is the statistics of each LULC class. Classified maps of 2001 and 2011 shown in appendix B.

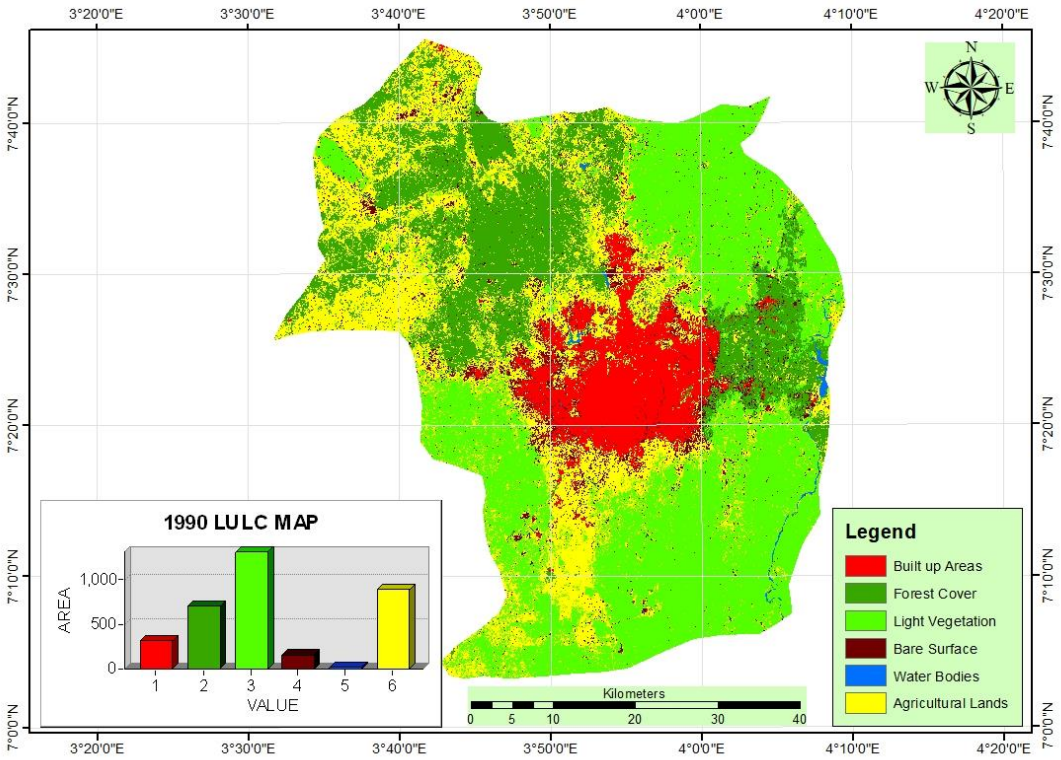


**Figure 4.1** Landuse/landcover of Ibadan Metropolis in 1990

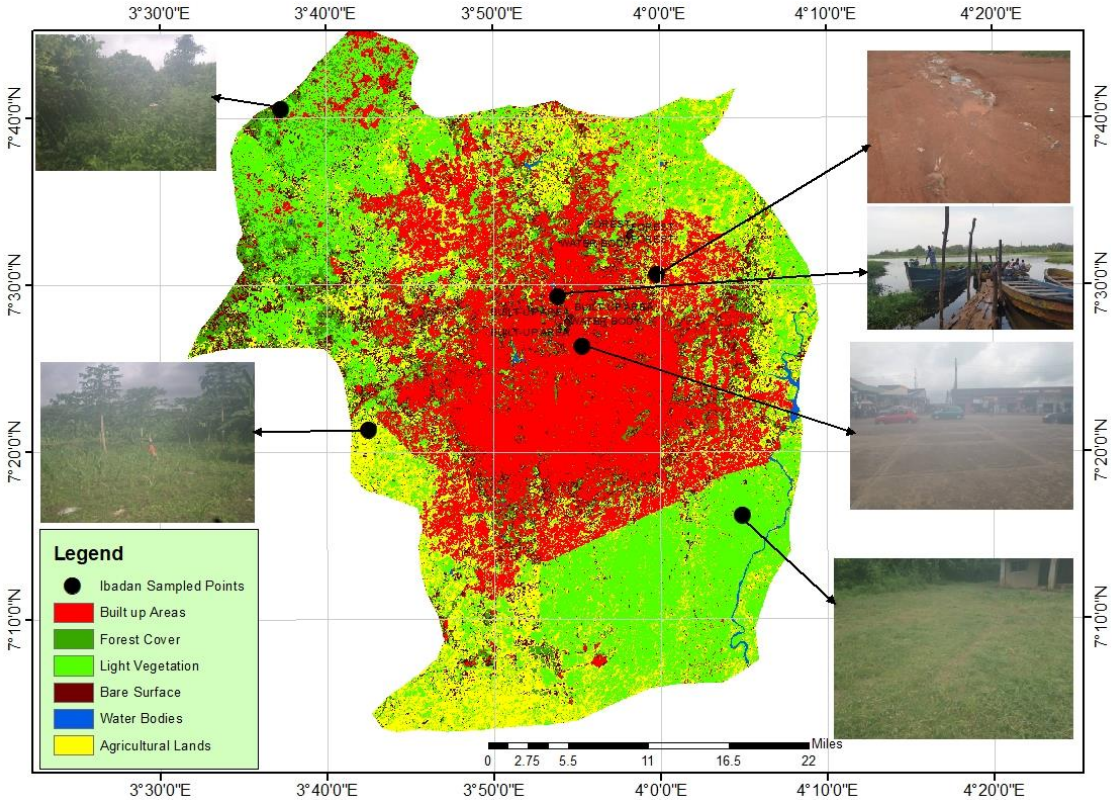


**Figure 4.2** Landuse/landcover of Ibadan Metropolis in 2019

Figure 4.3 revealed a progressive increase in built up areas from 1990 to 2019. It shows that in 1990 built up areas covered 312.90 km$^2$ and accounted for about 9.19 percent of the total coverage area. In 2001, it covered 479.45 km$^2$ and accounted for about 14.09 percent of the total area coverage.

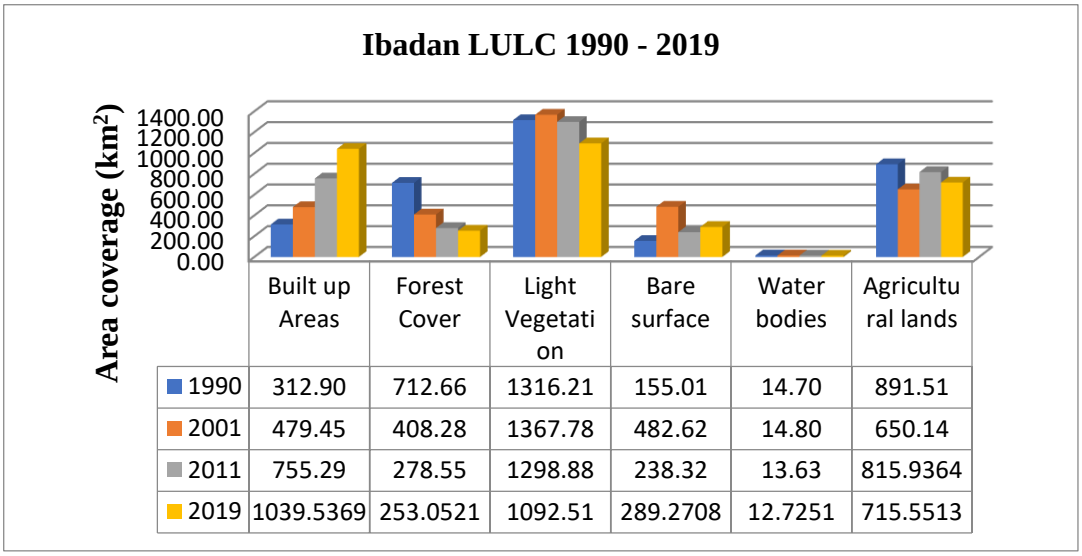


| | Built up Areas | Forest Cover | Light Vegetation | Bare surface | Water bodies | Agricultural lands |
|---|---|---|---|---|---|---|
| 1990 | 312.90 | 712.66 | 1316.21 | 155.01 | 14.70 | 891.51 |
| 2001 | 479.45 | 408.28 | 1367.78 | 482.62 | 14.80 | 650.14 |
| 2011 | 755.29 | 278.55 | 1298.88 | 238.32 | 13.63 | 815.9364 |
| 2019 | 1039.5369 | 253.0521 | 1092.51 | 289.2708 | 12.7251 | 715.5513 |

**Figure 4.3.** LULC of Ibadan 1990-2019

It further increased to 755.29 km$^2$ and accounted for about 22.21 percent of the total coverage in 2011, and finally, to 1,039.54 km$^2$ (30.55 percent) in 2019. The results are similar to those of Edobor and Bello (2017) whose study showed a progressive increase in built up from 107 km$^2$ in 1972 to 192 km$^2$ and 381 km$^2$ in 1986 and 2000 respectively. The rapid growth in built-up coverage may be attributed to the continuous increase in the population of the city occasioned by rural-urban and urban-urban migration as a result of perceived oppurtunities.

Ibadan has been acclaimed to be one of the rapidly expanding cities in Nigeria (Kasim *et al.*, 2020). Consequently, built-up areas seemed to have increased with corresponding decrease in vegetal cover; particularly forest cover, as well as other land cover classes. The growth in the built up area may be associated with increase in residential areas and human activities brought about by population growth. Mohammed *et al.* (2019) raised

concerns about the threat rapid increase in urban growth poses to urban green and blue spaces.

The result showed a progressive decrease in forest cover between 1990 and 2019. In 1990, forests covered an area of 712.66 $km^2$ and accounted for about 20.94 percent of the entire area. 1n 2001, forests covered an area of 408.28 $km^2$ and accounted for about 12 percent of the entire area. By 2011, forest cover had reduced to 278.55 $km^2$ (8.19 percent) of the entire area, while 2019 witnessed a further reduction in forest cover to 253.05 $km^2$ and accounted for about 7.44 percent of the entire area. The persistent decline in forest cover may suggest that agricultural lands and built up areas may have encroached on forest cover.

With the exception of 2001 which witnessed a higher coverage of light vegetation, Ibadan experienced continuous decrease in light vegetation from 1990 to 2019. Light vegetation occupied 1316.21 $km^2$ and accounted for 38.68 percent of the metropolitan area in 1990. In 2001, light vegetation increased and occupied 1367.78 $km^2$ (40.19 percent) of the metropolitan area. In 2001, light vegetation decreased to 1,298.88 $km^2$ (38.20 percent) of the metropolitan area and further decreased to 1,092.51 $km^2$ (32.11 percent) of the metropolitan area. The decrease in light vegetation may be attributable to expansion of built areas, conversion of land into farmlands, and firewood harvesting.

Bare surfaces did not exhibit any established pattern during the study period, nor was there any significant change. In 1990, they covered an area of 155.01 $km^2$ accounting for 4.56 percent of the land cover. In 2001, they covered an area of 482.62 $km^2$ (14.18 percent of the land cover) while in 2011, they covered an area of 238.32 $km^2$, accounting for 7.01 percent of the land cover. 1n 2019, bare surfaces covered an area of 289.27 $km^2$, accounting for 8.50 percent of the land cover. The absence of much change in bare surface

may be attributed to the fact that they consists largely of rock outcrops and exposed sand from the river bed which may only be visible in the absence of vegetation or water on the surface.

Water bodies occupied 14.70 $km^2$ (0.43 percent), 14.80 $km^2$ (0.43 percent), 13.63 $km^2$ (0.40 percent) and 12.73 $km^2$ (0.37 percent) of the land cover in 1990, 2001, 2011 and 2019 respectively.of the land cover in 1990. Thus water body did not experience any significant change throughout the study period. The slight decline in the percentage of water bodies may be attributed to encroachment on water bodies and wetlands by built surfaces. Agricultural lands covered 891.51 $km^2$, (26.20 percent), 650.14 $km^2$ (19.10 percent), 815.94 $km^2$ (23.99 percent) and 715.55 $km^2$ (21.03 percent) in 1990, 2001, 2011 and 2019 respectively. The seeming decrease in agricultural lands over the period may be attributed to annexation by built areas.

#### *4.1.1.2 Assessment of classification accuracy of LULC in Ibadan*

The accuracy of classification for the four periods of 1990, 2001, 2011 and 2019 for Ibadan showed an overall accuracy of 82.65 percent, 84.31 percent, 83.62 percent and 85.00 percent respectively (See Table 4.1). This was considered a decent overall accuracy and, therefore acceptable for the succeeding change detection and analysis. The user's accuracy for different land cover categories ranged between 62.03 percent and 92.00 percent while the producer's accuracy ranged between 68.49 percent and 90.99 percent.

The overall Kappa was also calculated for each of the classified maps to determine their accuracy. The results of the four periods 1990, 2001, 2011 and 2019 revealed Kappa statistics of 0.80, 0.84, 0.82 and 0.84 respectively. The Kappa coefficient for the four periods ranges from substantial agreement to almost perfect agreement on the kappa scale, an indication that it is usable.

#### *4.1.1.3 The magnitude and percentage change in LULC in Ibadan from 1990 to 2019*

The magnitude and percentage change in land use/land cover in Ibadan 1990 and 2019 are presented in Table 4.2, while those of 1990 – 2001, 2001 – 2011 and 2011 – 2019 respectively are shown in Appendix C1. Results showed that between 1990 and 2001, built up, increased in magnitude by 166.55km$^2$ (15.26 percent) at an annual change rate of 1.68 percent. between 2001 and 2011, built up increased in magnitude by 275. 84 km$^2$ (31.14 percent) at an annual change rate of 3.11 percent. Furthermore, between 2011 and 2019, built up areas in Ibadan increased in magnitude by 284.25 km$^2$ (42.53 percent) at an annual change rate of 3.40 percent. Generally, between 1990 and 2019, built up increased in magnitude by 726.64 km$^2$ (42.19 percent) from 312.90 km$^2$ in 1990 to 1039.54 km$^2$ in 2019 at an annual change rate of 12.24 percent (Table 4.2).

**Table 4.1 Classification Accuracy Assessment of Ibadan LULC Imageries (1990, 2001,2011 and 2019)**

| Class Name | 1990 | | 2001 | | 2011 | | 2019 | |
|---|---|---|---|---|---|---|---|---|
| | Producer's Accuracy (%) | User's Accuracy (%) | Producer's Accuracy (%) | User's Accuracy (%) | Producer's Accuracy (%) | User's Accuracy (%) | Producer's Accuracy (%) | User's Accuracy (%) |
| **Built-up areas** | 82.76 | 89.50 | 92.35 | 98.00 | 83.60 | 83.10 | 79.92 | 86.09 |
| **Forest cover** | 88.29 | 70.47 | 80.15 | 86.20 | 80.51 | 92.00 | 90.10 | 74.76 |
| **Light Vegetation** | 81.37 | 86.48 | 84.74 | 93.37 | 87.54 | 62.03 | 87.84 | 80.97 |
| **Bare Surface** | 80.21 | 78.61 | 93.20 | 86.01 | 84.31 | 85.5 | 75.78 | 87.65 |
| **Water Bodies** | 81.00 | 85.76 | 82.70 | 69.40 | 81.81 | 83.40 | 90.99 | 70.00 |
| **Agricultural lands** | 81.98 | 83.67 | 79.12 | 80.07 | 84.19 | 90.43 | 68.49 | 80.53 |
| **Overall Classification Accuracy (%)** | **82.65** | | **84.31** | | **83.62** | | **85.00** | |
| **Overall Kappa** | **0.801** | | **0.837** | | **0.823** | | **0.844** | |

**Source:** Author's Analysis (2023)

**Table 4.2 Magnitude and Percentage Change in LULCof Ibadan between 1990 and 2019**

| LULC Class | 1990 Extent ($km^2$) | 2019 Extent ($km^2$) | Magnitude of Change (km2) | Percentage of Change | Annual Rate % Change |
|---|---|---|---|---|---|
| Built up | 312.90 | 1039.54 | 726.64 | 42.19 | 12.24 |
| Forest cover | 712.66 | 253.05 | -459.61 | -26.69 | -7.74 |
| Light Vegetation | 1316.21 | 1092.51 | -223.7 | -13.57 | -3.94 |
| Bare surface | 155.01 | 289.27 | 134.26 | 7.79 | 2.26 |
| Water body | 14.70 | 12.73 | -1.97 | -0.11 | -0.03 |
| Agricultural lands | 891.51 | 715.55 | -175.96 | -10.22 | -2.96 |
| **Total** | 3402.98 | 3402.98 | 1722.14 | 100 | |

**Source:** Author's Analysis (2023)

The extent of built-up area coverage for 1990 and 2019 is shown in Figure 4.4. The increase in the urban built up area may be attributed to urban population explosion occasioned by the influx of rural dwellers to the urban and suburban areas in search of white collar jobs and presumed better quality of life which puts demand on urban residential houses, necessitating the expansion in the urban coverage.

Forest coverage for the periods 1990- 2001, 2001-2011, 2011- 2019 are shown in Appendix C1. It showed that between 1990 and 2001, forest cover changed in magnitude by -304.38 $km^2$ (27.89 percent) at an annual change rate of 3.07 percent. Between 2001 and 2011, it changed in magnitude by -129.73 $km^2$ (-14.65 percent) at an annual change rate of -1.47 percent. Lastly, between 2011 and 2019, forest cover changed in magnitude by 25.50 $km^2$ (-3.82 percent) at an annual change rate of -1.47 percent.

In general, during the study period between 1990 and 2019, forest cover decreased in magnitude by -459.61 $km^2$ (-26.69 percent), from 712.66$km^2$ in 1990 to 253.05 $km^2$ in 2019, at an annual change rate of -7.74 percent. The progressive decrease in forest cover may be attributed to demand for fuel wood, land clearance for urban infrastructural development, proliferation of educational institutions, and urban agriculture expansion.

Forest coverage for the periods 1990- 2001, 2001-2011, 2011- 2019 are shown in Appendix C1. It showed that between 1990 and 2001, light vegetation increased in magnitude by 51.57 $km^2$ (4.73 percent) at annual change rate of 0.52 percent. Between 2001 and 2011, it decreased in magnitude by -68.90 $km^2$ (-7.78 percent) at annual change rate of -0.78 percent.

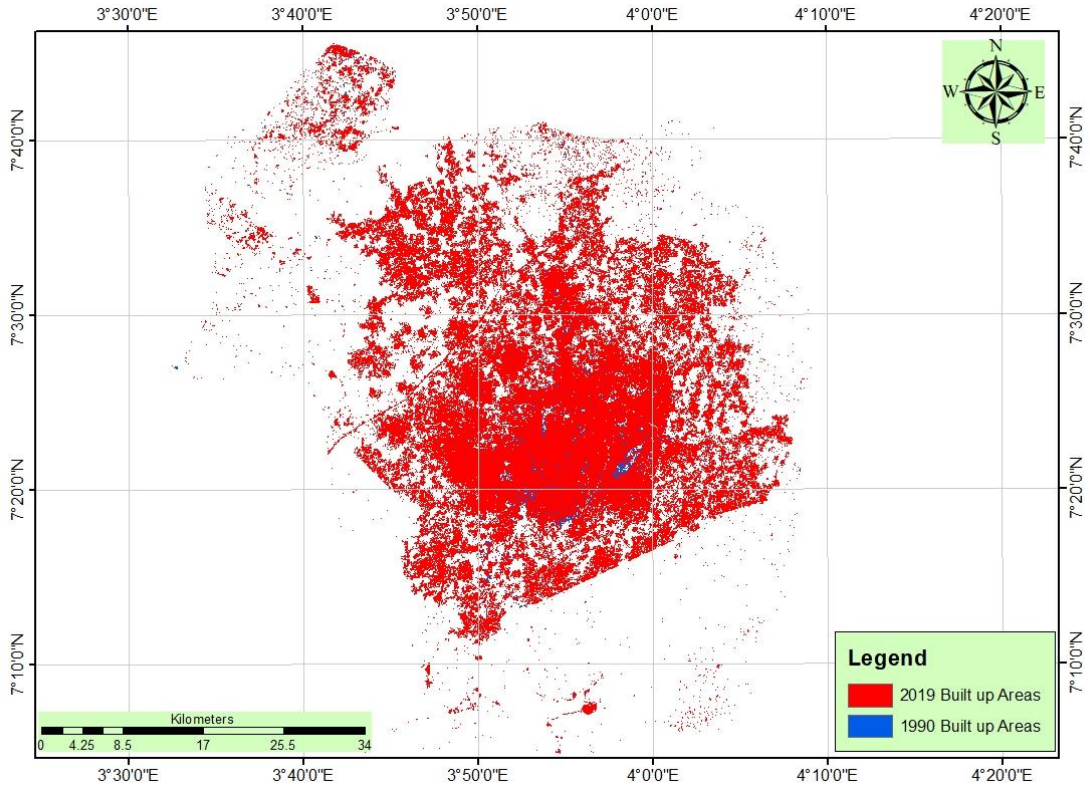


**Figure 4.4** Built-up Area Coverage of Ibadan Metropolis in 1990 and 2019

Lastly, between 2011 and 2019, it decreased in magnitude by -206.37 $km^2$ (-30.88 percent) at annual change rate of -2.47 percent. Generally, from 1990 to 2019, light vegetation decreased in magnitude by -223.70 $km^2$ (13.57 percent) from 1316.21 $km^2$ in 1990 to 1092.51 $km^2$ in 2019, at annual change rate of -3.94 percent (Table 4.2).

Bare surface coverage for the periods 1990- 2001, 2001-2011, 2011- 2019 are shown in Appendix C1. It showed that bare surfaces increased in magnitude between 1990 and 2001 by 327.61 $km^2$ (30.03 percent) at an annual change rate of 3.30 percent. It decreased in magnitude between 2001 and 2011 by -244.30 $km^2$ (-27.58 percent) at an

annual change rate of 2.76 percent. However, between 2011 and 2019, bare surfaces increased in magnitude by 50.95 $km^2$ (7.62 percent) at an annual change rate of 0.61 percent. Generally, from1990 to 2019, bare surfaces increased in magnitude by 134.26 $km^2$ (7.79 percent) from 155.01 $km^2$ in 1990 to 289.27 $km^2$ at an annual change rate of 2.26 percent (Table 4.2).

Water bodies coverage for the periods 1990- 2001, 2001-2011, 2011- 2019 are shown in Appendix C1. Results revealed that water bodies had a very insignificant decrease in magnitude of 0.01 $km^2$ (0.001 percent) between 1990 and 2001. Furthermore, it had a very insignificant magnitude of change of -1.21 $km^2$ (-0.14 percent) between 2001 and 2011. Water bodies further decreased in magnitude to -0.90 $km^2$ (-0.13 percent) between 2011 and 2019. By and large, water bodies decreased in magnitude to -1.97 $km^2$ (-0.11 percent) from 14.70 $km^2$ in 1990 to 12.73 $km^2$ in 2019, an annual change rate of -0.03 percent. The slight decrease in water bodies may be attributed to encroachment on floodplains by built surfaces.

Agricultural land coverage for the periods 1990- 2001, 2001-2011, 2011- 2019 are shown in Appendix C1. It depicted that agricultural lands increased in magnitude by 241.37 $km^2$ (22.12 percent) at an annual change rate of 2.43 percent between 1990 and 2001. The lands' area coverage further increased in magnitude by 165.80 $km^2$ (18.72 percent) at an annual change rate of 1.87 percent between 2001 and 2011. However, between 2011 and 2019, agricultural lands decreased in magnitude by -100.39 $km^2$ (-15.02 percent) at an annual change rate of -1.21 percent. By and large, between 1990 and 2019, agricultural lands generally decreased in magnitude by -175.96 $km^2$ (-10.22 percent) from 891.51 $km^2$ in 1990 to 715.55 $km^2$ at an annual change rate of -2.96 percent (Table 4.2). The decrease in agricultural land may be attributed to its annexation by built surfaces due to urban expansion.

#### *4.1.1.4 LULC Conversion model for Ibadan metropolis from 1990-2019*

Land Change Modeler in Idrisi software was used to generate land use conversion model for the various land use land cover classes of Ibadan between 1990 and 2019 as presented in Figure 4.5. The conversion model for the periods 1990 - 2000, 2000 -2010, and 2010 – 2019 respectively are depicted in Appendix D1. The result of LULC analysis for Ibadan city for the first period (1990 - 2001) showed that almost all the land cover classes lost and gained some grounds. Agricultural lands, light vegetation and bare surfaces recorded high losses of -393.14 $km^2$ (-39.44 percent), -347.87 $km^2$ (-19.92 percent) and -103.37 $km^2$ (-63.09 percent) respectively during the period.

High gains were recorded by agricultural lands, bare surfaces and forest with 410.77 $km^2$ (40.49 percent), 315.29 $km^2$ (83.91 percent) and 115.16 $km^2$ (41.24 percent) coverages respectively. Bare surfaces, forest, agricultural lands, and built up areas recorded positive gains of 211.92 $km^2$ (56.40 percent), 109.92 $km^2$ (39.36 percent), 17.64 $km^2$ (1.74 percent and 7.71 $km^2$ (2.41 percent) respectively, while light vegetation and water bodies had a net loss of -346.78 (-24.78 percent and -0.41 (-2.75 percent) respectively. Bare surfaces, agricultural lands and water bodies contributed positively to net changes in built up areas, with contributions of 4.64 $km^2$, (2.86 percent), 2.07 $km^2$ (0.21) and 1.64 $km^2$ (10.76 percent) respectively.

The second period (2001 – 2011) similarly recorded losses and gains in all land cover classes. Forest cover, light vegetation, and built up areas recorded net positive gains of 14 $km^2$ (52.36 percent), 13.39 $km^2$ (52.36 percent) and 7.08 $km^2$ (6.87 percent) respectively. The bare surfaces, water bodies, and agricultural lands recorded net losses of -46.41 $km^2$ (-29.59 percent), -20.74 $km^2$ (-0.66 percent), and -18.1 $km^2$ (-39.56) respectively. The result also shows that light vegetation (1.75 $km^2$ or 5.92 percent) and agricultural lands (1.61 $km^2$ or 4.5 percent) contributed positively to net change in the

urban areas while forest cover contributed negatively (-4.85 $km^2$ or -3.15 percent) to net change in urban.

The third period (2011-2019) also recorded losses and gains in all land cover classes. It shows that only built up areas recorded net positive gains of 590.47 $km^2$, while the forest cover, light vegetation, bare surfaces water bodies and agricultural lands recorded net losses of -51.74 $km^2$, -338.03 $km^2$, -24.33 km2, -2.67 $km^2$ and -173.7 $km^2$ respectively.

The result for the period also showed that all land cover classes contributed positively to net changes in built up areas with net contributions of 57.16 $km^2$, 317.74 $km^2$, 43.28$km^2$, 2.32 $km^2$ and 169.98 $km^2$ by forest cover, light vegetation, bare surfaces, water bodies and agricultural lands respectively. Generally, all land cover classes recorded net losses and gains during the entire study period (1990 – 2019). The general outlook is presented in Figure 4.5a. Built up areas lost -24.54 $km^2$ (-27.77 percent) and gained 623.69 $km^2$ (90.72 percent), forest cover lost -36.55 $km^2$ (-98.06 percent) and gained 23.05 $km^2$ (96.96 percent), light vegetation lost -401.54 $km^2$ (-94.49 percent) and gained 29.59 $km^2$ (55.81 percent), bare surfaces lost -41.04 $km^2$ (-94.32 percent) and gained 36.95 $km^2$ (93.74 percent) while agricultural lands lost -236.27 $km^2$ (-94.13 percent) and gained 30.11 $km^2$ (67.14 percent). Water bodies lost -3.97 $km^2$ and gained 0.52 $km^2$.

By and large, Figure 4.5b shows that only built up areas experienced a positive net change (gain) of 599.15 $km^2$ (87.15 percent). Other land cover classes experienced negative net changes (losses). Forest cover, light vegetation, bare surfaces and agricultural lands all experienced negative net changes of -13.5 $km^2$ (-56.79 percent), -371.95 $km^2$ (-701.45 percent), -4.09 $km^2$ (10.36 percent) -206.16 $km^2$ and (-459.74 percent) respectively. The result for the period also showed that all land cover classes

contributed positively to net changes in built up areas (Figure 4.5c) with net change contributions of 26.44 $km^2$ (70.92 percent), 348.38 $km^2$ (81.98 percent), 27.31 $km^2$ (62.76 percent), 3.14 $km^2$ (79.09 percent) and 193.88 $km^2$ (77.24 percent) by forest cover, light vegetation, bare surfaces, water bodies and agricultural lands respectively. Thus, light vegetation made the greatest contribution to the net changes in built up.

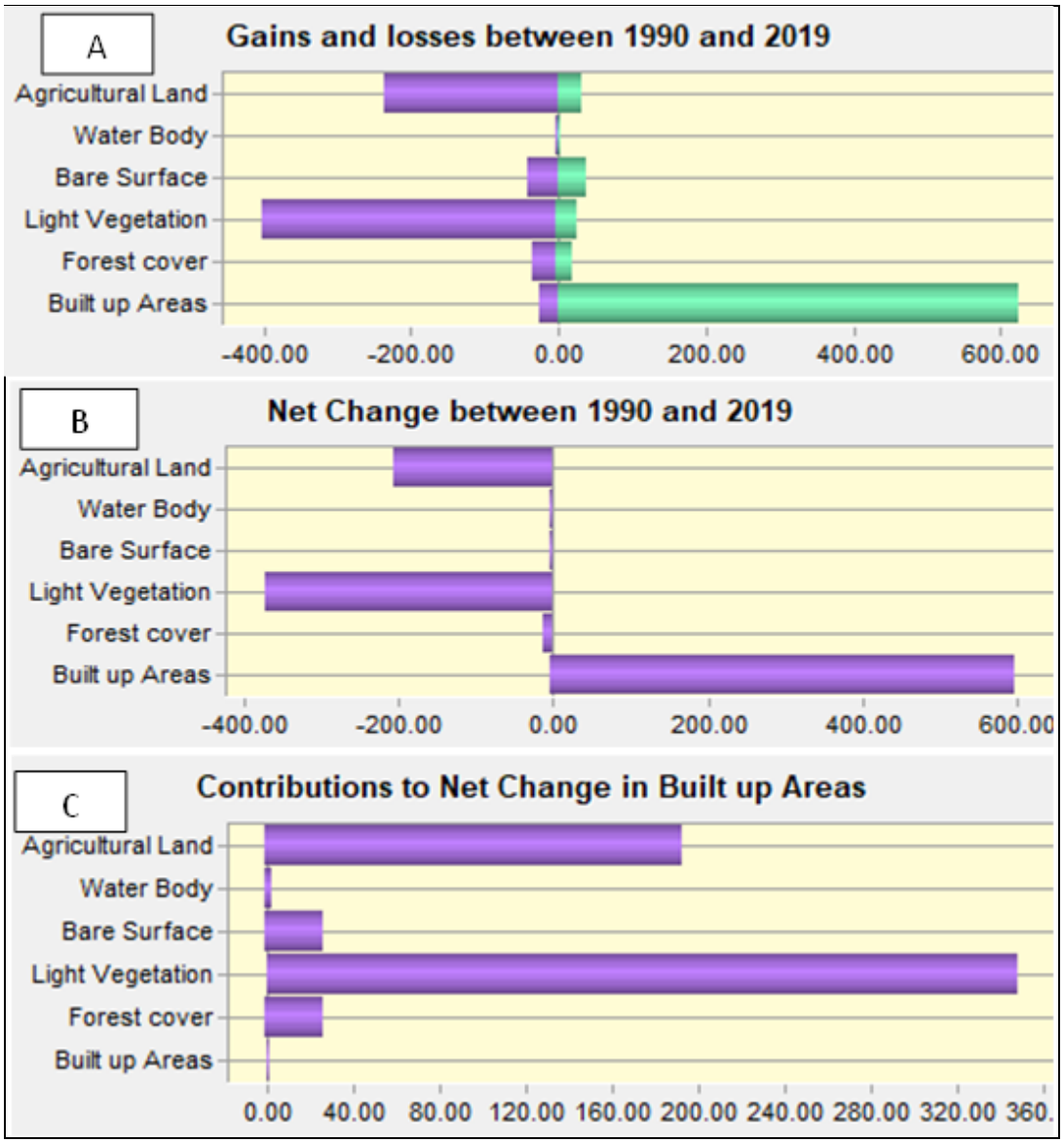


**Figure 4.5 Land cover transition for Ibadan for 1990-2019**

### 4. 1.2 LULC changes in Owerri

#### *4.1.2.1 LULC trends in Owerri Metropolis from 1990 to 2019*

The Landuse/landcover maps of Owerri metropolitan area in 1990 and 2019 are shown in Figures 4.6 and 4.7 while the statistics for the land use classes are presented in Figure 4.8. LULC maps of 2000, and 2011 are presented in Appendix B. Results showed that Owerri witnessed a progressive expansion of built up areas into other land use classes from 1990 to 2019. Figure 4.8 shows that built up areas occupied 70.32km$^2$ (12.94 percent), 166.55 km$^2$ (21.45 percent), 170.55 km$^2$ (31.39 percent), 209.16 km$^2$ (38.50 percent) of the coverage area in 1990, 2000, 2010 and 2019 respectively.

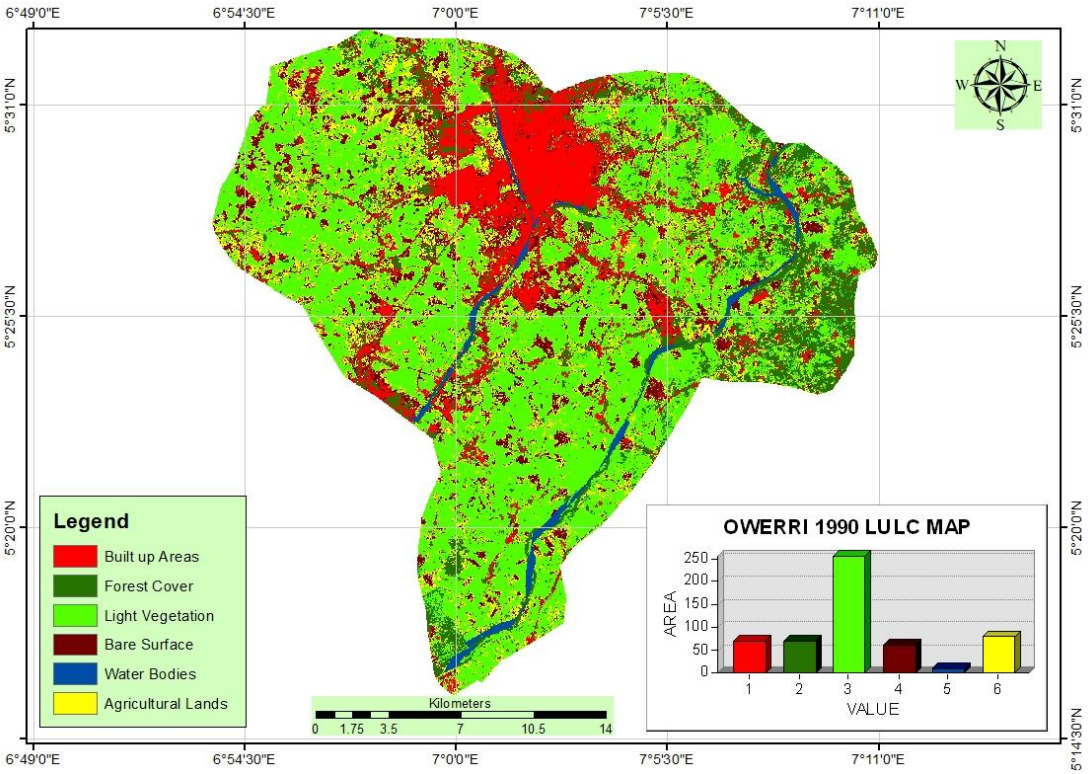


**Figure 4.6** Landuse/landcover of Owerri Metropolis in 1990

This is similar to the study by Echebima *et al*. (2019) whose study in parts of Owerri revealed that built up areas increased at a rate of 0.65 percent of the total land area annually between 1986 and 2016. The economic and industrial activities of Owerri, occasioned by its assemblage of well-developed road infrastructure, the surge in the

number of tertiary institutions, and the volume of activities in the city have been identified as factors that increase rural – urban migration (Emeribeole and Iheaturu, 2016) and resultant increase in the built environment.

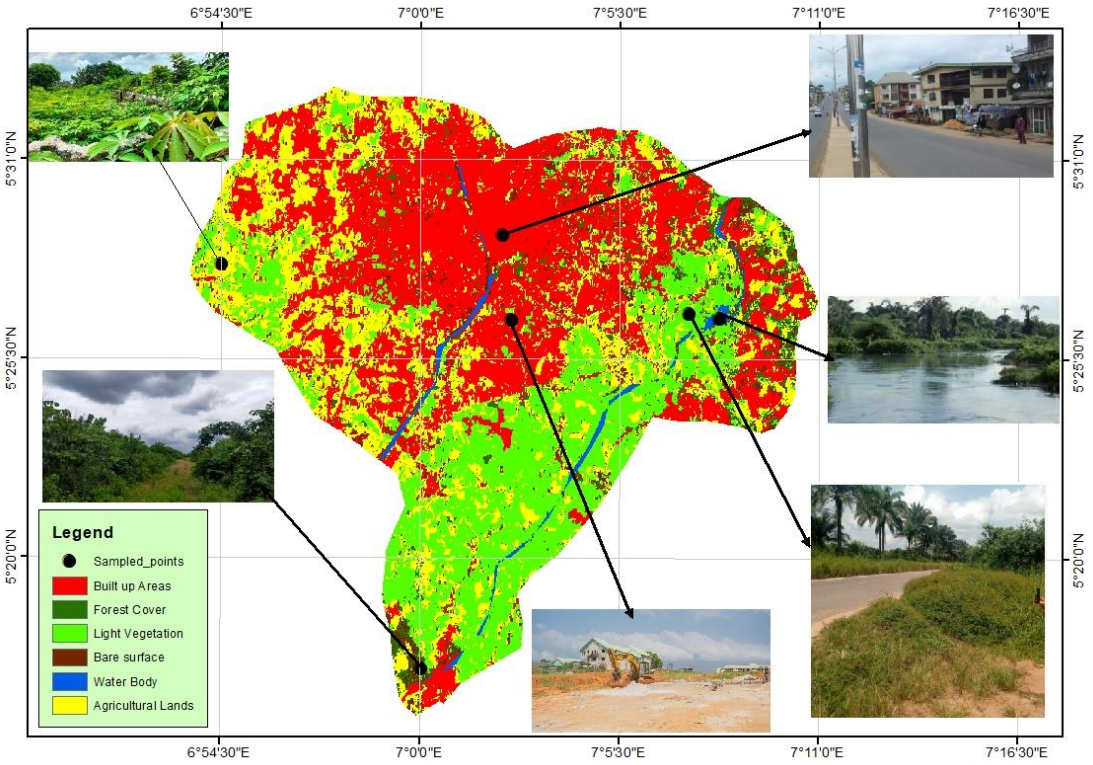


**Figure 4.7** Landuse/landcover of Owerri Metropolis in 2019

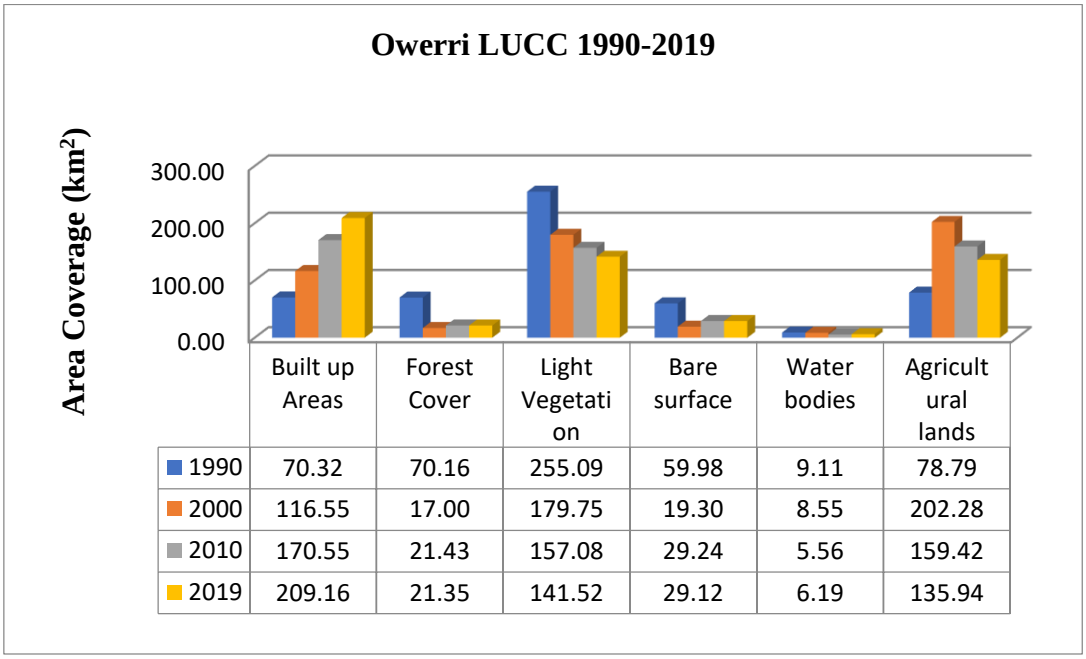


| | Built up Areas | Forest Cover | Light Vegetation | Bare surface | Water bodies | Agricultural lands |
|---|---|---|---|---|---|---|
| 1990 | 70.32 | 70.16 | 255.09 | 59.98 | 9.11 | 78.79 |
| 2000 | 116.55 | 17.00 | 179.75 | 19.30 | 8.55 | 202.28 |
| 2010 | 170.55 | 21.43 | 157.08 | 29.24 | 5.56 | 159.42 |
| 2019 | 209.16 | 21.35 | 141.52 | 29.12 | 6.19 | 135.94 |

**Figure 4.8 LULC of Owerri 1990-2019**

Forest cover decreased progressively between 1990 and 2019. Analysis shows that forest cover occupied 70.16 $km^2$ (12.91 percent), 17.00 $km^2$ (3.13 percent), 21.43 $km^2$ (3.94 percent) and 21.35 $km^2$ (3.93 percent) in 1990, 2000, 2010 and 2019 respectively. In the same vein, light vegetation decreased progressively between 1990 and 2019. It occupied 255.09 $km^2$ (46.94 percent), 179.75 $km^2$ (33.08 percent), 157.08 $km^2$ (28.91 percent) and 141.52 $km^2$ (26.05 percent) in 1990, 2000, 2010 and 2019 respectively; indicating a progressive decrease in light vegetation coverage. The continuous decrease in light vegetation coverage may be as a result of annexation by built up areas.

Echebima *et al*. (2019) also observed that forests and sparse vegetation decreased at a rate of 0.73 percent and 0.05 percent of the total land cover respectively annually over a period of three decades. A model of land land use and land cover by Echebima *et al*. (2019) depicted that Owerri metropolitan area may be devoid of vegetation cover by 2039 if the rate of conversion of vegetal cover to built surfaces continuous unabated and may trigger changes in the local climate of the metropolis. Construction and agricultural activities contributed to the continuous depletion and degradadation of the natural forest, as they lead to the removal of forest vegetal cover.

Bare surfaces did not follow a definite pattern between 1990 and 2019. Analysis shows that bare surfaces occupied 58.98 $km^2$ (11.04 percent), 19.30 $km^2$ (3.55 percent), 29.24 $km^2$ (5.38 percent) and 29.12 $km^2$ (5.36) in 1990, 2000, 2010 and 2019 respectively. This may be because they are easily converted ito built surfaces like roads, pavements and buildings. Water bodies decreased progressively between 1990 and 2010 but increased slightly in 2019. It occupied 9.11 $km^2$ (1.68 percent), 8.55 $km^2$ (1.57 percent), 5.56 $km^2$ (1.02 percent) and 6.19 $km^2$ (1.14 percent) in 1990, 2000, 2010 and 2019 respectively. The continuous decrease in coverage by water surfaces may have been as a result of encroachment on wet/marsh lands by urban infrastructures (roads and

buildings) and increased water usage for domestic and industrial activities by the spiralling urban population in and around the metropolis.

Agricultural lands increased progressively during the study period, except for the derease in 2019. They occupied 78.79 $km^2$ (14.50 percent), 202.28 $km^2$ (37.22 percent), 1.59 $km^2$ (29.34 percent) and 135.94 $km^2$ (25.02 percent) in 1990, 2000, 2010 and 2019 respectively. Rising food insecurity in urban areas may have resulted in intensification of agricultural activities as a means of augmenting food supply.

#### *4.1.2.2 Assessment of classification accuracy of LULC in Owerri*

The accuracy of classification for the four periods of 1990, 2000, 2010 and 2019 for Owerri showed an overall accuracy of 81.45 percent, 82.62 percent, 84.70 percent and 85.21 percent respectively (see Table 4.3). This was considered a decent overall accuracy and, therefore acceptable for the succeeding change detection and analysis. The user's accuracy for different land cover categories ranged between 72.29 percent and 93.73 percent while the producer's accuracy ranged between 73.60 percent and 93.55 percent. The overall Kappa was also calculated for each of the classified maps to determine their accuracy. The results of the four periods 1990, 2000, 2010 and 2019 revealed Kappa statistics of 0.78, 0.80, 0.82 and 0.81 respectively. The Kappa coefficient for the four periods ranges from substantial agreement to almost perfect agreement on the kappa scale, an indication that it is usable.

#### *4.1.2.3 The magnitude and percentage change in land use/land cover in Owerri from 1990-2019*

The magnitude and percentage change in Landuse/landcover in Owerri 1990 to 2019 are presented in Table 4.4 while those of 1990 - 2000, 2000 - 2010, and 2010 – 2019 and are presented in Appendix C2. Results revealed that between 1990 and 2000, built up, increased in magnitude by 13.62$km^2$ (1.36 percent) at an annual change rate of 1.68

percent. From 2000 to 2010, built up increased in magnitude by 54.00 $km^2$ (39.45 percent), at an annual change rate of 3.95 percent. Lastly, between 2010 and 2019, built up areas in Owerri increased in magnitude by 38.61 $km^2$ (49.20 percent) at an annual change rate of 4.43 percent. Generally, between 1990 and 2019, built up increased in magnitude by 138.84 $km^2$ (35.14 percent) from 70.32 $km^2$ in 1990 to 209.16 $km^2$ in 2019 at an annual change rate of 10.19 percent (Table 4.4).

The extent of built-up area coverage for 1990 and 2019 is shown in Figure 4.9. The persistent increase in the urban built up area may be attributed to urban population explosion occasioned by the influx of rural dwellers to the urban and suburban areas in search of white collar jobs and presumed better quality of life which puts demand on urban residential houses, necessitating the expansion in the urban coverage.

Between 1990 and 2001, forest cover decreased in magnitude by -53.16 $km^2$ (15.66 percent) at an annual change rate of 1.57 percent. Between 2000 and 2010, it increased in magnitude by 4.43 $km^2$ (3.24 percent) at an annual change rate of 3.20 percent. Lastly, between 2010 and 2019, forest cover decreased in magnitude by -0.08 $km^2$ (0.10 percent) at an annual change rate of 0.01 percent. In general, between 1990 and 2019, forest cover diminished in magnitude by -41.81 $km^2$ (12.45 percent) from 70.16 $km^2$ in 1990 to 21.35 $km^{2,}$ in 2019, at an annual change rate of 3.61 percent.

**Table 4.3 Classification Accuracy Assessment of Owerri LULC Imageries (1990, 2001,2011 and 2019)**

| | 1990 | | 2000 | | 2010 | | 2019 | |
|---|---|---|---|---|---|---|---|---|
| **Class Name** | Producer's Accuracy (%) | User's Accuracy (%) | Producer's Accuracy (%) | User's Accuracy (%) | Producer's Accuracy (%) | User's Accuracy (%) | Producer's Accuracy (%) | User's Accuracy (%) |
| **Built-up areas** | 83.32 | 93.50 | 90.35 | 93.73 | 73.60 | 83.10 | 80.87 | 84.82 |
| **Forest cover** | 81.20 | 72.29 | 81.95 | 88.24 | 79.96 | 91.19 | 66.43 | 87.95 |
| **Light Vegetation** | 79.71 | 83.10 | 80.74 | 92.38 | 91.33 | 75.63 | 85.11 | 80.69 |
| **Bare Surface** | 85.25 | 82.61 | 90.76 | 88.67 | 82.84 | 85.58 | 79.98 | 83.85 |
| **Water Bodies** | 82.29 | 84.13 | 85.70 | 83.50 | 93.55 | 80.40 | 91.68 | 83.25 |
| **Agricultural lands** | 80.11 | 82.99 | 79.01 | 82.47 | 85.10 | 89.43 | 80.75 | 92.52 |
| **Overall Classification Accuracy (%)** | **81.45** | | **82.62** | | **84.70** | | **85.21** | |
| **Overall Kappa** | **0.78** | | **0.802** | | **0.82** | | **0.81** | |

**Source:** Author's Analysis (2023)

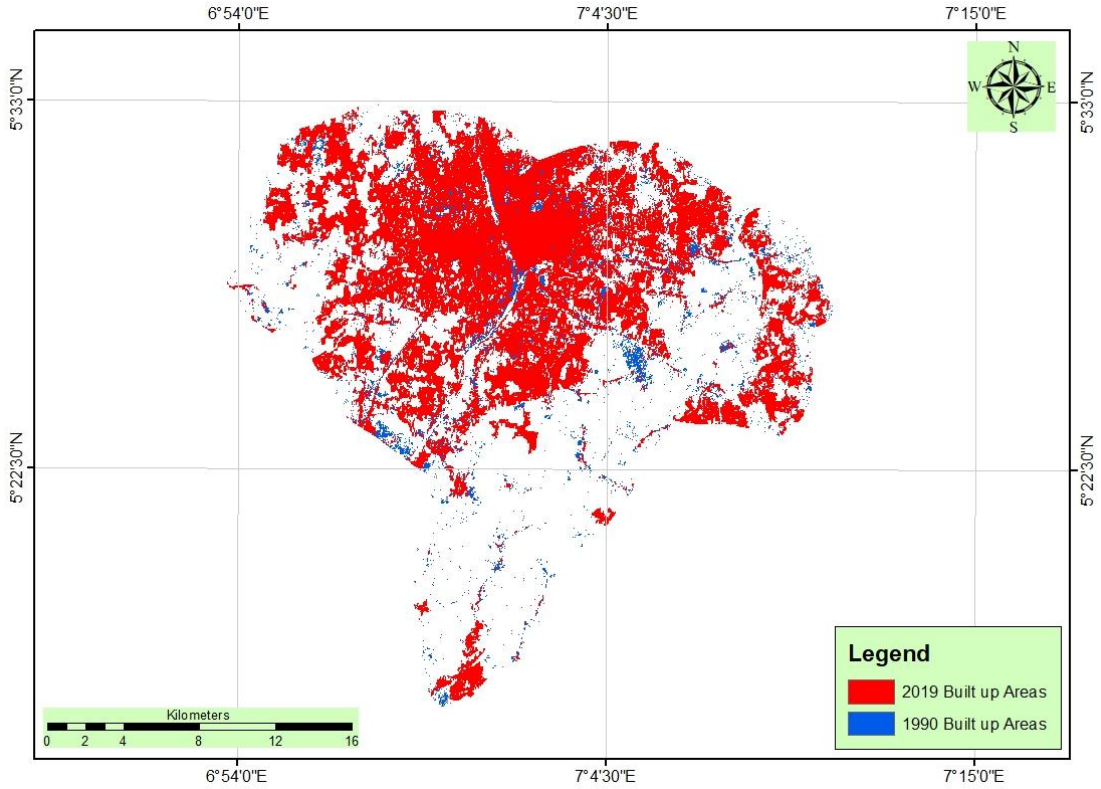


**Figure 4.9** Built-up Area Coverage of Owerri Metropolis from 1990 to 2019

The progressive decrease in forest cover may be attributed to demand for fuel wood, land clearance for urban infrastructural development, proliferation of educational institutions, and urban agriculture expansion. Results also showed that between 1990 and 2000, light vegetation decreased in magnitude by -75.34km$^2$ (22.19 percent) at annual change rate of 2.22 percent. Between 2000 and 2010, light vegetation further decreased in magnitude by -22.67 km$^2$ (16.56 percent) at annual change rate of 1.66 percent. In addition, between 2010 and 2019, light vegetation decreased in magnitude by -15.56 km$^2$ (19.83 percent) at annual change rate of 1.78 percent. Generally, By and large, light vegetation decreased in magnitude by -113.57 (28.96 percent) from 255.09 km$^2$ in 1990 to 141.52 km$^2$ in 2019 at annual change rate of 8.40 percent (Table 4.4).

**Table 4.4 Magnitude and Percentage Change in LULC of Owerri between 1990 and 2019**

| LULC Class | 1990 Extent (Sq. km) | 2019 Extent (Sq. km) | Magnitude of Change (Sq. km) | Percentage of Change | Annual Rate of Change % |
|---|---|---|---|---|---|
| Built up | 70.32 | 209.16 | 138.84 | 35.14 | 10.19 |
| Forest cover | 70.16 | 21.35 | -48.81 | 12.45 | 3.61 |
| Light Vegetation | 255.09 | 141.52 | -113.57 | 28.96 | 8.40 |
| Bare surface | 59.98 | 29.12 | -30.86 | 7.87 | 2.28 |
| Water body | 9.11 | 6.19 | -2.92 | 0.74 | 0.21 |
| Agricultural lands | 78.79 | 135.94 | 57.15 | 14.57 | 4.23 |
| **Total** | **543.45** | **543.45** | **392.15** | **100** | |

**Source:** Author's Analysis (2023)

Bare surfaces decreased in magnitude between 1990 and 2000 by -40.68 $km^2$ (11.98 percent) at an annual change rate of 1.20 percent. It further decreased in magnitude between 2000 and 2010 by -22.67 $km^2$ (16.56 percent) at an annual change rate of 1.66 percent. The period 2010 and 2019, also witnessed a slight decrease in the magnitude of bare surfaces by -0.12 $km^2$ (0.15 percent) at an annual change rate of 0.01 percent. The general trend in Owerri between 1990 and 2019 is that bare surfaces decreased in magnitude by -30.86 $km^2$ (7.87 percent) from 59.98 $km^2$ in 1990 to 29.12 $km^2$, at an annual change rate of 2.28 percent (Table 4.4). The general decrease in bare surfaces may be attributed to the incursion of built up areas into it.

Appendix C2 also depicts that between 1990 and 2000, water bodies had a very insignificant decrease in magnitude of -0.56 $km^2$ (0.16 percent) at an annual rate of 0.02 percent. It further decreased by a greater magnitude of -2.99 $km^2$ (2.18 percent) at an annual rate of 0.22 percent between 2000 and 2010. However, it increased slightly in magnitude between 2010 and 2019 by magnitude of 0.63 $km^2$ (0.80 percent) at the rate of 0.07 percent per annum. Summarily, from 1990 to 2019, water bodies decreased in magnitude to -2.92 $km^2$ (0.74 percent) from 9.11 $km^2$ in 1990 to 6.19 $km^2$ in 2019 at an annual change rate of 0.21 percent (Table 4.4).

Lastly, the study depicted that agricultural lands increased in magnitude by 123.49 $km^2$ (36.38 percent) at an annual change rate of 3.64 percent between 1990 and 2000. It however decreased in magnitude by -42.86 $km^2$ (31.31 percent) at an annual change rate of 3.13 percent between 2000 and 2010. The period 2010 to 2019 witnessed a further decrease in the magnitude of agricultural lands by -23.48 $km^2$ (29.21 percent) at an annual change rate of 2.70 percent. By and large, owing to the high magnitude of increase in the period 1990 to 2000, agricultural lands may be said to have generally increased in magnitude by 57.15 $km^2$ (14.57 percent) from 78.79 $km^2$ in 1990 to 135.94 $km^2$ in 2019, at an annual change rate of 4.23 percent (Table 4.4).

#### *4.1.2.4 LULC conversion model for Owerri metropolis between 1990 and 2019*

The results of LULC analysis for Owerri city between 1990 and 2019 are presented in Figure 4.10 while those periods 1990 to 2000, 2000 to 2010, and 2000 to 2019 are presented in Appendix D2. For the first period (1990 - 2000) shows that almost all the land cover classes lost and gained some grounds. Built-up areas lost -11.11 $km^2$ (-2.04 percent) and gained 25.01 $km^2$ (4.36 percent). Forest cover lost -28.93 $km^2$ (-41.24 percent) and gained 69.57 $km^2$ (62.79 percent). Light vegetation lost –68.62 $km^2$ (-26.90 percent) and gained 8.09 $km^2$ (4.16 percent). Bare surfaces lost 27.20 $km^2$ (-45.35 percent) and gained 21.18 $km^2$ (39 .25 percent). Water bodies lost 5.54 $km^2$ (-60.86 percent) and gained 4.96 $km^2$ (58.16 percent). Agricultural lands lost 28.91 $km^2$ (-36.60 percent) and gained 41.80 $km^2$ (45.60) during the period.

Built-up areas, forest cover and agricultural lands recorded net positive gains of 13.60 $km^2$ (36.68 percent), 40.64 $km^2$ (2.37 percent), and 12.89 $km^2$ (14.06 percent) respectively while light vegetation, bare surfaces and water bodies had net losses of -60.53 $km^2$ (-31.11 percent) -6.02 $km^2$ (-11.15 percent) and -0.58 $km^2$ (-6.83 percent) respectively. Only forest cover and water bodies contributed positively to net changes

in built-up areas; contributing 18.56 $km^2$ (26.20 percent) and 0.26 $km^2$(2.46 percent). Other land cover classes contributed negatively to net changes in built-up areas, though not significantly.

The second period (2000 – 2010) similarly recorded losses and gains in all land cover classes. Light vegetation, agricultural lands, forest cover, bare surfaces and water bodies recorded losses of -93.00 $km^2$ (-47.80 percent), 76.03 $km^2$ (-82.93 percent), 65.02 $km^2$ (-58.68 percent), 42.14 $km^2$ (78.09 percent) and -6.37 $km^2$ (-74.75 percent) respectively. The highest gain during the period of 580.49 $km^2$ (97.91 percent) was recorded by bare surfaces while water bodies recorded the least gain of 3.40 $km^2$ (61.24 percent). Light vegetation, forest cover, agricultural lands and built surfaces recorded gains of 85.41 $km^2$ (45.68 percent), 63.43 $km^2$ (58.08 percent) 60.69 $km^2$ (79.50 percent) and 35.91 $km^2$ (40.15 percent) respectively.

Only bare surfaces recorded net gain of 511.85 $km^2$ (90.46 percent). Built up areas, forest cover, light vegetation, water bodies and agricultural lands recorded net losses of -400. 00 $km^2$ (-541.64 percent), -1.59 $km^2$ (-1.46 percent), -7.59 $km^2$ (-4.06 percent), -2.91 $km^2$ (-53.49 percent) and -15.34 $km^2$ (-20.10 percent) respectively (Appendix D2). The result also shows that forest cover, light vegetation, water bodies and agricultural lands made positive contributions of 0.05 $km^2$ (0.04 percent), 2.19 $km^2$ (1.13 percent), 0.28 $km^2$ (3.34 percent), and 4.984 $km^2$ (5.43 percent) respectively to the net changes in built-up area while bare made a negative contribution of -491.85 $km^2$ ( -911.46 percent) to the net changes in built up area.

The third period (2010-2019) also recorded losses and gains in all land cover classes. The result shows that bare surfaces, light vegetation and forest cover recorded high losses of -563.62 $km^2$ (-99.61 percent), -113.95 $km^2$ (60.95) and -100.68 $km^2$ (-92.19 percent) respectively, while high gains of 582.87 $km^2$ (88.51 percent), 136.04 $km^2$

(83.46 percent) and 71.86 $km^2$ (49.60 percent) were recorded by built up, agricultural lands and light vegetation respectively. The study also revealed that only built–up areas and agricultural lands recorded positive net changes of 569.10 $km^2$ (86.42 percent) and 86.66 $km^2$ (53.16 percent) respectively, while bare surfaces recorded a high net negative change of -554.22 $km^2$ (-4,784.07 percent). The result for the period also shows that bare surfaces, light vegetation, forest cover and agricultural lands made positive contributions of 93.03 $km^2$ (526.35 percent), 12.01 $km^2$ (22.45 percent) 5.44 $km^2$ (5.94 percent) and 19.06 $km^2$ (14.55 percent) respectively to the net changes in the built up area.

Generally, all land cover classes recorded net losses and gains during the entire study period (1990 – 2019). The general outlook is presented in Figure 4.10A. Built up areas lost -14.80 $km^2$ (-2.64 percent) and gained 113.15 $km^2$ (17.18 percent), forest cover lost -60.72 $km^2$ (-86.54 percent) and gained 40.99 $km^2$ (81.28 percent), light vegetation lost -163.84 $km^2$ (-64.23 percent) and gained 53.62 $km^2$ (37.01 percent), bare surfaces lost -58.15 $km^2$ (-96.94 percent) and gained 9.75 $km^2$ (84.17 percent) agricultural lands lost -54.57 $km^2$ (-69.26 percent) and gained 138.78 (85.14 percent). Water bodies lost -6.66 $km^2$ (-73.14) and gained 2.45 $km^2$ (50.06 percent).

By and large, Figure 4.10B shows that only built up areas and agricultural lands experienced a positive net change (gain) of 98.35 $km^2$ (14.93 percent) and 84.21 $km^2$ (51.66 percent). Other land cover classes experienced negative net changes (losses). Light vegetation recorded the highest net negative change; losing an area of 110.22 $km^2$ (-76.08 percent). The result for the period also showed that all land cover classes contributed positively to net changes in built up areas (Figure 4.10C) with net change contributions of 18.69 $km^2$ (26.63 percent), 35.92 $km^2$ (14.08 percent), 24.06 $km^2$ (40.12 percent), 1.17 $km^2$ (12.85 percent) and 18.51 $km^2$ (23.49 percent) by forest

cover, light vegetation, bare surfaces, water bodies and agricultural lands respectively. Thus, light vegetation made the greatest contribution to the net changes in built up.

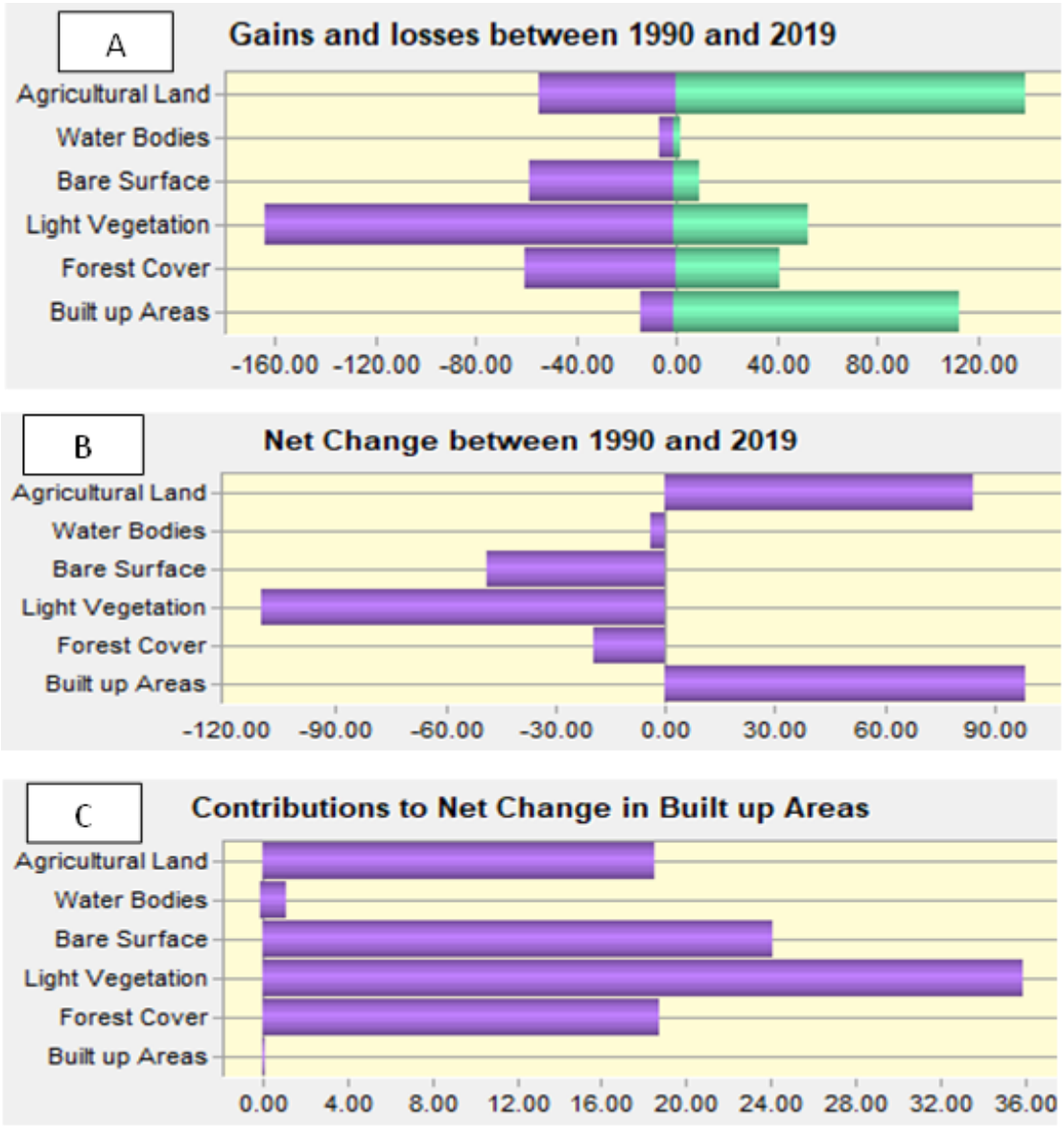


**Figure 4.10 Land cover transition for Owerri for 1990-2019**

### 4. 1.3 LULC changes in Kano

#### *4.1.3.1 LULC trends in Kano from 1991 to 2019*

The Landuse/landcover maps of Kano metropolitan area in 1991 and 2019 are shown in Figures 4.11 and 4.12 while the statistics for the land use classes are presented in Figure 4.13. LULC maps of 2001, and 2011 are presented in Appendix B. The results reveal a progressive increase in built up areas from 1991 to 2019. Figure 4.13 shows

that built up areas covered 58.48 km$^2$ and accounted for about 11.85 percent of the total coverage area. In 2001, it covered 102.66 km$^2$, comprising about 20.80 percent of the total area coverage. It further increased to 167.73 km$^2$ and accounted for about 33.99 percent of the total coverage in 2011, and finally, to 216.03 km$^2$ or 43.77 percent of the total area coverage in 2019.

The result shows that Kano Metropolis witnessed a progressive decrease in forest cover from 1991 to 2011 but a slight increase in 2019. The forest covered 19.61 km$^2$ (3.97 percent), 15.54 km$^2$ (3.15 percent), and 5.92 km$^2$ (1.20 percent) of the total coverage area in 1991, 2001 and 2011 respectively, while 2019 had forest area coverage of 11.12 km$^2$ (2.25 percent). The progressive decline in forest vegetal cover may be attributed to the expanding built-up areas in the metropolis which have led to the depletion of the already scanty vegetal cover of the metropolis.

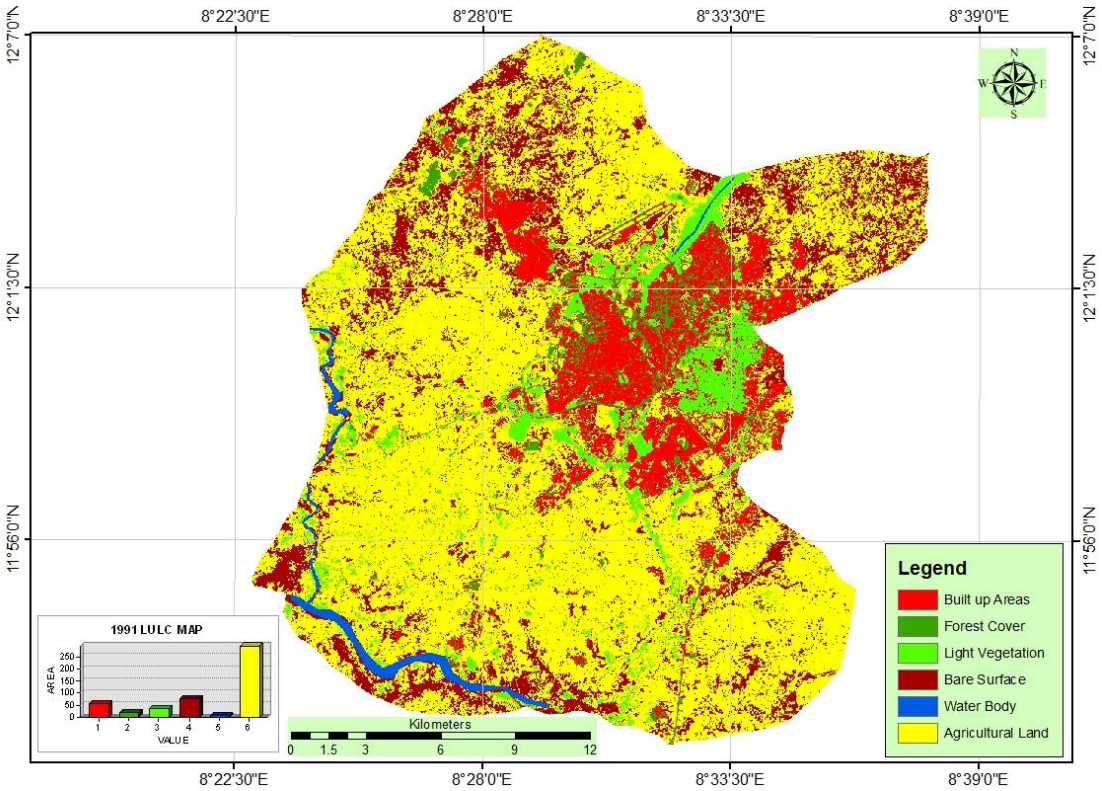


**Figure 4.11** Landuse/landcover of Kano Metropolis in 1991

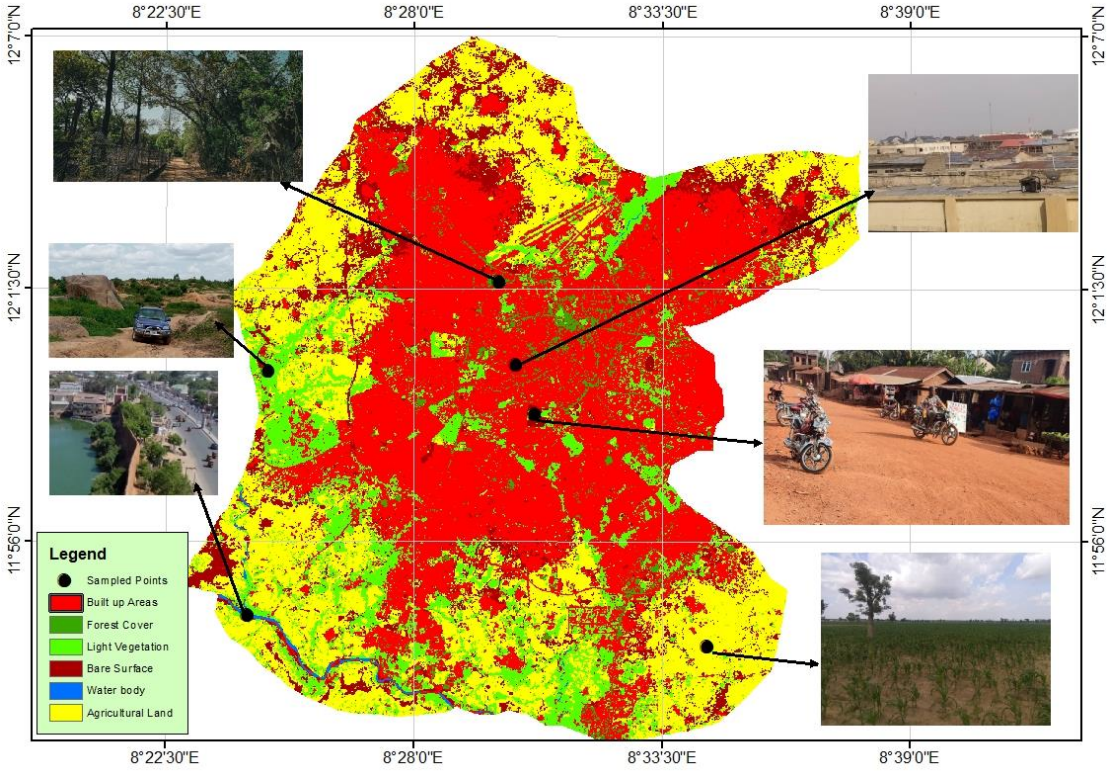


**Figure 4.12** Landuse/landcover of Kano Metropolis in 2019

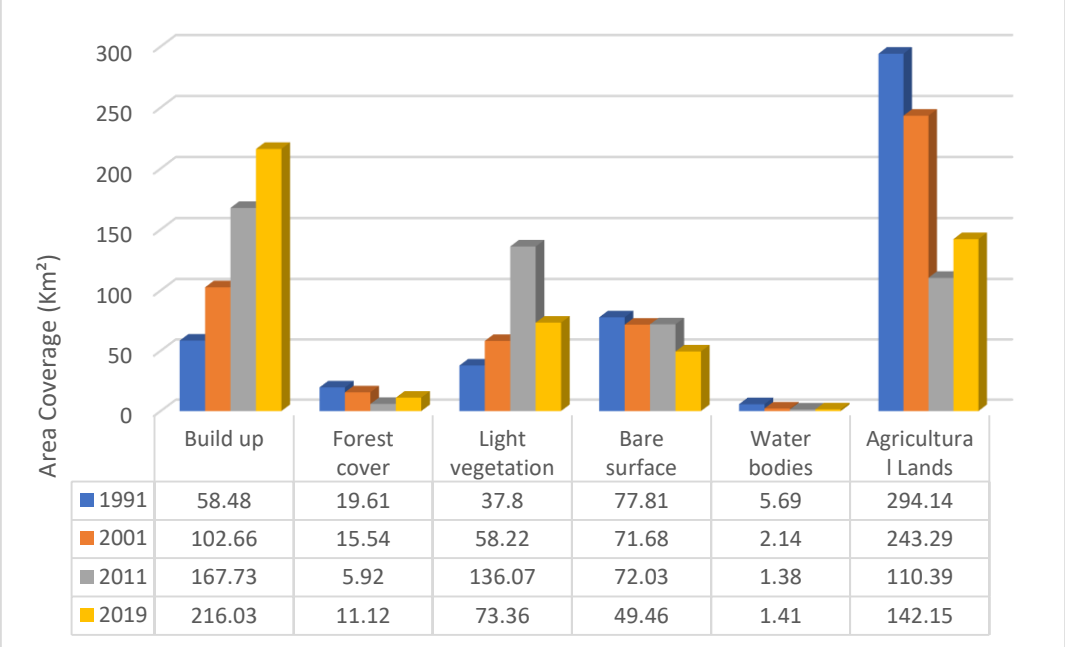


| | Build up | Forest cover | Light vegetation | Bare surface | Water bodies | Agricultural Lands |
|---|---|---|---|---|---|---|
| 1991 | 58.48 | 19.61 | 37.8 | 77.81 | 5.69 | 294.14 |
| 2001 | 102.66 | 15.54 | 58.22 | 71.68 | 2.14 | 243.29 |
| 2011 | 167.73 | 5.92 | 136.07 | 72.03 | 1.38 | 110.39 |
| 2019 | 216.03 | 11.12 | 73.36 | 49.46 | 1.41 | 142.15 |

**Figure 4.13 LULC of Kano 1991-2019**

Kano Metropolis witnessed a progressive increase in light vegetation from 1991 to 2011; covering 37.80 $km^{2,}$ (7.66 per cent), 58.22 $km^2$ (11.80 percent) and 136.07 $km^2$ (27.57 percent) in 1991, 2001 and 2011 respectively. 2019 however recorded higher

percentage coverage of light vegetation; covering an area of 73.56 $km^2$ (14.86 per cent). Bare surfaces did not seem to exhibit any established pattern during the study period; as the area coverage was nearly uniform from 1991 and 2011 but reduced markedly in 2019. They covered 77.81 $km^2$ (15.77 percent), 71.68 $km^2$ (14.52 percent), 72.03 $km^2$ (14.60 percent) and 49.46 $km^2$ (10.02 percent).

Water bodies occupied 5.69 $km^2$ (1.15 percent), 2.14 $km^2$ (0.43 percent), 1.38 $km^2$ (0.28 percent) and 1.41 km2 (0.29 percent) of the land cover in 1991, 2001, 2011 and 2019 respectively. This depicted a progressive decrease in area coverage between 1991 and 2011 but an increase in 2019. Agricultural lands covered 294.14 $km^2$ (59.60 percent), 243.29 $km^2$ (49.30 percent), 110.39 $km^2$ (22.37 percent) and 142.15 $km^2$ (28.80 percent) in 1991, 2001, 2011 and 2019 respectively. This depicted a progressive decrease in its area coverage from 1991 to 2011, and an increase in 2019. The general decrease in agricultural land may not be unconnected with the rapid urbanization taking place in Kano, sepecially the road infrastructure projects undertaken by the government which has taken over erstwhile farmlands.

#### *4.1.3.2 Assessment of classification accuracy of LULC in Kano*

The accuracy of classification for the four periods of 1991, 2001, 2011 and 2019 for Kano showed an overall accuracy of 83.65 percent, 84.99 percent, 85.62 percent and 87.90 percent respectively (see Table 4.5). This was considered a decent overall accuracy and, therefore acceptable for the succeeding change detection and analysis. The user's accuracy for different land cover categories ranged between 75.29 percent and 97.08 percent while the producer's accuracy ranged between 68.19 percent and 91.80 percent.

#### *4.1.3.3 The magnitude and percentage change in LULC in Kano from 1991-2019*

The magnitude and percentage changes in landuse/landcover of Kano in 1991 and 2019 are presented in Table 4.6 while those of 1991 – 2001, 2001 - 2011, and 2011 – 2019 respectively are presented in Appendix C3. Between 1991 and 2001, built up areas increased in magnitude by 44.18 $km^2$ (34.19 percent) at an annual change rate of 3.42 percent. Between 2001 and 2011, built up areas increased in magnitude by 65.07 $km^2$ (22.71 percent), at an annual change rate of 2.27 percent.

Lastly, between 2011 and 2019, built up areas in Kano increased in magnitude by 216.03 $km^2$ (23.81 percent) at an annual change rate of 2.26 percent. Generally, between 1991 and 2019, built up increased in magnitude by 157.55 $km^2$ (40.79 percent) at an annual change rate of 11.42 percent (Table 4.6).

The extent of built-up area coverage for 1991 and 2019 is shown in Figure 4.14. The persistent increase in the urban built up area may be attributed to urban population explosion occasioned by the influx of rural dwellers to the urban and suburban areas in search of white collar jobs and presumed better quality of life which puts demand on urban residential houses, necessitating the expansion in the urban coverage.

Between 1991 and 2001, forest cover decreased in magnitude by -4.07 $km^2$ (3.15 percent) at an annual change rate of 0.32 percent. Between 2001 and 2011, it further decreased in magnitude by -9.62 $km^2$ (3.36 percent) at an annual change rate of 0.34 percent. Lastly, between 2011 and 2019, forest cover increased in magnitude by 5.20 $km^2$ (3.05 percent) at an annual change rate of 0.24 percent. The general outlook of the forest cover between 1991 and 2019 is that it decreased in magnitude by -6.49 $km^2$ (2.19 percent) at an annual change rate of 0.61 percent. The progressive decrease in forest cover may be attributed to high urbanization and its attendantconsequences.

**Table 4.5** Accuracy Assessment of Kano LULC Imageries (1991, 2001,2011 and 2019)

| | 1991 | | 2001 | | 2010 | | 2019 | |
|---|---|---|---|---|---|---|---|---|
| **Class Name** | **Producer's Accuracy (%)** | **User's Accuracy (%)** | **Producer's Accuracy (%)** | **User's Accuracy (%)** | **Producer's Accuracy (%)** | **User's Accuracy (%)** | **Producer's Accuracy (%)** | **User's Accuracy (%)** |
| **Built-up areas** | 88.06 | 79.50 | 89.70 | 97.08 | 81.08 | 84.00 | 83.62 | 89.75 |
| **Forest cover** | 84.28 | 90.47 | 80.18 | 85.20 | 72.99 | 90.00 | 68.19 | 78.71 |
| **Light Vegetation** | 80.40 | 85.02 | 69.05 | 83.31 | 82.59 | 80.93 | 91.80 | 90.97 |
| **Bare Surface** | 87.00 | 81.91 | 90.23 | 85.01 | 84.31 | 86.15 | 69.79 | 84.85 |
| **Water Bodies** | 84.00 | 88.33 | 87.56 | 75.29 | 86.84 | 83.04 | 80.99 | 77.20 |
| **Agricultural limits** | 77.98 | 79.75 | 80.18 | 80.11 | 80.58 | 81.07 | 78.32 | 79.56 |
| **Overall Classification Accuracy (%)** | **83.65** | | **84.99** | | **85.62** | | **87.90** | |
| **Overall Kappa** | **0.76** | | **0.82** | | **0.85** | | **0.84** | |

**Source:** Author's Analysis (2023)

**Table 4.6 Magnitude and Percentage of Change in LULC of Kano between 1991 and 2019**

| LULC Class | 1991 Extent (Sq. km) | 2019 Extent (Sq. km) | Magnitude of Change (Sq. km) | Percentage of Change | Annual Rate of Change % |
|---|---|---|---|---|---|
| Built up | 58.48 | 216.03 | 157.55 | 40.79 | 11.42 |
| Forest cover | 19.61 | 11.12 | -8.49 | 2.19 | 0.61 |
| Light Vegetation | 37.80 | 73.36 | 35.56 | 9.21 | 2.57 |
| Bare surface | 77.81 | 49.46 | 28.35 | 7.34 | 2.05 |
| Water body | 5.69 | 1.41 | -4.28 | 1.11 | 0.31 |
| Agricultural lands | 294.14 | 142.15 | 151.99 | 39.35 | 11.02 |
| **Total** | **493.53** | **493.53** | **386.22** | **100** | |

**Source:** Author's Analysis (2023)

Between 1991 and 2001, light vegetation increased in magnitude by 20.42 $km^2$ (15.80 percent) at annual change rate of 1.58 percent. Between 2001 and 2011, it increased in magnitude by 77.85 $km^2$ (27.17 percent) at an annual change rate of 2.72 percent (Table 4.13). Lastly between 2011 and 2019, light vegetation decreased in magnitude by -62.71 $km^2$ (36.76 percent) at an annual change rate of 2.94 percent. Generally, from 1991 to 2019 light vegetation increased in magnitude by 35.56 $km^2$ (9.21 percent) at an annual change rate of 2.57 percent (Table 4.6).

Bare surfaces decreased in magnitude between 1991 and 2001 by -6.13 $km^2$ (4.74 percent) at an annual change rate of 0.47 percent. It increased in magnitude between 2001 and 2011 by 0.35 $km^2$ (0.12 percent) at an annual change rate of 0.01 percent. Between 2011 and 2019, bare surfaces decreased in magnitude by -22.57 $km^2$ (13.23 percent) at an annual change rate of 1.03 percent. Generally, from1990 to 2019, bare surfaces decreased in magnitude by 28.35 $km^2$ (7.34 percent) at an annual change rate of 2.05 percent.

Results also revealed that water bodies decreased in magnitude by -3.55 $km^2$ (2.75 percent) between 1991 and 2001 at an annual change rate of 0.28. It decreased in magnitude by -0.76 $km^2$ (0.27 percent) between 2001 and 2011, at an annual change

rate of 0.03 percent. It decreased in magnitude 0.03 km$^2$ (0.02 percent) between 2011 and 2019. By and large, from 1990 to 2019, water bodies decreased in magnitude by -4.28 km$^2$ (1.11 percent) an annual change rate of -0.31 percent (Table 4.6).

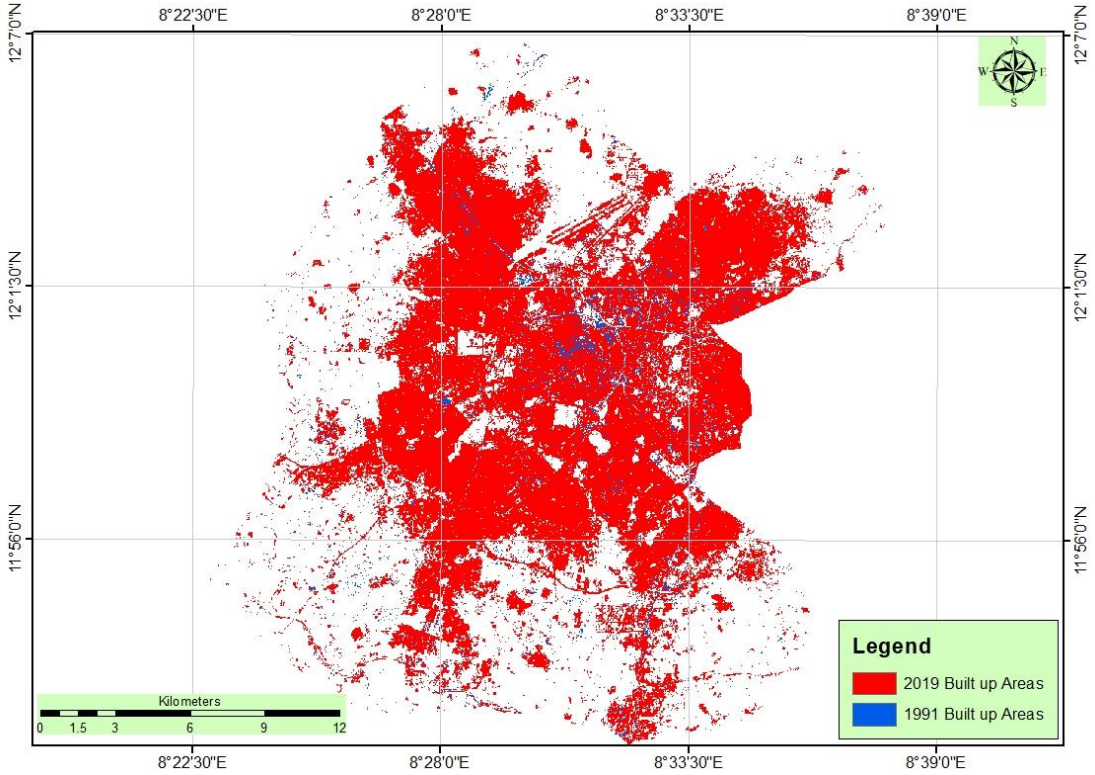


**Figure 4.14** Built-up Area Coverage of Kano Metropolis from 1990 to 2019

Agricultural lands decreased in magnitude by -50.85 km$^2$ (39.36 percent) at an annual change rate of 3.94 percent between 1991 and 2001. It decreased in magnitude by 132.9 km$^2$ (46.38 percent) at an annual change rate of 4.64 percent between 2001 and 2011. Between 2011 and 2019, agricultural lands decreased in magnitude by 31.76 km$^2$ (18.62 percent) at an annual change rate of 1.48 percent (Table 4.14). By and large, between 1990 and 2019, agricultural lands generally decreased in magnitude by 151.99 km$^2$ (39.35 percent) at an annual change rate of 11.02 percent (Table 4.15).

#### *4.1.3.4 LULC conversion model for Kano metropolis from 1991-2019*

The results of LULC analysis for Kano Metropolis between 1991 and 2019 are presented in Figure 4.15 while those of 1991 to 2001, 2001 to 2011, and 2011 to 2019 respectively are presented in Appendix D3. The results of LULC analysis of the city for the first period (1991 - 2001) showed that all the land cover classes lost and gained some grounds. Built-up areas lost -7.90 $km^2$ (-12.81 percent), forest cover lost -15.06 $km^2$ (-4.9 percent) and gained 10.99 $km^2$ (3.62 percent), light vegetation lost -14.35 $km^2$ (-37.96 percent) and gained 34.77 $km^2$ (59.72 percent), bare surfaces lost -48.44 $km^2$ (-62.26 percent) and gained 42.31 $km^2$ (59.03 percent), water surfaces lost -4.30 $km^2$ (-75.60 percent) and gained 0.75 $km^2$ (35.21 percent), and lastly, agricultural lands lost -98.42 $km^2$ (33.46 percent) and gained 47.56 $km^2$ (19.55 percent).

The second period (2001 – 2011) similarly recorded losses and gains in all land cover classes. The analysis showed that whereas the greatesr losses were recorded by forest cover, built up recorded the greatest gain. Forest cover lost – 301.28 $km^2$ and gained only 3.83 $km^2$ during the period. Bulit up areas lost just -11.70 $km^2$ and gained 364. 60 $km^2$. Light vegetation lost -30.43 $km^2$and gained 108.28 $km^2$.

Agricultural lands lost -160.31 $km^2$ and gained just 27.41 $km^2$. Water bodies also experienced more losses, as it gained only 0.72 $km^2$ and lost -1.48 $km^2$. Lastly, there was no significant change in bare surfaces during the period; as -50.68 $km^2$ was lost and 51.04 $km^2$ was gained. This implies that during this period, built up and light vegetation recorded net positive gains of 352.90 $km^2$ and 77.85 $km^2$ respectively, while forest cover and agricultural lands recorded net losses of -297.45 $km^2$ and 132.90 $km^2$ respectively. Water bodies and bare surfaces recorded insignifant negative (-.076 $km^2$) and positive (0.36 $km^2$) net changes respectively. Furthermore, the result showed that forest cover (294.21 $km^2$ ) was the highest net contributor to net changes in built up

areas while agricultural lands, bare surfaces and bare surfaces also made significant contributions of 31.15 $km^2$, 14.24 $km^2$ and 13.01 $km^2$ respectively.

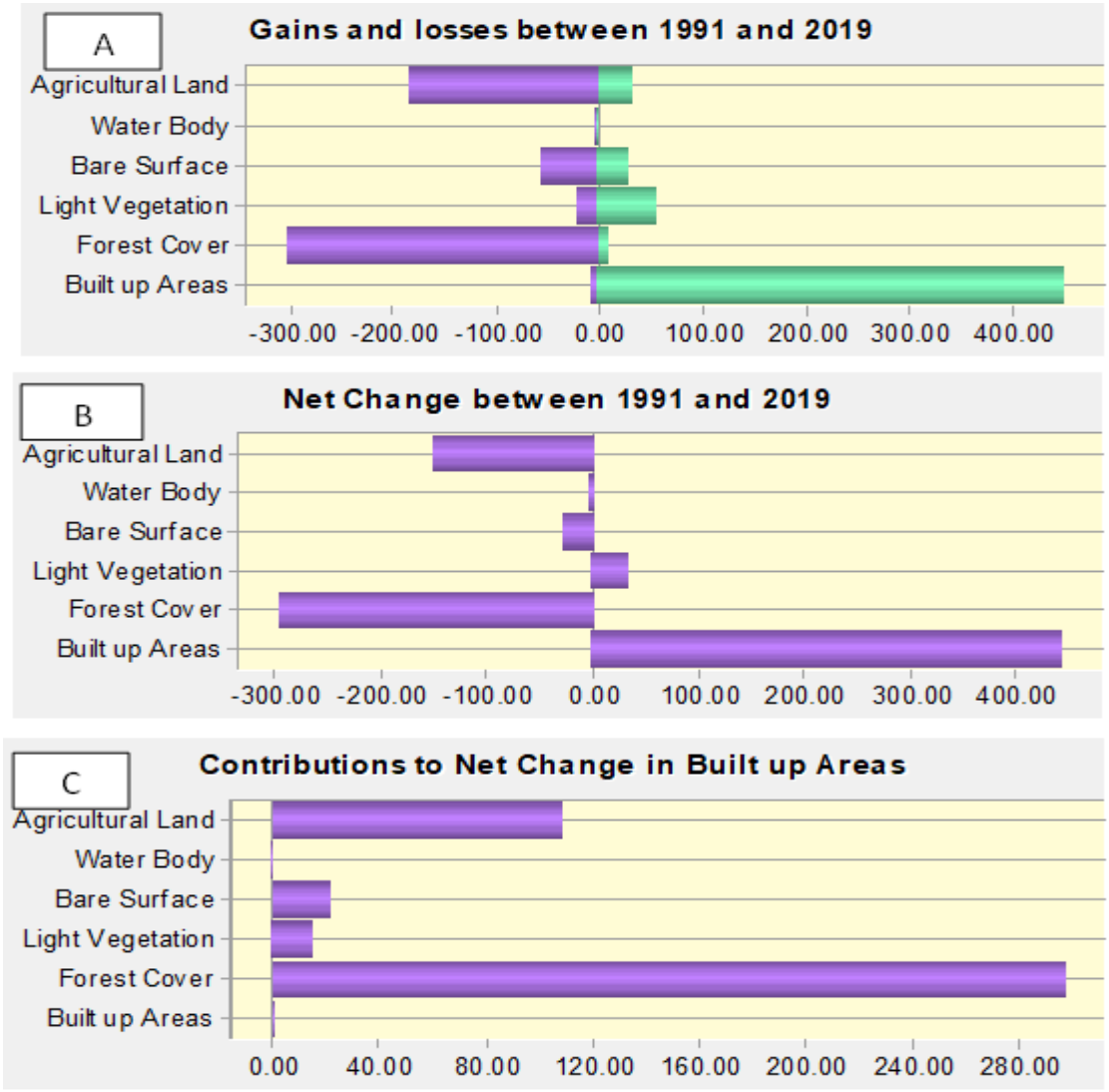


**Figure 4.15 Land cover transition for Kano for 1990-2019**

The third period (2011-2019) also recorded losses and gains in all land cover classes. It shows that built up areas lost -21.92 $km^2$ and gained 70.22 $km^2$ . Forest cover lost -3.69 and gained 8.89. light vegetation lost -97.66 $km^2$ and gained 34.95. bare surfaces lost -55.63 $km^2$.and gained 33.06 $km^2$. Agricultural lands lost -50.83 $km^2$ and gained 82.59 $km^2$. Lastly, water bodies lost -0.91 $km^2$ and gained 0.94 $km^2$. This implies that built up areas and agricultural lands recorded positive net changes (gains) of 48.30 $km^2$ and 31.76 $km^2$ respectively, while light vegetation and bare surfaces recorded significant

net losses of -62.71 $km^2$ and -22.57 $km^2$. The result for the period also shows that bare surfaces and agricultural lands made signifiacant contributuions of 29.22 $km^2$ and 16.63 $km^2$ respectively to the net changes in built up areas.

Generally, all land cover classes recorded net losses and gains during the entire study period (1991 – 2019). The general outlook is presented in Figure 4.15a. Built up areas lost -7.09 $km^2$ (-12.13 percent) and gained 452.48 $km^2$ (89.80 percent), forest cover lost -304.16 $km^2$ (-98.93 percent) and gained 7.84 $km^2$ (70.50 percent), light vegetation lost -22.91 $km^2$ (-60,59 percent) and gained 58.46 $km^2$ (79.69 percent), bare surfaces lost -58.02 $km^2$ (-74.57 percent) and gained 29.67 $km^2$ (59.99 percent), agricultural lands lost -184.45 $km^2$ (-62.71 percent) and gained 32.46 $km^2$ (22.84 percent) while water bodies lost -4.74 $km^2$ (-83.29 percent and gained 0.46 $km^2$.(32.61 percent).

By and large, Figure 4.15b shows that only built up area experienced a positive net change (gain) of 445.38 $km^2$ (88.39 percent). Other land cover classes experienced negative net changes (losses). Forest cover, agricultural lands, light vegetation, bare surfaces, and water bodies all experienced negative net changes of -296.33 $km^2$ (-2665.14 percent), -1591.99 $km^2$ (-106.92 percent), 35.56 $km^2$ (48.47 percent) -28.35 $km^2$ (-57.32 percent) and -4.28 $km^2$ (-303.25 percent) respectively. The result for the period also shows that all land cover classes contributed positively to net changes in built up areas (Figure 4.15c) with net contributions of 297.58 $km^2$ (96.79 percent), 109.09 $km^2$ (37.09 percent), 15.37 $km^2$ (40.66 percent), 22.48 $km^2$ (15.11 percent) and 0.86 $km^2$ (15.11 percent) by forest cover, agricultural lands, light vegetation, bare surfaces, and water bodies respectively. Thus, forest cover made the greatest contribution to the net changes in built up.

### 4.1.4 LULC changes in Birnin Kebbi

This section is the presentation of results of LULC analysis of Birnin Kebbi, also located in the Sudan Savanna ecological belt from 1990 to 2019.

#### *4.1.4.1 LULC trends in Birnin Kebbi from 1990 to 2019*

The Landuse/landcover maps of Kano metropolitan area in 1990 and 2019 are shown in Figures 4.16 and 4.17 while the statistics for the land use classes are presented in Figure 4.18. LULC maps of the city in 2000 and 2010 are presented in Appendix B. The results reveal a progressive increase in built up areas from 1990 to 2019. Figure 4.22 shows that in 1990, built up areas covered 14.06 km$^2$ and accounted for about 1.13 percent of the total coverage area. In 2000, it covered 26.96 km$^2$, comprising about 2.16 percent of the total area coverage.

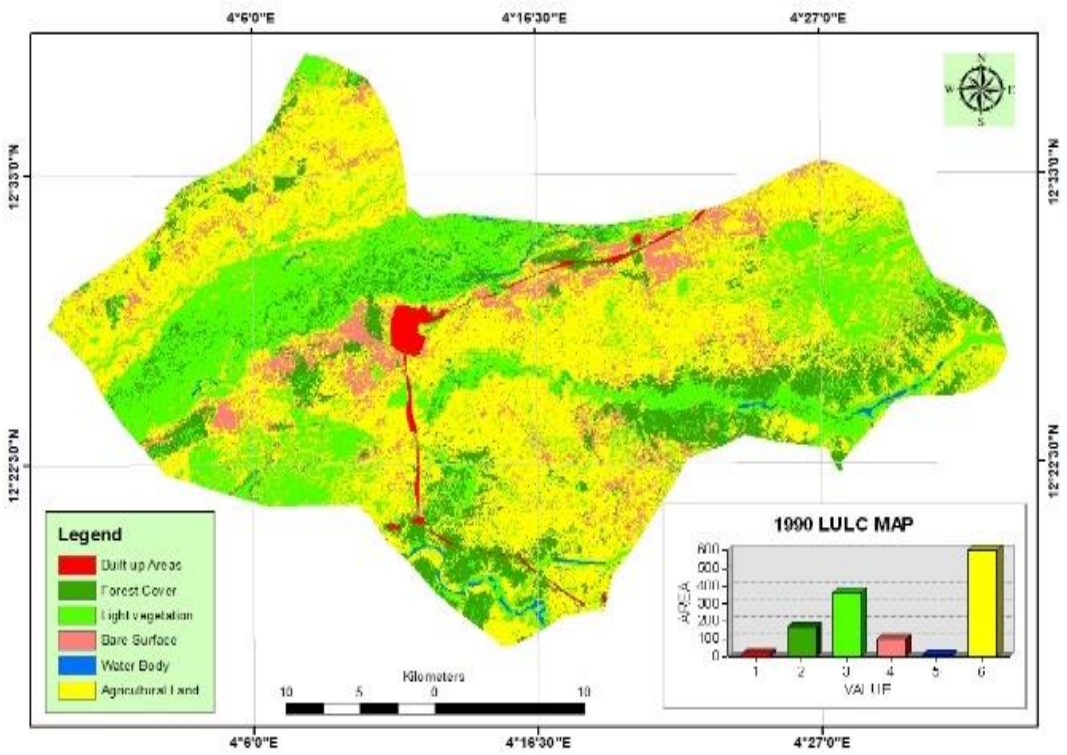


**Figure 4.16** Landuse/landcover of Birnin Kebbi Metropolis in 1990

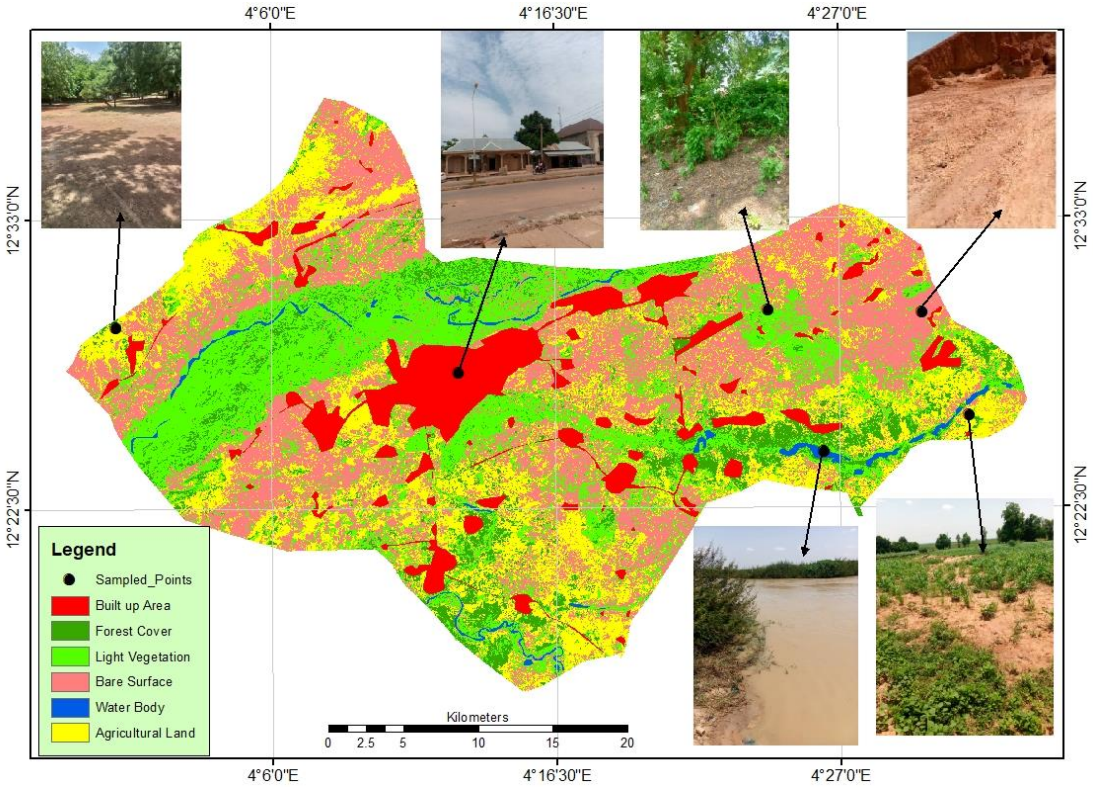


**Figure 4.17** Landuse/landcover of Birnin Kebbi Metropolis in 2019

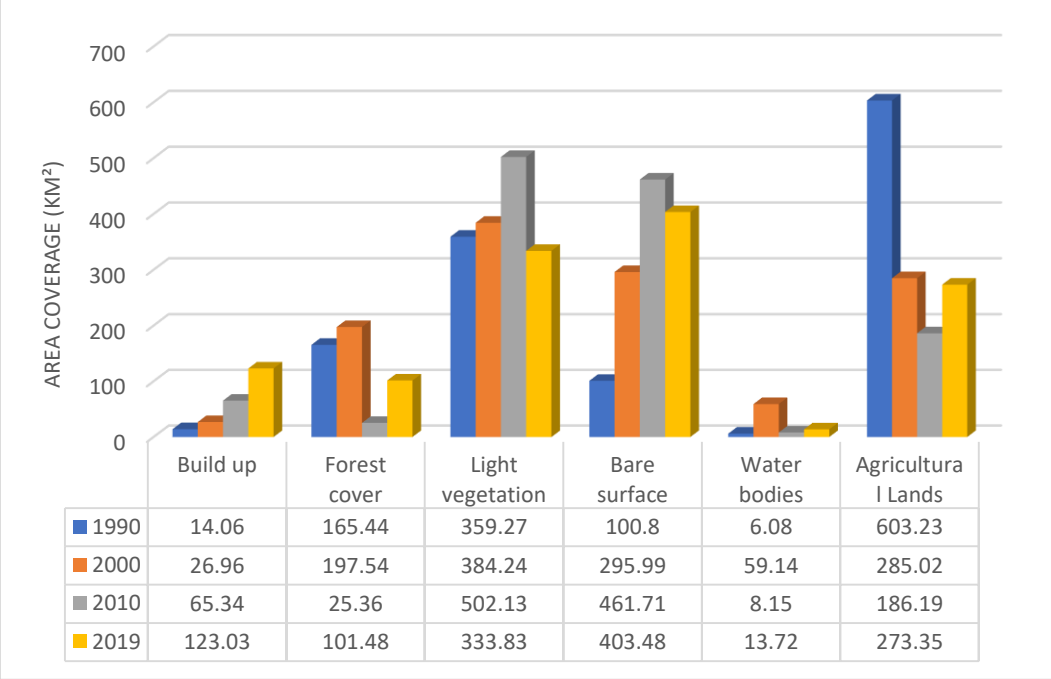


| | Build up | Forest cover | Light vegetation | Bare surface | Water bodies | Agricultural Lands |
|---|---|---|---|---|---|---|
| 1990 | 14.06 | 165.44 | 359.27 | 100.8 | 6.08 | 603.23 |
| 2000 | 26.96 | 197.54 | 384.24 | 295.99 | 59.14 | 285.02 |
| 2010 | 65.34 | 25.36 | 502.13 | 461.71 | 8.15 | 186.19 |
| 2019 | 123.03 | 101.48 | 333.83 | 403.48 | 13.72 | 273.35 |

**Figure 4.18** LULC of Birnin Kebbi 1990-2019

Built-up further increased to 65.34 km$^2$ and accounted for about 5.23 percent of the total coverage in 2010, and finally, to 123.03 km$^2$ or 9.85 percent of the total area coverage in 2019.

The result shows that forest cover in Birnin Kebbi Metropolis did not exhibit any definite pattern. It increased in coverage area from 165.44 $km^2$ (13 .25 percent) in 1990 to 197.54 $km^2$ (15.82 percent) in 2000. In 2010, it occupied only about 25.36 $km^2$ (2.03 percent) but in 2019 it increased to 101.48 $km^2$ (8.13 percent). Light vegetation increased progressively between 1990 and 2010 but witnessed a decrease between year 2010 and 2019. Light vegetation increased from 359.27 $km^2$ (28.77 percent) in 1990 to 384.24 $km^2$ (30.77 percent) in year 2000 and a further increase to 502.13 $km^2$ (40.21 percent) in 2010. However, between 2010 and 2019, it decreased to 333.83 $km^2$ (26.73 percent).

Bare surfaces did not seem to have exhibited any established pattern during the study period. It covered about 100.80 $km^2$ (8.07 percent) in 1990 but reduced to 295.99 $km^2$ (23.70 percent) 1n 2000. In 2010, the distribution of bare surfaces increased to 461.71 $km^2$ (38.97 percent) and decreased to 403.48 $km^2$ (32.31 percent). Water bodies occupied 6.08 $km^2$ (0.49 percent), 59.14 $km^2$ (4.74 percent), 8.15 $km^2$ (0.65 percent) and 13.72 $km^2$ (1.10 percent) of the land cover in 1990, 2000, 2010 and 2019 respectively. Agricultural lands decreased progressively from 1990 to 2010 but increased in 2019. It covered 603.23 $km^2$; (48.30 percent), 285.02 $km^2$ (22.82 percent), 186.19 $km^2$ (14.91 percent) and 273.35 $km^2$ (21.89 percent) in 1990, 2000, 2010 and 2019 respectively.

#### *4.1.4.2 Assessment of classification accuracy of LULC in Birnin Kebbi*

The accuracy of classification for the four periods of 1990, 2000, 2010 and 2019 for Birnin Kebbi showed an overall accuracy of 82.65 percent, 85.31 percent, 84.62 percent and 87.80 percent respectively (See Table 4.7). This was considered a decent overall accuracy and, therefore acceptable for the succeeding detection of change and analysis. The user's accuracy for different land cover categories ranged between 62.63 percent

and 96.38 percent while the producer's accuracy ranged between 78.20 percent and 93.35 percent.

The overall Kappa was also calculated for each of the classified maps to determine their accuracy. The results of the four periods 1990, 2000, 2010 and 2019 revealed Kappa statistics of 0.76 0.82, 0.85 and 0.84 respectively. The Kappa coefficient for the four periods ranges from substantial agreement to almost perfect agreement on the kappa scale, an indication that it is usable.

#### *4.1.4. 3 The magnitude and percentage change in LULC in Birnin Kebbi from 1990-2019*

The magnitude and percentage changes in landuse/landcover of Birnin Kebbi in 1990 and 2019 are presented in Table 4.8 while those of 1990 – 2000, 2000 - 2010, and 2010 – 2019 respectively are presented in Appendix C4. The results show that between 1990 and 2000, built up, increased in magnitude by 12.90 $km^2$ (91.75 percent) at an annual change rate of 9.18 percent. Between 2000 and 2010, built up areas increased in magnitude by 38.36 $km^2$ (142.28 percent), at an annual change rate of 14.23 percent. Lastly, between 2010 and 2019, built up areas in Birnin Kebbi increased in magnitude by 57.69 $km^2$ (88.29 percent) at an annual change rate of 9.81 percent. Generally, between 1990 and 2019, built up increased in magnitude by 108.97 $km^2$ (775.04 percent) at an annual change rate of 26.73 percent.

**Table 4.7 Magnitude and Percentage of Change in LULC between 1990 and 2019**

| LULC Class | 1990 Extent (Sq. km) | 2019 Extent (Sq. km) | Magnitude of Change (Sq. km) | Percentage of Change | Annual Rate of Change % |
|---|---|---|---|---|---|
| **Built up** | 14.06 | 123.03 | 108.97 | 775.04 | 26.73 |
| **Forest cover** | 165.44 | 101.48 | -63.96 | 38.66 | 1.33 |
| **Light Vegetation** | 359.27 | 333.83 | -25.44 | 7.08 | 0.24 |
| **Bare surface** | 100.80 | 403.48 | 302.68 | 300.28 | 10.35 |
| **Water body** | 6.08 | 13.72 | 7.64 | 125.66 | 4.33 |

| | | | | | |
|---|---|---|---|---|---|
| **Agricultural lands** | 603.23 | 273.35 | -329.88 | 54.69 | 1.89 |
| **Total** | **1248.88** | **1248.881** | **838.57** | **1301.41** | **44.84** |

**Source: Author's Analysis, 2023**

**Table 4.8 Classification Accuracy Assessment of Birnin Kebbi LULC Imageries (1990, 2001,2011 and 2019)**

| Class Name | 1990 | | 2000 | | 2010 | | 2019 | |
|---|---|---|---|---|---|---|---|---|
| | Producer's Accuracy (%) | User's Accuracy (%) | Producer's Accuracy (%) | User's Accuracy (%) | Producer's Accuracy (%) | User's Accuracy (%) | Producer's Accuracy (%) | User's Accuracy (%) |
| **Built-up areas** | 84.53 | 95.50 | 93.35 | 96.14 | 83.60 | 93.10 | 81.32 | 76.98 |
| **Forest cover** | 78.20 | 64.29 | 80.15 | 87.20 | 81.50 | 94.11 | 82.63 | 91.00 |
| **Light Vegetation** | 80.71 | 85.30 | 84.74 | 96.38 | 90.33 | 62.63 | 80.80 | 89.09 |
| **Bare Surface** | 83.21 | 80.65 | 93.20 | 85.67 | 85.55 | 85.5 | 79.20 | 81.15 |
| **Water Bodies** | 80.00 | 80.76 | 82.70 | 79.50 | 91.45 | 83.40 | 84.11 | 93.60 |
| **Agricultural limits** | 81.10 | 82.50 | 79.12 | 82.47 | 88.17 | 90.43 | 89.61 | 81.70 |
| **Overall Classification Accuracy (%)** | **82.65** | | **85.31** | | **84.62** | | **87.80** | |
| **Overall Kappa** | **0.801** | | **0.83** | | **0.823** | | **0.844** | |

**Source:** Author's Analysis, 202

The extent of built-up area coverage for 1990 and 2019 is shown in Figure 4.19. The persistent increase in the urban built up area may be attributed to urban population explosion occasioned by the influx of rural dwellers to the urban and suburban areas in search of white collar jobs and presumed better quality of life which puts demand on urban residential houses, necessitating the expansion in the urban coverage.

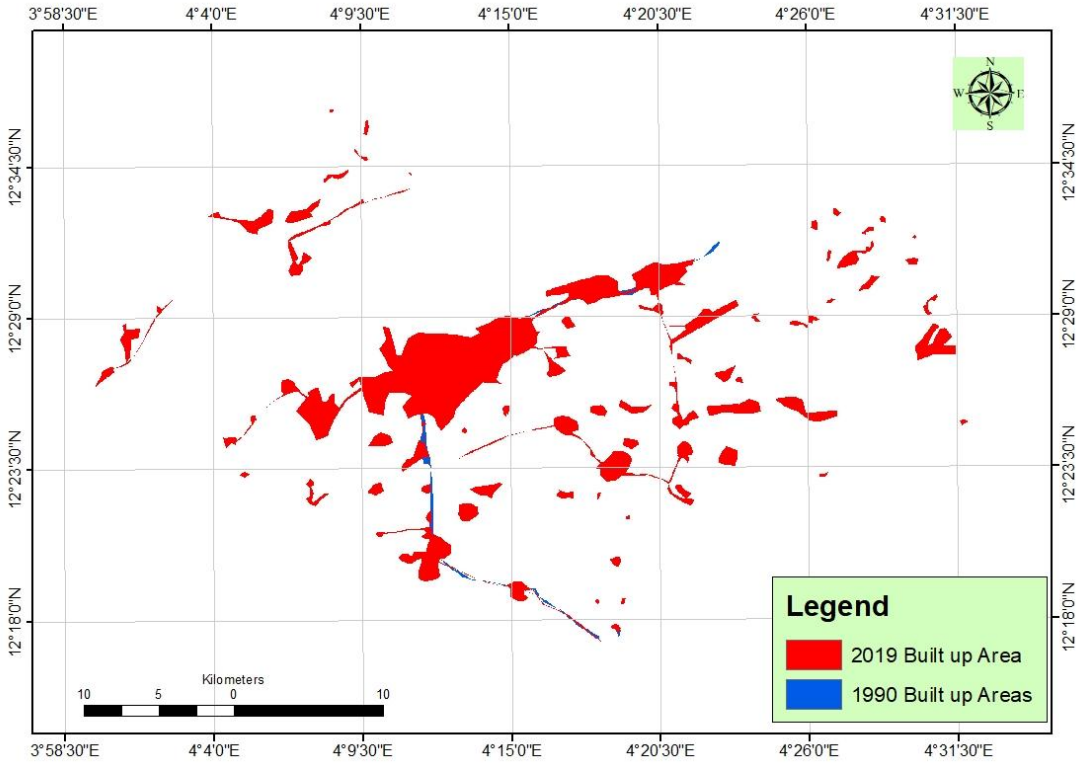


**Figure 4.19** Built-up Area Coverage of Birnin Kebbi from 1990 to 2019

Between 1990 and 2000, forest cover increased in magnitude by 32.10 km$^2$ (19.40 percent) at an annual change rate of 1.94 percent. Between 2000 and 2010, it decreased in magnitude by -172.18 km$^2$ (87.16 percent) at an annual change rate of 8.72 percent. Lastly, between 2010 and 2019, forest cover increased in magnitude by 72.16 km$^2$ (300.15 percent) at an annual change rate of 33.35 percent. The general outlook of the forest cover between 1990 and 2019 is that it decreased in magnitude by -63.96 km$^2$ (38.66 percent) at an annual change

rate of 1.33 percent. The progressive decrease in forest cover may be attributed to the increase in urban size which results in deforestation.

Between 1990 and 2000, light vegetation increased in magnitude by 24.97 $km^2$ (6.95 percent) at annual change rate of 0.70 percent. Between 2000 and 2010, it further increased in magnitude by 117.89 $km^2$ (30 .68 percent) at an annual change rate of 3.07 percent. Lastly between 2010 and 2019, light vegetation decreased in magnitude by -168.30 $km^2$ (33.52 percent) at an annual change rate of 3.72 percent. Generally, from 1990 to 2019 light vegetation decreased in magnitude by -25.44 $km^2$ (7.08 percent) at an annual change rate of 0.24 percent.

Bare surfaces increased in magnitude between 1990 and 2000 by 195.19 $km^2$ (193.64 percent) at an annual change rate of 19.36 percent. It further increased in magnitude between 2000 and 2010 by 165.72 $km^2$ (55.99 percent) at an annual change rate of 5.60 percent. However, between 2010 and 2019, bare surfaces decreased in magnitude by -58.23 $km^2$ (12.61 percent) at an annual change rate of 1.40 percent. Generally, from1990 to 2019, bare surfaces increased in magnitude by 302.68 $km^2$ (300.28 percent) at an annual change rate of 10.35 percent.

Water bodies increased in magnitude by 53.06 $km^2$ (872.70 percent) between 1990 and 2000 at an annual change rate of 0.28. It decreased in magnitude by -50.99 $km^2$ (86.22 percent) between 2000 and 2010 at an annual change rate of 8.62 percent. It increased in magnitude by 5.57 $km^2$ (68.34 percent) between 2010 and 2019. By and large, from 1990 to 2019, water bodies increased in magnitude by 7.64 $km^2$ (125.66 percent) an annual change rate of 4.33 percent.

Between 1990 and 2000, agricultural lands decreased in magnitude by -318.21 $km^2$ (52.75 percent) at an annual change rate of 5.28 percent. It further decreased in magnitude by -98.83 $km^2$ (34.67 percent) at an annual change rate of 3.47 percent between 2000 and 2010. However, between 2010 and 2019, agricultural lands increased in magnitude by 87.16 $km^2$ (46.81 percent) at an annual change rate of 5.20 percent. By and large, between 1990 and 2019, agricultural lands generally decreased in magnitude by -329.88 $km^2$ (54.69 percent) at an annual change rate of 1.89 percent (Table 4.8).

#### *4.1.4.4 LULC conversion model for Birnin Kebbi metropolis from 1990-2019*

The results of LULC analysis for Birnin Kebbi Metropolis between 1990 and 2019 are presented in Figure 4.20 while those of 1990 to 2000, 2000 to 2011 and 2010 to 2019 are presented in Appendix D4. The results of LULC analysis for Birnin Kebbi city for the first period (1990 - 2000) showed that almost all the land cover classes lost and gained some grounds. Forest cover lost -1444.39 $km^2$ (-96.03 percent) and gained 137.87 $km^2$ (69.77 percent). Light vegetation lost -165.84 $km^2$ (-46.16) and gained 1529.20 $km^2$ (88.77 percent). Agricultural lands lost -375.35 $km^2$ (-66.22 percent) and gained 57.25 $km^2$ (20.08 percent). Bare surfaces lost -51.23 $km^2$ (-43.07 percent) and gained 18.95 $km^2$ (70.30 percent). Water bodies lost -3.95 $km^2$ (-64.96 percent) and gained 57.01 $km^2$ (96.39 percent). Summarily, for the period 1990 to 2000, greater losses were recorded by forest cover, light vegetation and agricultural lands.

The net changes of the land use classes revealed that forest cover and agricultural lands recorded net negative changes of -1,306.53 $km^2$ (-661.23 percent) and -318.09 $km^2$ (-111.56 percent) respectively, while light vegetation, bare surfaces, built up areas and water bodies recorded positive net gains of 1,361.36 $km^2$ (79.14 percent), 195.31 $km^2$ (65.96 percent),

12.89 $km^2$ (47.83 percent) and 53.06 $km^2$ (89.71 percent) respectively. Forest cover, agricultural lands, light vegetation and bare surfaces contributed 6.53, 4.72, 1.29 and 0.35 $km^2$ respectively to net changes in built up areas while there was no contribution by water bodies.

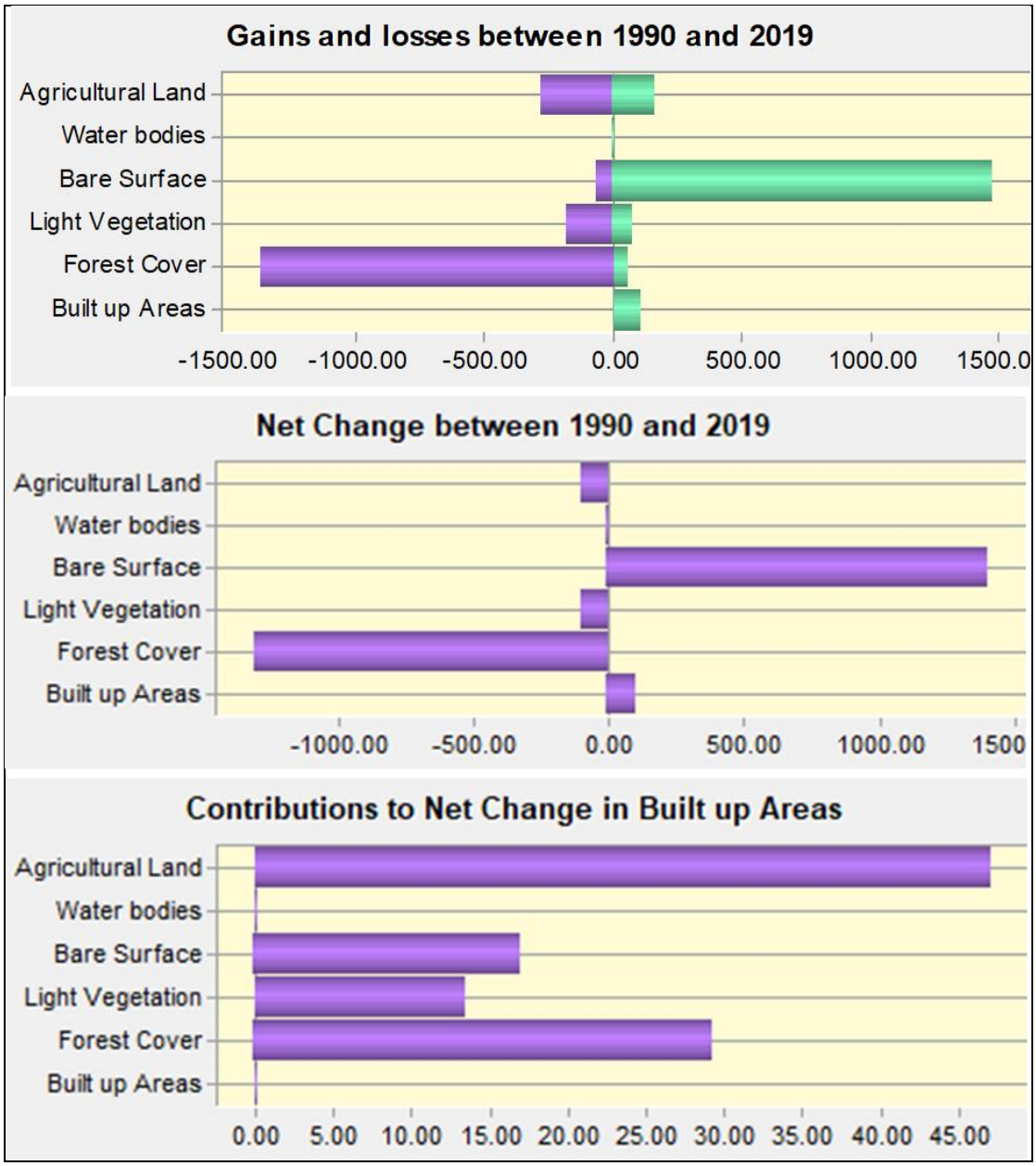


**Figure 4.20 Land cover transition for Birnin Kebbi for 1990-2019**

Statistics of losses and gains by the land use/land cover classes for the period 2000 – 2010 (Appendix D) showed that light vegetation lost -597.22 $km^2$ (-2.13 percent) and gained 726.52 $km^2$ (2.5 percent). Bare surfaces lost -258.92 $km^2$ (-93.71), and gained 443.29 (95.97 percent). Forest cover lost -184.18 $km^2$ (-99.59 percent) and gained 24.56 $km^2$. Water bodies lost 55.29 $km^2$ and gained 8.10 $km^2$. Forest cover, agricultural lands, water bodies and built up all recorded net losses of -159.62 $km^2$ (-678.95 percent), -81.45 $km^2$ (-53.1 percent), -47.20 $km^2$ (-625.86 percent) and 25.46 $km^2$ (-58.74 percent) respectively, while light vegetation and bare surfaces recorded net gains of 129.35 $km^2$ (0.38 percent) and 184.37 $km^2$ (35.89 percent) respectively. Light vegetation, bare surfaces, agricultural lands and forest cover contributed -22.60, -1.88, -0.84 and 0.1 $km^2$ respectively to the net losses in built up areas. The seeming loss of built up area over the period may be explained largely by the increased coverage of light vegetation which may have covered some built up surfaces.

Between 2010 – 2019 are 76.95, built up area gained 72.54 $km^2$ (100.00 percent) Bare surfaces lost -244.76 $km^2$ (-52.99) and gained 184.26 (45.90 percent). Forest cover lost -22.25 $km^2$ (-87.73 percent) and gained 95.75 $km^2$ (96.85 percent). Water bodies lost -2.70 $km^2$ (-33.17 percent) and gained 8.27 $km^2$(60.31 percent). Agricultural lands lost -120.23 $km^2$ (-64.55 percent) and gained 202.82 $km^2$ (60.31 percent).The net gains and losses of the various land use and land cover classes indicated that built-up, forest cover, agricultural lands and water bodies all recorded net gains of 72.54 $km^2$ (100.00 percent), 73.50 $km^2$ (74.34 percent), 82.58 $km^2$ (30.72 percent) and 5.57 $km^2$ (40.60 percent) respectively, while light vegetation and bare surfaces recorded net losses of -173.70 $km^2$ (-0.59 percent) and -60.50 $km^2$ (-15.07 percent) respectively. Light vegetation, bare surfaces, agricultural lands

and forest cover contributed 29.19, 27.22, 15.56 and 0.57 $km^2$ respectively to the net gains in built up area.

The general outlook of the land use /land cover transition of Birnin Kebbi between 1990 and 2019 is presented in Figures 4.20. The Statistics of losses and gains by the land use/land cover classes for the period 1990 -2019 are shown in Figure 4.20A. Between 1990 and 2019, built-up lost -2.51 $km^2$ and gained 109.37 $km^2$. Forest cover lost -1367.69 $km^2$ and gained 54.76 $km^2$. Light vegetation lost -180.42 $km^2$ and gained 78.54 $km^2$. Bare surfaces lost -68.54 $km^2$ and gained 1,477.46 $km^2$. Water bodies lost -3.40 $km^2$ and gained 10.72 $km^2$. The seeming gain in water bodies may be attributed to deforestation which may have exposed some water bodies initially covered by vegetation. Agricultural lands lost -82.12 $km^2$ and gained 173.82 $km^2$.

By and large, the net gains and losses of the various land use and land cover classes are presented in Figure 4.20B. Built-up, bare surfaces and water bodies recorded net gains of 106.89, 1,408.92 and 7.32 respectively $km^2$, whereas forest cover, light vegetation and agricultural lands recorded net losses of water bodies and built up all recorded net losses of -1,312.93 $km^2$, -101.88 $km^2$ and 108.30 $km^2$ respectively, while light vegetation and bare surfaces recorded net gains of 129.35 $km^2$ (0.38 percent) and 184.37 $km^2$ (35.89 percent) respectively. Lastly, during the period, forest cover (29.36 $km^2$), light vegetation (13.40 $km^2$), bare surfaces (17.04 $km^2$), water bodies (0.01 $km^2$) and agricultural lands (47.05 $km^2$) all contributed positively to the net change in built up (Figure 4.20C).

### 4.1.5 Urban built up coverage between 1990 and 2019

This section is a comparative analysis of urban built coverages for Ibadan, Owerri, Kano and Birnin Kebbi between 1990 and 2019. The percentage built up coverage for the four cities

from 1990 to 2019 is presented in Figure 4.21. It shows that Owerri Metropolis recorded the least increase in built-up surfaces. It increased by 297.53 percent from 12.94 percent in 1990 to 38.50 percent in 2019. In Ibadan, built-up surfaces increased in percent coverage by 332.43 percent from 9.19 percent in 1990 to 38.50 percent in 2019. Built-up surfaces in Kano metropolis increased in size by 369.37 percent from 11.85 percent in 1990 to 43.77 percent in 2019. Birnin Kebbi recorded the highest increase in built-up surfaces. It increased by 871.68 percent from 1.13 percent in 1990 to 9.85 percent in 2019. The high rate of increase in urban built surfaces may be attributed to its establishment as the capital of Kebbi State in 1991 and establishment of higher institutions of learning which has resulted in the influx of people into the city.

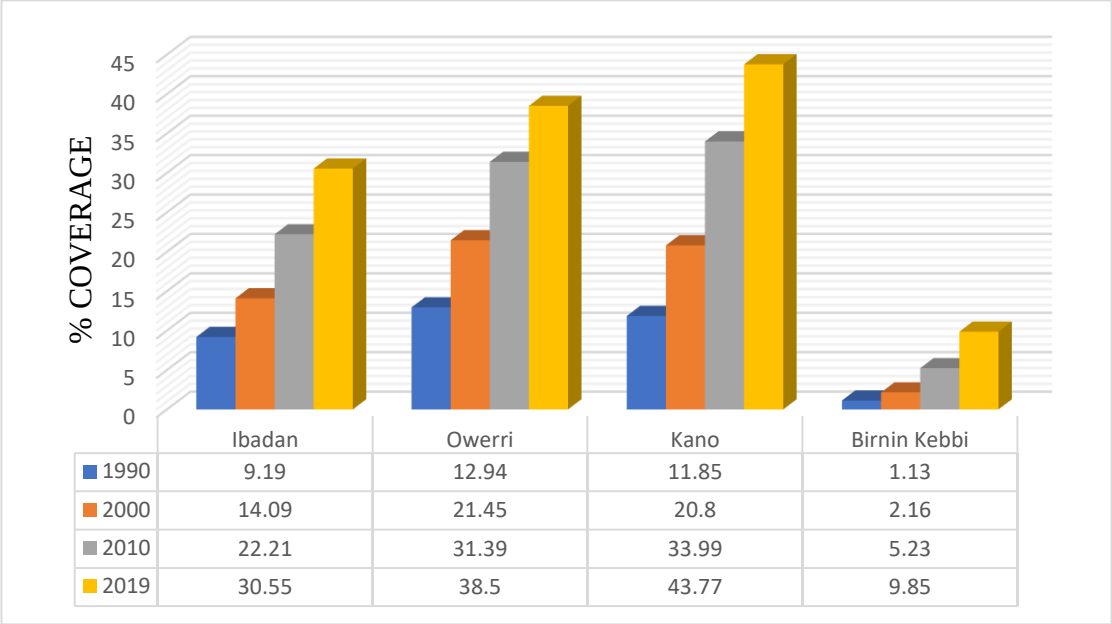


| | Ibadan | Owerri | Kano | Birnin Kebbi |
|---|---|---|---|---|
| 1990 | 9.19 | 12.94 | 11.85 | 1.13 |
| 2000 | 14.09 | 21.45 | 20.8 | 2.16 |
| 2010 | 22.21 | 31.39 | 33.99 | 5.23 |
| 2019 | 30.55 | 38.5 | 43.77 | 9.85 |

**Figure 4.21** Built up coverage of the four cities from 1990 to 2019

The high urbanization rate of Birnin Kebbi may have also contributed to the high rate of bare surfaces.

## 4.2 NDVI of Selected Cities from 1990 to 2019

The following section is the presentation of results of NDVI analysis of the Ibadan, Owerri, Kano and Birnin Kebbi from 1990 to 2019.

### 4.2.1 NDVI of Ibadan metropolis 1990-2019

NDVI images of Ibadan Metropolis in 1990 and 2019 are presented in Figures 4.22 and 4.23 while those of 2001 and 2011 are shown in Appendix E. Results showed that the maximum recorded NDVI of the city was 0.97, 0.25, 0.12 and 0.42 in 1990, 2001, 2011 and 2019 respectively, while the minimum was -0.95, -0.65, -0.39 and -0.02 in 1990, 2001, 2011 and 2019 respectively. This implied that both maximum (0.97) and minimum (-0.97) NDVI values in the city were recorded in Ibadan in 2019.

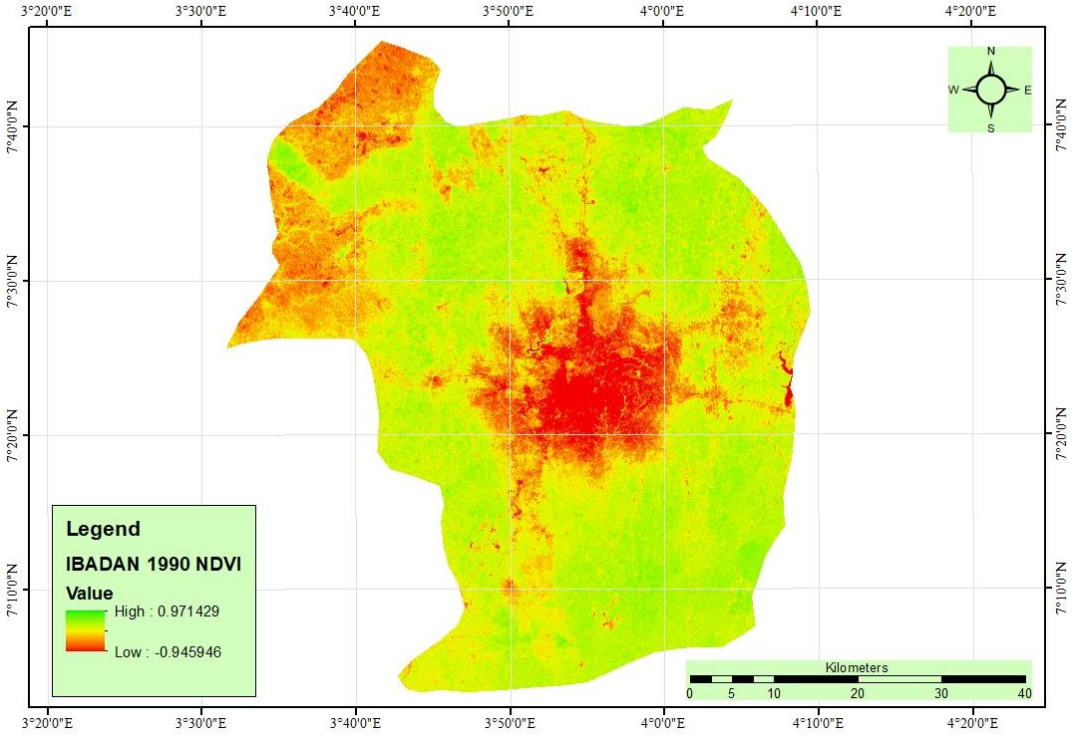


**Figure 4.22** NDVI of Ibadan Metropolis in 1990

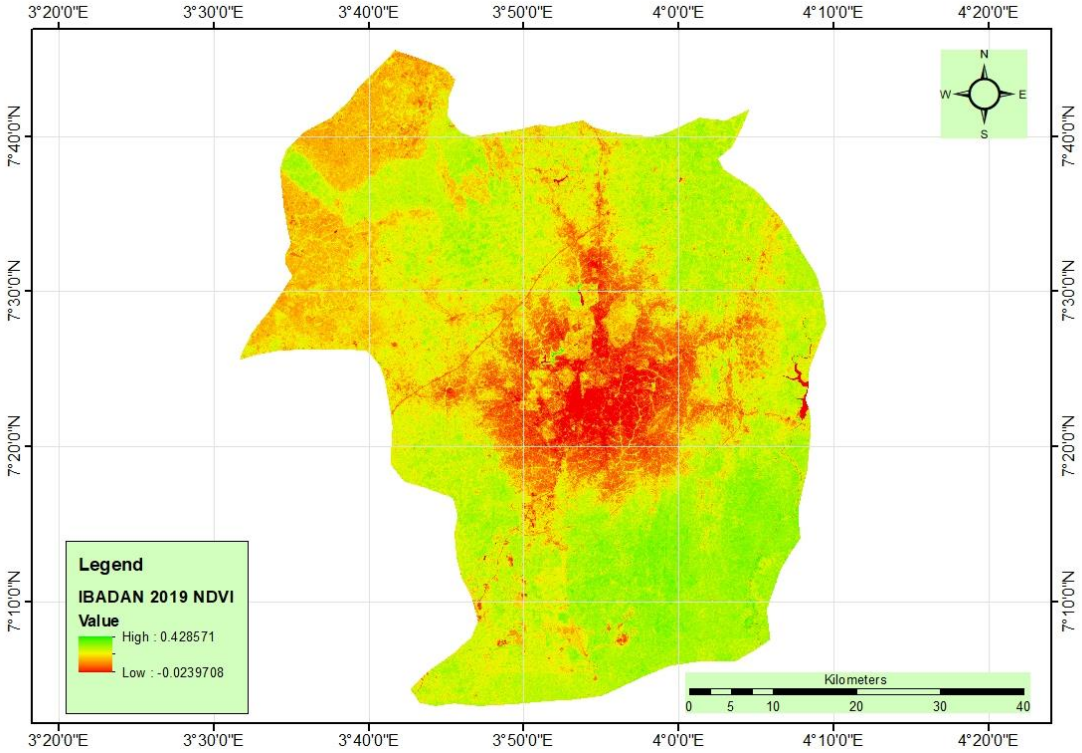


**Figure 4.23** NDVI of Ibadan Metropolis in 2019

The mean NDVI values of -0.08, -0.13, -0.08 and 0.24 were recorded in 1990, 2001, 2011 and 2019 respectively; indicating that the highest mean value was recorded in 2019, while the lowest mean value was recorded in 2001. For standard deviation, recorded values were 1.85, 0.09, 0.07, and 0.07 in 1990, 2001, 2011 and 2019 respectively, indicating that 1990 had the highest standard deviation. The high NDVI points were concentrated around the non-urbanized locations of the city such as thick and light vegetation areas of the city, which possessed insignificant concentrations of built up surfaces, while the lowest NDVI values were concentrated in the built areas (particularly the core of the city), bare surfaces, and water surfaces which devoid of vegetal cover.

Figure 4.24 shows the statistics of re-classified NDVI images of Ibadan in 1990, 2001, 2011 and 2019 respectively while the classification maps are shown in Appendix F. The statistics showed that in 1990, low NDVI areas (-0.95 to -0.23) occupied 253.64 $km^2$ (7.45 percent of

the total area). The secondary low NDVI areas (-0.23 to -0.15) occupied 596.06 km$^2$ (17.52 percent). The medium NDVI areas (-0.15 to -0.09) occupied 958.37 km$^2$ (28.16 percent). The secondary high NDVI areas (-0.09 to -0.04) covered 1205.39 km$^2$ (35.42 percent). The high NDVI areas (-0.04 to 0.97) covered 389.61 km$^2$ (11.45 percent). This implied that in 1990, high and secondary high NDVI areas (-0.09 to 0.97) collectively occupied 1595.00 km$^2$ and covered 46.87 percent of Ibadan. Low and secondary low NDVI areas (-0.95 to -0.15) collectively occupied 849.70 km$^2$ and covered 24.97 percent of the Metropolis. This implied that higher NDVI values dominated the scene of Ibadan Metropolis in 1990.

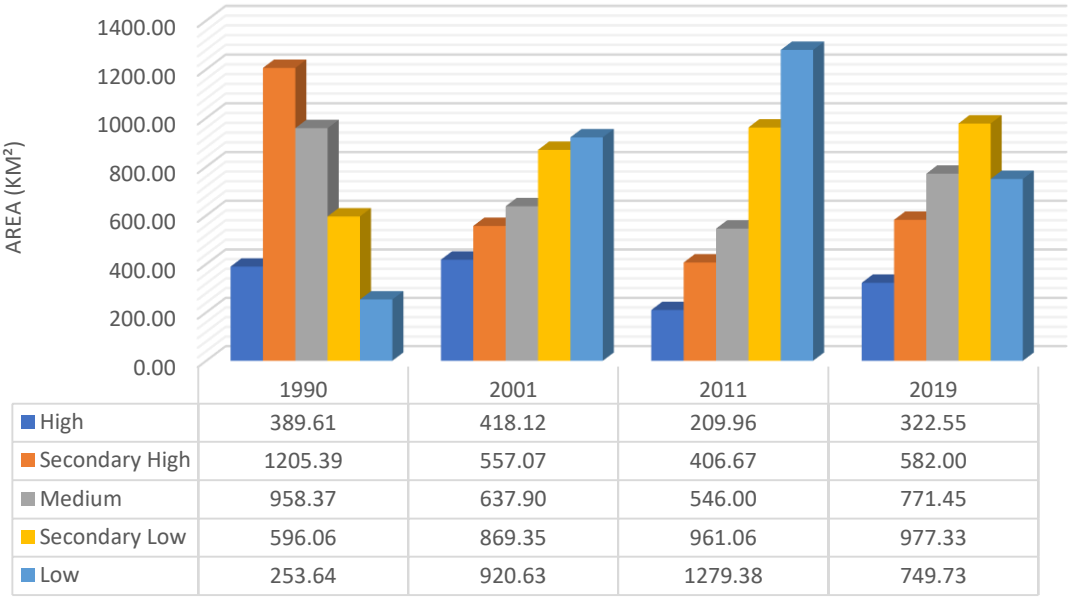


| | 1990 | 2001 | 2011 | 2019 |
|---|---|---|---|---|
| High | 389.61 | 418.12 | 209.96 | 322.55 |
| Secondary High | 1205.39 | 557.07 | 406.67 | 582.00 |
| Medium | 958.37 | 637.90 | 546.00 | 771.45 |
| Secondary Low | 596.06 | 869.35 | 961.06 | 977.33 |
| Low | 253.64 | 920.63 | 1279.38 | 749.73 |

**Figure 4.24** Ibadan NDVI Class Chart 1990 – 2019

In 2001, low NDVI areas (-0.65 to -0.25) occupied 920.63 km$^2$ (27.05 percent of the total area). The secondary low NDVI areas (-0.25 to -0.18) covered 869.35 km$^2$ (25.55 percent). The medium NDVI areas (-0.18 to -0.11) covered 637.90 km$^2$ (18.74 percent). The secondary high NDVI areas (-0.11 to -0.06) occupied 557.07 km$^2$ (16.37 percent). The high NDVI areas (-0.06 to 0.25) covered 418.12 km$^2$ (12.29 percent). This implied that in 2001,

high and secondary high NDVI areas (-0.09 to 0.97) collectively covered 975.19 $km^2$ and covered 28.66 percent of Ibadan Metropolis, indicating a coverage area decrease of 18.21 percent from 46.87 percent in 1990 to 28.66 percent in 2001.

Similarly, medium NDVI areas decreased in percentage coverage by 9.42 percent from 28.16 percent in 1990 to 18.74 percent in 2001. On the contrary low and secondary low NDVI areas (-0.95 to -0.15) collectively covered 1,789.98 $km^2$ and covered 52.60 percent of the Metropolis, indicating a coverage area increase of 27.63 percent from 24.97 percent in 1990 to 52.60 percent in 2001.

In 2011, low NDVI areas (-0.39 to -0.22) covered 1279.38 $km^2$ (37.59 percent of the total area). The secondary low NDVI areas (-0.25 to -0.18) occupied 961.06 $km^2$ (28.24 percent). The medium NDVI areas (-0.14 to -0.08) covered 546.00 $km^2$ (16.04 percent). The secondary high NDVI areas (-0.08 to -0.03) occupied 406.67 $km^2$ (11.95 percent). The high NDVI areas (-0.03 to 0.12) occupied 209.96 $km^2$ (6.17 percent). This implied that in 2011, high and secondary high NDVI areas (-0.08 to 0.12) collectively occupied 616.63 $km^2$ and covered 18.12 percent of Ibadan Metropolis, indicating a progressive coverage area decrease of 10.54 percent from 28.66 percent in 2001 to 18.12 percent in 2011. Similarly, medium NDVI areas decreased progressively in percentage coverage by 2.02 percent from 18.74 percent in 2001 to 16.04 percent in 2011.

In 2019, low NDVI areas (-0.02 to -0.14) occupied 749.73 $km^2$ (22.03 percent of the total area). The secondary low NDVI areas (-0.14 to 0.20) covered 977.33 $km^2$ (28.72 percent). The medium NDVI areas (0.20 to 0.25) occupied 771.45 $km^2$ (22.67 percent). The secondary high NDVI areas (0.25 to 0.29) covered 582.00 $km^2$ (17.10 percent). The high NDVI areas (0.29 to 0.43) occupied 322.55 $km^2$ (9.48 percent). This implied that in 2019, high and

secondary high NDVI areas (0.25 to 0.43) covered 904.55km$^2$ and covered 26.58 percent of Ibadan Metropolis, indicating a coverage area higher than 2011 by 8.46 percent.

Similarly, medium NDVI areas increased in percentage coverage by 6.63 percent from 16.04 percent in 2011 to 22.67 percent in 2019. On the contrary, low and secondary low NDVI areas (-0.02 to 0.20) collectively occupied 1727.06 km$^2$ and covered 50.75 percent of the Metropolis, indicating a lower coverage area of 15.09 percent, from 65.84 percent 2011 to 50.75 percent in 2019.

This result therefore demonstrated an association between land use/land cover in Ibadan city over the study period, and was corroborated with results of previous studies (Kasim *et al*., 2020; Seun *et al*., 2022) which revealed higher NDVI values over semi-urban areas and areas that had thicker vegetal cover, while lower NDVI values were recorded over water, bare and built surfaces across the city. The persistent increase in areas with very low and low NDVI values indicated that increase in built and bare surfaces during the study period resulted in reduced coverage areas of vegetal cover. This may be explained by heightened anthropogenic activities resulting from urbanization such as land clearing for agricultural activities or construction or tree felling for other purposes.

### 4.2.2 NDVI of Owerri metropolis 1990-2019

NDVI images of Owerri Metropolis in 1990 and 2019 are presented in Figures 4.25 and 4.26 while those of 2000 and 2010 are shown in Appendix E. Results showed that the maximum recorded NDVI of the city was 0.42, 0.28, 0.42 and 0.27 in 1990, 2000, 2010 and 2019 respectively, while the minimum was -0.12, -0.32, -0.17 and -0.01 in 1990, 2000, 2010 and 2019 respectively. This implied that maximum (0.42) was recorded in 1990 and 2010 while the minimum (-0.32) NDVI values in the city were recorded in Ibadan in 2000.

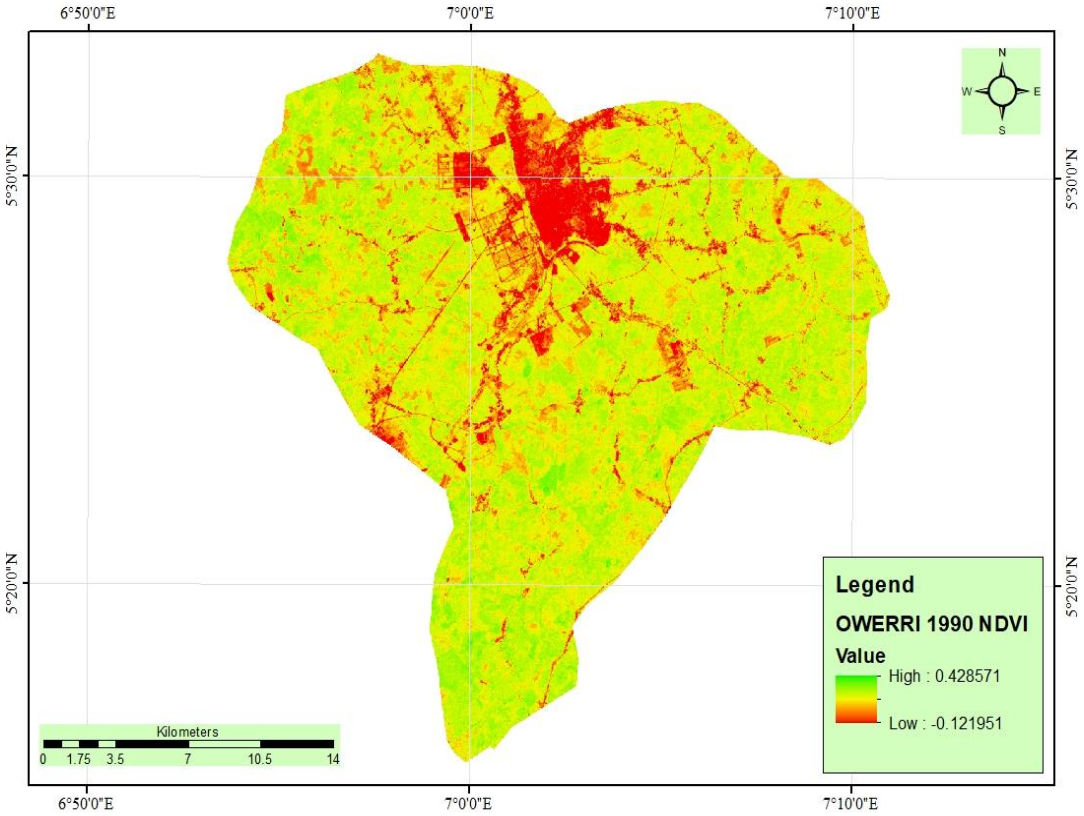


**Figure 4.25** NDVI of Owerri Metropolis in 1990

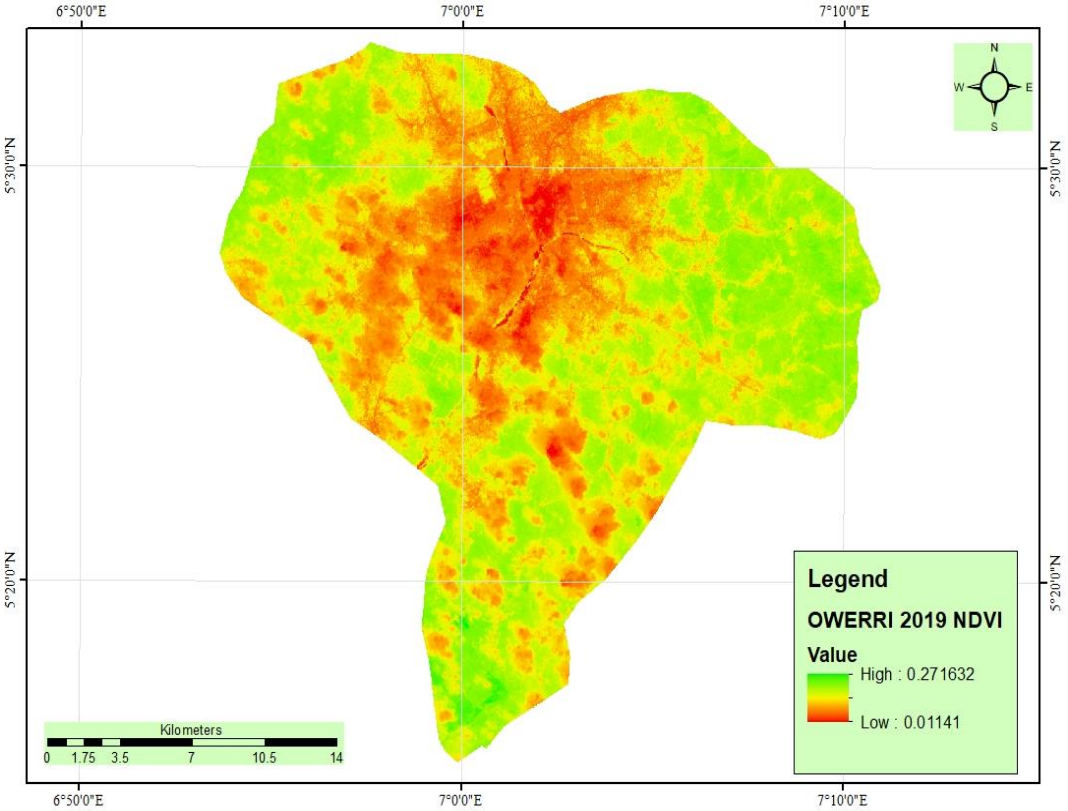


**Figure 4.26** NDVI of Owerri City in 2019

The mean NDVI values of 0.27, 0.05, 0.05 and 0.15 were recorded in 1990, 2000, 2010 and 2019 respectively; indicating that the highest mean value was recorded in 1990, while the lowest value was recorded in 2000 and 2010. For standard deviation, recorded values were 0.05, 0.08, 0.09, and 0.04 in 1990, 2000, 2010 and 2019 respectively, indicating that 2000 had the highest standard deviation. The low NDVI points are concentrated around the city core comprising of Owerri-North, Owerri-West and Owerri Municipal Local Government Areas which have the highest percentage of built-up area and vegetal cover.

Figure 4.27 shows the statistics of re-classified NDVI images of Owerri in 1990, 2000, 2010 and 2019 respectively while classification maps are shown in Appendix F. The statistics showed that in 1990, low NDVI areas (-0.12 to 0.13) 19.95 $km^2$ (3.67 percent). Secondary low areas (0.13 to 0.21) 38.41 $km^2$ (7.07 percent). The medium NDVI areas (0.21 to 0.26) occupied 88,275 points covering an area of 79.45 $km^2$ (14.62 percent). The secondary high NDVI areas (0.26 to 0.31) occupied 183.15 $km^2$ (33.70 percent). The high NDVI area (0.31 to 0.43) covered 222.45 $km^2$ (40.94 percent).

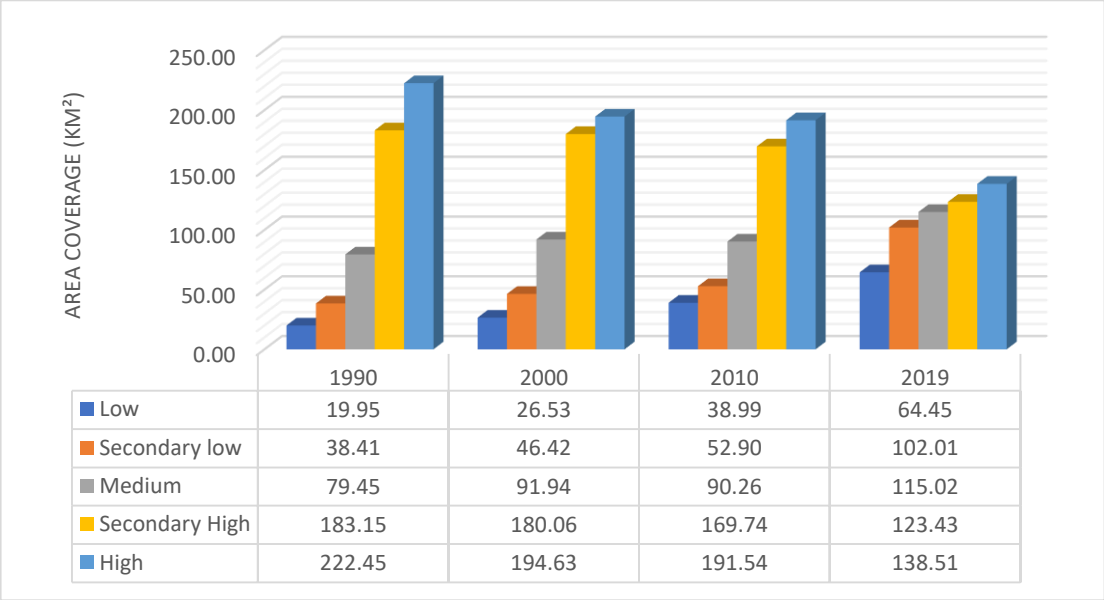


| | 1990 | 2000 | 2010 | 2019 |
|---|---|---|---|---|
| Low | 19.95 | 26.53 | 38.99 | 64.45 |
| Secondary low | 38.41 | 46.42 | 52.90 | 102.01 |
| Medium | 79.45 | 91.94 | 90.26 | 115.02 |
| Secondary High | 183.15 | 180.06 | 169.74 | 123.43 |
| High | 222.45 | 194.63 | 191.54 | 138.51 |

**Figure 4.27** Owerri NDVI Class Charts 1990 – 2019

This implied that in 1990 high and secondary high NDVI areas (0.26 to 0.43) collectively occupied 450,669 points (405.60km km$^2$) and covered 74.64 percent of Owerri Metropolis, whereas low and secondary low NDVI areas (-0.12 to 0.21) collectively occupied 58.37 km$^2$ and covered about 10.74 percent of the Metropolis.

In 2000, low NDVI areas (-0.32 to -0.13) occupied 26.53 km$^2$ (4.92 percent of the total area). The secondary low NDVI areas (-0.13 to -0.04) covered 46.42 km$^2$ (8.60 percent). The medium NDVI areas (-0.04 to 0.04) occupied 91.94 km$^2$ (17.04 percent). The secondary high NDVI areas (0.04 – 0.09) covered 180.06 km$^2$ (33.37 percent). The high NDVI areas (0.09 – 0.28) covered 194.63 km$^2$ (36.07 percent). This implied that in 2000, high and secondary high NDVI areas (0.04 – 0.28) collectively occupied 374.69 km$^2$ and covered 69.44 percent of Owerri Metropolis, indicating a coverage area lower than 1990 by 5.20 percent. On the contrary, low and secondary NDVI areas (72.95 km$^2$) increased slightly in percentage coverage by 2.78 percent from 10.74 percent in 1990 to 13.52 percent in 2000. Similarly, medium NDVI areas increased in coverage from 79.45 km$^2$ (14.62 percent) in 1990 to 91.94 km$^2$ (17.04 percent) in 2000, a difference of 2.42 percent.

In 2010, low NDVI areas (-0.17 to -0.02) covered 38.99 km$^2$ (7.17 percent of the total area). The secondary low NDVI areas (0.02 to 0.11) occupied covered 52.90 km$^2$ (9.73 percent). The medium NDVI areas (0.11 to 0.19) covered 90.26 km$^2$ (16.61 percent). The secondary high NDVI areas (0.19 to 0.25) covered 169.74 km$^2$ (31.24 percent). The high NDVI areas (0.25 to 0.42) occupied 191.54km$^2$ (32.25 percent).

This implied that in 2010, high and secondary high NDVI areas (0.19 to 0.42) collectively occupied 361.28 km$^2$ and covered 66.48 percent of Owerri Metropolis, indicating a coverage area lower than 2000 by 2.96 percent. Similarly, medium NDVI areas decreased in

percentage coverage from 17.04 percent in 2000 to 16.61 percent in 2010. On the other hand, low and secondary low NDVI areas (-0.17 to 0.11) collectively occupied 91.87 $km^2$ and covered 16.91 percent of the Metropolis, indicating a coverage area higher than year 2000 by 3.39 percent.

In 2019, low NDVI areas (0.01 - 0.10) occupied 64.45 $km^2$ (11.86 percent of the total area). The secondary low NDVI areas (0.10 – 0.13) covered 102.01 $km^2$ (18.77 percent). The medium NDVI areas (0.13 – 0.16) 115.02 $km^2$ (21.17 percent). The secondary high NDVI areas (0.16 – 0.19) covered 123.43 $km^2$ (22.71 percent). The high NDVI areas (0.12 – 0.27) 138.51 $km^2$ (25.49 percent). This implied that in 2019, high and secondary high NDVI areas (0.16 – 0.27) collectively occupied 261.95 $km^2$ and covered 48.20 percent of Owerri Metropolis, indicating a coverage area lower than 2010 by 18.28 percent. On the contrary, low and secondary low NDVI areas (0.01 – 0.13) collectively covered 166.46 $km^2$ and covered 30.63 percent of the Metropolis, indicating an increase in percentage coverage by 13.72 percent from 16.91 percent in 2010 to 30.63 percent in 2019. Similarly, medium NDVI areas increased in percentage coverage from 16.61 percent in 2010 to 21.17 in 2019.

As in the case of Ibadan, the study demonstrated an association between land use/land cover in Owerri metropolis during the period, and corroborated the results of Kasim *et al*., 2020 and Seun *et al*., 2022 which depicted higher NDVI values over semi-urban areas and areas that had thicker vegetal cover, while lower NDVI values were recorded over water, bare and built surfaces across the city. The city also witnessed a persistent increase in areas with very low and low NDVI values; indicating that increase in built and bare surfaces during the period resulted in reduced coverage areas of vegetation. This may be explained by heightened rate of deforestation occasioned by urbanization.

### 4.2.3 NDVI of Kano metropolis 1991-2019

NDVI images of Kano Metropolis in 1991 and 2019 are presented in Figures 4.28 and 4.29 while those of 2001 and 2011 are shown in Appendix E. Results showed that the maximum recorded NDVI of the city was 0.43, 0.17, 0.42 and 0.40 in 1991, 2001, 2011 and 2019 respectively, while the minimum was -0.34, -0.59, -0.37 and -0.24 in 1991, 2001, 2011 and 2019 respectively. This implied that maximum (0.43) was recorded in 1991 while the minimum (-0.59) NDVI values in the city were recorded in Ibadan in 2001. The mean NDVI values of 0.02, -0.22, 0.06 and 0.12 were recorded in 1991, 2001, 2011 and 2019 respectively; indicating that the highest mean value was recorded in 2019, while the lowest value was recorded in 2001.

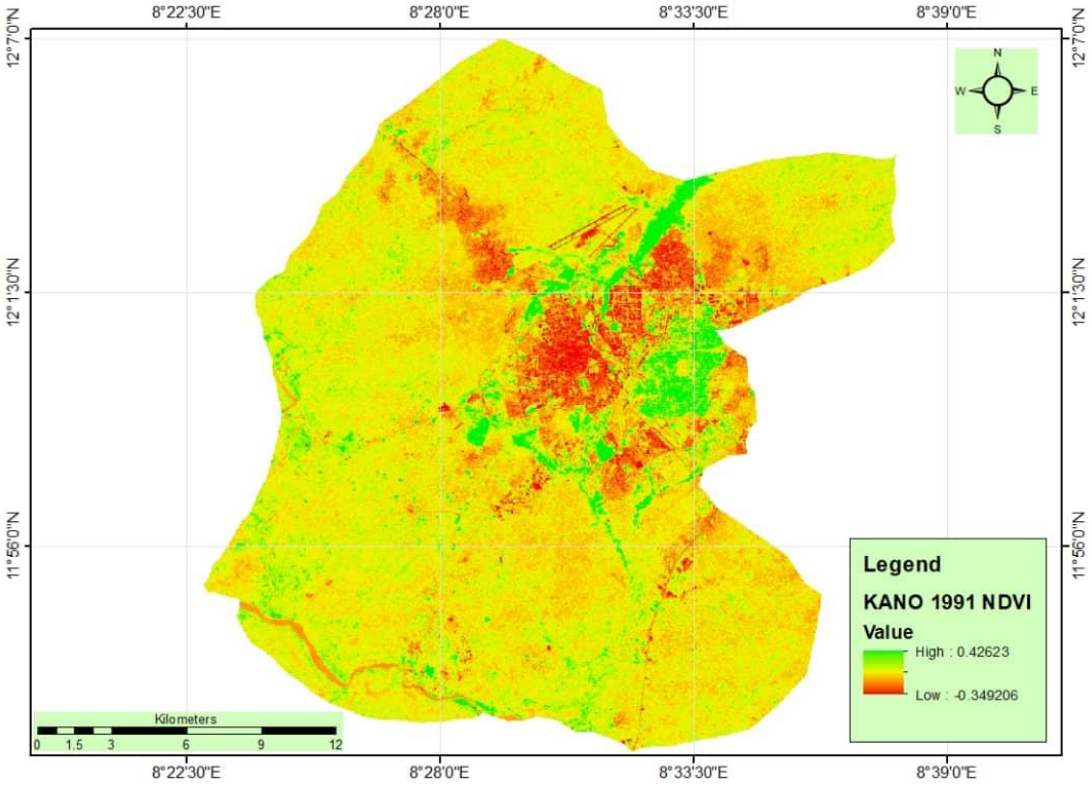


**Figure 4.28** NDVI of Kano Metropolis in 1991

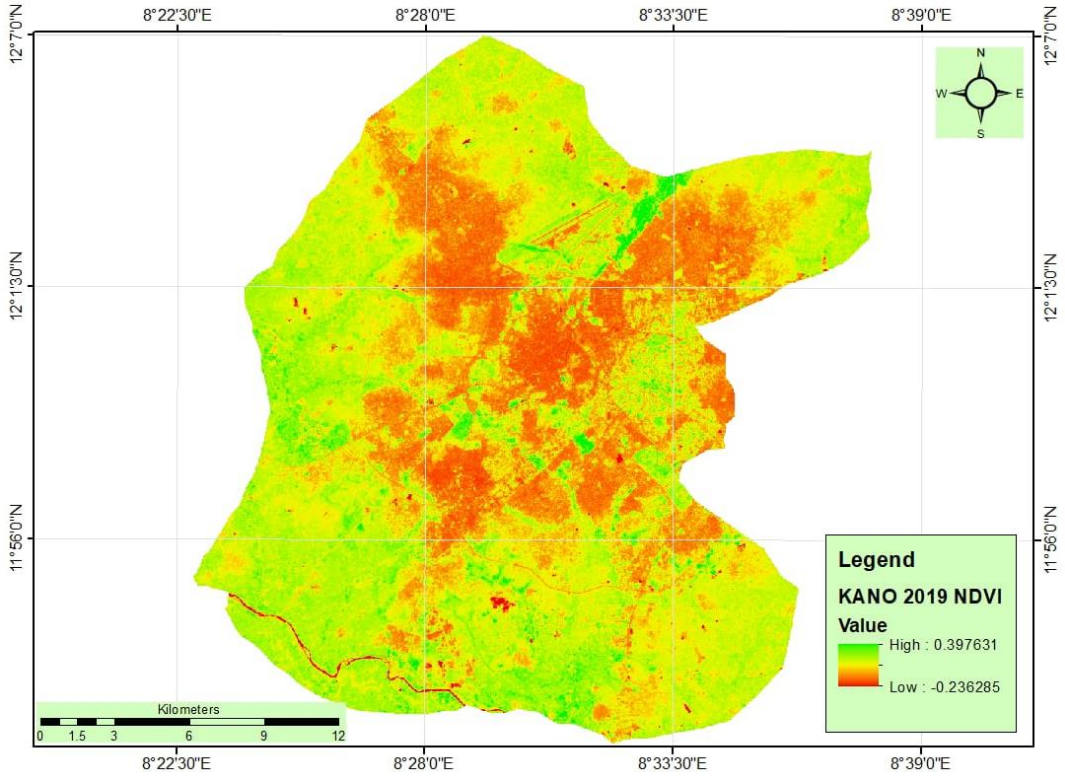


**Figure 4.29** NDVI of Kano City in 2019

For standard deviation, recorded values were 0.04, 0.05, 0.09, and 0.05 in 1991, 2001, 2011 and 2019 respectively, indicating that 2011 had the highest standard deviation while 1991 recorded the least. The lowest NDVI points are concentrated around the city core comprising of Dala, Fagge, Gwale, Kano Municipal, Nassarawa, Government Areas which have the highest percentage of built-up area and vegetal cover.

Figure 4.30 shows the statistics of re-classified NDVI images of Kano metropolis in 1991, 2001, 2011 and 2019 respectively while classification maps are shown in Appendix F. The statistics showed that in 1991, low NDVI areas (-0.35 to -0.27) occupied 8.61 $km^2$ (8.62 percent of the total area). The secondary low NDVI areas (-0.27 to 0.02) covered 191.91 $km^2$ (38.88 percent). The medium NDVI areas (0.02 to 0.05) covered 196093 $km^2$ (39.90 percent). The secondary high NDVI areas (0.05 to 0.13) covered an area of 50.85 $km^2$ (10.30 percent). The high NDVI areas (0.13 to 0.43) occupied 11.28 $km^2$ (2.28 percent).

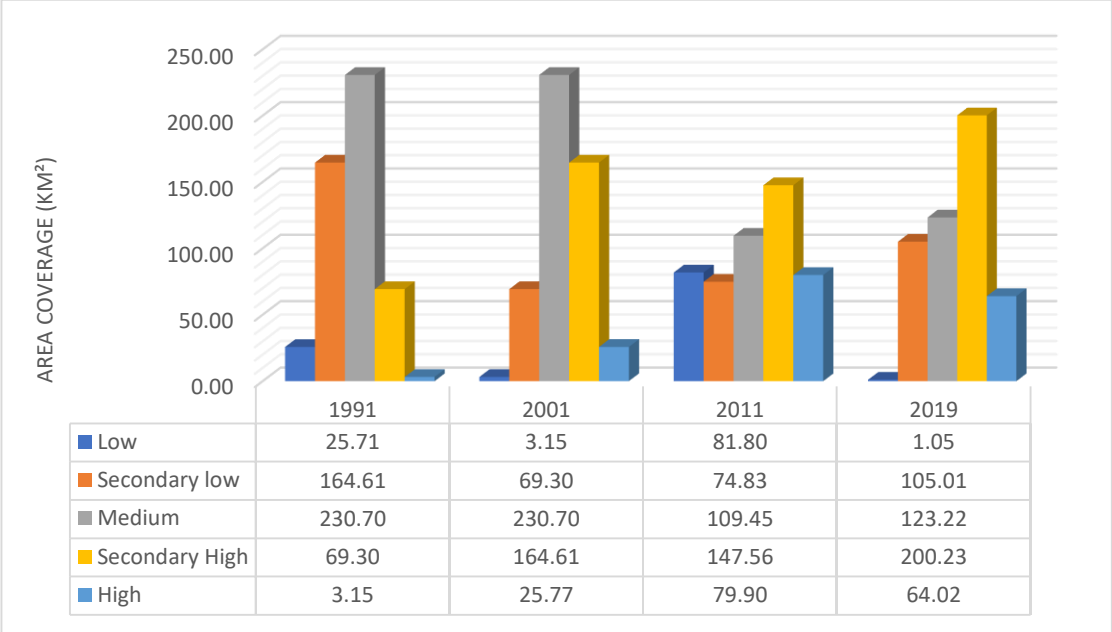


| | 1991 | 2001 | 2011 | 2019 |
|---|---|---|---|---|
| Low | 25.71 | 3.15 | 81.80 | 1.05 |
| Secondary low | 164.61 | 69.30 | 74.83 | 105.01 |
| Medium | 230.70 | 230.70 | 109.45 | 123.22 |
| Secondary High | 69.30 | 164.61 | 147.56 | 200.23 |
| High | 3.15 | 25.77 | 79.90 | 64.02 |

**Figure 4.30** Kano NDVI Class Charts 1991 – 2019

This implied that in 1991 high and secondary high NDVI areas (0.05 to 0.43) collectively occupied 11.12 $km^2$ and covered 2.26 percent of Kano Metropolis, whereas low and secondary low NDVI areas (-0.35 to 0.02) collectively occupied 386.84 $km^2$ and covered about 78.38 percent of the Metropolis. In 2001, low NDVI areas (-0.59 to -0.38) covered 25.77 $km^2$ (5.22 percent of the total area). The secondary low NDVI areas(-0.38 to -0.27) covered 164.61 $km^2$ (33.35 percent). The medium NDVI areas (-0.27 to -0.22) occupied 230.70 $km^2$ (46.75 percent). The secondary high NDVI areas (-0.22 to -0.15) covered 69.30 $km^2$ (14.04 percent).

The high NDVI areas (-0.15 to 0.17) occupied 3.15 $km^2$ (0.64 percent). This implied that in 2001, high and secondary high NDVI areas (-0.22 – 0.17) collectively occupied 72.45 $km^2$ and covered 14.68 percent of Kano Metropolis, indicating a coverage area higher than 1991 by 12.42 percent. Similarly, medium NDVI areas increased in coverage from 19.37 percent

in 1990 to 46.75 percent in 2001. On the contrary, low and secondary NDVI areas (-0.59 to -0.27) collectively covered 190.38 $km^2$ or 38.57 percent, a decrease of 39.81 percent.

In 2011, low NDVI areas (-0.08 to -0.06) covered 81.80 $km^2$ (16.58 percent of the total area). The secondary low NDVI areas (-0.06 to -0.20) occupied 74.83 $km^2$ (15.16 percent). The medium NDVI areas (-0.20 to 0.09) covered 109.45 $km^2$ (22.18 percent). The secondary high NDVI areas (0.09 to 0.15) covered 147.56 $km^2$ (29.90 percent). The high NDVI areas (0.15 to 0.42) covered 79.90 $km^2$ (16.19 percent). This implied that in 2011, high and secondary high NDVI areas (0.09 to 0.42) collectively occupied 227.45 $km^2$ and covered 46.09 percent of Kano Metropolis. Similarly, medium NDVI areas decreased in percentage coverage from 46.75 percent in 2001 to 22.18 percent in 2011. On the other hand, low and secondary low NDVI areas (-0.38 to -0.20) collectively covered 156.63 $km^2$ (31.74 percent) of the Metropolis, indicating a coverage area higher than year 2001 by 17.06 percent.

In 2019, low NDVI areas (-0.24 - 0.01) covered 1.05 $km^2$ (0.21 percent of the total area). The secondary low NDVI areas (-0.01 to 0.08) occupied 105.01 $km^2$ (21.28 percent). The medium NDVI areas (0.08 – 0.13) occupied 123.22 $km^2$ (24.97 percent). The secondary high NDVI areas (0.13 – 0.17) occupied 200.23 $km^2$ (40.57 percent). The high NDVI areas (0.17 – 0.40) covered 64.02 $km^2$ (12.97 percent). This implied that in 2019, high and secondary high NDVI areas (0.13 – 0.40) collectively occupied 264.25 $km^2$ and covered 53.54 percent of Kano Metropolis, indicating a coverage area higher than 2011 by 7.45 percent. Similarly, medium NDVI areas increased in percentage coverage from 22.18 percent in 2011 to 24.9 in 2019. On the contrary, low and secondary low NDVI areas (-0.24 – 0.08) collectively occupied 106.06 $km^2$ and covered 21.49 percent of the Metropolis, indicating an decrease in percentage coverage by 21.49 percent.

### 4.2.4 NDVI of Birnin Kebbi metropolis 1990-2019

NDVI images of Birnin Kebbi Metropolis in 1990 and 2019 are presented in Figures 4.31 and 4.32 while those of 2000 and 2010 are shown in Appendix E. Results showed that the maximum recorded NDVI value of the city was 0.17, 0.60, 0.48 and 0.56 in 1990, 2000, 2010 and 2019 respectively, while the minimum was -0.01, -0.39, -0.51 and -0.28 in 1990, 2000, 2010 and 2019 respectively. This implied that maximum value (0.60) was recorded in 2000 while the minimum (-0.51) NDVI values in the city were recorded in Ibadan in 2010. The mean NDVI values of 0.13, 0.14, 0.04 and 0.25 were recorded in 1990, 2000, 2010 and 2019 respectively; indicating that the highest mean value was recorded in 2019, while the lowest value was recorded in 2000.

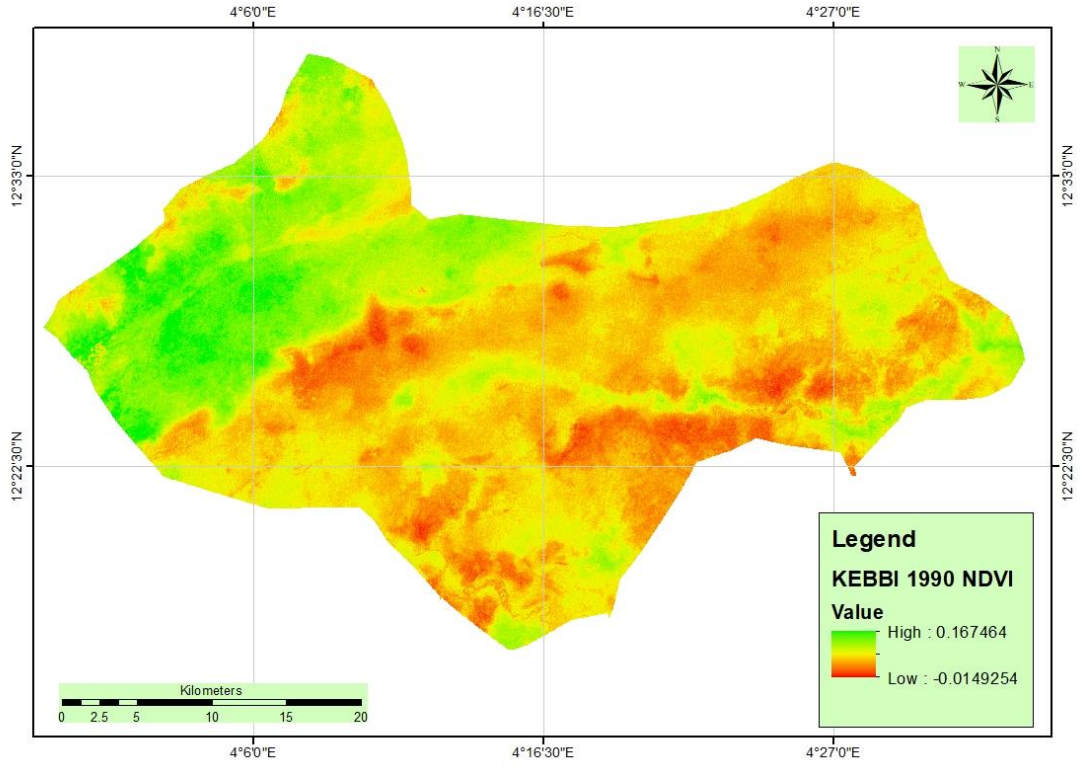


**Figure 4.31** NDVI of Birnin Kebbi Metropolis in 1990

For standard deviation, recorded values were 0.05, 0.10, 0.06, and 0.06 in 1990, 2000, 2010 and 2019 respectively, indicating that 2000 had the highest standard deviation while 1990 recorded the least. The high NDVI points were concentrated along the flood plains because of the cultivated agricultural crops, while lowest NDVI values occupied built surfaces and open/bare surfaces.

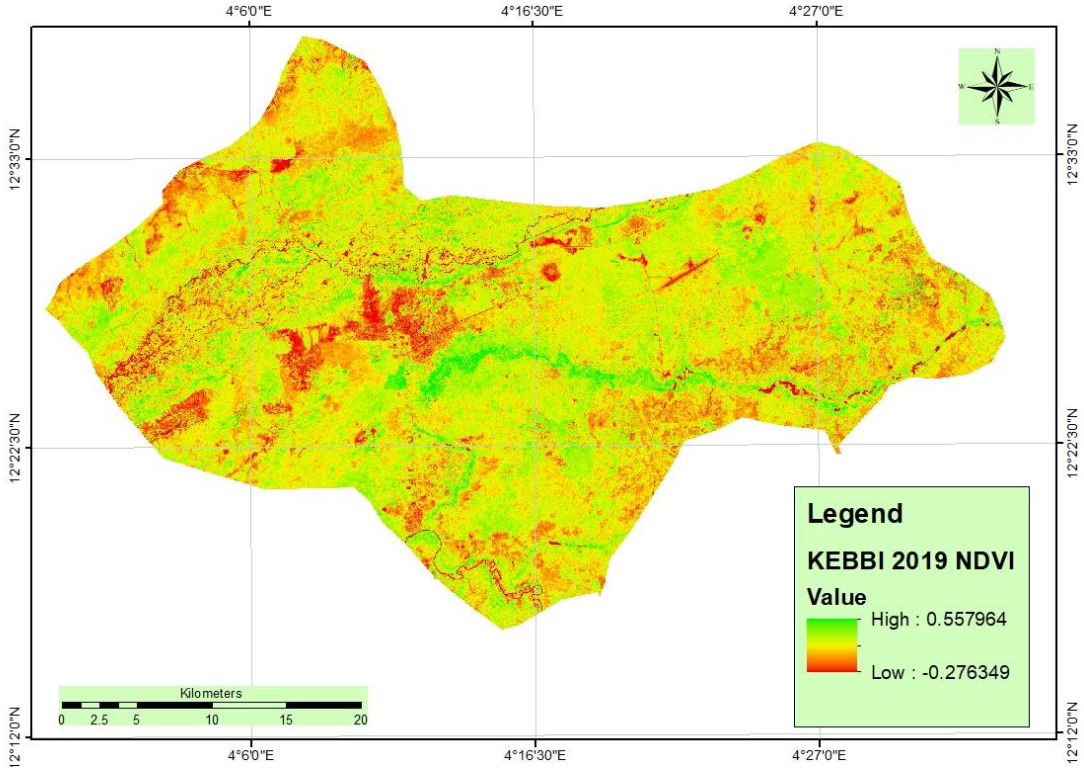


**Figure 4.32** NDVI of Birnin Kebbi City in 2019

Figure 4.33 shows the statistics of re-classified NDVI images of Birnin Kebbi metropolis in 1990, 2000, 2010 and 2019 respectively while classification maps are shown in Appendix F. The statistics showed that in 1990, low NDVI areas (-0.01 to 0.34) covered 185.41 $km^2$ (14.85 percent). Secondary low areas (0.34 to 0.05) covered 388.65 $km^2$ (31.12 percent). The medium NDVI areas (0.05 to 0.07) occupied 334.59 $km^2$ (26.79 percen). The secondary

high NDVI areas (0.07 to 0.10) covered 212.10 km$^2$ (16.98 percent). The high NDVI areas (0.10 to 0.17) covered 128.13 km$^2$ (10.26 percent).

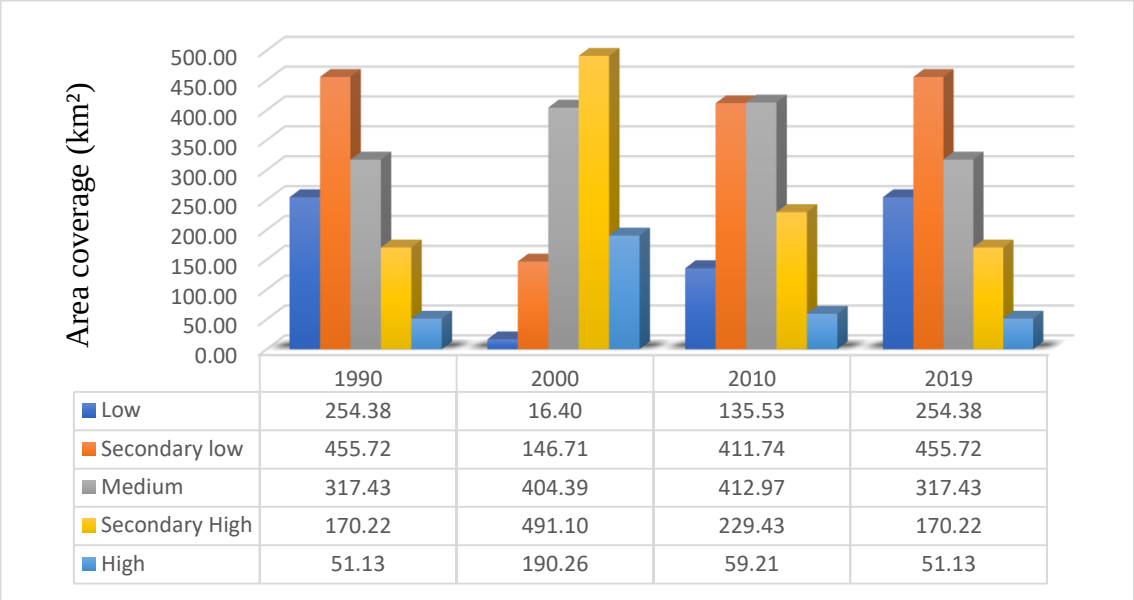


| | 1990 | 2000 | 2010 | 2019 |
|---|---|---|---|---|
| Low | 254.38 | 16.40 | 135.53 | 254.38 |
| Secondary low | 455.72 | 146.71 | 411.74 | 455.72 |
| Medium | 317.43 | 404.39 | 412.97 | 317.43 |
| Secondary High | 170.22 | 491.10 | 229.43 | 170.22 |
| High | 51.13 | 190.26 | 59.21 | 51.13 |

**Figure 4.33** Birnin Kebbi NDVI Class Charts 1991 – 2019

This implied that in 1990 High and secondary high NDVI areas (0.73 to 0.17) collectively occupied 340.23 km$^2$ and covered about 27.24 percent of the Metropolis, whereas low and secondary low NDVI areas (-0.01 to 0.53) collectively occupied 574.04 km$^2$ and covered 45.97 percent of Birnin Kebbi Metropolis.

In 2000, low NDVI areas (-0.39 to 0.01) covered 118.63 km$^2$ (9.50 percent of the total area). The secondary low NDVI areas (0.01 to 0.10) covered 334.28 km$^2$ (26.77 percent). The medium NDVI areas (0.01 to 0.18) covered 386.14 km$^2$ (30.92 percent). The secondary high NDVI areas (0.18 – 0.28) occupied 285.99 km$^2$ (22.90 percent). The high NDVI areas (0.28 – 0.60) covered 123.84 km$^2$ (9.92 percent). This implied that in 2000, high and secondary high NDVI areas (0.18 – 0.60) collectively occupied 409.83 km$^2$ and covered 32.82 percent of Birnin Kebbi Metropolis, indicating a coverage area higher than 1990 by 5.58 percent. Similarly, medium NDVI areas increased in coverage from 334.59 km$^2$ (26.79 percent) in

1990 to 386.14 $km^2$ (30.92 percent) in 2000, a difference of 4.13 percent. On the contrary, low and secondary NDVI areas (536.26 $km^2$) decreased slightly in percentage coverage by 9.71 percent from 45.97 percent in 1990 to 36.26 percent in 2000.

In 2010, low NDVI areas for the year (-0.51 to -0.04) covered 123.03 $km^2$ (9.85 percent of the total area). The secondary low NDVI areas (-0.04 to 0.02) occupied 412.95 $km^2$ (33.00 percent). The medium NDVI areas (0.02 to 0.07) covered 418.74 $km^2$ (33.53 percent). The secondary high areas (0.07 to 0.14) covered 233.90 $km^2$ (18.73 percent). Finally, the high NDVI areas (0.14 to 0.48) covered 61.06 $km^2$ (4.89 percent). Collectively, in 2010, secondary high and high NDVI areas (0.07 to 0.48) occupied 294.96 $km^2$ and covered 23.62 percent of Birnin Kebbi Metropolis, indicating a coverage area lower than 2000 by 9.20 percent. On the contrary, medium NDVI areas increased in percentage coverage from 30.92 percent in 2000 to 33.53 percent in 2010. Similarly, low and secondary low NDVI areas (-0.51 to 0.02) collectively occupied 535.17 $km^2$ and covered 42.85 percent of the Metropolis, indicating a coverage area higher than year 2000 by 6.59 percent.

In 2019, low NDVI areas (-0.28 - 0.09) covered 16.40 $km^2$ (1.31 percent of the total area). The secondary low areas (0.09 – 0.19) occupied 146.71 $km^2$ (11.75 percent). The medium NDVI areas (0.19 – 0.25) occupied 404.39 $km^2$ (32.38 percent). The secondary high NDVI areas (0.25 – 0.31) 491.10 $km^2$ (39.32 percent). The high NDVI areas (0.31 – 0.56) covered 190.26 $km^2$ (15.23 percent). This implied that in 2019, secondary high and high NDVI areas (0.25 – 0.56) collectively occupied 681.36 $km^2$ and covered 54.56 percent of Birnin Kebbi Metropolis, indicating a coverage area higher than 2010 by 30.94 percent. On the contrary, low and secondary low NDVI areas (-0.28 – 0.19) collectively occupied (163.12 $km^2$) and covered 13.06 percent of the Metropolis, indicating a decrease in percentage coverage by

29.19 percent from 42.85 percent in 2010 to 32.38 percent in 2019. Similarly, medium NDVI areas decreased in percentage coverage by 1.15 percent from 33.53 percent in 2010 to 32.38 in 2019.

Summarily, the NDVI values across the four locations varied from year to year; with a successive decline in areas with high NDVI in all locations. The high NDVI values were found in areas within the metropolis of the cities that had higher concentration of vegetal coverage, such as forests, light vegetation, and agricultural lands while bare surfaces, water bodies and bare surfaces which were void of vegetation recorded the lowest NDVI values. Results were similar to those of Kasim *et al*. (2020) whose work revealed a higher NDVI in surb-urban settlements in Ibadan with thicker vegetal cover in 2009, and a decline in the communities with high NDVI in 2009 when compared to 2000. This may be a function of several factors, such as yearly rainfall amount which determines the availalabity of moisture for foliage, agricultural activities which resulted in the loss of vegetal cover, and urbanization. The reduction in the locations with high values over time may be a consequent of rising urbanization, which has led to increase in built-up and bare surfaces.

### 4.2.5 Analysis of variance (ANOVA) in mean NDVI of Ibadan, Owerri, Kano and Birnin Kebbi 1990-2019

The Analysis of variance in NDVI for Ibadan, Owerri, Kano and Birnin Kebbi from 1990 to 2019 were computed from Appendices K1-4 and presented in Table 4.9 and Figure 4.33. The table indicates that the p-value was greater than 0.00 but less than significance value of 0.05; depicting a significance difference in NDVI for the four locations. That is, NDVI differed across the four location.

**Table 4.9 Analysis of Variance in NDVI for Ibadan, Owerri, Kano and Birnin Kebbi from 1990 to 2019**

**Analysis of Variance for NDVI**

| Source | DF | SS | MS | F | P |
|---|---|---|---|---|---|
| LOCAT | 3 | 1.53977 | 0.51326 | 15.49 | 0.000 |
| year | 3 | 1.60591 | 0.53530 | 16.15 | 0.000 |
| Error | 313 | 10.37257 | 0.03314 | | |
| Total | 319 | 13.51825 | | | |

Grouping Information Using the Tukey Method and 95% Confidence

| **LOCAT** | **N** | **Mean** | **Grouping** |
|---|---|---|---|
| 1 | 80 | 0.1333 | A |
| 4 | 80 | 0.1137 | A B |
| 2 | 80 | 0.0369 | B |
| 3 | 80 | -0.0422 | C |

*Means that do not share a letter are significantly different
1=Kebbi, 2=Kano, 3=Ibadan, 4=Owerri
**Source:** Author's work (2023)

Using Tukey pairwise comparison test, the study established that Birnin Kebbi had the highest mean NDVI (0.1333), followed by Owerri (0.1137) but the difference in the mean NDVI for Birnin Kebbi and Owerri were not statistically significant at 5 percent significance level. Kano (0.0369) followed Owerri in the mean NDVI but the difference between mean NDVI for Kano and Owerri were statistically the same but Birnin Kebbi was statistically different from Kano. Lastly, Ibadan (-0.0422) had the least mean NDVI which was statistically different from all other three locations.

This implied that NDVI values were generally higher in Birnin Kebbi, probably as a result of the two rich fertile extensive flood plains of the Rima and Shella Rivers (Ogunbajo *et al*., 2015) which constitute a large portion of the city and are largely cultivatedand were still green as at the time the imageries were acquired. It also implied that the smaller towns (Birnin Kebbi and Owerri) recorded high mean NDVI values than the larger cities (Kano

and Ibadan); depicting urbanization effects on NDVI. The implication is that increase in the urban sizes negatively affects NDVI values.

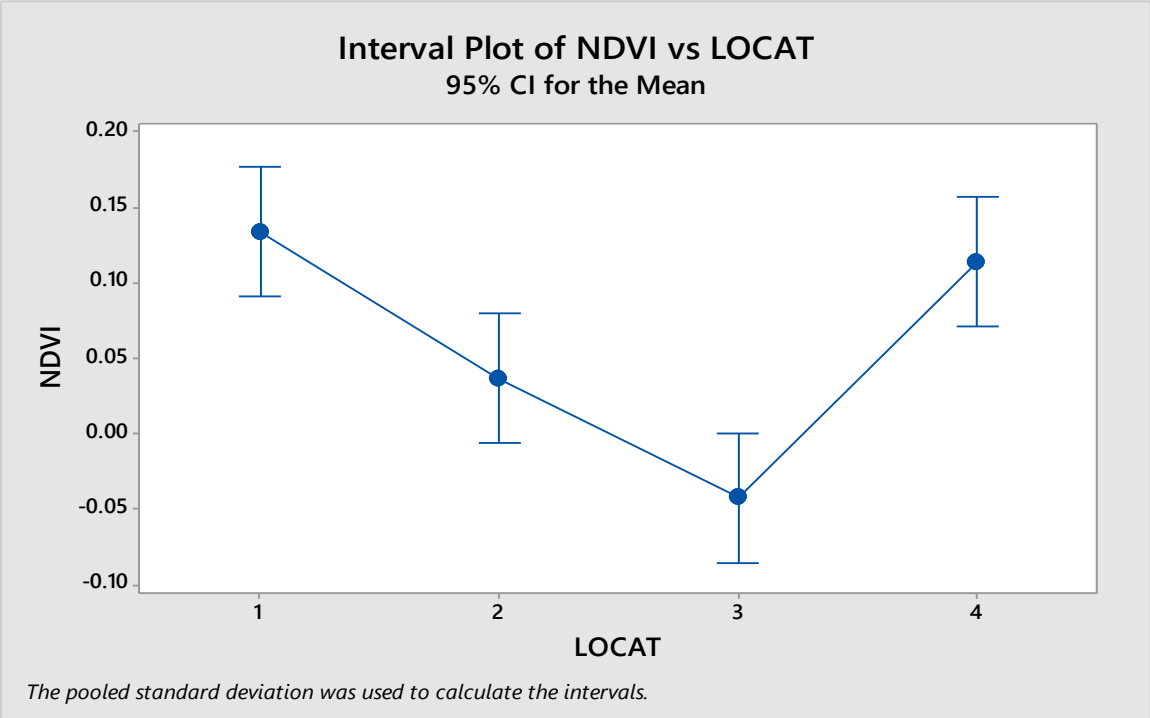


**Figure 4.34** Interval Plot for NDVI versus location for the cities (1990-2019)

### 4.3. NDBI of study cities from 1990 – 2019

This section presents the rsults of NDBI analysis of Ibadan, Owerri, Kano and Birnin Kebbi from 1990 to 2019.

#### 4.3.1 NDBI of Ibadan metropolis 1990-2019

NDBI images of Ibadan Metropolis in 1990 and 2019 are presented in Figures 4.35 and 4.36 while those of 2001 and 2011 are shown in Appendix G. Results showed that the maximum recorded NDBI of the city was 0.95, 0.68, 0.65 and 0.50 in 1990, 2001, 2011 and 2019 respectively, while the minimum was -0.09, -0.39, -0.25 and -0.28 in 1990, 2001, 2011 and 2019 respectively. This implied that maximum (0.95) was recorded in 2001 while the minimum (-0.39) NDBI values in the city were recorded in 2001.

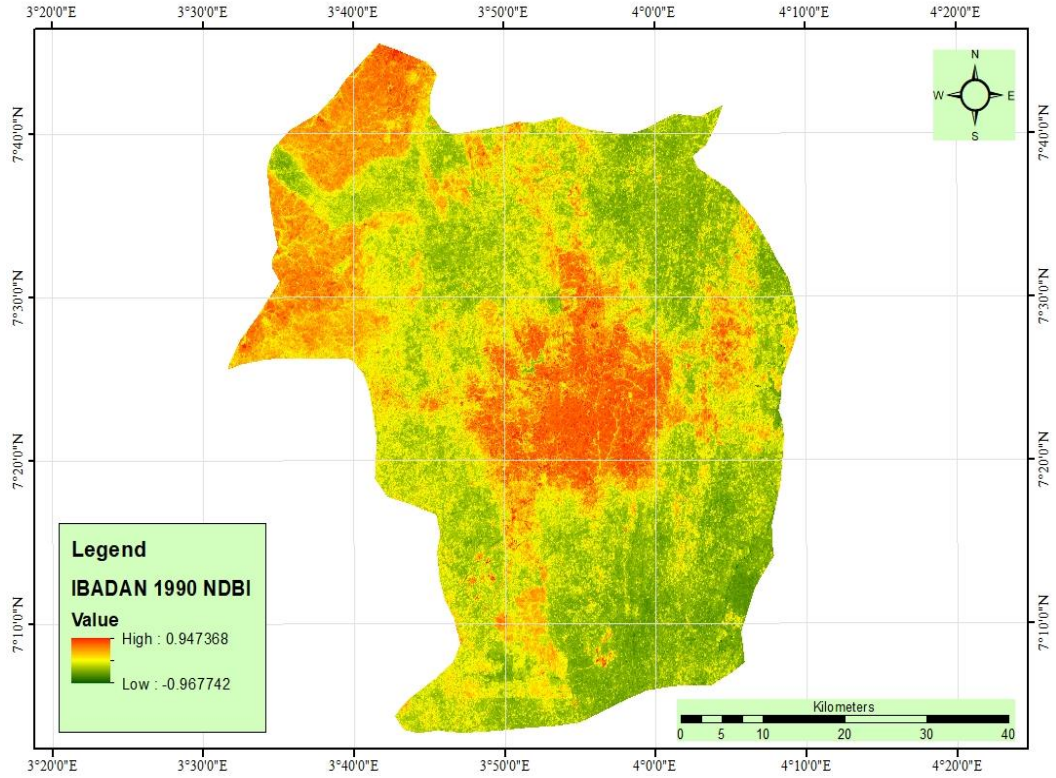


**Figure 4.35** NDBI of Ibadan Metropolis in 1990

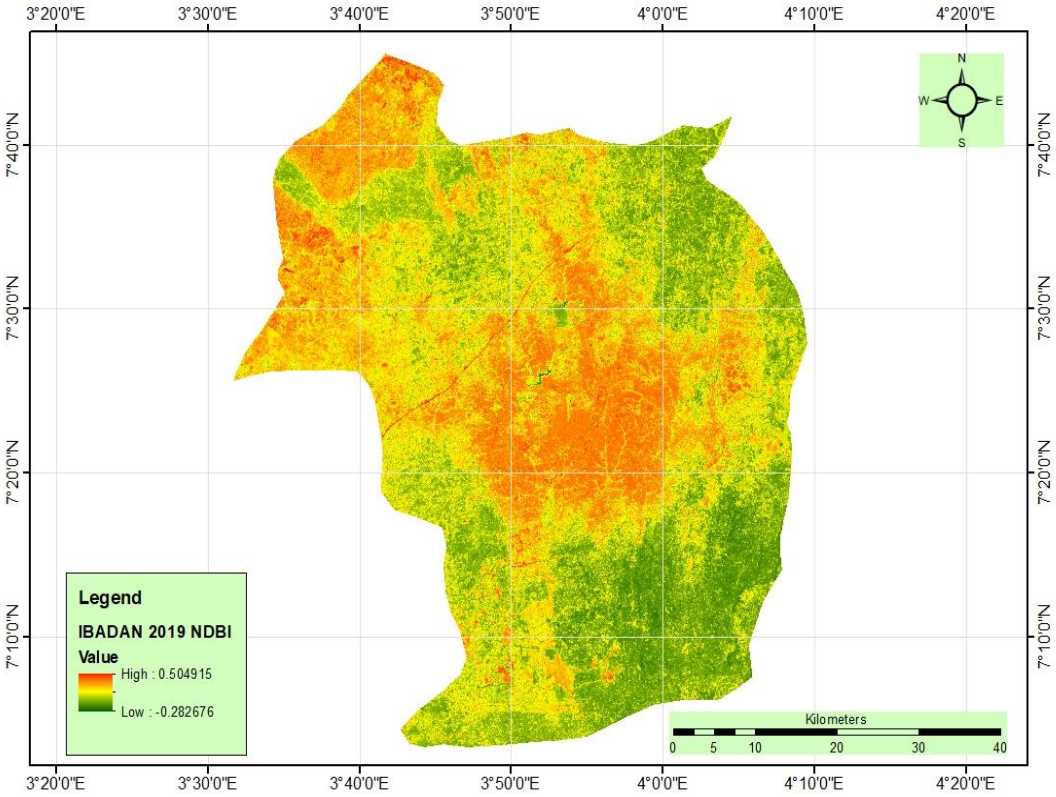


**Figure 4.36** NDBI of Ibadan Metropolis in 2019

The mean NDBI values of 0.12, 0.19, 0.12 and -0.07 were recorded in 1990, 2001, 2011 and 2019 respectively; indicating that the highest mean value was recorded in 2001, while the lowest value was recorded in 2019. For standard deviation, recorded values were 0.09, 0.09, 0.08, and 0.08 in 1990, 2001, 2011 and 2019 respectively, indicating that 1990 and 2001 had the highest standard deviation while 2011 and 2019 recorded the least. The high NDBI points were concentrated around the urbanized areas of the city, particularly the core local government areas which have significant concentrations of built up areas.

Figure 4.37 shows the statistics of re-classified NDBI images of Ibadan metropolis in 1990, 2001, 2011 and 2019 respectively while classification maps are shown in Appendix H. The statistics showed that in 1990, low NDBI areas (-0.97 to 0.05) occupied 920.63 $km^2$ (27.05 percent of the total area). The secondary low NDBI areas (0.05 to 0.11) covered 869.34 $km^2$ (25.55 percent). The medium NDBI areas (0.11 to 0.17) occupied 708,780 points covering an area of 637.90 $km^2$ (18.74 percent).

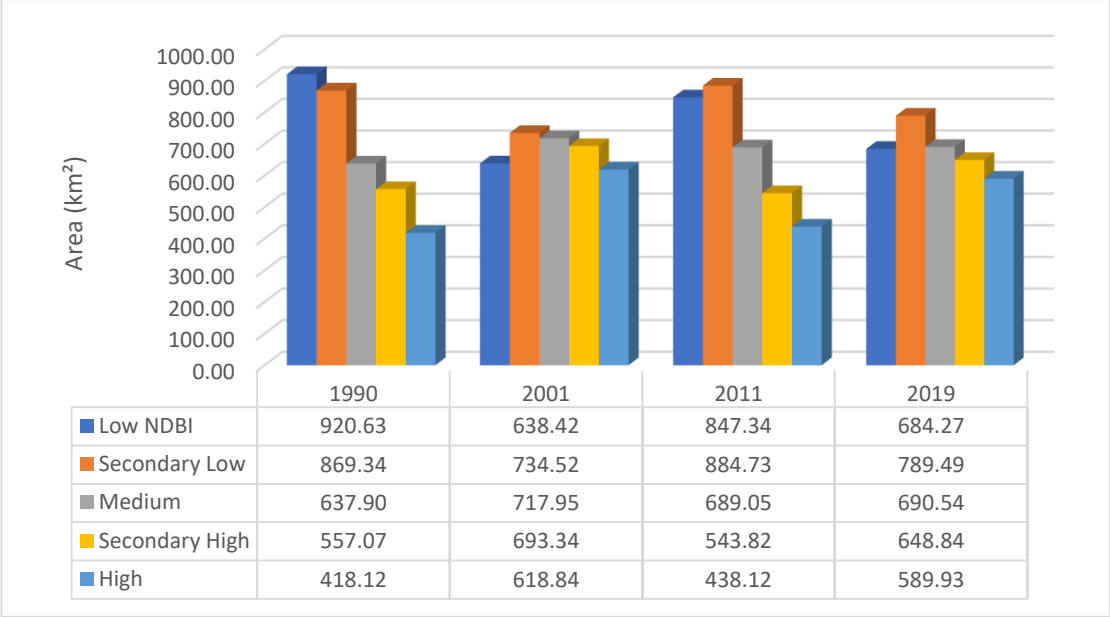


| | 1990 | 2001 | 2011 | 2019 |
|---|---|---|---|---|
| Low NDBI | 920.63 | 638.42 | 847.34 | 684.27 |
| Secondary Low | 869.34 | 734.52 | 884.73 | 789.49 |
| Medium | 637.90 | 717.95 | 689.05 | 690.54 |
| Secondary High | 557.07 | 693.34 | 543.82 | 648.84 |
| High | 418.12 | 618.84 | 438.12 | 589.93 |

**Figure 4.37** Ibadan NDBI 1990 – 2019

The secondary high NDBI areas (0.17 to 0.24) occupied 557.07 $km^2$ (16.37 percent). The high NDBI areas (0.24 to 0.95) covered 418.12 $km^2$ (12.29 percent). This implied that in 1990, high and secondary high NDBI areas (0.17 to 0.95) collectively occupied 975.19$km^2$ and covered 28.66 percent of Ibadan. Low and secondary low NDBI areas (-0.97 to 0.11) collectively had occupied 1789.98 $km^2$ and covered 56.20 percent of the Metropolis. This implied that low NDBI values dominated the scene of Ibadan Metropolis in 1990.

In 2001, low NDBI areas (-0.09 to 0.10) occupied 638.42 $km^2$ (18.76 percent of the total area); lower than 1990 by 8.29 percent. The secondary low NDBI areas (0.10 to 0.17) occupied 734.52 $km^2$ (21.58 percent), lower than 1990 by 3.97 percent. The medium NDBI areas (0.17 to 0.23) occupied 717.95 $km^2$ (21.10 percent), higher than 1990 by 2.36 percent. The secondary high NDBI areas (0.23 to 0.30) occupied 693.34 $km^2$ (20.38 percent), higher than 1990 by 4.01 percent. The high NDBI areas (0.30 to 0.68) covered 618.84 $km^2$ (18.18 percent), 5.89 percent higher than 1990. This implied that in 2001, high and secondary high NDBI areas (0.23 to 0.68) collectively occupied 1,312.17 $km^2$ and covered 38.56 percent of Ibadan, indicating a coverage area increase of 9.9 percent higher than 1990. Similarly, medium NDBI areas increased in coverage area by 2.36 percent. On the contrary low and secondary low NDBI areas (-0.09 to - 0.17) collectively 1,372.94 $km^2$ and covered 40.34 percent of the Metropolis, which was 15.86 percent lower than 1990.

In 2011, low NDBI areas (-0.25 to 0.06) occupied 847.34 $km^2$ (24.9 percent of the total area). The secondary low NDBI areas (0.06 to 0.11) covered 884.73 $km^2$ (26.00 percent). The medium NDBI areas (0.11 to 0.18) occupied 689.05 $km^2$ (20.25 percent). The secondary high NDBI areas (0.18 to 0.25) covered 543.82 $km^2$ (15.98 percent). The high NDBI areas (0.25 to 0.65) occupied 438.12 $km^2$ (12.87 percent). This implied that in 2011, high and

secondary high NDBI areas (0.18 to 0.65) collectively occupied 981.94 $km^2$ and covered 28.85 percent of Ibadan Metropolis. The low and secondary low NDBI areas (-0.25 to 0.11) collectively occupied 1,988,864 points (1,732.08 $km^2$) and covered 50.90 percent of the area.

1n 2019, low NDBI areas for the year (-0.28 to -0.15) occupied 684.27 $km^2$ (20.11 percent of the total area). The secondary low NDBI areas for the year (-0.15 to -0.10) occupied 789.49 $km^2$ (23.20 percent). The medium NDBI areas for the year (-0.10 to -0.04) occupied 690.54 $km^2$ (20.29 percent). The secondary high NDBI areas (-0.04 to 0.01) occupied 648.84 $km^2$ (19.07 percent). The high NDBI areas of the year (0.01 to 0.50) occupied 589.93 $km^2$ (17.34 percent). This implied that in 2019, high and secondary high NDBI areas (-0.04 to 0.05) collectively occupied 1.238.77 $km^2$ and covered 36.40 percent of Ibadan Metropolis, indicating a coverage area higher than 2011 by 7.74 percent. Similarly, medium NDBI areas increased in percentage coverage by 1.55 percent between 2011 and 2019. On the contrary low and secondary low NDBI areas (-0.28 to -0.10) collectively covered 1,473.76 $km^2$ and covered 43.31 percent of the Metropolis, indicating a coverage area decrease of 9.29 percent between 2011 and 2019.

### 4.3.2 NDBI of Owerri 1990-2019

NDBI images of Owerri Metropolis in 1990 and 2019 are presented in Figures 4.38 and 4.39 while those of 2000 and 2010 are shown in Appendix G. Results showed that the maximum recorded NDBI of the city was 0.47, 0.60, 0.36 and 0.13 in 1990, 2000, 2010 and 2019 respectively, while the minimum was -0.12, -0.25, -0.48 and -0.26 in 1990, 2000, 2010 and 2019 respectively.

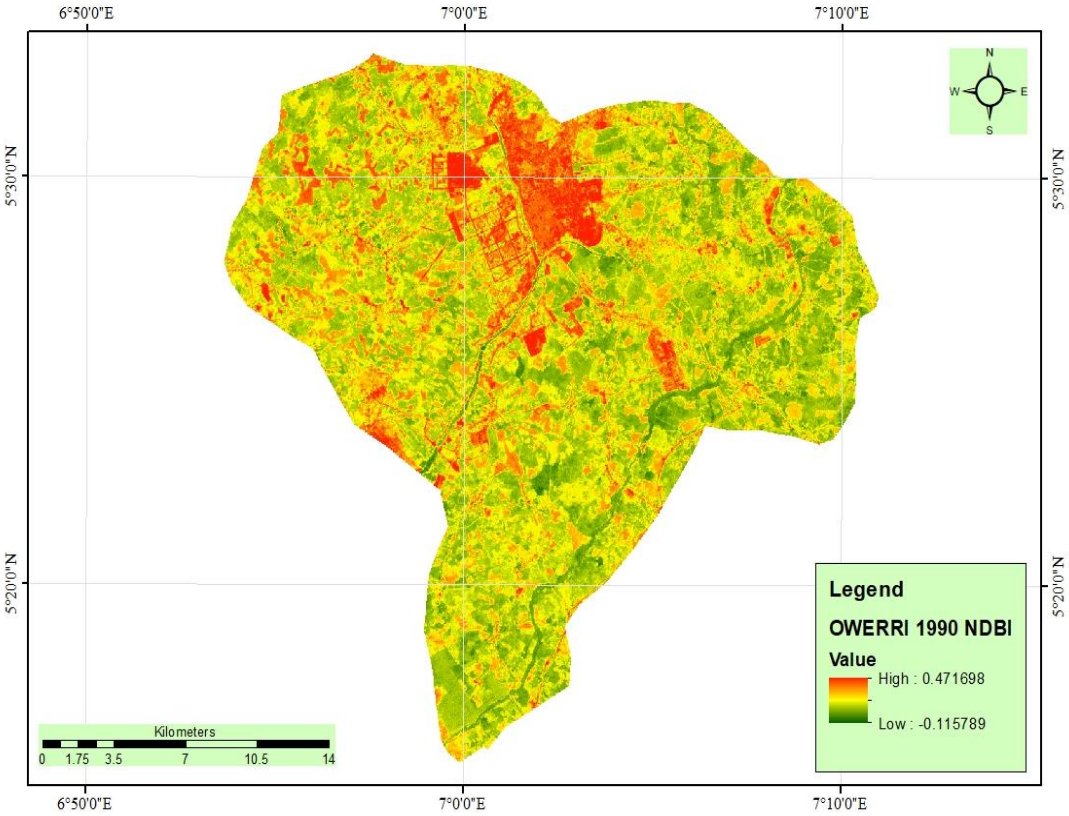


**Figure 4.38** NDBI of Owerri Metropolis in 1990

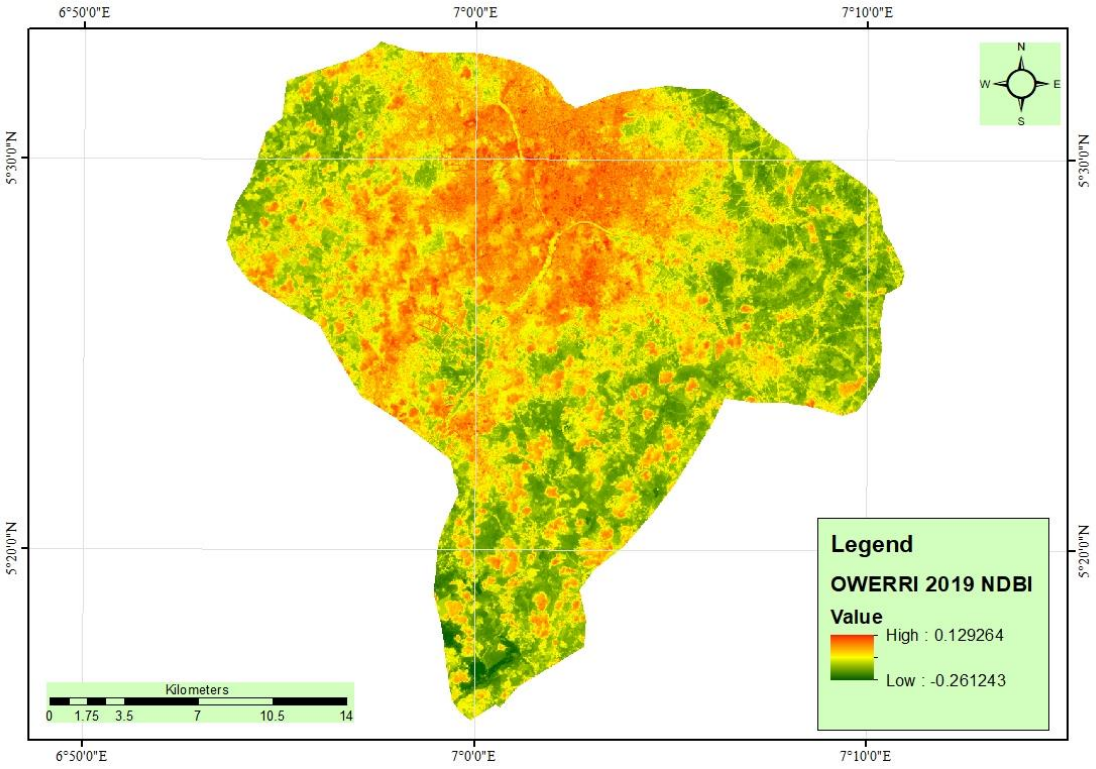


**Figure 4.39** NDBI of Owerri City in 2019

This implied that the maximum (0.60) value for the city was recorded in 2000 while the minimum values (-0.48) was recorded in 2010. The mean NDBI values of 0.09, 0.19, 0.07 and -0.09 were recorded in 1990, 2000, 2010 and 2019 respectively; indicating that the highest mean value was recorded in 2000, while the lowest value was recorded in 2019. For standard deviation, recorded values were 0.08, 0.08, 0.08, and 0.05 in 1990, 2000, 2010 and 2019 respectively, indicating only 2019 standard deviation less than 0.08 had the highest standard deviation while 2011 and 2019 recorded the least. The high NDBI points were concentrated around the urbanized areas of the city, particularly the core three local government areas which have significant concentrations of built-up areas.

Figure 4.40 shows the statistics of re-classified NDBI images of Ibadan metropolis in 1990, 2001, 2011 and 2019 respectively while classification maps are shown in Appendix H. The statistics showed that in 1990, that low NDBI area (-0.12 to 0.03) occupied 157.85 km$^2$ (29.05 percent). Secondary low areas (0.03 to 0.09) covered 160.79 km$^2$ (29.59 percent).

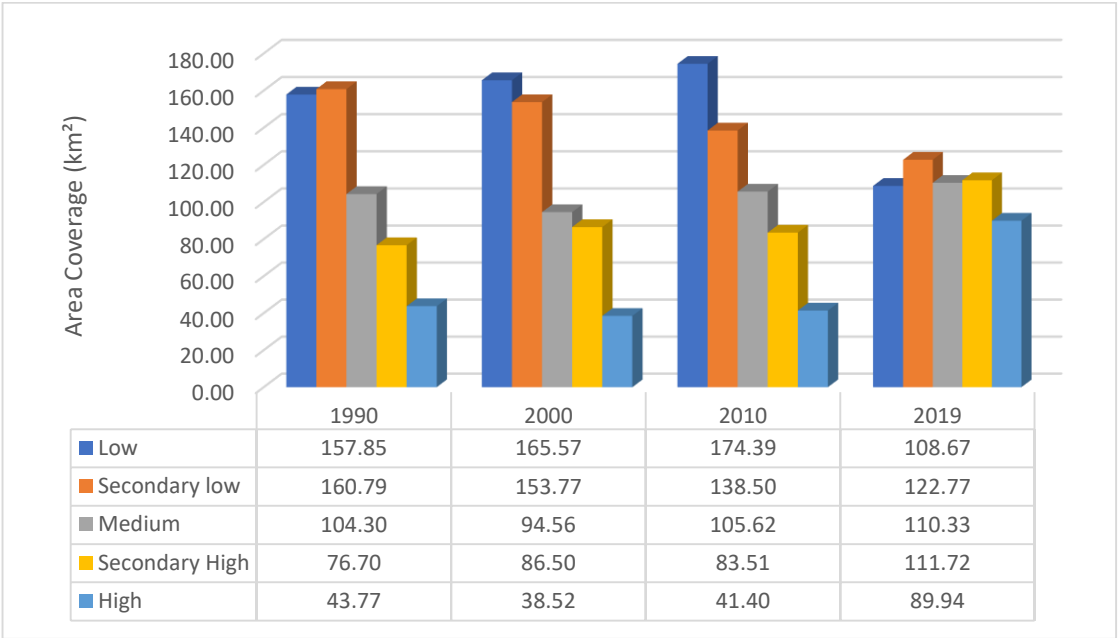


| | 1990 | 2000 | 2010 | 2019 |
|---|---|---|---|---|
| Low | 157.85 | 165.57 | 174.39 | 108.67 |
| Secondary low | 160.79 | 153.77 | 138.50 | 122.77 |
| Medium | 104.30 | 94.56 | 105.62 | 110.33 |
| Secondary High | 76.70 | 86.50 | 83.51 | 111.72 |
| High | 43.77 | 38.52 | 41.40 | 89.94 |

**Figure 4.40** Owerri NDBI 1990 – 2019

The medium NDBI area (0.09 to 0.15) occupied 104.30 $km^2$ (19.19 percent). The secondary high NDBI area (0.15 to 0.23) covered 76.70 $km^2$ (14.11 percent). The high NDBI area (0.23 to 0.47) occupied 43.77 $km^2$ (8.05 percent). This implied that in 1990 high and secondary high NDBI areas (0.15 to 0.47) collectively occupied 120.47 $km^2$ (22.17 percent of Owerri Metropolis), whereas low and secondary low NDBI areas (-0.12 to 0.09) covered 318.65 $km^2$ (58.64 percent of the Metropolis).

In 2000, low NDBI areas (-0.25 to 0.04) occupied 165.57 $km^2$ (30.72 percent of the total area). The secondary low NDBI areas (0.04 to 0.10) occupied 153.77 $km^2$ (28.53 percent). The medium NDBI areas (0.10 – 0.16) occupied 94.56 $km^2$ (17.55 percent). The secondary high NDBI areas (0.16 -0.24) covered 86.50 $km^2$ (16.05 percent). The high NDBI areas of the year (0.24 – 0.60) occupied 38.52 $km^2$ (7.15 percent). This implied that in 2000, high and secondary high NDBI areas (0.16 – 0.60) collectively occupied 125.02 $km^2$ (23.20 percent of Owerri Metropolis); indicating a coverage area higher than 1990 by 1.03 percent. Similarly, low and secondary NDBI areas (354,827 points or 319.34 $km^2$) increased slightly in percentage coverage by 0.62 percent from 58.64 percent in 1990 to 59.26 percent in 2000. On the contrary medium NDBI areas reduced in coverage from 104.30 $km^2$ (19.19 percent) in 1990 to 94.56 (17.55) in 2000, a difference of 1.64 percent.

In 2010, low NDBI areas (-0.48 to -0.14 occupied 174.39 $km^2$ (32.09 percent of the total area). The secondary low NDBI areas (-0.14 to -0.09) occupied 138.50 $km^2$ (25.49 percent). The medium NDBI areas 44 percent). The secondary high NDBI areas (-0.22 to 0.06) covered 83.51 $km^2$ (15.37 percent). The high NDBI areas (0.06 to 0.36) covered 41.4 $km^2$ (7.62 percent). This implied that in 2010, high and secondary high NDBI areas (-0.22 to 0.36) collectively occupied 124.91 $km^2$ (22.99 percent of Owerri Metropolis); indicating a

coverage area lower than 2000 by 0.21 percent. Similarly, low and secondary low NDBI areas (-0.48 to -0.09) collectively occupied312.90 $km^2$ and covered 57.58 percent of the Metropolis; indicating a coverage area lower than year 2000 by 1.68 percent. On the contrary, medium NDBI areas (99.09 $km^2$) increased in percentage coverage from 17.55 percent in 2000 to 19.44 percent in 2010.

In 2019, low NDBI areas (-0.26 to -0.15) occupied 108.67 $km^2$ (20.00 percent of the total area). The secondary low NDBI areas (-0.15 to 0.11) covered 122.77 $km^2$ (22.59 percent). The medium NDBI areas (-0.11 to -0.07) covered 110.33 $km^2$ (20.30 percent). The secondary high NDBI areas (-0.07 to -0.03) occupied 111.72 $km^2$ (20.56 percent). The high NDBI areas (-0.03 to 0.13) covered 89.94 $km^2$ (16.55 percent). This implied that in 2019, high and secondary high NDBI areas (-0.07 to 0.13) collectively occupied 201.65 $km^2$ (about 37.11 percent of Owerri Metropolis), indicating a coverage area higher than 2010 by 14.12 percent. Similarly, medium NDBI areas (110.33 $km^2$) increased in percentage coverage from 19.44 percent in 2010 to 20.30 in 2019. On the contrary, low and secondary low NDBI areas (-0.26 to -0.11) collectively occupied 231.44 $km^2$ (42.59 percent of the Metropolis), indicating a decrease in percentage coverage by 14.99 percent from 57.58 percent in 2010 to 42.59 percent in 2019.

### 4.3.3 NDBI of Kano metropolis 1991- 2019

NDBI images of Kano Metropolis in 1991 and 2019 are presented in Figures 4.41 and 4.42 while those of 2001 and 2011 are shown in Appendix G. Results showed that the maximum recorded NDBI of the city was 0.52, 0.99, 0.46 and 0.33 in 1991, 2001, 2011 and 2019 respectively, while the minimum was -0.38, 0.97, -0.49 and -0.30 in 1991, 2001, 2011 and 2019 respectively.

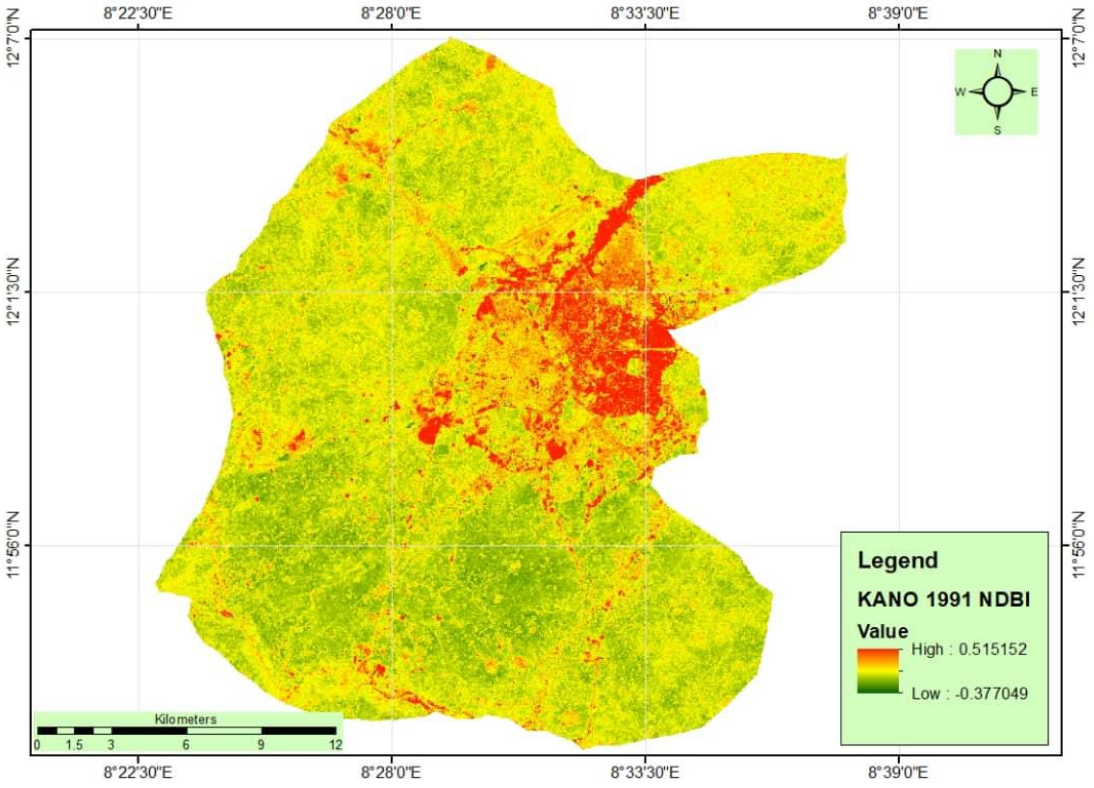


**Figure 4.41** NDBI of Kano in 1991

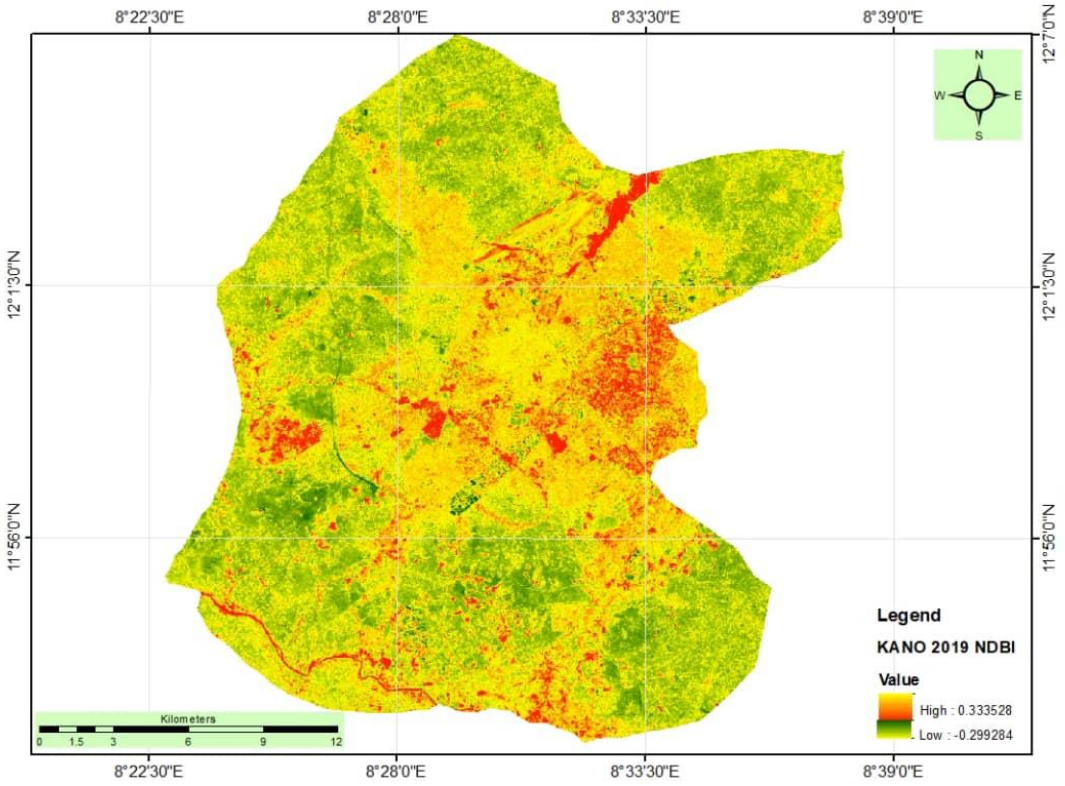


**Figure 4.42** NDBI of Kano in 2019

This implied that the maximum (0.99) value for the city was recorded in 2001 while the minimum value (-0.49) was recorded in 2011. The high NDBI in 2001 may be attributed to the large presence of bare surfaces during the year. The mean NDBI values of 0.31, 0.97, 0.05 and 0.05 were recorded in 1991, 2001, 2011 and 2019 respectively; indicating that the highest mean value was recorded in 2001, while the lowest values were recorded in 2011 and 2019.

For standard deviation, recorded values were 0.05, 0.01, 0.06, and 0.04 in 1991, 2001, 2011 and 2019 respectively, indicating a higher standard deviation in 2011 and the lowest in 2001 standard deviation less than 0.08 had the highest standard deviation while 2011 and 2019 recorded the least. The high NDBI points concentrated around the urbanized areas of the city, particularly the core areas which have significant concentrations of built-up surfaces such as Tudun Wada, Gwagwarwa, Dakata, Kawaji, Gama (all in Nassarawa LGA) and Kurna Asabe, Jakara and Sanka settlements (all in Dala), other locations in Kano Municipal, Fagge, Gwale and Tarauni, as well as commercial locations (markets) such as Kurmi, Sabon Gari, Kantin Kwari, Yankaba, Kofar Ruwa, Kasuwar Rimi and Yanlemo markets.

Figure 4.43 shows the statistics of re-classified NDBI images of Kano metropolis in 1991, 2001, 2011 and 2019 respectively while classification maps are shown in Appendix H. The statistics showed that in 1991, low NDBI area (-0.38 to 0.14) occupied 173.98 $km^2$ (2.13 percent). Secondary low areas (0.14 to 0.23) covered 198.87 $km^2$ (40.30 percent). The medium NDBI area (0.23 to 0.29) occupied 80.52 $km^2$ (16.32 percent).

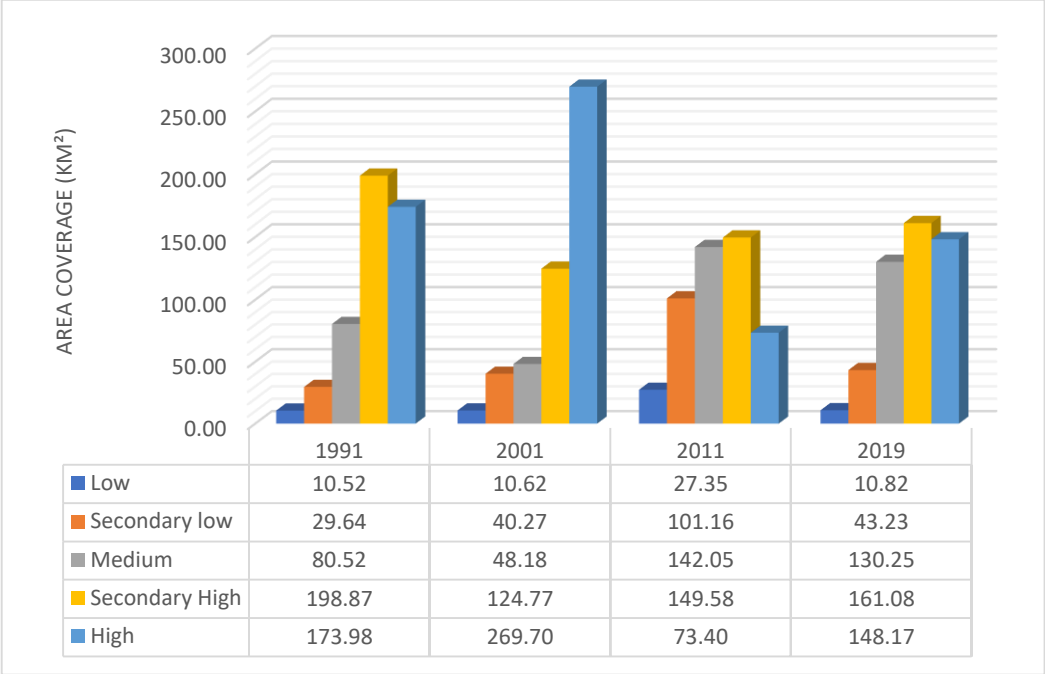


| | 1991 | 2001 | 2011 | 2019 |
|---|---|---|---|---|
| Low | 10.52 | 10.62 | 27.35 | 10.82 |
| Secondary low | 29.64 | 40.27 | 101.16 | 43.23 |
| Medium | 80.52 | 48.18 | 142.05 | 130.25 |
| Secondary High | 198.87 | 124.77 | 149.58 | 161.08 |
| High | 173.98 | 269.70 | 73.40 | 148.17 |

**Figure 4.43** Kano NDBI 1991 – 2019

The secondary high NDBI area (0.29 to 0.33) covered 29.64 km$^2$ (6.01 percent). The high NDBI area (0.33 to 0.51) occupied 10.52 km$^2$ (2.13 percent). This implied that in 1991 high and secondary high NDBI areas (0.29 to 0.51) collectively occupied 40.16 km$^2$ (8.14 percent of Kano), whereas low and secondary low NDBI areas (-0.38 to 0.23) collectively 372.85 km$^2$ and covered about 75.55 percent of the Metropolis.

In 2001, low NDBI areas (0.971 – 0.986) occupied 10.62 km$^2$ (2.15 percent of the total area). The secondary low NDBI areas (0.986 to 0.988) covered 40.27 km$^2$ (8.16 percent). The medium NDBI areas (0.988 to 0.989) occupied 48.18 km$^2$ (9.76 percent). The Secondary high NDBI areas (0.989 to 0.991) occupied 24.77 km$^2$ (25.28 percent). The high NDBI areas (0.991 – 0.998) occupied 269.70 km$^2$ (54.65 percent). This implied that in 2001, secondary high and high NDBI areas (0.989 to 0.998) collectively covered 194.46 km$^2$ (79.93 percent of Kano), indicating a coverage area higher than 1990 by 4.38 percent. On the contrary, low

and secondary NDBI areas (0.971 - 0.988) covered 50.89 $km^2$ and increased in percentage coverage by 2.17 percent in 2001.

In 2011, low NDBI areas (-0.49 to -0.07 occupied 27.35 $km^2$ (5.54 percent of the total area). The secondary low NDBI areas (-0.07 to 0.001) covered 101.16 $km^2$ (20.50 percent). The medium NDBI areas (0.001 to 0.05) occupied 142.06 $km^2$ (28.78 percent). The secondary high NDBI areas (0.054 to 0.11) occupied 149.58 $km^2$ (30.31 percent). The high NDBI areas (0.11 to 0.46) covered 73.40 $km^2$ (14.87 percent). This implied that in 2011, high and secondary high NDBI areas (0.05 to 0.46) collectively covered 222.97 $km^2$ (45.18 percent of Kano), while low and secondary low NDBI areas (-0.49 to 0.001) collectively occupied 128.51 $km^2$ (26.04 percent of the Metropolis).

In 2019, low NDBI areas for the year (-0.30 to -0.56) occupied 148.17 $km^2$ (30.02 percent of the total area). The secondary low NDBI areas (-0.56 to 0.003) covered 161.08 $km^2$ (32.64 percent). The medium NDBI areas (0.003 to 0.05) covered 130.25 $km^2$ (26.39 percent). The secondary high NDBI areas (0.05 to 0.07 covered 43.23 $km^2$ (8.76 percent). The high NDBI areas (0.07 to 0.33) occupied 10.81 $km^2$ (2.19 percent), This implied that in 2019, high and secondary high NDBI areas (0.41 to 0.33) collectively occupied 54.04 $km^2$ (10.95 percent of Kano); indicating a coverage area lower than 2011 by 34.23 percent. On the contrary, low and secondary low NDBI areas (-0.30 to 0.003) collectively covered 154.62 $km^2$ (62.66 percent of the Metropolis); indicating an increase in percentage coverage by 36.62 percent in 2019.

### 4.3.4 NDBI of Birnin Kebbi metropolis 1990-2019

NDBI images of Birnin Kebbi Metropolis in 1990 and 2019 are presented in Figures 4.44 and 4.45 while those of 2000 and 2010 are shown in Appendix G. Results showed that the maximum recorded NDBI of the city was 0.24, 0.36, 0.64 and 0.27 in 1990, 2000, 2010 and 2019 respectively, while the minimum was -0.01, -0.54, -0.82, and -0.44 in 1990, 2000, 2010 and 2019 respectively. This implied that both maximum (0.64) and minimum (-0.82) values for the city were recorded in 2010. The mean NDBI values of 0.13, -0.01, 0.07 and -0.02 were recorded in 1990, 2000, 2010 and 2019 respectively; indicating that the highest mean value was recorded in 2000, while the lowest value was recorded in 2019. For standard deviation, recorded values were 0.05, 0.13, 0.18, and 0.08 in 1990, 2000, 2010 and 2019 respectively, indicating a higher standard deviation in 2010 and the lowest in 1990.

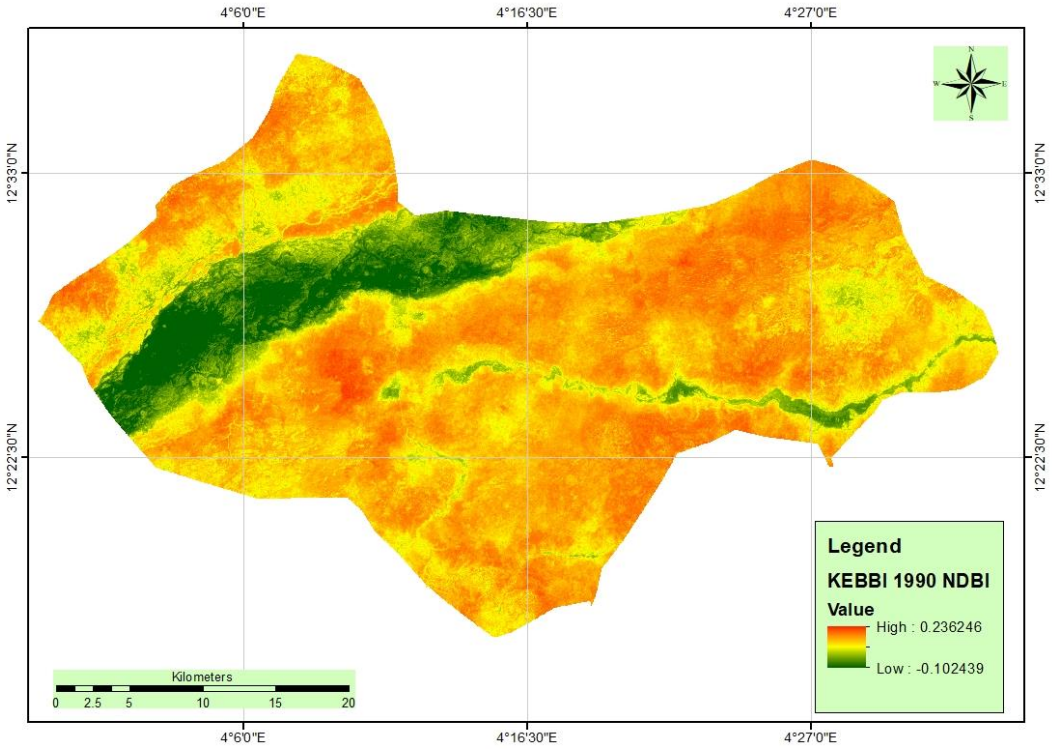


**Figure 4.44** NDBI of Birnin Kebbi in 1990

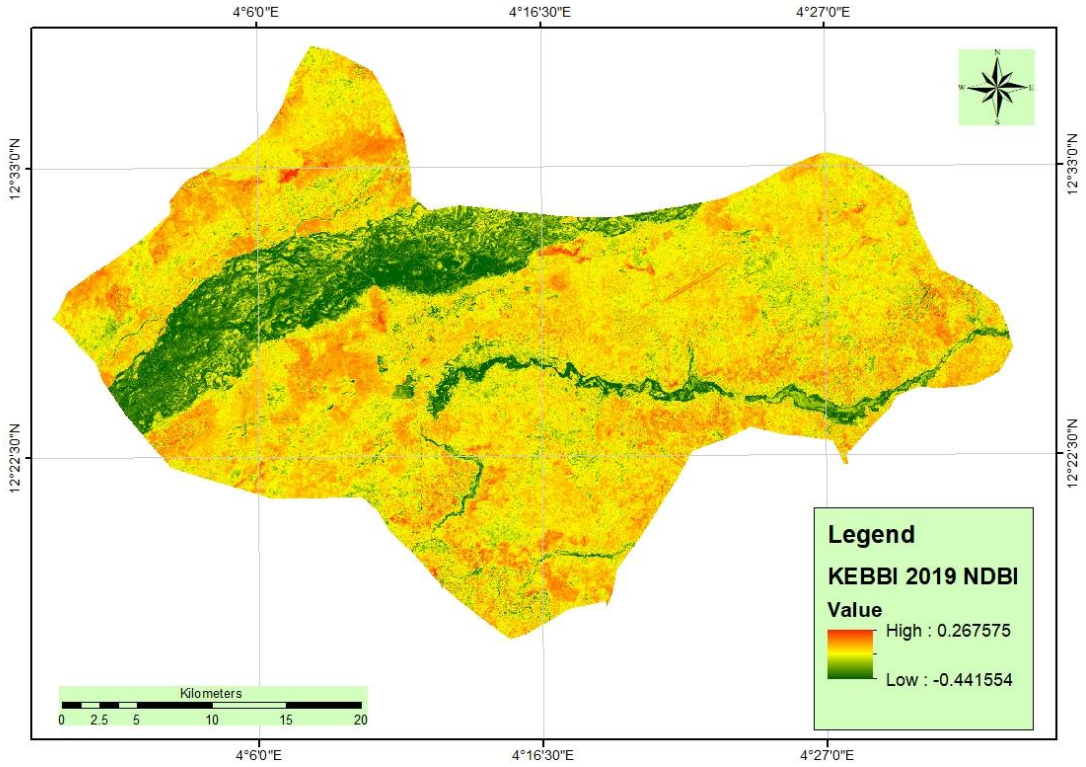


**Figure 4.45** NDBI of Birnin Kebbi in 2019

The high NDBI points concentrated around the urbanized and densely populated residential, high Traffic, industrial, and market areas such as the CBD, Makerar Gwandu, Kofar Kola, Rafin Atiku, Badariya, Bayan Kara, Takalau,Tudun Wada, Nasarawa 1, Nasarawa 2 and Gwadangwaji.

Figure 4.46 shows the statistics of re-classified NDBI images of Birnin Kebbi metropolis in 1990, 2000, 2010 and 2019 respectively while classification maps are shown in Appendix H. The statistics showed that in 1990, low NDBI areas (-0.10 to 0.01) covered 80.73 $km^2$ (6.46 percent). Secondary low areas (0.01 to 0.08) occupied 107.19 $km^2$ (8.58 percent). The medium NDBI areas (0.03 to 0.13) covered 222.31 $km^2$ (17.80 percent). The secondary high NDBI areas (0.13 to 0.17) occupied 445.61 $km^2$ (35.68 percent). The high NDBI areas (0.17 to 0.24) covered 393.04 $km^2$ (31.47 percent).

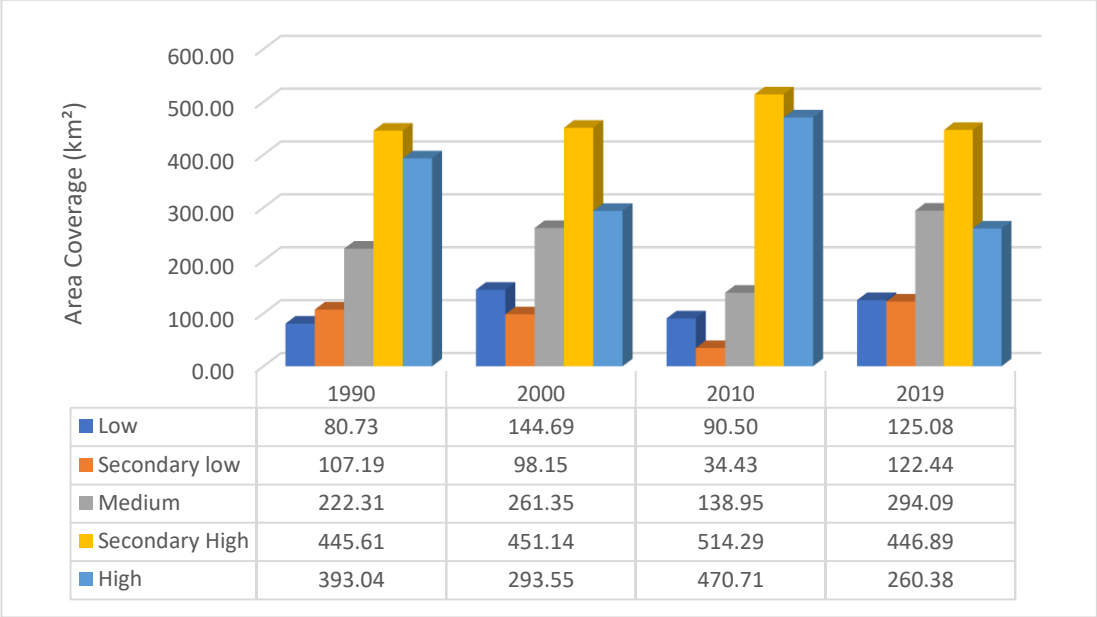


| | 1990 | 2000 | 2010 | 2019 |
|---|---|---|---|---|
| Low | 80.73 | 144.69 | 90.50 | 125.08 |
| Secondary low | 107.19 | 98.15 | 34.43 | 122.44 |
| Medium | 222.31 | 261.35 | 138.95 | 294.09 |
| Secondary High | 445.61 | 451.14 | 514.29 | 446.89 |
| High | 393.04 | 293.55 | 470.71 | 260.38 |

**Figure 4.46** Birnin Kebbi NDBI 1990 – 2019

This implied that in 1990, high and secondary high NDBI areas (0.13 to 0.24) collectively occupied 419.32 km$^2$ (67.15 percent of the city), whereas low and secondary low NDBI areas (-0.10 to 0.08) collectively covered 187.92 km$^2$ (15.05 percent of the Metropolis).

In 2000, low NDBI areas (-0.54 to -0.24) occupied 144.69 km$^2$ (11.59 percent of the total area). The secondary low NDBI areas (-0.24 to -0.01) covered 98.15 km$^2$ (7.86 percent). The medium NDBI areas (-0.10 to -0.00) occupied 261.35 km$^2$ (20.93 percent). The Secondary high NDBI areas (0.00 to 0.08) covered 451.14 km$^2$ (36.12 percent). The high NDBI areas (0.08 – 0.36) occupied 293.55 km$^2$ (23.51 percent). This implied that in 2000, secondary high and high NDBI areas (0.00 to 0.36) collectively covered 744.69 km$^2$ (59.81 percent of the area), indicating a coverage area lower than 1990 by 7.34 percent. On the contrary, low and secondary NDBI areas (-0.54 to -0.01) which covered 558.34 km$^2$ increased in percentage coverage by 4.39 percent from 15.05 percent in 1990 to 19.44 percent in 2000. Similarly, medium NDBI areas increased in coverage from 222.31 km$^2$ (17.80 percent) in 1990 to 261.35 km$^2$ (20.93 percent) in 2000, a difference of 3.13 percent.

In 2010, low NDBI areas (-0.82 to -0.54 occupied 90.50 $km^2$ (7.25 percent of the total area). The secondary low NDBI areas (-0.54 to -0.28) covered 34.43 $km^2$ (2.76 percent). The medium NDBI areas (-0.28 to -0.00) occupied 138.95 $km^2$ (11.13 percent). The secondary high NDBI areas (-0.00 to 0.12) covered 514.29 $km^2$ (41.18 percent). The high NDBI areas (0.12 to 0.64) occupied 470.71 $km^2$ (37.69 percent). This implied that in 2010, high and secondary high NDBI areas (-0.00 to 0.64) collectively occupied 985.00 $km^2$ (78.87 percent of the city), indicating a coverage area higher than 2000 by 11.72 percent. On the contrary, low and secondary low NDBI areas (-0.82 to -0.28) collectively covered 124.93 $km^2$ (10 percent of the Metropolis), indicating a coverage area lower than year 2000 by 5.05 percent. Similarly, medium NDBI areas decreased in percentage coverage by 9.80 percent from 20.93 percent in 2000 to 11.13 percent in 2010.

In 2019, low NDBI areas (-0.44 to -0.16) 125.08 $km^2$ (10.02 percent of the total area). The secondary low NDBI areas (-0.16 to -0.07) covered 122.44 $km^2$ (9.80 percent). The medium NDBI areas (-0.07 to -0.01) covered 294.09 $km^2$ (23.55 percent). The secondary high NDBI areas (-0.01 to 0.05) occupied 446.89 $km^2$ (37.78 percent). The high NDBI areas (0.05 to 0.27) covered 260.38 $km^2$ (20.85 percent). This implied that in 2019, high and secondary high NDBI areas (-0.01 to 0.27) collectively occupied 707.27 $km^2$ (56.63 percent of the city), indicating a coverage area lower than 2010 by 22.24 percent. On the contrary, low and secondary low NDBI areas (-0.44 to -0.07) collectively occupied 247.52 $km^2$ (19.82 percent of the Metropolis), indicating an increase in percentage coverage by 9.82 percent in 2019. Similarly, medium NDBI areas increased in percentage coverage by 11.42 percent from 12.13 percent in 2010 to 23.55 percent in 2019.

For the four cities, high/positive NDBI values occupied the highly urbanized core areas of the cities which were either bare/open or possessed very sparce vegetal cover, while the lowest negative NDBI values occupied the suburban areas which were characterized by vegetal cover or water bodies. This is similar to the study by Kasim *et al*. (2020) who established high NDBI recorded high NDBI readings in the core settlements in Ibadan metropolis and negative values in settlements with characterized by more vegetal cover.

### 4.3.5 Analysis of variance (ANOVA) in mean NDBI of Ibadan, Owerri, Kano and Birnin Kebbi 1990-2019

The Analysis of variance in NDBI for Ibadan, Owerri, Kano and Birnin Kebbi from 1990 to 2019 computed from Appendices K1-4 is presented in Table 4.10 and Figure 4.46. The table established that the p-value was greater than 0.00 but less than significance value of 0.05, indicating a significance difference in NDBI for the four locations.

**Table 4.10 Analysis of Variance in NDVI for Ibadan, Owerri, Kano and Birnin Kebbi from 1990 to 2019**

**Analysis of Variance for NDBI**

| Source | DF | SS | MS | F | P |
|---|---|---|---|---|---|
| LOCAT | 3 | 25.4771 | 8.4924 | 124.11 | 0.000 |
| year | 3 | 7.7456 | 2.5819 | 37.73 | 0.000 |
| Error | 313 | 21.4173 | 0.0684 | | |
| Total | 319 | 54.6399 | | | |

Grouping Information Using the Tukey Method and 95% Confidence

| LOCAT | N | Mean | Grouping |
|---|---|---|---|
| 2 | 80 | 0.2836 | A |
| 3 | 80 | 0.1578 | B |
| 4 | 80 | 0.0589 | B |
| 1 | 80 | -0.4584 | C |

*Means that do not share a letter are significantly different.
1=Kebbi, 2=Kano, 3=Ibadan, 4=Owerri

**Source:** Author's work (2023)

The Tukey pairwise comparison test revealed that Kano had the highest mean NDBI (0.2836), which was statistically different from all other three locations. Kano was followed by Ibadan and Owerri which recorded mean NDBI values of 0.1578 and 0.0589 respectively. The mean NDBI for Ibadan was higher than that of Owerri but was not statistically significant.

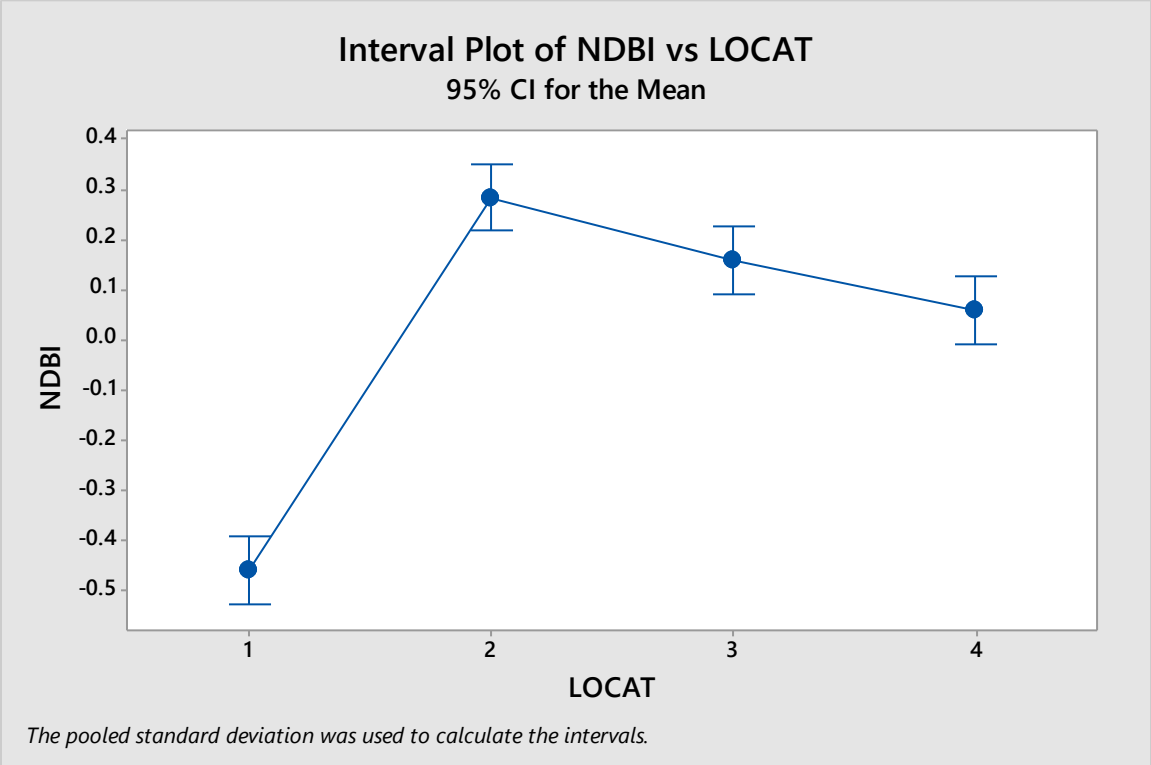


**Figure 4.47** Interval plot of NDBI versus Locations 1990 -2019

Lastly, Birnin Kebbi had the least mean NDBI (-0.4584 ) which was statistically significantly different from all other three locations. This analysis therefore revealed the relationship between the urbanizarion and NDBI. Kano, which had the highest population density among the four cities and is higly congested recorded the highest mean NDBI followed by Ibadan which is the largest in terms of landmass but possesses lower density. Consequently, Birnin Kebbi which was the least in terms of size also had the least mean NDBI.

## 4.4. Analysis and Results of Trends in Air Temperature

The descriptive analysis of maximum noon-time temperature, the time plots for the four cities, trend analysis for the period 1990-2019 using Mann-Kendall, Sen's slope estimator, Pettitt tests for change point and Seasonal Mann-Kendall test were investigated using R statistical package 3.6.1 version. The results and discussions are as follows:

### 4.4.1 Descriptive statistics for the maximum noon-time temperatures for the four cities

Table 4.11 shows the descriptive statistics of the maximum noontime temperature in Birnin Kebbi, Kano, Ibadan and Owerri. It shows that Birnin Kebbi had the highest mean temperature followed by Kano, Ibadan and Owerri respectively. This depicts the implication of latitudinal location on the temperature of the cities; as Birnin Kebbi which is located at a higher latitude in the Sudan recorded the highest mean, while Owerri located in the lower latitude of the Rainforest recorded the least mean temperature.

**Table 4.11 Descriptive Statistics for the Maximum Noon-Time Temperatures**

| Statistics | Birnin Kebbi | Kano | Ibadan | Owerri |
|---|---|---|---|---|
| Mean | 27.49 | 25.56 | 24.08 | 23.17 |
| Skew | 0.39 | -0.09 | 0.47 | 0.60 |
| Kurtosis | -0.72 | -0.69 | -0.59 | -0.06 |
| Minimum | 21.41 | 18.66 | 22.07 | 21.49 |
| Maximum | 33.12 | 31.84 | 27.51 | 26.67 |
| Range | 11.71 | 13.18 | 5.44 | 5.18 |
| 1st Quartile | 25.69 | 23.54 | 23.04 | 22.32 |
| Median | 26.86 | 25.44 | 23.98 | 23.03 |
| 3rd Quartile | 29.58 | 27.83 | 24.96 | 23.85 |
| Standard Deviation | 2.66 | 3.16 | 1.18 | 0.97 |
| Coefficient of Variation | 0.097 | 0.12 | 0.05 | 0.04 |

**Source: Author's Work (2023)**

The standard deviation and the coefficient of variation from the mean value were higher for Kano than those of Birnin Kebbi, Ibadan and Owerri in that order.

### 4.4.2 Time and box plots of maximum noon-time temperature for the four cities

Figures 4.48a, b, c and d present the maximum temperature plots against the time (years) for the four cities. The graphs reveal that the maximum temperatures of the cities do not depict any temporal trend especially for Birnin Kebbi. For Kano, Ibadan and Owerri trends are not quite discernible, although trends are suspected to be present.

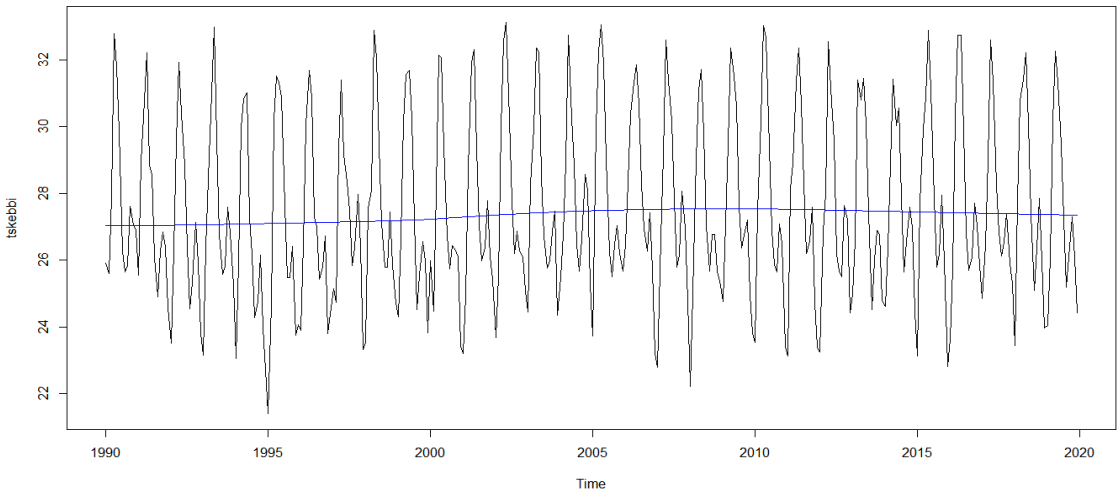


**Figure 4. 48a:** Time plot of the time series observation of Birnin Kebbi in Nigeria against months for the period 1990 – 2019

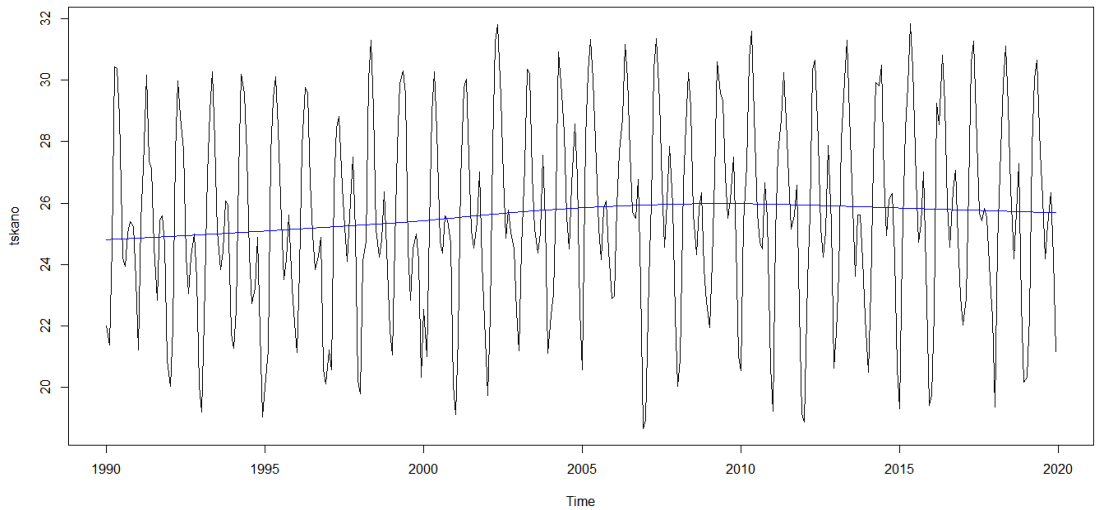


**Figure 4. 48b:** Time plot of the time series observation of Kano in Nigeria against Months for the period 1990 – 2019

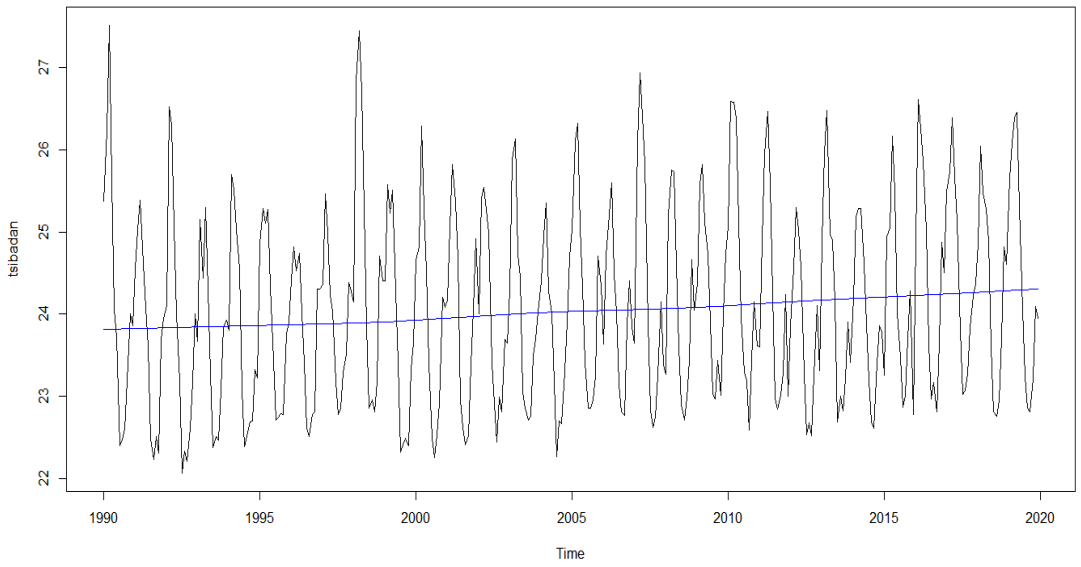


**Figure 4. 48c:** Time plot of the time series observation of Ibadan in Nigeria against months for the period 1990 – 2019

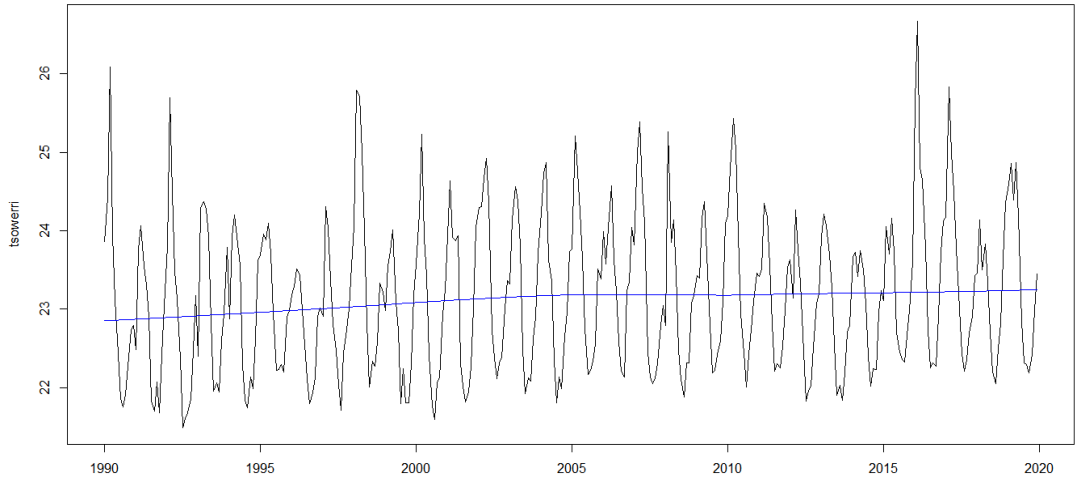


**Figure 4. 48d: Time plot of the time series observation of Owerri in Nigeria against months for the period 1990 – 2019**

The box plot for the four cities is shown in Figure 4.49. It revealed five important statistics namely: minimum value, 25$^{th}$ percentile, median, 75$^{th}$ percentile, and the maximum value of the distribution as well as identification of potential outliers in the observations. From the boxplot, it is apparent that only one observation was found to be above the upper adjacent value in Owerri. No outliers were detected for every other city. The plot also revealed that

more data is lying in the upper half of the range in Birnin Kebbi and Kano while those of Ibadan and Owerri were around the middle and lower half of the range respectively. In other words the upper half of the maximum temperature was heavily weighted for Sudan Savanna cities (Birnin Kebbi and Kano) while those of Tropical Rainforest cities (Ibadan and Owerri) are otherwise.

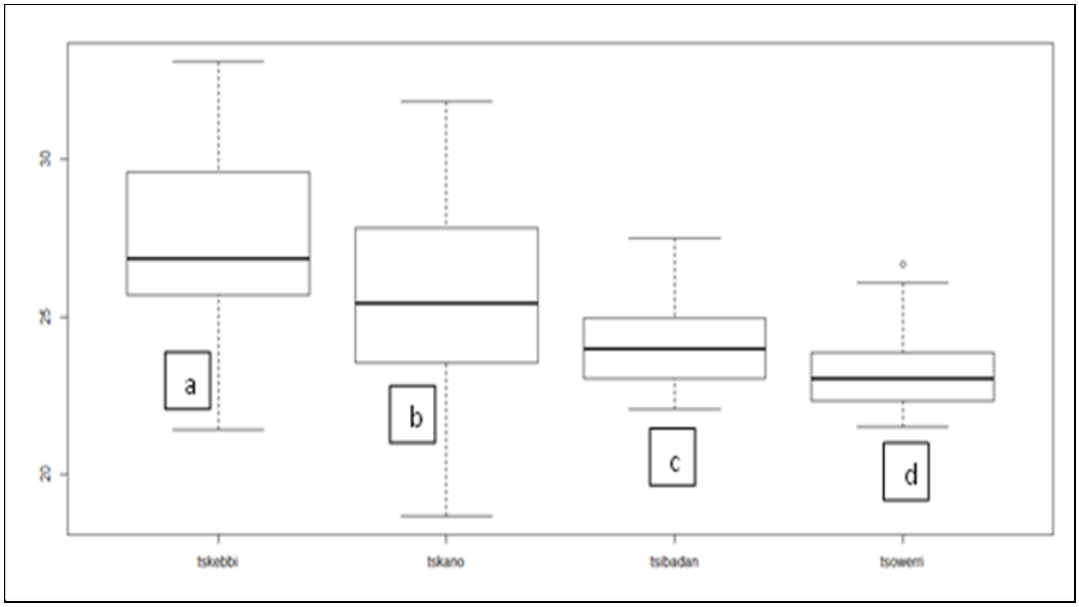


**Figure 4.49** Box plots of Maximum Noon-time temperature against time for Birnin Kebbi (a), Kano (b), Ibadan (c) and Owerri (d).

### 4.4.3 Normal probability plots and Shapiro Wilk normality test of maximum temperature series for the four cities

The normal probability plots of maximum temperature series for the four cities are depicted in Figure 4.50. The plots reveal significant deviations from straight line on the normal probability plots.

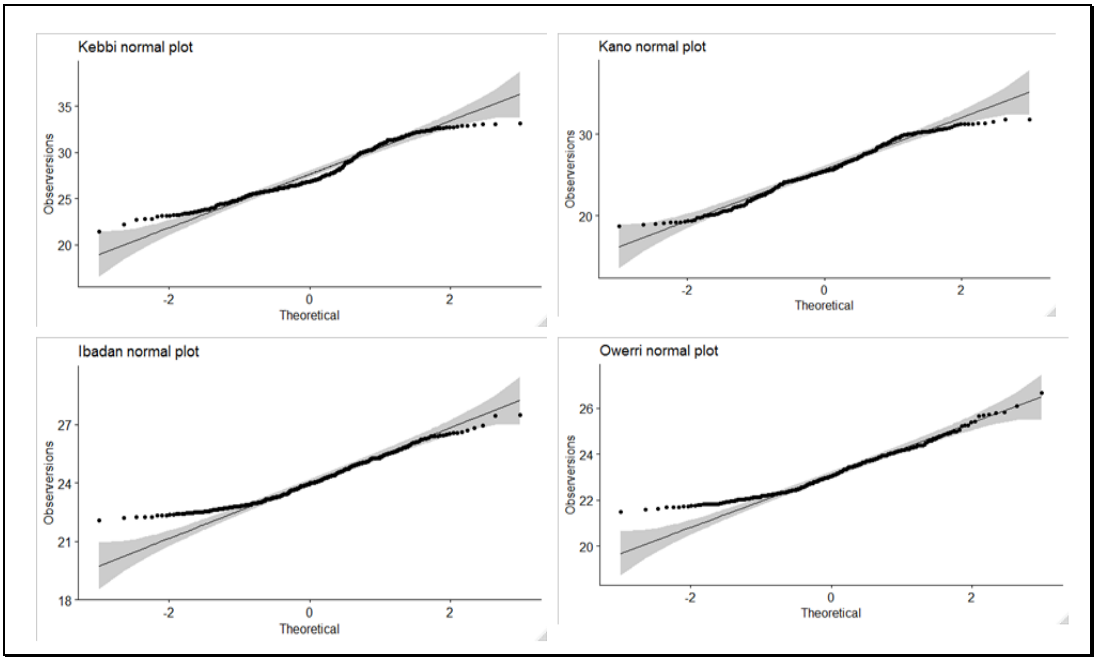


**Figure 4. 50** Normal Probability Plot of Maximum Noon-time temperature for Birnin Kebbi, Kano, Ibadan and Owerri

Therefore, the series may not be normally distributed. The results of Shapiro Wilk normality test presented in Table 4.12 is a further validation of non-normality of the maximum temperature series for Birnin Kebbi, Kano, Ibadan and Owerri from the normal probability plots. Since the p-values are all less than 0.05 significant value, it is concluded that the maximum temperature series collected for the period of 1990 to 2019 in the for the four cities are not normally distributed.

### 4.4.4 Mann-Kendall and Sen's slope estimate results of maximum temperature for the four cities

Mann-Kendall and Sen's slope estimate results of maximum noon-time temperature for the four cities are presented in Table 4.13. From the result, the Tau statistic for Birnin Kebbi is 0.045 and the corresponding p-value is 0.1976. Since the p-value is greater than 0.05, it is concluded that there is no significant trend in Birnin Kebbi. However, the Tau statistics results for Kano, Ibadan and Owerri were 0.071, 0.098 and 0.091 and the corresponding p-values are 0.045, 0.005 and 0.010, indicating significant trends in the three cities.

**Table 4.12 Shapiro Wilk Normality Test Result**

| City | W-Statistic | P-Value |
|---|---|---|
| Birnin Kebbi | 0.9591 | 1.8e-08 |
| Kano | 0.9801 | 7.15e-05 |
| Ibadan | 0.9620 | 4.7e-08 |
| Owerri | 0.9620 | 4.729e-08 |

**Source: Author's Analysis (2023)**

Since the p-values were less than 0.05 alpha value, the implication is that a trend was present in the data for Kano, Ibadan and Owerri respectively; with greater trends in the cities located within the Tropical Rainforest (Ibadan and Owerri).

**Table 4.13 Mann-Kendall Trend and Sen's slope Results of Maximum Noon-Time Temperature for Birnin Kebbi, Kano, Ibadan and Owerri**

| City | Tau | p-value | Sen's Slope | p-value | 95percent Confident Interval | |
|---|---|---|---|---|---|---|
| Birnin Kebbi | 0.0455 | 0.1976 | 0.0013 | 0.2849 | -0.0011 | 0.003703 |
| Kano | 0.0708 | 0.0447 | 0.0023 | 0.0609 | -0.0001 | 0.006089 |
| Ibadan | 0.0985 | 0.0053 | 0.0015 | 0.0136 | 0.0003 | 0.002624 |
| Owerri | 0.0911 | 0.0098 | 0.0011 | 0.0224 | 0.0002 | 0.001979 |

**Source: Author's Analysis (2023)**

For the Sen's slope estimates, the slopes are all positive, indicating increasing trends over the years for the four cities. However, Ibadan and Owerri slopes showed significant differences at 5 percent significant level, Kano at 10 percent level, while slope for Birnin Kebbi is not statistically different from zero. These are further validated from the 95 percent confident interval reported. Any interval that contained zero is reported not statistically different from zero at 95 percent, indicating that the slope estimate is not statistically significant. The results are similar to those of Amadi *et al.* (2014) whose Mann-Kendall's test results for 20 synoptic weather cities across Nigeria (1950-2012) showed general warming trends across the locations and indicated that 17 cities had significant increasing trends in the minimum temperature at the 0.01 level of significance while 16 cities revealed

significant increasing trends in the maximum temperature at the 0.01 and 0.05 significance levels.

The mean annual maximum noon-time temperature trends for the four cities are presented in Figure 4.51. It shows higher temperature values in the two Sudan Savanna Cities (Birnin Kebbi and Kano) than the cities in the Tropical Rainforest (Ibadan and Owerri).

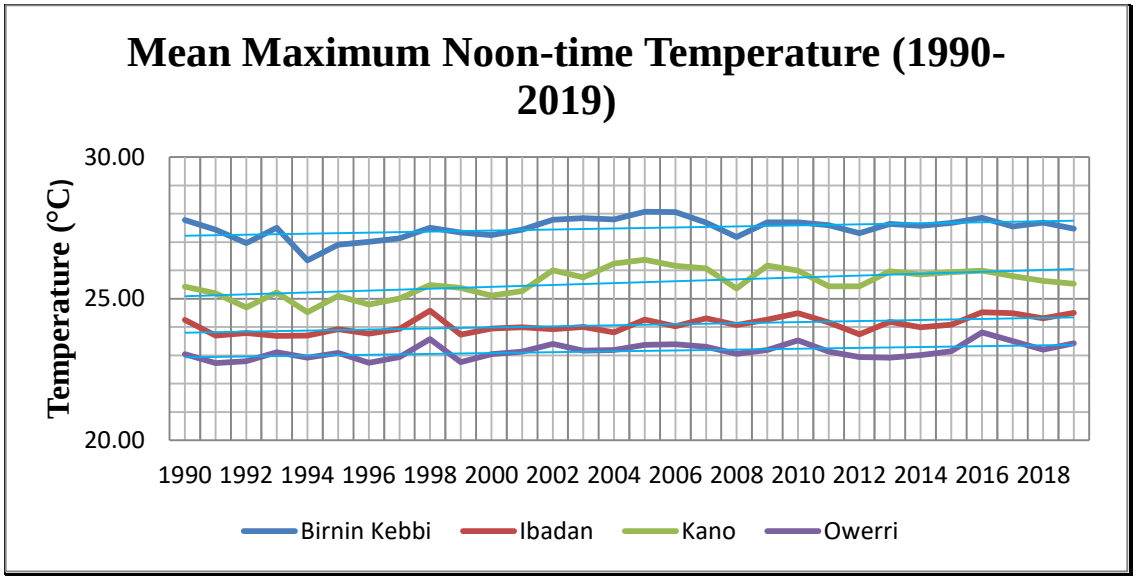


**Figure 4.51: Annual temperature trends across the four cities from 1990-2019**

According to Najib *et al.* (2017), temperature in Nigeria had higher values in the far north, occasioned by the effect of the Sahara Desert, which is characterized by fewer cloud cover, resulting in more solar irradiation; while, lower temperature values in the south are attributable to much higher cloud cover and abundant vegetal cover.

### 4.4.5 Mann-Kendall seasonal trend test results

Mann-Kendall Seasonal Trend Test Results for the four cities are presented in Table 4.14. The results indicate a sufficient statistical evidence of a significant seasonal increase at 0.05 significant level in maximum noon-time temperature series for the four cities from 1990 - 2019.

**Table 4.14 Seasonal Mann-Kendall Trend Test Results of Maximum Noon-Time Temperature for Birnin Kebbi, Kano, Ibadan and Owerri**

| City | S | Var S | Z | p-value |
|---|---|---|---|---|
| Birnin Kebbi | 695 | 37678.33 | 3.5753 | 0.0003498 |
| Kano | 1047 | 37677.00 | 5.3888 | 7.092e-08 |
| Ibadan | 1490 | 37659.33 | 7.6729 | 1.682e-14 |
| Owerri | 1259 | 37663.67 | 6.4822 | 9.042e-11 |

**Source: Author's Analysis (2023)**

In Table 4.15, the seasonal Mann-Kendall trend result indicates increasing trend in almost all the months of the year. For Birnin Kebbi, there are eleven months of increasing trend of which only July was statistically significant at 5 percent level, while the month of January witnessed a decrease in trend, although not statistically significant. The rising trend may be attributed to the urbanization trend in these cities which has resulted in the removal of vegetal cover, and subsequent release of carbon dioxide and other greenhouse gases.

**Table 4.15 Seasonal Mann-Kendall trend Results for Individual Seasons (Months)**

| | Birnin Kebbi | | Kano | | Ibadan | | Owerri | |
|---|---|---|---|---|---|---|---|---|
| Months | Z(trend) | P-Value | Z(trend) | P-Value | Z(trend) | P-Value | Z(trend) | P-Value |
| January | -0.250 | 0.8027 | -1.035 | 0.3007 | 0.464 | 0.6426 | 1.998 | 0.0457 |
| February | 1.106 | 0.2687 | 1.142 | 0.2535 | 0.375 | 0.7078 | 0.517 | 0.6048 |
| March | 0.786 | 0.4321 | 1.374 | 0.1693 | 0.928 | 0.3534 | -0.553 | 0.5801 |
| April | 0.161 | 0.8724 | 0.000 | 1.0000 | 1.840 | 0.0657 | 1.588 | 0.1123 |
| May | 0.981 | 0.3263 | 2.481 | 0.0131 | 4.069 | 4.72e-5 | 1.481 | 0.1385 |
| June | 1.802 | 0.0715 | 1.945 | 0.0518 | 2.554 | 0.0106 | 1.304 | 0.1923 |
| July | 1.963 | 0.0496 | 4.158 | 3.2e-05 | 4.052 | 5.07e-5 | 3.194 | 0.0014 |
| August | 1.250 | 0.2114 | 3.248 | 0.0012 | 3.714 | 0.0002 | 2.588 | 0.0096 |
| September | 1.856 | 0.0634 | 3.105 | 0.0019 | 2.534 | 0.0112 | 2.643 | 0.0082 |
| October | 1.802 | 0.0715 | 2.320 | 0.0203 | 3.676 | 0.0002 | 2.802 | 0.0051 |
| November | 0.607 | 0.5440 | -0.518 | 0.6047 | 2.356 | 0.0184 | 2.644 | 0.0081 |
| December | 0.161 | 0.8724 | 0.339 | 0.7345 | -0.143 | 0.8865 | 2.089 | 0.0366 |

**Source: Author's Analysis (2023)**

Kano witnessed a decreasing trend in the months of January and November, and increasing trends in the months of February - April and December but not statistically significant at 5 percent alpha level. However, from the months of May to October in Kano, there has been a significant increasing trend of temperature with the p-value <.05 alpha value. In Ibadan,

December showed a decreasing trend over the years while, January to March are increasing but not significant statistically. However, there has been significant increase in temperature from the months of April to November for the period under consideration. In Owerri, January, and July - December have witnessed increasing trends of temperature over the years and are statistically significant at 5 percent alpha value. The months of February to June witnessed increasing trend in temperature but not statistically significant. These increases might be attributed partly due to the general increase in the size of the cities, and partly due to the global rise in temperature due to anthropogenic forcings.

A graphical representation of the mean monthly temperature of the four cities during the period under consideration is presented in Figure 4.52.

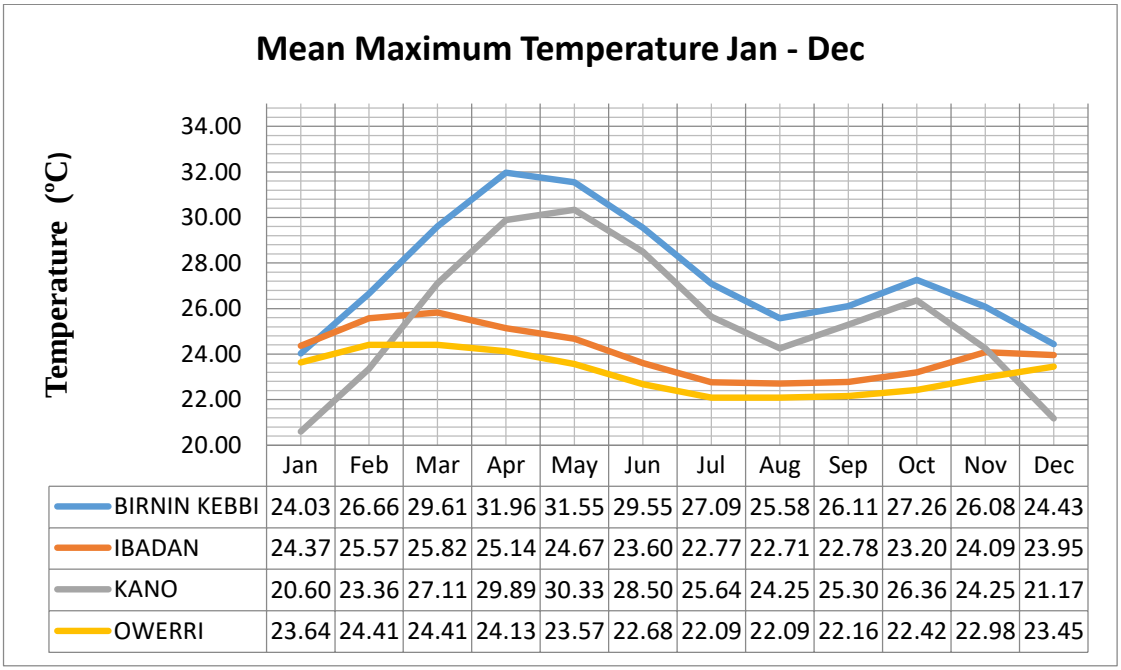


| | Jan | Feb | Mar | Apr | May | Jun | Jul | Aug | Sep | Oct | Nov | Dec |
|---|---|---|---|---|---|---|---|---|---|---|---|---|
| BIRNIN KEBBI | 24.03 | 26.66 | 29.61 | 31.96 | 31.55 | 29.55 | 27.09 | 25.58 | 26.11 | 27.26 | 26.08 | 24.43 |
| IBADAN | 24.37 | 25.57 | 25.82 | 25.14 | 24.67 | 23.60 | 22.77 | 22.71 | 22.78 | 23.20 | 24.09 | 23.95 |
| KANO | 20.60 | 23.36 | 27.11 | 29.89 | 30.33 | 28.50 | 25.64 | 24.25 | 25.30 | 26.36 | 24.25 | 21.17 |
| OWERRI | 23.64 | 24.41 | 24.41 | 24.13 | 23.57 | 22.68 | 22.09 | 22.09 | 22.16 | 22.42 | 22.98 | 23.45 |

**Figure 4.52** Mean monthly noon-time temperature of the cities from 1990 to 2019

It shows that not only are temperature values higher in the two Sudan Savanna cities (Birnin Kebbi and Kano); they are more variable seasonally compared to the two cities in the Tropical Rainforest (Ibadan and Owerri). The higher values in the Sudan cities may be

attributed to their location in the drier latitudes, the continuous loss of vegetal cover to natural factors and anthropogenic activities, as well as desertification. Birnin Kebbi and Kano recorded the highest monthly mean temperature values between the months of March and June. The results are also in consonance with Amadi *et al.* (2014) whose study demonstrated latitudinal dependence of basic temperature characteristics; with the northern region of Nigeria showing higher temperature variability than the southern region.

With low temperature values of 20.60°C and 21.17°C in the months of January and December for Kano and Birnin Kebbi respectively, Kano Metropolis particularly recorded temperatures much lower than those of the Tropical Rainforest which are generally characterized by lower temperatures. The lower temperature in Kano city is attributable to the Harmattan season which occurs between the end of November and mid-March (Okeahialam, 2016) and is more severe in the Sudan ecological zone. The Harmattan dust is largely made up of dense silicon content which reduces radiation from the sun, and its attendant warmth, hence the associated low temperature (Enete *et al.,* 2012). For the cities in the Rainforest ecological zone, temperature peaks in March (25.82 °C for Ibadan and 24.41°C in Owerri) and declines steadily till July from when a near uniform temperature is sustained until September, after which the temperature rises following the cessation of the rainy season.

### 4.4.6 Pettitt Test for Single Change-Point in Temperature for the cities

Results for the Pettitt Test for Single change-Point in temperature for the four cities are presented in Table 4.16 and Figure 4.53.

**Table 4.16** Pettitt test for single change-point in maximum temperature for the cities

| City | U | p-vale | K | Year-Month |
|---|---|---|---|---|
| Birnin Kebbi | 3943 | 0.2723 | 146 | February, 2002 |
| Kano | 5544 | 0.0388 | 146 | February, 2002 |
| Ibadan | 5251 | 0.0583 | 179 | November, 2004 |
| Owerri | 5342 | 0.0515 | 143 | November, 2001 |

**Source: Author's Analysis (2023)**

The results reveal that the general rising trend began in the month of February 2002 for Birnin Kebbi and Kano, both located in the same ecological zone. However, Birnin Kebbi is not statistically significant at 5 percent level. For Ibadan and Owerri both in the same ecological zone, an increasing trend was experienced in the month of November. The change in trend in Owerri was earlier (2001), while that of Ibadan occurred later. Also, an increasing change point was observed in November 2004 and 2001 in Ibadan and Owerri. The results for Ibadan and Owerri were statistically significant only at 10 percent significance level with p-values of .058 and .051 respectively.

Conclusively, these analysis is in agreement with documented evidences from several studies. For instance, analysis of temperature data of Agios Nikolaos, Evrytania central Greece, from 1973 to 2019 by Kaoukis *et al*. (2022), aside showing a significant rising trend in temperature values on yearly and seasonal basis; particularly during summer, also indicated a rise in the daily temperature range and the number of days which recorded very high temperature.

Results of the study are also in tandem with Ajaaj *et al*. (2017) who utilized multiple statistical tests in examining long term tendencies in yearly and seasonal temperature in 18 sampled mega cities cutting across six continents of the world, with the urban and peri-urban areas classified based using percentage of land imperviousness.

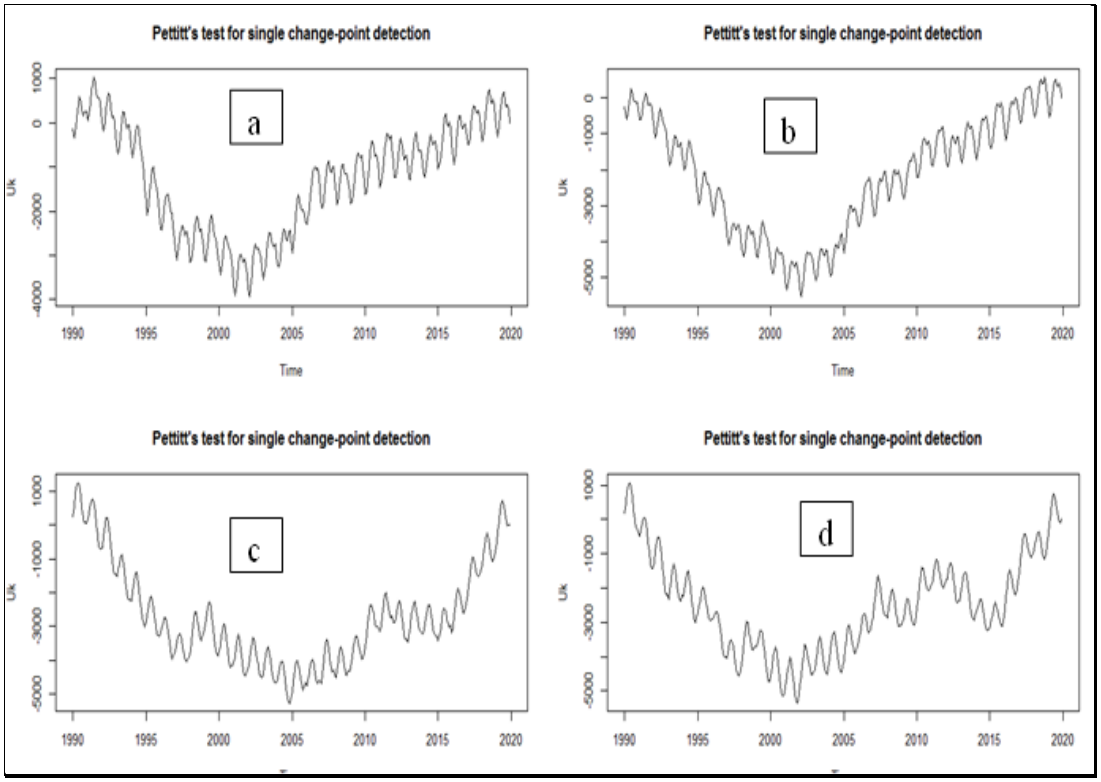


**Figure 4.53** Pettitt's Test for Single Change-Point Detection in Maximum temperature for Birnin Kebbi (a), Kano (b), Ibadan (c) and Owerri (d) for the period 1990-2019

Results of the study indicated that approximately seventy percent of the urban locations revealed higher positive air temperature trends when compared with peri-urban locations. Results are also similar to the works of Subarna (2017) who carried out an evaluation of temporal changes in temperature in Jakarta from 1901 to 2002 with the use of Mann-Kendall trend test and the statistical linear trend test method, with the results of the two tests indicating an increase in the monthly mean values in the air surface temperature at a decadal rate of approximately 0.152°C. Furthermore, the study was corroborated by Song and Park (2021) whose study in South Korea revealed temperature rise of 2°C rise in stations with high trend slope and 0.5°C rise at stations with low trend slopes. The study also established a positive relationship between city locations and the trend slope; and an inverse relationship between forest areas and the trend slope, implying that expansion of urban areas into forested areas was a key factor in the long-term rise in urban temperature.

## 4.5 Trends in LST of the Study Locations from 1990 to 2019

This section presents the results for the analysis of LST in Ibadan, Owerri, Kano and Birnin Kebbi cities from 1990 to 2019.

### 4.5.1 LST of Ibadan 1990-2019

LST images of Ibadan Metropolis in 1990 and 2019 are presented in Figures 4.54 and 4.55 while those of 2001 and 2011 are shown in Appendix I. Results showed that the maximum recorded LST of the city was 40.50℃, 79.24℃, 46.42℃ and 37.42℃ in 1990, 2001, 2011 and 2019 respectively, while the minimum was 13.45℃, -31.04℃, 18.64℃, and 23.31℃ in 1990, 2001, 2011 and 2019 respectively. This implied that both maximum (79.24℃) and minimum (-31.04℃) LST values of the city were recorded in 2001.

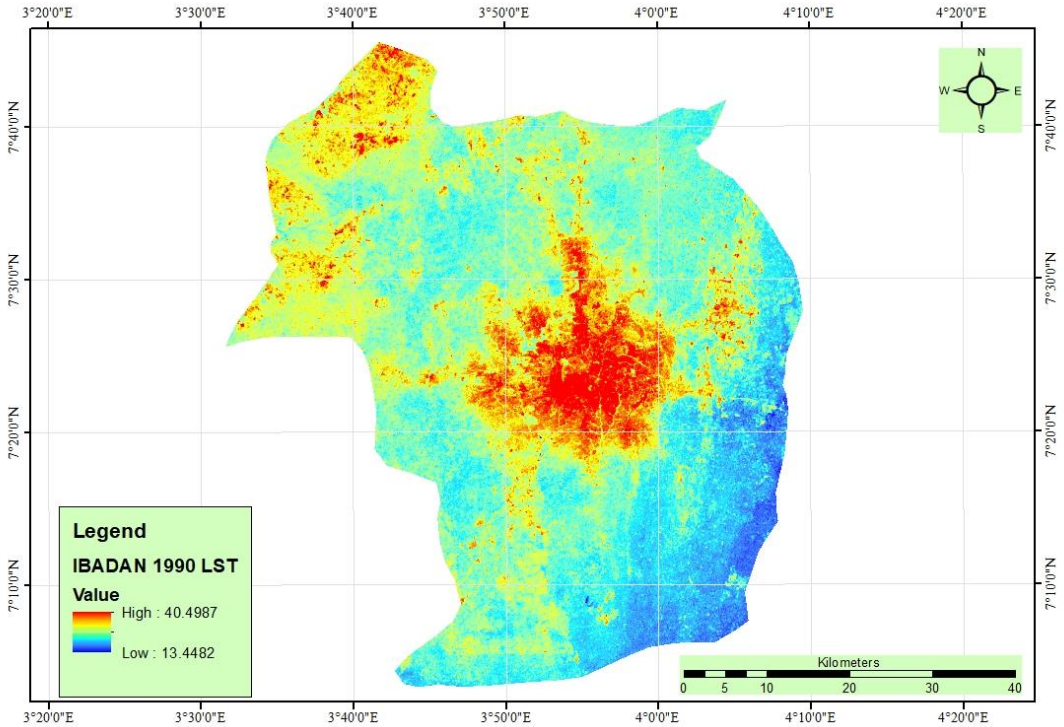


**Figure 4.54** LST of Ibadan Metropolis in 1990

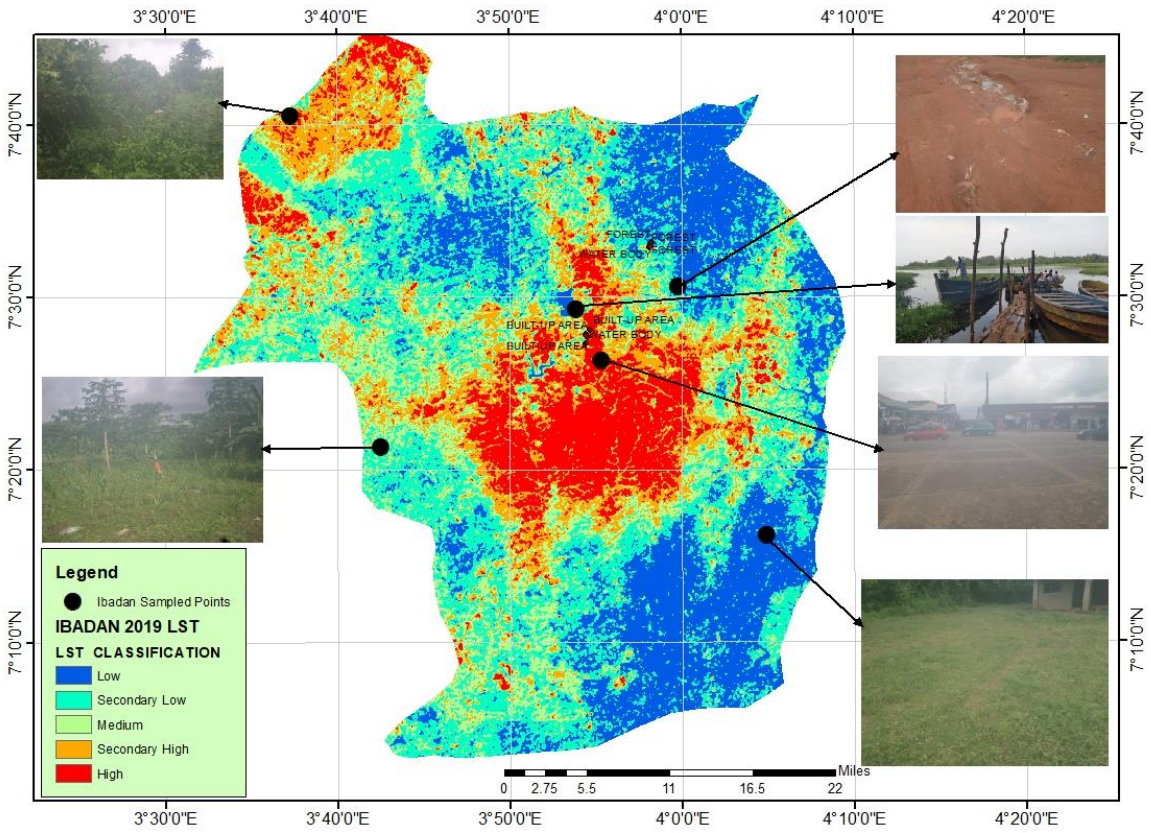


**Figure 4.55** LST of Ibadan Metropolis in 2019

The mean LST values of 24.89℃, 3.40℃, 30.44℃ and 27.69℃ were recorded in 1990, 2001, 2011 and 2019 respectively; indicating that the highest mean value was recorded in 2010, while the lowest value was recorded in 2001. Figure 4.55 shows the statistics of re-classified LST images of Ibadan metropolis in 1990, 2001, 2011 and 2019 respectively while classification maps are shown in Appendix J. The statistics showed that in 1990, low LST areas areas (13.45 – 22.78℃) occupied 1279.38 km$^2$ (37.59 percent). The secondary low temperature areas (22.78– 24.16℃) covered 961.06 km$^2$ (28.24 percent).

The medium temperature areas (24.16 – 25.54℃) covered 546.00 km$^2$ (16.04 percent). The secondary high temperature areas (25.54– 27.88℃) covered 406.67 km$^2$ (11.95 percent). The high temperature areas (27.88 – 40.50℃) occupied 209.96 km$^2$ (6.17 percent). This implied that in 1990 high and secondary high temperature areas (25.54 – 40.50℃)

collectively occupied 616.63 km$^2$ (18.12 percent of Ibadan Metropolis), whereas low and secondary low temperature areas (13.45 - 24.16℃) collectively occupied 2,240.44 km$^2$ (65.84 percent of the Metropolis). The remaining 546.00 km$^2$ (16.04 percent) was characterised by moderate temperature.

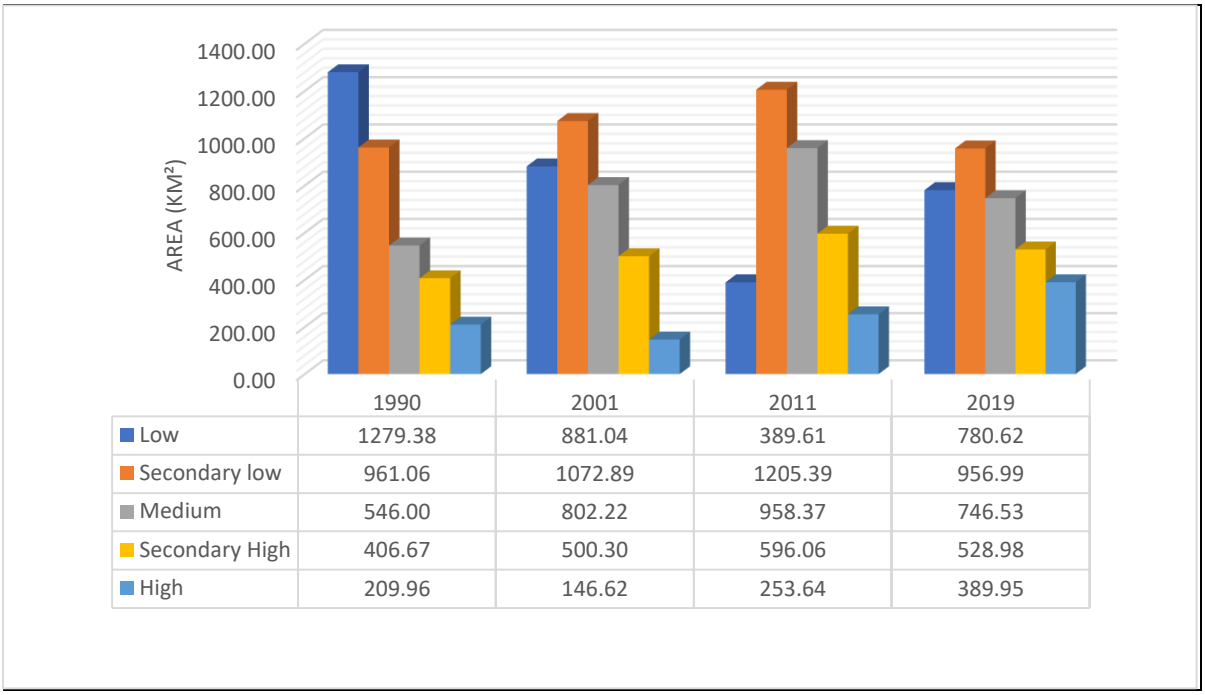


| | 1990 | 2001 | 2011 | 2019 |
|---|---|---|---|---|
| Low | 1279.38 | 881.04 | 389.61 | 780.62 |
| Secondary low | 961.06 | 1072.89 | 1205.39 | 956.99 |
| Medium | 546.00 | 802.22 | 958.37 | 746.53 |
| Secondary High | 406.67 | 500.30 | 596.06 | 528.98 |
| High | 209.96 | 146.62 | 253.64 | 389.95 |

**Figure 4.56** Ibadan LST 1990 – 2019

In 2001, low temperature areas (-31.04 to -1.95℃) covered 1072.89 km$^2$ (31.53 percent). The medium temperature areas (4.12 – 8.90℃) occupied 802.22 km$^2$ (23.57 percent). The secondary high temperature areas (8.90 – 14.55 covered 500.30 km$^2$ (14.70 percent). The high temperature areas (14.55 – 79.24℃) 146.62 km$^2$ (4.31 percent). This implied that in 2001 high and secondary high temperature areas (89.90 – 79.24℃) collectively occupied 646.92 km$^2$ (19.01 percent of Ibadan Metropolis), indicating a coverage area higher than year 1990 by 12.84 percent. Similarly, medium temperature areas 802.22 km$^2$ increased in percentage coverage from 16.04 percent in 1990 to 23.57 percent in 2001. On the contrary, low and secondary low temperature areas (-31.04 – 4.12℃) collectively covered 1,953.93

$km^2$ (57.42 percent of the Metropolis), indicating a coverage area lower than year 1990 by 8.42 percent. The remaining 802.22 $km^2$ (23.57 percent) occupied by medium temperature.

In 2011, low temperature areas (18.64 – 28.26℃) covered 389.61 $km^2$ (11.45 percent). The secondary low temperature areas (28.26 – 29.68℃) occupied 1,205.39 $km^2$ (35.42 percent). The medium temperature area (29.68 – 31.11℃) covered 958.37 $km^2$ (28.16 percent). The secondary high temperature areas (31.11 – 33.51℃) occupied 596.06 $km^2$ (17.52 percent). The high temperature areas (33.51– 46.42℃) covered 253.64 $km^2$ (7.45 percent). This implied that in 2011 high and secondary high temperature areas (31.11 – 46.42℃) collectively covered 849.70 $km^2$ (24.97 percent of Ibadan Metropolis), indicating a coverage area higher than 2001 by 5.96 percent. Similarly, medium temperature areas (958.37 $km^2$) increased in percentage coverage from 23.57 percent in 2001 to 28.16 percent in 2011. On the contrary, low and secondary low temperature areas (18.64 – 29.68℃) collectively occupied 1,595.00 $km^2$ (46.87 percent of the Metropolis), indicating a coverage area lower than year 2001 by 10.55 percent.

In 2019, low temperature areas (23.31–26.02℃) occupied 780.62 $km^2$ (22.94 percent). The secondary low temperature areas (26.02 – 27.40℃) covered 956.99 $km^2$ (28.12 percent). The medium temperature areas (27.40 – 28.90℃) occupied 746.53 $km^2$ (21.94 percent). The secondary high temperature areas (28.90 – 30.61℃) covered 528.98 $km^2$ (15.54 percent). The high temperature areas (30.61 – 37.42℃) 389.95 $km^2$ (11.46 percent). This implied that in 2019 high and secondary high temperature areas (28.90 – 37.42℃) collectively occupied 918.93 $km^2$ (27.00 percent of Ibadan Metropolis), indicating an area coverage higher than year 2011 by 2.03 percent. Similarly, low and secondary low temperature areas (23.31 – 27.40℃) collectively covered 1,737.61 $km^2$ (51.06 percent of the Metropolis), indicating a

coverage area higher than year 2011 by 4.19 percent. On the contrary, medium temperature areas (746.53 $km^2$) decreased in percentage coverage from 28.16 percent in 2011 to 21.94 percent in 2019.

### 4.5.2 LST of Owerri 1990 to 2019

LST images of Owerri Metropolis in 1990 and 2019 are presented in Figures 4.57 and 4.58 while those of 2000 and 2010 are shown in Appendix I. Results showed that the maximum recorded LST of the city was 39.16℃, 41.75℃, 43.07℃ and 29.50℃ in 1990, 2001, 2011 and 2019 respectively, while the minimum was 29.50℃, 29.75℃, 20.73℃, and 15.83℃ in 1990, 2000, 2010 and 2019 respectively.

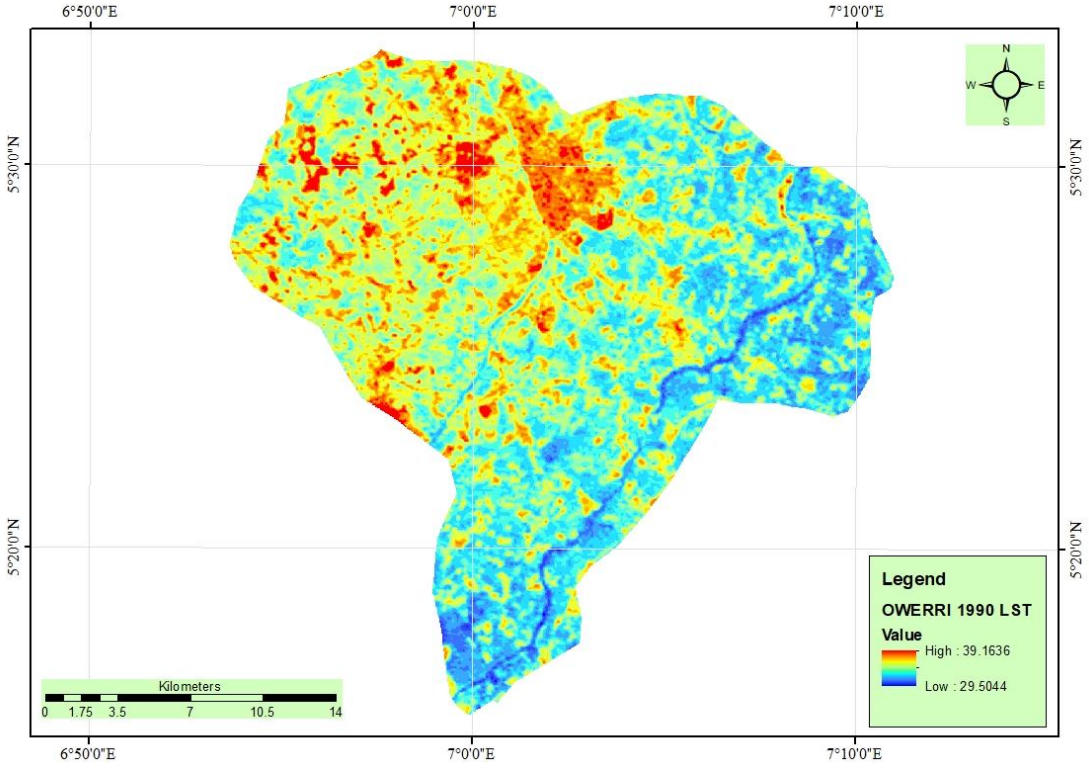


**Figure 4.57** LST of Owerri Metropolis in 1990

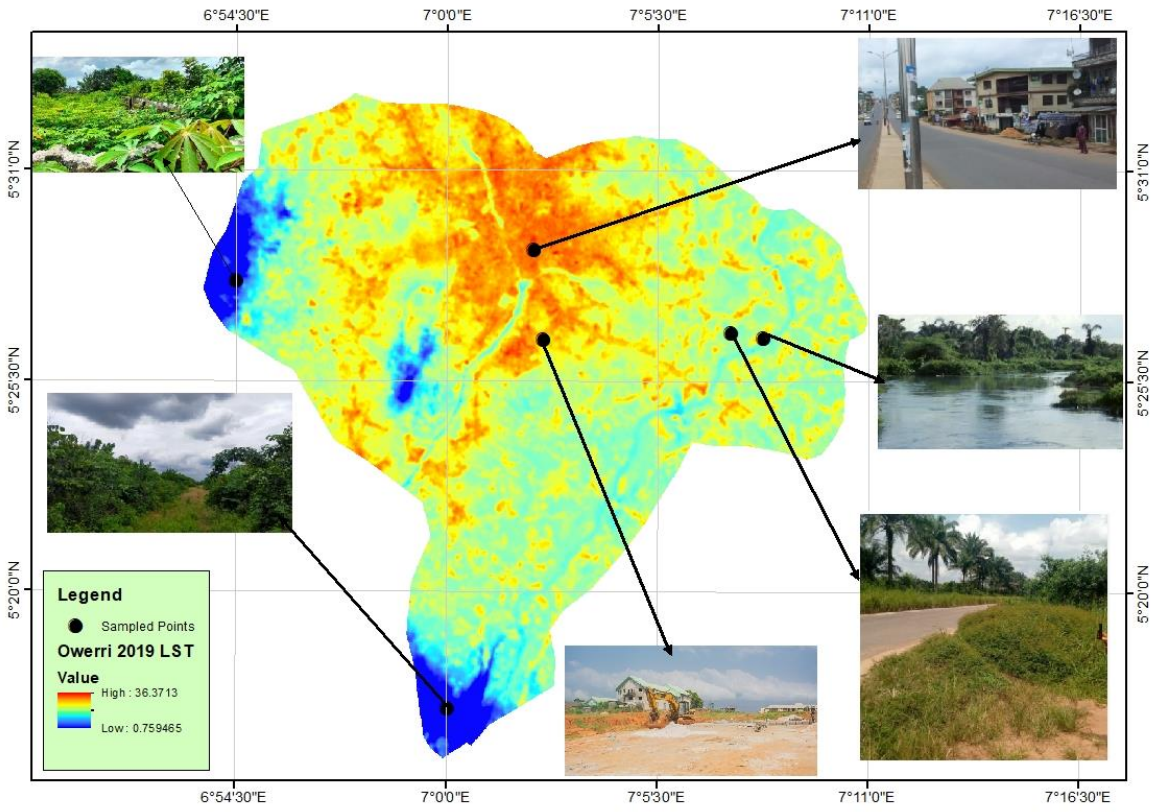


**Figure 4.58** LST of Owerri City in 2019

This implied the maximum LST (43.07℃) value was recorded in 2010 while the minimum (15.83℃) value of the city was recorded in 2019. The mean LST values of 32.89℃, 33.13℃, 34.86℃ and 25.19℃ were recorded in 1990, 2000, 2010 and 2019 respectively; indicating that the highest mean value was recorded in 2010, while the lowest value was recorded in 2019. For standard deviation, recorded values were 1.35, 1.66, 2.03, and 1.74 in 1990, 2000, 2010 and 2019 respectively, indicating a higher standard deviation in 2010 and the lowest in 1990.

The high LST areas were largely located within the core LGAs (Owerri Municipal, Owerri West and Owerri North) that make up Owerri metropolis, which characteristically comprise densely populated residential, high Traffic, industrial, and market areas. The high LST areas include Eke Onunwa and new markets, Ikenebu, Wetheral, Warehouse, Nekede, Amakaohia,

Relief, Egbu, New Owerri, Concorde Area, World Bank Estate (Area C), Eziobodo Area, FUTO-Obinze Area, Avu, and Irete among others.

Figure 4.59 shows the statistics of re-classified LST images of Owerri metropolis in 1990, 2000, 2010 and 2019 respectively while classification maps are shown in Appendix J. The statistics showed that in 1990, low temperature areas (29.50 – 31.97℃) occupied 199.24 $km^2$ (36.67 percent).

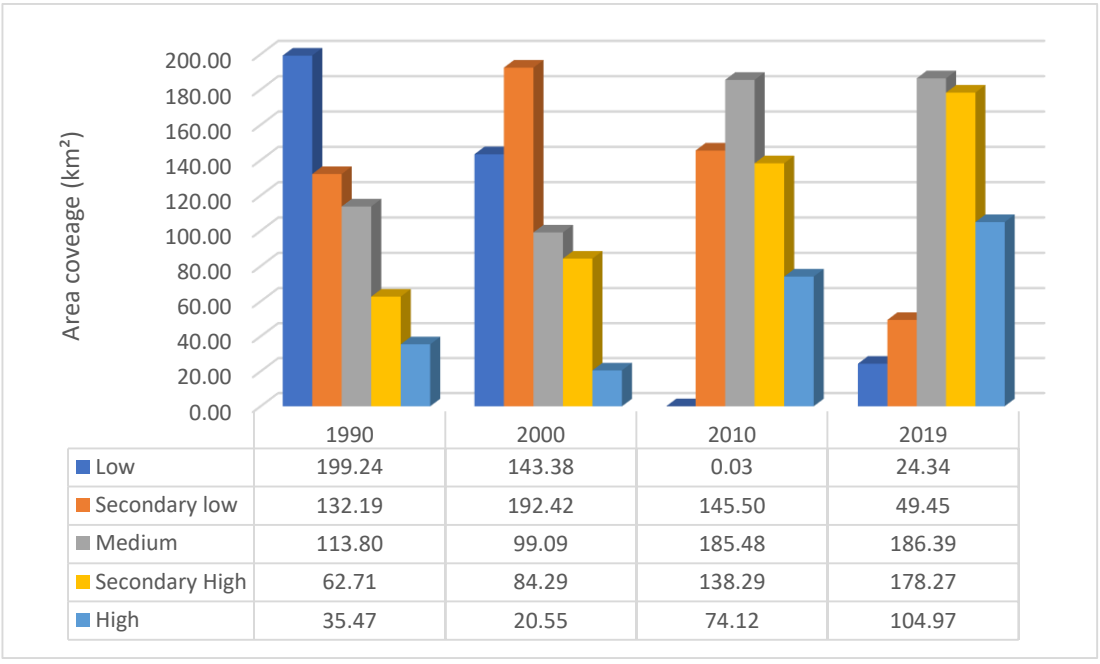


| | 1990 | 2000 | 2010 | 2019 |
|---|---|---|---|---|
| Low | 199.24 | 143.38 | 0.03 | 24.34 |
| Secondary low | 132.19 | 192.42 | 145.50 | 49.45 |
| Medium | 113.80 | 99.09 | 185.48 | 186.39 |
| Secondary High | 62.71 | 84.29 | 138.29 | 178.27 |
| High | 35.47 | 20.55 | 74.12 | 104.97 |

**Figure 4.59** Owerri LST 1990 – 2019

Secondary low temperature areas (31.97 – 32.95℃) covered 132.19 $km^2$ (24.33 percent). The medium temperature areas (32.95 – 33.90℃) occupied 113.80 $km^2$ (20.94 percent). The secondary high temperature areas (33.90 – 34.88℃) occupied 62.71 $km^2$ (11.54 percent). The high temperature areas (34.88 – 39.16℃) covered 35.47 $km^2$ (6.53 percent). This implied that in 1990 high and secondary high temperature areas (33.90 – 39.16℃) collectively occupied 98.18 $km^2$ and (8.07 percent of Owerri Metropolis), whereas low and

secondary low temperature areas (29.50 – 32.95℃) 331.44 $km^2$ (60.99 percent of the Metropolis).

In 2000, low temperature areas (29.75 – 32.10℃) 143.38 $km^2$ (26.56 percent of the total area). The secondary low temperature areas (32.10 – 33.51℃) covered 192.42 $km^2$ (35.65 percent). The medium temperature areas (33.51 – 34.93℃) occupied 99.09 $km^2$ (18.36 percent). The secondary high temperature areas (34.93 – 36.76℃) covered 84.29 $km^2$ (15.62 percent). The high temperature areas (36.76 – 41.75℃) 20.55 $km^2$ (3.81 percent). This implied that in 2000, high and secondary high temperature areas (29.75 - 33.51℃) collectively covered 104.84 $km^2$ (19.42 percent of Owerri Metropolis), indicating a coverage area higher than year 1990 by 1.35 percent. Similarly, low and secondary low temperature areas (29.74 – 33.51℃) collectively covered 335.79 $km^2$ (62.22 percent of the Metropolis), indicating an area coverage higher than year 1990 by 1.23 percent. On the contrary, medium temperature areas decreased in percentage coverage from 20.94 percent in 1990 to 18.36 percent in 2000.

In 2010, low temperature areas (20.73 – 28.27℃) covered 0.03 $km^2$ (0.01 percent of the total area). The secondary low temperature areas (28.27 – 33.08℃) occupied 145.50 $km^2$ (26.77 percent). The medium temperature areas (33.08 – 34.92℃) covered 185.48 $km^2$ (34.13 percent). The secondary high temperature areas (34.92– 37.20℃) covered 138.29 $km^2$ (25.45 percent). The high temperature areas (37.20 – 43.07℃) covered 74.12 $km^2$ (13.64 percent). This implied that in 2010, high and secondary high temperature areas (34.92 – 43.07℃) collectively occupied 212.41 $km^2$ (39.09 percent of Owerri Metropolis), indicating an area coverage higher than year 2000 by 19.67 percent. Similarly, medium temperature areas increased in percentage coverage from 18.36 percent in 2000 to 34.13 percent in 2010.

On the contrary, low and secondary low temperature areas (20.73 – 33.08℃) collectively occupied 145.53 $km^2$ (26.78 percent of the Metropolis), indicating a coverage area lower than year 2000 by 35.44 percent.

In 2019, low temperature areas (15.83 – 21.46℃) covered 24.34 $km^2$ (4.48 percent of the total area). The secondary low temperature areas (21.46 – 23.71℃) occupied 49.45 $km^2$ (9.10 percent). The medium temperature areas (23.71 – 25.27℃) covered 186.39 $km^2$ (34.30 percent). The secondary high temperature areas (25.27– 26.61℃) occupied 178.27 $km^2$ (32.81 percent). The high temperature areas (26.61 – 29.50℃) covered 104.97 $km^2$ (19.32 percent). This implied that in 2010, high and secondary high temperature areas (25.27 – 29.50℃) collectively covered 283.25 $km^2$ (52.12 percent of Owerri Metropolis); indicating a coverage area higher than year 2010 by 13.03 percent. Similarly, medium temperature areas increased in percentage coverage from 34.13 percent in 2010 to 34.30 percent in 2019. On the contrary, low and secondary low temperature areas (15.83 – 23.71℃) collectively covered 73.79 $km^2$ (13.58 percent of the Metropolis), indicating a coverage area lower than year 2010 by 13.20 percent.

### 4.5.3 LST of Kano 1991 to 2019

LST images of Owerri Metropolis in 1991 and 2019 are presented in Figures 4.60 and 4.61 while those of 2001 and 2011 are shown in Appendix I. Results showed that the maximum recorded LST of the city was 30.92°C, 42.19°C, 46.53°C and 21.59°C in 1991, 2001, 2011 and 2019 respectively, while the minimum was -0.27°C, 14.32°C, 18.11°C, and -1.94°C in 1991, 2001, 2011 and 2019 respectively. This implied that the maximum LST (46.53°C) value was recorded in 2011 while the minimum (-0.27°C) value of the city was recorded in 1991.

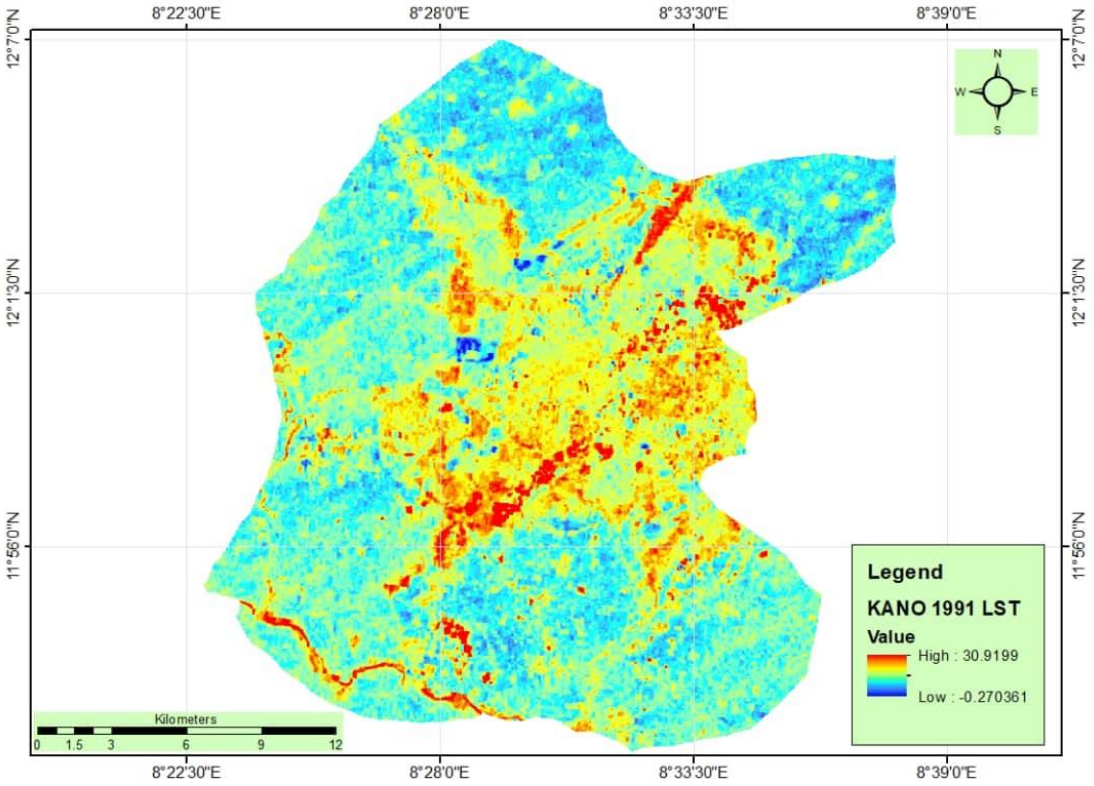


**Figure 4.60** LST of Kano Metropolis in 1991

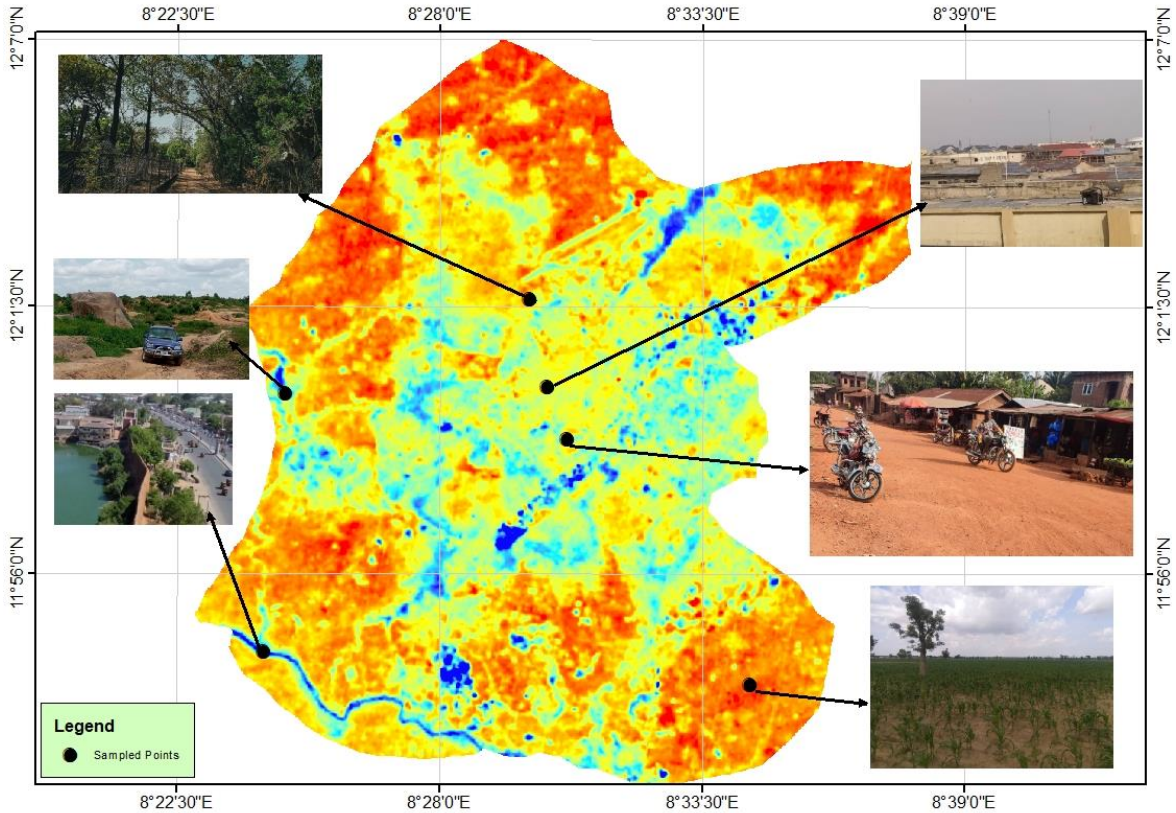


**Figure 4.61** LST of Kano City in 2019

The mean LST values of 25.18°C, 35.77°C, 39.22°C and 16.02°C were recorded in 1991, 2001, 2011 and 2019 respectively; indicating that the highest mean value was recorded in 2011, while the lowest value was recorded in 2019. For standard deviation, recorded values were 1.44, 1.65, 1.59, and 1.64 in 1991, 2001, 2011 and 2019 respectively, indicating a higher standard deviation in 2001 and the lowest in 1991. The high LST areas were largely located within the core LGAs, which characteristically comprise densely populated residential, high Traffic, industrial, and market areas.

Figure 4.62 shows the statistics of re-classified LST images of Kano metropolis in 1991, 2001, 2011 and 2019 respectively while classification maps are shown in Appendix J. The statistics showed that in 1991, low LST areas (-0.27°C to 17.34°C) occupied 1.06 km$^2$ (0.22 percent). Secondary low areas (17.34°C to 22.11°C) covered 10.05 km$^2$ (2.04 percent). The medium LST areas (22.11°C to 24.07°C) occupied of 95.58 km$^2$ (19.37 percent).

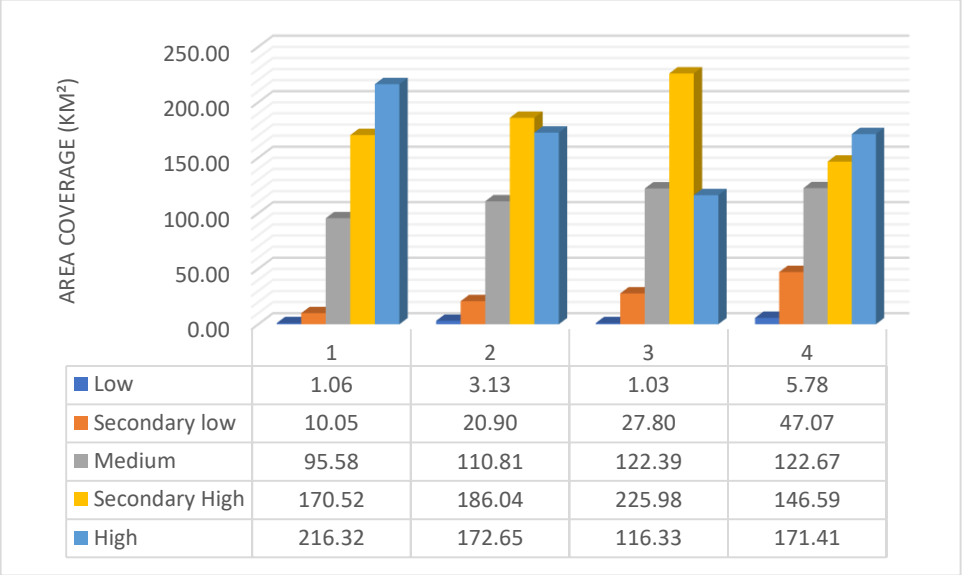


| | 1 | 2 | 3 | 4 |
|---|---|---|---|---|
| Low | 1.06 | 3.13 | 1.03 | 5.78 |
| Secondary low | 10.05 | 20.90 | 27.80 | 47.07 |
| Medium | 95.58 | 110.81 | 122.39 | 122.67 |
| Secondary High | 170.52 | 186.04 | 225.98 | 146.59 |
| High | 216.32 | 172.65 | 116.33 | 171.41 |

**Figure 4.62** Kano LST 1991 – 2019

The secondary high LST areas 24.07°C to 25.42°C) covered 170.52 km$^2$ (34.55 percent). The high LST area (25.42°C to 30.92°C) occupied 216.32 km$^2$ (43.83 percent). This implied

that in 1991 high and secondary high LST areas (24.07°C to 30.92°C) collectively covered 386. 84 $km^2$ (78.38 percent of Kano Metropolis), whereas low and secondary low LST areas (-0.27°C to 22.11°C) collectively covered 11.12 $km^2$ (2.26 percent of the Metropolis).

In 2001, low LST areas (14.32°C to 29.19°C) occupied 3.18 $km^2$ (0.63 percent of the total area). The secondary low LST areas (29.19°C to 32.57°C) covered 20.90 $km^2$ (4.24 percent). The medium LST areas (32.57°C to 34.87°C) occupied 110.81 $km^2$ (22.45 percent). The secondary high LST areas (34.87°C – 36.29°C) covered 186.04 $km^2$ (37.70 percent). The high LST areas (36.29°C – 42.19°C) occupied 172.65 $km^2$ (34.98 percent). On the contrary, low and secondary LST areas (14.32°C to 32.57°C) covered 24.03 $km^2$ and increased slightly in percentage coverage by 2.61 percent from 2.26 percent in 1991 to 4.87 percent in 2001. Similarly, medium LST areas increased in coverage from 19.37 percent in 1991 to 22.45 percent.

In 2011, low LST areas (18.11°C to 34.38°C) covered 1.03 $km^2$ (0.21 percent of the total area). The secondary low LST areas (34.38°C to 37.61°C) occupied 27.80 $km^2$ (5.63 percent). The medium LST areas (37.61°C to 39.51°C) covered 122.39 $km^2$ (24.80 percent). The secondary high LST areas (39.51°C to 40.85°C) covered 225.98 $km^2$ (45.79 percent). The high LST areas (40.85°C to 46.53°C) occupied 116.33 $km^2$ (23.57 percent). This implied that in 2011, secondary high and high LST areas (39.51°C to 46.53°C) collectively occupied 342.31 $km^2$ (69.36 percent of Kano Metropolis), indicating a coverage area lower than 2001 by 3.32 percent. On the contrary, medium LST areas increased in percentage coverage by 2.35 percent from 22.45 percent in 2001 to 24.80 percent in 2011. similarly, low and secondary low LST areas (18.11°C to 37.61°C) collectively covered 28.83 $km^2$ (5.84 percent of the Metropolis), indicating a coverage area higher than year 2001 by 0.97 percent.

In 2019, low LST areas (-1.94°C to 11.53°C) occupied 5.78 $km^2$ (1.17 percent of the total area). The secondary low LST areas (11.53°C – 14.12°C) covered 47.07 $km^2$ (9.54 percent). The medium LST areas (14.12°C – 15.59°C) occupied 122.67 $km^2$ (24.86 percent). The secondary high LST areas (15.59°C – 17.07°C) covered 171.41 $km^2$ (34.37 percent). The high LST areas (17.07°C – 29.53) covered 146.59 $km^2$ (29.70 percent). This implied that in 2019, high and secondary high LST areas (15.59°C – 21.59°C) collectively occupied 318.00 $km^2$ (64.43 percent of Kano Metropolis), indicating a coverage area lower than 2011 by 4.93 percent. On the contrary, low and secondary low LST areas (-1.94°C – 14.12°C) collectively occupied 52.86 $km^2$ (10.71 percent of the Metropolis), indicating an increase in percentage coverage by 4.87 percent from 5.84 percent in 2011 to 10.71 percent in 2019. Similarly, medium LST areas increased in percentage coverage from 24.80 percent in 2011 to 24.86 percent in 2019.

### 4.5.4 LST of Birnin Kebbi 1990-2019

LST images of Birnin Kebbi Metropolis in 1990 and 2019 are presented in Figures 4.63 and 4.64 while those of 2000 and 2010 are shown in Appendix I. Results showed that the maximum recorded LST of the city was 29.03℃, 40.82℃, 47.13℃ and 42.63℃ in 1990, 2000, 2010 and 2019 respectively, while the minimum was -1.22℃, 26.81℃, 29.51℃, and 27.00℃ in 1990, 2000, 2010 and 2019 respectively. This implied that the maximum LST (47.13℃) value was recorded in 2010 while the minimum (-122℃) value of the city was recorded in 1990. The mean LST values of 9.05℃, 35.73℃, 41.22℃ and 33.60℃ were recorded in 1990, 2000, 2010 and 2019 respectively; indicating that the highest mean value was recorded in 2010, while the lowest value was recorded in 1990. For standard deviation, recorded values were 2.53, 2.11, 2.40, and 2.47 in 1990, 2000, 2010 and 2019 respectively, indicating a higher standard deviation in 1990 and the lowest in 2000.

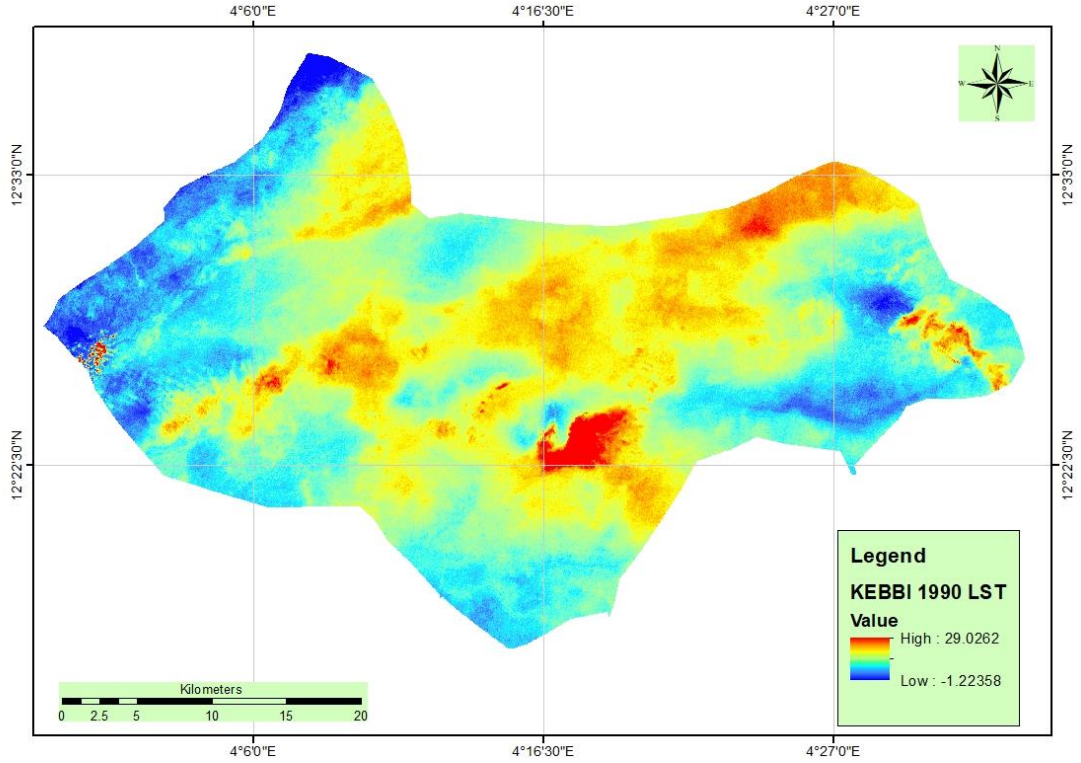


**Figure 4.63** LST of Birnin Kebbi Metropolis in 1990

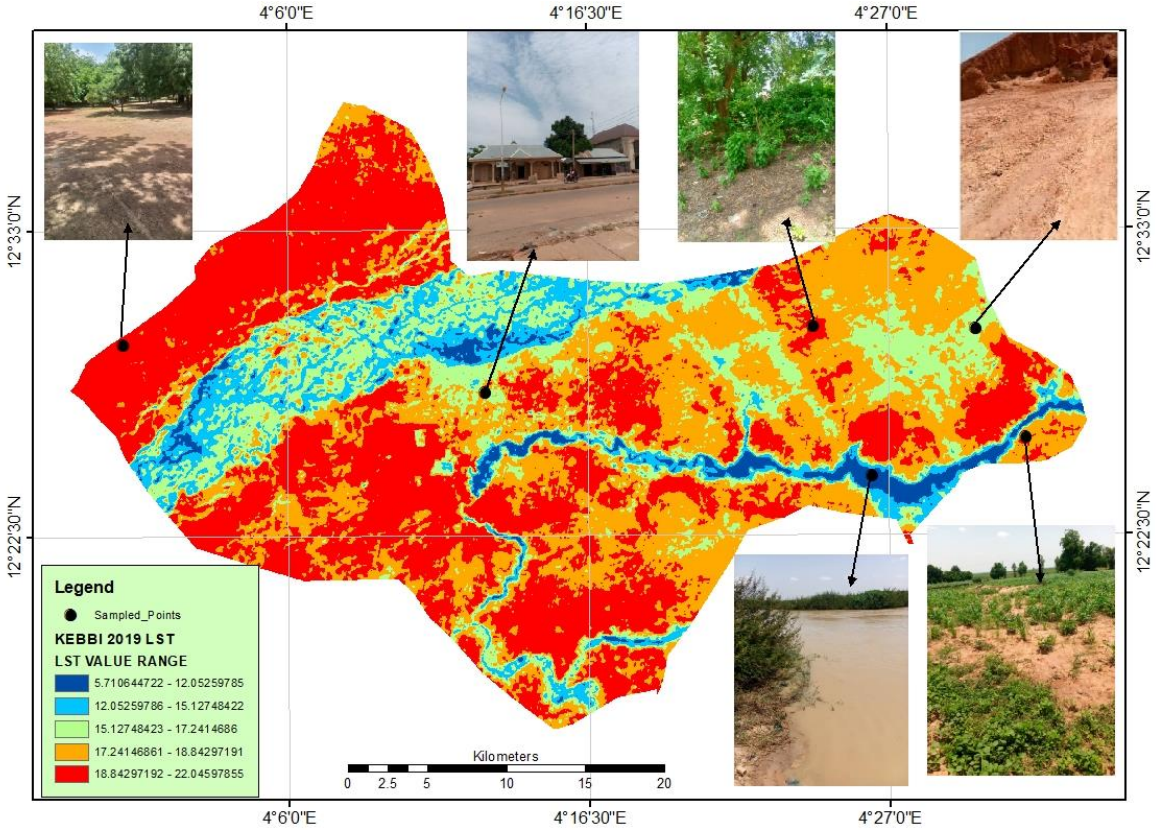


**Figure 4.64** LST of Birnin Kebbi City in 2019

The high LST areas were largely located within the core areas of Birnin Kebbi, which characteristically comprise densely populated residential, high Traffic, and market areas such as CBD, Makerar Gwandu, Kofar Kola, Rafin Atiku, Badariya, Bayan Kara, Takalau,Tudun Wada, Nasarawa 1, Nasarawa 2, Gwadangwaji.

Figure 4.65 shows the statistics of re-classified LST images of Birnin Kebbi metropolis in 1990, 2000, 2010 and 2019 respectively while classification maps are shown in Appendix J. In 1990, low temperature areas (-1.22 – 6.61℃) occupied 257.50 km$^2$ (20.62 percent). Secondary low temperature areas (6.61 – 8.98℃) covered 434.43 km$^2$ (34.79 percent). The medium temperature areas (8.98 – 11.23℃) occupied 373.21 km$^2$ (29.88 percent). The secondary high temperature areas (11.23 – 15.62℃) covered 174.37 km$^2$ (13.96 percent). The high temperature areas (15.62 – 29.03℃) occupied 9.37 km$^2$ (0.75 percent). This implied that in 1990 high and secondary high temperature areas (11.23 – 29.03℃) collectively covered 183.74 km$^2$ (14.71 percent of Birnin Kebbi Metropolis), whereas low and secondary low temperature areas (-122 – 8.98℃) collectively covered 691.93 km$^2$ (55.40 percent of the Metropolis).

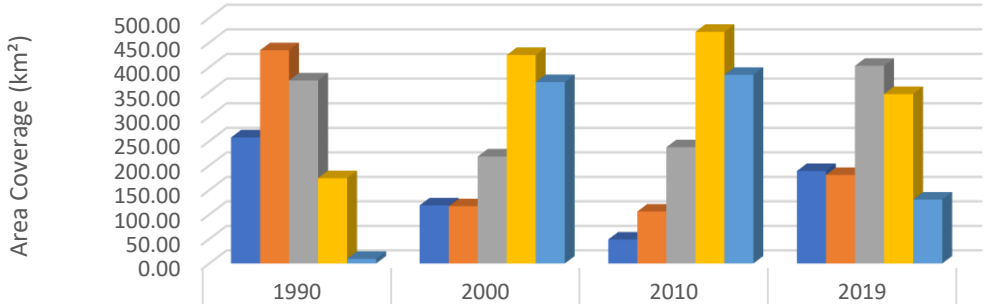


| | 1990 | 2000 | 2010 | 2019 |
|---|---|---|---|---|
| Low | 257.50 | 118.68 | 49.04 | 188.96 |
| Secondary low | 434.43 | 117.01 | 106.10 | 180.88 |
| Medium | 373.21 | 218.64 | 237.52 | 402.87 |
| Secondary High | 174.37 | 424.73 | 471.68 | 345.58 |
| High | 9.37 | 369.82 | 384.53 | 130.57 |

**Figure 4.65** Birnin Kebbi LST 1990 – 2019

In 2000, low temperature areas (26.81 – 31.66℃) occupied 118.68 $km^2$ (9.50 percent of the total area). The secondary low temperature areas (31.66 – 33.52℃) covered 117.01 $km^2$ (9.37 percent). The medium temperature areas (33.52 – 35.41℃) occupied 218.64 $km^2$ (17.51 percent). The secondary high temperature areas (33.41– 36.78℃) covered 424.73 $km^2$ (34.01 percent). The high temperature areas (36.78 – 40.86℃) occupied 369.82 $km^2$ (29.61 percent). This implied that in 2000, high and secondary high temperature areas (35.41 – 40.86 ℃) collectively covered 794.55 $km^2$ (63.62 percent of Birnin Kebbi Metropolis), indicating a coverage area higher than year 1990 by 48.91 percent.

On the contrary, low and secondary low temperature areas (26.81 – 33.52℃) collectively covered 235.69 $km^2$ (18.87 percent of the Metropolis), indicating a coverage area lower than year 1990 by 36.53 percent. Similarly, medium temperature areas decreased in percentage coverage by 12.37 percent from 29.88 percent in 1990 to 17.51 percent in 2000. In 2010, low temperature areas (29.51 – 35.59℃) occupied 49.04 $km^2$ (3.93 percent of the total area). The secondary low temperature areas (35.59 – 38.36℃) covered 106.10 $km^2$ (8.50 percent). The medium temperature areas (38.36 – 40.57℃) occupied 237.52 $km^2$ (19.02 percent).

The secondary high temperature areas (40.57– 42.36℃) 471.68 $km^2$ (37.77 percent). The high temperature areas (42.36 – 47.13℃) occupied 384.53 $km^2$ (30.79 percent). Thus in 2010, high and secondary high temperature areas (40.57 – 47.13℃) collectively covered 856.21 $km^2$ (68.56 percent of the metropolis), indicating a coverage area higher than year 2000 by 4.94 percent. Similarly, medium temperature areas for the year increased in percentage coverage by 1.51 percent from 17.51 percent in 2000 to 19.02 in 2010. On the contrary, low and secondary low temperature areas (29.51 – 38.36℃) collectively occupied 172,386 points (155.15 $km^2$) and covered 12.42 percent of the metropolis, indicating a coverage area lower than year 2000 by 6.45 percent.

In 2019, low temperature areas (27.00 – 30.56℃) occupied 188.96 $km^2$ (15.13 percent of the total area). The secondary low temperature areas (30.56 – 32.95℃) covered 180.88 $km^2$ (14.48 percent). The medium temperature areas (32.95 – 34.60℃) covered 402.87 $km^2$ (32.26 percent). The secondary high temperature areas (34.60– 36.32℃) occupied 345.58 $km^2$ (27.67 percent). The high temperature areas (36.32 – 42.63℃) covered 130.57 $km^2$ (10.46 percent). Hence in 2019, high and secondary high temperature areas (34.60 – 42.63℃) collectively covered 476.16 $km^2$ (38.13 percent of the metropolis), indicating a coverage area lower than year 2010 by 30.43 percent.

On the contrary, low and secondary low temperature areas (27.00 – 32.95℃) collectively covered 369.85 $km^2$ (29.61 percent of the Metropolis), indicating a coverage area higher than year 2010 by 17.19 percent. Similarly, medium temperature areas increased in percentage coverage by 13.24 percent from 19.02 percent in 2010 to 32.26 percent in 2019.

### 4.5.5 Analysis of variance (ANOVA) in mean LST of Ibadan, Owerri, Kano and Birnin Kebbi 1990-2019

The Analysis of variance in LST for Ibadan, Owerri, Kano and Birnin Kebbi from 1990 to 2019 computed from Appendices K1-4 is presented in Table 4.17 and Figure 4.66.

**Table 4.17 Analysis of Variance in mean LST for Ibadan, Owerri, Kano and Birnin Kebbi from 1990 to 2019**

**Analysis of Variance for LST**

| Source | DF | SS | MS | F | P-value |
|---|---|---|---|---|---|
| LOCAT | 3 | 7924.8 | 2641.6 | 25.40 | 0.000 |
| year | 3 | 8472.5 | 2824.2 | 27.16 | 0.000 |
| Error | 313 | 32547.4 | 104.0 | | |
| Total | 319 | 48944.7 | | | |

S = 10.1973 R-Sq = 33.50% R-Sq(adj) = 32.23%

Grouping Information Using the Tukey Method and 95% Confidence

| LOCAT | N | Mean | Grouping |
|---|---|---|---|
| 1 | 80 | 33.47 | A |
| 4 | 80 | 31.377 | A B |
| 3 | 80 | 27.42 | B |
| 2 | 80 | 20.42 | C |

*Means that do not share a letter are significantly different
1=Kebbi,2=Kano,3=Ibadan,4=Owerri

**Source:** Author (2023)

The table established that the p-value was greater than 0.00 but less than significance value of 0.05, indicating a significance difference in LST for the four regions. This implied that

LST differed across the four regions. Tukey pairwise comparison test revealed that Birnin Kebbi recorded the highest mean LST (33.47°C) followed by Owerri(31.38°C) but the difference in the mean LST for Birnin Kebbi and Owerri were not statistically significant at 5 percent significance level.

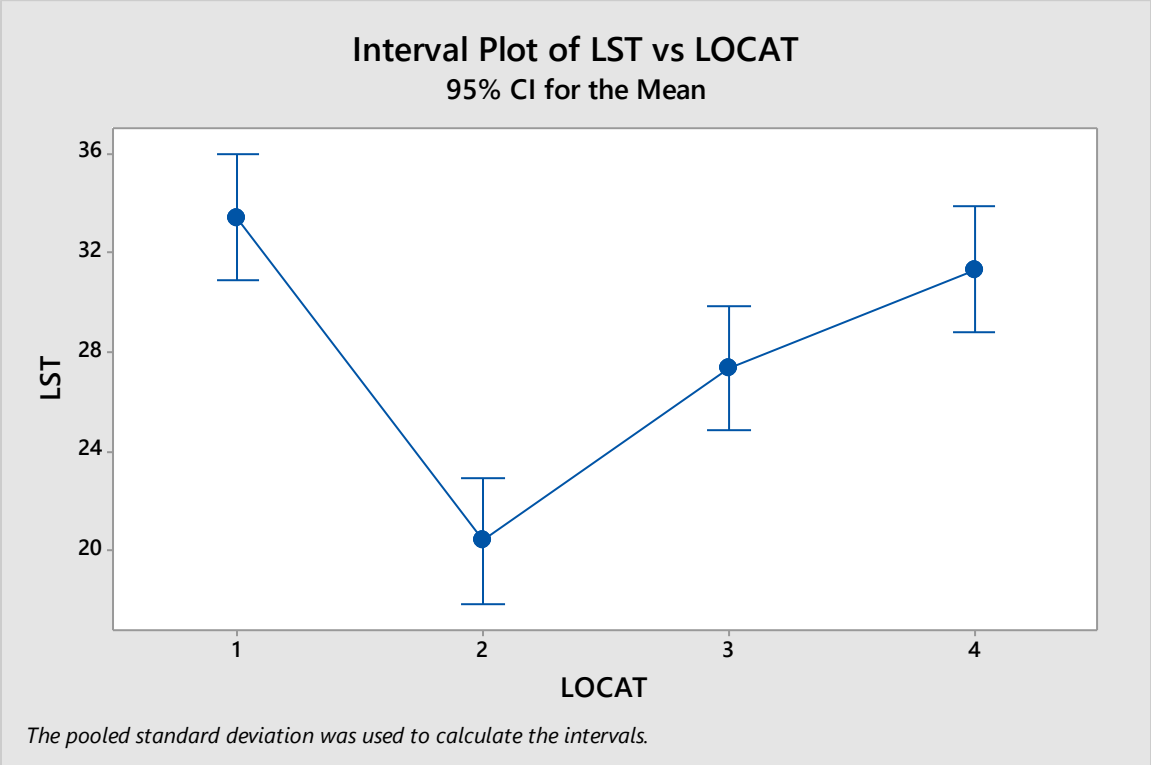


**Figure 4.66** Interval plot of LST versus Locations 1990 -2019

Ibadan metropolis followed Owerri with a mean LST of 27.42°C but the difference between mean LST for Ibadan and Owerri were statistically the same. Birnin Kebbi was however statistically different from Ibadan. Lastly, Kano had the least mean LST (20.42°C), which was statistically different from all other three locations.

Results of the LST analysis in the four cities is related to those of similar studies elsewhere. The work of Rahman *et al*. (2022) did not only suggest that bigger districts in Bangladesh possessed greater urban heat islands than smaller ones because of high population and unplanned urban expansion, but further showed that high land surface temperature areas in

all districts increased as urban expansion increased. Similar to the results from the four cities, the work of Çolakkadıoğlu (2023) showed an expansion in urban surfaces, decreased vegetal cover, and an increase in average LST values over a 30-year period in Osmaniye Province, Turkey. Li *et al*. (2021) showed that the area of sub-urban heat island intensity in Kampala increased tremendously from 22,910 hectres in 2003 to 27,900 hectres in 2016.

However, the annual daytime sub-urban heat island intensity in some areas decreased from of 2.2˚C in 2003 to 1.9˚C in 2017; probably due to the closeness of those areas to Lake Victoria. Similarly, the role of vegetation in mitigating the effects of LST was substantiated by Sohail *et al*. (2023) whose study revealed decreasing trends in the LST records of Islamabad between 2000 and 2020, as vegetation over the study area increased.

However, a study by Al Blooshi *et al*. (2020) in Al-Ain, a desert city in Abu Dhabi Emirate, United Arab Emirate revealed a surprising result; as overall LST in the city decreased by between of 3˚C-5˚C between 1988 and 2017 despite urban expansion in the desert environment. This drop in LST values was not unconnected with the increase in green spaces in the recently developed urban areas, and the extension of date plantations around the city. This study therefore demonstrated the mitigative roles that urban greening can pay in the study cities, particularly the drier cities in Sudan Savanna.

## 4.6. Variation in LST trend across the two Ecological Zones from 1990 -2019

### 4.6.1. LST trends in the two cities in Sudan Savanna from 1990 to 2019

Figure 4.67 shows the comparison of maximum LST trends in the two cities in Sudan Savanna from 1990 to 2019. It shows a rising trend in LST of the ecological zone between 1990 and 2010 and a decline in 2019. Kano recorded higher LST of 30.92°C, 42.19°C, and 46.53°C in 1990, 2000, and 2010 respectively and a declined value of 21.9°C in 2019. Birnin

Kebbi recorded somewhat lower LST than Kano Metropolis. It recorded higher LST of 29.03°C, 40.86°C, and 47.13°C in 1990, 2000, and 2010 respectively and a declined value of 43.32°C in 2019. It generally shows that the size of the built up area with its concomitant commercial, industrial and domestic activities may be largely responsible for the higher LST recorded in Kano Metropolis.

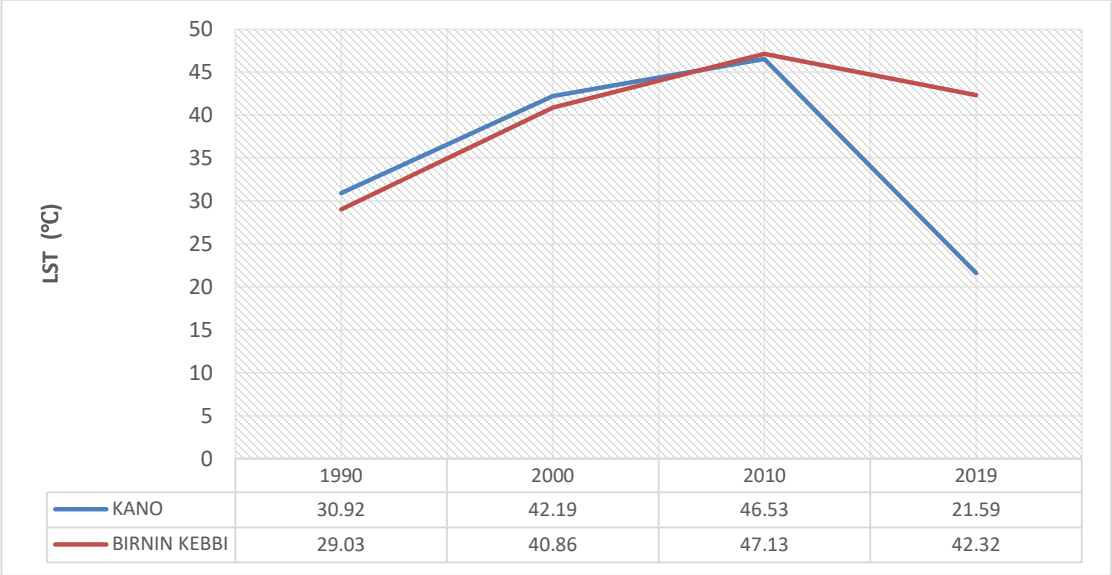


**Figure 4.67** Maximum LST of Sudan Savanna Cities from 1990-2019

### 4.6.2. LST trends in the two cities in the Rainforest from 1990 to 2019

Figure 4.68 shows the comparison of maximum LST trends in the two cities in Rainforest from 1990 to 2019. It shows that the LST for the two cities in the zone did not follow any particular pattern. Generally, Ibadan recorded higher LST than Owerri. It recorded LST of 40.50°C, 79.24°C, and 46.42°C and 37.42°C in 1990, 2000, 2010 and 2019 respectively. Owerri recorded LST of 39.16°C, 41.75°C, 43.07°C and 29.50°C in 1990, 2000, 2010 and 2019 respectively. The size of the built up area with its concomitant commercial, industrial and domestic activities may be largely responsible for the higher LST recorded in Ibadan Metropolis.

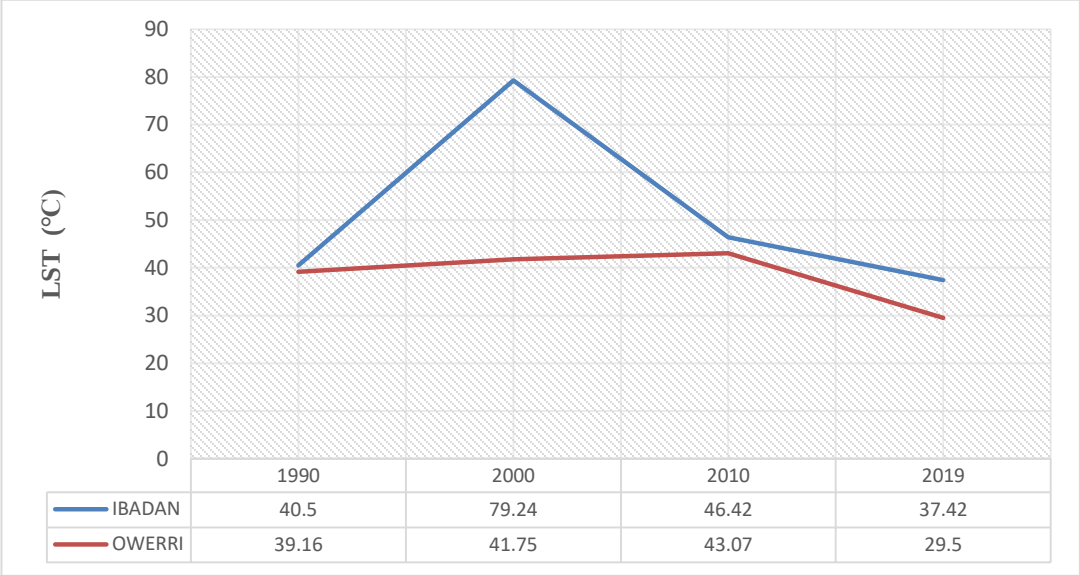


**Figure 4. 68** Maximum LST of Rainforest Cities from 1990-2019

### 4.6.3. Mean maximum LST trends in Sudan Savanna and the Rainforest from 1990 to 2019

Figure 4.69 shows the comparison of mean maximum LST trend for the cities in the Sudan Savanna and Rainforest ecological zones from 1990 to 2019. It generally shows that Tropical Rainforest recorded higher LST than the Sudan Savanna. It recorded LST of 39.83°C, 60.50°C, 44.75°C and 33.46°C in 1990, 2000, 2010 and 2019 respectively, whereas, the Sudan Savanna recorded LST of 29.98°C, 41.53°C, 46.83°C and 31.96°C in 1990, 2000, 2010 and 2019 respectively. The satellite images for the Tropical Rainforest were mostly acquired between December and March, while those of the Sudan Savanna were acquired in October, which marks the early onset of dry season in the zone. The higher LST in the Tropical rainforest may therefore be explained by the fact that the influence of the Harmattan is less severe in the zone. It may also be as a result of higher commercial / industrial activities in the zone.

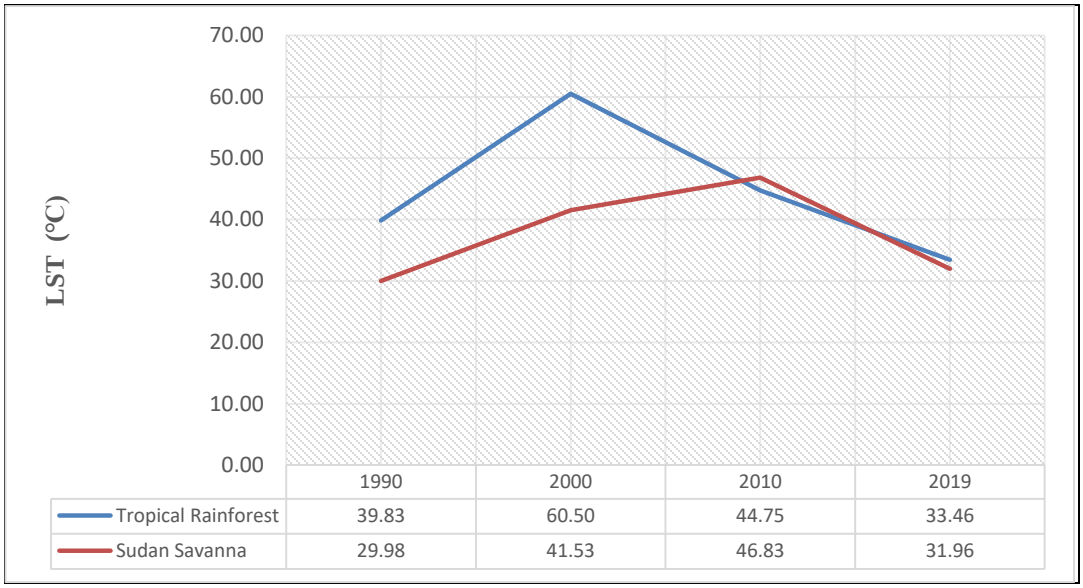


**Figure 4.69** Mean Maximum Yearly LST for the Rainforest and Sudan Ecological Zones 1990 -2019

The larger size of the urban centres in the Tropical Rainforest may be responsible for the higher LST in the zone.

## 4.7 Relationship between LST and NDBI/NDVI

This section presents the results of the analysis of the relationship between LST and NDBI and NDVI in Ibadan, Owerri, Kano and Birnin Kebbi cities from 1990 to 2019.

### 4.7.1 Relationship between LST and NDBI in Ibadan 1990-2019

The scatter plots for LST-NDBI relationships of Ibadan from 1990 to 2019 were plotted using 20 interval classes generated from the computed LST and NDVI imageries presented in Appendix K1. The results are presented in Figure 4.70. They show strong positive correlations of $R^2$ = 0.87, 0.97, 0.98 and 0.93 for 1990, 2001, 2011 and 2019 respectively, with the strongest correlation in 2011 and the weakest in 1990.

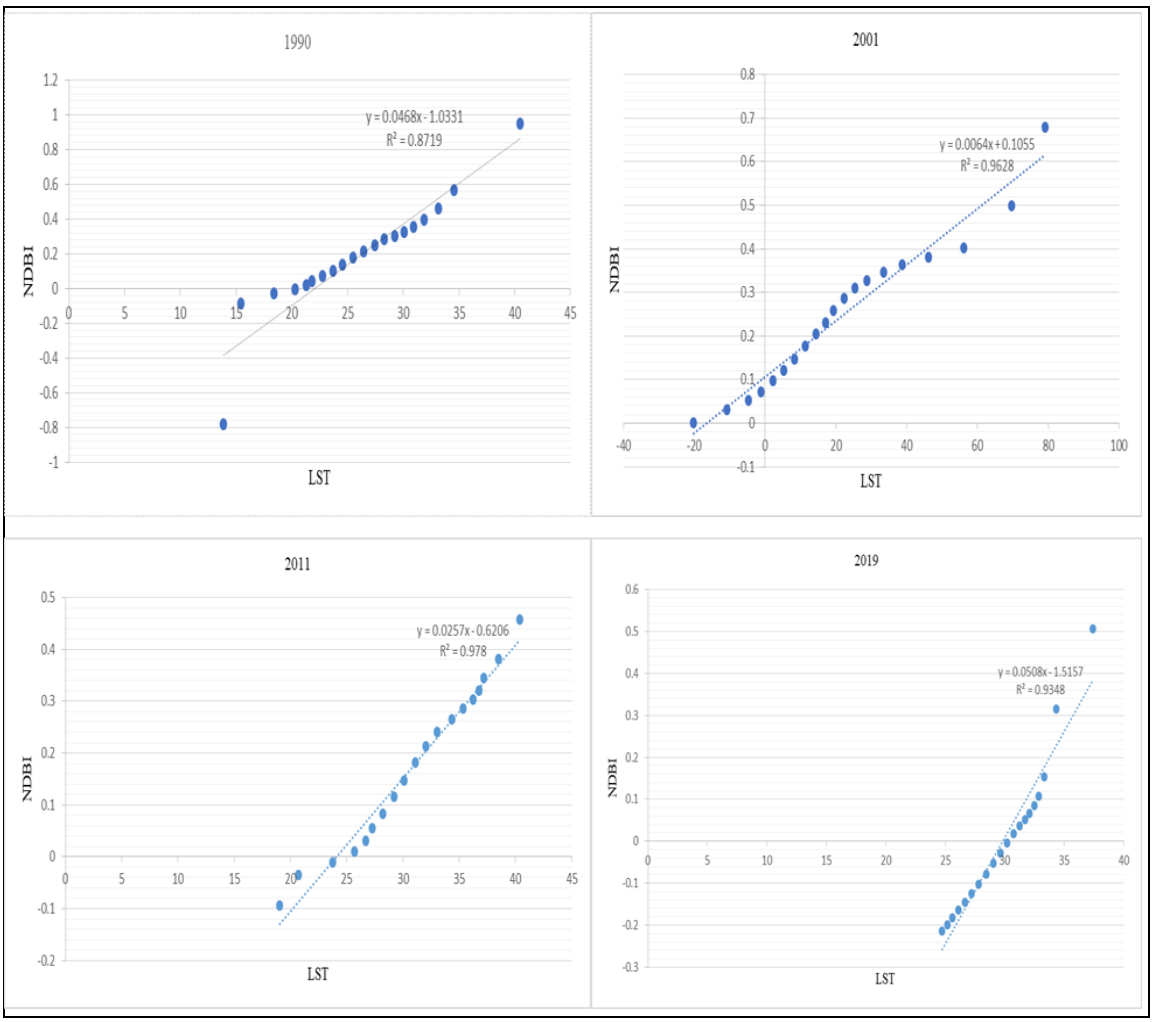


**Figure 4.70** Ibadan scatter plots for LST-NDBI Relationship (1990 -2019)

### 4.7.2 Relationship between LST and NDBI in Owerri 1990-2019

The scatter plots for LST-NDBI relationships of Owerri from 1990 to 2019 were plotted using 20 interval classes generated from the computed LST and NDVI imageries presented in Appendix K2. The results are presented in Figure 4.71. They show strong positive correlations of $R^2$ = 0.99, 0.97, 0.96 and 0.99 for 1990, 2000, 2010 and 2019 respectively, with the strongest correlation in 1990 and 2019, and the weakest in 2010.

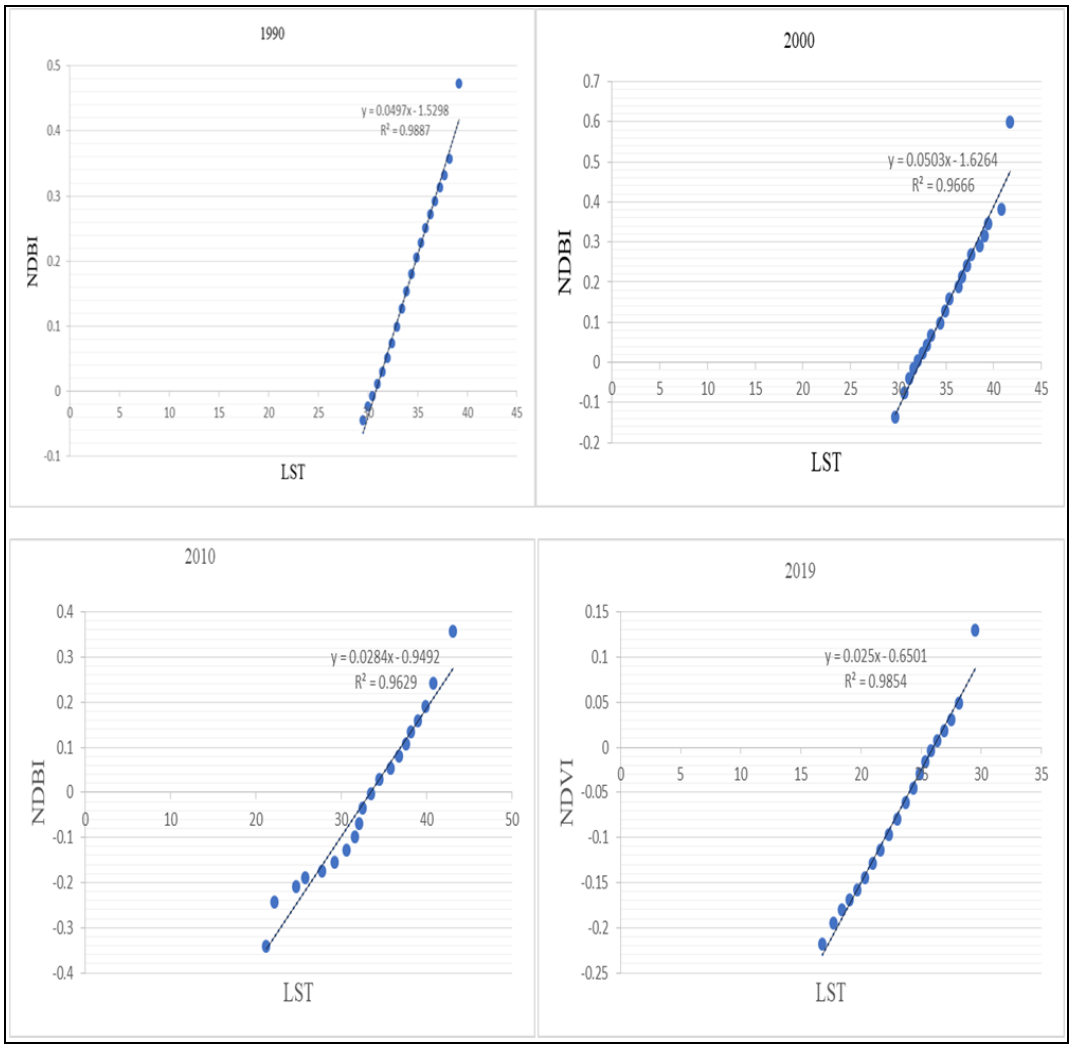


**Figure 4.71** Owerri scatter plots for LST-NDBI Relationship (1990 -2019)

### 4.7.3 Relationship between LST and NDBI in Kano 1991-2019

The scatter plots for LST-NDBI relationships of Kano from 1991 to 2019 were plotted using 20 interval classes generated from the computed LST and NDVI imageries presented in Appendix K3. The results are presented in Figure 4.72. They show strong positive correlations of $R^2$ = 0.967, 0.966, 0.948 and 0.955 for 1991, 2001, 2011 and 2019 respectively, with the strongest correlation in 1991, and the weakest in 2010.

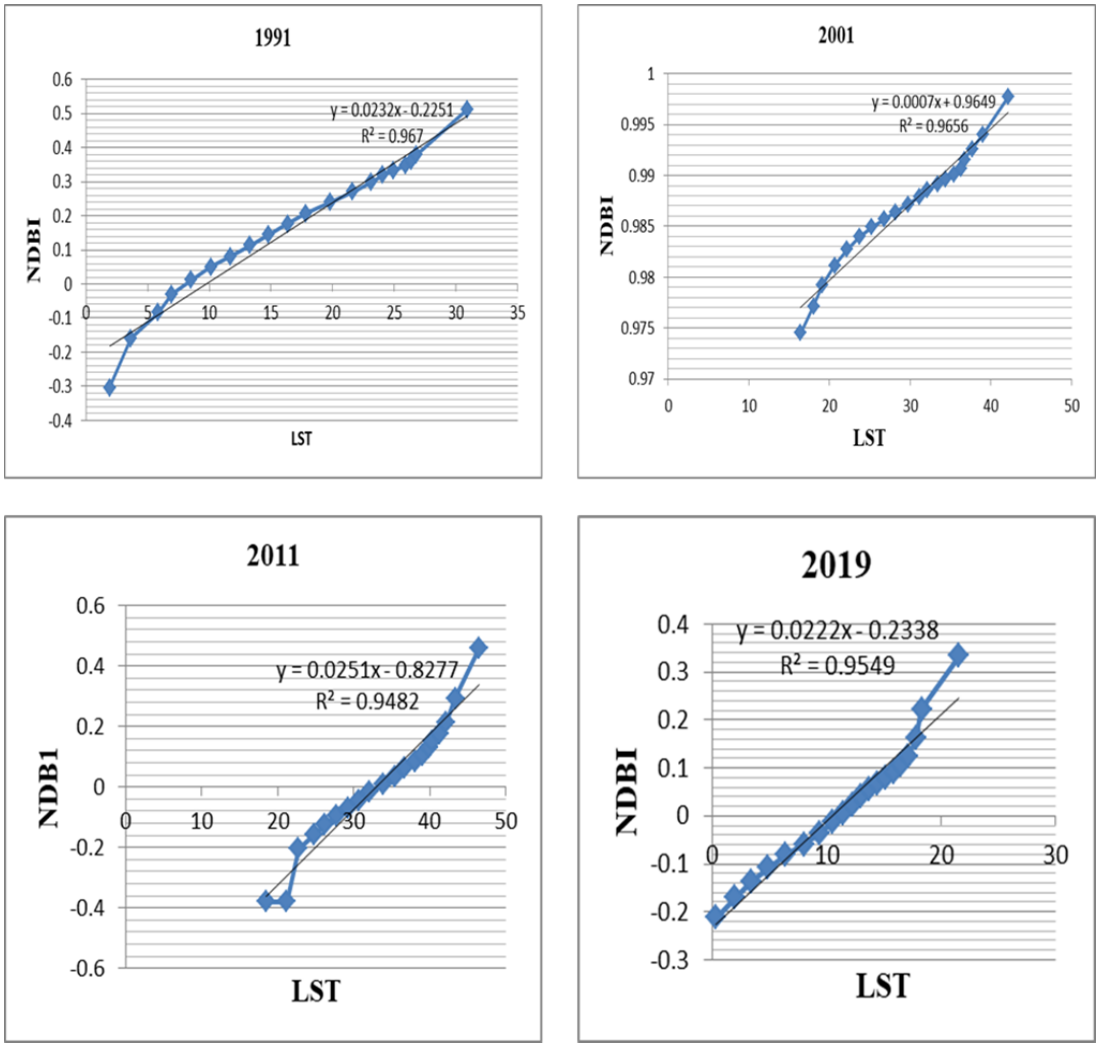


**Figure 4.72** Kano LST-NDBI Correlation 1990-2019

### 4.7.4 Relationship between LST and NDBI in Birnin Kebbi 1990-2019

The scatter plots for LST-NDBI relationships of Birnin Kebbi from 1990 to 2019 were plotted using 20 interval classes generated from the computed LST and NDVI imageries presented in Appendix K4. Results are presented in Figure 4.73. They show strong positive correlations of $R^2$ = 0.988, 0.994, 0.969 and 0.996 for 1991, 2001, 2011 and 2019 respectively, with the strongest correlation in 2019, and the weakest in 2010.

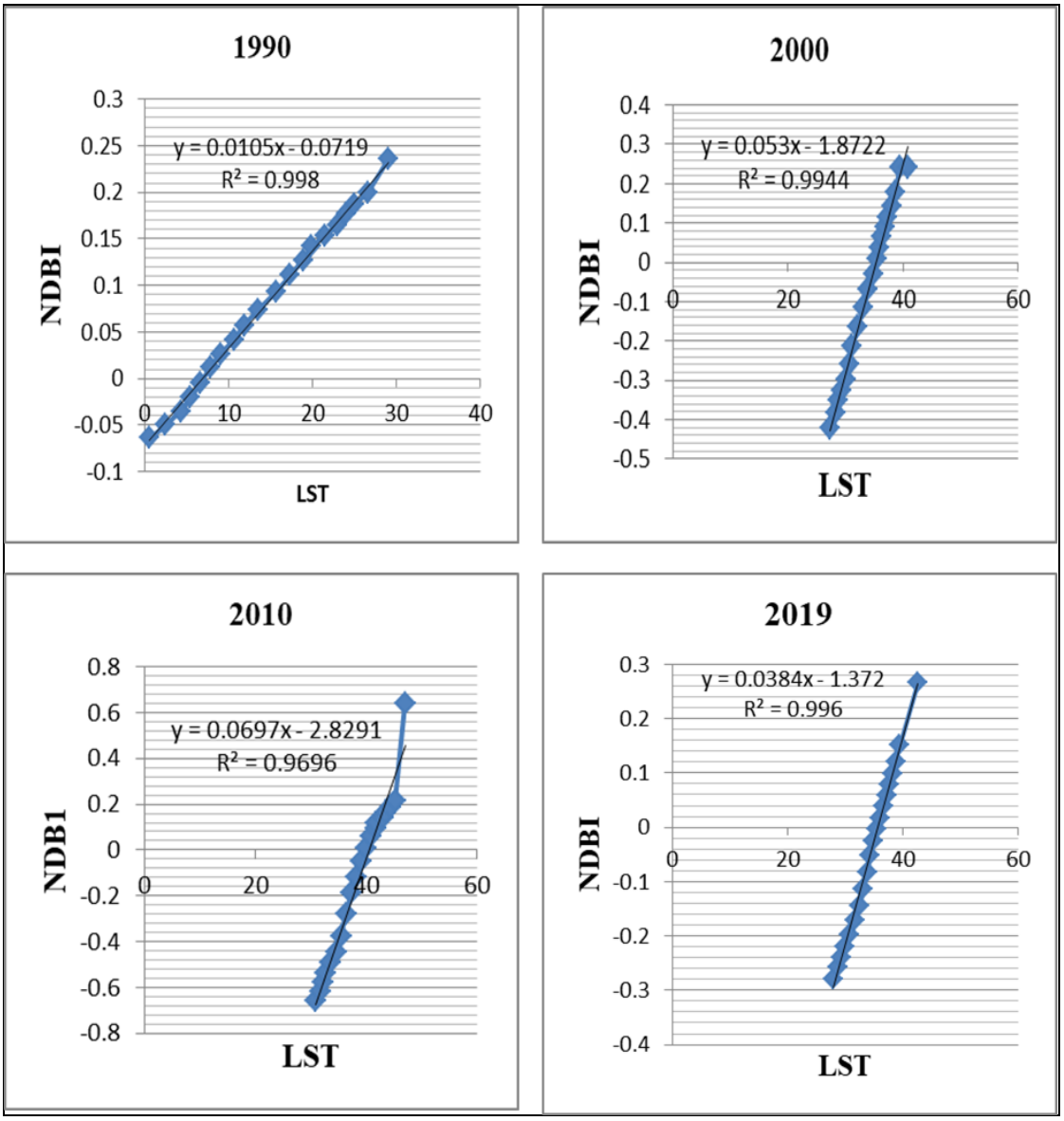


**Figure 4.73** Birnin Kebbi LST-NDBI Correlation 1990-2019

The NDBI-LST correlation results for the four cities were in consonance with the studies by Malik *et al*. (2019) and Tanaji *et al*. (2021) whose studies established strong positive relationships between NDBI and LST. The strong correlation implied that increase in built surfaces in the cities led to increase in LST, and is therefore a major contributor to UHI. Thus, the continued removal of vegetal cover in the four cities and consequent transformation of land cover into impervious artificial surfaces resulted in LST increase in the cities.

### 4.7.5 Relationship between LST and NDVI in Ibadan 1990-2019

The scatter plots for LST-NDVI relationships of Ibadan from 1990 to 2019 were plotted using 20 interval classes generated from the computed LST and NDVI imageries in Appendix K1. They are presented in Figure 4.74. They show strong negative correlations of $R^2$ = 0.76, 0.85, 0.961 and 0.96 for 1990, 2001, 2011 and 2019 respectively, with the strongest correlation in 2011, and the weakest in 1990.

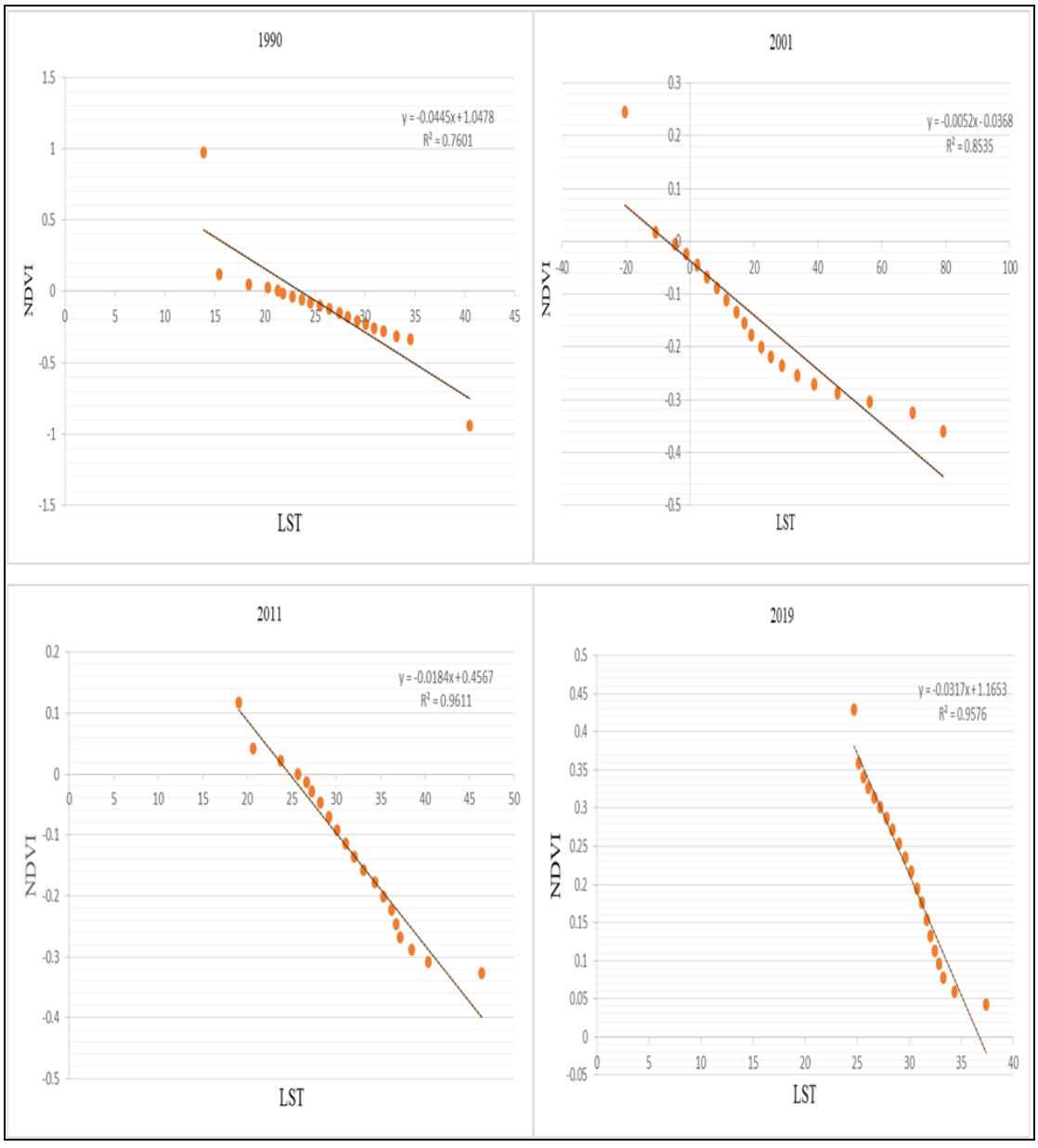


**Figure 4.74** Ibadan scatter plots for LST-NDVI Relationship (1990 -2019)

### 4.7.6 Relationship between LST and NDVI in Owerri 1991-2019

The scatter plots for LST-NDVI relationships of Owerri from 1990 to 2019 were plotted using 20 interval classes generated from the computed LST and NDVI imageries presented in Appendix K2 are presented in Figure 4.75. They show strong negative correlations of $R^2$ = 0.993, 0.988, 0.973 and 0.933 for 1990, 2000, 2010 and 2019 respectively, with the strongest correlation in 1990, and the weakest in 2010.

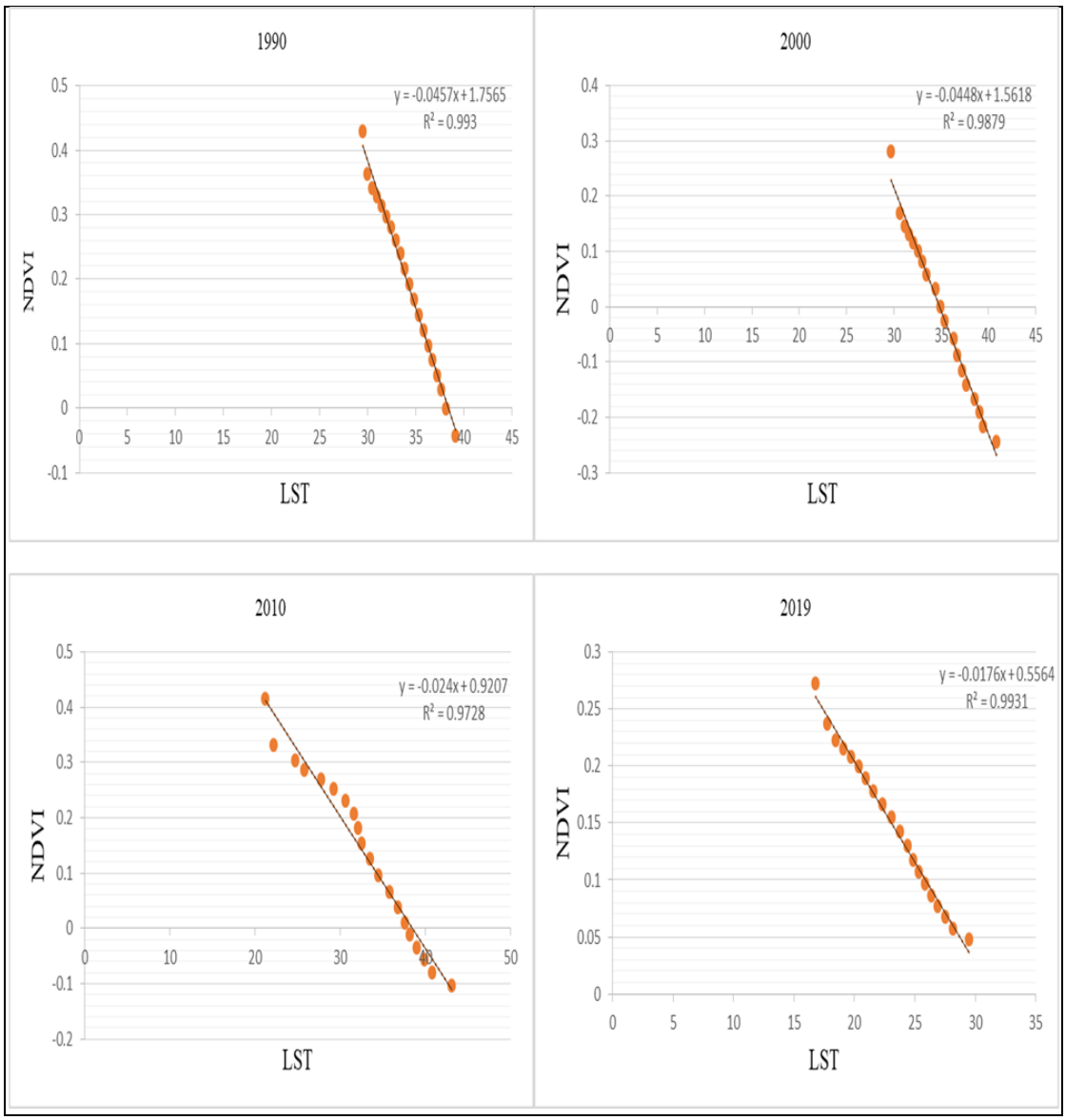


**Figure 4.75** Owerri scatter plots for LST-NDVI Relationship (1990 -2019)

### 4.7.7 Relationship between LST and NDVI in Kano 1991-2019

The scatter plots for LST-NDVI relationships of Birnin Kebbi from 1990 to 2019 were plotted using 20 interval classes generated from the computed LST and NDVI imageries presented in Appendix K3. They are presented in Figure 4.76. They show strong negative correlations of $R^2$ = 0.960, 0.964, 0.985 and 0.963 for 1991, 2001, 2011 and 2019 respectively, with the strongest correlation in 2019, and the weakest in 2010.

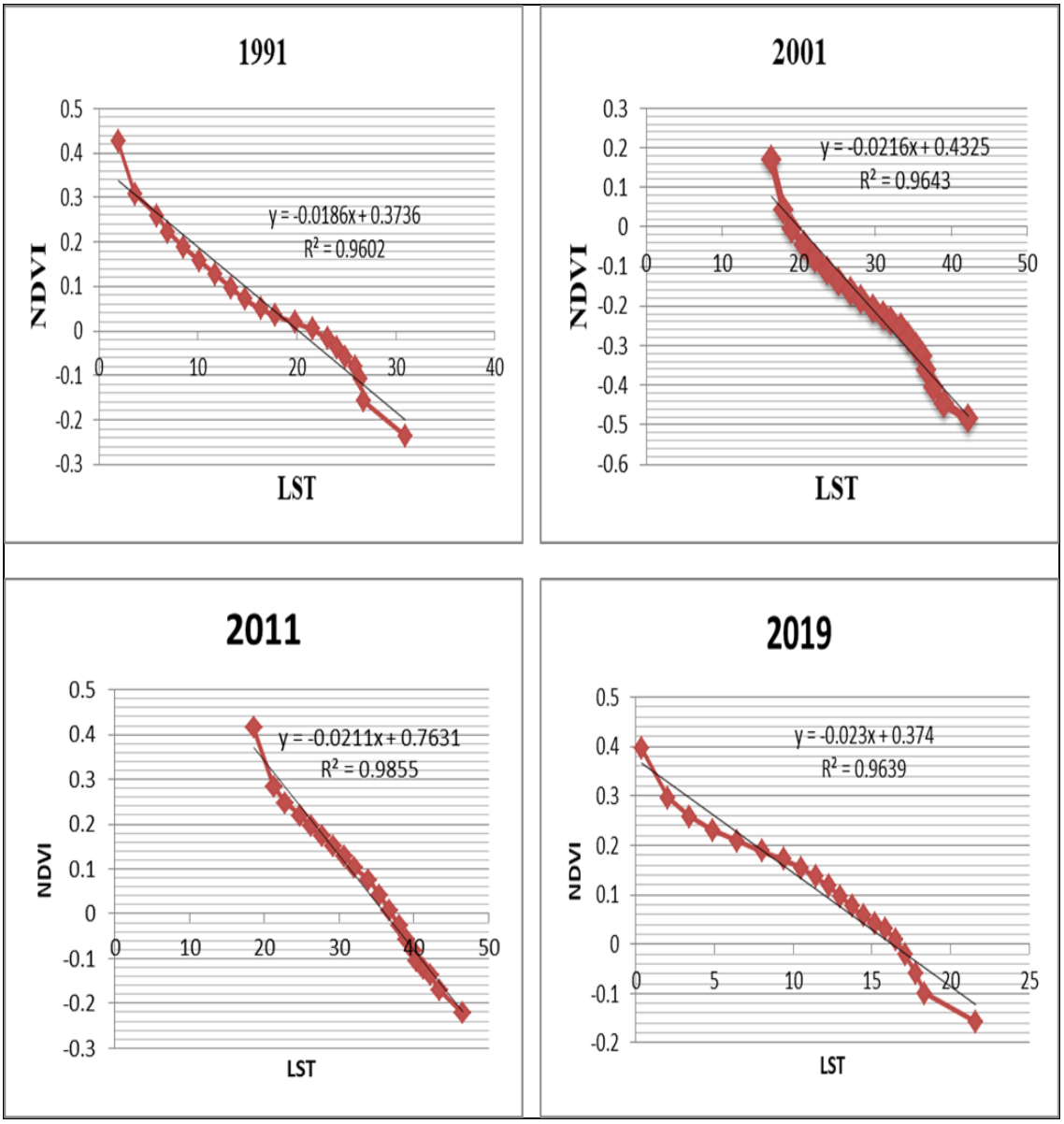


**Figure 4.76** Kano scatter plots for LST-NDVI Relationship (1990 -2019)

### 4.7.8 Relationship between LST and NDVI in Birnin Kebbi 1990-2019

The scatter plots for LST-NDVI relationships of Birnin Kebbi from 1990 to 2019 were plotted using 20 interval classes generated from the computed LST and NDVI imageries presented in Appendix K4. They are presented in Figure 4.77. They show strong negative correlations of $R^2$ = 0.99, 0.98, 0.95 and 0.97 for 1990, 2000, 2010 and 2019 respectively, with the strongest correlation in 1990, and the weakest in 2010.

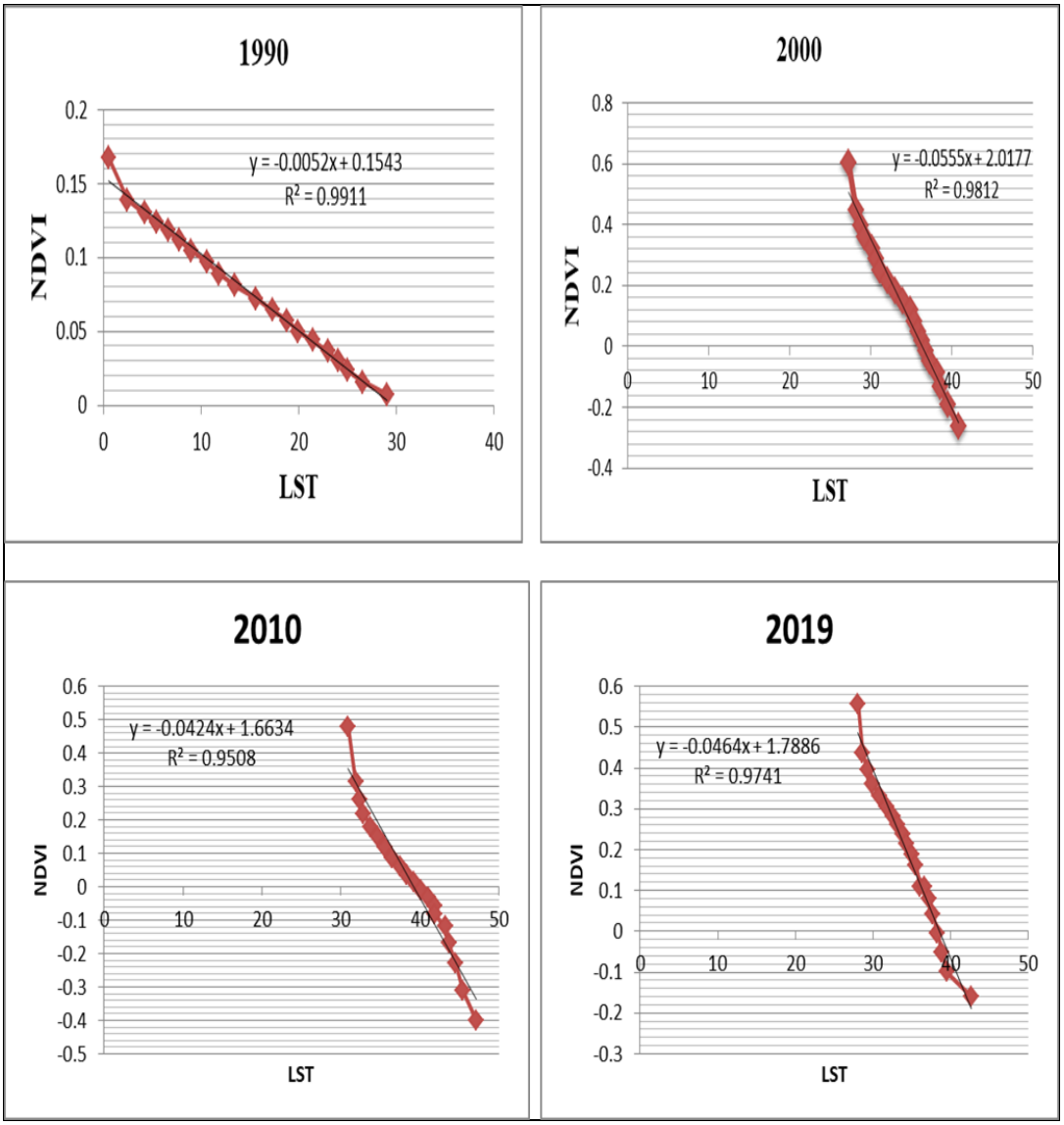


**Figure 4.77** Birnin Kebbi scatter plots for LST-NDVI Relationship (1990 -2019)

The NDVI-LST correlation results for the four cities were in consonance with the studies by Malik *et al*. (2019) and Tanaji *et al*. (2021) whose studies established strong negative relationships between NDVI and LST. The strong inverse relationship implied that areas with the least vegetal cover in the cities experienced greater LST values and vice-versa. Thus, as the cities lose their vegetal cover to urban expansion, LST may continue to rise and become widespread in the cities. In other words, an increase in vegetal cover in these cities reduces the intensity of land surface temperatures in them and may therefore be exploited as measures to mitigate its effects in the urban areas.

Results of this study were also compared with other scientific studies across the globe. Çolakkadıoğlu (2023) revealed a strong inverse correlation between land surface temperature and normalized difference vegetation index, and a strong positive correlation between LST and NDBI. In the same vein, study by Seun *et al*. (2022) revealed an inverse relationship between land surface temperature and normalized difference vegetation index over south-west Nigeria with $r^2$ of −0.8738, −0.8594, and −0.8546 for 1986, 2002, and 2017 respectively, suggesting that depletion in vegetal cover in geographical locations increases the intensity of the LST over the locations. Similarly, Kaiser *et al*. (2022) observed increasing strong inverse relationships between normalized difference vegetation index and land surface temperature (R = −0.55, −0.58, −0.59, and −0.76) in 1989, 1999, 2008 and 2018 respectively for four urban districts of Porto Alegre City, Brazil.

## 4.8 Urbanization Effects on LST Values

### 4.8.1 Temperature values of urban built-up in Ibadan metropolis from 1990 to 2019

This section discusses the effects of urbanization on the LST values in Ibadan Metropolis from 1990 to 2019. The temperature values over the different LULC types in the metropolis

during the period are presented in Figure 4.78. The recorded maximum and minimum temperature values for Ibadan in 1990 as presented earlier in section 4.5.1 are 40.50℃ and 13.45℃ respectively. An overlay of the LST map on the LULC map showed that the built areas accounted for much of the highest temperature areas, falling within the high LST class range of 27.88℃ to 40.50℃. Moderate temperatures were recorded over agricultural lands and bare surfaces, while vegetated areas and water bodies recorded the lowest temperatures.

The recorded maximum and minimum temperature values for Ibadan in 2001 as presented earlier in section 4.5.1 were 79.24℃ and -31.04℃ respectively. An overlay of the LST map on the LULC map of 2001 shows that the highest temperature points were located within the heavily built areas while the very low temperature points were situated within the vegetated areas and water bodies. The areas of high temperature fell within the temperature range of 14.55℃ to 79.24℃.

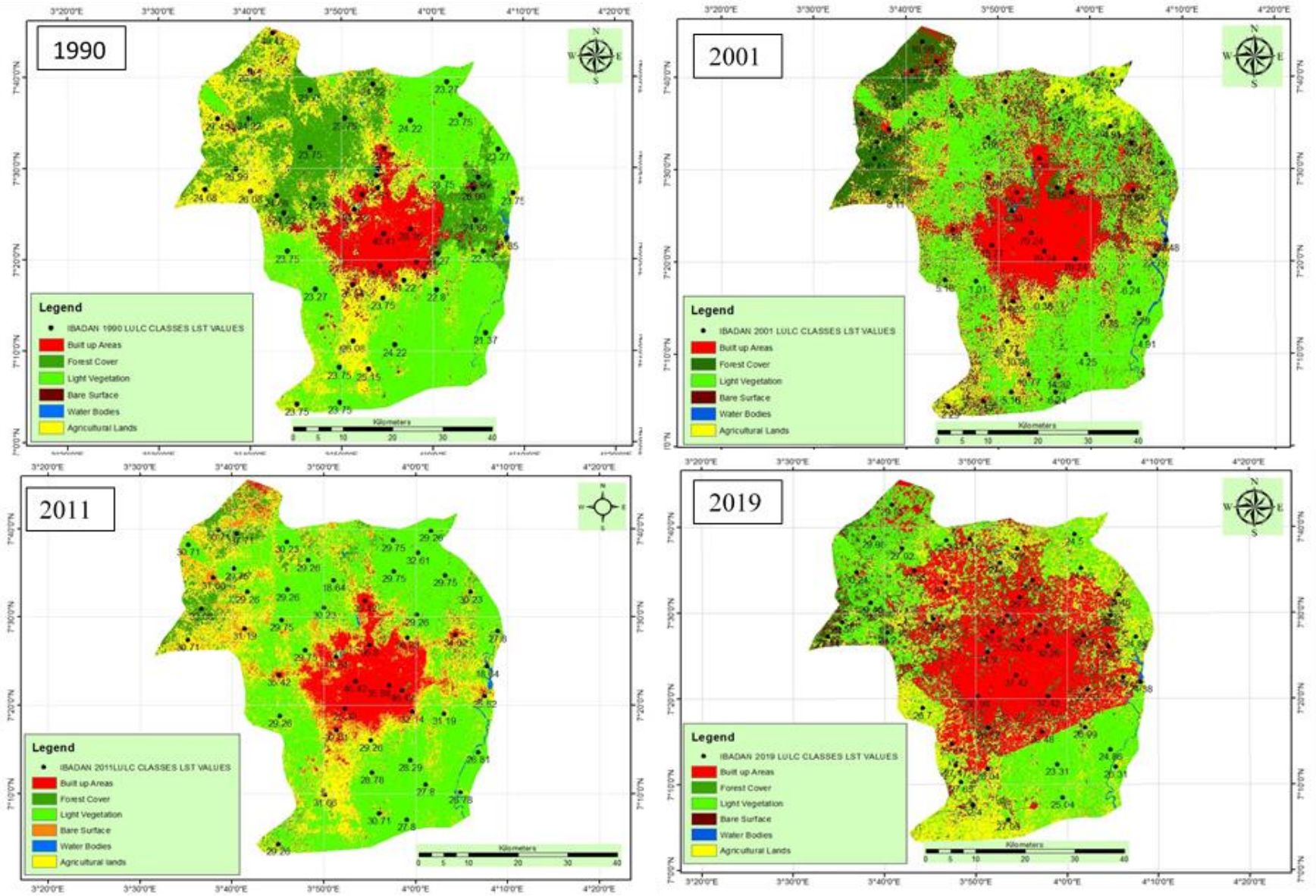


**Figure 4.78** LULC LST Values of Ibadan from 1990-2019

The recorded maximum and minimum temperature values for Ibadan in 2011 as presented earlier in section 4.5.1 were 46.42℃ and 18.64℃ respectively. An overlay of the LST map on the LULC map 2011 shows that high temperature points were located within the heavily built areas while the very low temperature points were situated within the vegetated areas and water bodies. The areas of high temperature areas largely fall within the temperature range of 33.51– 46.42℃. Water bodies accounted for the lowest temperature of 18.64℃.

The recorded maximum and minimum temperature values for Ibadan in 2019 as presented earlier in section 4.5.1 were 37.42℃ and 23.31℃ respectively. An overlay of the LST map on the LULC map of 2019 showed that highest temperature points were equally located within the heavily built areas while the very low temperature points were situated within the vegetated areas and water bodies. The temperature of the urban built-up for the year fell within the temperature range of 30.61 to 37.42℃.

The high LST areas were largely located within the core local government areas that make up Ibadan metropolis, which characteristically comprise densely populated residential, high Traffic, industrial, and market areas such as Mokola, Adeoyo-Yemetu, Bere, Ojoba, Kudeti, Bode, Yejide, Salvation Army, Sabo, Challenge, Liberty, Sweetco, Molete, Bode Market, Dugbe Market, Moniya, Ojo, Idi-Ape areas, among others. The result on high temperature coverage as presented in section *4.5.1* showed that high LST over built surfaces covered 6.17 percent, 4.35 percent, 7.45 percent and 11.46 percent for 1990, 2001, 2011 and 2019 respectively. This implied that with the exception of 2001, percentage coverage of high temperature areas seemed to have increased as the urban built-up increased in areal coverage.

Having presented the results of the effects of urbanization on LST in Ibadan Metropolis from 1990 to 2019, the next section presents the result of urbanization effects in Owerri, another city in the Tropical Rainforest Ecological zone of Nigeria.

### 4.8.2 Temperature values of urban built-up in Owerri metropolis from 1990 to 2019

This section discusses the effects of urbanization on the LST values in Owerri Metropolis from 1990 to 2019. The temperature values over the different LULC types in the metropolis during the period are presented in Figure 4.79. The recorded maximum and minimum temperature values for Owerri in 1990 as presented earlier in section 4.5.2 are 39.16℃ and 29.50℃ respectively. An overlay of the LST map on the LULC map showed that the built areas accounted for much of the highest temperature areas, falling within the high LST class ranging of 34.88℃ to 39.16℃. Moderate temperatures were recorded over agricultural lands and bare surfaces, while vegetated areas and water bodies recorded the lowest temperatures.

The recorded maximum and minimum temperature values for Ibadan in 2000 as presented earlier in section 4.5.2 were 41.75℃ and 29.75℃ respectively. An overlay of the LST map on the LULC map of 2000 shows that the highest temperature points were located within the heavily built areas while the very low temperature points were situated within the vegetated areas and water bodies. The areas of high temperature fell within the temperature range of 36℃ to 41.75℃. Water bodies recorded mean temperature of 30.71℃.

The recorded maximum and minimum temperature values for Owerri in 2010 as presented earlier in section 4.5.2 were 43.07℃ and 20.73℃ respectively. An overlay of the LST map on the LULC map 2010 shows that highest temperature point of 43.07℃ was located within the heavily built metropolitan area while the very low temperature points were situated within the vegetated areas and water bodies.

The recorded maximum and minimum temperature values for Ibadan in 2019 as presented earlier in section 4.5.2 were 29.50℃ and 15.83℃ respectively. An overlay of the LST map on the LULC map of 2019 showed that highest temperature points were equally located within the heavily built areas while the very low temperature points were situated within the vegetated areas and water bodies. The temperature of the urban built-up for the year fell within the temperature range of 26.61℃ to 29.50℃.

The high LST areas were largely located within the core local government areas that make up Owerri metropolis namely Owerri Municipal, Owerri West and Owerri North local government areas, which characteristically comprise densely populated residential, high Traffic, industrial, and market areas, such as the commercial areas of Douglas (which houses most commercial activities such like markets such as Eke Onunwa and new markets; banks, illegal roadside shops, schools, fuel stations, churches, and so on), Ikenebu, Wetheral, and Warehouse. Other highly populated residential and commercial areas with concomitant higher LSTs inlude Nekede, Amakaohia, Relief, Egbu, New Owerri, Concorde Area, World Bank Estate (Area C), Eziobodo Area, FUTO-Obinze Area, Avu, and Irete among others.

The result on high temperature coverage as presented in section *4.5.2* showed that high LST over built surfaces covered 6.53 percent, 3.81 percent, 13.64 percent and 19.32 percent for 1990, 2000, 2010 and 2019 respectively. This implied that with the exception of 2000, percentage coverage of high temperature areas seemed to have increased as the urban built-up increased in areal coverage.

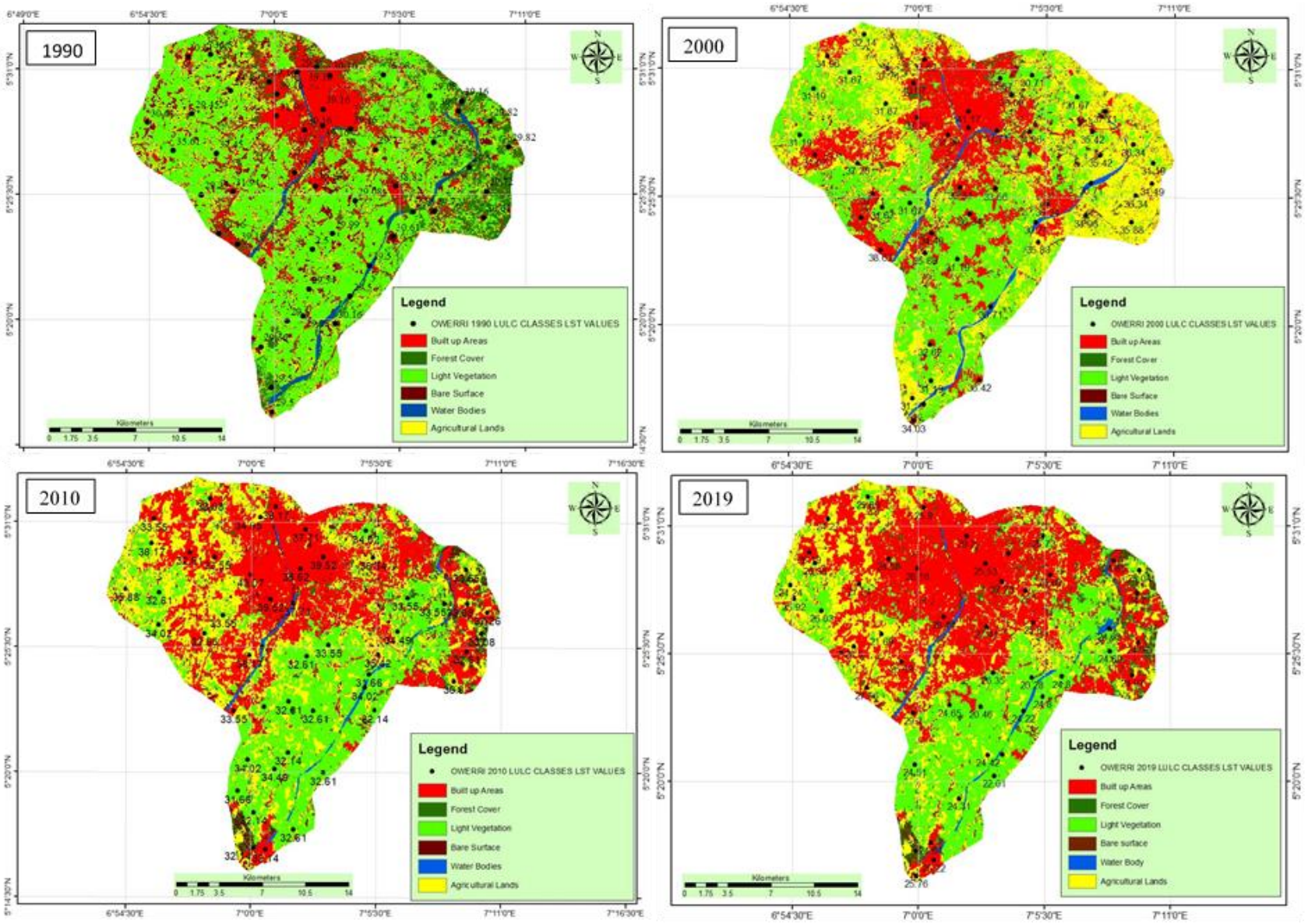


**Figure 4.79** LULC LST Values of Owerri from 1990-2019

### 4.8.3 Temperature values of urban built-up in Kano metropolis from 1991 to 2019

This section discusses the effects of urbanization on the LST values in Kano Metropolis from 1991 to 2019. The temperature values over the different LULC types in the metropolis during the period are presented in Figure 4.80. The recorded maximum and minimum temperature values for Kano in 1991 as presented earlier in section 4.5.3 are 30.92℃ and -0.27℃ respectively. An overlay of the LST map on the LULC map showed that the built areas and bare surfaces accounted for much of the highest temperature areas of 30.92℃ were recorded in the core of the metropolis. Moderate LST of 25 ℃ and 30 ℃ were recorded agricultural lands and bare surfaces, while water bodies recorded the lowest temperatures of -0.27℃.

The recorded maximum and minimum temperature values for Kano in 2001 as presented earlier in section 4.5.3 were 42.19℃ and 14.32℃ respectively. An overlay of the LST map on the LULC map of 2001 showed that the highest temperature points were located within the heavily built areas while the very low temperature points were situated within the forested areas and water bodies. The areas of high LST fell within the neighbourhood of 32.61℃.

The recorded maximum and minimum temperature values for Kano in 2011 as presented earlier in section 4.5.3 were 46.53℃ and 18.11℃ respectively. An overlay of the LST map on the LULC map 2011 showed that high temperature points were located within the heavily built areas while the very low temperature points were situated within the vegetated areas and water bodies. The areas of high temperature areas largely fell within the temperature range of 40.85– 46.53℃). Moderately low LST falling within the range of 37.61 – 39.51℃

The recorded maximum and minimum temperature values for Kano in 2019 as presented earlier in section 4.5.3 were 21.60℃ and -.94℃ respectively. An overlay of the LST map on the LULC map of 2019 showed that highest temperature points were equally located within the heavily built areas while the very low temperature points were situated within the vegetated areas and water bodies. The temperature of the urban built-up for the year hovered around 21.60 ℃. High temperature points were recorded at heavily built residential areas such as such as Tudun Wada, Gwagwarwa, Dakata, Kawaji, Gama (all in Nassarawa LGA) and Kurna Asabe, Jakara and Sanka settlements (all in Dala) as well as other locations in Kano Municipal, Fagge, Gwale and Tarauni. Similarly, commercial locations (markets) such as Kurmi, Sabon Gari, Kantin Kwari, Yankaba, Kofar Ruwa, Kasuwar Rimi and Yanlemo markets and so on, as well as industrial estates like Sharada, Challawa and Bompai industrial estates are were locations of high LSTs.

The result on high temperature coverage as presented in section 4.5.3 showed that high LST over built surfaces covered 43.83 percent, 34.98 percent, 23.57 percent and 29.70 percent for 1991, 2001, 2011 and 2019 respectively. Mohammed *et al*. (2019) attributed rising temperature in Kano Metropolis to rapid urban expansion and poor planning, while Tanko *et al.* (2017) concluded that urbanization is the key factor leading to the occurrence of surface UHI in Kano Metropolis.

### 4.8.4 Temperature values of urban built-up in Birnin Kebbi metropolis from 1990 to 2019

This section discusses the effects of urbanization on the LST values in Birnin Kebbi Metropolis from 1990 to 2019.

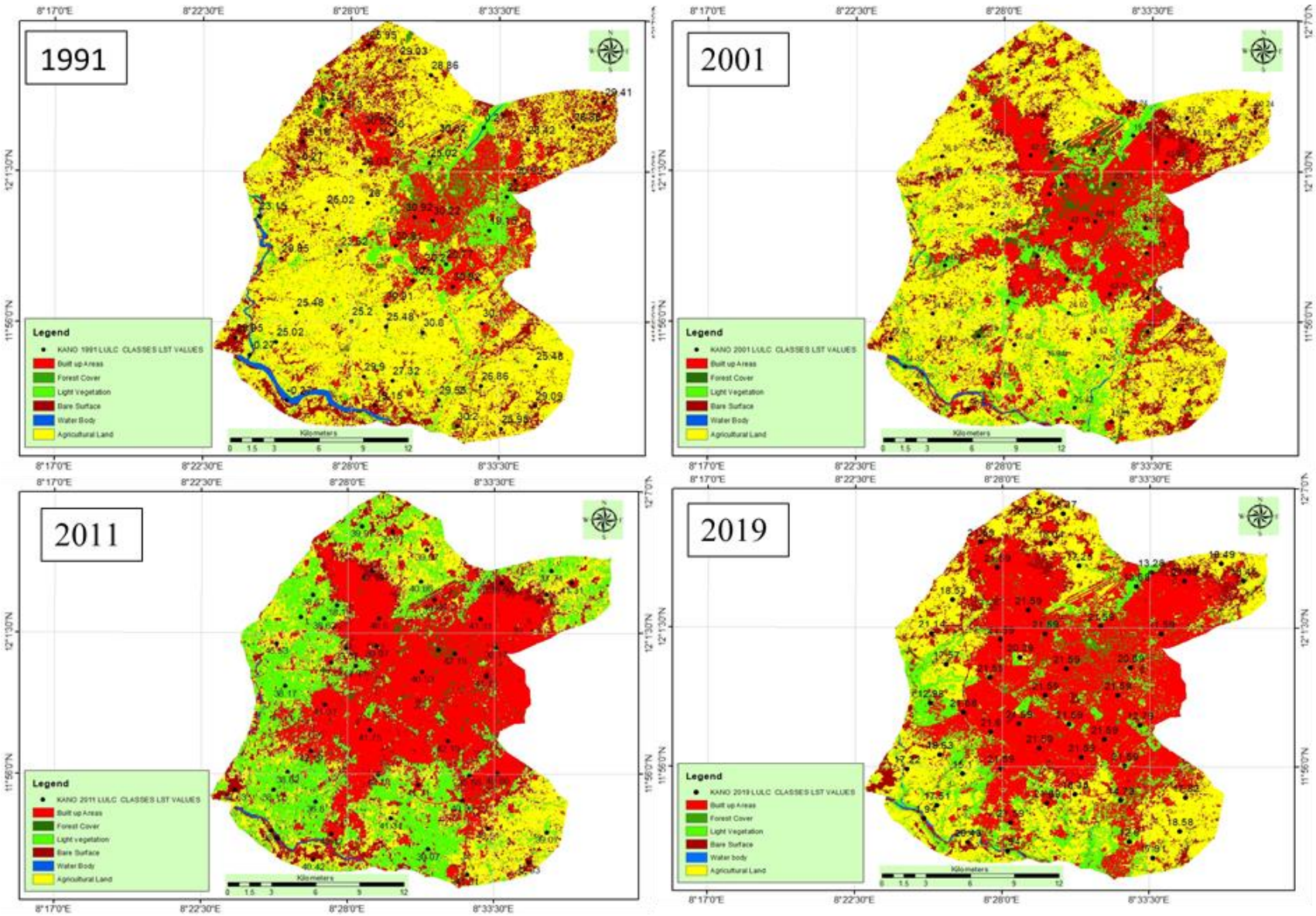


**Figure 4.80** LULC LST Values of Kano from 1991 - 2019

The temperature values over the different LULC types in the metropolis during the period are presented in Figure 4.81 The recorded maximum and minimum temperature values for Birnin Kebi in 1990 as presented earlier in section *4.6.4.1* are 29.02℃ and -1.22℃ respectively. An overlay of the LST map on the LULC map showed that the built areas accounted for much of the highest temperature areas, hovering around 29.02℃. Moderate, low and very low (-1.22℃) LSTs were recorded on agricultural lands, vegetated flood plains and water bodies respectively.

The recorded maximum and minimum temperature values for Birnin Kebbi in 2000 as presented earlier in section 4.5.4 were 40.86℃ and 26.81℃ respectively. An overlay of the LST map on the LULC map of 2000 showed that the highest temperature points were located within the built areas, hovering between 38.17℃ and 40.86℃.

The recorded maximum and minimum temperature values for Birnin Kebbi in 2010 as presented earlier in section 4.5.4 were 47.13℃ and 29.51℃ respectively. An overlay of the LST map on the LULC map 2010 showed that highest temperature point (47.13℃) were located within the heavily built areas; while the lowest temperature points were situated on water bodies.

The recorded maximum and minimum temperature values for Ibadan in 2019 as presented earlier in section 4.5.4 were 42.63℃ and 27.00℃ respectively. An overlay of the LST map on the LULC map of 2019 showed that highest temperature points were equally located within the heavily built areas and bare surfaces while the very low temperature points were recorded within the vegetated flood plains and water bodies.

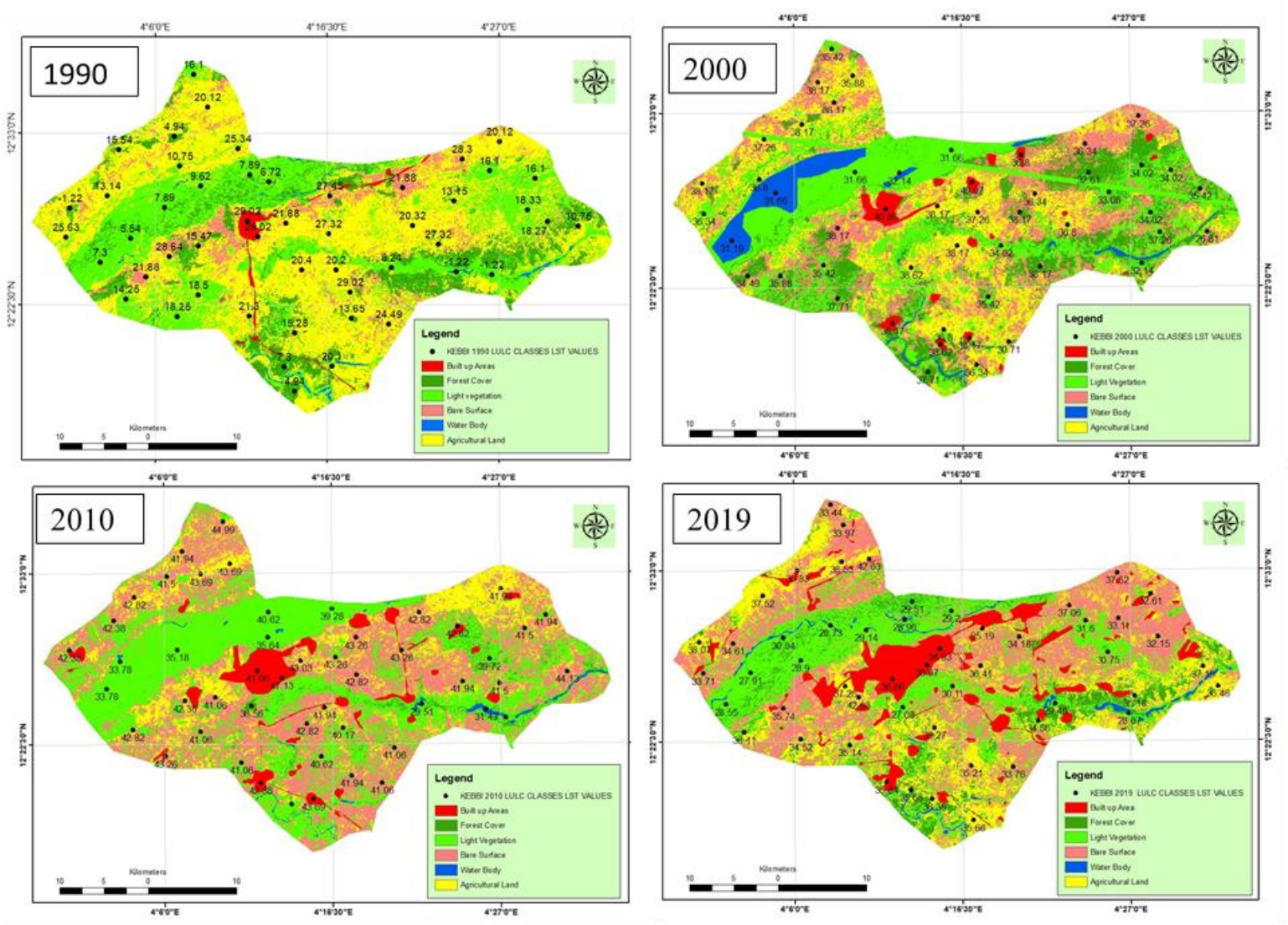


**Figure 4.81** LULC LST Values of Birnin Kebbi from 1990 - 201

The high LST areas were largely located within the densely populated residential, high Traffic, industrial, and market areas such as the CBD, Makerar Gwandu, Kofar Kola, Rafin Atiku, Badariya, Bayan Kara, Takalau,Tudun Wada, Nasarawa 1, Nasarawa 2, Gwadangwaji The result on high temperature coverage as presented in section 4.5.4 showed that high LST over built surfaces covered 0.75 percent, 29.61 percent, 30.79 percent and 10.46 percent for 1990, 2000, 2010 and 2019 respectively. This implied that with the exception of 2019, percentage coverage of high temperature areas seemed to have increased as the urban built-up increased in areal coverage.

In all the cities, the study established the interesting relationship between LST and distribution of vegetation, as vegetation and water bodies demonstrated the ability to reduce LST. This is because across all the cities, low LST was recorded over vegetal cover and water bodies. On the other hand, LST profiles showed that the core of the cities where built-surfaces and bare grounds are highly concentrated recorded the highest LST. The higher LSTs are as a result of the construction materials with varying surface properties such as albedo, thermal, capacity, and heat conductivity, which have the capability to raise the LST of the cities.

Results from the four cities are similar to the work of Baram *et al*. (2021) whose study depicted LULC change as a key influence on rise in LST in Halabja City, Iraq between 1999 and 2019. The work showed that low temperatures of 30°C and 31°C coincided with areas with vegetal cover while high temperatures varying between 44°C and 53°C coincided with barren lands and built surfaces. Similarly, the work of Ali *et al*. (2017) revealed that green spaces like parks with dense tree cover in Bhopal city (India) recorded the lowest surface temperature of about while possessing highest mean normalized difference vegetation index value of about 0.5.

## 4.9 Summary of findings

The Study analysed the LULC changes in Ibadan and Owerri in the Rainforest, and Kano and Birnin Kebbi in the Sudan savanna from 1990 to 2019, using multi-temporal Landsat imageries. It also analysed two biophysical parameters of urban LULCC, specifically NDVI and NDBI. The study went further to analyse the spatio-temporal dynamics/trends of noon time ERA Interim temperatures of the four cities from 1990 to 2019. The study also carried out mapping of LSTs of the locations using the Landsat data of the same period. The study also examined relationships between LSTs and NDVI and NDBI in the cities over the period. In addition, the study compared the variation in LST trend across the two ecological Rainforest and Sudan Savanna during the period. Finally, the study analysed the effect of urbanization on the LSTs of the cities during the said period.

For urban LULCC analysis, six LULC classes for each of the cities were produced for 1990/199, 2000/2001, 2010/2011 and 2019, using maximum likelihood supervised classification scheme. Rigorous procedures were employed in ensuring the accuracy and efficacy of the classified maps. The analysis revealed progressive expansion in built-up in all the cities during the 30 year period from the base year of 1990. The analysis revealed that built up areas in Ibadan, Owerri, Kano and Birnin Kebbi increased from 312.90 $km^2$, (9.19 percent), 70.32$km^2$ (12.94 percent), 58.48 $km^2$ (11.85 percent) and 14.06 $km^2$ (1.13 percent) respectively in 1990 to 1,039.54 $km^2$ (30.55 percent), 209.16 $km^2$ (38.50 percent), 216.03 $km^2$ (43.77 percent) and 123.03 $km^2$ (9.85 percent) in 2019. The increase in the urban built areas was at the detriment of all other LULC types.

The study also examined the temporal changes of vegetation and built-up indices of the four cities during the period. The results of the NDVI analysis did not have any established pattern

in all the four cities during the period. The result showed that in Ibadan, the highest maximum NDVI values (0.97) were recorded in 1990 while the lowest maximum values (0.12) in 2011. In Owerri, highest maximum NDVI values (0.43) were recorded in 1990 while the lowest maximum values (0.27) were recorded in 2019.

Kano, highest maximum NDVI values (0.43) were recorded in 1991 while the lowest maximum values (0.17) were recorded in 2001. In Birnin Kebbi, highest maximum NDVI values (0.60) were recorded in 2001 while the lowest maximum values (0.17) were recorded in 2001. Generally, the results showed a progressive percentage decrease in coverage areas of high and secondary high NDVI values in all the cities during the thirty-year period, and a corresponding percentage increase in coverage areas of low and secondary low NDVI values.

The progressive decrease in percentages coverage area of high NDVI values in all the cities were attributed to the progressive expansion of the urban built environments and conversion of vegetal covers into other land use types. For NDBI, the progressive increase in built surfaces led to a progressive percentage increase in coverage areas of high and secondary high NDBI values in all the cities during the thirty-year period, and a corresponding percentage decrease in coverage areas of low and secondary low NDBI values.

The results of the analysis of noon-time temperature showed positive Sen's slope estimates, indicating increasing trends over the years for the four cities, with Ibadan and Owerri showing significant differences at 5 percent significant level, while Kano was significant at 10 percent level, Mann-Kendall Seasonal trend test results for the four cities also indicate a sufficient statistical evidence of a significant seasonal increase at 0.05 significant level in maximum noon-time temperature series for the four cities from 1990 - 2019.

The results of the LST analysis for Ibadan did not have any established pattern, as it recorded the highest maximum LST in 2000 and lowest in 2019. However, Owerri, Kano, and Birnin Kebbi seemed to have a rising pattern as they recorded higher maximum LSTs as evidenced between 1990 and 2011. Generally, the results showed a progressive percentage increase in coverage areas of high and secondary high LST values in all the cities during the thirty-year period, and a corresponding percentage decrease in coverage areas of low and secondary low LST values. The progressive increase in percentages coverage area of high LST values in these cities were attributed to the progressive expansion of the urban built environments and conversion of vegetal covers into other land use types.

The study showed very strong positive correlation ($R^2$ = 0.87- 0.99) between LST and NDBI in all the surveyed cities, and very strong negative correlation ($R^2$ = 0.76 - 0.99) between LST and NDVI. The study also generally showed that Tropical Rainforest recorded higher LST than the Sudan Savanna.

# CHAPTER FIVE

# 5.0 CONCLUSIONS AND RECOMMENDATIONS

## 5.1. Conclusion

This study aimed at examining the effects of urbanization on land surface temperature in parts of Sudan Savanna and Rainforest Zones of Nigeria. To achieve this aim, the study assessed land use/land cover change in four cities in the two ecological zones and analysed the NDVI, NDBI and air temperature of the cities from 1990 to 2019. It also assessed the LST of the four cities over the same period and established relationships between LST and NDVI/NDBI in these cities. Furthermore the study examined the relationship between urbanization and LST, and made comparisons between LST across the cities and the two ecological zones. Conclusively, the study established that expansion of built up areas in the four cities led to depletion in the vegetal cover of the cities and resulted in air higher temperatures and LST over increasing areas of the cities. It also established very strong positive and negative relationships between LST and NDVI and NDI respectily.

## 5.3 Recommendations

Based on the findings of this study the following recommendations are considered worthwhile:

i. With the general rising trend in LST across the cities of Ibadan, Kano, Owerri and Birnin Kebbi, there is a need for urban planners, ministries, departments, agencies, and international donor organizations to properly and adequately plan cities and initiate green and blue infrastructures in the cities. The greening processes may have cooling effect and serve as mitigating measures for high urban LSTs, in the cities of

Ibadan, Kano, Owerri and Birnin Kebbi, but also vigorously pursue the sustenance of their implementation.

ii. Also, there is need for government at all levels, civil society organizations, development partners, and community heads/local authorities to motivate community participation in urban greening processes, particularly in Sudan Savanna located cities of Kano and Ibadan whose vegetion are naturally sparse and are characteristically warmer. The motivation should go beyond community sensitization and enlightenment. It should be holistic by incorporating the provision of finances, urban greening infrastructure, technical support, and monitoring of progresses made.

iii. Aside, the provision of green infrastructures, this study suggests the massive adoption of clean energy sources to provide power for the urban environment in Ibadan, Kano, Owerri and Birnin Kebbi in place of fossil fuels. Funding sources may be explored by planners, development partners, administrators, communities/community leaders, and city dwellers for the provision of infrastructure for exploiting the opportunities provided by the vast solar energy in Tropical Africa as a source of domestic and commercial power supply. This may reduce the level of greenhouse gases (GHGs) in the city centres and ameliorate their urban heat highland (UHI) effects.

iv. Development planners in the cities of Ibadan, Kano, Owerri and Birnin Kebbi may decongest city centres through proper and adequate planning, provision and access to affordable landed properties, provision of mortgage services, infrastructural development (road/drainage infrastructures, communication infrastructures, establishment of greenies and recreational parks) and provision of social amenities

(public water and electricity supply, hospitals, markets) in rural areas and at urban fringes or satellite communities. These will encourage and facilitate outmigration to the planned urban fringes.

v. This study also recommends the integration of Landsat images with those of higher spatial/spectral resolution passive optical imageries and active sensors like Radio Detection and Ranging (RADAR) and Light Detection and Ranging (LIDAR) for more adequate and comprehensive surveys of the urban environments, with view to improving their livability.

## 5.4 Contributions to Knowledge

The thesis established that built-up areas increased from 312.90 $km^2$ (9.19%), 70.32 $km^2$ (12.94%), 58.48 $km^2$ (11.85 %) and 14.06 $km^2$ (1.13%) in Ibadan, Owerri, Kano and Birnin Kebbi respectively in 1990 to 1,039.54 $km^2$ (30.55%), 209.16 $km^2$ (38.50%), 216.03 $km^2$ (43.77%) and 123.03 $km^2$ (9.85%) in 2019 respectively. This implied a high rate of urbanization process in all the cities, and a concomitant decrease in other land cover types; with a resultant imbalance in the ecosystem of the urban environment. The study also established differences in values of the mean noon-time air temperature; indicating higher temperature values in Birnin Kebbi (27.49°C) and Kano (25.56°C) both in the Sudan, in contrast to lower temperature values of 24.08°C and 23.17°C for Ibadan and Owerri respectively located in the Rainforest.

Furthermore, the thesis established a Tau statistic of 0.070, 0.098 and 0.091 with corresponding p-values of 0.045, 0.005 and 0.0098 which are less than 0.05 confidence level for Kano, Ibadan and Owerri respectively; indicating significant rising trends of noon-time

temperature in the three cities. Aside the mean LST-NDBI correlation of 0.94, 0.98, 0.96, 0.98 in Ibadan, Owerri, Kano and Birnin Kebbi respectively, the study established an increase in coverage areas of high LST areas from 18.12%, 18.07% and 14.71% respectively in Ibadan, Owerri and Birnin Kebbi in 1990 to 27.00%, 52.12% and 64% in 2019. This implied that as the urban sizes increase in the cities, the coverage area of higher LST increase.

## REFERENCES


Abubakar A. Z. (2015). Effects of Urbanization on Landuse/Landcover Changes in Birnin Kebbi, Kebbi State, Nigeria. An unpublished M.Sc Thesis submitted the School of Post Graduate Studies, Ahmadu Bello University, Zaria.

Abubakar A. Z. and Sawa B. A (2016). Analysis of Land Use/Land Cover Changes in Birnin Kebbi, Kebbi State, Nigeria. Katsina *Journal of Natural and Applied Sciences*, 5 (1) 163-174.

Aburasa M. M., Abdullaha S. H., Ramlia M. F., Ash'aaria Z. H. (2015). Measuring Land Cover Change in Seremban, Malaysia using NDVI Index. International Conference on Environmental Forensics 2015 (iENFORCE2015). *Procedia Environmental Sciences* 30 (2015) 238 – 243.

Abutaleb K., Ngie A., Darwish A., Ahmed M. Arafat S., and Ahmed F. (2015). Assessment of Urban Heat Island Using Remotely Sensed Imagery over Greater Cairo, Egypt. *Advances in Remote Sensing*, 2015, 4, 35-47.

Adaohuru A. R., Obiefuna J.C, Ibeawuchi I. I., Okoli N. A (2012). Evoking the Knowledge of Tree Tenure in the Humid Tropics: A Review of Dimensions in Agro-Plantation System in Nigeria. *Journal of Agriculture and Social Research* (JASR) 12 (1) 171-182.

Adekunle, V. A. J., Olagoke, A. O. and Ogundare, L. F. (2013). Timber Exploitation Rate in Tropical Rainforest Ecosystem of Southwest Nigeria and Its Implications on Sustainable Forest Management. *Applied Ecology and Environmental Research* 11(1): 123-136.

Adepoju K. A and Salami A. T. (2017). Geospatial Assessment of Forest Fragmentation and Its Implications for Ecological Processes in Tropical Forests. *Journal of Landscape Ecology*, 10 (2) 19-34.

Ajaaj A. A; Mishra A. K & Khan A. A (2017). Urban and peri-urban precipitation and air temperature trends in mega cities of the world using multiple trend analysis methods. *Theoretical* and *Applied Climatology, 1-16.* DOI 10.1007/s00704-017-2096-7.

Akpan-Ebe I. N (2017). Reforestation in Nigeria: History, Current Practice and Future Perspectives. *Reforesta*, 3:105-115.

Alabi M. O. (2012). The Built-Up Environment and Micro-Climate Variation in Lokoja, Nigeria. *American International Journal of Contemporary Research* 2(12), 150-158.

Al-Ahmadi, F. S. and Hames, A. S. (2009). Comparison of Four Classification Methods to Land Use and Land Cover from Raw Satellite Images for Some Remote Arid Areas, Kingdom of Saudi Arabia. *Earth Science*, 20(1), 167-191

Alavipanah S., Wegmann M., T Qureshi S., Weng Q., and Koellner T. (2015). The Role of Vegetation in Mitigating Urban Land Surface Temperatures: A Case Study of

Munich, Germany during the Warm Season. *Sustainability*, 7, 4689-4706. Doi:10.3390/su7044689.

Alemayehu F., Tolera M., Tesfaye G. (2019). Land Use Land Cover Change Trend and Its Drivers in Somodo Watershed South Western, Ethiopia. *African Journal of Agricultural Research*, 14(2) 102-117. DOI: 10.5897/AJAR2018.13672 102-117.

Al Blooshi, L.S., Abuelgasim, A., Nassar, A. and Ksiksi, T. (2020). Impact of Desert Urbanization on Urban Heat Islands Effect. *Open Journal of Geology*, 10, 760-770. https://doi.org/10.4236/ojg.2020.107034.

Al-Gretawee H., Rayburg S., and Neave M. (2016). The Cooling Effect of a Medium Sized Park on an Urban Environment. *International Journal of GEOMATE*, 11(26) 2541-2546.

Alhawiti R. A and Mitsova D. (2016). Using Landsat-8 Data to Explore the Correlation between Urban Heat Island and Urban Land Uses. *International Journal of Research in Engineering and Technology*, 5 (3) 457-466.

Almeida T., de Souza Filho, C., and Rossetto R. (2006). Aster and landsat ETM+ Images Applied to Sugarcane Yield Forecast. *International Journal of Remote Sensing*, *27*, 4057–4069.

Alexandri E., and Jones P. (2008). Temperature Decreases in an Urban Canyon Due to Green Walls and Green Roofs in Diverse Climates. *Building and Environment*, 43 (4) 480-93.

Ali S.B, Patnaik S., and Madguni O. (2017). Microclimate land surface temperatures across urban land use/ land cover forms. *Global Journal of Environmental Science Management* 3(3): 231-242, Summer 2017 DOI: 10.22034/gjesm.2017.03.03.001.

Aliyu A. A. and Amadu L. (2017). Urbanization, Cities, and Health: The Challenges to Nigeria: A Review. *Annals of African Medicine* 16(4): 149–158.

Amadi S.O., Udo S.O. & Ewona I.O. (2014). Trends and Variations of Monthly Mean Minimum and Maximum Temperature Data over Nigeria for the Period 1950-2012. *International Journal of Pure and Applied Physics*, 2 (4) 1-27.

Ambe, B. A., and Onnoghen, U. N. (2019). Ecosystems Services of the Tropical Rain Forest Environment: Lessons from the Cross River National Park, Nigeria. *Journal of Geoscience and Environment Protection*, 7, 1-10.

Anderson, M.C.; Allen, R.G.; Morse, A.; Kustas, W.P. (2012). Use of Landsat Thermal Imagery in Monitoring Evapotranspiration and Managing Water Resources. *Remote Sensing of the Environment*, *122*, 50–65.

Angel, S., Parent, J., Civco, D.L., Blei, A., Potere, D. (2011). The Dimensions of Global Urban Expansion: Estimates and Projections for All Countries, 2000–2050. *Programme Planning* 75, 53–107.

Araujo R.V., Albertini M. R., Costa-da-Silva A.L., Suesdek L., Franceschi N.C.S., Bastos N.M., Katz G., ...., Allegro V.L.A.C (2015). São Paulo Urban Heat Islands Have a Higher Incidence of Dengue than Other Urban Areas. *The Brazilian Journal of Infectious Disease* 1 9(2): 146–155.

Aremu O., Bello E., Aremu P., Aganbi B., and Machoko J. (2017). Monitoring and Analysis of Urban Heat Island using Remote Sensing Data – A Case Study of Akure, Ondo State, Nigeria. *International Journal of Environmental Sciences and Natural Resources,* 4 (5) 1-9. DOI: 10.19080/IJESNR.2017.04.555647.

Arnfield A.J. (2000). A Simple Model of Urban Canyon Energy Budget and its Validation. *Physical Geography* 23 (1) 305–326.

Arohunsoro S. J. Owolabi J. T. and Omotoba N. I. (2017).Watershed Management and Ecological Hazards in an Urban Environment: The Case of River Ajilosun in Ado Ekiti, Nigeria. *European Journal of Academic Essays* 1(2) 17-23.

Arohunsoro S. J. and Omotoba N. I. (2017). Causes, Effect and Abatement Measures of Flooding in River Ajilosun Drainage Basin in Ado-Ekiti, Nigeria. *Donnish Journal of Ecology and the Natural Environment*, 4(1) 001-010

Arsiso B. K., Tsidu G. M., Stoffberg G. H., Tadesse T (2018) Influence of Urbanization-Driven Land Use/Cover Change on Climate: The Case of Addis Ababa, Ethiopia. *Physics and Chemistry of Earth* 105:212–223.

Ashie Y. and Kono T. (2011). Urban-scale CFD Analysis in Support of a Climate-sensitive Design for the Tokyo Bay Area. *International Journal of Climatology* 31 (2), 174–199.

Ashley R. and Cashman A. (2006). Infrastructure to 2030: Telecommunication, Land Transport, Water and Electricity. OECD

Ashraf M. (2015). A Study of Temporal Change in Land Surface Temperature and Urban Heat Island Effect in Patna Municipal Corporation Over a Period of 25 years (1989 – 2014) Using Remote Sensing and GIS Technique. *International Journal of Remote Sensing & Geoscience* (IJRSG) 4 (1), 71-77.

Aslan N. and Koc-San D. (2016). Analysis of Relationship between Urban Heat Island Effect and Land Use/Cover Type Using Landsat 7 Etm+ and Landsat 8 OLI Images. *The International Archives of the Photogrammetry, Remote Sensing and Spatial Information Sciences*, Volume XLI-B8, 2016 XXIII ISPRS Congress, 12–19 July 2016, Prague, Czech Republic.

Awopetu M. S and Baruwa A. (2017). Appraisal of Groundwater Quality in Ado-Ekiti Metropolitan Area, Nigeria. *International Journal of Advanced Engineering, Management and Science* (IJAEMS) 3 (2) 117-121.

Ayila A. E. , Oluseyi F. O and Anas B. Y. (2014). Statistical Analysis of Urban Growth in Kano Metropolis, Nigeria. *International Journal of Environmental Monitoring and Analysis*, 2(1) 50-56

Azmi R., Alami O. B., Saadane A. E., Kacimi I., and Chafiq T. (2016). A Modified and Enhanced Normalized built-up Index using Multispectral and Thermal Bands. *Indian Journal of Science and Technology*, 9(28) 1-11.

Babalola O.S and Akinsanola A. A. (2016). Change Detection in Land Surface Temperature and Land Use Land Cover over Lagos Metropolis, Nigeria. *Journal of Remote Sensing & GIS*, 5:31-7.

Bach E., Walde I., Hese S., Schmullius C. and Denzler J. (2013). Land Cover Classification of Satellite Images Using Contextual Information. *ISPRS Annals of the Photogrammetry, Remote Sensing and Spatial Information Sciences*, Volume II-3/W1, 2013 VCM 2013 - The ISPRS Workshop on 3D Virtual City Modelling, 28 May 2013, Regina, Canada.

Bai Y., Wong M.S., Shi W., Wu L. and Qin K. (2015). Advancing of Land Surface Temperature Retrieval Using Extreme Learning Machine and Spatio-Temporal Adaptive Data Fusion Algorithm. *Remote Sensing*, *7*, 4424-4441. Doi:10.3390/rs70404424.

Bakr, N., Weindorf, D. C., Bahnassy, M. H., Marei, S. M. and EI-Badawi, M. M. (2010), Monitoring Land Cover Changes in a Newly Reclaimed Area of Egypt Using Multi-temporal Landsat Data. *Applied Geography*, 30: (4), 592-605.

Baram H. O; Mohammed O. A.; Hamaamin H. K.; Hamid A. A ; Mustafa R. L (2021). Urbanization and its Effect on Land Surface Temperatures in Halabja City. *Technium* 3(7) 87-98

Barata M., Ligeti E., De Simone G., T. Dickinson T., Jack, D., Penney, J., Rahman M., R. Zimmerman R. (2011): Climate change and human health in cities. *Climate Change and Cities: First Assessment Report of the Urban Climate Change Research Network*, Rosenzweig C., Solecki W. D., Hammer S. A., Mehrotra S. Eds., Cambridge University Press, Cambridge, UK, 179–21.

Bates B., Kundzewicz Z. W., Wu S., and Palutikof J. P (2008). *Climate Change and Water*, Technical Paper of the Intergovernmental Panel on Climate Change, Geneva: IPCC Secretariat.

Bechtel B., Langkamp T., Böhner J., Daneke C., Oßenbrügge J., Schempp S. (2012). Classification and Modelling of Urban Micro-Climates Using Multisensoral and Multitemporal Remote Sensing Data. International Archives of the Photogrammetry, Remote Sensing and Spatial Information Sciences, Volume XXXIX-B8, 2012 XXII ISPRS Congress, 25 August – 01 September 2012, Melbourne, Australia.

Bekele B., Wu W., Yirsaw E. (2019). Drivers of Land Use-Land Cover Changes in the Central Rift Valley of Ethiopia. *Sains Malaysiana* 48(7) 1333–1345.

Benali, A.; Carvalho, A.C.; Nunes, J.P.; Carvalhais, N.; Santos, A. (2012). Estimating Air Surface Temperature in Portugal Using MODIS LST Data. *Remote Sensing of Environment, 124, 108- 121*.

Benjamin, K.; Luo, Z.; Wang, X. (2021). Crowdsourcing Urban Air Temperature Data for Estimating Urban Heat Island and Building Heating/Cooling Load in London. *Energies*, 14, 5208. 1-26.

Benz U. C., Hofmann P., Willhauck G., Lingenfelde I. and Markus H., (2004). Multi-resolution, Object-oriented Fuzzy Analysis of Remote Sensing Data for GIS-ready Information. ISPRS *Journal of Photogrammetry and Remote Sensing* 58, 239–258.

Bettencourt L. M., Lobo J., Helbing D., Kühnert C., West G. B (2007). Growth, Innovation, Scaling, and the Pace of Life in Cities. *PNAS*. 2007;104:7301–6.

Bhatta B. (2010). Analysis of Urban Growth and Sprawl from Remote Sensing Data. *Advances in Geographic Information Science,* DOI 10.1007/978-3-642-05299-6_2

Bhatti S. S. and Tripathi N.K (2014). Built-up Area Extraction using Landsat 8 OLI Imagery. *GIScience & Remote Sensing* 51(4) 445-467. Doi: 10.1080/15481603.2014.939539.

Bissadu K. D. (2015). Remote Sensing and GIS-Based Assessment of Land Degradation Driven by Climate and Land Use Changes in Nasarawa State, Nigeria. Unpublished MTech Thesis Submitted to West African Science Service Centre on Climate Change and Adapted Land Use (WASCAL), Federal of University of Technology, Minna, Nigeria.

Blake R., Grimm A., Ichinose T., Horton R., Gaffin S., Jiong S., Bader D. and Cecil L. (2011). *Urban climate: processes, trends, and projections*. Climate Change and Cities: First Assessment Report of the Urban Climate Change Research Network. Cambridge University Press, Cambridge, UK, 43-81.

Blaschke T (2010). Object Based Image Analysis for Remote Sensing. *ISPRS Journal of Photogrammetry and Remote Sensing* 65 (1) 2–16.

Blaschke T., Hay G. J., Weng Q., and Resch B. (2011). Collective Sensing: Integrating Geospatial Technologies to Understand Urban Systems—An Overview. *Remote Sensing, 3,* 1743-1776. Doi:10.3390/rs3081743

Bloch R., Fox S., Monroy J., and Ojo A. (2015) Urbanisation and Urban Expansion in Nigeria. Urbanization Research Nigeria (URN) Research Report. London: ICF International. Creative Commons Attribution-Non- Commercial-Share Alike CC BY-NC-SA.

Block R. L. (1978). Development of Thermal Infrared Imagery to the Detection of Urban Heat Islands" (1978). Open-Access Master's Theses from the University of Nebraska-Lincoln. Paper 16.

Bodo T. (2019). Rapid Urbanisation: Theories, Causes, Consequences and Coping Strategies *Annals of Geographical Studies* (2)13, 32-45.

Bohnenstengel, S. I., Hamilton I., Davies M., and Belcher S. E. (2014). Impact of Anthropogenic Heat Emissions on London's Temperatures, *Q J R Meteorological Society* 140 (679), 687-698.

Bosilovich, M.G. (2013). Regional Climate and Variability of NASAMERRA and Recent Reanalyses: U.S. Summertime Precipitation and Temperature. *Journal of Applied Meteorology and Climatology* 52, 1939–1951.

Brazel, A.J., and D. Quatrocchi. 2005. *Urban Climatology.* 766–779. *In* Encyclopedia of World Climatology. Springer, New York.

Bouchama, A., Dehbi M., Mohamed G., Matthies F., Shoukri M., and Menne, B. (2007). Prognostic Factors in Heat Wave-related Deaths: A Meta-analysis. *Archives of Internal Medicine*, 167, 2170-2176.

Bozorgi M & Nejadkoorki F (2019). Spatiotemporal Monitoring of Thermal Environment in Isfahan Metropolitan area. *Environmental Risk Assessment and Remediation*;3(1):15-32.

Buccola N. and Spolek G. (2011). Pilot-Scale Evaluation of Green roof Runoff Retention, Detention, and Quality. *Water, Air and Soil Pollution*, 216 (1-4) 83-92.

Burke, M., Hsiang, S. M., and Miguel, E. (2015). Global Non-Linear Effect of Temperature on Economic Production, *Nature*, 527, 235–239, doi:10.1038/nature15725, 2015.

Butu A. W. and Emeribe C. N. (2019). Spatial patterns of climatic variability and water budget over Sudan Savannah Region of Nigeria. *African Journal of Environmental Science and Technology*, 13(12) 464-480. DOI: 10.5897/AJEST2019.2726.

Byomkesh T., Nakagoshi N., and Dewan A. M. (2012). Urbanization and Green Space Dynamics in Greater Dhaka, Bangladesh. *Landscape Ecology Engineering* 8:45-58. DOI 10.1007/s11355-010-0147-7.

Campbell-Lendrum, D. and Corvalan C. (2007). Climate Change and Developing Country Cities: Implications for Environmental Health and Equity. *Journal of Urban Health*, 84 (1), 109-117.

Cardoso R. D., Dorigon L. P., Teixeira D. C. F., and Amorim M.C. D.T (2017). Assessment of Urban Heat Islands in Small- and Mid-Sized Cities in Brazil. *Climate* 5, 14; doi:10.3390/cli5010014.

Cendese, A., and Monti P. (2003). Interaction between an Inland Urban Heat Island and a Sea-breeze Flow: A Laboratory Study, *Journal of Applied Meteorology*, 42:1569–1583.

Chaithanya, V.V. Binoy, B.V and Vinod, T.R (2017). Estimation of the Relationship between Urban Vegetation and Land Surface Temperature of Calicut City and Suburbs, Kerala, India using GIS and Remote Sensing data. *International Journal of Advanced Remote Sensing and GIS* 6 (1) 2088-2096.

Chakraborty S. B., Kant Y. and Mitra D. (2013). Assessment of Land Surface Temperature and Heat Fuxes over Delhi using Remote Sensing Data. *Journal of Environmental Management* xxx (2013) 1-10.

Chander G. and Markham, B. (2003). Revised Landsat-5 TM Radiometric Calibration Procedures and Post-calibration Dynamic Ranges. *IEEE Transactions on Geoscience and Remote Sensing* 41 (11) 2674–2677.

Chander G., Markham B. L., and Helder D. L. (2009). Summary of Current Radiometric Calibration Coefficients for Landsat MSS, TM, ETM+, and E0-1 ALI Sensors *Remote Sensing of Environment,*113 (5) 893-903.

Chang T., Liou Y, Lin C., Liu, S., and Wang, Y. (2010). Evaluation of surface heat fluxes in Chiayi plain of Taiwan by remotely sensed data. *International Journal of Remote Sensing,* 31 (14) 3885–3898.

Chapman L. and Thornes J. E. (2003). The use of geographical information systems in climatology and meteorology. *Progress in Physical Geography* August 2003 DOI: 10.1191/030913303767888464.

Chen J., Li Q., Niu J., and Sun L. (2011). Regional climate change and local urbanization effects on weather variables in Southeast China. *Stochastic Environmental Research and Risk Assessment* 25(4), 555-565.

Chen L., Jiang R., and Xiang W. (2016). Surface Heat Island in Shanghai and Its Relationship with Urban Development from 1989 to 2013. *Advances in Meteorology* Volume 2016, Article ID 9782686.

Chen G., Zhao L. and Mochida A. (2016b). Urban Heat Island Simulations in Guangzhou, China, Using the Coupled WRF/UCM Model with a Land Use Map Extracted from Remote Sensing Data. *Sustainability* 2016, 8, 628; doi:10.3390/su8070628www.

Chen Y., Quan J. Zhan W. and Guo Z. (2016c). Enhanced Statistical Estimation of Air Temperature Incorporating Nighttime Light Data. *Remote Sensing* 2016, 8, 656. doi:10.3390/rs8080656.

Cheval S., Micu D., Dumitrescu A., Irimescu A., Frighenciu M., Iojă C., Tudose N. C., Davidescu S., and Antonescu B. (2020). Meteorological and Ancillary Data Resources for Climate Research in Urban Areas. *Climate* 8, 37, 1-26.

Chudnovsky, A., Ben-Dor E., and Saaroni H. (2004). Diurnal Thermal Behavior of Selected Urban Objects using Remote Sensing Measurements, *Energy and Buildings*, 36:1063–1074.

Childe, V.G. (1950). The Urban Revolution. *Town Planning Review*, 21(1) 3, Routledge, London.

Chukwuocha N. A. C., Ogbenna Uchechukwu O., Chizoba O., and Emenike Nnedinma E. (2021). Erosion Sensitivity Assessment of Communities in Owerri, Nigeria Using Geographic Information System and Revised Universal Soil Loss Equation- Based Model. *American Journal of Geographic Information System*, 5(2) 55-67. DOI: 10.5923/j.ajgis.20160502.03.

Clinton N., Yu L., Fu H., He C., and Gong P. (2014). Global-Scale Associations of Vegetation Phenology with Rainfall and Temperature at a High Spatio-Temporal Resolution. *Remote Sensing*, *6*, 7320–7338.

Cohen B. (2006). Urbanization in developing countries: Current Trends, Future Projections, and Key Challenges for Sustainability. *Technology in Society* 28 (2006) 63–80.

Çolakkadıoğlu, D. (2023). The Effects of Urbanization and Vegetation Cover on Urban Heat Island: A Case Study in Osmaniye Province, *International Journal of Environment and Geoinformatics* (IJEGEO), 10(1):120-131. Doi. 10.30897/ijegeo.1144167.

Coll C., Caselles V., Galve J.M., Mira M., Bisquert M., and Vicente G.S. (2011). Long-term Accuracy Assessment of Land Surface Temperatures Derived from the Advanced Along-Track Scanning Radiometer. *Remote Sensing of Environment*, 116, 211–225.

Congalton, R.G., and K.Green K. (1999). *Assessing the Accuracy of Remotely Sensed Data: Principle and Practices*, CRS Press, Boca Raton, Florida

Cornes, R. C., and P. D. Jones (2013). How Well Does The ERA-Interim Reanalysis Replicate Trends in Extremes of Surface Temperature Across Europe? *Journal of Geophysical Research: Atmospere*, 118, 10,262–10,276. Doi:10.1002/jgrd.50799.

Cousins S. A. O., Auffret A. G., Lindgren J., Trank L. (2015). Regional-scale Land-Cover Change During the 20th Century and Its Consequences for Biodiversity. *AMBIO*, 44(Suppl. ): S17–S27. DOI 10.1007/s13280-014-0585-9.

Coutts A.M., Beringer J. and Tapper N.J (2007). Impact of Increasing Urban Density on Local Climate: Spatial and Temporal Variations in the Surface Energy Balance in Melbourne, Australia. *Journal of Applied Meteorology and Climatology*, 46 (4), 477-493.

Coutts A. M., Beringer J. and Tapper N. J (2008). Investigating the Climatic Impact of Urban Planning Strategies through the use of Regional Climate Modelling: A Case Study for Melbourne, Australia. *International Journal of Climatology* 28: 1943 – 1957.

Cui, L. and Shi J. (2012). Urbanization and Its Environmental Effects in Shanghai, China. *Urban Climate*, 2 (2012) 1–15.

Damisa M. A., Sanni S. A., Abdoulaye T., Kamara A.Y and A. Ayanwale A. (2010). Household Typology Based Analysis of Livelihood Strategies and Poverty Status in the Sudan Savannah of Nigeria: *Baseline Conditions. Learning Publics Journal of Agriculture and Environmental Studies,* 2 (1) 146- 160.

Danboyi, A.J. (2006) Reclamation of Derelict ponds of Birnin Kebbi. An Unpublished M.Tech Dissertation submitted to the Department of Geography, Federal University of Technology, Minna, Nigeria.

Dankani, I. M and Abubakar, S. D (2011). Uncontrolled urban growth around Dorayi area of Kano Metropolis: The planning and infrastructural development implications. *Ife Research Publications in Geography* 10 (1) 36-44.

Daramola, A. and Ibem, E. O (2010). Urban Environmental Problems in Nigeria: Implications for Sustainable Development. *Journal of Sustainable Development in Africa*, 12 (1) 124 – 145.

Dash, P., Göttsche, F. M., Olesen, F.S., Fischer, H. (2002). Land Surface Temperature and Emissivity Estimation from Passive Sensor Data: Theory and practice-current trends. *International Journal of Remote Sensing*, 23, 2563–2594.

Davis R. G, Barbosa O., Fuller Sobrino R. A, Tratalos J, Burke N., Lewis D, Warren P. H, Gaston K. J (2008). City-wide Relationships between Green Spaces, Urban Land use and Topography. *Urban Ecosystem* 11:269–287.

Dawson, R.J., Hall, J.W., Barr, S.L., Batty, M., Bristow, A.L., Carney, S., Dagoumas, A., Evans, S., Ford, A., Harwatt, H., Köhler, J., Tight, M.R., Walsh, C.L., and Zanni, .M. (2009). A Blueprint for the Integrated Assessment of Climate Change in Cities. Tyndall Working Paper 129, 26.

De Joanna P. and Francese D. (2012). *Sustainable Environment in the Mediterranean Region: From Housing to Urban and Land Scale Construction.* Franco Angeli, Italy, Milano.

Department of Geography, Federal University of Technology, Minna (2019). Unpublished Maps from the Map Repository of the Remote Sensing and GIS Laboratory, Department of Geography, Federal University of Technology, Minna.

Ding, H.; Shi, W. (2013). Land-use/land-cover Change and Its Influence on Surface Temperature: A Case Study in Beijing City. *International Journal of Remote Sensing*, 34, 5503–5517.

Dissanayake, D.M.S.L.B, Morimoto T., Murayama Y., Ranagalage M., and Handayani H. H. (2019). Impact of Urban Surface Characteristics and Socio-Economic Variables on the Spatial Variation of Land Surface Temperature in Lagos City, Nigeria. *Sustainability*, 11 (25). 1-23. Doi:10.3390/su11010025.

Dobesch H., Dumolard P., Dyras I. (2007). *Spatial Interpolation for Climate Data: The Use of GIS in Climatology and Meteorology.* ISTE Ltd UK, London.

Dobrovolný P. and Krahula L. (2015). The Spatial Variability of Air Temperature and Nocturnal Urban Heat Island Intensity in the City of Brno, Czech Republic. *Moravian Geographical Reports*, 23 (3), 8-16.

Dodgen, D., Donato D., Kelly N., La Grecan A., Morganstein J., Reser J., Ruzek J., Schweitzer S., Shimamoto M.M., Thigpen Tart K., and Ursano R. (2016). Chapter 8: Mental Health and Well-Being. *The Impacts of Climate Change on Human Health in the United States: A Scientific Assessment.* U.S. Global Change Research Program, Washington, DC, 217–246.

Doick K. and T. Hutchings (2013). Air temperature regulation by urban trees and green infrastructure. Forestry Research, Forestry Commission, UK, 10 pp.

Donat, M.G.; Sillmann, J.; Wild, S.; Alexander, L.V.; Lippmann, T.; Zwiers, F.W. (2014). Consistency of Temperature and Precipitation Extremes across Various Global Gridded in situ and Reanalysis Datasets. *Journal of Climatology*, 27, 5019–5035.

Donoghue D. N. M. (2002). Remote sensing: Environmental Change. *Progress in Physical Geography,* 26 (1) 144–151.

Du P., Liu P., Xia J., Feng L., Liu S., Tan Tan K., and Cheng L. (2014). Remote Sensing Image Interpretation for Urban Environment Analysis: Methods, System and Examples. *Remote Sensing*, *6*, 9458-9474. Doi:10.3390/rs6109458

Dunne, J. P., Stouffer, R. J., and John, J. G. (2013). Reductions in labour capacity from heat stress under climate warming, *Nature Climate Change*, 3, 563–566, doi:10.1038/nclimate1827, 2013.

Echebima, S.I., Obafemi, A.A. and Ndukwu, B.C. (2019). Assessment and Trend of Land Cover Land Use Changes in Owerri and Environs, South Eastern Nigeria. *Natural Resources*, 10, 284-298. DOI: 10.4236/nr.2019.107018.

Edobor W. W & Bello I. E. (2017). Remote Sensing and GIS Assessment of a Typical African Urban City: A Case Study of Ibadan, Nigeria. *American Journal of Geographical Research and Reviews,* 1(2) 1-9.

Effat H. A, Taha L. G, and Mansour K.F. (2014). Change Detection of Land cover and Urban Heat Islands Using Multi-Temporal Landsat Images, Application in Tanta City, Egypt. *Open Journal of Remote Sensing and Positioning* 1(2). 1-15.

Efe S. I and Eyefia O. A (2014). Urban Warming in Benin City, Nigeria. *Atmospheric and Climate Sciences*, 4, 241-252.

Eliasson I. and Svensson M. K. (2003). Spatial Air Temperature Variations and Urban Land Use: A Statistical Approach. *Meteorological Applications* 2003, 10 (2) 135–149. DOI:10.1017/S1350482703002056.

Elsayed I.S.M (2012). Mitigation of the Urban Heat Island of the City of Kuala Lumpur, Malaysia. *Middle-East Journal of Scientific Research* 11 (11): 1602-1613. DOI: 10.5829/idosi.mejsr.2012.11.11.1590.

Emeribeole A. and Iheaturu C. J (2016). Land Use/ Land Cover Dynamics and Urban Sprawl Movement: A Case Study of Owerri, Imo State Nigeria. *International Journal for Research in Emerging Science and Technology*, 3 (3), 54-60.

Emmanuel M. R. (2005). *An Urban Approach to Climate-sensitive Design: Strategies for the tropics*. Spon Press, Oxfordshire, 208.

Enete J.C, Obienusi E.A, Igu IN, Ayadiulo R. (2012). Harmattan Dust: Composition, Characteristics and Effects on Soil fertility in Enugu, Nigeria. *British Journal of Applied Science and Technology*, 2(1):72–81.

Essa W.; Verbeiren B.; van der Kwast J.; van de Voorde T.; and Batelaan O. (2012). Evaluation of the DisTrad Thermal Sharpening Methodology for Urban Areas. *International Journal of Applied Earth Observations and Geoinfomatics, 19*, 163–172.

Essou, G.R., F. Sabarly, P. Lucas-Picher, F. Brissette, and Poulin A. (2016). Can Precipitation and Temperature from Meteorological Reanalyses Be Used for Hydrological Modelling? *Journal of Hydrometeorology*, 17, 1929–1950. https://doi.org/10.1175/JHM-D-15-0138.1

Fabrizi R., Bonafoni S., and Biondi R. (2010). Satellite and Ground-Based Sensors for the Urban Heat Island Analysis in the City of Rome. *Remote Sensing*, 2, 1400-1415. Doi:10.3390/rs2051400.

Falahatkar, S. Hosseini, S. M. and Soffianian, A. R. (2011). The Relationship between Land Cover Changes and Spatial-temporal Dynamics of Land Surface Temperature. *Indian Journal of Science and Technology*, 4 (2) 76–81, 2011.

Fanan, U., Dlama, K. I., and Oluseyi, I. O. (2011), Urban Expansion and Vegetal Cover Loss in and around Nigeria's Federal Capital City. *Journal of Ecology and the Natural Environment*, 3(1), 1-10.

Fasona M. J. and Omojola A. S. (2004). GIS and Remote Sensing for Urban Planning: A Case of Festac Town, Lagos, Nigeria. *Proceedings of the 12th International Conference on Geoinformatics − Geospatial Information Research: Bridging the Pacific and Atlantic.* University of Gävle, Sweden, 7-9 June 2004, 45.

Fecht D., Fortunato L., Morley D., Hansell A. L and Gulliver J. (2016) Associations between Urban Metrics and Mortality Rates in England. *Environmental Health*, 15 (Suppl 1):34. DOI 10.1186/s12940-016-0106-3.

Federal Department of Forestry (FDF, 2019). National Forest Reference Emission Level (FREL) for the Federal Republic of Nigeria. Federal Department of Forestry, Federal Ministry of Environment Federal Republic of Nigeria.

Feizizadeh, B. and Blaschke, T. (2013). Examining Urban Heat Island Relations to Land Use and Air Pollution: Multiple Endmember Spectral Mixture Analysis for Thermal Remote Sensing. *IEEE Journal of Selected Topics in Applied Earth Observations and Remote Sensing, 6* 1749-1756.

Fire and Disaster Management Agency of Japan (2011). Fire and Disaster Management Agency of Japan.

Fisk, W. J., Lei-Gomez Q., and Mendell M. J. (2007). Meta-analyses of the Associations of Respiratory Health Effects with Dampness and Mold in Homes. *Indoor Air,* 17**,** 284-296, Doi:10.1111/j.1600-0668.2007.00475.x

Frey, C.M.; Parlow, E. (2012). Flux Measurements in Cairo. Part 2: On The Determination of the Spatial Radiation and Energy Balance Using Aster Satellite Data. *Remote Sensing* 4, 2635–2660.

Fujibe, F. (2009). Detection of Urban Warming in Recent Temperature Trends in Japan. *International Journal of Climatology* 29 (11), 1811–1822.

Gallo, K.; McNab, A.; Karl, T.R.; Brown, J.; Hood, J.; Tarpley, J. (1993). The use of NOAA AVHRR Data for Assessment of the Urban Heat Island Effect. *Journal of Applied Meteorology*, 32, 899–908.

Garcia-Herrera R., Díaz J., Trigo R. M., Luterbacher J., Fischer E. M. (2010). A Review of the European Summer Heat Wave of 2003. *Critical Review of Environmental Science and Technology*, 40(4):267–306.

Gbiri, I. A, Idoko, I. A, Okegbola, M. O and Oyelakin L. O (2019). Analysis of Forest Vegetal Characteristics of Akure Forest Reserve from Optical Imageries and Unmanned Aerial Vehicle Data. *European Journal of Engineering Research and Science* 4 (6) 58-61.

Ghent, D. (2012). Land Surface Temperature Validation and Algorithm Verification; Report to European Space Agency; European Space Agency: Paris, France, 2012.

Gilbert, RO. (1987). *Statistical Methods for Environmental Pollution Monitoring*. John Wiley and Sons, New York, 1987.

Goddard I. L.M and Tett S. F.B (2019). How Much Has Urbanisation Affected United Kingdom Temperatures? *Atmosperic Science Letters* 2019;20:e896.

Goldreich, Y. (2006). Ground and Top of Canopy Layer Urban Heat Island Partitioning on an Airborne Image. *Remote Sensing of Environment*, 104, 247–255.

Gonzales N. (2016). Sustainable Tourism and the impact of climate Change in the Caribbean. Occasional Paper Series No. XVII November, 2016. Institute of Air and Space Law (IASL), McGill University.

Gorgani S. A., Panahi M., and Rezaie F. (2013). The Relationship between NDVI and LST in the Urban Area of Mashhad, Iran. International Conference on Civil Engineering Architecture & Urban Sustainable Development 27 & 28 November 2013, Tabriz , Iran.

Goswami J., Roy S., and Sudhakar S. (2013). A Novel Approach in Identification of Urban Hot Spot Using Geospatial Technology: A Case Study in Kamrup Metro District of Assam. *International Journal of Geosciences*, 4, 898-903.

Grimmond S., Blackett M., Best M., Baik J.J., Belcher S., Bohnenstengel S.I., *et al*. (2010). The International Urban Energy Balance Models Comparison Project: First Results from Phase 1. *Journal of Applied Meteorology and Climatology* 49 (6), 1268–1292.

Gu C., Wu L. and Cook I. (2012). Progress in Research on Chinese Urbanization. *Frontiers of Architectural Research*, 1, 101–149.

Guha S. & Govil H. (2021) A Long-Term Monthly Analytical Study on The Relationship of LST with Normalized Difference Spectral Indices. *European Journal of Remote Sensing*, 54:1, 487-512. DOI: 10.1080/22797254.2021.1965496.

Gusso A., Silva A., Boland J., Lenz L., Philipp C. (2017). Income Driven Patterns of the Urban *Environment. Sustainability*, 9, 275, 1-20. Doi:10.3390/su9020275 1-20.

Hajat S., Vardoulakis S., Heaviside C., Eggen, B. (2014). Climate Change Effects on Human Health: Projections of Temperature-Related Mortality for the UK During the 2020s, 2050s and 2080s. *Journal of Epidemiology and Community Health* 68 (7) 641–648.

Hamilton B. and Erickson C. L (2012). Urban Heat Islands and Social Work: Opportunities for Intervention. *Advances in Social Work* 13 (2) 420-430.

Harris H. and Coutts A. (2011). Airborne Thermal Remote Sensing for Analysis of the Urban Heat Island. A Technical Report. Victorian Centre for Climate Change Adaptation Researchhttp://www.vcccar.org.au/sites/default/files/publications/VCCCAR%20Urban%20Heat%20Island%20Technical%20Report%20-%20WEB.pdf. Accessed on 17 March, 2017.

Hart M. A., and Sailor D. J. (2009). Quantifying the Influence of Land-Use and Surface Characteristics on Spatial Variability in the Urban Heat Island. *Theoretical Applications in Climatology,* 95, 397–406.

Haruna S. and Murtala M.R (2019). Assessing the Length of Growing Season in the Sudan Savanna Ecological Zone of Nigeria as a Challenge to Food Security for Sustainable Development. *Journal of Tropical Agriculture, Food, Environment and Extension*, 18 (3) 5-10.

Hassan Z., Shabbir R., Ahmad S. S., Malik A.H., Aziz N., Butt A. and Erum S. (2016). Dynamics of Land use and Land Cover Change (LULCC) using Geospatial Techniques: A Case Study of Islamabad Pakistan. *SpringerPlus* (2016) 5:812. DOI 10.1186/s40064-016-2414-z.

He C., Shi P., Xie D. and Zhao Y. (2010) Improving the Normalized Difference Built-Up Index to Map Urban Built-Up Areas Using A Semiautomatic Segmentation Approach. *Remote Sensing Letters*, 1:4, 213-221. DOI: 10.1080/01431161.2010.481681.

He Q., Wang M., Liu K., Li K., Jiang Z. (2022). GPRChinaTemp1km: A High-Resolution Monthly Air Temperature Data Set for China (1951–2020) Based on Machine Learning. *Earth System Science Data*, 14, 3273–3292. https://doi.org/10.5194/essd-14-3273-2022.

Heaviside, C, Vardoulakis, S., Cai, X (2016). Attribution of Mortality to the Urban Heat Island during Heatwaves in the West Midlands, UK. *Environmental Health*; 15 (Suppl 1):27.

Hebbert M. and Mackillop F. (2013). Urban Climatology Applied to Urban Planning: A Postwar Knowledge Circulation Failure. *International Journal of Urban and Regional Research* 37.5, 1542–58. DOI:10.1111/1468-2427.12046.

Heisler G. M. and Brazel A.J. (2010). The Urban Physical Environment: Temperature and Urban Heat Islands. Urban Ecosystem Ecology. Aitkenhead-Peterson J. and A. Volder A. (ed.) doi:10.2134/agronmonogr55.c2.

Henderson J. V, Storeygard A, and Deichmann U. (2017). Has Climate Change Driven Urbanization in Africa? *Journal of Development Economics* 12, 60–82

Herold M., Schiefer S., Hostert P., Roberts D. A. (2006). Applying imaging spectrometry in urban areas. In: Weng, Q., Quattrochi, D. (Eds.), Urban Remote Sensing. CRC Press, Florida, 137–162.

Hirsch, R.M., Slack, J.R. and Smith, R.A. (1982). Techniques of Trend Analysis for Monthly Water Quality Data. *Water Resources Research*, 18 (1), 107-121.

Howard, L. (1833). *The climate of London, deduced from meteorological observations*. Three Volumes, Brazel Harvey & Darton, London.

Hsiang, S.M., Burke M., and Miguel E. (2013). Quantifying the Influence of Climate on Human Conflict. *Science*, 341, 1235367. http://dx.doi.org/10.1126/science.1235367.

Huang C., Barnett A.G, Wang X, Vaneckova P., FitzGerald G., Tong S. (2011). Projecting Future Heat-related Mortality under Climate Change Scenarios: A Systematic Review. *Environmental Health Perspective*,119 (12) 1681–1690.

Huang, T., Uchihama D., Ochi S., and Yasuoka Y. (2006). Assessment with Satellite Data of the Urban Heat Island Effect in Asian Mega Cities. *International Journal of Applied Earth Observation and Geoinformation* 8: 34–48.

Hughes K. (2006). The Impact of Urban Areas on Climate in the UK: A Spatial and Temporal Analysis, with an Emphasis on Temperature and Precipitation Effects. *Earth & Environment* 2: 54-83.

Ifatimehin O. O, Ujoh F., and Magaji J. Y (2009). An Evaluation of the Effect of Land Use/cover Change on the Surface Temperature of Lokoja Town, Nigeria. *African Journal of Environmental Science and Technology*, 3(3),086-090. DOI: 10.5897/AJEST09.014.

Ifatimehin, O. O Ishaya, S and Fanan, U (2010). An Analysis of Temperature Variations Using Remote Sensing Approach in Lokoja Area, Nigeria. *Production Agriculture and Technology (PAT)*, 6 (2): 35-44.

Ifatimehin O. O., Ismail N. A., and Balogun M. (2015). Bioclimatic Conditions of Urban Residents through Deteriorating Ecosystem Practices in an Emerging City of Nigeria. *International Journal of Ecosystem* 2015, 5(3): 75-79 DOI: 10.5923/j.ije.20150503.01.

Iwasokun G.B, and Akinyokun O.C (2014). Image Enhancement Methods: A Review. *British Journal of Mathematics & Computer Science* 4(16), 2251-2277.

Iwuji, M. C., Ibe, C. P., Njoku J. D., Anyanwu S. O., Amangabara, G. T., Ac-Chukwuocha N., Ukaegbu, K. O. E. (2017). Analysis of Land Use and Land Cover Dynamics in Orlu, Nigeria. *Asian Journal of Environment & Ecology* 4(1): 1-10.

Izquierdo, M., A. Moreno-Rodriguez, A. Gonzalez-Gil, and N. Garcia-Hernando. (2011). Air Conditioning in the Region of Madrid, Spain: An Approach to Electricity Consumption, Economics and $CO_2$ Emissions. *Energy* 36: 1630-1639.

Jahan M. (2012). Impact of rural urban migration on physical and social environment: The case of Dhaka city. *International Journal of Development and Sustainability* 1 (2)186-194

James M. M. and Charles N. M. (2014). Dynamism of Land use Changes on Surface Temperature in Kenya: A Case Study of Nairobi City. *International Journal of Science and Research* (IJSR), 3 (4) 39-41.

Jeong J. J. (2012). Higher Temperature Effects of Impervious Surface Due to Urbanization in South Berkeley, California. *Impervious Surface & Temperature*, 1-12.

Jiang Y., Fu P., and Weng Q. (2015). Assessing the Impacts of Urbanization-Associated Land Use/Cover Change on Land Surface Temperature and Surface Moisture: A Case Study in the Midwestern United States. *Remote Sensing*, 7, 4880-4898. Doi:10.3390/rs70404880.

Jiang Y., Fu P. and Weng Q. (2015b). Downscaling GOES Land Surface Temperature for Assessing Heat Wave Health Risks. *IEEE Geoscience and Remote Sensing Letters*, 12(8) 1605-1609.

Jibril I. U. (2010). The Return of the Greens in Abuja, Nigeria's New Capital City. TS 9E - Sustainable Planning and Urban Renewal. FIG Congress 2010: Facing the Challenges – Building the Capacity Sydney, Australia, 11-16 April 2010.

Jim C. Y., Chen W. Y (2006) Perception and Attitude of Residents Towards Urban Green Spaces in Guangzhou (China). *Environmental Management* 38(3):338–349.

Jime´nez-Munoz J. C. and Sobrino J. A. (2003). A Generalized Single- Channel Method for Retrieving Land Surface Temperature from Remote Sensing Data. *Journal of Geophysical Research*: *Atmospheres*, 108 (22) 4688–4697.

Jime´nez-Munoz, J.C.; Sobrino J.A. (2008). Split-window coefficients for land surface temperature retrieval from low-resolution thermal infrared sensors. *IEEE Geosci. Remote Sensing Letters* 5, 806–809.

Jin M. and Dickinson R.E (2010). Land Surface Skin Temperature Climatology. *Environmental Research Letters*, 5, 44004.

Jin, M.S.; Kessomkiat, W.; Pereira, G. (2011). Satellite-observed Urbanization Characters in Shanghai, China: Aerosols, Urban Heat Island Effect, and Land-Atmosphere Interactions. *Remote Sensing, 3*, 83–99.

Josh J. P and Bhatta B. (2012). Estimating Temporal Land Surface Temperature Using Remote Sensing: A Study of Vadodara Urban Area, Gujarat. *International Journal of Geology, Earth and Environmental Sciences*, 2 (1) 23-130

Joshi, R., Raval, H., Pathak, M., Prajapati, S., Patel, A., Singh, V. and Kalubarme, M.H. (2015) Urban Heat Island Characterization and Isotherm Mapping Using Geo-Informatics Technology in Ahmedabad City, Gujarat State, India. *International Journal of Geosciences*, 6, 274-285. http://dx.doi.org/10.4236/ijg.2015.63021.

Joshi N., Baumann M., Ehammer A., Fensholt R., Grogan K., Hostert P., Jepsen M.R. Kuemmerle T…..Waske B. (2016). A Review of the Application of Optical and Radar Remote Sensing Data Fusion to Land Use Mapping and Monitoring. *Remote Sensing*, 8, 70. Doi:10.3390/rs8010070.

Jothimani M., Gunalan J., Duraisamy R., and Abebe A. (2021). Study the Relationship Between LULC, LST, NDVI, NDWI and NDBI in Greater Arba Minch Area, Rift Valley, Ethiopia. Proceedings of the 3rd International Conference on Integrated Intelligent Computing Communication & Security (ICIIC 2021).

Jurairat P., and Seng L. (2018). A Review of Mobile Crowdsourcing Architectures and Challenges: Toward Crowd-Empowered Internet-of-Things. *IEEE Access* 7, 304-324.

Kaiser, M.F. (2014). Impact of the Human Activities on the Local Climate and Environment of the Suez City in Egypt. *International Journal of Geosciences*, 5, 700-709.

Kaiser, E.A.; Rolim, S.B.A.; Grondona, A.E.B.; Hackmann, C.L.; de Marsillac Linn, R.; Käfer, P.S.; da Rocha, N.S.; Diaz, L.R. (2022). Spatiotemporal Influences of LULC Changes on Land Surface Temperature in Rapid Urbanization Area through Landsat-TM and TIRS Images. *Atmosphere*, 13, 460, 1-18 https://doi.org/10.3390/ atmos13030460.

Kanda N., Negi H.S., Rishi M. S. and Kumar A. (2020). Performance of various gridded temperature and precipitation datasets over Northwest Himalayan Region. *Environmental Research Communications*, 2 (2020) 085002, 1-20.

Kankara, I. A (2019). Ground and Surface Water Potentials and Accessibility in Kano Municipal, Nigeria: Implication for Geological Constraints. *Annals of Geographical Studies* 2, (1), 2019 1-7.

Kaoukis K., Bourletsikas A., Tsagari C., Baloutsos G., Karetsos G., and Michopoulos P. (2022), Trend Analysis of Long-lasting Air Temperature and Precipitation Time Series in a Mountainous Fir Forest in Central Greece: Implications for Nitrogen uptake by Plants. *Global NEST Journal*, 24(4), 553-561.

Kasarda J. D. and Crenshaw E. D. (1991). Third World Urbanization: Dimensions, Theories, and Determinants. *Annual Review of Sociology*, 17, 467-501.

Kasim, O., Agbola, S. & Oweniwe, M. (2020). Land Use Land Cover Change and Land Surface Emissivity in Ibadan, Nigeria. *Town and Regional Planning*,77. 71-88.

Kaya S, Basar U. G, Karaca M, Seker D. Z (2012) Assessment of Urban Heat Islands Using Remotely Sensed Data. *Ekoloji* 21 (84): 107-113.

Kenney, W.L.; DeGroot, D.W.; and Alexander H. L. (2004). Extremes of Human Heat Tolerance: Life at the Precipice of Thermoregulatory Failure. *Journal of Thermal Biology* 2, 479–485.

Kerle N., Janssen L. F. F and Huurneman G. C (eds.) (2004). Principles of Remote Sensing. Third edition. A publication by International Institute for Geo-Information Science and Earth Observation (ITC), Enschede, The Netherlands.

Kinney P. L, O'Neill M. S., Bell M.L, Schwartz J. (2008). Approaches For Estimating Effects of Climate Change on Heat-related Deaths: Challenges and Opportunities. *Environmental Science Policy*,11(1):87–96.

Knowlton K., Rotkin-Ellman M., King G., Margolis H. G., Smith D., Solomon G., Trent R., and English P. (2009). The 2006 California heat wave: Impacts on hospitalizations and emergency department visits. *Environmental Health Perspectives*, 117**,** 61-67, doi:10.1289/ehp.11594.

Kok, P., O'Donovan M., Bouare O., and van Zyl J. (2003). *Post-apartheid Patterns of Internal Migration in South Africa*. HSRC Publishers, Cape Town, South Africa, pp 33.

Kong F. and Nakagoshi N. (2006). Spatial-temporal Gradient Analysis of Urban Green Spaces in Jinan, China. *Landscape Urban Planning* 78:147–164.

Kotharkar R. and Bagade A. (2018). Evaluating urban heat island in the critical local climate zones of an Indian city. *Landscape and Urban Planning* 169 (2018) 92–104.

Krehbiel C., and Henebry G. (2016). Comparison of Multiple Datasets for Monitoring Thermal Time in Urban Areas over the U.S. Upper Midwest. *Remote Sensing*, 8, 297; Doi:10.3390/rs8040297.

Kumar, K.S, Deepak, B. A, Kumar, A.C., Mounika, C. and Prasad, T. V (2015). Study on Urban Surface Temperature Changes of Vijayawada City using Remote Sensing and GIS *International Journal of Innovative Research in Advanced Engineering (IJIRAE)* 3(2), 98-102

Kumi-Boateng B., Stemn E., and Agyapong E.A (2015). Effect of Urban Growth on Urban Thermal Environment: A Case Study of Sekondi-Takoradi Metropolis of Ghana. *Journal of Environment and Earth Science* 5 (2) 32-41.

Kustas W. P.; Norman J.M.; Anderson M.C.; and French A.N. (2003). Estimating subpixel surface temperatures and energy fluxes from the vegetation index–radiometric temperature relationship. *Remote Sensing of the Environment* 2003, *85*, 429–440.

Lehoczky A., Sobrino J.A., Skoković D., and Aguilar E. (2017). The Urban Heat Island Effect in the City of Valencia: A Case Study for Hot Summer Days. *Urban Science* 2017, *1*(1), 9; Doi:10.3390/urbansci1010009.

Le Tertre A., Lefranc A., Eilstein D., Declercq C., Medina S., Blanchard M. (2006). Impact of the 2003 Heatwave on All-cause Mortality in 9 French Cities. *Epidemiology* M17 (1):75–9.

Li H. and Liu Q. (2008). Comparison of NDBI and NDVI as Indicators of Surface Urban Heat Island Effect in MODIS Imagery. International Conference on Earth Observation Data Processing and Analysis (ICEODPA). Proceedings of SPIE Vol. 7285, 728503

Li X., Stringer LC, Chapman S., and Dallimer M. (2021) How Urbanisation Alters the Intensity of the Urban Heat Island in a Tropical African City. *PLoS ONE* 16(7): e0254371. https://doi.org/10.1371/ journal.pone.025437.

Li X. and Norford L. K (2016). Evaluation of Cool Roof and Vegetation in Mitigating Urban Heat Island in a Tropical City, Singapore. *Urban Climate* 16, 59–74

Li X., Koh T.Y., Panda J. and Norford L.K. (2016). Impact of Urbanization Patterns on the Local Climate of a Tropical City Singapore: An Ensemble Study. *American Geophysical Union* Doi: 10.1002/2015JD024452.

Li, Z. L., Tang B.H., Wu H., Ren H., Yan G., Wan Z., Trigo I. F., Sobrino J.A. (2013). Satellite-derived Land Surface Temperature: Current Status and Perspectives. *Remote Sensing of the Environment*, *131*, 14–37.

Lillesand T, Kiefer R, Chipman J. (2004). *Remote Sensing and Image Interpretation*. Chichester: John Wiley.

Lin, C.Y., Chen F., Huang J., Liou Y.A., Chen W.C., Chen W. N., and Liu S. C. (2008), Urban Heat Island Effect and its Impact on Boundary Layer Development and Land-sea circulation over northern Taiwan, *Atmos. Environ*, 42, 5639-5649.

Lin M. Luo S., Walker R. J., Liu X., Hwang S. A., and Chinery R. (2009). Extreme High Temperatures and Hospital Admissions for Respiratory and Cardiovascular Diseases. *Epidemiology,* 20**,** 738-746.

Limin Y. & George X. (2003). Urban Land-Cover Change Detection through Sub-Pixel Imperviousness Mapping Using Remotely Sensed Data. *Photogrammetric Engineering and Remote Sensing*, 69 (9) 1003–1010.

Lin, Y.; Yang, L.; Zheng, W.; and Ren, Y. (2015). Study on Human Physiological Adaptation of Thermal Comfort under Building Environment. *Procedia Engineering,* 121, 1780–1787.

Liu M., Hu Y., Chang Y., He X., and Zhang W. (2009). Land Use and Land Cover Change Analysis and Prediction in the Upper Reaches of the Minjiang River, China. *Environmental Management*, 43(5), 899–907.

Liu L., and Zhang Y. (2011). Urban Heat Island Analysis Using the Landsat TM Data and ASTER Data: A Case Study in Hong Kong. *Remote Sensing*. 3,1535-1552.Doi:10.3390/rs3071535.

Liu, K., Zhang, X., Li, X., Jiang, H. (2014) Multiscale Analysis of Urban Thermal Characteristics: Case Study of Shijiazhuang, China. *Journal of Applied Remote Sensing. Society of Photo- Optical Instrumentation Engineers* (SPIE), 083649-1 - 083649-15. DOI: 10.1117/1.JRS.8.083649

Liu K., Su H., Zhang L., Zhang R., Li X. (2015). Analysis of the Urban Heat Island Effect in Shijiazhuang, China Using Satellite and Airborne Data. *Remote Sensing*, 7, 4804-4833. Doi:10.3390/rs70404804.

Liu T, & Yang X (2015). Monitoring Land Changes in an Urban Area Using Satellite Imagery, GIS and Landscape Metrics. *Applied Geography* 56:42–54.

Liu K., Fang J., Zhao D., Liu X., Zhang X., Wang X., and Li X. (2016). An Assessment of Urban Surface Energy Fluxes Using a Sub-Pixel Remote Sensing Analysis: A Case Study in Suzhou, China. *ISPRS International Journal of Geo-Informatics*, 5, 11. Doi:10.3390/ijgi5020011.

Lobl E.S; Spencer R. W; Shibata A.; Imaoka K.; Sasaki, M. (2013). Global Climate Monitoring with the Advanced Microwave Scanning Radiometer (AMSR and AMSR-E). *Proceedings of SPIE 4894, Microwave Remote Sensing of the Atmosphere and Environment* III, (104). Doi:10.1117/12.466518.

Lorenz, C., and Kunstmann H. (2012). The Hydrological Cycle in Three State-of-the-art Reanalyses: Inter-comparison and Performance Analysis. *Hydrometeorology*, 13, 1397–1420.

Loughnan, M. E., Nicholls N., and Tapper N. (2009). Hot Spots Project: A Spatial Vulnerability Analysis of Urban Populations to Extreme Heat Events, Victorian Department of Health,

Melbourne. Accessed 2011: http://www.health.vic.gov.au/environment/heatwave/agencies/research_pubs.htm

Lu D., and Weng Q. (2006). Spectral Mixture Analysis of ASTER Images for Examining the Relationship between Urban Thermal Features and Biophysical Descriptors in Indianapolis, Indiana, USA. *Remote Sensing of Environment* 104, 157-167.

Luber, G., K. Knowlton, J. Balbus, H. Frumkin, M. Hayden, J. Hess, M. McGeehin, N. Sheats, L. Backer, C. B. Beard, K. L. Ebi, E. Maibach, R. S. Ostfeld, C. Wiedinmyer, E. Zielinski-Gutiérrez, and L. Ziska (2014). Ch. 9: Human Health. *Climate Change Impacts in the United States: The Third National Climate Assessment*, J. M. Melillo, Terese (T.C.) Richmond, and G. W. Yohe, Eds., U.S. Global Change Research Program, 220-256. Doi:10.7930/J0PN93H5.

Luederitz, C., Brink, E., Gralla, F., Hermelingmeier, V., Meyer, M., Niven, L., von Wehrden, H. (2015). A Review of Urban Ecosystem Services: Six Key Challenges for Future Research. *Ecosystem Services*, 14, 98-112. https://doi.org/10.1016/j.ecoser.2015.05.001.

Lundholm J.T. and Richardson P.J. (2010). Habitat Analogues for Reconciliation Ecology in Urban and Industrial Environments. *Journal of Applied Ecology*, 47 (5) 966-975.

Maghsoudi Y., Collins M. J., and Leckie, D. (2012). Speckle Reduction for the Forest Mapping Analysis of Multi-temporal Radarsat-1 Images. *International Journal of Remote Sensing*, 33, 1349–1359.

Mahmoud M. I., Duker A., Conrad C., Thiel M., and Ahmad H. S. (2016). Analysis of Settlement Expansion and Urban Growth Modelling Using Geoinformation for Assessing Potential Impacts of Urbanization on Climate in Abuja City, Nigeria. *Remote Sensing*, 8, 220.

Maigari A. I. (2016). Road Network: The Silent Treasures of Kano Metropolis. *International Journal of Innovative Environmental Studies Research* 4 (1), 1-8.

Makido Y., Shandas V., Ferwati S. and Sailor D. (2016). Daytime Variation of Urban Heat Islands: The Case Study of Doha, Qatar. *Climate* 2016, 4, 32; doi:10.3390/cli4020032.

Malik M. S., Shukla J. P., & Mishra S. (2019). Relationship of LST, NDBI and NDVI using Landsat-8 data in Kandaihimmat Watershed, Hoshangabad, India. *Indian Journal of Geo Marine Sciences* 48 (01) 25-31

Mallam I, Iguisi E.O., and Tasi'u .Y.R (2016). An Assessment of Gully Erosion in Kano Metropolis, Nigeria. *Global Advanced Research Journal of Agricultural Science*, 5(1) 014-027.

Mallick, J., Rahman, A., and Singh, C.K. (2013). Modelling Urban Heat Islands in Heterogeneous Land Surface and its Correlation with Impervious Surface Area by

Using Night-time ASTER Satellite Data in Highly Urbanizing City, Delhi-India. *Advances in Space Research, 52*, 639-655.

Manik T. K and Syaukat S. (2015). The impact of Urban Heat Islands. Assessing Vulnerability in Indonesia. Asian Cities Climate Resilience. Working Paper Series 13: 2015.

Manzanas R. L., Amekudzi K., Preko S., and Gutiérrez J. M. (2014). Precipitation Variability and Trends in Ghana: An Intercomparison of Observational and Reanalysis Products. *Climatic Change*, 124, 805–819.

Martiello M. A and Giacchi M. V (2010). Review Article: High Temperatures and Health Outcomes: A Review of the Literature, *Scandinavian Journal of Public Health*, 38 (8) 826-837.

McCarthy H., and Pataki D. (2010). Drivers of Variability in Water use of Native and Non-native Urban Trees in the Greater Los Angeles Area. *Urban Ecosystems*, (4) 393-414.

McGranahan G. and Satterthwaite D. (2014). *Urbanization Concepts and Trends*. International Institute for Environment and Development (IIED) Working Paper London.

McMichael, A. J., Wilkinson P., Kovats R. S., Pattenden S., Hajat S., Armstrong B., Vajanapoom N., Niciu E. M., Mahomed H., Kingkeow C., Kosnik M., O'Neill M. S., Romieu I., Aguilar M.R., Barreto M. L., Gouveia N., and 12 and Nikiforov B. (2008). International study of temperature, heat and urban mortality: the 'ISOTHURM' project. *International Journal of Epidemiology* 2008;1–11 doi:10.1093/ije/dyn086.

Meera G. G., Parthiban S., Nagaraj T., Christy. A (2015). NDVI: Vegetation Change Detection Using Remote Sensing and GIS. A Case study of Vellore District. *Procedia Computer Science* 57, 1199 – 1210.

Melesse A.S., Weng Q., Thenkabail P. S. Senay G. B. (2007). Remote Sensing Sensors and Applications in Environmental Resources Mapping and Modelling. *Sensors, 7*, 3209-3241.

Mendes M., and Pala, A. (2003). Type 1 Error Rate and Power of Three Normality Tests. Pakistan *Journal of Information and Technology*, 2003, 2(2), 135-139.

Merchant J. W and Narumalani S. (2009). Integrating Remote Sensing and Geographic Information Systems. Papers in Natural Resources, 216. Published in *The SAGE Handbook of Remote Sensing*, 2009, Chapter 18 DOI: 10.4135/978-1-8570-2105-9.n18

Mildrexler, D.J., Zhao, M., Owe, M., Running, S.W. (2011). A Global Comparison between Station Air Temperatures and MODIS Land Surface Temperatures Reveals the Cooling Role of Forests. *Journal of Geophysical Research*, 116, G03025.

Miles V. and Nansen I. E. (2017). Seasonal and Spatial Characteristics of Urban Heat Islands (UHIs) in Northern West Siberian Cities. *Remote Sensing* 2017, 9, 989; Doi:10.3390/rs9100989.

Mills, G. (2007). Cities as Agents of Global Change. *International Journal of Climatology* 27:1849–1857.

Mirzaei P.A, Haghighat F. (2010) Approaches to study Urban Heat Island – Abilities and Limitations. *Built Environment* 2010, 45(10) 2192-2201.

Mirzaei P. A (2015). Recent Challenges in Modelling of Urban Heat Island. *Sustainable Cities and Society* 19 (2015) 200–206.

Mitraka Z., Chrysoulakis, N., Doxani, G., Del Frate, F., and Berger, M. (2015). Urban Surface Temperature Time Series Estimation at the Local Scale by Spatial-Spectral Unmixing of Satellite Observations. *Remote Sensing*, *7*, 4139-4156. Doi:10.3390/rs70404139.

Mohan M., Pathan S. K., Narendrareddy K., Kandya A., and Pandey S. (2011). Dynamics of Urbanization and Its Impact on Land-Use/Land-Cover: A Case Study of Megacity Delhi. *Journal of Environmental Protection*. 2011, (2) 1274-1283. Doi:10.4236/jep.2011.29147.

Mohammed B. N and Jeb D. N. (2014). Analysis of Flood Risk Inundation Hazard in Birnin Kebbi Town, Kebbi State, Nigeria. *International Journal of Geomatics and Geosciences*, 5 (1) 119-131.

Mohammed M. U., Hassan N. & Badamasi M. M. (2019). In search of missing links: urbanisation and climate change in Kano Metropolis, Nigeria. *International Journal of Urban Sustainable Development*, 11:3, 309-318, DOI: 10.1080/19463138.2019.1603154

Moonen P., Defraeye T., Dorer V; Blocken B., and Carmeliet J. (2012). Urban Physics: Effect of the Micro-climate on Comfort, Health and Energy Demand. *Frontiers of Architectural Research*, 1, 197–228.

Morabito M., Crisci A., Messeri A., Orlandini S., Raschi A., Maracchi G., and Munafò M. (2016).The impact of Built-up Surfaces on Land Surface Temperatures in Italian Urban Areas. *Science of the Total Environment* 551–552, 317–326.

Morris, K. I., Chan A., Salleh, S.A., Ooi, M. C. G., Oozeer, M. Y. & Abakr, Y. A (2016). Numerical Study on the Urbanisation of Putrajaya and Its Interaction with the Local Climate Over a Decade. *Urban Climate* 16, 1–24.

Mukaka M. M. (2012). Statistics Corner: A guide to appropriate use of Correlation coefficient in medical research. *Malawi Medical Journal*, 24 (3): 69-71.

Mwakapuja F., Liwa E., and Kashaigili J. (2013).Usage of Indices for Extraction of Built-up Areas and Vegetation Features from Landsat TM Image: A Case of Dar Es Salaam

and Kisarawe Peri-Urban Areas, Tanzania. *International Journal of Agriculture and Forestry*, 3(7): 273-283. DOI: 10.5923/j.ijaf.20130307.04.

Myint S. W., Gober P., Brazel A., Grossman-Clarke S. and Weng, Q. (2011). Per-pixel vs. Object-Based Classification of Urban Land Cover Extraction Using High Spatial Resolution Imagery. *Remote Sensing of Environment*, 115(5) 1145–1161.

Nabegu A. B. (2010). An Analysis of Municipal Solid Waste in Kano Metropolis, Nigeria. *Journal of Human Ecology* 31(2): 111-119.

Nádudvari A. (2021). The Localization of Urban Heat Island in the Katowice Conurbation (Poland) Using the Combination of Land Surface Temperature, Normalized Difference Vegetation Index and Normalized Difference Built-Up Index. *Geographia Polonica*, 94 (1) 111-129.

Najib Y., Okoh D., Musa I., Adedoja S., and Said R. A (2017) Study of the Surface Air Temperature Variations in Nigeria. *The Open Atmospheric Science Journal*, 11, 54-70. DOI: 10.2174/1874282301711010054.

Naipal V., Naipal S., and Samson R. (2013). Estimating the Evapotranspiration Rates of Wetlands in Suriname: A Case Study of the Nani Swamp. *Academic Journal of Suriname*, 4, 332-338.

Namugize J. N., Jewitt G., Graham M. (2018) Effects of Land Use and Land Cover Changes on Water Quality in the Mngeni River Catchment, South Africa. *Physics and Chemistry of Earth*, 105:247–264.

Nastos, P. and Matzarakis A. (2012). The effect of air temperature and human thermal indices on mortality in Athens, Greece. *Theoretical Applications in Climatology*, 2012 (108) 591–599.

Nguyen L. H. and Henebry G. M. (Urban Heat Islands as Viewed by Microwave Radiometers and Thermal Time Indices. *Remote Sensing* 2016, 8, 831. Doi:10.3390/rs8100831.

Nichol J. E. and Wong M. S. (2009). High Resolution Remote Sensing of Densely Urbanised Regions: A Case Study of Hong Kong. *Sensors*, *9*, 4695–4708.

Nichol J. E. and Hang T. P. (2012). Temporal Characteristics of Thermal Satellite Images for Urban Heat Stress and Heat Island Mapping. *ISPRS Journal of Photogrammetry and Remote Sensing*, 74, 153-162.

Nieuwenhuijsen M. J (2016). Urban and Transport Planning, Environmental Exposures and Health. New Concepts, Methods and Tools to Improve Health in Cities. *Environmental Health* 2016, 15 (Suppl 1):38 DOI 10.1186/s12940-016-0108-1.

Nieuwolt S. (1966). The Urban Microclimate of Singapore. *The Journal of Tropical Geography* 22**,** 30–37.

Nigeria Bureau of Statistics (NBS, 2012). Annual Abstracts of Statistics (2012). National Bureau of Statistics. Federal Republic of Nigeria.

Niyogi D., Mahmood R. and Adegoke, J. O. (2009). Land Use/Land-Cover Change and Its Impacts on Weather and Climate. *Boundary Layer Meteorology* 133(3), 297-298.

Nnaji A. O., Iro S.I. and Onyekuru S.O (2014). Application of Geographic Information System in the Mapping of Otamiri River Watershed in Owerri, Nigeria. *International Journal of Engineering Sciences*. 3(1) 1-5.

Norton B. A., Coutts A.M., Livesley S.J., Harris R.J., Hunter A.M., and Williams N.S. G (2015). Planning for Cooler Cities: A Framework to Prioritise Green Infrastructure to Mitigate High Temperatures in Urban Landscapes. *Landscape and Urban Planning,* 134, 127-138.

National Population Commission (NPC,2007). Extraordinary Federal Republic of Nigeria Official Gazette, 91 ( 212007), 175-198.

Nwaerema P., Moses O. N (2019). Assessment of Normalized Difference Vegetation Index (NDVI) of Port Harcourt Metropolis and Environs, from 1986 to 2018: Implication to Urban Greening and Management. *Annals of Geographical Studies,* 2(2) 25-34.

Nwanya A. C., Alagbe S. A., and Garba M.L (2019). Evaluation of Total Groundwater Reserves (Water Budget) of Owerri and Environs, Southeastern Nigeria. *International Journal of Advanced Academic Research Sciences, Technology and Engineering*, I5(6) 31-42.

Obeidat M., Awawdeh M., and Lababneh A. (2019). Assessment of Land Use/Land Cover Change and Its Environmental Impacts Using Remote Sensing and GIS Techniques, Yarmouk River Basin, North Jordan. *Arabian Journal of Geosciences* (2019) 12:685, 1-15.

Odindi, J. O. Bangamwabo, V. and Mutanga, O (2015). Assessing the Value of Urban Green Spaces in Mitigating Multi-Seasonal Urban Heat using MODIS Land Surface Temperature (LST) and Landsat 8 data. *International Journal of Environmental Research., 9(1):9-18,*

Ogashawara I. & A Bastos V. S. B. (2012). Quantitative Approach for Analyzing the Relationship between Urban Heat Islands and Land Cover. *Remote Sensing* 2012, (*4*) 3596-3618. Doi:10.3390/rs4113596.

Ogbomida E. T. and Emeribe C. N (2013). Impact of Urbanization on Nwaorie and Otamiri Rivers in Owerri, Imo State, Nigeria. *Advances in Environmental Research*, 2(2) 119-129. DOI: http://dx.doi.org/10.12989/aer.2013.2.2.119.

Ogunbajo, R. A., Ajayi, M. T. A., Usman B. S. and Wali R. I. (2015). Spatial Variations in Residential Property Development in Birnin- Kebbi, Nigeria. *Ethiopian Journal of Environmental Studies & Management* 8(2): 206 – 224.

Ogunjobi K. O, Adamu Y, Akinsanola A.A, Orimoloye I. R. (2018). Spatiotemporal Analysis of Land Use Dynamics and Its Potential Indications on Land Surface Temperature in Sokoto Metropolis, Nigeria. Royal. *Society Open Science*, 5, 1-10.

Oguro Y., Ito S., and Tsuchiya K. (2011). Comparisons of Brightness Temperatures of Landsat-7/ETM+ and Terra/MODIS around Hotien Oasis in the Taklimakan Desert. *Applied and Environmental Soil Science* Volume 2011, 1-11. Doi:10.1155/2011/948135.

Ohashi, Y., Genchi, Y., Kondo, H., Kikegawa, Y., Yoshikado, H., Hirano, Y., (2007). Influence of Air-conditioning Waste Heat on Air Temperature in Tokyo during Summer: Numerical Experiments Using an Urban Canopy Model Coupled with a Building Energy model. *Journal of Applied Meteorology and Climatology* 46, (1) 66-81.

Ohwo O. and Abotutu A. (2015). Environmental Impact of Urbanization in Nigeria. *British Journal of Applied Science & Technology* 9(3): 212-221.

Ojeh V.N., Balogun A.A. and Okhimamhe A. A. (2016). Urban-Rural Temperature Differences in Lagos. *Climate* 2016, 4, 29. Doi:10.3390/cli4020029.

Oke T.R. (1973) City Size and the Urban Heat Island. *Atmospheric Environment* 7: 769-779.

Oke, T.R. (1987). *Boundary Layer Climates*. Second edition Routledge, London.

Oke, T.R., Spronken-Smith R.A. Jauregui E., and Grimmond C.S.B. (1999). The energy Balance of Central Mexico City During the Dry Season, *Atmospheric Environment*, 33:3919–3930.

Oke, T. R. (2004). Initial Guidance to Obtain Representative Meteorological Observations at Urban Sites. Instruments and Methods of Observation Program. Geneva: World Meteorological Organization.

Oke, T. R. (2009). The Need to Establish Protocols in Urban Heat Island Work. 8th Symposium on Urban Environments. Phoenix, Arizona.

Okeahialam, B.N (2016). The Cold Dusty Harmattan: A Season of Anguish for Cardiologists and Patients. *Environmental Health Insights*, 10, 143-146.

Okeke, P. N (2015). An Assessment of two Decades of Land use Changes in Owerri Town Imo State Nigeria. *Sky Journal of Soil Science and Environmental Management*, 4(7), 079 – 086.

Okere K. J., Abu G. O., and Ndukwu B. (2018). Estimation and Characterization of Municipal Solid Waste in Nekede Landfill, Owerri Metropolis, Nigeria. *International Journal of Engineering and Applied Sciences (IJEAS)*, 5(3) 93-100.

Olatoye T. A., Mazinyo S. P., Odeyemi A. S., Orimoloye I. P and Busayo E. T. (2021). Forest Systems Services Provisioning in Africa: Case of Gambari Forest Reserve, Ibadan, Nigeria. *International Journal of Forestry Research* 2021, 1-6.

Omran E. E (2012). Detection of Land-Use and Surface Temperature Change at Different Resolutions. *Journal of Geographic Information System*, 2012, 4, 189-203.

O'Malley C., Piroozfarb P.A.E., Farr E.R.P and Gates J. (2014). An Investigation into Minimizing Urban Heat Island (UHI) Effects: A UK perspective. 6th International Conference on Sustainability in Energy and Buildings, SEB-14. *Energy Procedia* 62, 72-80.

Onyebuchi C., Okeke H., Adeyemi S., Abayomi A., and Olatunji B. (2016). Landuse and Urban Sprawl Assessment of Ibadan Metropolis using Geospatial Techniques. *International Journal of Trend in Research and Development*, 3(6), 395-402.

Opoko, A. P and Oluwatayo, A. (2014). Trends in Urbanization: Implication for Planning and Low-Income Housing Delivery in Lagos, Nigeria. *Architecture Research*, 4 (1A): 15-26.

Orimoogunje, O.O.I, Ekanade, O. and Adesina F. A. (2019). Land use changes and forest reserve management in a changing environment: South-western Nigeria experience. *Journal of Geography and Regional Planning*, 2(11) 283-290.

Oriye O. (2013). Urban Expansion and Urban Land Use in Ado Ekiti, Nigeria. *American Journal of Research Communication*, 1 (2) 128-139.

Ouyang X., Chen D., Duan S., Lei Y., Dou Y., and Hu G. (2017). Validation and Analysis of Long-Term AATSR Land Surface Temperature Product in the Heihe River Basin, China. *Remote Sensing*, 9, 152. Doi:10.3390/rs9020152.

Owolabi J. T. and Adebayo W. O. (2016). The Extent of Urban Forestry in Ado-Ekiti, Nigeria. *Donnish Journal of Geography and Regional Planning*, 2(2) 015-021.

Oyeleye, O I. (2013). Challenges of Urbanization and Urban Growth in Nigeria. *American Journal of Sustainable Cities and Society*, 2 (1) 79-95.

Paranunzio R., Ceola S., Laio F. and Montanari A. (2019). Evaluating the Effects of Urbanization Evolution on Air Temperature Trends Using Nightlight Satellite Data. *Atmosphere*, 10, 117. Doi:10.3390/atmos10030117www

Parham, A. M. and Haghighat, F. (2010). Approaches to Study Urban Heat Island – Abilities and Limitations. *Building and Environment*, 45, 2192-2201.

Patel S. K., Verma P., and Singh G. S. (2019). Agricultural Growth and Land Use Land Cover Change in Peri-Urban India. *Environment Monitoring and Assessment*, (2019) 191: 600.

Pearson, E. S. & Hartley, H.O. (1972) Tables for Statisticians. *Biometrika* Vol 2, University Press, Cambridge.

Peters E. B., McFadden J. P., and Montgomery R. A. (2010). Biological and Environmental Controls on Tree Transpiration in a Suburban Landscape. *Journal of Geophysical Research-Biogeosciences*,115, G04006.

Pettitt, A.N. (1979). A Non-parametric Approach to the Change-Point Problem. *Journal of the Royal Statistical Society*, 28 (2), 126-135.

Polydoros A., Mavrako, T., Cartalis, C. (2018). Quantifying the Trends in Land Surface Temperature and Surface Urban Heat Island Intensity in Mediterranean Cities in View of Smart Urbanization. *Urban Science*, 2, 16, 1-16. Doi:10.3390/urbansci2010016.

Pongracz, R., J. Bartholy J., and Dezso Z. (2006). Remotely Sensed Thermal Information Applied to Urban Climate Analysis. *Advances in Space Research* 37: 2191–2196.

Potgieter J., Nazarian N., Lipson M.J., Hart M. A., Ulpiani G., Morrison W. and Benjamin K. (2021). Combining High Resolution Land Use Data with Crowdsourced Air Temperature to Investigate Intra-Urban Microclimate. *Frontiers in Environmental Science*, 9:720323 1-19. Doi: 10.3389/fenvs.2021.720323.

Prakash A. (2000). Thermal Remote Sensing: Concepts, Issues and Applications. *International Archives of Photogrammetry and Remote Sensing*. Vol. XXXIII, Part B1. Amsterdam 2000. 239-243.

Qin Z. H., Li W., Xu B., Chen Z., Liu J. (2004). *Remote Sensing for Land and Resources*, 3, 28–42.

Qing C, Shuangcheng L, Yanglin W., Jiansheng W., and Miaomiao X. (2013). Spatial process of green infrastructure changes associated with rapid urbanization in Shenzhen, China. *Chinese Geographical Science*, 23(1): 113–128. Doi: 10.1007/s11769-012-0568-3.

Quah, A.K. and Roth M. (2012). Diurnal and Weekly Variation of Anthropogenic Heat Emissions in a Tropical City, Singapore. *Atmospheric Environment*, 46, 92-103.

Quattrochi D.A and Luvall J.C (1997). Application of High-resolution Thermal Infrared Remote Sensing and GIS to Assess the Urban Heat Island Effect. *International Journal of Remote Sensing*, 18 (2) 287—304.

Quegan, S. and Yu, J. J. (2001). Filtering of Multichannel SAR Images. *IEEE Transactions Geoscience and Remote Sensing* 2001, 39, 2373–2379.

Ra P. K., Nathawat M.S., and Onagh M. (2012). Application of Multiple Linear Regression Model through GIS and Remote Sensing for Malaria Mapping in Varanasi District, *India Health Science Journal*, 6 (4)

Rahman, M.N.; Rony, M.R.H.; Jannat, F.A.; Chandra Pal, S.; Islam, M.S.; Alam, E.; Islam, A.R.M.T. (2022). Impact of Urbanization on Urban Heat Island Intensity in Major Districts of Bangladesh Using Remote Sensing and Geo-Spatial Tools. *Climate*, 10, 3,1-32. https://doi.org/ 10.3390/cli10010003.

Redman, C. L., & Jones, N. S. (2005). The Environmental, Social, and Health Dimensions of Urban Expansion. *Population and Environment* 26, 505–520.

Rehman U. R., Kazmi S. J. H., Khanum F., and Samoon Z.A (2015). Analysis of Land Surface Temperature and NDVI Using Geo-SpatialTechnique: A Case Study of Keti Bunder, Sindh, Pakistan. *Journal of Basic & Applied Sciences, 11,* 514-527.

Revi, A., Satterthwaite D.E., Aragón-Durand F., Corfee-Morlot J., Kiunsi R.B.R., Pelling M., Roberts D.C., and Solecki W., (2014). Urban areas. In: Climate Change 2014: Impacts, Adaptation, and Vulnerability. Part A: Global and Sectoral Aspects. Contribution of Working Group II to the Fifth Assessment Report of the Intergovernmental Panel on Climate Change Change [Field, C.B., Barros V.R., Dokken D.J., Mach K.J., Mastrandrea M.D., Bilir T.E., Chatterjee M., Ebi K.L., Estrada Y.O., Genova R.C., Girma B., Kissel E.S., Levy A.N., MacCracken S., Mastrandrea P.R., and White L.L. (eds.)]. Cambridge University Press, Cambridge, United Kingdom and New York, NY, USA, pp. 535-612.

Rey, G., Jougla E., Fouillet A., Pavillon G., Bessemoulin P., Frayssinet P., Clavel J., and Hémon D. (2007). The Impact of Major Heat Waves on All-Cause and Cause-Specific Mortality in France From 1971 to 2003. *International Archives of Occupational and Environmental Health*, 80, 615-626. Doi: 10.1007/s00420-007-0173-4.

Richards J.A (1999). *Remote Sensing Digital Image Analysis*, Springer-Verlag, Berlin, p. 240.

Robine J. M, Cheung S. L. K., Le Roy S., Van Oyen H., Griffiths C. , Michel J. P. (2008). Death Toll Exceeded 70,000 in Europe During the Summer of 2003. *Comptes Rendus Biologies,* 331(2):171–178.

Rosenqvist A., Shimada M., Ito N., and Watanabe M. (2007). ALOS PALSAR: A Pathfinder Mission for Global-scale Monitoring of the Environment. *IEEE Trans. Geoscience and Remote Sensing*, 45, 3307–3316.

Roth M. (2013). Urban Heat Island. *Handbook of Environmental Fluid Dynamics*, Volume Two. Fernando H. J. S (Ed.). CRC Press/Taylor & Francis Group, LLC, 143-159

Roth M. and Chow W.T.L (2012). A Historical Review and Assessment of Urban Heat Island Research in Singapore. *Singapore Journal of Tropical Geography* 33, 381–397. Doi:10.1111/sjtg.12003.

Rowe D. R. (2011). Green Roofs as a Means of Pollution Abatement. *Environmental Pollution* 159, 2100-10.

Roy P. S., Dwivedi R.S and Vijayan D. (2010). *Remote Sensing Applications*. National Remote Sensing Centre, Indian Space Research Organisation (NRSC / ISRO) Dept. of Space, Government of India, Balanagar, Hyderabad.

Roy P. S. and Roy A. (2010). Land Use and Land Cover Change in India: A Remote Sensing and GIS Perspective. *Journal of the Indian Institute of Science*, 90:4, 489-502.

Rozenstein O., Qin Z., Derimian Y., and Karnieli A. (2014). Derivation of Land Surface Temperature for Landsat-8 TIRS Using a Split Window Algorithm. *Sensors*, *14*, 5768-5780. Doi:10.3390/s140405768.

Rusticucci, M., N. Zazulie, and Raga G. B. (2014). Regional Winter Climate of the Southern Central Andes: Assessing the Performance of ERA-Interim for Climate Studies. *Journal of Geophys. Res. Atmos*, 119, 8568–8582, doi:https://doi.org/10.1002/2013JD021167.

Saaroni, H., Ben-Dor, E., Bitan, A. & Potchter, O. (2000). Spatial distribution and microscale characteristics of the urban heat island in Tel-Aviv, Israel. Landscape and Urban Planning, 48, 1-18.

Sabel C.E., Hiscock R., Asikainen A., Bi J., Depledge M., Elshout S.V. Friedrich R., …. Willers S. (2016). Public Health Impacts of City Policies to Reduce Climate Change: Findings from the URGENCHE EU-China project. *Environmental Health* 2016, 15 (Suppl 1):25, 5-21.

Shapiro, S.S. (1980). How to Test Normality and other Distributional Assumptions. In: The ASQC Basic References in Quality Control. *Statistical Techniques*, 1980, 3, 1–78

Shapiro, S.S. & Wilk, M.B. (1965). An Analysis of Variance Test for Normality (complete samples), *Biometrika*, 52 (3–4): 591–611.

Sen, P. K. (1968). Estimates of the regression coefficient based on Kendall's tau. *Journal of American Statistics Association*. 63(324), 1379-1389.

Şahin, M., Yildiz, B.Y., Şenkal, O., Peştemalci, V. (2011). Modelling and Remote Sensing of Land Surface Temperature in Turkey. *Journal of Indian Society of Remote Sensing*, 1 (*40*) 399–409.

Sailor D., Shepherd M., Sheridan S., Stone B., Kalkstein L., Russell A., Vargo J., and Andersen T. (2016). Improving Heat-Related Health Outcomes in an Urban Environment with Science-Based Policy. *Sustainability* 2016, 8, 1015; Doi:10.3390/su8101015.

Saitoh, T.S., Shimada T., and Hoshi H. (1996). Modeling and Simulation of the Tokyo Urban Heat Island, *Atmospheric Environment*, 30:3431–3442.

Saleh S. A. H (2010). Remote Sensing and GIS Techniques for Urban Growth Monitoring of Basarah City. *International Journal of Remote Sensing and Earth Sciences*, 7: 73-83.

Sameen M. I. and Al Kubaisy M.A. (2014). Automatic Surface Temperature Mapping in ArcGIS using landsat- 8 TIRS and ENVI Tools, Case Study: Al Habbaniyah Lake. *Journal of Environment Earth Science*, *4*, 12–17.

Santamouris, M., Papanikolaou, N., Livada, I., Koronakis, I., Georgakis, C., Argiriou, A., and Assimakopoulos, D.N. (2001). On the Impact of Urban Climate on the Energy Consumption of Buildings. *Solar Energy* 70 (3), 201–216.

Sarrat C., Lemonsu A., Masson V. and Guedalia D. (2006). Impact of Urban Heat Island on Regional Atmospheric Pollution. *Atmospheric Environment,* 40 (2006) 1743–1758.

Satterthwaite, D., G. McGranahan, and C. Tacoli (2010). Urbanization and its implications for food and farming. *Philosophical Transactions of the Royal Society* B, 365(1554), 2809-2820.

Schatz J. and Kucharik C. J. (2015). Urban Climate Effects on Extreme Temperatures in Madison, Wisconsin, USA. *Environmental Research Letters* 10(2015)094024. Doi:10.1088/1748-9326/10/9/094024.

Senanayake I., Welivitiya W. and Nadeeka P. (2014) Remote Sensing Based Analysis of Urban Heat Islands with Vegetation Cover in Colombo City, Sri Lanka using Landsat-7 ETM+ data. *Urban Climate, 5,19–35.*

Seto, K. C. (2009). Global urban issues: A Primer in Global Mapping of Human Settlement: Experiences, Datasets, and Prospect; Gamba, P., Herold, M., Eds.; Taylor and Francis Group: CRC Press: Boca Raton, FL, USA, 2009; 3–9.

Seto, K.C., Güneralp, B., Hutyra, L.R., (2012). Global Forecasts of Urban Expansion to 2030 and Direct Impacts on Biodiversity and Carbon Pools. *Proceedings of National. Academy of Science,* 109, 16083–16088.

Seun A. I., Ayodele A. P, Koji D., Akande S.O (2022). The Potential Impact of Increased Urbanization on Land Surface Temperature over South-West Nigeria. *Current Research in Environmental Sustainability* 4, 100142, 1-10.

Shen L., Guo., X and Xiao K. (2015). Spatiotemporally Characterizing Urban Temperatures Based on Remote Sensing and GIS Analysis: A Case Study in the City of Saskatoon (SK, Canada). *Open Geoscience; 7:27–39.*

Sherwood S.C. and Huber M. (2010). An Adaptability Limit to Climate Change Due to Heat stress *Proceedings of National Academy of Science*, USA 107, 9552–9555.

Shukla K. N., Potnis A., and Dwivedy (2017). A Review on Image Enhancement Techniques. *International Journal of Engineering and Applied Computer Science (IJEACS)*, 2 (7) 232-235.

Silva F. B., Longo K. L., and Andrade F. M. (2017). Spatial and Temporal Variability Patterns of the Urban Heat Island in São Paulo. *Environments* 2017, 4, 27. Doi:10.3390/environments4020027.

Singh, R. B., Grover, A., and Zhan J. (2014). Inter-Seasonal Variations of Surface Temperature in the Urbanized Environment of Delhi Using Landsat Thermal Data *Energies 2014, 7, 1811-1828*; doi:10.3390/en7031811

Singh R. P., Singh N., Singh S., Mukherjee S. (2016). Normalized Difference Vegetation Index (NDVI) Based Classification to Assess the Change in Land Use/Land Cover

(LULC) in Lower Assam, India. *International Journal of Advanced Remote Sensing and GIS*, 5(10) 1963-1970.

Skoulikaris C., Anagnostopoulou C. and Lazoglou G. (2020). Hydrological Modeling Response to Climate Model Spatial Analysis of a South Eastern Europe International Basin. *Climate*, 8(1) 1-17. Doi:10.3390/cli8010001.

Smith C.; Webb, A.; Levermore, G. J.; Lindley, S. J.; and Beswick, K. (2011). Fine-scale Spatial Temperature Patterns across a UK Conurbation. *Climate Change* 109, 269–286.

Sobrino J. A., Jiménez-Muñoz, J. C., and Paolini, L. (2004). Land Surface Temperature Retrieval from LANDSAT TM *5*. *Remote Sensing Environment*, 90 (4): 434-440.

Sobrino J. A., Jiménez-Muñoz J. C., Zarco-Tejada P. J., Sepulcre-Cantó G. and de Miguel E. (2006). Land surface temperature derived from airborne hyperspectral scanner thermal infrared data. *Remote Sensing of Environment* 102, 99– 115

Sobrino J. A., Jiménez-Muñoz J.C., Sòria G., Romaguera R. and Guanter L. (2008). Land Surface Emissivity Retrieval from Different VNIR and TIR Sensors. *IEEE Transactions on Geoscience and Remote Sensing*, 46 (2) 316-327.

Sobrino J. A., Jime´nez-Mun˜ oz J. C. , Zarco-Tejada P. J., Sepulcre-Canto´ G., de Miguel E., So`ria G., Romaguera M., Julien y. (2009). Thermal remote sensing from Airborne Hyperspectral Scanner Data in the Framework of the SPARC and SEN2FLEX Projects: an overview. *Hydrological Earth System Science*, 13, 2031–2037.

Sobrino, J.A.; Oltra-Carrió, R.; Sòria, G.; Jiménez-Muñoz, J.C.; Franch, B.; Hidalgo, V.; Mattar, C.; Julien, Y.; Cuenca, J.; Romaguera, M.; *et al*. (2013). Evaluation of the Surface Urban Heat Island Effect in the City of Madrid. *International Journal of Remote Sensing*, 34, 3177–3192.

Solecki W.D. and Rosenzweig C. (2004). Biodiversity, biosphere reserves, and the Big Apple: A Study of the New York Metropolitan Region. *Annals of the New York Academy of Sciences*, 1023, 105-124.

Song B. & Park K. (2021). Temperature Trend Analysis Associated with Land-Cover Changes Using Time-Series Data (1980–2019) from 38 Weather Stations in South Korea. *Sustainable Cities and Society*, 65, 102615

Sòria G. and Sobrino, J.A. (2007). ENVISAT/AATSR Derived Land Surface Temperature over a Heterogeneous Region. *Remote Sensing of Environment*, 111, 409–422.

Srivanit M. and Hokao (2012). Thermal Infrared Remote Sensing for Urban Climate and Environmental Studies: An Application for the City of Bangkok, Thailand. *JARS* 9 (1) 84-100.

Srivanit M., Hokao K. and Phonekeo V. (2012). Assessing the Impact of Urbanization on Urban Thermal Environment: A Case Study of Bangkok Metropolitan. *International Journal of Applied Science and Technology*, 2 (7) 243-256.

Srivastava P.K., Majumdar T.J., Bhattacharya A. K. (2010). Study of Land Surface Temperature and Spectral Emissivity using Multi-sensor Satellite Data. *Journal of Earth System Science* 119 (1) 67–74.

Stathopoulou M., Cartalis C, and Keramitsoglou I (2004). Mapping Micro-urban Heat Islands using NOAA/AVHRR Images and CORINE Land Cover: An Application to Coastal Cities of Greece. *International Journal of Remote Sensing*, 25(12) 2301–2316.

Stone, B. and Norman, J. M. (2006). Land Use Planning and Surface Heat Island Formation: A Parcel-Based Radiation Flux Approach. *Atmospheric Environment* 40, 3561–3573. Doi:10.1016/j.atmosenv.2006.01.015.

Streutker, D.R. (2003). Satellite-measured Growth of the Urban Heat Island of Houston, Texas, *Remote Sensing of Environment*, 85:282–289.

Sohail M. T., Manzoor Z., Ehsan M., Al-Ansari N., Khan M.B., Shafi A., Ullah J., Hussain A., Raza D., Usman U., Akbar S., and Elbeltagi A. (2023), Impacts of Urbanization, LULC, LST, and NDVI Changes on the Static Water Table with Possible Solutions and Water Policy Discussions: A case from Islamabad, Pakistan. *Frontiers in Environmental Science*, 11:1018500. Doi: 10.3389/fenvs.2023.1018500.

Subarna D. (2017). Analysis of Long-Term Temperature Trend as an Urban Climate Change Indicator. *Forum Geografi*, 31 (2) 196-208.

Suresh S., Suresh A. V., and Mani. K. (2014). Estimation of Land Surface Temperature of High Range Mountain Landscape of Devikulam Taluk Using Landsat 8 Data. *International Journal of Research in Engineering and Technology* (IJRET), 5 (1)92-96.

Swanwick C., Dunnett N., and Woolley H. (2003). Nature, Role and Value of Green Spaces in Towns and Cities: An Overview. *Built Environment* 29 (2):94–106.

Szymanowski M., and Kryza M. (2009). GIS-based Techniques for Urban Heat Island Spatialization. *Climate Research*, 38, 171–187.

Tanaji P. P., Ajit C. V., & Vishnu D. S. (2021). Urban weather assessment using LST, NDBI and NDVI of Kolhapur city, Maharashtra. *Disaster Advances* 14 (4) 76-84

Tanko I. A, Suleiman Y. M., Yahaya T. I. and Kasim A. A. (2017). Urbanization Effect on the Occurrence of Urban Heat Island over Kano Metropolis, Nigeria. *Journal of Scientific & Engineering Research* 8 (9),293-299.

Tewabe D. and Fentahun T. (2020) Assessing Land Use and Land Cover Change Detection Using Remote Sensing in the Lake Tana Basin, Northwest Ethiopia. *Cogent Environmental Science*, 6:1, 1778998, 1-11. DOI: 10.1080/23311843.2020.1778998.

Tomlinson, C.J.; Chapman, L.; Thornes, J.E.; Baker, C. J (2011). Remote Sensing Land Surface Temperature for Meteorology and Climatology: A Review. *Meteorological Applications*, 18, 296–306. Doi:10.1002/met.287.

Tomlinson C. J.; Chapman L.; Thornes J.E.; and Baker C. J (2011b). Including the Urban Heat Island in Spatial Heat Health Risk Assessment Strategies: A Case Study for Birmingham, UK. *International Journal of Health Geographics* 2011, 10:42.

Tomlinson, C.J.; Chapman, L.; Thornes, J.E.; Baker, C.J. (2012). Derivation of Birmingham's Summer Surface Urban Heat Island from MODIS Satellite Images. *International Journal of Climatology* 2012, (32) 214–224.

Trotter L. Dewan A., & Robinson T. (2017). Effects of Rapid Urbanization on the Urban Thermal Environment between 1990 and 2011 in Dhaka Megacity, Bangladesh *AIMS Environmental Science* 4 (1): 145- 167.

Tsin P. K., Knudby A., Krayenhoff, E. S., Ho H. C., Brauer M., and Henderson S. B (2016). Microscale Mobile Monitoring of Urban Air Temperature. *Urban Climate* 18 (2016) 58–72.

Tzoulas K., Korpela K., Venn S., Yli-Pelkonen V., Kazmierczak A., Niemela J., and James P. (2007). Promoting Ecosystem and Human Health in Urban Areas using Green Infrastructure: A Literature Review. *Landscape and Urban Planning*, 81 (3) 167-78.

Ukaegbu, K. O. E., Iwuji M. Uche C. C., Osumgborogwu, I. E. and Amangabara G. T. (2017). Spatial Assessment of Temperature and Land Cover Change as Climate Change Monitoring Strategies in Owerri, Nigeria. *Journal of Geography, Environment and Earth Science International*, 11(1) 1-9.

Ukoje J. E. (2016). Impacts of rapid urbanization in the urban fringe of Lokoja. *Nigeria Journal of Geography and Regional Planning*, 9 (10) 185-194, DOI: 10.5897/JGRP2016.0591.

United Nations (2010). Department of Economic and Social Affairs. Population Division. World Urbanisation Prospects. The 2009 Revision. CD-ROM.

United Nations (2010b) World Population Prospects: The 2010 Revision.

United Nations (2014) World urbanization prospects: the 2014 revision highlights (ST/ESA/SER. A/352). UN Department of Economic and Social Affairs Population Division.

United Nations (UN, 2018). World Urbanization Prospects: The 2018 Revision. Department of Economic and Social Affairs, Population Division, United Nations, New York.

United Nations (UN, 2020). World Population Prospects. https://www.macrotrends.net/cities/22015/owerri/population'>Owerri, Nigeria Metro Area Population 1950-2020</a>. www.macrotrends.net. Retrieved 2020-06-06.

UN DESA Population Division (2012). World Urbanization Prospects: The 2011 Revision. United Nations Department of Economic and Social Affairs (UN DESA) Population Division, New York, NY, USA, esa.un.org/unpd/wup/index.htm.

United Nations Development Project (UNDP, 2016). Sustainable Urbanization Strategy: UNDP's Support to Sustainable, Inclusive and Resilient Cities in the Developing World. United Nations Development Programme. New York, USA

UN-Habitat (2012). State of the World's Cities 2012/2013. Prosperity of Cities. Nairobi Kenya.

United State Geological Survey (USGS 2016). Landsat 8 (L8) Data Users Handbook

van Hove, L.W.A., Jacobs, C.M.J., Heusinkveld B.G., Elbers J.A., van Driel B.L., and Holtslag A.A. M (2015). Temporal and Spatial Variability of Urban Heat Island and Thermal Comfort within the Rotterdam Agglomeration. *Building and Environment* 83, 91-103.

Van, T.T. and Bao H.D.X (2015). Characteristics of Urban Thermal Environment from Satellite Remote Sensing Data in Ho Chi Minh City, Vietnam. Conference Proceeding Paper. 1st International Electronic Conference on Remote Sensing 22 June – 5 July 2015.

Vardoulakis S. and Heaviside, C. (2012). Health Effects of Climate Change in the UK 2012– Current Evidence, Recommendations and Research Gaps. Health Protection Agency. Centre for Radiation, Chemical and Environmental Hazards. London, UK 2012

Vardoulakis S., Dear K, Hajat S., Heaviside C., Eggen B, McMichael A.J. (2014). Comparative Assessment of the Effects of Climate Change on Heat-and Cold-related Mortality in the United Kingdom and Australia. *Environmental Health Perspectives*; 122(12)1285–92.

Vida, S., Durocher M., Ouarda T.B.M.J., and Gosselin P. (2012). Relationship between Ambient Temperature and Humidity and Visits to Mental Health Emergency Departments in Québec. *Psychiatric Services*, 63, 1150-1153.

Villeneuve P. J., Jerrett M., Su J. G., Burnett R. T., Chen H., Wheeler A. J, .... (2012). A Cohort Study Relating Urban Green Space with Mortality in Ontario, Canada. *Environmental Research*, 115:51–58.

Vineis P. (2010). Climate Change and the Diversity of Its Health Effects. *International Journal of Public Health* 55, 81– 82.

Voogt J. A. (2002). Urban Heat Island, *Encyclopaedia of Global Environmental Change, Vol. 3* (T. Munn, Editor), John and Wiley Sons, Chichester, 660–666.

Voogt, J. A. and Oke, T. R. (2003). Thermal Remote Sensing of Urban Climates. *Remote Sensing of Environment*, 86 (3) 370–384.

Vose R. S., S. Applequist M. J., Menne, Williams C. N. and Thorne P. (2012). An Intercomparison of Temperature Trends in the U.S. Historical Climatology Network and Recent Atmospheric Reanalyses. *Geophysical Research Letters*, 39, L10703, doi:https://doi.org/10.1029/2012GL051387

Wagner T. J., Klein P. M., and Turner D. D. (2019). A New Generation of Ground-Based Mobile Platforms for Active and Passive Profiling of the Boundary Layer. *American Meteorological Society*, 137–153. https://doi.org/10.1175/BAMS-D-17-0165.1

Walsund E. (2013). Geographical Information Systems as a Tool in Sustainable Urban Development Unpublished Master Thesis in Built Environment. Department of Urban Studies, Faculty of Culture and Society, Malmö University.

Walawender J. P., Szymanowski M., Hajto M.J and Bokwa A (2014). Land Surface Temperature Patterns in the Urban Agglomeration of Krakow (Poland) Derived from Landsat-7/ETM+ Data. *Pure and Applied Geophysics* 171, 913–940.

Walton D. and Hall A. (2018). An Assessment of High-Resolution Gridded Temperature Datasets over California. *Journal of Climate*, 31(10) 3789–3810.

Wan Z., Zhang Y., and Zhang Q. (2004). Quality Assessment and Validation of the MODIS Global Land Surface Temperature. *International Journal of Remote Sensing* 25 (1) 261–274.

Wang, K. C., Wang, J.K., Wang P. C., Sparrow, M., Yang J. and Chen H. B. (2007). Influences of Urbanization on Surface Characteristics as Derived from the Moderate-Resolution Imaging Spectroradiometer: A Case Study for the Beijing Metropolitan Area. *Journal of Geophysical Research* 112. Doi:10.1029⁄2006JD007997.

Wang, X., Lavigne E., Ouellette-kuntz H., and Chen B.E., (2014). Acute Impacts of Extreme Temperature Exposure on Emergency Room Admissions Related to Mental and Behaviour Disorders in Toronto, Canada. *Journal of Affective Disorders*, 155, 154-161.

Wang F., Qin Z., Li W., Song C., Karnieli A., and Zhao (2015). An Efficient Approach for Pixel Decomposition to Increase the Spatial Resolution of Land Surface Temperature Images from MODIS Thermal Infrared Band Data. *Sensors* 2015, *15*, 304-330; doi:10.3390/s150100304.

Wang J., Zhan Q. and Guo H. (2016). The Morphology, Dynamics and Potential Hotspots of Land Surface Temperature at a Local Scale in Urban Areas. *Remote Sensing* 2016 (8) 18

Wang, W., P. Xie, S.-H. Yoo, Y. Xue, A. Kumar, and Wu X (2011). An Assessment of the Surface Climate in the NCEP Climate Forecast System Reanalysis. *Climate Dynamics* 37, 1601–1620.

Ward T. C., Roe J., Aspinall P., Mitchell R., Clow A., Miller D. (2012). More Green Space is Linked to Less Stress in Deprived Communities: Evidence from Salivary Cortisol Patterns. *Landscape Urban Planning*, 105:221–229.

Weeks J.R. (2013). New Forms of Urbanization: Beyond the Urban-Rural Dichotomy Champion T. and Hugo G. (Eds). Aldershot, UK: Ashgate Publishing Co., 2003. A Publication of the International Union for the Scientific Study of Population.

Weng Q. (2003). Fractal Analysis of Satellite-detected Urban Heat Island Effect. *Photogrammetric Engineering and Remote Sensing*, 69 (5), 555–566

Weng Q., Lu D., Schubring J. (2004). Estimation of Land Surface Temperature– Vegetation Abundance Relationship for Urban Heat Island Studies. *Remote Sensing of Environment* 89, 467 – 483. Doi:10.1016/j.rse.2003.11.005.

Weng Q. & Yang S. (2004). Managing the Adverse Thermal Effects of Urban Development in a Densely Populated Chinese City. *Journal of Environmental Management*, 70**,** 145-56.

Weng Q., and D. Quattrochi (2006). Thermal Remote Sensing of Urban areas: An Introduction to the Special Issue, *Remote Sensing of Environment*, 104 (2):119–122.

Weng Q. (2009). Thermal Infrared Remote Sensing for Urban Climate and Environmental Studies: Methods, Applications, and Trends. *ISPRS Journal of Photogrammetry and Remote Sensing*, 64 (4) 335–344.

Wheatley. P (1971). *The Pivot of the Four Quarters.* The University of Chicago Press, Chicago.

Wilhelmi O.V., Purvis K. L., and Harriss R. C. (2004). Designing a Geospatial Information Infrastructure for Mitigation of Heat Wave Hazards in Urban Areas. *Natural Hazards Review*, 5 (3) 147-158.

World Bank (2008). World Development Report 2009: Reshaping Economic Geography. The International Bank for Reconstruction and Development / The World Bank, Washington DC, USA, 383 pp.

Wu J., Xiang W., and Zhao J. (2014). Urban Ecology in China: Historical Developments and Future Directions. *Landscape and Urban Planning* 125 (2014) 222–233.

Wu, J. G. (2008). Making the Case for Landscape Ecology: An Effective Approach to Urban Sustainability. *Landscape Journal* 27(1), 41–50.

Wu Q. S.; Liu H. X.; Wang L.; Deng, C.B. (2016). Evaluation of AMSR2 Soil Moisture Products over the Contiguous United States using In Stu Fata from the International

Soil Moisture Network. *International Journal of Applied Earth Observation and Geoinformatics*, 45, 187–199.

Wubie M. A., Assen M., and Nicolau M. D (2016). Patterns, Causes and Consequences of Land Use/Cover Dynamics in the Gumara Watershed of Lake Tana Basin, North-western Ethiopia. *Environmental System Research*, 5:8, 1-12. DOI 10.1186/s40068-016-0058-1.

Xiao R., Weng Q., Ouyang Z., Li W., Schienke E.W and Zhang Z. (2008). Land Surface Temperature Variation and Major Factors in Beijing, China. *Photogrammetric Engineering and Remote Sensing*, 74 (4), 451–461.

Xie, Q and Zhou, Z. (2015). Impact of Urbanization on Urban Heat Island Effect Based on TM Imagery in Wuhan, China *Environmental Engineering and Management Journal* 14(3), 647-655.

Xiong, Y.; Huang, S.; Chen, F.; Ye, H.; Wang, C.; Zhu, C. (2012). The Impacts of Rapid Urbanization on the Thermal Environment: A Remote Sensing Study of Guangzhou, South China. *Remote Sensing*, *4*, 2033–2056.

Xu, W., Wooster, M.J., Grimmond, C.S.B (2008). Modelling of Urban Sensible Heat flux At Multiple Spatial Scales: A Demonstration Using Airborne Hyperspectral Imagery of Shanghai and A Temperature–Emissivity Separation Approach. *Remote Sensing of Environment* 112, 3493–3510.

Yadav S. K., Raj S. and Roy S. S (2013). Remote Sensing Technology and Its Applications. *International Journal of Advancements in Research & Technology,* 2 (10) 25-30.

Yang C., He X., Yan F., Yu L., Bu K., Yang J., Chang L., and Zhang S. (2017). Mapping the Influence of Land Use/Land Cover Changes on the Urban Heat Island Effect—A Case Study of Changchun, China. *Sustainability* 2017 (9) 312. Doi:10.3390/su9020312.

Yang J., Gong P., Fu R., Zhang M., Chen J., Liang S., Xu B., Shi J., and Dickinson R. (2013). The Role of Satellite Remote Sensing in Climate Change Studies. Nature climate Change 1-15. Doi: 10.1038/NCLIMATE1908. Accessed online from www.nature.com/natureclimatechange on 23 December, 2016.

Yasutomi N., Hamada A. and Yatagai A. (2011). Development of a Long-term Daily Gridded Temperature Dataset and Its Application to Rain/Snow Discrimination of Daily. *Global Environmental Research,* AIRIES 15/2011: 165-172.

Yow D.M. (2007). Urban heat islands: Observations, Impacts, and Adaptation. *Geography Compass* 1 (6), 1227–1251.

Yu X., Guo X., and Wu Z. (2014). Land Surface Temperature Retrieval from Landsat 8 TIRS—Comparison between Radiative Transfer Equation-Based Method, Split Window Algorithm and Single Channel Method. *Remote Sensing* 2014, *6*, 9829-9852; Doi:10.3390/rs6109829.

Yuan, F. and Bauer, M.E. (2007). Comparison of Impervious Surface Area and Normalized Difference Vegetation Index as Indicators of Surface Urban Heat Island Effects in Landsat Imagery. *Remote Sensing of Environment* 106 (2007) 375–386.

Yue W., XU J., Tan W., and Xu. L. (2007). The relationship between land surface temperature and NDVI with remote sensing: application to Shanghai Landsat 7 ETM+ data. *International Journal of Remote Sensing*, 28 (15), 3205–3226.

Zaitunah A. and Sahara S. F. (2021). Mapping and Assessment of Vegetation Cover Change and Species Variation in Medan, North Sumatra. *Heliyon* 7(7) E07637, 1-8.

Zander, K. K.; Botzen, W. J. W.; Oppermann, E.; Kjellstrom, T.; and Garnett, S.T. (2015). Heat stress Causes Substantial Labour Productivity Loss in Australia. *Natural Climate Change* 2015, (5) 647–651.

Zha, Y.; Gao, J.; Ni, S. (2005). Use of Normalized Difference Built-up Index in Automatically Mapping Urban Areas from TM imagery. *International Journal of Remote Sensing*, 24, 583–594.

Zhan W., Chen, Y. Zhou J., Wang J., Liu W., Voogt J., Zhu X., Quan J., and Li J. (2013). Disaggregation of Remotely Sensed Land Surface Temperature: Literature Survey, Taxonomy, Issues, and Caveats. *Remote Sensing of the Environment*, (131,119–139.

Zhang, Q., H. Körnich, and Holmgren K. (2013). How Well Do Reanalyses Represent the Southern African Precipitation? *Climate Dynamics*, 40, 951–962, doi:https://doi.org/10.1007/s00382-012-1423-z.

Zhang P. (2015). Spatiotemporal Features of the Three-Dimensional Architectural Landscape in Qingdao, China. *PLoS ONE* 10(9): e0137853. Doi:10.1371/journal.pone.0137853.

Zhang X., Fried M. A., Schaaf C. B., Strahler A. H. and Schneider A. (2014). The Footprint of Urban Climates on Vegetation Phenology. *Geophysical Research Letters* 31. DOI: 10.1029/2004GL020137.

Zhang, Y., Odeh, I.O.A. and Han, C. (2009). Bi-temporal Characterization of Land Surface Temperature in Relation to Impervious Surface Area, NDVI and NDBI, using a Sub-pixel Image Analysis. *International Journal of Applied Earth Observation and Geoinformation*, 11, 256–264.

Zhao P., Gao L., Jianhui W., Ma M., Deng H. Gao J. and Chen X. (2020). Evaluation of ERA-Interim Air Temperature Data over the Qilian Mountains of China. *Advances in Meteorology*, 2020, Article ID 7353482, 1-11.

Zhou, J., Chen, Y. H. Li, J. Weng, Q. H. and Yi W. B. (2008). A Volume Model for Urban Heat Island Based on Remote Sensing Imagery and its Application: A Case Study in Beijing. *Journal of Remote Sensing* 12: 734–742.

Zhou, J., Chen Y, Wang J., and Zhan W. (2011). Maximum Night-time Urban Heat Island (UHI) Intensity Simulation by Integrating Remotely Sensed Data and Meteorological

Observations. *IEEE Journal of Selected Topics in Applied Earth Observations and Remote Sensing* 4: 138–146.

Zhou J., Chen Y., Zhang X., and Zhan W. (2013) Modelling the Diurnal Variations of Urban Heat Islands with Multi-source Satellite Data, *International Journal of Remote Sensing, 34:21, 7568-7588,* DOI: 10.1080/01431161.2013.821576.

Zhou, D.; Zhang, L.; Hao, L.; Sun, G.; Liu, Y and Zhu, C. (2016). Spatiotemporal Trends of Urban Heat Island Effect along the Urban Development Intensity Gradient in China. *Science of the Total Environment* 544 (2016) 617–626.

Zhu S.; Guan H.; Millington A.C.; Zhang G. (2013). Disaggregation of land surface temperature over a heterogeneous urban and surrounding suburban area: A case study in Shanghai, China. *International Journal of Remote Sensing* 2013, *34*, 1707–1723.

Zipper S., Schatz J., Singh A., Kucharik C., Townsend P. A., and LoheideII S. P. (2016). Urban Heat Island Impacts on Plant Phenology: Intra-urban Variability and Response to Land Cover. *Environmental Research Letters* 11(2016)054023. Doi:10.1088/1748-9326/11/5/054023.

Zoran M. (2011). Satellite Observation of Urban Heat Island Effect. *Proceedings of the Global Conference on Global Warming* 2011 11-14 July, 2011, Lisbon, Portugal.

Zupancic T., Westmacott C., and Bulthuis M. (2015). The Impact of Green Space on Heat and Air Pollution in Urban Communities: A Meta-narrative Systematic Review. David Suzuki Foundation, Canada, Vancouver B.C.

# APPENDICES

## Appendix A 1 Coordinates of Sample Points for Owerri

| S/N | Feature (LULC) | Lat. | Long. | S/N | Feature (LULC) | Lat. | Long. |
|---|---|---|---|---|---|---|---|
| 1 | Bare Surface | 5.46533 | 7.07518 | 34 | Forest Cover | 5.473039 | 7.041181 |
| 2 | Light Vegetation | 5.46534 | 7.07537 | 35 | Bare Surface | 5.473378 | 7.049872 |
| 3 | Agricultural land | 5.46513 | 7.07527 | 36 | Bare Surface | 5.470004 | 7.029702 |
| 4 | Agricultural land | 5.46494 | 7.07508 | 37 | Built Up | 5.470895 | 7.033708 |
| 5 | Light Vegetation | 5.46499 | 7.07517 | 38 | Built Up | 5.469546 | 7.02674 |
| 6 | Agricultural land | 5.46412 | 7.07519 | 39 | Bare Surface | 5.46844 | 7.033264 |
| 7 | Thick Vegetation | 5.46233 | 7.07456 | 40 | Built Up | 5.368029 | 7.005325 |
| 8 | Light Vegetation | 5.46242 | 7.07448 | 41 | Forest Cover | 5.365709 | 7.012705 |
| 9 | Bare Surface | 5.46154 | 7.07407 | 42 | Bare Surface | 5.362098 | 7.011231 |
| 10 | Bare Surface | 5.46274 | 7.07218 | 43 | Bare Surface | 5.380063 | 6.997097 |
| 11 | Bare Surface | 5.46262 | 7.07226 | 44 | Thick Vegetation | 5.381839 | 7.002201 |
| 12 | Bare Surface | 5.47758 | 7.06884 | 45 | Forest Cover | 5.376003 | 6.979951 |
| 13 | Water Body | 5.465217 | 7.06997 | 46 | Water Body | 5.378106 | 6.981661 |
| 14 | Bare Surface | 5.47678 | 7.14303 | 47 | Bare Surface | 5.37435 | 6.976538 |
| 15 | Bare Surface | 5.474531 | 7.127077 | 48 | Built Up | 5.404729 | 6.970064 |
| 16 | Forest Cover | 5.489637 | 7.145844 | 49 | Farmland | 5.404651 | 6.967412 |
| 17 | Agricultural land | 5.487121 | 7.129159 | 50 | Thick Vegetation | 5.409891 | 6.963892 |
| 18 | Built Up | 5.477361 | 7.124337 | 51 | Built Up | 5.445873 | 6.962909 |
| 19 | Bare Surface | 5.471672 | 7.139487 | 52 | Forest Cover | 5.444535 | 6.962609 |
| 20 | Forest Cover | 5.49567 | 7.131887 | 53 | Light Vegetation | 5.487703 | 7.012364 |
| 21 | Light Vegetation | 5.485743 | 7.090795 | 54 | Built Up | 5.489303 | 7.016731 |
| 22 | Built Up | 5.494851 | 7.086001 | 55 | Forest Cover | 5.484381 | 7.009179 |
| 23 | Forest Cover | 5.504095 | 7.108276 | 56 | Thick Vegetation | 5.536924 | 6.97646 |
| 24 | Bare Surface | 5.51974 | 7.061865 | 57 | Forest Cover | 5.514376 | 6.978298 |
| 25 | Light Vegetation | 5.521701 | 7.072176 | 58 | Light Vegetation | 5.515701 | 6.975298 |
| 26 | Bare Surface | 5.515832 | 7.053697 | 59 | Bare Surface | 5.517596 | 6.98111 |
| 27 | Bare Surface | 5.47758 | 7.06884 | 60 | Built Up | 5.516976 | 6.98107 |
| 28 | Bare Surface | 5.48008 | 7.05491 | 61 | Built Up | 5.517075 | 7.019761 |
| 29 | Light Vegetation | 5.48416 | 7.05377 | 62 | Forest Cover | 5.501632 | 7.017419 |

## Appendix A 2 Coordinates of Sample Points for Kano

| Lat | Long | Location_Feature |
|---|---|---|

| | | |
|---|---|---|
| 12.11556 | 8.660492 | Water body |
| 11.9685 | 8.524282 | Thick vegetation |
| 11.9673 | 8.525878 | Thick vegetation |
| 11.96831 | 8.523694 | Bare Surface |
| 11.97127 | 8.526096 | Built Up |
| 11.97281 | 8.525096 | Agricultural Land |
| 12.00692 | 8.514679 | Built Up |
| 12.01497 | 8.512146 | Built Up |
| 12.05045 | 8.536135 | Light Vegetation |
| 12.04725 | 8.531594 | Light Vegetation |
| 12.04937 | 8.527986 | Bare Surface |
| 11.96395 | 8.471813 | Bare Surface |
| 11.98354 | 8.468001 | water body |
| 11.98439 | 8.467811 | Light Vegetation |
| 11.98561 | 8.468958° | Agricultural Land |
| 11.9861 | 8.468644 | Light Vegetation |
| 11.99828 | 8.553832 | Bare Surface |
| 11.9984 | 8.558875 | Built Up |
| 11.99869 | 8.559514 | Light Vegetation |
| 12.00028 | 8.55956 | Light Vegetation |
| 12.0045 | 8.560162 | Light Vegetation |
| 12.00766 | 8.559359 | Thick vegetation |
| 12.00782 | 8.558491 | Agricultural Land |
| 12.04537 | 8.519893 | Built Up |
| 12.06139 | 8.545934 | Built Up |
| 12.04063 | 8.5312 | Thick vegetation |
| 12.03992 | 8.53172 | Bare Surface |
| 12.05518 | 8.486676 | Built Up |
| 12.06589 | 8.558551 | Agricultural Land |
| 12.06264 | 8.562201 | Agricultural Land |
| 12.02289 | 8.536798 | Built Up |
| 12.02223 | 8.540711 | Bare Surface |

Appendix B: Landuse/Landcover classified images of the four cities from 2000 - 2010

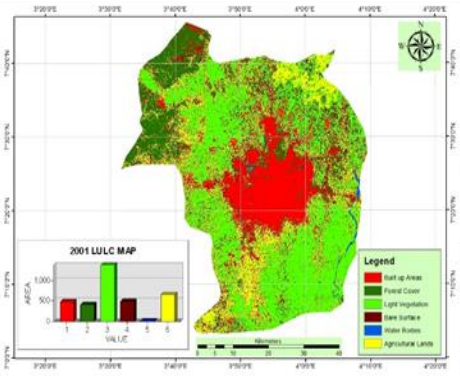


Landuse/landcover of Ibadan Metropolis in 2001

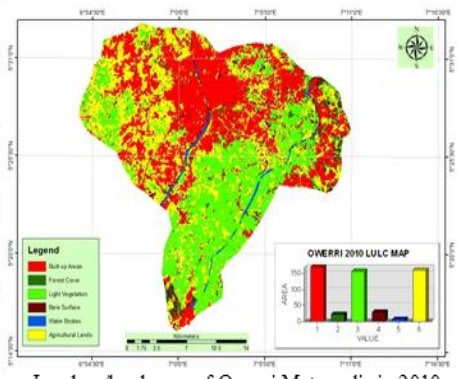


Landuse/landcover of Owerri Metropolis in 2010

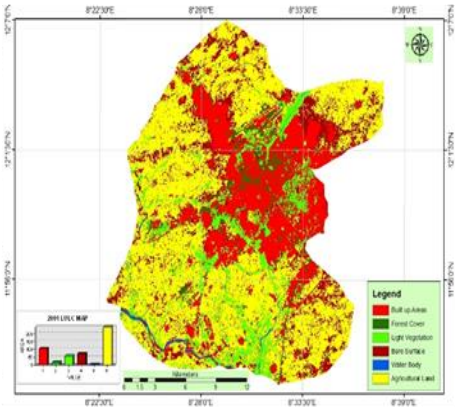


Landuse/landcover of Kano Metropolis in 2001

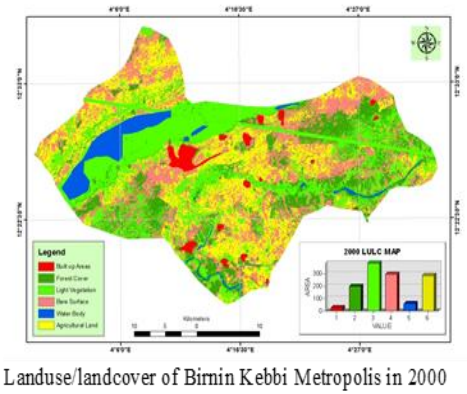


Landuse/landcover of Birnin Kebbi Metropolis in 2000

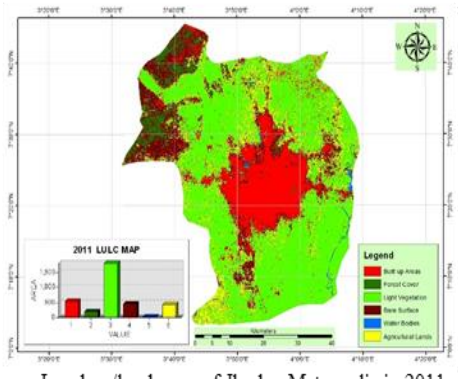


Landuse/landcover of Ibadan Metropolis in 2011

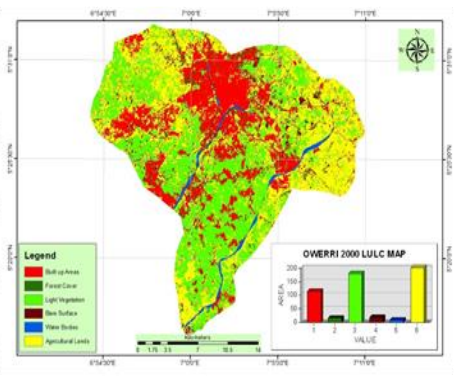


Landuse/landcover of Owerri Metropolis in 2000

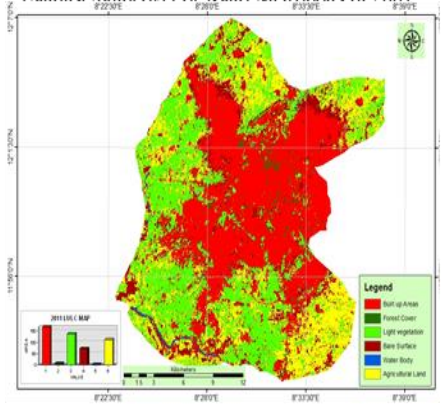


Landuse/landcover of Kano Metropolis in 2011

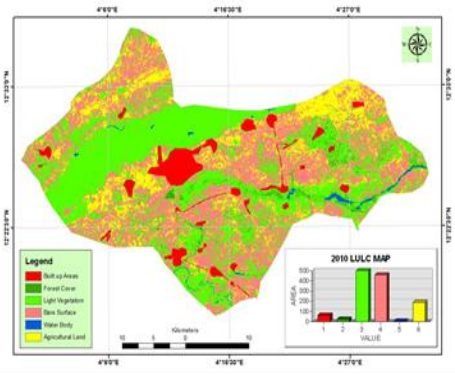


Landuse/landcover of Birnin Kebbi Metropolis in 2010

**Appendix C 1: LULC Classes of Ibadan from 1991 – 2019**

**Magnitude and Percentage Change in LULCof Ibadan between 1990 and 2001**

| LULC Class | 1990 Extent ($km^2$) | 2001 Extent ($km^2$) | Magnitude of Change ($km^2$) | Percentage of Change | Annual Rate of % Change |
|---|---|---|---|---|---|
| Built up | 312.90 | 479.45 | 166.55 | 15.26 | 1.68 |
| Forest cover | 712.66 | 408.28 | -304.38 | 27.89 | 3.07 |
| Light Vegetation | 1316.21 | 1367.78 | 51.57 | 4.73 | 0.52 |
| Bare surface | 155.01 | 482.62 | 327.61 | 30.03 | 3.30 |
| Water body | 14.70 | 14.80 | 0.01 | 0.001 | 0.00 |
| Agricultural lands | 891.51 | 650.14 | 241.37 | 22.12 | 2.43 |
| Total | **3402.98** | **3402.98** | **1091.19** | **100** | |

**Magnitude and Percentage of Change in LULC of Ibadan between 2001 and 2011**

| LULC Class | 2001 Extent ($km^2$) | 2011 Extent ($km^2$) | Magnitude of change ($km^2$) | % Change | Annual Rate of % Change |
|---|---|---|---|---|---|
| Built up | 479.45 | 755.29 | 275.84 | 31.14 | 3.11 |
| Forest cover | 408.28 | 278.55 | -129.73 | -14.65 | -1.47 |
| Light Vegetation | 1367.78 | 1298.88 | -68.9 | -7.78 | -0.78 |
| Bare surface | 482.62 | 238.32 | -244.3 | -27.58 | 2.76 |
| Water body | 14.80 | 13.63 | -1.21 | -0.14 | -0.01 |
| Agricultural lands | 650.14 | 815.94 | 165.8 | 18.72 | 1.87 |
| Total | **3402.98** | **3402.98** | **885.78** | **100** | |

**Magnitude and Percentage Change in LULC of Ibadan between 2011 and 2019**

| LULC Class | 2011 Extent ($km^2$) | 2019 Extent ($km^2$) | Magnitude of Change ($km^2$) | Percentage of Change | Annual Rate of % Change |
|---|---|---|---|---|---|
| Built up | 755.29 | 1039.54 | 284.25 | 42.53 | 3.40 |
| Forest cover | 278.55 | 253.05 | 25.5 | 3.82 | 0.31 |
| Light Vegetation | 1298.88 | 1092.51 | -206.37 | -30.88 | -2.47 |
| Bare surface | 238.32 | 289.27 | 50.95 | 7.62 | 0.61 |
| Water body | 13.63 | 12.73 | -0.9 | -0.13 | -0.13 |
| Agricultural lands | 815.94 | 715.55 | -100.39 | -15.02 | -1.21 |
| Total | 3402.98 | 3402.98 | 668.36 | 100 | |

**Appendix C 2: LULC Classes of Owerri from 1990 – 2019**

**Magnitude and Percentage Change in LULC of Owerri between 1990 and 2000**

| LULC Class | 1990 Extent (Sq. km) | 2000 Extent (Sq. km) | Magnitude of Change (Sq. km) | Percentage of Change | Annual Rate of Change % |
|---|---|---|---|---|---|
| Built up | 70.32 | 116.55 | 46.23 | 13.62 | 1.36 |
| Forest cover | 70.16 | 17.00 | -53.16 | 15.66 | 1.57 |
| Light Vegetation | 255.09 | 179.75 | -75.34 | 22.19 | 2.22 |
| Bare surface | 59.98 | 19.30 | -40.68 | 11.98 | 1.20 |
| Water body | 9.11 | 8.55 | -0.56 | 0.16 | 0.016 |
| Agricultural lands | 78.79 | 202.28 | 123.49 | 36.38 | 3.64 |
| Total | 543.45 | 543.45 | 339.46 | 100 | |

**Magnitude and Percentage of Change in LULC of Owerri between 2000 and 2010**

| LULC Class | 2000 Extent (Sq. km) | 2010 Extent (Sq. km) | Magnitude of Change (Sq. km) | Percentage of Change | Annual Rate of Change % |
|---|---|---|---|---|---|
| Built up | 116.55 | 170.55 | 54.00 | 39.45 | 3.95 |
| Forest cover | 17.00 | 21.43 | 4.43 | 3.24 | 0.32 |
| Light Vegetation | 179.75 | 157.08 | -22.67 | 16.56 | 1.66 |
| Bare surface | 19.30 | 29.24 | 9.94 | 7.26 | 0.76 |
| Water body | 8.55 | 5.56 | -2.99 | 2.18 | 0.22 |
| Agricultural lands | 202.28 | 159.42 | -42.86 | 31.31 | 3.13 |
| Total | **543.45** | **543.45** | **136.87** | **100** | |

**Magnitude and Percentage Change in LULC of Owerri between 2010 and 2019**

| LULC Class | 1990 Extent (Sq. km) | 2019 Extent (Sq. km) | Magnitude of Change (Sq. km) | Percentage of Change | Annual Rate of Change % |
|---|---|---|---|---|---|
| Built up | 70.32 | 209.16 | 138.84 | 35.14 | 10.19 |
| Forest cover | 70.16 | 21.35 | -48.81 | 12.45 | 3.61 |
| Light Vegetation | 255.09 | 141.52 | -113.57 | 28.96 | 8.40 |
| Bare surface | 59.98 | 29.12 | -30.86 | 7.87 | 2.28 |
| Water body | 9.11 | 6.19 | -2.92 | 0.74 | 0.21 |
| Agricultural lands | 78.79 | 135.94 | 57.15 | 14.57 | 4.23 |
| **Total** | **543.45** | **543.45** | **392.15** | **100** | |

**Appendix C 3: LULC Classes of Kano from 1991 - 2019**

**Magnitude and Percentage of Change in LULC of Kano between 1991 and 2001**

| LULC Class | 1991 Extent ($km^2$) | 2001 Extent ($km^2$) | Magnitude of Change ($km^2$) | Percentage of Change | Annual Rate of Change % |
|---|---|---|---|---|---|
| Built up | 58.48 | 102.66 | 44.18 | 34.19 | 3.42 |
| Forest cover | 19.61 | 15.54 | -4.07 | 3.15 | 0.32 |
| Light Vegetation | 37.80 | 58.22 | 20.42 | 15.80 | 1.58 |
| Bare surface | 77.81 | 71.68 | -6.13 | 4.74 | 0.47 |
| Water body | 5.69 | 2.14 | -3.55 | 2.75 | 0.28 |
| Agricultural lands | 294.14 | 243.29 | -50.85 | 39.36 | 3.94 |
| **Total** | **493.53** | **494.53** | **129.2** | **100** | |

**Magnitude and Percentage of Change in LULC of Kano between 2001 and 2011**

| LULC Class | 2001 Extent ($km^2$) | 2011 Extent ($km^2$) | Magnitude of Change ($km^2$) | Percentage of Change | Annual Rate of Change % |
|---|---|---|---|---|---|
| Built up | 102.66 | 167.73 | 65.07 | 22.71 | 2.27 |
| Forest cover | 15.54 | 5.92 | -9.62 | 3.36 | 0.34 |
| Light Vegetation | 58.22 | 136.07 | 77.85 | 27.17 | 2.72 |
| Bare surface | 71.68 | 72.03 | 0.35 | 0.12 | 0.01 |
| Water body | 2.14 | 1.38 | -0.76 | 0.27 | 0.03 |
| Agricultural lands | 243.29 | 110.39 | 132.9 | 46.38 | 4.64 |
| **Total** | **493.53** | **496.53** | **286.55** | **100** | **10** |

**Magnitude and Percentage of Change in LULC of Kano between 2011 and 2019**

| LULC Class | 2011 Extent ($km^2$) | 2019 Extent ($km^2$) | Magnitude of Change ($km^2$) | Percentage of Change | Annual Rate of Change % |
|---|---|---|---|---|---|
| Built up | 167.73 | 216.03 | 48.3 | 28.31 | 2.26 |
| Forest cover | 5.92 | 11.12 | 5.2 | 3.05 | 0.24 |
| Light Vegetation | 136.07 | 73.36 | -62.71 | 36.76 | 2.94 |
| Bare surface | 72.03 | 49.46 | -22.57 | 13.23 | 1.06 |
| Water body | 1.38 | 1.41 | 0.03 | 0.02 | 0.00 |
| Agricultural lands | 110.39 | 142.15 | 31.76 | 18.62 | 1.48 |
| **Total** | **493.52** | **493.53** | **170.57** | **100** | 8 |

**Appendix C 4: LULC Classes of Birnin Kebbi from 1990 - 2019**

**Birnin Kebbi Magnitude and Percentage of Change in LULC between 1990 and 2000**

| LULC Class | 1990 Extent (Sq. km) | 2000 Extent (Sq. km) | Magnitude of Change (Sq. km) | Percentage of Change | Annual Rate of Change % |
|---|---|---|---|---|---|
| Built up | 14.06 | 26.96 | 12.9 | 91.75 | 9.18 |
| Forest cover | 165.44 | 197.54 | 32.1 | 19.40 | 1.94 |
| Light Vegetation | 359.27 | 384.24 | 24.97 | 6.95 | 0.70 |
| Bare surface | 100.80 | 295.99 | 195.19 | 193.64 | 19.36 |
| Water body | 6.08 | 59.14 | 53.06 | 872.70 | 87.27 |
| Agricultural lands | 603.23 | 285.02 | -318.21 | 52.75 | 5.28 |
| Total | **1248.88** | **1248.88** | **636.43** | **1237.19** | **123.73** |

**Birnin Kebbi Magnitude and Percentage of Change in LULC between 2000 and 2010**

| LULC Class | 2000 Extent (Sq. km) | 2010 Extent (Sq. km) | Magnitude of Change (Sq. km) | Percentage of Change | Annual Rate of Change % |
|---|---|---|---|---|---|
| Built up | 26.96 | 65.34 | 38.36 | 142.28 | 14.23 |
| Forest cover | 197.54 | 25.36 | -172.18 | 87.16 | 8.72 |
| Light Vegetation | 384.24 | 502.13 | 117.89 | 30.68 | 3.07 |
| Bare surface | 295.99 | 461.71 | 165.72 | 55.99 | 5.60 |
| Water body | 59.14 | 8.15 | -50.99 | 86.22 | 8.62 |
| Agricultural lands | 285.02 | 186.19 | -98.83 | 34.67 | 3.47 |
| Total | **1248.88** | **1248.88** | **643.97** | **437.00** | **43.71** |

**Birnin Kebbi Magnitude and Percentage of Change in LULC between 2010 and 2019**

| LULC Class | 2010 Extent (Sq. km) | 2019 Extent (Sq. km) | Magnitude of Change (Sq. km) | Percentage of Change | Annual Rate of Change % |
|---|---|---|---|---|---|
| Built up | 65.34 | 123.03 | 57.69 | 88.29 | 9.81 |

| | | | | | |
|---|---|---|---|---|---|
| Forest cover | 25.36 | 101.48 | 76.12 | 300.15 | 33.35 |
| Light Vegetation | 502.13 | 333.83 | -168.3 | 33.52 | 3.72 |
| Bare surface | 461.71 | 403.48 | -58.23 | 12.61 | 1.40 |
| Water body | 8.15 | 13.72 | 5.57 | 68.34 | 7.59 |
| Agricultural lands | 186.19 | 273.35 | 87.16 | 46.81 | 5.20 |
| Total | **1248.88** | **1248.88** | **365.91** | **549.72** | **61.07** |

## Appendix D1 LULC Transitions in Ibadan between 1990 and 2019

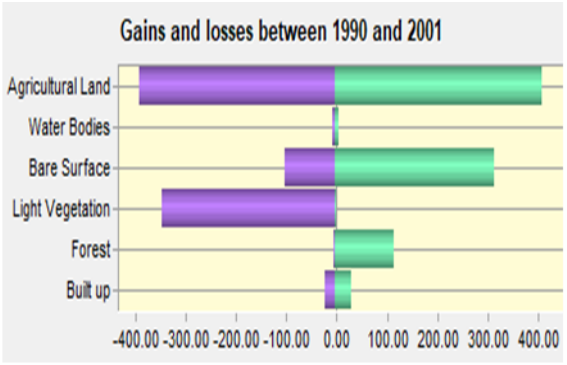


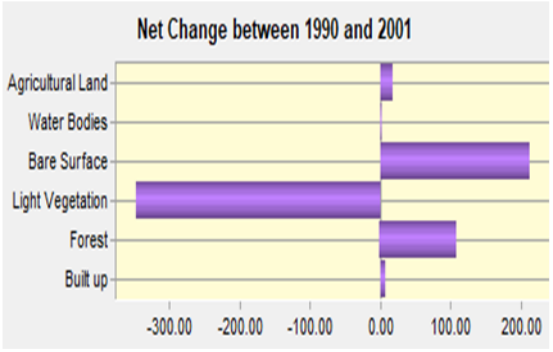


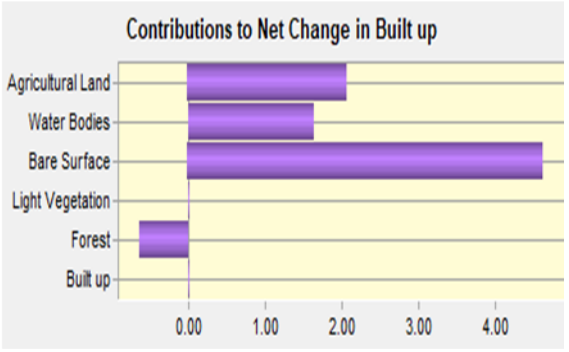


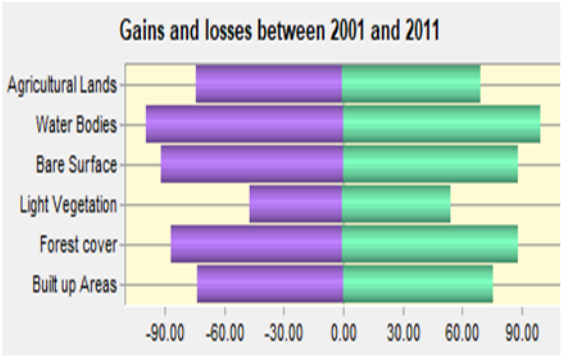


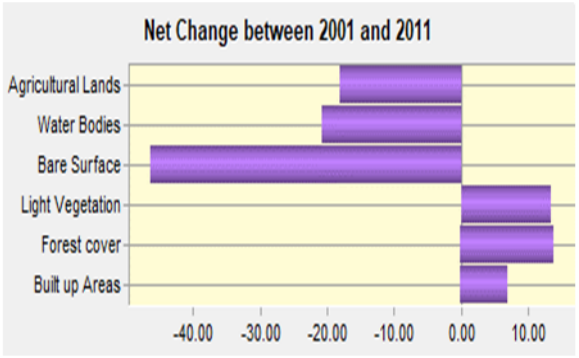


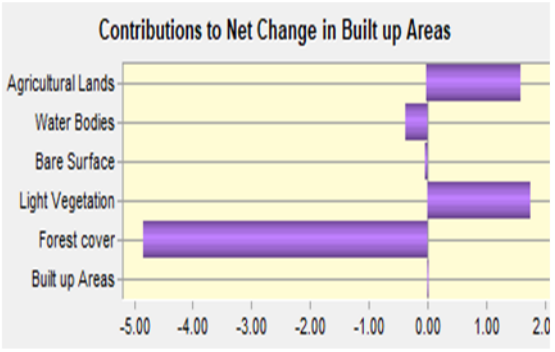


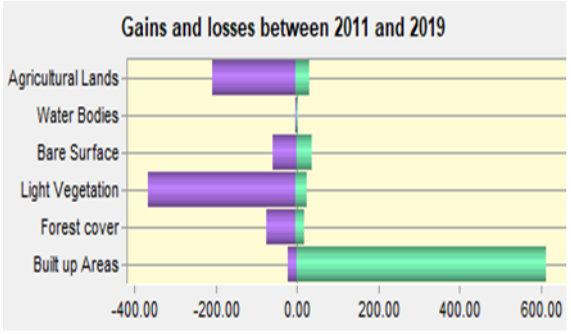


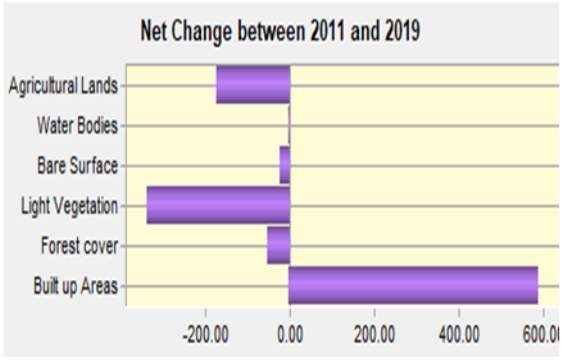


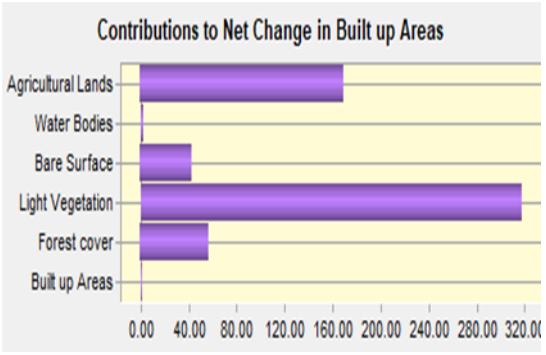

## Appendix D2 LULC Transitions in Owerri between 1990 and 2019

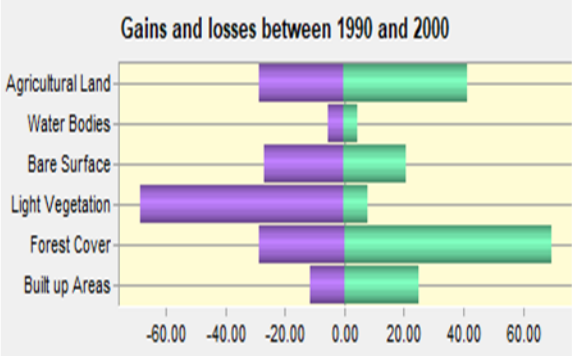


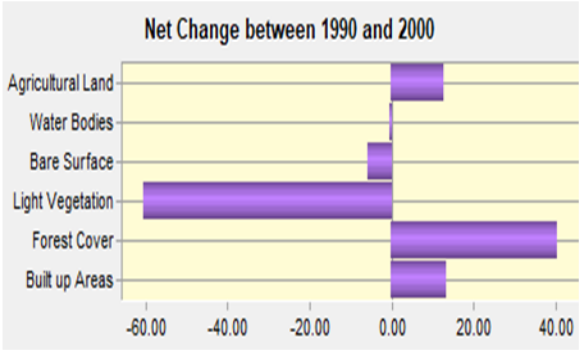


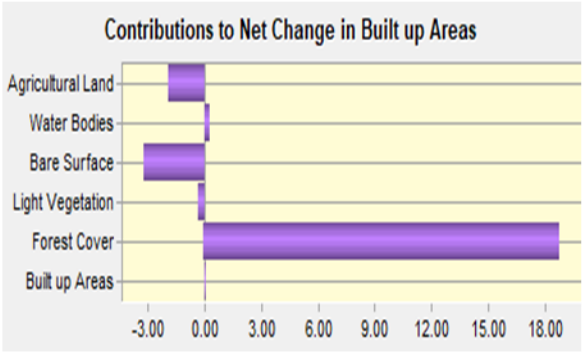


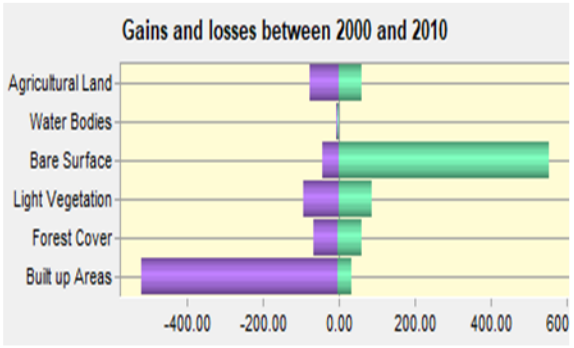


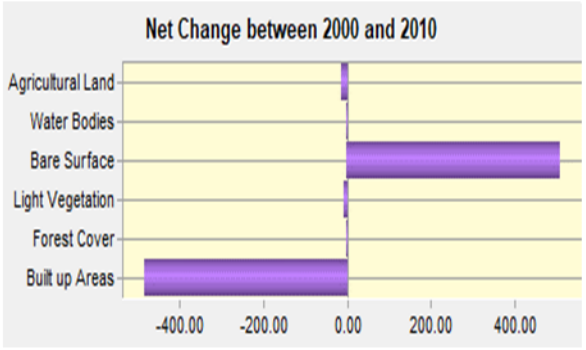


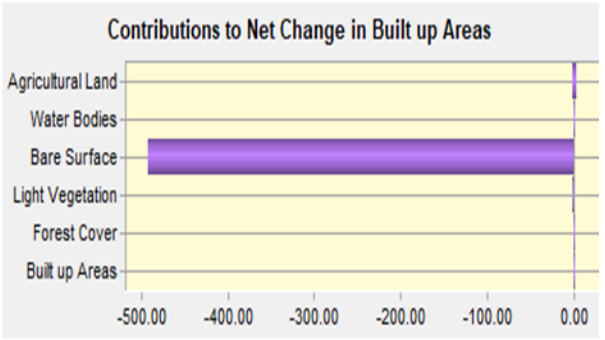


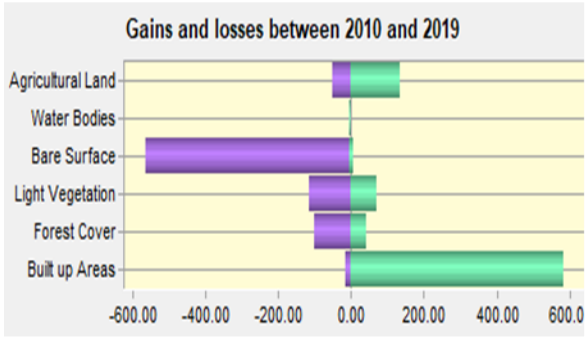


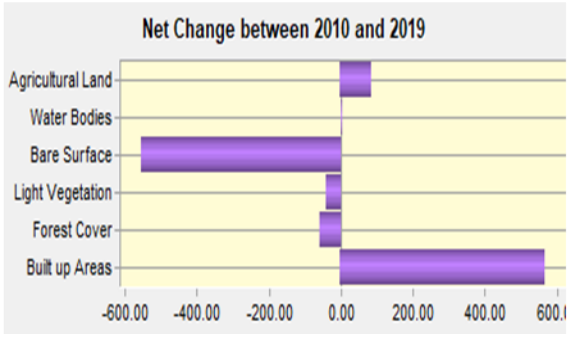


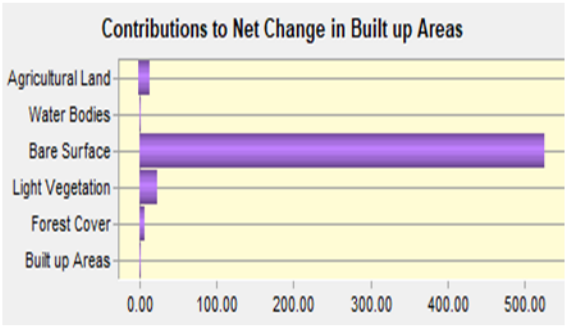

## Appendix D3 LULC Transitions in Kano between 1991 and 2019

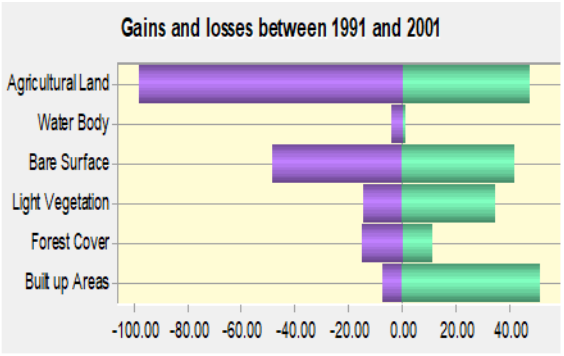


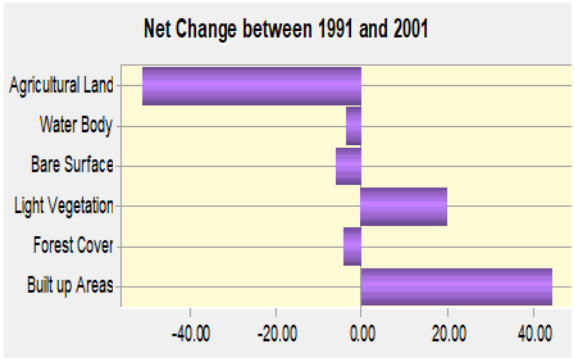


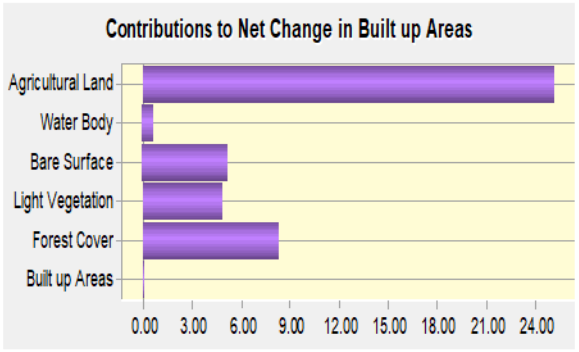


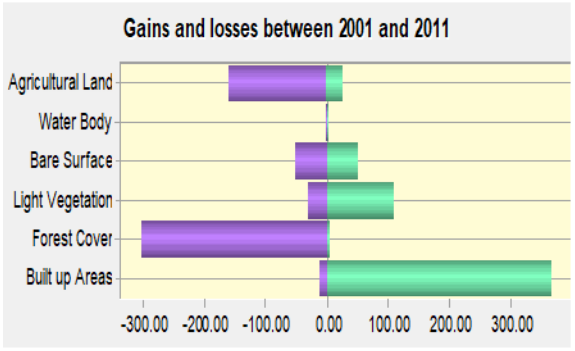


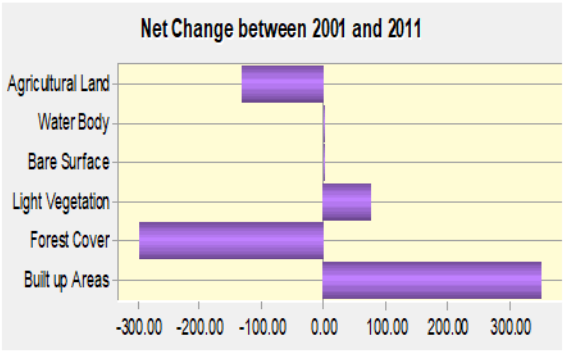


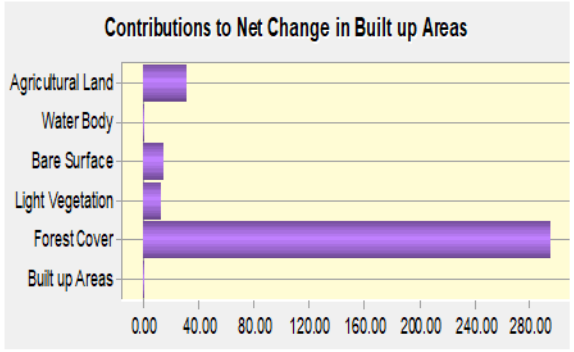


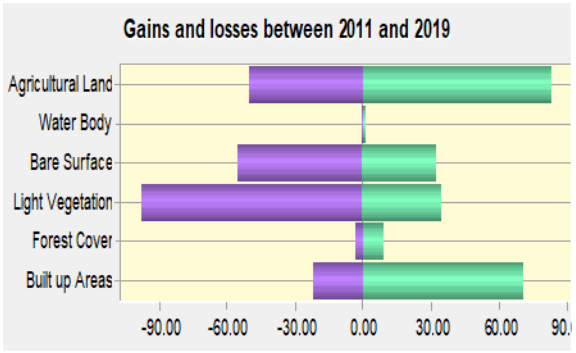


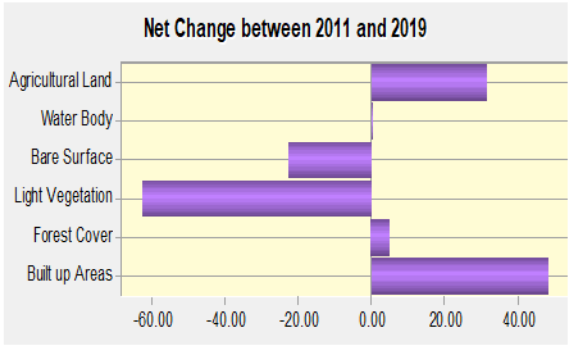


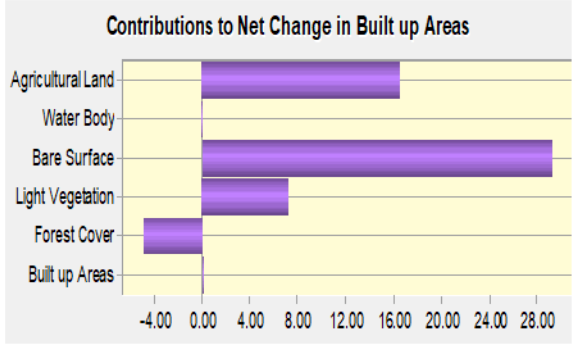

## Appendix D4 LULC Transitions in Birnin Kebbi between 1990 and 2019

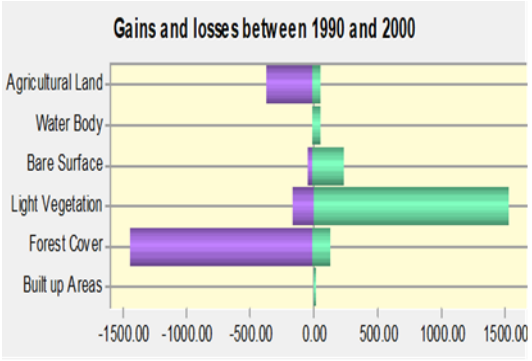


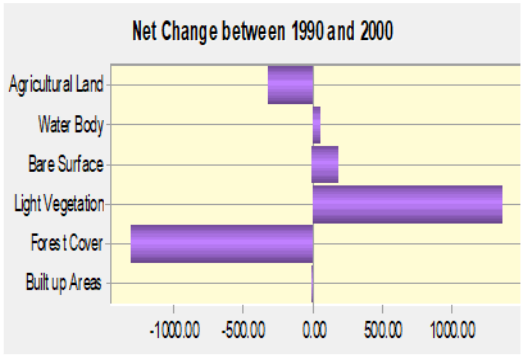


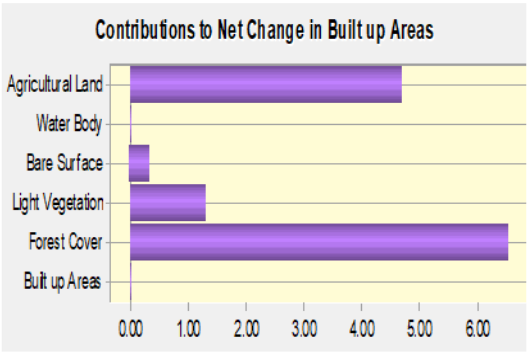


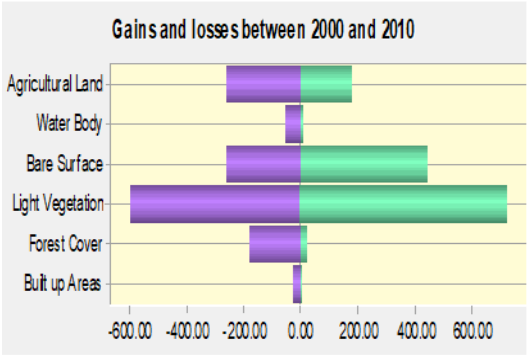


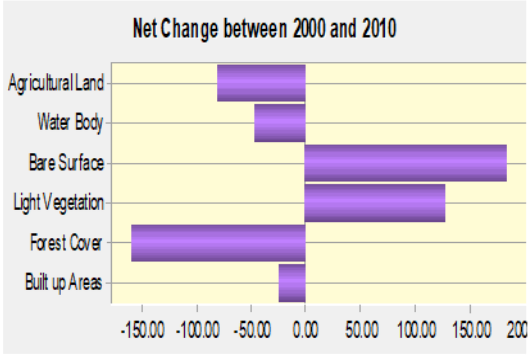


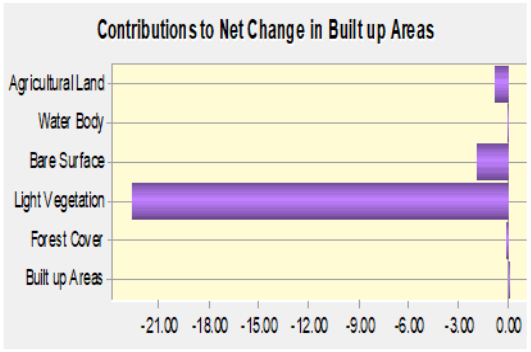


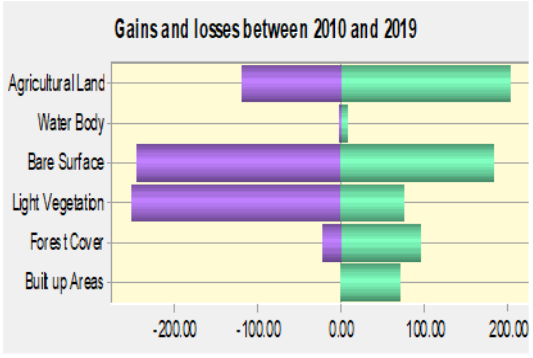


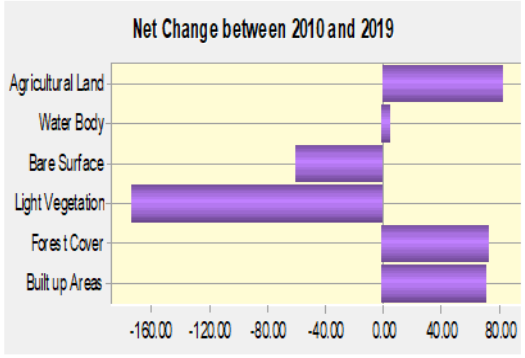


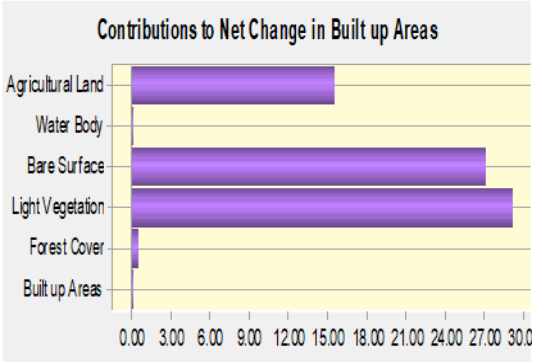

## Appendix E: NDVI of the four cities from 2000 – 2010

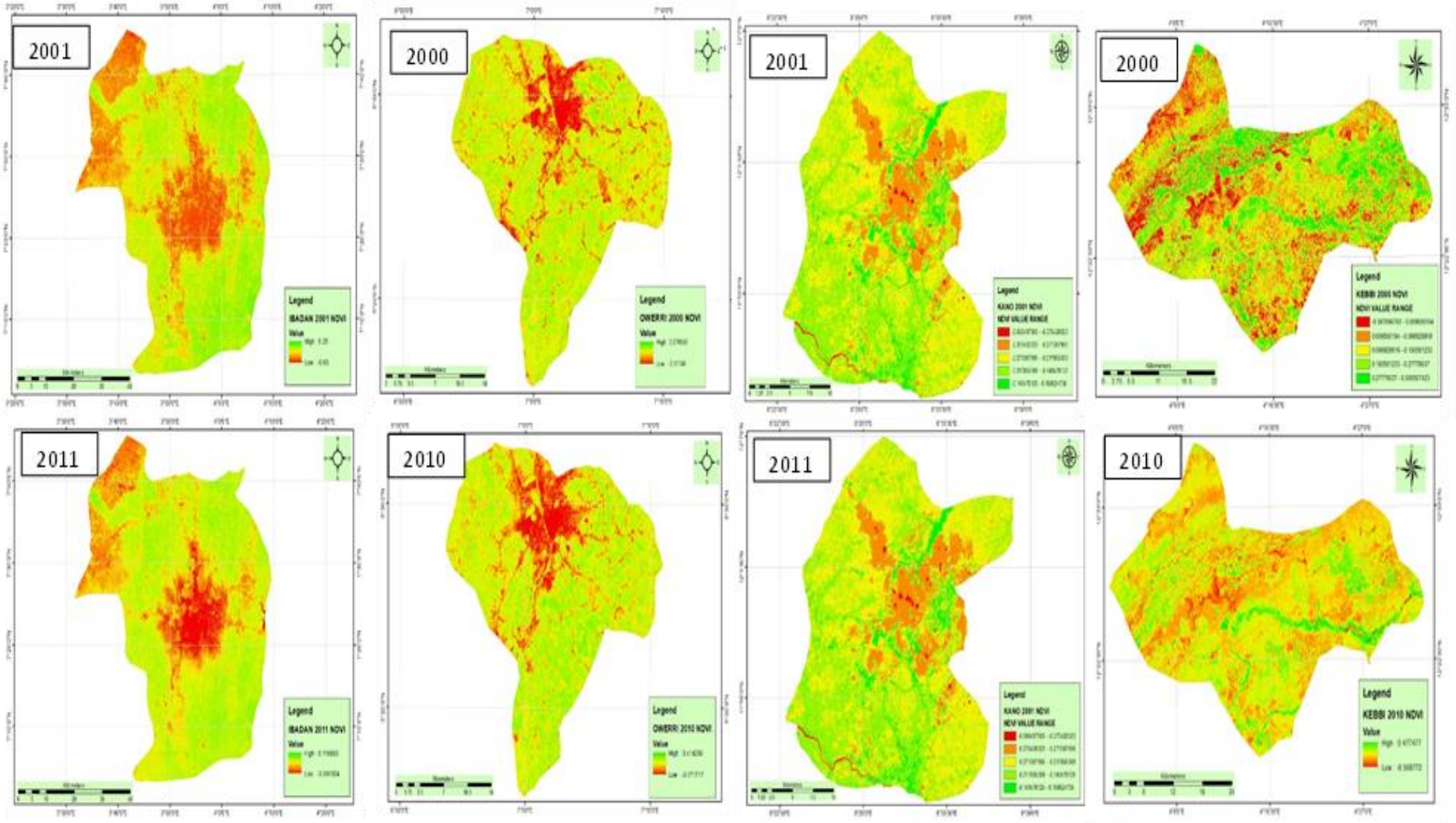

## Appendix F: Classified NDVI of the four cities from 2000 – 2010

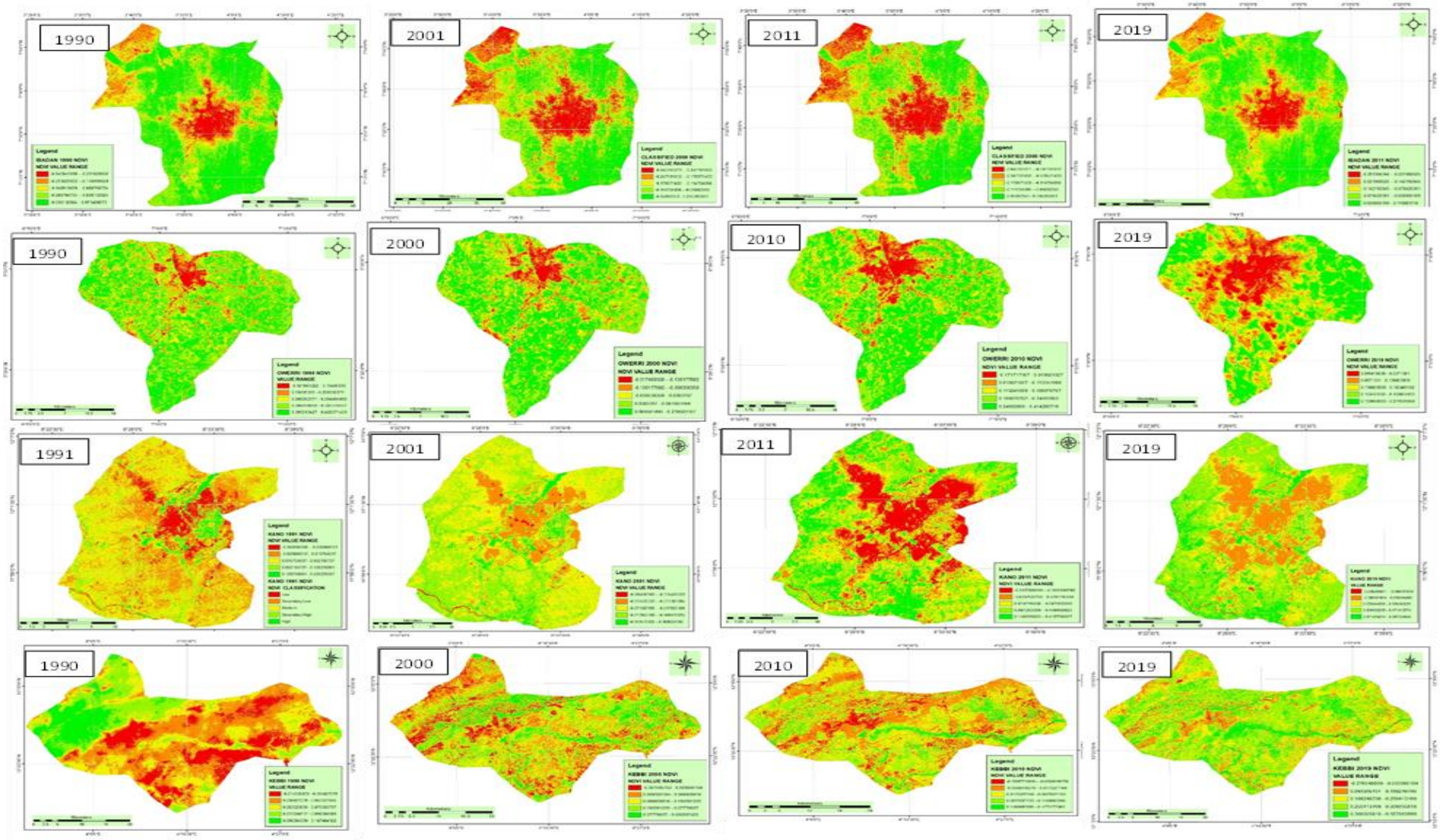

## Appendix G: NDBI of the four cities from 2000 – 2010

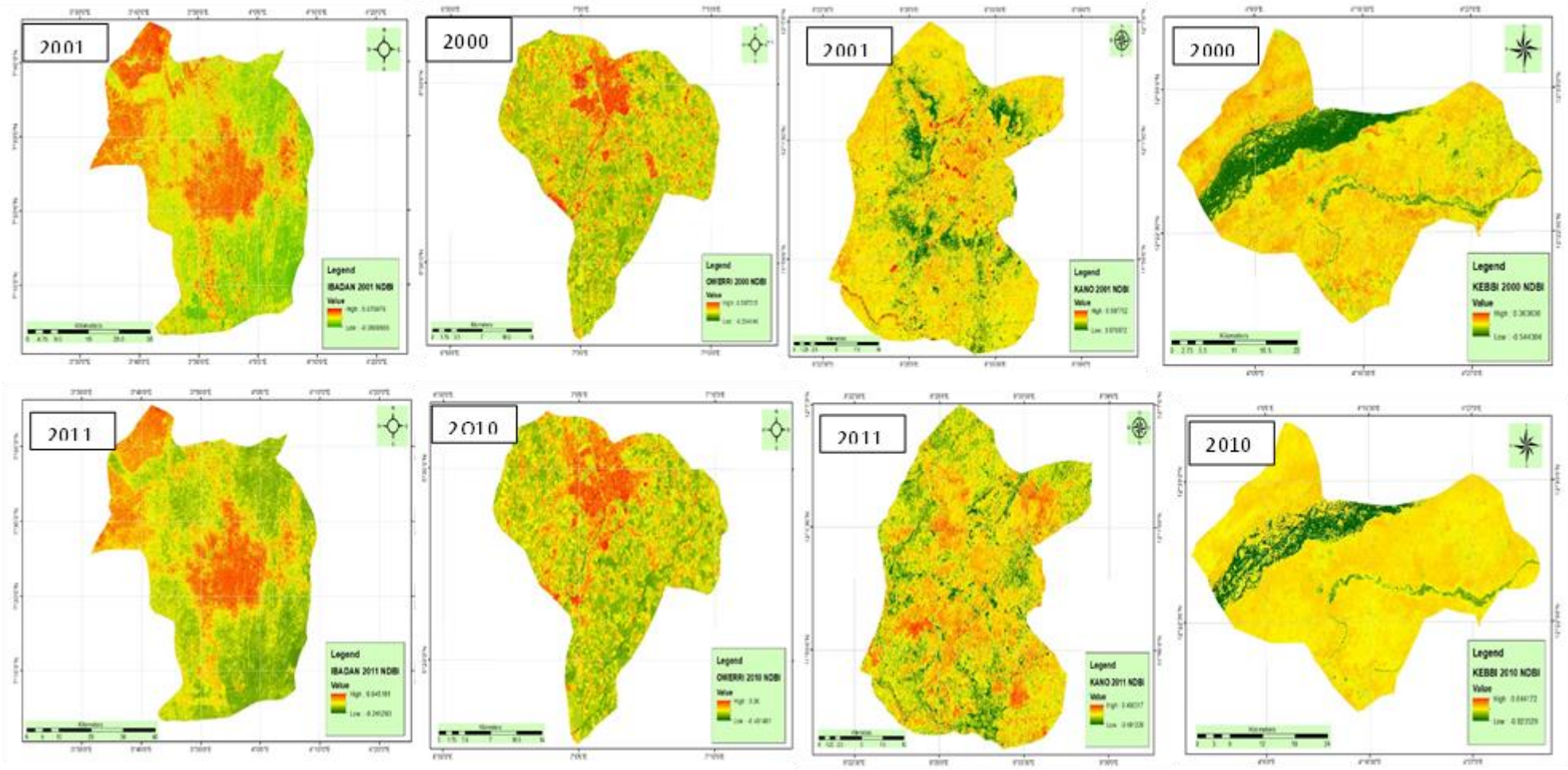

**Appendix H: Classified NDBI of the four cities from 2000 – 2010**

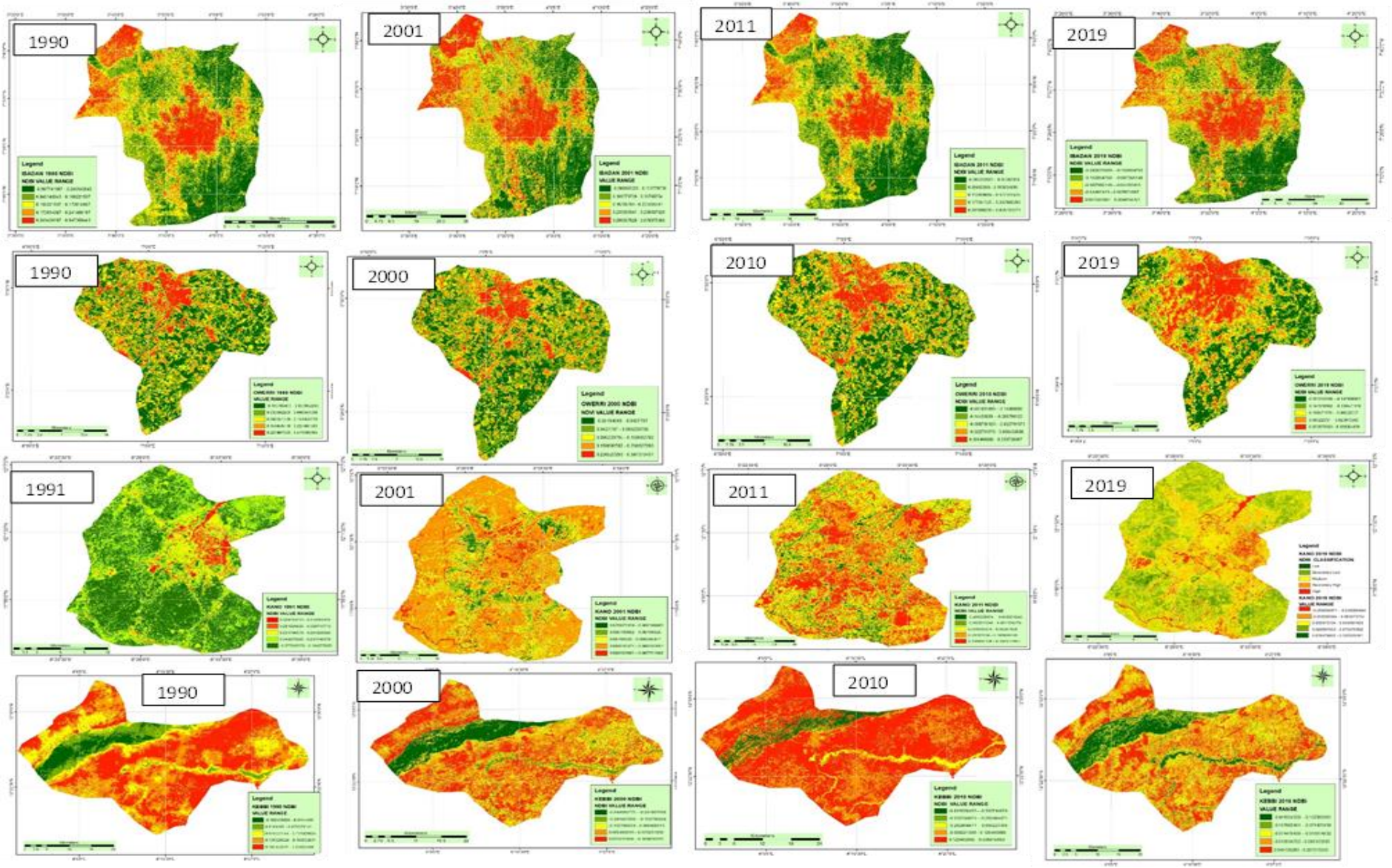

## Appendix I: LST of the four cities from 2000 – 2010

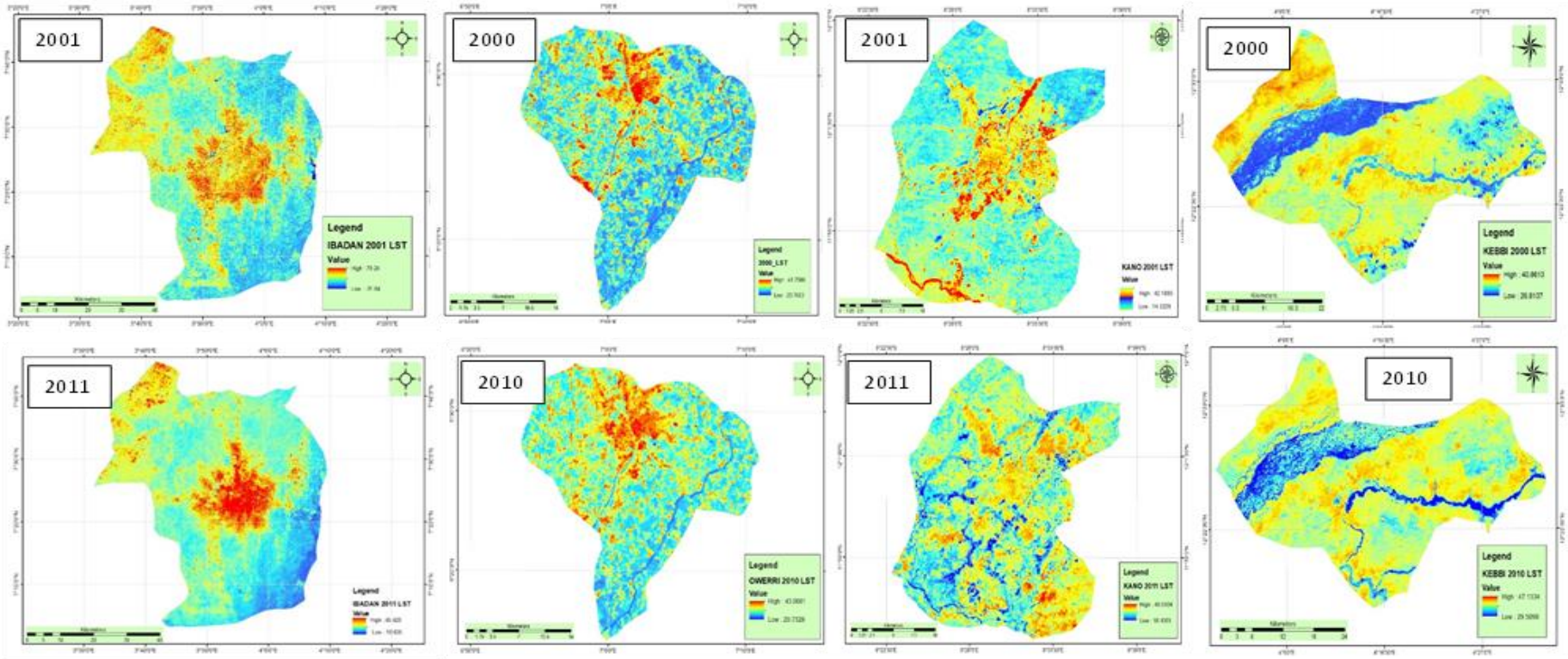

## Appendix J: Classified LST of the four cities from 2000 – 2010

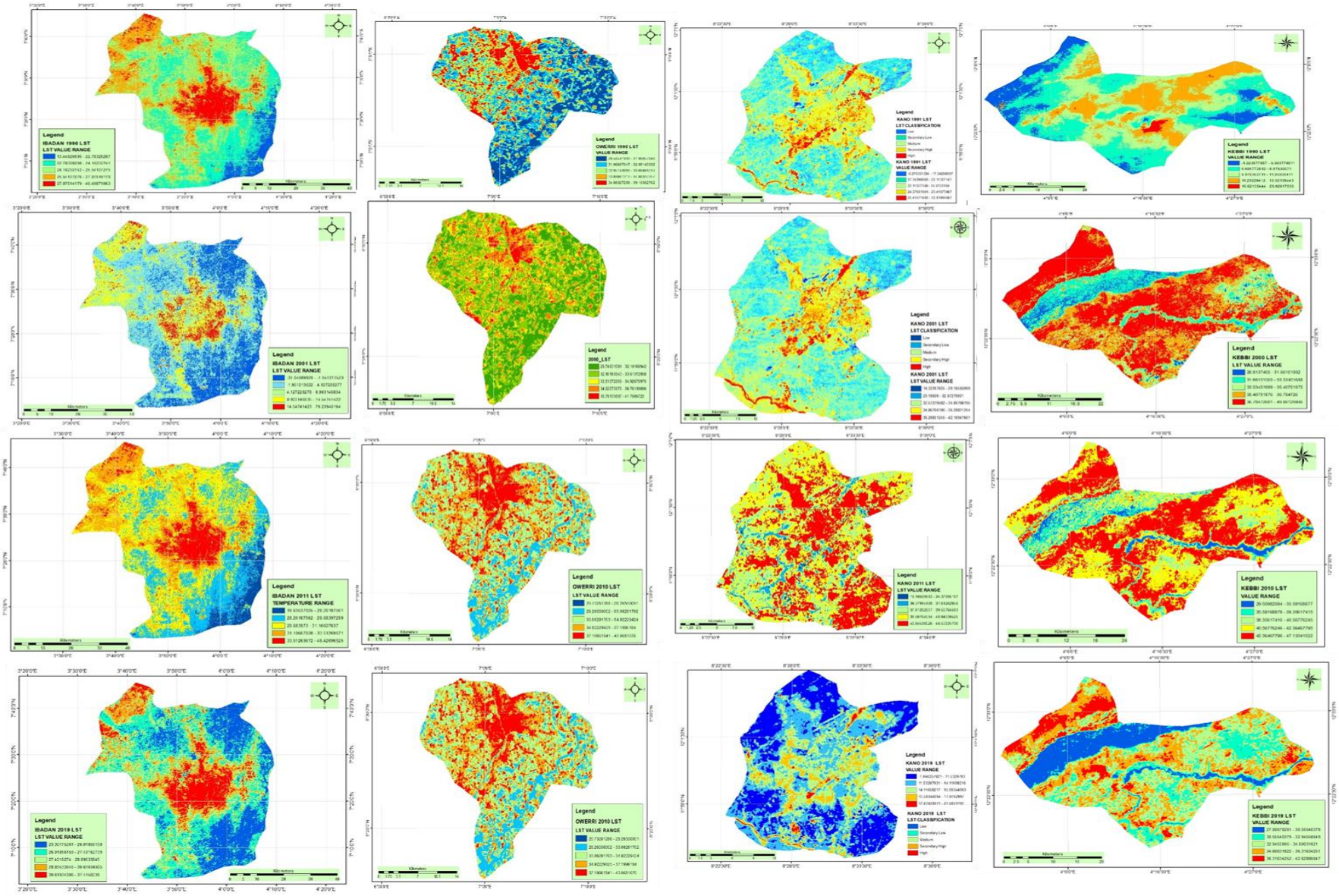

**Appendix K1: Values for LST (°C), NDVI and NDBI Classes for Ibadan 1990 - 2019**

| | 1990 | | | 2001 | | | 2011 | | | 2019 | | |
|---|---|---|---|---|---|---|---|---|---|---|---|---|
| SN | LST | NDVI | NDBI | LST | NDVI | NDBI | LST | NDVI | NDBI | LST | NDVI | NDBI |
| 1 | 13.87253 | -0.94595 | -0.7875 | -20.1865 | -0.36111 | -0.000078 | 19.07294 | -0.327532 | -0.09513 | 24.74614 | 0.041692196 | -0.21473 |
| 2 | 15.46373 | -0.3369 | -0.08904 | -10.6347 | -0.3262 | 0.029880 | 20.71382 | -0.309596 | -0.03577 | 25.18872 | 0.05943895 | -0.19928 |
| 3 | 18.43399 | -0.31434 | -0.02896 | -4.55626 | -0.30526 | 0.050851 | 23.7768 | -0.289667 | -0.01132 | 25.6313 | 0.077185704 | -0.18384 |
| 4 | 20.34343 | -0.28426 | -0.00643 | -1.08286 | -0.28796 | 0.071822 | 25.74586 | -0.269738 | 0.009628 | 26.12921 | 0.094932458 | -0.16531 |
| 5 | 21.29816 | -0.26171 | 0.016099 | 2.390531 | -0.27174 | 0.095788 | 26.73039 | -0.247816 | 0.03058 | 26.68243 | 0.112679212 | -0.14678 |
| 6 | 21.82856 | -0.23163 | 0.03863 | 5.429752 | -0.2551 | 0.119755 | 27.27735 | -0.223901 | 0.055024 | 27.23566 | 0.132200641 | -0.12516 |
| 7 | 22.78328 | -0.20907 | 0.068671 | 8.468972 | -0.23757 | 0.146717 | 28.26188 | -0.201980 | 0.082959 | 27.84421 | 0.153496746 | -0.10354 |
| 8 | 23.73801 | -0.179 | 0.098712 | 11.50819 | -0.21978 | 0.176675 | 29.2464 | -0.178065 | 0.114387 | 28.45276 | 0.174792851 | -0.07883 |
| 9 | 24.58665 | -0.15644 | 0.136263 | 14.54741 | -0.20225 | 0.203637 | 30.12154 | -0.158136 | 0.145814 | 29.06131 | 0.19431428 | -0.05412 |
| 10 | 25.54137 | -0.12636 | 0.173814 | 17.15246 | -0.1791 | 0.230600 | 31.10607 | -0.136214 | 0.180733 | 29.66986 | 0.215610385 | -0.02941 |
| 11 | 26.4961 | -0.1038 | 0.211365 | 19.32333 | -0.15663 | 0.257562 | 32.0906 | -0.114292 | 0.212161 | 30.22308 | 0.235131814 | -0.0047 |
| 12 | 27.45082 | -0.08125 | 0.248916 | 22.36255 | -0.13402 | 0.284524 | 33.07513 | -0.092371 | 0.240096 | 30.77631 | 0.252878568 | 0.016918 |
| 13 | 28.29946 | -0.05869 | 0.278957 | 25.40177 | -0.11236 | 0.308491 | 34.38783 | -0.070449 | 0.26454 | 31.27421 | 0.270625322 | 0.035449 |
| 14 | 29.25419 | -0.03613 | 0.301488 | 28.87517 | -0.08982 | 0.326466 | 35.37236 | -0.048527 | 0.285492 | 31.71679 | 0.286597401 | 0.050892 |
| 15 | 30.10283 | -0.02109 | 0.324019 | 33.65109 | -0.06796 | 0.344441 | 36.2475 | -0.028598 | 0.302951 | 32.10405 | 0.300794804 | 0.066335 |
| 16 | 30.95147 | 0.001463 | 0.35406 | 38.86118 | -0.04651 | 0.362416 | 36.79446 | -0.014648 | 0.320411 | 32.49131 | 0.313217532 | 0.084867 |
| 17 | 31.9062 | 0.02402 | 0.391611 | 46.24215 | -0.02597 | 0.380390 | 37.23203 | -0.000698 | 0.344855 | 32.87857 | 0.32564026 | 0.106487 |
| 18 | 33.17916 | 0.046577 | 0.459203 | 56.22816 | -0.00592 | 0.401361 | 38.54473 | 0.021224 | 0.379774 | 33.32115 | 0.339837663 | 0.152816 |
| 19 | 34.55821 | 0.114249 | 0.564346 | 69.68756 | 0.016667 | 0.497227 | 40.4044 | 0.041153 | 0.456597 | 34.37228 | 0.357584417 | 0.313422 |
| 20 | 40.49871 | 0.971429 | 0.947368 | 79.2394 | 0.245283 | 0.676976 | 46.42097 | 0.116883 | 0.645161 | 37.41502 | 0.428571433 | 0.504915 |

## Appendix K2 Values for LST (°C), NDVI and NDBI Classes for Owerri 1990 - 2019

| | 1990 | | | 2000 | | | 2010 | | | 2019 | | |
|---|---|---|---|---|---|---|---|---|---|---|---|---|
| **SN** | **LST** | **NDVI** | **NDBI** | **LST** | **NDVI** | **NDBI** | **LST** | **NDVI** | **NDBI** | **LST** | **NDVI** | **NDBI** |
| 1 | 29.50442 | -0.04423 | -0.04437 | 29.74832 | -0.27532 | -0.13762 | 21.17076 | -0.10507 | -0.34288 | 16.79441 | 0.047127 | -0.21836 |
| 2 | 29.99685 | -0.00105 | -0.02363 | 30.68967 | -0.24489 | -0.07749 | 22.22183 | -0.0798 | -0.24389 | 17.75955 | 0.057331 | -0.19539 |
| 3 | 30.48928 | 0.027014 | -0.00751 | 31.16035 | -0.2168 | -0.04075 | 24.76192 | -0.05681 | -0.21089 | 18.45659 | 0.067536 | -0.18008 |
| 4 | 30.98171 | 0.050762 | 0.010924 | 31.63102 | -0.19104 | -0.01736 | 25.813 | -0.03613 | -0.19109 | 19.10001 | 0.076721 | -0.16936 |
| 5 | 31.47414 | 0.07451 | 0.029355 | 32.1017 | -0.16763 | 0.002683 | 27.73996 | -0.01315 | -0.17459 | 19.74344 | 0.085905 | -0.15864 |
| 6 | 31.96657 | 0.096099 | 0.050089 | 32.57238 | -0.14188 | 0.022727 | 29.22898 | 0.009829 | -0.15479 | 20.38686 | 0.09611 | -0.14486 |
| 7 | 32.459 | 0.119847 | 0.073128 | 33.04305 | -0.11613 | 0.042771 | 30.63041 | 0.037405 | -0.12839 | 20.97667 | 0.106314 | -0.12954 |
| 8 | 32.95143 | 0.143595 | 0.098471 | 33.51373 | -0.08804 | 0.066155 | 31.5939 | 0.064982 | -0.09869 | 21.62009 | 0.11754 | -0.11423 |
| 9 | 33.44386 | 0.167343 | 0.126117 | 34.45508 | -0.05761 | 0.096221 | 32.11943 | 0.094857 | -0.06899 | 22.31713 | 0.129785 | -0.09738 |
| 10 | 33.89841 | 0.191091 | 0.153764 | 34.92576 | -0.02717 | 0.126286 | 32.55738 | 0.124731 | -0.03599 | 23.06779 | 0.142031 | -0.08054 |
| 11 | 34.39084 | 0.214839 | 0.179106 | 35.39644 | -0.00142 | 0.156352 | 33.52086 | 0.152308 | -0.00299 | 23.76484 | 0.154277 | -0.06216 |
| 12 | 34.88327 | 0.238587 | 0.204449 | 36.33779 | 0.031354 | 0.186418 | 34.48435 | 0.179885 | 0.026707 | 24.40826 | 0.166523 | -0.04532 |
| 13 | 35.3757 | 0.260176 | 0.227488 | 36.7614 | 0.057105 | 0.213143 | 35.79819 | 0.207461 | 0.053107 | 24.89083 | 0.177748 | -0.03 |
| 14 | 35.83025 | 0.279606 | 0.250526 | 37.23208 | 0.080515 | 0.239868 | 36.76167 | 0.230442 | 0.079506 | 25.3734 | 0.188973 | -0.01622 |
| 15 | 36.32268 | 0.296878 | 0.271261 | 37.70275 | 0.099244 | 0.266593 | 37.63757 | 0.251124 | 0.105906 | 25.85597 | 0.199178 | -0.00397 |
| 16 | 36.77723 | 0.31199 | 0.291996 | 38.59704 | 0.115631 | 0.289977 | 38.1631 | 0.269509 | 0.132305 | 26.39215 | 0.207342 | 0.006752 |
| 17 | 37.26967 | 0.327103 | 0.312731 | 39.06771 | 0.129677 | 0.313362 | 39.039 | 0.285595 | 0.158704 | 26.92834 | 0.214485 | 0.017472 |
| 18 | 37.72422 | 0.340056 | 0.331162 | 39.49132 | 0.146064 | 0.343427 | 39.91489 | 0.303979 | 0.188404 | 27.51814 | 0.222649 | 0.029723 |
| 19 | 38.21665 | 0.361645 | 0.356504 | 40.85629 | 0.169475 | 0.380174 | 40.79078 | 0.331556 | 0.241203 | 28.16157 | 0.236935 | 0.0481 |
| 20 | 39.16363 | 0.428571 | 0.471698 | 41.75057 | 0.279503 | 0.597315 | 43.06811 | 0.414286 | 0.3567 | 29.50204 | 0.271632 | 0.129264 |

## Appendix K3 Values for LST (°C), NDVI and NDBI Classes for Kano 1990 - 2019

| | 1991 | | | 2001 | | | 2011 | | | 2019 | | |
|---|---|---|---|---|---|---|---|---|---|---|---|---|
| **SN** | **LST** | **NDVI** | **NDBI** | **LST** | **NDVI** | **NDBI** | **LST** | **NDVI** | **NDBI** | **LST** | **NDVI** | **NDBI** |
| 1 | 1.931307 | 0.42623 | -0.30357 | 6.832704 | 0.233766 | 0.974116 | 12.31695 | 0.435897 | -0.65826 | 0.363335 | 0.397631 | -0.21243 |
| 2 | 3.643717 | 0.307633 | -0.16012 | 8.602885 | 0.15902 | 0.976886 | 13.98159 | 0.31679 | -0.53467 | 2.024801 | 0.295708 | -0.17024 |
| 3 | 5.845385 | 0.258979 | -0.08315 | 10.87883 | 0.124851 | 0.978658 | 16.70553 | 0.255315 | -0.44869 | 3.409356 | 0.258418 | -0.13798 |
| 4 | 6.94622 | 0.222488 | -0.03067 | 12.01681 | 0.097088 | 0.98032 | 19.42948 | 0.201524 | -0.36808 | 4.886215 | 0.231073 | -0.1082 |
| 5 | 8.536314 | 0.189037 | 0.011321 | 13.66054 | 0.073597 | 0.982093 | 21.39677 | 0.155418 | -0.28747 | 6.455377 | 0.208699 | -0.0809 |
| 6 | 10.12641 | 0.158628 | 0.049808 | 15.30428 | 0.052241 | 0.983644 | 23.06141 | 0.113154 | -0.21224 | 8.02454 | 0.188812 | -0.05857 |
| 7 | 11.7165 | 0.128219 | 0.081297 | 16.94802 | 0.03302 | 0.984863 | 25.0287 | 0.074732 | -0.14776 | 9.409095 | 0.17141 | -0.03623 |
| 8 | 13.3066 | 0.09781 | 0.112786 | 18.59176 | 0.015935 | 0.98586 | 26.99599 | 0.040152 | -0.09402 | 10.51674 | 0.154009 | -0.0139 |
| 9 | 14.77438 | 0.070441 | 0.144276 | 20.10906 | -0.00115 | 0.986635 | 28.96329 | 0.013257 | -0.04565 | 11.43978 | 0.136607 | 0.005955 |
| 10 | 16.36447 | 0.049155 | 0.175765 | 21.7528 | -0.0161 | 0.9873 | 30.93058 | -0.0098 | -0.00266 | 12.27051 | 0.116719 | 0.023326 |
| 11 | 17.83225 | 0.03395 | 0.207255 | 23.2701 | -0.03318 | 0.987965 | 33.20054 | -0.02901 | 0.034952 | 13.00894 | 0.096832 | 0.040697 |
| 12 | 19.78929 | 0.018746 | 0.238744 | 25.29316 | -0.05027 | 0.988629 | 35.47049 | -0.04822 | 0.072568 | 13.74737 | 0.076944 | 0.055587 |
| 13 | 21.62401 | 0.003541 | 0.270234 | 27.18979 | -0.06949 | 0.989183 | 37.43779 | -0.07127 | 0.104811 | 14.4858 | 0.057057 | 0.067995 |
| 14 | 23.09179 | -0.01775 | 0.298224 | 28.70708 | -0.08871 | 0.989627 | 38.79976 | -0.09817 | 0.131679 | 15.22423 | 0.042141 | 0.080403 |
| 15 | 24.07031 | -0.03903 | 0.319217 | 29.71862 | -0.10793 | 0.989959 | 40.0104 | -0.12506 | 0.153174 | 15.87035 | 0.029711 | 0.092811 |
| 16 | 24.92651 | -0.06032 | 0.333213 | 30.60371 | -0.12288 | 0.990513 | 41.37237 | -0.14811 | 0.174669 | 16.51648 | 0.009824 | 0.105219 |
| 17 | 25.90503 | -0.0816 | 0.347208 | 31.61524 | -0.13783 | 0.991178 | 42.28036 | -0.17885 | 0.201538 | 17.1626 | -0.02249 | 0.125072 |
| 18 | 26.39429 | -0.10897 | 0.361203 | 32.121 | -0.15278 | 0.992175 | 43.18834 | -0.23264 | 0.239154 | 17.80873 | -0.05978 | 0.162297 |
| 19 | 26.76124 | -0.15763 | 0.378697 | 32.50033 | -0.18054 | 0.993726 | 44.39898 | -0.30949 | 0.314387 | 18.36255 | -0.09956 | 0.221855 |
| 20 | 30.91995 | -0.23669 | 0.511653 | 36.79934 | -0.22966 | 0.997493 | 48.78756 | -0.39786 | 0.572327 | 21.59318 | -0.15673 | 0.333528 |

## Appendix K4: Values for LST (°C), NDVI and NDBI Classes for Birnin Kebbi 1990 – 2019

| | 1990 | | | 2000 | | | 2010 | | | 2019 | | |
|---|---|---|---|---|---|---|---|---|---|---|---|---|
| SN | LST | NDVI | NDBI | LST | NDVI | DBI | LST | NDVI | NDBI | LST | NDVI | NDBI |
| 1 | 36.27589 | 0.575342 | -0.73926 | 31.66409 | 0.494505 | -0.82646 | 31.12926 | 0.459294 | -0.78531 | 6.863727 | 0.557964 | -0.9584 |
| 2 | 37.23493 | 0.451874 | -0.68541 | 32.1371 | 0.376664 | -0.76952 | 32.09759 | 0.330395 | -0.73501 | 7.696509 | 0.436907 | -0.9151 |
| 3 | 37.74642 | 0.405156 | -0.63984 | 32.61012 | 0.338445 | -0.72682 | 32.58175 | 0.279513 | -0.69245 | 8.40117 | 0.394373 | -0.88263 |
| 4 | 38.64152 | 0.368449 | -0.59841 | 33.08314 | 0.303411 | -0.68886 | 33.06591 | 0.238808 | -0.65376 | 9.169892 | 0.361655 | -0.85377 |
| 5 | 39.15301 | 0.331742 | -0.55699 | 33.98617 | 0.274747 | -0.6509 | 33.96508 | 0.204887 | -0.61894 | 9.938613 | 0.332209 | -0.82852 |
| 6 | 39.60056 | 0.295035 | -0.51557 | 34.9322 | 0.246082 | -0.61294 | 34.9334 | 0.174358 | -0.58412 | 10.70734 | 0.306034 | -0.79965 |
| 7 | 40.49566 | 0.261665 | -0.47414 | 35.40522 | 0.217418 | -0.57498 | 35.83256 | 0.143829 | -0.5493 | 11.54012 | 0.283131 | -0.7744 |
| 8 | 41.4547 | 0.228295 | -0.43272 | 35.87824 | 0.188754 | -0.53228 | 36.73172 | 0.113300 | -0.51448 | 12.3729 | 0.260229 | -0.74914 |
| 9 | 42.3498 | 0.194925 | -0.39543 | 36.30825 | 0.16009 | -0.49432 | 37.70005 | 0.086164 | -0.48353 | 13.20568 | 0.237326 | -0.72028 |
| 10 | 43.2449 | 0.164892 | -0.36229 | 36.78127 | 0.131426 | -0.45636 | 38.59921 | 0.062419 | -0.45644 | 14.03846 | 0.214423 | -0.68781 |
| 11 | 44.20394 | 0.138196 | -0.32916 | 37.6843 | 0.099576 | -0.41365 | 39.49837 | 0.038674 | -0.42936 | 14.87124 | 0.188249 | -0.65534 |
| 12 | 45.09904 | 0.114838 | -0.29602 | 38.15732 | 0.067727 | -0.37095 | 40.39753 | 0.014929 | -0.39841 | 15.70403 | 0.162074 | -0.62287 |
| 13 | 45.99415 | 0.091479 | -0.26702 | 38.58733 | 0.035878 | -0.32824 | 41.2967 | -0.005423 | -0.37132 | 16.53681 | 0.1359 | -0.5904 |
| 14 | 46.82531 | 0.06812 | -0.23802 | 39.06035 | 0.000844 | -0.2808 | 42.12669 | -0.029168 | -0.34424 | 17.30553 | 0.109725 | -0.55432 |
| 15 | 47.27286 | 0.048098 | -0.20902 | 39.49037 | -0.03419 | -0.2286 | 42.61085 | -0.052913 | -0.31716 | 18.01019 | 0.080279 | -0.51464 |
| 16 | 47.72042 | 0.028076 | -0.17588 | 39.96338 | -0.07241 | -0.17166 | 43.44085 | -0.076657 | -0.2862 | 18.58673 | 0.041017 | -0.47134 |
| 17 | 48.16797 | 0.00138 | -0.13446 | 40.3934 | -0.11381 | -0.11472 | 43.92501 | -0.103794 | -0.24751 | 19.09921 | -0.00479 | -0.42444 |
| 18 | 49.06307 | -0.03866 | -0.08061 | 41.29643 | -0.15522 | -0.05778 | 44.75501 | -0.144499 | -0.20108 | 19.67575 | -0.05059 | -0.37393 |
| 19 | 49.89424 | -0.09206 | 0.002241 | 41.72645 | -0.19662 | -0.00085 | 45.65417 | -0.198773 | -0.13531 | 20.25229 | -0.09967 | -0.30899 |
| 20 | 51.68444 | -0.15546 | 0.167939 | 42.62948 | -0.24121 | 0.203186 | 47.38332 | -0.259831 | 0.046535 | 22.04598 | -0.15856 | -0.16829 |